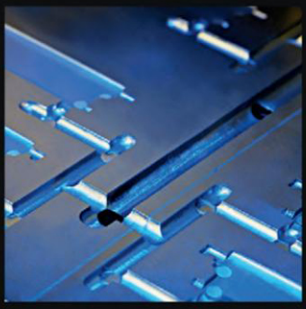
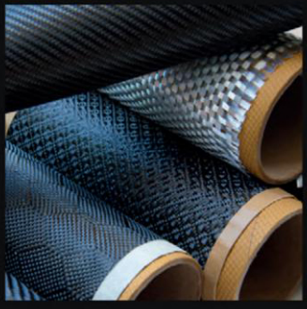
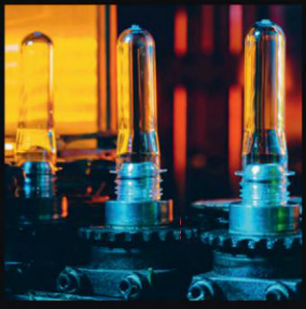
PLASTICS ENGINEERING

FOURTH EDITION




ROY J. CRAWFORD
PETER J. MARTIN

B
H

Plastics Engineering

Fourth Edition

R. J Crawford
Former Vice Chancellor, University of Waikato,
Hamilton, Waikato, New Zealand

P. J Martin
Reader in Mechanical Engineering,
Queen's University Belfast, Belfast, United Kingdom





Butterworth-Heinemann
An imprint of Elsevier

Butterworth-Heinemann is an imprint of Elsevier
The Boulevard, Langford Lane, Kidlington, Oxford OX5 1GB, United Kingdom
50 Hampshire Street, 5th Floor, Cambridge, MA 02139, United States

Copyright © 2020 Elsevier Ltd. All rights reserved.

No part of this publication may be reproduced or transmitted in any form or by any means, electronic or mechanical, including photocopying, recording, or any information storage and retrieval system, without permission in writing from the publisher. Details on how to seek permission, further information about the Publisher's permissions policies and our arrangements with organizations such as the Copyright Clearance Center and the Copyright Licensing Agency, can be found at our website: www.elsevier.com/permissions.

This book and the individual contributions contained in it are protected under copyright by the Publisher (other than as may be noted herein).

Notices
Knowledge and best practice in this field are constantly changing. As new research and experience broaden our understanding, changes in research methods, professional practices, or medical treatment may become necessary.

Practitioners and researchers must always rely on their own experience and knowledge in evaluating and using any information, methods, compounds, or experiments described herein. In using such information or methods they should be mindful of their own safety and the safety of others, including parties for whom they have a professional responsibility.

To the fullest extent of the law, neither the Publisher nor the authors, contributors, or editors, assume any liability for any injury and/or damage to persons or property as a matter of products liability, negligence or otherwise, or from any use or operation of any methods, products, instructions, or ideas contained in the material herein.

Library of Congress Cataloging-in-Publication Data
A catalog record for this book is available from the Library of Congress

British Library Cataloguing-in-Publication Data
A catalogue record for this book is available from the British Library

ISBN: 978-0-08-100709-9

For information on all Butterworth-Heinemann publications visit our website at https://www.elsevier.com/books-and-journals

Publisher: Matthew Deans
Acquisition Editor: Edward Payne
Editorial Project Manager: John Leonard
Production Project Manager: Kamesh Ramajogi
Cover Designer: Mark Rogers

Typeset by TNQ Technologies



Preface to the fourth edition

Plastics continue to be one of the most important materials in use today and over the past 20 years their breadth of applications and volumes of consumption have continued to rise at an astonishing pace. They are now so essential to modern life that it is virtually impossible to imagine how society could function without them. However, over the past few years the world's view of plastics has begun to change dramatically with the realisation that we have taken them for granted for the sake of convenience and in doing so we have created huge environmental problems. Their once cherished properties of variety, adaptability, inertness and indestructibility are now the same characteristics that are causing them to pollute our oceans and damage the eco-systems of our planet. The challenges that are emerging are immense and profound, and as never before require innovative engineers with a strong knowledge of the properties and processing of plastics.

In this new edition the structure of the previous edition has been largely retained, although all chapters have been thoroughly updated to reflect the numerous changes that have occurred in the types and formulations of plastic and composite materials over the last 23 years. New sections and sub-sections have been added throughout each chapter to introduce new technologies and chapter 4 has been expanded substantially to include a variety of new processing technologies. As before each chapter includes numerous worked example problems with solutions provided at the end of the book. One of the largest changes in this edition is to the figures, which have been almost entirely replaced, and which are now available in colour in the e-book version of the textbook.

I first became aware of the textbook 'Plastics Engineering' whilst being taught by Professor R. J Crawford at Queen's University Belfast in 1984, and since then it is a book that I have consistently turned to throughout my career. It remains the textbook that I recommend to our undergraduate engineers studying plastics and it is an essential reference source for our research students. I was absolutely delighted when Roy first approached me in 2015 about the possibility of producing a new edition of the book and I had no hesitation in accepting the challenge. Throughout 2015 we made ambitious plans for the new edition and we began work on chapter 1 in 2016. However, as the year progressed Roy unfortunately became increasingly ill and he sadly passed away in June 2016. At this point my progress did slow with the realisation of the enormity of the task in front

of me, but I hope that the completion of this new edition is a fitting tribute to my dear friend and colleague R. J Crawford. His foresight in identifying a need for a textbook of this kind and its continuing appeal after almost 40 years stand as testaments to his remarkable life and legacy.

P. J Martin
January 2020

Preface to the third edition

Plastics continue to be exciting materials to use and a dynamic area in which to work. Every year new application areas are being developed to utilise more fully the unique properties of this class of materials. In addition, new processing technologies are emerging to exploit the versatility of plastics and to take advantage of their ease of manufacture into all types of end products. It is very important that students and those already working in the industry are kept fully informed about these new developments. In this new edition an attempt has been made to bring existing subject material up to date and many new sections have been added to cover the innovations introduced over the past decade. The number of Worked Examples has been increased and there are many more Set Questions at the end of each Chapter. As in the previous editions, a full set of solutions to the Set Questions is provided at the end of the book.

In this new edition, some re-structuring of the content has taken place. The subject material on Fracture that previously formed Chapter 3 has been brought forward to Chapter 2. This chapter now provides a more unified approach to the deformation and fracture behaviour of non-reinforced plastics. Chapter 3 is new and deals with all aspects of the mechanical behaviour of composites in much more detail than the previous editions. Composites are an extremely important class of material for modern design engineers and they must form an integral part of undergraduate and postgraduate teaching. There are many excellent textbooks devoted to this subject, but it was felt that an introduction to the analysis of laminates would be a valuable addition to this text. It is hoped that the many worked examples in this new chapter will help the student, and the practising engineer, to gain a better understanding of this apparently complex subject area. Chapters 4 and 5 are essentially as before but they have been extensively updated. A more unified approach to the analysis of processing has also been adopted.

As other authors will know, the preparation of a textbook is a demanding, challenging and time-consuming occupation. I have been very fortunate to receive many encouraging comments on the previous editions and this has given me the enthusiasm to continue developing the subject material in the book. I am

very grateful to all of those who have taken the trouble to contact me in the past and I continue to welcome comments and advice as to how the book could be improved in the future.

R. J Crawford
September 1997

Preface to the second edition

In this book no prior knowledge of plastics is assumed. The text introduces the reader to plastics as engineering materials and leads on to the design procedures which are currently in use. Since the publication of the first edition the subject has developed in some areas, particularly processing and so this second edition contains the new and up-to-date information. Other modifications have also been made to improve the presentation of the contents. In particular, Chapter 1 has been completely re-written as an introduction to the general behaviour characteristics of plastics. The introduction to the structure of plastics which formed the basis of Chapter 1 in the first edition has been condensed into an Appendix in the new edition. Chapter 2 deals with the deformation behaviour of plastics. It has been expanded from the first edition to include additional analysis on intermittent loading and fibre composites. Chapter 3 deals with the fracture behaviour of plastics and here the importance of fracture mechanics has been given greater emphasis.

Chapter 4 describes in general terms the processing methods which can be used for plastics. All the recent developments in this area have been included and wherever possible the quantitative aspects are stressed. In most cases a simple Newtonian model of each of the processes is developed so that the approach taken to the analysis of plastics processing is not concealed by mathematical complexity.

Chapter 5 deals with the aspects of the flow behaviour of polymer melts which are relevant to the processing methods. The models are developed for both Newtonian and Non-Newtonian (Power Law) fluids so that the results can be directly compared.

Many more worked examples have been included in this second edition and there are additional problems at the end of each chapter. These are seen as an important aspect of the book because in solving these the reader is encouraged to develop the subject beyond the level covered in the text. To assist the reader a full set of solutions to the problems is provided at the back of the book.

R. J Crawford
January 1987

Preface to the first edition

This book presents in a single volume the basic essentials of the properties and processing behaviour of plastics. The approach taken and terminology used has been deliberately chosen to conform with the conventional engineering approach to the properties and behaviour of materials. It was considered that a book on the engineering aspects of plastics was necessary because there is currently a drive to attract engineers into the plastics industry and although engineers and designers are turning with more confidence to plastics there is still an underlying fear that plastics are difficult materials to work with. Their performance characteristics fall off as temperature increases and they are brittle at low temperatures. Their mechanical properties are time dependent and in the molten state they are non-Newtonian fluids. All this presents a gloomy picture and unfortunately most texts tend to analyse plastics using a level of chemistry and mathematical complexity which is beyond most engineers and designers. The purpose of this text is to remove some of the fears, by dealing with plastics in much the same way as traditional materials. The major part of this is to illustrate how quantitative design of plastic components can be carried out using simple techniques and how apparently complex moulding operations can be analysed without difficulty.

Many of the techniques illustrated have been deliberately simplified and so they will only give approximate solutions but generally the degree of accuracy can be estimated and for most practical purposes it will probably be acceptable. Once the engineer/designer has realised that there are proven design procedures for plastics which are not beyond their capabilities then these materials will be more readily accepted for consideration alongside established materials such as woods and metals. On these terms plastics can expect to be used in many new applications because their potential is limited only by the ingenuity of the user.

This book is intended primarily for students in the various fields of engineering, but it is felt that students in other disciplines will welcome and benefit from the engineering approach. Since the book has been written as a general introduction to the quantitative aspects of the properties and processing of plastics, the depth of coverage is not as great as may be found in other texts on the physics, chemistry and stress analysis of viscoelastic materials. this has been done deliberately because it is felt that once the material described here has been studied and understood the reader will be in a better position to decide if he requires the more detailed viscoelastic analysis provided by the advanced texts.

In this book no prior knowledge of plastics is assumed. Chapter 1 provides a brief introduction to the structure of plastics and it provides an insight to the way in which their unique structure affects their performance. There is a resume of the main types of plastics which are available. Chapter 2 deals with the mechanical properties of unreinforced and reinforced plastics under the general heading of deformation. The time dependent behaviour of the materials is introduced and simple design procedures are illustrated. Chapter 3 continues the discussion on properties but concentrates on fracture as caused by creep, fatigue and impact. The concepts of fracture mechanics are also introduced for reinforced and unreinforced plastics.

Chapter 4 describes in general terms the processing methods which can be used for plastics and wherever possible the quantitative aspects are stressed. In most cases a simple Newtonian model of each of the processes is developed so that the approach taken to the analysis of plastics processing is not concealed by mathematical complexity. Chapter 5 deals with the aspects of the flow behaviour of polymer melts which are relevant to the processing methods. The models are developed for both Newtonian and Non-Newtonian (Power Law) fluids so that the results can be directly compared.

Throughout the book there are worked examples to illustrate the use of the theory and at the end of each chapter there are problems to be solved by the reader. These are seen as an important part of the book because in solving the problems the reader is encouraged to develop the subject material beyond the level covered in the text. Answers are given for all the questions.

R. J Crawford

Chapter 1

General properties of plastics

1.1 Introduction

Plastics were undoubtedly the revolutionary material of the late 20th Century and in the early part of this century they have continued their inexorable rise in terms of importance and breadth of applications. In less than 150 years they have grown from being a chemical curiosity at the end of the 19th century, through a period of very rapid growth and development as a largely cheap alternative to other materials in the mid-20th century, to the point today where they are regarded as essential materials in their own right.

Today plastics surround us in every aspect of our lives and in numerous modern products it is difficult to imagine how they could have been manufactured without the unique properties of plastics. Their importance is most obvious in areas such as textiles, packaging and consumer electronics. It is estimated that there are now more mobile phones in the world than people (more than 7 billion) and every one of these devices uses plastic materials to either a greater or lesser extent. At the most basic level plastics are essential for creating the numerous case designs for mobile phones, but they are also employed more subtly as internal fixtures, screens or coatings on screens, or as insulators within or around numerous electronic components.

Therefore today designers and engineers readily turn to plastics because they offer combinations of properties not available in any other materials. Plastics offer advantages such as lightness, resilience, resistance to corrosion, colour fastness, transparency, ease of processing, etc., and although they have their limitations, their exploitation is limited only by the ingenuity of the designer.

The term *plastic* refers to a family of materials which includes nylon, polyethylene and PTFE just as zinc, aluminium and steel fall within the family of *metals*. This is an important point because just as it is accepted that zinc has quite different properties from steel, similarly nylon has quite different properties from PTFE. Few designers would simply specify *metal* as the material for a particular component so it would be equally unsatisfactory just to recommend *plastic*. This analogy can be taken still further because in the same way that there are different grades of steel there are also different grades of, say, polypropylene. In both cases the good designer will recognise this and

Plastics Engineering. https://doi.org/10.1016/B978-0-08-100709-9.00001-7
Copyright © 2020 Elsevier Ltd. All rights reserved.

select the most appropriate material and grade on the basis of processability, toughness, chemical resistance, etc.

It is usual to think that plastics are a relatively recent development but in fact, as part of the larger family called *polymers,* they are a basic ingredient of animal and plant life. Polymers are different from metals in the sense that their structure consists of very long chain-like molecules. Natural materials such as silk, shellac, bitumen, rubber and cellulose have this type of structure. However, it was not until the 19th century that attempts were made to develop a synthetic polymeric material and the first success was based on cellulose. This was a material called *Parkesine,* after its inventor Alexander Parkes, and although it was not a commercial success it was a start and it led to the development of *Celluloid.* This material was an important breakthrough because it became established as a good replacement for natural materials which were in short supply – for example, ivory for billiard balls.

During the early 20th century there was considerable interest in these new synthetic materials. Phenol-formaldehyde (*Bakelite*) was introduced in 1909, and at about the time of the Second World War materials such as nylon, polyethylene and acrylic (*Perspex*) appeared on the scene. Unfortunately many of the early applications for plastics earned them a reputation as being cheap substitutes. It took much of the latter half of the 20th century to overcome this image but nowadays the special properties of plastics have placed them at the forefront of much of our modern world's technological developments. Plastics are now firmly established as important materials in their own right, and they are often the first materials to be considered for many applications. This ever increasing use of plastics in all kinds of environments means that it is essential for designers and engineers to become familiar with the ever-expanding range of modern plastics and the types of performance characteristics to be expected so that these can be used to the best advantage.

This chapter is written as a general introduction to design with plastics. It outlines the range of plastics available, describes the types of behaviour which they exhibit and illustrates the design process involved in selecting the most appropriate plastic for a particular application.

1.2 Polymeric materials

Synthetic large molecules are made by joining together thousands of small molecular units known as **monomers**. The process of joining the molecules is called **polymerisation** and the number of these units in the long molecule is known as the **degree of polymerisation**. The names of many polymers consist of the name of the monomer with the suffix **poly-**. For example, the polymers polypropylene and polystyrene are produced from propylene and styrene respectively. Names, and symbols for common polymers are given in Appendix F.

It is an unfortunate fact that many design engineers are uncomfortable with plastics compared to other materials because they have an image of complicated structures described by complex chemical formulae. In fact it is not necessary to have a detailed knowledge of the structure of plastics in order to make good use of them. Perfectly acceptable designs are achieved provided one is familiar with their performance characteristics in relation to the proposed service conditions. An awareness of the structure of plastics can assist in understanding why they exhibit a time-dependent response to an applied force, or why acrylic is transparent and stiff whereas polyethylene is opaque and flexible, etc., but it is not necessary for one to be an expert in polymer chemistry in order to use plastics. Those who wish to have a general introduction to the structure of plastics may refer to Appendix A.

The words **polymers** and **plastics** are often taken as synonymous but in fact there is a distinction. The polymer is the pure material which results from the process of polymerisation and is usually taken as the family name for materials which have long chain-like molecules. This definition includes a range of naturally occurring polymers such as collagen, cellulose, keratin and rubber, which are still used widely today. In the case of rubber, newer synthetic varieties are increasingly replacing the natural material, and all types may be classified as **elastomers** due to their highly elastic mechanical behaviour. Pure polymers are seldom used on their own and it is when additives are present that the term plastic is applied. Polymers contain additives for a number of reasons. The following alphabetical list outlines the purpose of the main additives used in plastics:

Antioxidants. Antioxidants are used in plastics to inhibit their oxidative degradation and their thermal oxidation. Common plastics such as polyethylene and polypropylene are prone to oxidative degradation during processing at elevated temperatures.

Antistatic agents. Most polymers, because they are poor conductors of current, build up a charge of static electricity that can have undesirable effects. Problems include interference with electrical devices, attraction of dirt and sticking of surfaces. Antistatic agents attract moisture from the air to the plastic surface, improving its surface conductivity and reducing the likelihood of a spark or a discharge.

Blowing agents. Blowing agents are added to plastics to create foam or cellular structures in the final product. They may either take the form of physical blowing agents (where a gas is injected at high pressure directly into the plastic melt during processing), or chemical blowing agents (where a chemical agent is added to the plastic, which then decomposes during processing to evolve gas).

Coupling agents. Coupling agents are added to improve the bonding of the plastic to inorganic filler materials, such as glass fibres. They are very important in most polymer-based composite materials. Inorganic materials such as silane, titanate and zirconia are used for this purpose.

Fillers. Fillers are solid particles of usually inorganic materials that are added to plastics to improve properties and costs. Some, such as short fibres or flakes, improve the mechanical properties of a plastic. Others, called *extenders,* permit a large volume of a plastic to be produced with relatively little actual polymer resin. Low cost solids such as calcium carbonate, silica and clay are frequently used extenders.

Flame retardants. Most polymers, because they are organic materials, are flammable. Additives that contain chlorine, nitrogen, bromine, phosphorous or metallic salts reduce the likelihood that combustion will occur or spread.

Heat stabilisers. Heat stabilisers protect polymers during thermal processing and avoid product deterioration in short and long-term use at elevated temperatures. They are an essential additive for PVC, which is susceptible to rapid thermal degradation.

Lubricants. Lubricants such as wax or calcium stearate reduce the viscosity and stickiness of the molten plastic and improve its forming characteristics.

Nucleating agents. Nucleating agents are important for controlling the structure and properties of semi-crystalline plastics. They promote nucleation and crystallisation and they ensure that crystal structures are regular with smaller and more numerous spherulites. They include inorganic agents such as talc, mica and calcium carbonate, and organic agents such as mineral oils.

Pigments. Pigments and dyes are used to produce colours in plastics. Many provide secondary benefits, e.g. carbon black and titanium dioxide (white) act as UV stabilisers. Pigments are insoluble and may be organic or inorganic. Dyes are soluble and invariably organic.

Plasticisers. Plasticisers are added to plastics to aid flow and processing. They are low molecular weight materials which alter the properties and forming characteristics of the plastic. They help to develop new, improved properties not present in the original plastic, e.g. the production of flexible grades of PVC by the use of plasticisers.

Reinforcement. The strength, stiffness and toughness of polymers are improved by adding fibres of glass, carbon, aramid etc. Natural fibres, such as hemp, flax and jute, may also be used. Reinforcement with nano-clay particles, carbon nanotubes and graphene are leading to the development of new nanocomposite materials.

Release agents. Release agents can play a vital role in preventing plastics from sticking to processing machinery and in some cases are often more appropriately termed as ‘mould release agents’.

UV stabilisers. UV stabilisers are used to prevent or protect plastics from degradation by ultraviolet rays and thereby extend the life of the end products. Discoloration and brittleness are the key problems they address.

There are two important classes of plastics:

(a) Thermoplastic materials

In a thermoplastic material the very long chain-like molecules are held together by relatively weak van der Waals forces. A useful image of the structure is a mass of randomly distributed long strands of sticky wool. When a thermoplastic material is heated the intermolecular forces are weakened so that it becomes soft and flexible and eventually, at high temperatures, it is a viscous melt. When the material is allowed to cool it solidifies again. This cycle of softening by heat and solidifying on cooling can be repeated more or less indefinitely and is a major advantage in that it is the basis of most processing methods for these materials. It does have its drawbacks, however, because it means that the properties of thermoplastics are heat sensitive. A useful analogy which is often used to describe these materials is that, like candle wax, they can be repeatedly softened by heat and will solidify when cooled.

The properties of thermoplastics are greatly influenced by the lengths of the individual polymer chains and whether they contain side branches. Chain lengths are normally quantified by the molecular weight and the molecular weight distribution of the polymer. During the polymerisation process, steps can be taken to adjust both the lengths of the growing chains and to encourage side branches to form. This enables thermoplastic materials that have the same chemical formula to exist in quite different molecular arrangements that can give rise to very different properties. This is known as isomerism. Polyethylene, which is the most widely used thermoplastic, is a very good example of this. When it exists in the form of a largely linear chain, as shown in Fig. 1.1(a), the chains can be packed tightly together and the material is known as high density polyethylene (HDPE). When longer side branches are encouraged to grow (shown in Fig. 1.1(b), the chains can no longer pack together so tightly and the material is known as low density polyethylene (LDPE). Other variations include linear low density polyethylene (LLDPE) and ultra-high molecular weight polyethylene (UHMWPE). Other examples of common commercial thermoplastics are polyvinyl chloride (PVC), polystyrene, nylon, cellulose acetate, polycarbonate, polyethylene terephthalate (PET), polymethyl methacrylate, polylactic acid (PLA) and polypropylene.

An important subdivision within the thermoplastic group of materials is related to whether they have a **crystalline** (ordered) or an **amorphous** (random) structure. In practice, of course, it is not possible for a moulded plastic to have a completely crystalline structure due to the complex physical nature of the molecular chains (see Appendix A). Some plastics, such as polyethylene and nylon, can achieve a high degree of crystallinity but they are probably more accurately described as *partially crystalline* or *semi-crystalline.* Other plastics such as acrylic and polystyrene are always amorphous. The presence of crystallinity in those plastics capable of crystallising is very

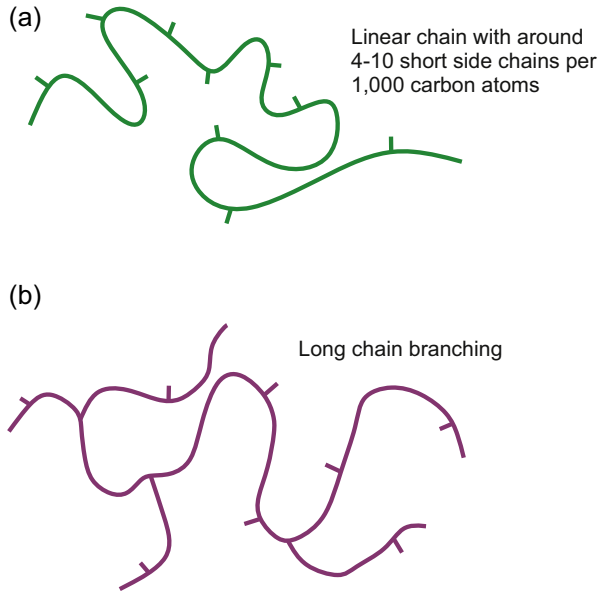


FIG. 1.1 Chain structures of polyethylene.

dependent on their thermal history and hence on the processing conditions used to produce the moulded article. In turn the mechanical properties of the moulding are very sensitive to whether or not the plastic possesses crystallinity.

In general, plastics have a higher density when they crystallise due to the closer packing of the molecules. Typical characteristics of crystalline and amorphous plastics are shown below:

Amorphous	Crystalline
• **Broad softening range** Thermal agitation of the molecules breaks down the weak secondary bonds. The rate at which this occurs throughout the formless structure varies producing a broad temperature range for softening.	• **Sharp melting point** The regular close-packed structure results in most of the secondary bonds being broken down at the same time. This results in a sharp crystalline melting point.
• **Usually transparent** The looser structure transmits light so the material appears transparent.	• **Usually opaque** The difference in refractive indices between the two phases (amorphous and crystalline) causes interference to light so the material appears translucent or opaque.

—cont'd

Amorphous	Crystalline
• **Low shrinkage** All thermoplastics are processed in the amorphous state. On solidification, the random arrangement of molecules produces little volume change and hence low shrinkage.	• **High shrinkage** As the material solidifies from the amorphous state the polymers take up a closely packed, highly aligned structure. This produces a significant volume change manifested as high shrinkage.
• **Low chemical resistance** The more open random structure enables chemicals to penetrate deep into the material and to destroy many of the secondary bonds.	• **High chemical resistance** The tightly packed structure prevents chemical attack deep within the material.
• **Poor fatigue and wear resistance** The random structure contributes little to fatigue or wear properties.	• **Good fatigue and wear resistance** The uniform structure is responsible for good fatigue and wear properties.

Examples of amorphous and crystalline thermoplastics

Amorphous	Crystalline
Polyvinyl chloride (PVC)	Polyethylene (PE)
Polystyrene (PS)	Polypropylene (PP)
Polycarbonate (PC)	Polyamide (PA)
Acrylic (PMMA)	Acetal (POM)
Acrylonitrile-butadiene-styrene (ABS)	Polyesters (PET, PBT)
Polyphenylene (PPO)	Fluoropolymers (PTFE, PFA, FEP & ETFE)
	Polylactic acid (PLA)

(b) Thermosetting plastics

A thermosetting plastic is produced by a chemical reaction which has two stages. The first stage results in the formation of long chain-like molecules similar to those present in thermoplastics, but still capable of further reaction. The second stage of the reaction (**cross-linking** of chains) takes place during moulding, usually under the application of heat, pressure or in some cases by exposure to UV light. The resultant moulding will be rigid when cooled and a close network structure has been set up within the material. During the second stage the long molecular chains have been interlinked by strong bonds so that

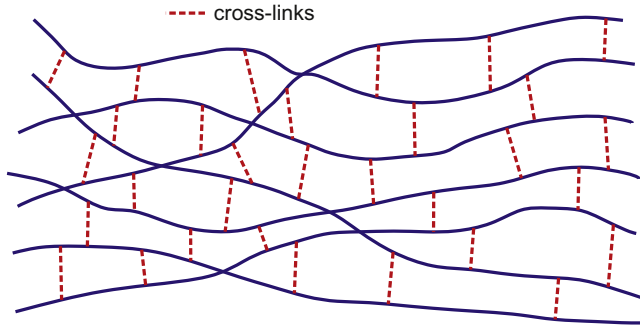


FIG. 1.2 Cross-linked structure of a typical thermoset.

the material cannot be softened again by the application of heat. The cross-linked structure of a typical thermoset is shown in Fig. 1.2. If excess heat is applied to these materials they will char and degrade. This type of behaviour is analogous to boiling an egg. Once the egg has cooled and is hard, it cannot be softened again by the application of heat.

Since the cross-linking of molecules is by strong chemical bonds, thermosetting plastics are characteristically quite rigid materials and their mechanical properties are not heat sensitive. Examples of thermosets are phenol formaldehyde, melamine formaldehyde, urea formaldehyde, epoxy, silicone and some polyesters.

1.3 Plastics available to the designer

Plastics, more than any other design material, offer such a wide spectrum of properties that they must be given serious consideration in most component designs. However, this does not mean that there is sure to be a plastic with the correct combination of properties for every application. It simply means that the designer must have an awareness of the properties of the range of plastics available and keep an open mind. One of the most common faults in design is to be guided by preconceived notions. For example, an initial commitment to plastics based on an irrational approach is itself a serious design fault. A good design always involves a judicious selection of a material from the whole range available, including non-plastics. Generally, in fact, it is only against a background of what other materials have to offer that the full advantages of plastics can be realised.

In the following sections most of the common plastics will be described briefly to give an idea of their range of properties and applications. However, before going on to this it is worthwhile considering briefly several of the special categories into which plastics are divided.

1.3.1 Commodity thermoplastics

The largest category of plastics are termed commodity plastics, since they are used in very high volumes across a wide range of applications. They are

selected to exploit some of the unique advantages of thermoplastics over alternative materials such as their low density, high flexibility, good transparency and ease of mouldability. Typically such plastics exhibit relatively low mechanical properties and are of low cost. The major applications of commodity plastics include packaging, toys, clothing, transportation and household products where mechanical properties and service environments are not critical. The most important commodity plastics are polyethylene, polypropylene, polyvinyl chloride (PVC), polystyrene, and polyethylene terephthalate (PET).

1.3.2 Engineering thermoplastics

Thermoplastics are now firmly established as engineering materials and many are distinguished by the description **engineering thermoplastics**. The term probably originated as a classification distinguishing those that could be substituted satisfactorily for metals such as aluminium in small devices and structures from those with inadequate mechanical properties. This demarcation is clearly artificial because the properties on which it is based are very sensitive to the ambient temperature, so that a thermoplastic might be a satisfactory substitute for a metal at a particular temperature and an unsatisfactory substitute at a different one. There are also an increasing number of thermoplastics that are further classified as high performance materials due to one or more properties that are exceptional compared to a general engineering plastic. These are explored in more detail in the next section but it is worth pointing out that the distinction of 'high performance' has changed considerably over the years. For example, in the early days of plastics nylon was regarded as a high performance material when compared to the alternatives at that time, but these days it is quite an ordinary engineering thermoplastic.

A useful definition of an engineering material is that it is able to support loads more or less indefinitely. By such a criterion thermoplastics are at a disadvantage compared with metals because they have low time-dependent moduli and inferior strengths except in rather special circumstances. However, these disadvantages are off-set by advantages such as low density, resistance to many of the liquids that corrode metals and above all, easy processability. Thus, where plastics compete successfully with other materials in engineering applications it is usually because of a favourable balance of properties rather than because of an outstanding superiority in some particular respect, although the relative ease with which they can be formed into complex shapes tends to be a particularly dominant factor. In addition to conferring the possibility of low manufacturing costs, this ease of processing permits imaginative designs that commonly enable plastics to be used as a superior alternative to metals rather than merely as a tolerated substitute.

Currently the materials generally regarded as making up the **engineering thermoplastics** group are Nylon (or polyamide), acetal (or polyoxymethylene

POM), polycarbonate (PC), acrylonitrile butadiene styrene (ABS), polyphenylene oxide (PPO), thermoplastic polyesters and polysulphone (PSU). However, this list is not exclusive and it is continually subject to change with material developments. Newer grades of many of the commodity thermoplastics can possess good *engineering* performance such as in the use of unplasticised polyvinyl chloride (uPVC) in industrial pipework or ultra-high molecular weight polyethylene (UHMWPE) in artificial hip joints. Plastics may also be given substantially enhanced engineering properties through process-induced orientation of the polymer chains. Examples are biaxially orientated polypropylene (BOPP) and injection blow moulded PET. Hence it is unwise to exclude any plastic from consideration as an engineering material even though there is a sub-group specifically identified for this area of application.

1.3.3 High performance plastics

High performance plastics are defined as materials that meet higher requirements than standard engineering plastics because of their better mechanical properties, higher chemical resistance and/or higher heat stability. Usually such plastics have exceptional properties in one or two key areas, as opposed to the more balanced general performance of the engineering thermoplastics. Elevated thermal performance is most often the key distinctive property of this class of thermoplastics and a general rule of thumb is that a plastic may be considered high performance if it has a short-term heat resistance of 250°C and a long term heat resistance of 160°C. However, such improvements in thermal properties make processing more difficult and often special machines are required. In some cases the plastics are so viscous in the melt state that they cannot be processed by any of the normal processing techniques, and as a result their practical applications are severely limited. Many of the materials are also substantially more expensive than other thermoplastics. For example, on a cost per weight basis PEEK can be more than 50 times more expensive than commodity plastics such as PE or PP. Nevertheless new high performance plastics are constantly emerging and demand for them is being fuelled by strong growth in key market sectors such as aerospace, IT/telecom and automotive.

Some of the most important types and classes of high performance plastics are: Polyarylethersulfones (PAES), Polyphthalamides (PPA), Polyphenylene sulphide (PPS), Polyaryletherketones (PAEK) such as polyetherketones (PEK, PEEK), Polyimides (PI), Polybenzimidazole (PBI), and Fluoropolymers such as polytetrafluoroethylene (PTFE), fluorinated ethylene propylene (FEP) and perfluoroalkoxy (PFA).

1.3.4 Thermosets

Although many of the earliest synthetic polymers developed were thermosets (e.g. Bakelite (introduced in 1907)), their share of the rapidly growing plastics

market has consistently declined since the mid-twentieth century. Markets for thermosetting plastics have continued to grow over the years and new materials have been introduced. However, in comparison to thermoplastics, which can be exceptionally easy to process, many thermosets require specialised processing equipment and as a result they have become unattractive for mass production. Typically their production costs are much higher and their production volumes are much lower than thermoplastics, and crucially their production scrap cannot be reprocessed. Therefore thermoplastics have come to dominate all of the very high volume markets for plastics in areas such as packaging and consumer goods, and thermosets have instead found more-modestly growing applications in niche market sectors. Thermosets have also lost some market share due to the rise of high performance thermoplastics, which have enhanced properties that can approach those of thermosets in key applications. Thermosets are generally stronger, stiffer and harder than thermoplastics and are best-suited to applications that require high temperature service. They are chemically resistant, non-flammable and dimensionally stable. However, they are normally brittle and they can only be recycled as a filler material.

The main types of thermosetting plastics are: Phenolics (e.g. phenol formaldehyde or Bakelite), Amino plastics (e.g. urea formaldehyde (UF) or melamine formaldehyde (MF)), thermosetting Polyesters, Epoxies (EP), thermosetting Polyimides, and Polyurethanes (PU). It should be pointed that some materials may be either thermoplastic or thermoset, as is the case with polyesters, polyimides and polyurethanes.

1.3.5 Composites

One of the key factors which make plastics attractive for engineering applications is the possibility of property enhancement through reinforcement. Most commonly this is achieved by the introduction of fibres, but increasingly new nanocomposite plastics are starting to emerge in which reinforcement is provided by a range of nano-scale materials such as nano-clays, carbon nanotubes and graphene. In all cases the reinforcement is designed to either enhance the mechanical properties of the original plastic or to provide other specific property improvements such as gas barrier enhancement or improved electrical conductivity. From the early days of plastics manufacturers were quick to turn to reinforcing fibres to offset the brittle nature of many of the original thermosetting plastics, but this trend has continued with widening applications for reinforced thermoplastics. Reinforcement can be hidden as short fibres within the plastic during conventional processing or they can be in the form of plastic impregnated long fibres or woven fibre mats that require specialised manufacturing techniques. Demand has been particularly driven by the needs of the automotive and aerospace sectors for light-weight recyclable materials with lower production costs. Change has been most evident in

aircraft production where the percentage of composite materials used has risen from less than 5% in the 1980s to over 50% in the latest passenger aircraft produced by both Boeing and Airbus. Traditionally aircraft composites have been based on long or woven fibre reinforced thermosets such as epoxy resin, but these generally require slow and labour-intensive production methods and the use of very expensive equipment such as an autoclave. With parts now being produced in much larger numbers, there is increasing interest in using readily mouldable reinforced thermoplastics as alternatives. A number of new thermoplastic composites have been introduced which are largely based on combining either engineering or high performance thermoplastics (e.g. PC, PA, PPS, PEI, PEEK and PEKK) with reinforcing fibres. In some cases the fibres are provided as woven mats pre-impregnated with thermoplastic that largely resemble the common form of thermosetting composite pre-pregs. Although thermoplastic matrix composites require much simpler manufacturing processes, they cannot yet compete with the best thermosetting composites in terms of ultimate mechanical properties and they are susceptible to serious property deterioration at elevated temperatures. For these reasons they are largely confined to weight-saving applications and they are not yet ready to replace thermosetting composites in the main structural components.

The automotive industry has had a much longer relationship with composites, and here the predominant materials have been reinforced thermoplastics due to their greater suitability for the mass production methods required for very high volume vehicle production. By introducing short fibres (usually of glass) thermoplastics can be significantly strengthened whilst retaining the capacity to melt and flow so that rapid and efficient production methods such as injection moulding may be employed. Originally thermoplastics were introduced to automobiles as replacements for natural materials such as wood and leather in decorative panels and upholstery, but nowadays they are used throughout a vehicle's interior and increasingly short fibre-reinforced thermoplastics are being used in structural components such as bumpers or panelling, where they have the advantage of enabling large coloured body parts to be produced in a single moulding operation. Longer fibre or woven fibre thermoplastic composite have also been used for many years but these require manufacturing processes such as stamping or compression moulding. Materials of this kind include glass-mat thermoplastics (GMT) and more recently developed long fibre reinforced thermoplastics (LFRT), which can be processed by injection moulding and are based on a wide variety of thermoplastics that include PP, PE and PET. Reinforced thermosets have tended to be used to a much lesser extent, but have found applications in heat resistant fixtures and housings around the engine and exhaust systems. Some small volume vehicle manufacturers have produced major structural components and body panels using either hand lay-up or processes similar to thermosetting composite manufacturing for aircraft, but these are simply not economically viable for larger production runs.

There are some alternative materials such as bulk moulding compound (BMC) or sheet moulding compound (SMC). In both cases these consist of a pre-prepared mixture of uncured thermosetting polyester with glass fibre reinforcement, which acts as a feedstock or preform for subsequent processing by compression moulding or injection moulding. In the case of SMC the polyester paste/fibre mixture is sandwiched between fine thermoplastic films to create a sheet preform, and this material is now showing promise for the high volume manufacture of automotive body panels. Further details of the major processing techniques for composites are included in chapter 4.

Glass fibres are the principal form of reinforcement used for plastics because they offer a good combination of strength, stiffness and price. Improved strengths and stiffnesses can be achieved with other fibres such as aramid (**Kevlar**) or carbon fibres but these are expensive. Hybrid systems consisting of combinations of fibres of different types can provide a good balance of properties at an acceptable price. For example, the impact properties of carbon fibre-reinforced plastics (CFRP) can be improved by the addition of glass fibres and the stiffness of glass fibre-reinforced plastics (GFRP) can be increased by the addition of carbon fibres. There is also a growing interest in the use of natural fibres such as flax, jute, hemp, sisal and banana. Typically these do not perform as well as the synthetic fibres from an engineering point of view but their principal attractions are to exploit untapped economic resources in agricultural waste and to provide sustainable bio-degradable reinforcement for new bio-degradable plastics.

1.3.6 Structural foam

The concept of structural foams offers an unusual but exciting opportunity for designers. Many plastics can be foamed by the introduction of a blowing agent so that when moulded the material structure consists of a cellular rigid foam core with a solid tough skin. This type of structure is of course very efficient in material terms and offers an excellent stiffness-to-weight ratio.

The foam effect is achieved by the dispersion of inert gas throughout the molten resin directly before moulding. Introduction of the gas is usually carried out by one of two types of blowing agent: (1) Chemical blowing agents. The resin is pre-blended with a chemical blowing agent (e.g. azodicarbon-amides) which releases gas when heated; (2) Physical blowing agents. A gas (usually nitrogen) is directly injected into the polymer melt at high pressure. In both cases the gas is initially dissolved as a supersaturated solution within the high pressure plastic melt and only when the melt emerges into the mould does it form gas bubbles that expand explosively to fill the mould cavity and typically create an internal cellular structure with a solid skin.

ABS, polycarbonate, polypropylene and modified PPO are common materials for structural foam moulding. One of the main application areas is housings for business equipment and domestic appliances because the number

of component parts can be kept to the absolute minimum due to integral moulding of wall panels, support brackets, etc. Other components include vehicle body panels and furniture.

Structural foam mouldings may also include fibres to enhance further the mechanical properties of the material. Typical performance data for foamed polypropylene relative to other materials is given in Table 1.1.

1.3.7 Elastomers

Natural rubbers (Polyisoprenes) are members of the polymer family in that athey consist of long chain-like molecules. These chains are coiled and twisted in a random manner and have sufficient flexibility to allow the material to undergo very large deformations. In the *green* state the rubber would not be able to recover fully from large deformations because the molecules would have undergone irreversible sliding past one another. In order to prevent this sliding, the molecules are anchored together by a curing process known as vulcanisation. This creates cross-links between adjacent molecules as shown in Fig. 1.3 and the reaction is similar to that which occurs in thermosets. These cross-links do not detract from the random disposition of the molecules nor their coiled and twisted nature so that when the rubber is deformed the molecules stretch and unwind but do not slide. Thus when the applied force is removed the rubber will snap back to its original shape. Over the years a large number of synthetic polymers were developed to provide alternative sources of rubber and these developments were particularly intense during periods of world crises such as the Second World War. The new 'elastic polymer' materials were given the name **Elastomers**, although the terms rubber and elastomer are often used interchangeably. Some examples of these synthetic rubbers (or elastomers) are: Styrene-butadiene rubber (SBR), Butyl rubber, Ethylene-propylene rubber, Silicone rubber and Neoprene.

Vulcanised rubbers possess a range of very desirable properties such as resilience, resistance to oils, greases and ozone, flexibility at low temperatures and resistance to many acids and bases. However, they require careful (slow) processing and they consume considerable amounts of energy to facilitate moulding and vulcanisation. These disadvantages led to the development of **thermoplastic rubbers (or elastomers)**. These are materials which exhibit the desirable physical characteristics of rubber but with the ease of processing of thermoplastics.

There are two main types of thermoplastic elastomers (TPE), or thermoplastic rubber (TPR). The first of these are termed segmented block copolymers in that they consist of thermoplastic molecules grafted to the rubbery molecules. Some examples of these are thermoplastic polyurethane, styrenic block copolymer, thermoplastic copolyester and thermoplastic polyamide. The typical structure of these is illustrated by the styrenic block copolymer shown in Fig. 1.4. At room temperature the thermoplastic molecules clump together

TABLE 1.1 Comparison of structural foams based on various grades of polypropylene with some traditional materials.

	Unfilled copolymer		40% talc-filled homopolymer		30% coupled glass-reinforced		Chip-board	Pine	Aluminium	Mild steel
	Solid	Foam	Solid	Foam	Solid	Foam				
Flexural modulus (MPa)	1.4	1.2	4.4	2.5	6.7	3.5	2.3	7.9	70	207
Specific gravity	0.905	0.72	1.24	1.00	1.12	0.90	0.650	0.641	2.7	7.83
Relative thickness at equivalent rigidity	1	1.05	0.68	0.81	0.59	0.74	0.85	0.56	0.27	0.19
Relative weight at equivalent rigidity	1	0.84	0.94	0.90	0.74	0.73	0.61	0.40	0.81	1.65

to anchor the rubbery molecules. When heat is applied the thermoplastic molecules are capable of movement so that the material may be shaped using conventional thermoplastic moulding equipment.

The second type of TPEs are elastomeric alloys. These consist of fine rubber particles in a thermoplastic matrix which is most commonly a polyolefin (such as polypropylene or polyethylene). The structure for a polypropylene elastomer is shown in Fig. 1.5 and it is the matrix which melts

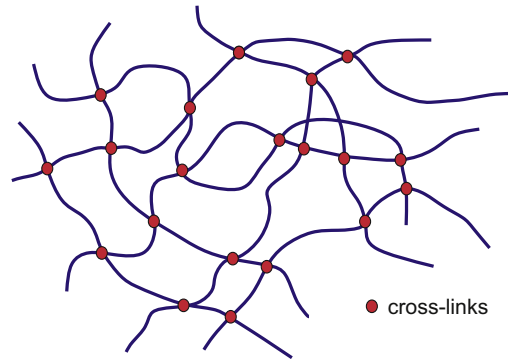


FIG. 1.3 Cross-linking of chains in an elastomer.

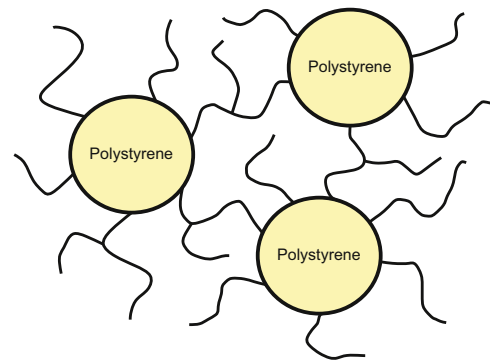


FIG. 1.4 Structure of a styrenic block copolymer elastomer.

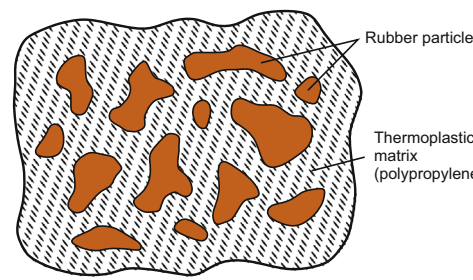


FIG. 1.5 Typical structure of olefinic TPR.

during processing to permit shaping of the material. The rubber filler particles then contribute the flexibility and resilience to the material. The properties of five TPEs are summarised in Table 1.11.

1.3.8 Polymer alloys

The principle of alloying plastics is similar to that of alloying metals, i.e. to achieve in one material the advantages possessed by several others. Blending or alloying of plastics has been exploited commercially for many years and one of its major successes is ABS, which is in fact an alloy of acrylonitrile, butadiene and styrene. Numerous other blends of materials are now commercially available and advances in blending technologies for plastics are enabling alloys to be created from plastics which were previously considered to be incompatible. Advances are also being driven by keen competition for a share of new market areas, particularly in the automotive sector. Here many applications call for combinations of properties not previously available in a single plastic and it has been found that it is less expensive to combine existing plastics than to develop a new monomer on which to base the new plastic.

In designing an alloy, polymer chemists choose candidate resins according to the properties, cost, and/or processing characteristics required in the end product. Next, compatibility of the constituents is studied, tested, and either optimised or accommodated. Polymer blends may be divided into three main types: (1) Compatible polymer blends (e.g. natural rubber and polybutadiene); (2) Partially incompatible blends (e.g. polyethylene and polypropylene, polycarbonate and polybutylene terephthalate); (3) Incompatible blends (polystyrene and polyolefins, polyamide and polyethylene).

Certain polymers have come to be considered standard building blocks of the polyblends. For example, impact strength may be improved by using polycarbonate, ABS and polyurethanes. Heat resistance is improved by using polyphenylene oxide, polysulphone, PVC, polyester (PET and PBT) and acrylic. Barrier properties are improved by using plastics such as ethylene vinyl alcohol (EVA). Elastomers are used to produce some types of thermoplastic elastomers (see section 1.3.7). Some modern plastic alloys and their main characteristics are given in Table 1.2.

1.3.9 Liquid crystal polymers

Liquid crystal polymers (LCP) are a relatively recent arrival on the plastics materials scene. They have outstanding dimensional stability, high strength, stiffness, toughness and chemical resistance all combined with ease of

TABLE 1.2 Typical plastic alloys.

Alloy	Features
PVC/acrylic	Tough with good flame and chemical resistance
PVC/ABS	Easily processed with good impact and flame resistance
Polycarbonate/ABS	Hard with high heat distortion temperature and good notch impact strength
ABS/Polysulphone	Less expensive than unmodified polysulphone
Polyphenylene oxide/HIPS	Improved processability, reduced cost
SAN/olefin	Good weatherability
Nylon/elastomer	Improved notched impact strength
Modified amorphous nylon	Easily processed with excellent surface finish and toughness
Polycarbonate/PBT	Tough engineering plastic

processing. They are named after the fact that they can retain a highly ordered (or crystalline) structure even in the molten state. When these materials are subjected to stress the molecular chains slide over one another but the ordered structure is retained. It is the retention of the highly crystalline structure which imparts the exceptional properties to LCPs. Many LCPs are based on thermoplastic aromatic polyesters but probably the best-known LCP is the aromatic polyamide or aramid polymer Kevlar, which in fibre form is renowned for its exceptional properties in bullet-proof vests and aircraft composites.

1.3.10 Shape memory polymers

Shape memory polymers (SMP) are an emerging technology and are classified as a form of smart material. They are plastics that are specifically designed to return from a deformed state (temporary shape) to their original (permanent) shape on the application of an external stimulus. This can be a temperature change, where heat is used to soften part of the structure so that the remaining part containing the original shape memory can return the softened part to its original shape. Alternatively some SMPs use optical or electrical stimuli to trigger the shape memory effect. Many of the current shape memory polymers employ either physical or chemical cross-linking processes to prevent the polymer chains from slipping. Polymers used to create SMPs include polyurethanes, polyesters and various elastomers.

1.3.11 Bio-degradable plastics

Many natural materials such as proteins, starches and cellulose are forms of polymer that are biodegradable. This means that they will break down after use into natural byproducts that will readily disperse into the environment. Biodegradable plastics are therefore not new and early plastics such as cellulose acetate were first manufactured from cellulose extracted from wood pulp over 100 years ago. However, developments in such materials waned for many years due to the ready availability of crude oil but this has now been replaced by an expansion of interest in new biodegradable plastics for two reasons: Firstly, the desire to replace the non-biodegradable, and in many cases non-recyclable, plastics derived from fossil fuels with naturally-derived and carbon neutral alternatives; Secondly, the growing interest in functional materials for medical use that could biodegrade naturally within the body without further medical intervention.

The most important group of new biodegradable plastics are aliphatic polyesters that may be produced either naturally or synthetically. These include: Polyhydroxyalkanoates (PHAs) (e.g. poly-3-hydroxybutyrate (PHB)), which are produced commercially by scaled up natural bacterial fermentation of sugars and vegetable oils; Polylactic Acid (PLA), which is synthesised from corn starch, sugar cane or other plant starches; Polybutylene succinate (PBS) and polycaprolactone (PCL), which are wholly synthetic. Other significant classes of biodegradable plastics include: Starch derived biopolymers; polyanhydrides; and cellulose esters, which include cellulose acetate. The currently available materials provide a very wide range of mechanical properties and degradation rates. For example, some starch biopolymers disintegrate immediately on the application of water, whereas PLA will only biodegrade when subjected to industrial composting conditions. Some of the materials (e.g. PHA, PHB, PLA and PBS) are seen as direct replacements for commodity thermoplastics as they show similar mechanical properties and processability. In terms of basic properties PHB is comparable to polypropylene and PLA is comparable to PET. Other materials such as PCL and polyanhydrates have comparatively poor mechanical properties but are being exploited mainly for their biodegradability in bioactive or bioresorbable implants such as tissue scaffolds.

1.4 Selection of plastics

The previous section has given an indication of the range of plastics available to the design engineer. The important question then arises *How do we decide which plastic, if any, is best for a particular application?* Material selection is not as difficult as it might appear but it does require an awareness of the

general behaviour of plastics as a group, as well as a familiarity with the special characteristics of individual plastics.

The first and most important steps in the design process are to define clearly the purpose and function of the proposed product and to identify the service environment. Then one has to assess the suitability of a range of candidate materials. The following are generally regarded as the most important characteristics requiring consideration for most engineering components.

(1) mechanical properties—strength, stiffness, specific strength and stiffness, fatigue and toughness, and the influence of high or low temperatures on these properties;
(2) corrosion susceptibility and degradation;
(3) wear resistance and frictional properties;
(4) thermal properties;
(5) special properties, for example, electrical, optical and magnetic properties, damping capacity, etc.;
(6) moulding and/or other methods of fabrication;
(7) recyclability;
(8) total costs attributable to the selected material and manufacturing route.

In the following sections these factors will be considered briefly in relation to plastics.

1.4.1 Mechanical properties

Strength and stiffness. Thermoplastic materials are viscoelastic which means that their mechanical properties reflect the characteristics of both viscous liquids and elastic solids. Thus when a thermoplastic is stressed it responds by exhibiting viscous flow (which dissipates energy) and by elastic displacement (which stores energy). The properties of viscoelastic materials are time, temperature and strain rate dependent. Nevertheless the conventional stress—strain test is frequently used to describe the (short-term) mechanical properties of plastics. It must be remembered, however, that as described in detail in Chapter 2 the information obtained from such tests may only be used for an initial sorting of materials. It is not suitable, or intended, to provide design data which must usually be obtained from long term (e.g. creep) tests.

In many respects the stress—strain graph for a plastic is similar to that for a metal (see Fig. 1.6). At low strains there is an elastic region whereas at high strains there is a nonlinear relationship between stress and strain and there is a permanent element to the strain. In the absence of any specific information for a particular plastic, design strains should normally be limited to 1%.

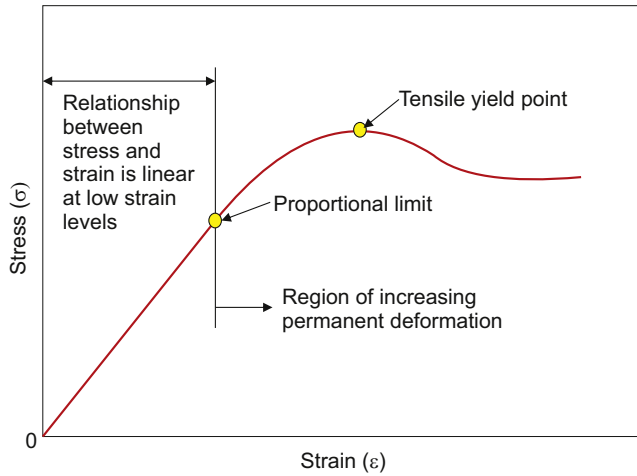


FIG. 1.6 Typical stress–strain graph for plastics.

Lower values ($\simeq 0.5\%$) are recommended for the more brittle thermoplastics such as acrylic, polystyrene and values of 0.2–0.3% should be used for thermosets.

The effect of material temperature is illustrated in Fig. 1.7. As temperature is increased the material becomes more flexible and so for a given stress the material deforms more. Another important aspect to the behaviour of plastics is the effect of strain rate. If a thermoplastic is subjected to a rapid change in strain it appears stiffer than if the same maximum strain were applied but at a slower rate. This is illustrated in Fig. 1.8.

It is important to realise also that within the range of grades that exist for a particular plastic, there can be significant differences in mechanical properties. For example, with polypropylene for each 1 kg/m^3 change in density there is typically a corresponding 4% change in modulus. Fig. 1.9 illustrates the stress-strain behaviour of the different grades of ABS. It may be seen that very often a grade of material selected for some specific desirable feature (e.g. high impact strength) results in a decrease in some other property of the material (e.g. tensile strength).

The stiffness of a plastic is expressed in terms of a modulus of elasticity. Most values of this modulus quoted in technical literature represent the slope of a tangent to the stress–strain curve at the origin (see Fig. 1.10). This is often referred to as Young's modulus, E, but it should be remembered that for a plastic this will not be a constant and, as mentioned earlier, is only useful for quality control purposes, not for design. Since the tangent modulus at the origin is sometimes difficult to determine precisely, a secant modulus is often quoted to remove any ambiguity. A selected strain value of,

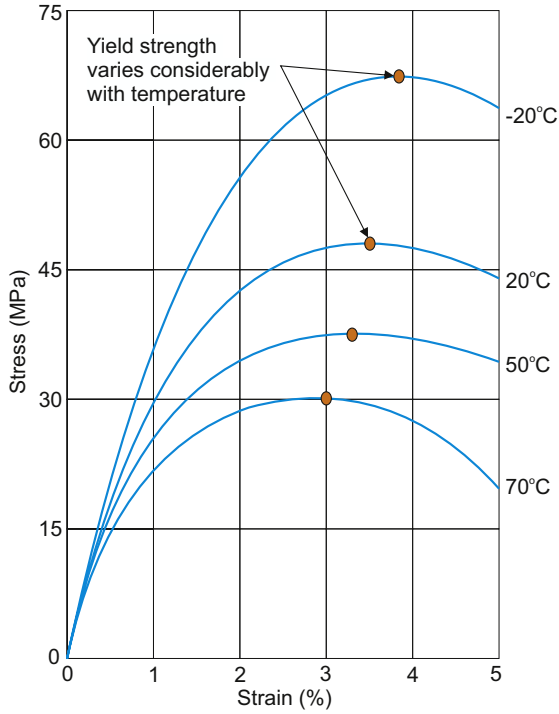


FIG. 1.7 Effect of material temperature on stress–strain behaviour of plastics.

say 2% (point C′, Fig. 1.10) enables a precise point, C, on the stress–strain curve to be identified. The slope of a line through C and O is the secant modulus. Typical short-term mechanical properties of plastics are given in Table 1.3. These are given for illustrative purposes. For each type of plastic there are many different grades and a wide variety of properties and costs are possible. The literature supplied by the manufacturers should be consulted in specific instances.

Material selection for strength

If, in service, a material is required to have a certain strength in order to perform its function satisfactorily then a useful way to compare the structural efficiency of a range of materials is to calculate their **strength desirability factor**.

Consider a structural member which is essentially a beam subjected to bending (Fig. 1.11). Irrespective of the precise nature of the beam loading the maximum stress, σ, in the beam will be given by

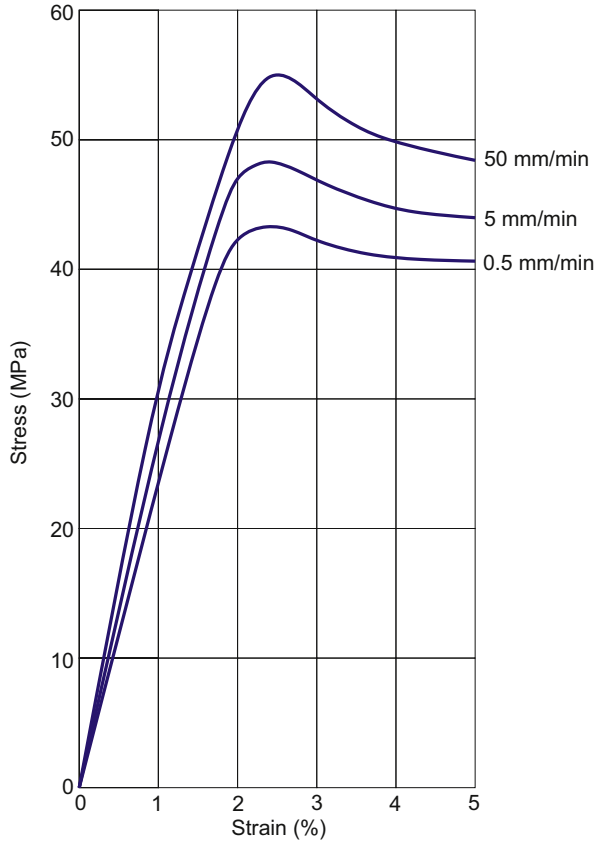


FIG. 1.8 Effect of strain rate on stress–strain behaviour of plastics.

$$\sigma = \frac{M_{\max}(d/2)}{I} = \frac{M_{\max}(d/2)}{bd^2/12} \tag{1.1}$$

Assuming that we are comparing different materials on the basis that the mean length, width and loading is fixed but the beam depth is variable then Eq. (1.1) may be written as

$$\sigma = \beta_1/d^2 \tag{1.2}$$

where β_1 is a constant.

But the weight, w, of the beam is given by

$$w = \rho bdL \tag{1.3}$$

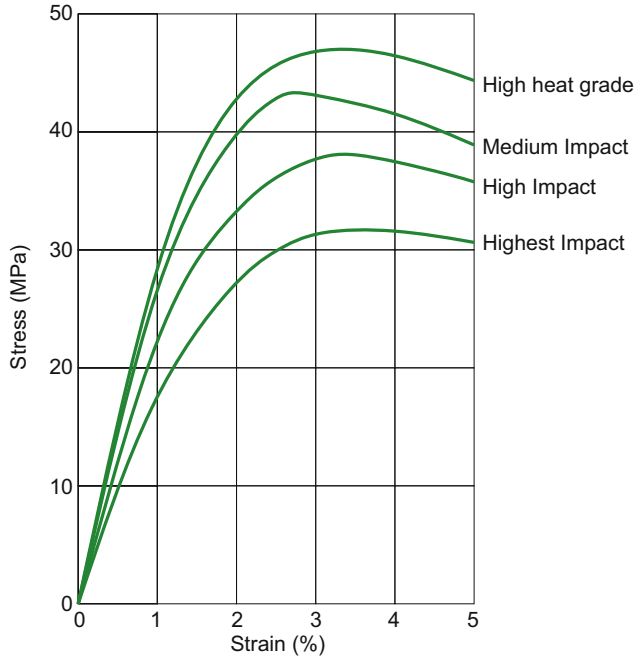


FIG. 1.9 Effect of grade on mechanical properties of ABS.

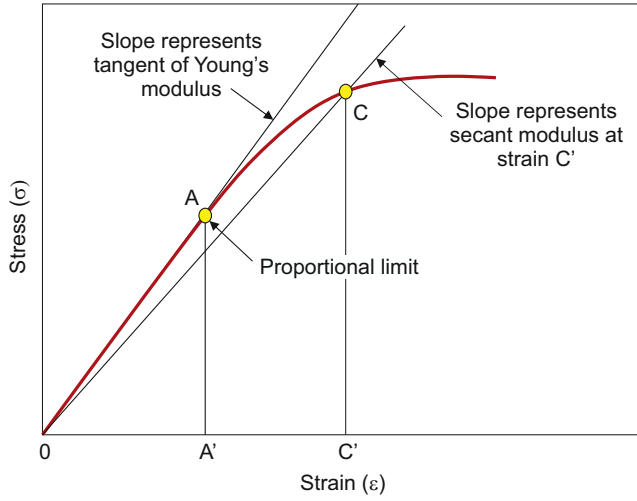


FIG. 1.10 Tangent and secant modulus.

TABLE 1.3 Short-term properties of some important plastics.

Material	Density (kg/m^3)	Tensile strength (MPa)	Flexural modulus (GPa)	% Elongation at break	Price[a]
ABS (high impact)	1040	38	2.2	8	1.7
Acetal (homopolymer)	1420	68	2.8	40	2.1
Acetal (copolymer)	1410	70	2.6	65	2.5
Acrylic	1180	70	2.9	2	2
Cellulose acetate	1280	30	1.7	30	3
Epoxy	1200	70	3.0	3	6.5
Liquid crystal polymer	1600	100	12.5	4	25
Modified PPO	1060	45	2.3	70	4
Nylon 66	1140	70	2.8	60	2.5
Nylon 66 (33% glass)	1380	115	5.1	4	2.8
PEEK	1300	62	3.8	4	62
PEEK (30% carbon)	1400	240	14	1.6	60
PET	1360	75	3	70	1.0
PET (36% glass)	1630	180	12	3	1.5
PHB	1250	26	1.6	8	2.5
Phenolic (mineral filled)	1690	55	8.0	0.8	1.5
PLA	1300	50	4.0	6	1.8
Polyamide-imide	1400	185	4.5	12	73
Polycarbonate	1150	65	2.8	100	2.2
Polyetherimide	1270	105	3.3	60	13.5
Polyethersulphone	1370	84	2.6	60	14
Polyimide	1420	72	2.5	8	70
Polypropylene	905	33	1.5	150	1
Polysulphone	1240	70	2.6	80	10
Polystyrene	1050	40	3.0	1.5	1.05

Continued

TABLE 1.3 Short-term properties of some important plastics.—cont'd

Material	Density (kg/m^3)	Tensile strength (MPa)	Flexural modulus (GPa)	% Elongation at break	Price[a]
Polyethylene (LD)	920	10	0.2	400	1.1
Polyethylene (HD)	950	32	1.2	150	1.1
PTFE	2100	25	0.5	200	10
PVC (rigid)	1400	50	3.0	80	0.8
PVC (flexible)	1300	14	0.007	300	0.85
SAN	1080	72	3.6	2	1.6
DMC (polyester)	1800	40	9.0	2	1.5
SMC (polyester)	1800	70	11.0	3	1.3

[a]*On a weight basis, relative to polypropylene.*

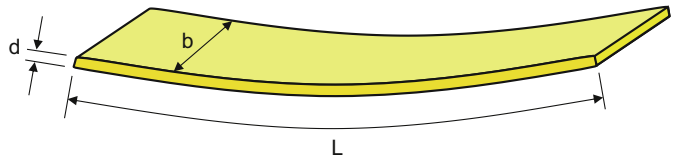


FIG. 1.11 Beam subjected to bending.

So substituting for d from (1.2) into (1.3)

$$w = \beta_2 \rho / \sigma^{1/2} \tag{1.4}$$

where β_2 is the same constant for all materials.

Hence, if we adopt loading/weight as a desirability factor, D_f, then this will be given by

$$D_f = \frac{\sigma_y^{1/2}}{\rho} \tag{1.5}$$

where σ_y and ρ are the strength and density values for the materials being compared.

Similar desirability factors may be derived for other geometries such as struts, columns etc. This concept is taken further later where material costs are taken into account and Tables 1.4 and 1.5 give desirability factors for a range of loading configurations and materials.

Material selection for stiffness

If in the service of a component it is the deflection, or stiffness, which is the limiting factor rather than strength, then it is necessary to look for a different desirability factor in the candidate materials. Consider the beam situation described above. The deflection, δ, will be given by

$$\delta = \alpha_1 \left(\frac{WL^3}{EI} \right) \tag{1.6}$$

where α_1 is a constant and W represents the loading.

The stiffness may then be expressed as

$$\begin{aligned} \frac{W}{\delta} &= \left(\frac{1}{\alpha_1} \right) \frac{EI}{L^3} \\ \frac{W}{\delta} &= \alpha_2 \left(Ed^3 \right) \end{aligned} \tag{1.7}$$

where α_2 is a constant and again it is assumed that the beam width and length are the same in all cases.

Once again the beam weight will be given by Eq. (1.3) so substituting for d from Eq. (1.7)

$$w = \alpha_3 \rho / E^{1/3} \tag{1.8}$$

Hence, the desirability factor, D_f, expressed as maximum stiffness for minimum weight will be given by

$$D_f = \frac{E^{1/3}}{\rho} \tag{1.9}$$

where E is the elastic modulus of the material in question and ρ is the density.

As before a range of similar factors can be derived for other structural elements and these are illustrated in Section 1.4.8 (Tables 1.8 and 1.9). where the effect of material cost is also taken into account. Note also that since for plastics the modulus, E, is not a constant it is often necessary to use a long-term (creep) modulus value in Eq. (1.9) rather than the short-term quality control value usually quoted in trade literature.

Ductility. A load-bearing device or component must not distort so much under the action of the service stresses that its function is impaired, nor must it fail by rupture, though local yielding may be tolerable. Therefore, high modulus and high strength, with ductility, is the desired combination of attributes. However, the inherent nature of plastics is such that high modulus tends to be associated with low ductility and steps that are taken to improve the one will cause the other to deteriorate. The major effects are summarised in Table 1.4. Thus it may be seen that there is a general situation in which increased modulus is accompanied by decreased ductility and vice versa.

TABLE 1.4 Balance between stiffness and ductility in thermoplastics.

	Effect on	
	Modulus	**Ductility**
Reduced temperature	Increase	Decrease
Increased straining rate	Increase	Decrease
Multiaxial stress field	Increase	Decrease
Incorporation of plasticiser	Decrease	Increase
Incorporation of rubbery phase	Decrease	Increase
Incorporation of glass fibres	Increase	Decrease
Incorporation of particulate filler	Increase	Decrease

Creep and recovery behaviour. Plastics exhibit a time-dependent strain response to a constant applied stress. This behaviour is called **creep**. In a similar fashion if the stress on a plastic is removed it exhibits a time dependent recovery of strain back towards its original dimensions. This is illustrated in Fig. 1.12 and because of the importance of these phenomena in design they are dealt with in detail in Chapter 2.

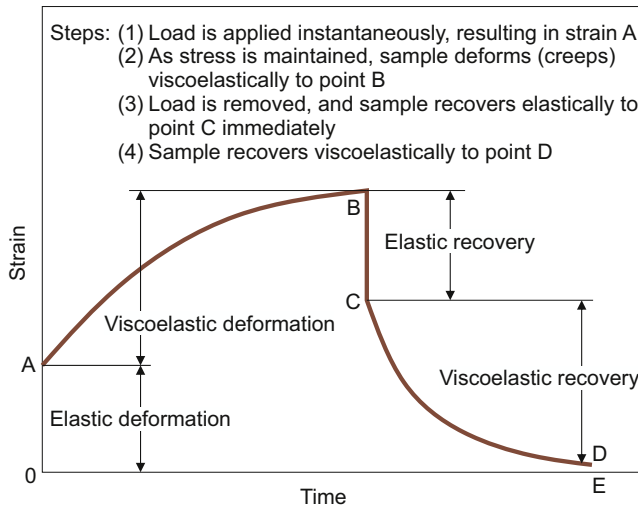


FIG. 1.12 Typical creep and recovery behaviour of a plastic.

Stress relaxation. Another important consequence of the viscoelastic nature of plastics is that if they are subjected to a particular strain and this strain is held constant it is found that as time progresses, the stress necessary to maintain this strain decreases. This is termed stress relaxation and is of vital importance in the design of gaskets, seals, springs and snap-fit assemblies. This subject will also be considered in greater detail in chapter 2.

Creep rupture. When a plastic is subjected to a constant tensile stress its strain increases until a point is reached where the material fractures. This is called creep rupture or, occasionally, static fatigue. It is important for designers to be aware of this failure mode because it is a common error, amongst those accustomed to dealing with metals, to assume that if the material is capable of withstanding the applied (static) load in the short term then there need be no further worries about it. This is not the case with plastics where it is necessary to use long-term design data, particularly because some plastics which are tough at short times tend to become embrittled at long times.

Fatigue. Plastics are susceptible to brittle crack growth fractures as a result of cyclic stresses, in much the same way as metals are. In addition, because of their high damping and low thermal conductivity, plastics are also prone to thermal softening if the cyclic stress or cyclic rate is high. The plastics with the best fatigue resistance are polypropylene, ethylene-propylene copolymer and PVDF. The fatigue failure of plastics is described in detail in Chapter 2.

Toughness. By toughness we mean the resistance to fracture. Some plastics are inherently very tough whereas others are inherently brittle. However, the picture is not that simple because those which are nominally tough may become embrittled due to processing conditions, chemical attack, prolonged exposure to constant stress, etc. Where toughness is required in a particular application it is very important therefore to check carefully the service conditions in relation to the above type of factors. At room temperature the toughest unreinforced plastics include nylon 66, LDPE, LLDPE, EVA and polyurethane structural foam. At sub-zero temperatures it is necessary to consider plastics such as ABS, polycarbonate and EVA. The whole subject of toughness will be considered more fully in Chapter 2.

1.4.2 Degradation

Physical or chemical attack

Although one of the major features which might prompt a designer to consider using plastics is corrosion resistance, nevertheless plastics are susceptible to chemical attack and degradation. As with metals, it can

sometimes be difficult to predict the performance of a plastic in an unusual environment so it is essential to check material specifications and where possible carry out proving trials. Clearly, in the space available here it is not possible to give precise details on the suitability of every plastic in every possible environment. Therefore the following sections give an indication of the general causes of polymer degradation to alert the designer to a possible problem.

The degradation of a plastic occurs due to a breakdown of its chemical structure. It should be recognised that this breakdown is not necessarily caused by concentrated acids or solvents. It can occur due to apparently innocuous mediums such as water (**hydrolysis**), or oxygen (**oxidation**). Degradation of plastics is also caused by heat, stress and radiation. During moulding the material is subjected to the first two of these and so it is necessary to incorporate stabilisers and antioxidants into the plastic to maintain the properties of the material. These additives also help to delay subsequent degradation for an acceptably long time.

As regards the general behaviour of polymers, it is widely recognised that crystalline plastics offer better environmental resistance than amorphous plastics. This is as a direct result of the different structural morphology of these two classes of material (see Appendix A). Therefore engineering plastics which are also crystalline e.g. Nylon 66 are at an immediate advantage because they can offer an attractive combination of load-bearing capability and an inherent chemical resistance. In this respect the arrival of crystalline plastics such as PEEK and polyphenylene sulphide (PPS) set new standards in environmental resistance, albeit at a price. At room temperature there is no known solvent for PPS, and PEEK is only attacked by 98% sulphuric acid.

Weathering. The deterioration of the properties of some plastics when subjected to outdoor conditions occurs as a result of the combined effects of water absorption and exposure to ultraviolet (UV) radiation. Absorption of water can have a plasticising action on plastics which increases flexibility but ultimately (on elimination of the water) results in embrittlement, while UV causes breakdown of the bonds in the polymer chain. The result is general deterioration of physical properties. A loss of colour or clarity (or both) may also occur. Absorption of water reduces dimensional stability of moulded articles. Most thermoplastics, in particular cellulose derivatives, are affected, and also polyethylene, PVC, and nylons.

Oxidation. This is caused by contact with oxidising acids, exposure to UV, prolonged application of excessive heat, or exposure to weathering. It results in a deterioration of mechanical properties (embrittlement and possibly stress cracking), increase in power factor, and loss of clarity. It affects most thermoplastics to varying degrees, in particular polyolefins, PVC, nylons, and cellulose derivatives.

Environmental stress cracking (ESC). In some plastics, brittle cracking occurs when the material is in contact with certain substances whilst under stress. The stress may be externally applied in which case one would be prompted to take precautions. However, internal or residual stresses introduced during processing are probably the more common cause of ESC. Most organic liquids promote ESC in plastics but in some cases the problem can be caused by a liquid which one would not regard as an aggressive chemical. The classic example of ESC is the brittle cracking of polyethylene washing-up bowls due to the residual stresses at the moulding gate (see injection moulding, Chapter 4) coupled with contact with the aqueous solution of washing-up liquid. Although direct attack on the chemical structure of the plastic is not involved in ESC the problem can be alleviated by controlling structural factors. For example, the resistance of polyethylene is very dependent on density, crystallinity, melt flow index (MFI) and molecular weight. As well as polyethylene, other plastics which are prone to ESC are ABS and polystyrene.

The mechanism of ESC is considered to be related to penetration of the promoting substance at surface defects which modifies the surface energy and promotes fracture. It is secondary bonds between the polymer chains that are broken and this leads to the formation and growth of micro-cracks that propagate rapidly in the harsh environmental conditions. It is thought that diffusion of liquids or chemicals into the plastic may play a role in this. ESC is more often seen in amorphous plastics rather than semi-crystalline plastics.

Biodegradation. Although most plastics are designed to resist degradation, biodegradable plastics are specifically formulated so that can eventually break down and return to natural compounds with minimal environmental impact. However, there is a very wide range of such materials available, and there is an equally large range of degradation rates. These are generally very dependent on the intended application of the material. For example, packaging grades of PLA will not degrade under normal environmental conditions and instead industrial composting is required (typically 60°C over several months). In comparison thermoplastic starches are readily biodegraded and rapidly absorb water that causes them to disintegrate very quickly. Special grades of PCL, PHB and PLA for medical scaffold and implant use are specifically designed to controllably biodegrade in vitro over a period of days or weeks.

1.4.3 Wear resistance and frictional properties

Plastics are widely used in bearing applications and in situations where there is sliding contact e.g. gears, piston rings, seals, cams, etc. The advantages of plastics are low rates of wear in the absence of conventional lubricants, low coefficients of friction, the ability to absorb shock and vibration and the ability

to operate with low noise and power consumption. Also when plastics have reinforcing fibres they offer high strength and load carrying ability. Typical reinforcements include glass and carbon fibres and fillers include PTFE and molybdenum disulphide in plastics such as nylon, polyethersulphone (PES), polyphenylene sulphide (PPS), polyvinylidene fluoride (PVDF) and polyetheretherketone (PEEK).

The friction and wear of plastics are complex subjects which depend markedly on the nature of the application and the properties of the material. The frictional properties of plastics differ considerably from those of metals. Even reinforced plastics have modulus values which are much lower than metals. Hence metal/thermoplastic friction is characterised by adhesion and deformation which results in frictional forces that are not proportional to load but rather to speed. Table 1.5 gives some typical coefficients of friction for plastics.

The wear rate of plastics is governed by several mechanisms. The primary one is adhesive wear which is characterised by fine particles of polymer being removed from the surface. This is a small-scale effect and is a common occurrence in bearings which are performing satisfactorily. However, the other mechanism is more serious and occurs when the plastic

TABLE 1.5 Coefficients of friction and relative wear rates for plastics.

	Coefficient of friction		
Material	Static	Dynamic	Relative wear rate
Nylon	0.2	0.28	33
Nylon/glass	0.24	0.31	13
Nylon/carbon	0.1	0.11	1
Polycarbonate	0.31	0.38	420
Polycarbonate/glass	0.18	0.20	5
Polybutylene terephthalate (PBT)	0.19	0.25	35
PBT/glass	0.11	0.12	2
Polyphenylene sulphide (PPS)	0.3	0.24	90
PPS/glass	0.15	0.17	19
PPS/carbon	0.16	0.15	13
Acetal	0.2	0.21	–
PTFE	0.04	0.05	–

becomes overheated to the extent where large troughs of melted plastic are removed. Table 1.5 shows typical primary wear rates for different plastics, the mechanism of wear is complex and the relative wear rates may change depending on specific circumstances.

In linear bearing applications the suitability of a plastic is usually determined from its PV rating. This is the product of P (the bearing load divided by the projected bearing area) and V (the linear shaft velocity). Fig. 1.13 shows the limiting PV lines for a range of plastics – combinations of P and V above the lines are not permitted. The PV ratings may be increased if the bearing is lubricated or the mode of operation is intermittent. The PV rating will be decreased if the operating temperature is increased. Correction factors for these variations may be obtained from material/bearing manufacturers. The plastics with the best resistance to wear are ultra-high molecular weight polyethylene (UHMWPE) (used in hip joint replacements) and PTFE lubricated versions of nylon, acetal and PBT. It is not recommended to use the same plastic for both mating surfaces in applications such as gear wheels.

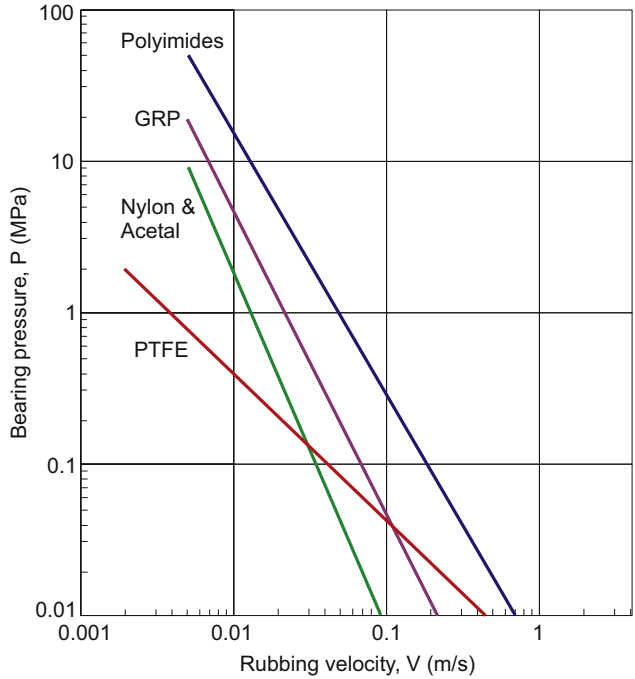


FIG. 1.13 Typical P–V ratings for plastics rubbing on steel.

1.4.4 Thermal properties

Before considering conventional thermal properties such as conductivity it is appropriate to consider briefly the effect of temperature on the mechanical properties of plastics. It was stated earlier that the properties of plastics are markedly temperature dependent. This is as a result of their molecular structure. Consider first an amorphous plastic in which the molecular chains have a random configuration. Inside the material, even though it is not possible to view them, we know that the molecules are in a state of continual motion. As the material is heated up the molecules receive more energy and there is an increase in their relative movement. This makes the material more flexible. Conversely if the material is cooled down then molecular mobility decreases and the material becomes stiffer.

With plastics there is a certain temperature, called the **glass transition temperature**, T_g, below which the material behaves like glass i.e. it is hard and rigid. As can be seen from Table 1.6 the value for T_g for a particular plastic is not necessarily a low temperature. This helps to explain some of the differences which we observe in plastics. For example, at room temperature polystyrene and acrylic are below their respective T_g values and hence we observe these materials in their glassy state. Note, however, that in contrast, at room temperature, polyethylene is above its glass transition temperature and so we observe a very flexible material. When cooled below its T_g it then becomes a hard, brittle solid. Plastics can have several transitions.

The main T_g is called the glass−rubber transition and signifies a change (when temperature falls) from a flexible, tough material to a glassy state in which the material exhibits stiffness, low creep and toughness although with a sensitivity to notches. At lower temperatures there is then a secondary transition characterised by a change to a hard, rigid, brittle state.

It should be noted that although Table 1.6 gives specific values of T_g for different polymers, in reality the glass−transition temperature is not a material constant. As with many other properties of polymers it will depend on the testing conditions used to obtain it.

In the so-called crystalline plastics the structure consists of both crystalline (ordered) regions and amorphous (random) regions. When these materials are heated there is again increased molecular mobility but the materials remain relatively stiff due to the higher forces between the closely packed molecules. When the crystalline plastics have their temperature reduced they exhibit a glass transition temperature associated with the amorphous regions. At room temperature polypropylene, for example, is quite rigid and tough, not because it is below its T_g but because of the strong forces between the molecules in the crystalline regions. When it is cooled below $-10°C$ it becomes brittle because the amorphous regions go below their T_g.

TABLE 1.6 Typical thermal properties of materials.

Material	Density (kg/m^3)	Specific heat (kJ/kg K)	Thermal conductivity (W/m/K)	Coeff. of therm exp ($\mu m/m/^\circ C$)	Thermal diffusivity (m^2/s) $\times 10^{-7}$	Glass transition Temp, T_g (° C)	Max. operating, Temp (°C)
ABS	1040	1.3	0.25	90	1.7	115	70
Acetal (homopolymer)	1420	1.5	0.2	80	0.7	−85	85
Acetal (copolymer)	1410	1.5	0.2	95	0.72	−85	90
Acrylic	1180	1.5	0.2	70	1.09	105	50
Cellulose acetate	1280	1.6	0.15	100	1.04	–	60
CAB	1190	1.6	0.14	100	1.27	–	60
Epoxy	1200	0.8	0.23	70	–	–	130
Modified PPO	1060	–	0.22	60	–	–	120
Nylon 66	1140	1.7	0.24	90	1.01	56	90
Nylon 66 (33% glass)	1380	1.6	0.52	30	1.33	–	100
PEEK	1300	–	–	48	–	143	204
PEEK (30% carbon)	1400	–	–	14	–	–	255

Continued

TABLE 1.6 Typical thermal properties of materials.—cont'd

Material	Density (kg/m^3)	Specific heat (kJ/kg K)	Thermal conductivity (W/m/K)	Coeff. of therm exp (μm/m/°C)	Thermal diffusivity (m^2/s) × 10^{-7}	Glass transition Temp, T_g (° C)	Max. operating, Temp (°C)
PET	1360	1.0	0.2	90	–	75	110
PET (36% glass)	1630	–	–	40	–	–	150
PHB	1230	1.5	0.22	100	1.19	15	80
Phenolic (glass filled)	1700	–	0.5	18	–	–	185
PLA	1250	1.2	0.13	70	0.87	55	80
Polyamide-imide	1400	–	0.25	36	–	260	210
Polycarbonate	1150	1.2	0.2	65	1.47	149	125
Polyester	1200	1.2	0.2	100	–	–	
Polyetherimide	1270	–	0.22	56	–	200	170
Polyethersulphone	1370	–	1.18	55	–	230	180
Polyimide	1420	–	–	45	–	400	260
Polyphenylene sulphide	1340	–	–	49	–	85	150
Polypropylene	905	2.0	0.20	100	0.65	−10	100

Polysulphone	1240	1.3	–	56	–	180	170
Polystyrene	1050	1.3	0.15	80	0.6	100	50
Polythene (LD)	920	2.2	0.24	200	1.17	−120	50
Polyethylene (HD)	950	2.2	0.25	120	1.57	−120	55
PTFE	2100	1.0	0.25	140	0.7	−113	250
PVC (rigid)	1400	0.9	0.16	70	1.16	80	50
PVC (flexible)	1300	1.5	0.14	140	0.7	80	50
SAN	1080	1.3	0.17	70	0.81	115	60
DMC (polyester)	1800	–	0.2	20	–	–	130
SMC (polyester)	1800	–	0.2	20	–	–	130
Polystyrene foam	32	–	0.032	–	–	–	–
PU foam	32	–	0.032	–	–	–	–
Stainless steel	7855	0.49	90	10	–	–	800
Nickel chrome alloy	7950	–	12	14	–	–	900
Zinc	7135	0.39	111	39	–	–	–
Copper	8940	0.39	400	16	–	–	–

In the past a major limitation to the use of plastics materials in the engineering sector has been temperature. This limitation arises not only due to the reduction in mechanical properties at high temperatures, including increased propensity to creep, but also due to limitations on the continuous working temperature causing permanent damage to the material as a result of thermal and oxidative degradation. Significant gains in property retention at high temperatures with crystalline polymers have been derived from the incorporation of fibrous reinforcement, but the development of new polymer matrices is the key to further escalation of the useful temperature range.

Table 1.6 indicates the service temperatures which can be used with a range of plastics. It may be seen that there are now commercial grades of unreinforced plastics rated for continuous use at temperatures in excess of 200°C. When glass or carbon fibres are used the service temperatures can approach 300°C.

The other principal thermal properties of plastics which are relevant to design are thermal conductivity and coefficient of thermal expansion. Compared with most materials, plastics offer very low values of thermal conductivity, particularly if they are foamed. Fig. 1.14 shows comparisons between the thermal conductivity of a selection of metals, plastics and building materials. In contrast to their low conductivity, plastics have high coefficients of expansion when compared with metals. This is illustrated in Fig. 1.15 and Table 1.6 gives fuller information on the thermal properties of plastics and metals.

An understanding of thermal properties is also very important when considering the wide variety of manufacturing processes for plastics. Thermosets typically generate their own internal heat as they cross-link and cure, and must then be cooled. Thermoplastics on the other hand are heated

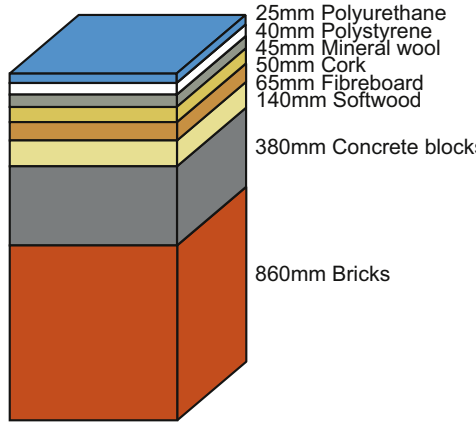


FIG. 1.14 Comparative Thermal conductivities for a range of materials.

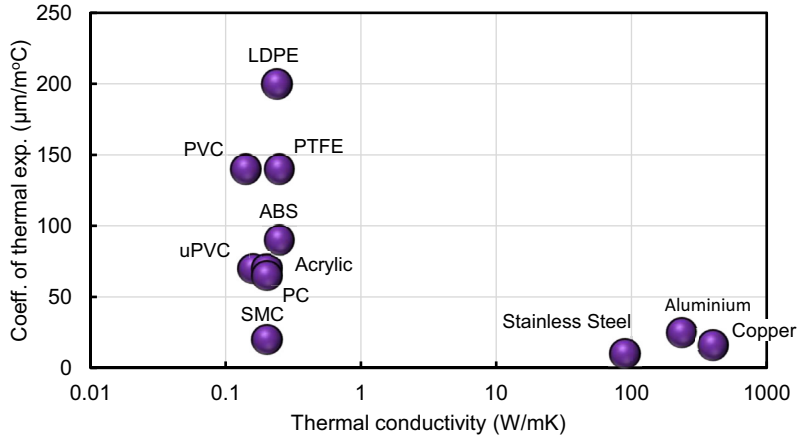


FIG. 1.15 Typical thermal properties of plastics.

sufficiently to soften them for forming before they are cooled to take the final shape of the product. In both cases the lengths of these heating and cooling times are crucial for determining production cycle times and they are driven by the thermal properties of the plastics and the forms of heat transfer employed. For cooling, thermal conduction (in the form of direct mould contact) is the predominant form of heat transfer employed, although thermal convection (e.g. air or water cooling) is also employed with some processes. For heating there is a much wider range of heat transfer mechanisms employed ranging from radiation (e.g. infrared lamps), convection (e.g. heated air-blowers or convection ovens), to conduction (e.g. direct contact with heated barrels and screws in an extruder). The effects of heat transfer in processes are explored in more detail in chapter 4.

1.4.5 Special properties

Electrical properties. Traditionally plastics have established themselves in applications which require electrical insulation. PTFE and polyethylene are among the best insulating materials available. The material properties which are particularly relevant to electrical insulation are *dielectric strength, resistance and tracking.*

The insulating property of any material will break down in a sufficiently strong electric field. The dielectric strength is defined as the electric strength (V/m) which an insulating material can withstand. For plastics the dielectric strength can vary from 1 to 1000 MV/m. Materials may be compared on the basis of their relative permittivity (or dielectric constant). This is the ratio of the permittivity of the material to the permittivity of a vacuum. The ability of a material to resist the flow of electricity is

determined by its volume resistivity, measured in ohm m. Insulators are defined as having volume resistivities greater than about $10^4\ \Omega$ m. Plastics are well above this, with values ranging from about 10^8 to $10^{16}\ \Omega$ m. These compare with a value of about $10^{-8}\ \Omega$ m for copper. Although plastics are good insulators, local breakdown may occur due to tracking. This is the name given to the formation of a conducting path (arc) across the surface of the polymer. It can be caused by surface contamination (for example dust and moisture) and is characterised by the development of carbonised destruction of the surface carrying the arc. Plastics differ greatly in their propensity to tracking – PTFE, acetal, acrylic and PP/PE copolymers offer very good resistance.

It is interesting to note that although the electrical insulation properties of plastics have generally been regarded as one of their major advantages, in recent years there has been significant advances in the development of electrically conducting plastics. This has been recognised as an exciting development area for plastics because electrical conduction would offer advantages in designing against the build-up of static electricity, in shielding of computers, etc. from electro-magnetic interference (EMI), and in the development of smart materials. Originally two approaches were used – coating or compounding. In the former the surface of the plastic is treated with a conductive coating (e.g. carbon or metal) whereas in the latter, fillers such as brass, aluminium or steel are incorporated into the plastic. It is important that the filler has a high aspect ratio (length:diameter) and so fibres or flakes of metal or metal-coated glass have been used. The conductive filler concentration must be high enough to produce a continuously conducting network (known as a percolation network). Most recently development work has been focussing on the use of nano-sized conductive fillers of metal or carbon such as carbon nanotubes or graphene. Since the filler aspect ratio is critical in the performance of conductive plastics there can be problems due to breaking up of fillers during processing. In this regard thermosetting plastics have an advantage because their simpler processing methods cause less damage to the filler. With all forms of compounded, conductive plastics the challenge is to balance the quantity of filler required to give a meaningful increase in electrical conductivity with the severely detrimental effects on the mechanical properties of excessive filler. Conductive grades of DMC are available with resistivities as low as $7 \times 10^{-3}\ \Omega$ m.

New forms of truly conductive plastics have started to emerge following the introduction of doped polyacetylene, in the year 2000. This material has a relatively low resistivity of about $10^2\ \Omega$ m but this can be substantially reduced to around $10^{-4}\ \Omega$ m by doping the plastic with electron-accepting or electron-rejecting compounds. However, the plastic is unstable and difficult to process, which has so far limited its commercial applications. Other similar plastics have been developed such as polythiophene and polyaniline.

Optical properties. Plastics have long been used specifically for their optical properties in applications such as lenses, light fittings and transparent packaging. Often they are chosen to replace glass. The optical properties of a plastic which are important are refraction, transparency, gloss and light transfer. Table 1.7 gives data on the optical properties of a selection of plastics. Some plastics may be optically clear (e.g. acrylic, cellulosics and ionomers) whereas others may be made transparent. These include epoxy, polycarbonate, polystyrene, polysulphone and PVC. Semi-crystalline thermoplastics, such as polypropylene or polyethylene, are naturally either opaque or translucent (hazy) due to the light scattering effects of the crystal structure, but additives that reduce crystal size and control crystallinity can provide them with a high degree of transparency.

Flammability. The fire hazard associated with plastics has always been difficult to assess and numerous tests have been devised which attempt to grade materials as regards flammability by standard small scale methods under controlled but necessarily artificial conditions. Descriptions of plastics as *self-extinguishing, slow burning, fire retardant* etc. have been employed to describe their behaviour under such standard test conditions, but could never be regarded as predictions of the performance of the material in real fire situations, the nature and scale of which can vary so much.

Currently there is a move away from descriptions such as *fire-retardant* or *self-extinguishing* because these could imply to uninformed users that the material would not burn. The most common terminology for describing the flammability characteristics of plastics is currently the **Critical Oxygen Index (COI)** (also called **Limiting Oxygen Index (LOI)**). This is defined as the minimum concentration of oxygen, expressed as volume percent, in a mixture of oxygen and nitrogen that will just support combustion under the conditions of test. Since air contains 21% oxygen, plastics having a COI of greater than 0.21 are regarded as self-extinguishing. In practice a higher

TABLE 1.7 Typical optical properties of plastics.

Material	Refractive index	Light transmission	Dispersive power
Acrylic	1.49	92	58
Polycarbonate	1.59	89	30–35
Polystyrene	1.59	88	31
CAB	1.49	85	–
SAN	1.57	–	36
Nylon 66	1.54	0	–

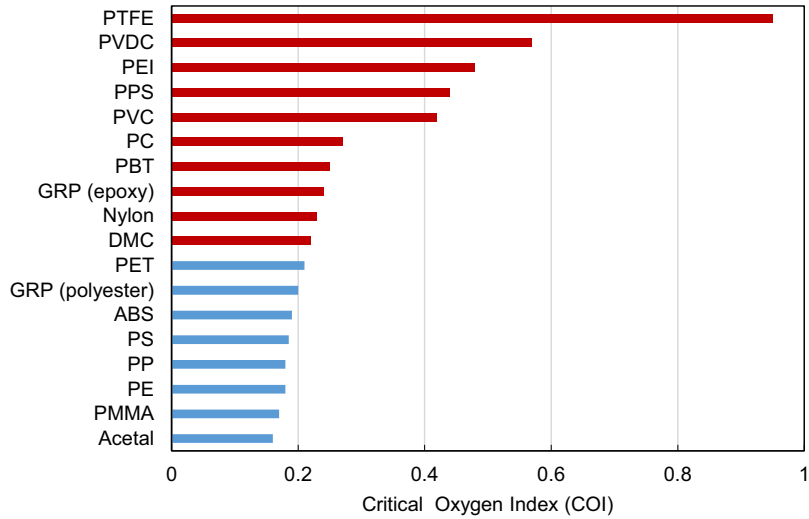


FIG. 1.16 Oxygen index values for plastics.

threshold (say 0.27) is advisable to allow for unforeseen factors in a particular fire hazard situation. Fig. 1.16 shows the typical COI values for a range of plastics.

Permeability. The low density of plastics is an advantage in many situations but the relatively loose packing of the molecules means that gases and liquids can permeate through the plastic. This can be important in many applications such as packaging or fuel tanks. It is not possible to generalise about the performance of plastics relative to each other or in respect to the performance of a specific plastic in contact with different liquids and gases.

Some plastics are poor at offering resistance to the passage of fluids through them whereas others are excellent. Their relative performance may be quantified in terms of a permeation constant, k, given by

$$k = \frac{Qd}{Atp} \tag{1.10}$$

where Q = volume of fluid passing through the plastic, d = thickness of plastic, A = exposed area, t = time, p = pressure difference across surfaces of plastic.

The main fluids of interest with plastics are oxygen and water vapour (for packaging applications) and CO_2 (for carbonated drinks applications). Figs. 1.17 and 1.18 illustrate the type of behaviour exhibited by a range of plastics. In some cases it is necessary to use multiple layers of plastics because

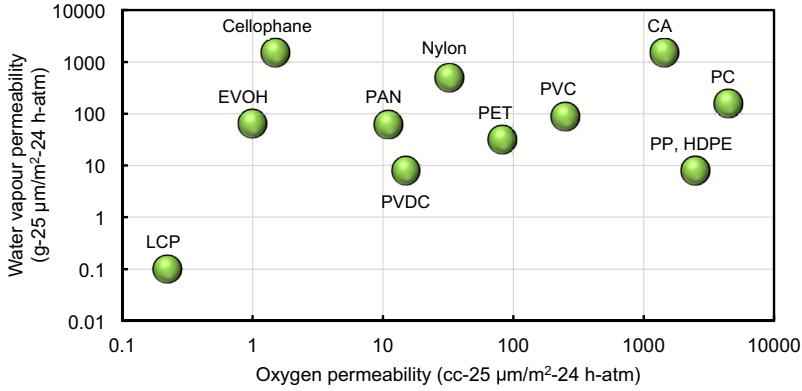


FIG. 1.17 Permeability data for a range of plastics.

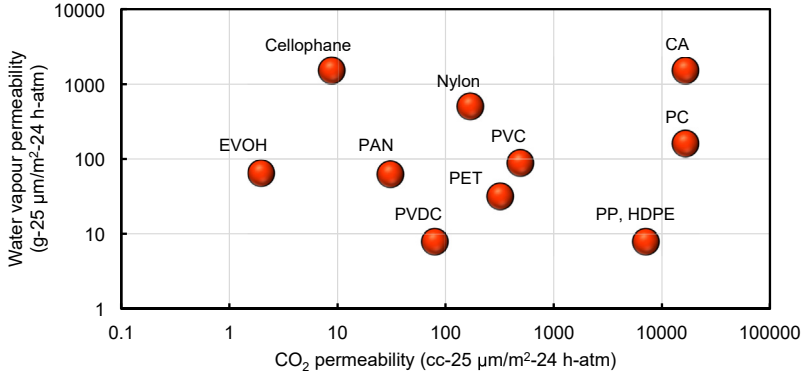


FIG. 1.18 Permeability data for a range of plastics.

no single plastic offers the combination of price, permeation resistance, printability, etc. required for the application. When multi-layers are used, an overall permeation constant for the composite wall may be obtained from

$$\frac{1}{k}=\frac{1}{d}\sum_{i=1}^{i=N}\frac{d_i}{k_i} \tag{1.11}$$

1.4.6 Processing

A key decision in designing with plastics is the processing method employed. The designer must have a thorough knowledge of processing methods because plastics are unique in design terms in that they offer a wider choice of

conversion techniques than are available for any other material. A simple container for example could be made by injection moulding, blow moulding or rotational moulding; light fittings could be thermoformed or injection moulded. In this brief introduction to designing with plastics it is not possible to do justice to the range of processing methods available for plastics. Therefore Chapter 4 will be devoted to processing. This describes the suitability of particular plastics for each moulding method and considers the limitations which these place on the designer.

1.4.7 Recyclability

Sustainability and environmental protection are of increasing concern to both legislators and the general public, and this change in attitudes has started to have profound effects on many areas of manufacturing. Plastic materials are in particular focus for two main reasons:

(1) Plastics are hydrocarbons and most types of plastics rely on crude oil as the raw resource for their manufacture. As such they are not sustainable materials and they have a very large carbon footprint. In addition through processes such as combustion, waste plastics can be readily turned into carbon dioxide and other greenhouse gases with very negative effects on the climate.

(2) Plastics are typically very resistant to environmental degradation and most are not biodegradable. As a result they can potentially remain in the environment for many years after their useful lifetime as products. With increasing use of plastics, this has created an ever-expanding mountain of plastic waste that has become a serious challenge to dispose of without causing environmental harm. Plastics are also notoriously difficult to recycle economically due to the very large number of variations in types of plastics, grades within family groups and the many different additives that may be present. A particular problem with plastics is that a small amount of colorant (e.g. from printing on the outside of a product) will discolour the recycled plastic and is very difficult to remove. Often these problems mean that recycled plastics have seriously compromised properties compared to new or virgin plastics.

Designers using plastics are therefore being increasingly asked to consider recyclability in their selection of plastics and their manufacturing processes. Use of biodegradable materials are an obvious solution but at present these are simply not produced in sufficient quantities and with sufficient variety of properties to address more than a small percentage of the current demand. The alternative is for the designer to more carefully select the types and grades of plastic used and by minimising the number of these make it easier for end of lifetime products to be collected and separated into different plastics so that these materials to be recycled. Heavy users of plastics such as the automotive

and packaging industries have already introduced targets for use of recycled plastics in new products and this trend is set to increase in the coming years.

1.4.8 Costs

It is a popular misconception that plastics are cheap materials. They are not. On a weight basis most plastics are more expensive than steel and only slightly less expensive than aluminium. Prices for plastics can range from about £1000 per tonne for polypropylene to about £60,000 per tonne for carbon fibre reinforced PEEK. Table 1.3 compares the costs of a range of plastics.

However, it should always be remembered that it is bad design practice to select materials on the basis of cost per unit weight. In the mass production industries, in particular, the raw material cost is of relatively little importance. It is the *in-position* cost which is all important. The in-position cost of a component is the sum of several independent factors i.e. raw material costs, fabrication costs and performance costs.

It is in the second two of these cost components that, in relation to other materials, plastics can offer particular advantages. Fabrication costs include power, labour, consumables, etc. and Fig. 1.19 shows that, in terms of the overall energy consumption, plastics come out much better than metals. Performance costs relate to servicing, warranty claims, etc. On this basis plastics can be very attractive to industries manufacturing consumer products because they can offer advantages such as colour fastness, resilience, toughness, corrosion resistance and uniform quality − all features which help to ensure a reliable product.

However, in general these fabrication and performance advantages are common to all plastics and so a decision has to be made in regard to which plastic would be best for a particular application. Rather than compare the basic raw material costs it is better to use a cost index on the basis of the cost to achieve a certain performance. Consider again the material selection procedures illustrated in Section 1.4.1 in relation to strength and stiffness.

Selection for strength at minimum cost

If the cost of a material is C per unit weight then from Eq. (1.3) the cost of the beam considered in the analysis would be

$$C_b = (\rho bdL)C \tag{1.12}$$

Substituting for d from (1.2) then the cost of the beam on a strength basis would be

$$C_b = \beta_3 \left(\frac{\rho C}{\sigma_y^{1/2}} \right) \tag{1.13}$$

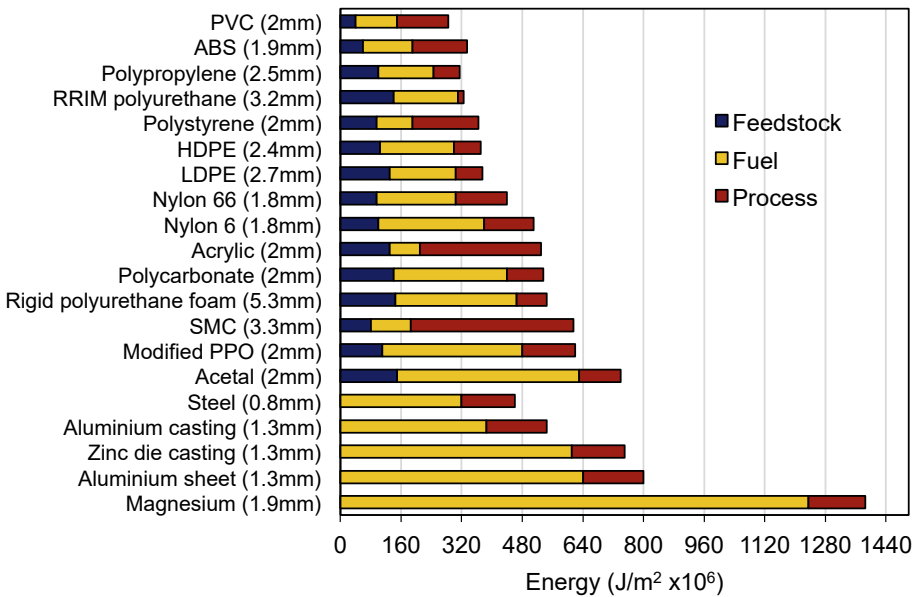


FIG. 1.19 Energy required to manufacture and process a range of materials at typical design thickness.

TABLE 1.8 Desirability factors for some common loading configurations.

Component	Desirability factor, D_f	
	Strength basis	**Stiffness basis**
Rectangular beam with fixed width	$\sigma_y^{1/2}/\rho C$	$E^{1/3}/\rho C$
Struts or ties	$\sigma_y/\rho C$	$E/\rho C$
Thin wall cylinders under pressure	$\sigma_y/\rho C$	–
Thin wall shafts in tension	$\tau_m/\rho C$	$G/\rho C$
Long rods in compression (buckling)	–	$E^{1/2}/\rho C$

where β_3 is a constant, which will be the same for all materials. Therefore we can define a cost factor, C_f, where

$$C_f = \left(\frac{\rho C}{\sigma_y^{1/2}}\right) \tag{1.14}$$

which should be minimised in order to achieve the best combination of price and performance. Alternatively we may take the reciprocal of C_f to get a desirability factor, D_f,

$$D_f = \left(\frac{\sigma_y^{1/2}}{\rho C}\right) \tag{1.15}$$

and this may be compared to D_f given by Eq. (1.5).

Selection for stiffness at minimum cost

Using Eq. (1.7) and an analysis similar to above it may be shown that on the basis of stiffness and cost, the desirability factor, D_f, is given by

$$D_f = \left(\frac{E^{1/3}}{\rho C}\right) \tag{1.16}$$

Tables 1.8 and 1.9 give desirability factors for configurations other than the beam analysed above and typical numerical values of these factors for a range of materials.

Typical Characteristics of Some Important Plastics

(a) Semi-crystalline plastics

Low density polyethylene (LDPE). This is one of the most widely used plastics. It is characterised by a density in the range 918–935 kg/m^3 and is

TABLE 1.9 Desirability factors for a range of materials.

Material	Density, ρ kg/m^3	Proof or fracture stress σ_y (MPa)	Modulus E (GPa)	$\frac{\sigma_y}{\rho}$	$\frac{E}{\rho}$	$\frac{\sigma_y^{1/2}}{\rho}\left(\times 10^{-3}\right)$	$\frac{E^{1/2}}{\rho}\left(\times 10^{-3}\right)$	$\frac{E^{1/3}}{\rho}\left(\times 10^{-3}\right)$
Aluminium (pure)	2700	90	70	0.033	0.026	3.51	3.12	1.53
Aluminium alloy	2810	500	71	0.178	0.025	7.95	3.0	1.47
Stainless steel	7855	980	185	0.125	0.024	4.0	1.73	0.73
Titanium alloy	4420	900	107	0.204	0.024	6.78	2.34	1.07
Spruce	450	35	9	0.078	0.020	13.15	6.67	4.62
GRP (80% unidirectional glass in polyester)	2000	1240	48	0.62	0.024	17.6	3.46	1.82
CFRP(60% unidirectional fibres in epoxy)	1500	1050	189	0.7	0.126	21.6	9.16	3.82
Nylon 66	1140	70	0.78[a]	0.061	6.8×10^{-4}	8.34	0.77	0.81
ABS	1040	35	1.2[a]	0.034	11.5×10^{-4}	5.68	1.05	1.02
Polycarbonate	1150	60	2.0[a]	0.052	17.4×10^{-4}	6.73	1.23	1.09
PEEK (+30% C)	1450	215	15.5	0.19	0.011	10.1	2.7	1.72

[a] *1500 h creep modulus.*

very tough and flexible. Its major application is in packaging film although its outstanding dielectric properties means it is also widely used as an electrical insulator. Other applications include domestic ware, tubing, squeeze bottles and cold water tanks.

Linear low density polyethylene (LLDPE). LLDPE has a regular linear structure with short chain branches, as opposed to the long chain branches of LDPE (shown in Fig. 1.1(b)), and it is produced by a low pressure process. Depending on the cooling rate from the melt, the material forms a structure in which the molecules are linked together. Hence for any given density, LLDPE is stiffer than LDPE and exhibits a higher yield strength and greater ductility. For processing LLDPE has higher shear viscosity, but lower shear sensitivity than LDPE, and importantly its short side branches make it softer in extension and it can be drawn to higher strains. It is increasingly replacing LDPE in some of its traditional markets such as packaging films, where it can be drawn down to much lower thicknesses for plastic bags, shrink wrap etc.

High density polyethylene (HDPE). This material has a density in the range 935−965 kg/m^3 and is more crystalline than LDPE. It has a linear chain structure, without side-branching (as shown in Fig. 1.1(a)), which makes it stronger, stiffer and harder than LDPE. It is also slightly more expensive but its greater strength and durability give it a much wider range of applications. These range from piping and furniture to kitchenware, toys and food containers.

Developments in polyethylenes and particularly the introduction of new material grades with enhanced properties has been made possible over the years through the introduction of new manufacturing technologies. A good example of this was the increasing use of metallocene catalysts in the polymerisation of polyethylenes from the 1980s onwards. The big advantage of metallocenes is that they are single site catalysts so that the polymer molecules which are produced tend to be all the same − a fact which offers an array of superior properties. Traditional catalysts for polyethylene (e.g. Ziegler Natta catalysts) are multi-sited so that they produce polymers with short, medium and long molecules. In metallocene grades of polyethylene, the absence of low molecular weight species results in low extractables, a narrow melting range and free-flowing material even at low densities. The absence of high molecular weight species contributes excellent melting point control, clarity and improved flexibility/toughness at low temperatures. Metallocene grades are generally indicated by the prefix ‘m’ as in ‘mLDPE’.

Cross-linked polyethylene (XLPE). Some thermoplastic materials such as polyethylene can have their structure altered so that the molecular chains become cross-linked and the material then behaves like a thermoset. In the case of polyethylene, a range of cross-linking methods are available. These include the use of radiation, peroxides and silanes. In some cases the cross-linking can occur during moulding whereas in other cases the end-product

shape is created before the cross-linking is initiated. The action of cross-linking has a number of beneficial effects including improved stress crack resistance, improved creep resistance, better chemical resistance, improved toughness and better general thermo-mechanical stability.

Polypropylene (PP). Polypropylene is an extremely versatile plastic and is available in many grades and also as a copolymer (ethylene/propylene). It has the lowest density of all thermoplastics (in the order of 900 kg/m^3) and this combined with strength, stiffness and excellent fatigue and chemical resistance make it attractive in many situations. These include crates, small machine parts, car components (fans, fascia panels etc.), chair shells, TV and computer cabinets, tool handles, etc. Its excellent fatigue resistance is utilised in the moulding of integral hinges (e.g. accelerator pedals and forceps/tweezers). Polypropylene is also available in fibre form (for ropes, carpet backing) and as a film (for packaging).

Polyamides (nylon). There are several different types of nylon (e.g., nylon 6, nylon 66, nylon 11) but as a family their characteristics of strength, stiffness and toughness have earned them a reputation as *engineering plastics*. Table 1.10 compares the relative merits of light metal casting alloys and nylon. Typical applications for nylon include small gears, bearings, bushes, sprockets, housings for power tools, terminal blocks and slide rollers. An important design consideration is that nylon absorbs moisture which can affect its properties and dimensional stability. Glass reinforcement reduces this problem and produces an extremely strong, impact resistant material. Another major application of nylon is in fibres which are notoriously strong. The density of nylon is about 1100 kg/m^3.

Polyoxymethylene (POM or acetals). The superior properties of acetal in terms of its strength, stiffness and toughness have also earned it a place as an *engineering plastic*. At 1420 kg/m^3 it is denser than nylon but in many respects their properties are similar and they can be used for the same types of light engineering application. A factor which may favour acetal in some cases is its relatively low water absorption. The material is available as both a homopolymer and a copolymer. The former is slightly stronger and stiffer whereas the copolymer has improved high temperature performance.

Polytetrafluoroethylene (PTFE). The major advantages of this material are its excellent chemical resistance and its extremely low coefficient of friction. Not surprisingly its major area of application is in bearings and it is particularly suited to situations where the environment is aggressive. It is also widely used in areas such as insulating tapes, gaskets, pumps, diaphragms and of course non-stick coatings on cooking utensils.

Polyethylene terephthalate (PET). PET is naturally highly crystalline and in this form (known as cPET) it exhibits toughness, strength, abrasion resistance, low friction, chemical resistance and low moisture absorption. Traditionally its main application is as a textile fibre (e.g. Terylene). However, by rapid cooling the material can be induced to remain in a largely amorphous

TABLE 1.10 Comparison between die casting alloys and nylons.

Points for comparison	Die casting alloys	Nylon
Cost of raw material/tonne	Low	High
Cost of mould	High	Can be lower – no higher
Speed of component production	Slower than injection moulding of nylon	Lower component production costs
Accuracy of component	Good	Good
Post moulding operations	Finishing – painting. Paint chips off easily	Finishing – not required – painting not required. Compounded colour retention permanent.
Surface hardness	Low – scratches easily	Much higher. Scratch resistant.
Rigidity	Good to brittleness	Glass reinforced grades as good or better
Elongation	Low	GR grades comparable unfilled grades excellent
Toughness (flexibility)	Low	GR grades comparable unfilled grades excellent
Impact	Low	All grades good
Notch sensitivity	Low	Low
Young's modulus (E)	Consistent	Varies with load
General mechanical properties	Similar to GR grades of 66 nylon	Higher compressive strength
Heat conductivity	High	Low
Electrical insulation	Low	High
Weight	High	Low
Component assembly	Snap fits difficult	Very good

state (known as aPET), where it retains its transparency and its processability is improved. Over the past 20 years this has been exploited to great advantage in the manufacture of plastic bottles, where aPET has largely replaced glass in most applications. PET is also relatively easy to recycle and as a result of this it is now rapidly growing as a general packaging material. PET is hygroscopic and must be dried prior to melt processing.

Polybutylene terephthalate (PBT). PBT is closely related to PET, but has slightly lower strength and rigidity, slightly higher impact resistance and better mouldability. Applications include slide bearings, valve mouldings, gears, cams, plug connectors, shower heads and LCD/LEDs.

Polyetheretherketone (PEEK). PEEK is a high performance plastics which offer the possibility of elevated service temperatures. It is crystalline in nature which accounts in part for its high resistance to attack from acids, alkalis and organic solvents. It melts at a relatively high temperature compared to most thermoplastics (343°C). It is easily processed and may be used continuously at 200°C where it offers good abrasion resistance, low flammability, toughness, strength and good fatigue resistance. Its density is 1300 kg/m^3. Applications include items used in demanding applications such as bearing, valves, pistons, impellors, wire, coatings, and medical implants, as well as small load bearing parts in the aerospace, automotive and chemical processing industries.

Polylactic acid (PLA). PLA is a rigid semi-crystalline thermoplastic with a density in the range 1200−1400 kg/m^3. It is the most important of the new bio-degradable plastics and it is now being produced in commercial quantities that are large enough to replace commodity plastics in key markets. PLA is not a natural material, but it is made from natural renewable sources, such as corn starch, and it is bio-degradable. The material is therefore promoted as being environmentally friendly, carbon neutral and from sustainable resources. PLA is readily mouldable and has properties similar to PET apart from its lower melting point. The principal applications for PLA are currently in disposable food packaging, but it has also been used as fibres, medical implants and the feedstock for 3D printers.

(b) Amorphous plastics

Polyvinyl chloride (PVC). This material is the most widely used of the amorphous plastics. It is available in two forms that are distinguished by whether a plasticiser has been added (i.e. plasticised or unplasticised). Both types are characterised by good weathering resistance, excellent electrical insulation properties, good surface properties and they are self-extinguishing. Plasticised PVC is flexible and finds applications in wire covering, floor tiles, toy balls, gloves and rainwear. Originally this material was used extensively in packaging but in these markets and others its use has declined significantly in recent years due to health concerns and legislation surrounding the presence of

phthalate plasticisers in PVC. Unplasticised PVC (uPVC) is a hard, tough, strong material which is widely used in the building industry. For example, pipes, gutters, window frames and wall claddings are all made in this material. The familiar credit cards are also made from uPVC.

Polymethyl methacrylate (PMMA). This material has exceptional optical clarity and resistance to outdoor exposure. It is resistant to alkalis, detergents, oils and dilute acids but is attacked by most solvents. Its peculiar property of total internal reflection is useful in advertising signs and some medical applications. PMMA is most often used as a replacement for glass and may be better known by its trade names Plexiglass or Perspex. Typical uses include illuminated notices, control panels, dome-lights, lighting diffusers, baths, face guards, nameplates, lenses and display models.

Polystyrene (PS). Polystyrene is available in a range of grades with varying impact strengths but naturally it is quite a brittle material. By forming a graft copolymer with polybutadiene rubber its brittleness may be significantly reduced to produce high impact polystyrene (HIPS). The non-pigmented grades of PS have crystal clarity and overall their low cost coupled with ease of processing makes them useful for such things as model aircraft kits, drinking cups, yoghurt containers, light fittings, CD cases, disposable razors and ballpoint pens. Polystyrene is also available in an expanded form which is used for such things as ceiling tiles and is excellent as a packaging material and thermal insulator.

Acrylonitrile-butadiene-styrene (ABS). ABS materials have superior strength, stiffness and toughness properties to many plastics and so they are often considered in the category of engineering plastics. They compare favourably with nylon and acetal in many applications and are generally less expensive. However, they are susceptible to chemical attack by chlorinated solvents, esters, ketones, acids and alkalis. Typical applications are housings and facia panels for a wide range of consumer electronics goods, kitchenware and automotive parts, luggage, helmets, toys and sporting goods.

Polycarbonates. These materials also come within the category of engineering plastics and their outstanding feature is extreme toughness. They are also optically transparent and have good temperature resistance but are attacked by alkaline solutions and hydrocarbon solvents. Typical applications include architectural light fittings and covers, eyeglasses and eye protection, baby feeding bottles, machine housings and guards, camera parts, LCD/LED screens, mobile phone cases and covers, CDs, DVDs and Blu-ray discs.

Polyethersulphone (PES). This high performance plastic is known for its toughness and stability at high temperature. It is recommended for load bearing applications up to 180°C. Even without flame retardants it offers low flammability and there is little change in dimensions or electrical properties in the temperature range 0−200°C. It is easily processed on conventional moulding equipment. Applications include aircraft heating ducts, terminal blocks, engine manifolds, durable filters and membranes,

bearings, grilles, tool handles, non-stick coatings. PES can be fibre-reinforced and some new thermoplastic composites consist of woven fibres in a PES matrix.

Modified polyphenylene oxide (PPO). The word *modified* in this material refers to the inclusion of high impact polystyrene (HIPS) to improve processability and reduce the cost of the basic PPO. This material offers a range of properties which make it attractive for a whole range of applications. For example, it may be used at 100−150°C where it is rigid, tough and strong with good creep resistance and hydrolytic stability. Water absorption is very small and there is excellent dimensional stability. Applications include business machine parts, flow valves, headlight parts, engine manifolds, fascia panels, grilles, pump casings, hair dryer housings, etc.

(c) Thermoplastics rubbers (TPRs or TPEs)

There are a wide variety of materials that are classified as thermoplastic rubbers (TPRs) or thermoplastic elastomers (TPEs). They are either elastomeric alloys consisting of rubber particles embedded in plastics such as polyolefins, or they are segmented block co-polymers of rubbers with plastics such as polyurethanes, styrenics, polyesters or polyamides. Some examples of these materials are: *Alcryn, Santoprene* (Olefinics); (e.g. *Elastollan, Pellethane* (Polyurethanes); *Hytrel, Arnitel* (Polyesters); *Solprene, Cariflex* (Styrenics); and *Pebax, Vestamid* (Polyamides). Some typical properties of TPRs are given in Table 1.11.

(d) Thermosetting plastics

Amino plastics. There are two basic types of amino plastics − urea formaldehyde and melamine formaldehyde. They are hard, rigid materials with good abrasion resistance and their mechanical characteristics are sufficiently good for continuous use at moderate temperatures (up to 100°C). Urea formaldehyde is relatively inexpensive but moisture absorption can result in poor dimensional stability. It is generally used for adhesives (such as in particle board or medium density fibreboard (MDF)), bottle caps, electrical switches, plugs, utensil handles and trays. Melamine formaldehyde has lower water absorption and improved temperature and chemical resistance. It is typically used for tableware, laminated worktop and furniture surfaces, and electrical fittings.

Phenolics. Phenol-formaldehyde (*Bakelite*) is one of the oldest synthetic materials available. It is a strong, hard, brittle material with good creep resistance and excellent electrical properties, but it is susceptible to attack by alkalis and oxidising agents. It is used for a wide variety of applications but normally it is combined with fillers or reinforcement. Its applications include: domestic electrical fittings, snooker/billiard balls, saucepan handles, bearings, brake shoes or clutch discs (as a binder), and worktop surfaces.

TABLE 1.11 Physical characteristics of thermoplastic rubbers.

Type	Olefinic	Polyurethane	Polyester	Styrenic	Polyamide
Hardness (Shore A–D)	60A to 60D	60A to 60D	40D to 72D	30A to 45D	40D to 63D
Resilience (%)	30 to 40	40 to 50	43 to 62	60 to 70	–
Tensile strength (MPa)	8 to 20	30 to 55	21 to 45	25 to 45	–
Resistances					
Chemicals	F	P/G	E	E	P/E
Oils	F	E	E	F	–
Solvents	P/F	F	G	P	P/E
Weathering	E	G	E	P/E	E
Specific gravity	0.97–1.34	1.11–1.21	1.17–1.25	0.93–1.0	1.0–1.12
Service temperature (°C)	−50–130	−40–130	−65–130	−30–120	−65–130

KEY: P = poor, F = fair, G = good, E = excellent.

Polyurethanes. Polyurethanes are a very versatile family of polymers and they can be either thermosetting or thermoplastic. The thermosetting types are the most important commercially and they are available in three main forms – rigid foam, flexible foam and elastomer. They are characterised by high strength and good chemical and abrasion resistance. The rigid foam is widely used as an insulation material, the flexible foam is an excellent cushion material for furniture and the elastomeric material is used in solid tyres and shock absorbers. Polyurethanes are also widely used in coatings and in polyurethane paints.

Polyesters. Although there are many types of thermoplastic polyesters (e.g. PET, PLA, PHA, PHB), unsaturated polyesters are thermosetting resins. These are mainly used as casting materials and as a matrix for glass fibre reinforcement. This can take many forms and is probably most commonly known as a DIY type material used for the manufacture of small boats, chemical containers, tanks and repair kits for cars, etc.

Epoxides. Epoxy resins are a range of polymers containing epoxide groups that may be cross-linked either with themselves or other polymers when mixed together or in the presence of a catalyst. They are more expensive than other equivalent thermosets (e.g. polyesters) but they generally out-perform these materials due to better strength and toughness, less shrinkage during curing, better weatherability and lower moisture absorption. One of their major applications is in the manufacture of structural aircraft composites because of the combination of properties offered when they are reinforced with fibres. Epoxies are also used for high quality coatings, two-part adhesives, electronic printed circuit boards and for filling and repairing. High temperature epoxy resins have an operating temperature range of −50 to 200°C.

Bibliography

Bastiola C: *Handbook of biodegradable polymers*, ed 2, Shrewsbury, 2014, Smithers.

Belofsky H: *Plastics: product design and process engineering*, Munich, 1995, Hanser.

Benham PP, Crawford RJ, Armstrong CG: *Mechanics of engineering materials*, Longmans.

Birley AW, Haworth B, Batchelor J: *Physics of plastics*, Munich, 1992, Hanser.

Blythe AR, Bloor D: *Electrical properties of polymers*, ed 2, Cambridge Univ. Press.

Charrier JM: *Polymeric materials and processing*, New York, 1990, Hanser.

Compton TR: *Engineering plastics*, Shrewsbury, 2014, Smithers.

Crane FAC, Charles JA: *Selection and use of engineering materials*, ed 3, Oxford, 1997, Butterworth-Heinemann.

Dominghaus H: *Plastics for engineers*, New York, 1993, Hanser.

Ehrenstein GW: *Polymeric materials: structure-properties-applications*, Munich, 2001, Hanser.

Erhard G: *Designing with plastics*, Munich, 2006, Hanser.

Gent NG: *Engineering with rubber: how to design rubber components*, ed 3, Munich, 2012, Hanser.

Gruenwald G: *Plastics: how structure determines properties*, Munich, 1992, Hanser.

Harper CA, Petrie EM: *Plastics materials and processes: a concise encyclopedia*, Hoboken, 2003, Wiley.

Kemmish DJ: *Practical guide to high performance engineering plastics*, Shrewsbury, 2011, iSmithers.

Koo JH: *Polymer nanocomposites: processing, characterization and applications*, New York, 2006, McGraw-Hill.

Kutz M: *Applied plastics engineering handbook: processing and materials*, Oxford, 2011, Elsevier.

Oswald TA, Menges G: *Materials Science of Polymers for engineers*, ed 3, Munich, 2012, Hanser.

Painter PC, Coleman MM: *Essentials of polymer science and engineering*, Lancaster, 2009, DEStech.

Platt DK: *Engineering and high performance plastics market report*, Shrewsbury, 2003, Rapra Technology.

Powell PC, Housz AJI: *Engineering with polymers*, ed 2, 1998. Cheltenham.

Progelhof RC, Throne JL: *Polymer engineering principles*, New York, 1993, Hanser.

Smith R: *Biodegradable polymers for industrial applications*, Cambridge, 2005, Woodhead.

Strong AB: *Plastics: materials and processing*, ed 3, New Jersey, 2006, Pearson Prentice Hall.

Subramanian MN: *Plastics additives and testing*, Hoboken, 2013, Wiley.

Van Krevelen DW, te Nijenhuis K: *Properties of polymers*, ed 4, Amsterdam, 2009, Elsevier.

Chapter 2

Mechanical behaviour of plastics

2.1 Introduction

In Chapter 1 the general mechanical properties of plastics were introduced. In order to facilitate comparisons with the behaviour of other classes of materials the approach taken was to refer to standard methods of data presentation, such as stress–strain graphs, etc. However, it is important to note that when one becomes involved in engineering design with plastics, such graphs are of limited value. The reason is that they are the results of relatively short-term tests and so their use is restricted to quality control and, perhaps, the initial sorting of materials in terms of stiffness, strength etc. Designs based on, say, the modulus obtained from a short-term test would not predict accurately the long-term behaviour of plastics because they are viscoelastic materials. This viscoelasticity means that quantities such as modulus, strength, ductility and coefficient of friction are sensitive to straining rate, elapsed time, loading history, temperature, etc. It will also be shown later that the manufacturing method used for the plastic product can create changes in the structure of the material which have a pronounced effect on properties. The behaviour of the moulded product may therefore be different from the behaviour of a moulded test-piece of the same material.

The time-dependent change in the dimensions of a plastic article when subjected to a constant stress is called **creep**. As a result of this phenomenon the modulus of a plastic is not a constant, but provided its variation is known then the creep behaviour of plastics can be allowed for using accurate and well established design procedures. Metals also display time dependent properties at high temperatures so that designers of turbine blades, for example, have to allow for creep and guard against creep rupture. At room temperature the creep behaviour of metals is negligible and so design procedures are simpler in that the modulus may be regarded as a constant. In contrast, thermoplastics at room temperature behave in a similar fashion to metals at high temperatures so that design procedures for relatively ordinary load-bearing applications must always take into account the viscoelastic behaviour of plastics.

For most traditional materials, the objective of the design method is to determine stress values which will not cause fracture. However, for plastics it

Plastics Engineering. https://doi.org/10.1016/B978-0-08-100709-9.00002-9
Copyright © 2020 Elsevier Ltd. All rights reserved.

is more likely that excessive deformation will be the limiting factor in the selection of working stresses. Therefore this chapter looks initially at the deformation behaviour of plastics and later fracture is examined at the end of the chapter.

2.2 Viscoelastic behaviour of plastics

For a component subjected to a uniaxial force, the engineering stress, σ, in the material is the applied force (tensile or compressive) divided by the original cross-sectional area. The engineering strain, ε, in the material is the extension (or reduction in length) divided by the original length. In a perfectly elastic (Hookean) material the stress, σ, is directly proportional to the strain, ε, and the relationship may be written, for uniaxial stress and strain, as

$$\sigma = \text{constant} \times \varepsilon \tag{2.1}$$

where the constant is referred to as the **modulus** of the material.

In a perfectly viscous (Newtonian) fluid the shear stress, τ is directly proportional to the rate of strain ($d\gamma/dt$ or $\dot{\gamma}$) and the relationship may be written as

$$\tau = \text{constant} \times \dot{\gamma} \tag{2.2}$$

where the constant in this case is referred to as the **viscosity** of the fluid.

Polymeric materials exhibit mechanical properties which come somewhere between these two ideal cases and hence they are termed **viscoelastic**. In a viscoelastic material the stress is a function of strain and time and so may be described by an equation of the form

$$\sigma = f(\varepsilon, t) \tag{2.3}$$

This type of response is referred to as non-linear viscoelastic but as it is not amenable to simple analysis it is often reduced to the form

$$\sigma = \varepsilon \cdot f(t) \tag{2.4}$$

This equation is the basis of linear viscoelasticity and simply indicates that, in a tensile test for example, for a fixed value of elapsed time, the stress will be directly proportional to the strain. The different types of response described are shown schematically in Fig. 2.1.

The most characteristic features of viscoelastic materials are that they exhibit a time dependent strain response to a constant stress (**creep**) and a time dependent stress response to a constant strain (**relaxation**). In addition when the applied stress is removed the materials have the ability to **recover** slowly over a period of time. These effects can also be observed in metals but the difference is that in plastics they occur at room temperature whereas in metals they only occur at very high temperatures.

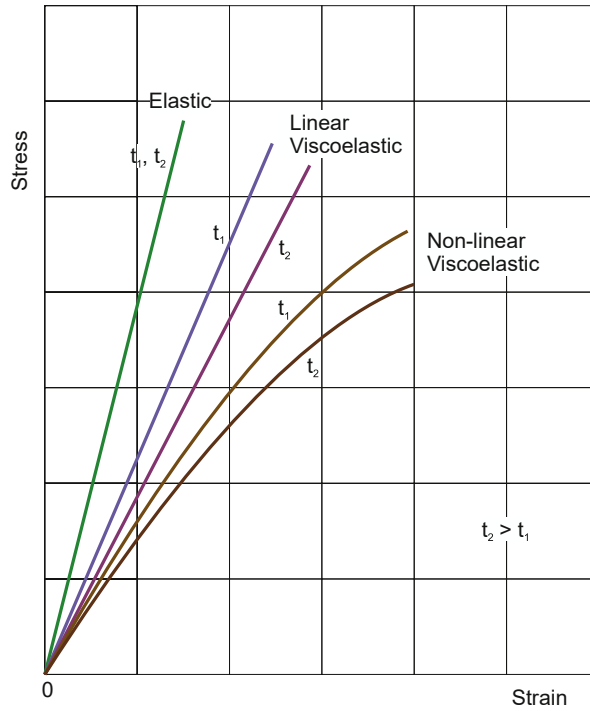


FIG. 2.1 Stress–strain behaviour of elastic and viscoelastic materials at two values of elapsed time, *t*.

2.3 Short-term testing of plastics

The simple tensile test is probably the most popular method for characterising metals and so it is not surprising that it is also widely used for plastics. However, for plastics the tensile test needs to be performed very carefully and the results of the single test should only be used as a means of quality control – not as design data. This is because, with plastics it is possible to obtain quite different results from the same material simply by changing the test conditions. Fig. 2.2 shows that at high extension rates (>1 mm/s) unplasticised PVC is almost brittle with a relatively high modulus and strength. At low extension rates (<0.05 mm/s) the same material exhibits a lower modulus and strength but its ductility is now very high. Therefore a single tensile test could be quite misleading if the results were used in design formulae but the test conditions were not similar to the service conditions.

Fig. 2.2 also illustrates an interesting phenomenon observed in some plastics. This is *cold drawing* and it occurs because at low extension rates the molecular chains in the plastic have time to align themselves under the influence of the applied stress. Thus the material is able to flow at the same rate

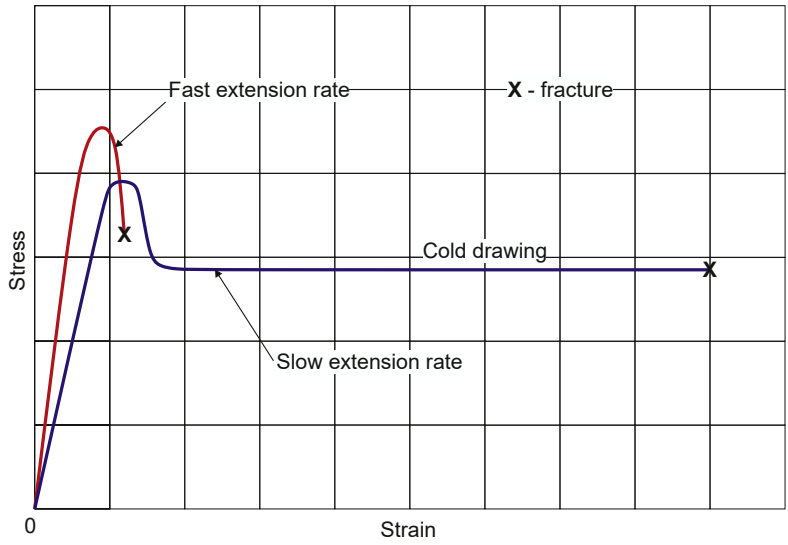


FIG. 2.2 Typical tensile behaviour of unplasticised PVC.

as it is being strained. Nowadays this phenomena is utilised in some forming methods for plastics. It creates highly aligned molecular structures which exhibit excellent strength and stiffness properties in the alignment direction.

Occasionally, materials are tested in tension by applying the loads in increments. If this method is used for plastics then special caution is needed because during the delay between applying the load and recording the strain, the material creeps. Therefore if the delay is not uniform there may appear to be excessive scatter or non-linearity in the material. In addition, the way in which the loads are applied constitutes a loading history which can affect the performance of the material. A test in which the increments are large would quite probably give results which are different from those obtained from a test in which the increments were small or variable.

As a result of these special effects in plastics it is not reasonable to quote properties such as modulus, yield strength, etc. as a single value without qualifying these with details of the test method. Standard short-term test methods for plastics are described in BS 2782, ASTM D638 and ASTM D790. These relate to both tensile and flexural short-term tests. It should be noted that, as pointed out above, in uniaxial loading the stress, σ, is simply the force divided by the cross-sectional area and the strain, ε, is the deformation divided by the original length. The modulus of the material is then the ratio of stress/strain.

Hence,

$$\text{stress, } \sigma = \frac{W}{A}$$

$$\text{strain, } \varepsilon = \frac{\delta}{L_0}$$

$$\text{modulus, } E = \frac{\sigma}{\varepsilon} = \frac{WL_0}{A\delta}$$

In flexure (bending) situations, these equations do not apply. For the three-point loading shown in Fig. 2.3, the relevant equations are

$$\text{stress, } \sigma = \frac{My}{I}$$

where M = bending moment at loading point (= $WL/4$)
y = half depth of beam (= $d/2$)
I = second moment of area ($bd^3/12$)

$$\text{hence stress, } \sigma = \frac{3WL}{2bd^2} \tag{2.5}$$

Also deflection, $\delta = \frac{WL^3}{48EI}$ (see Benham et al.)

$$= \sigma\left(\frac{L^2}{6Ed}\right) = \varepsilon\left(\frac{L^2}{6d}\right)$$

$$\text{hence strain, } \varepsilon = \frac{6\delta d}{L^2} \tag{2.6}$$

$$\text{modulus, } E = \frac{\sigma}{\varepsilon} = \frac{WL^3}{4bd^3\delta} \tag{2.7}$$

Note that these stress, strain and modulus equations are given for illustration purposes. They apply to three-point bending as shown in Fig. 2.3. Other types of bending can occur (e.g. four-point bending, cantilever, etc.) and different equations will apply. Some of these are illustrated in the worked

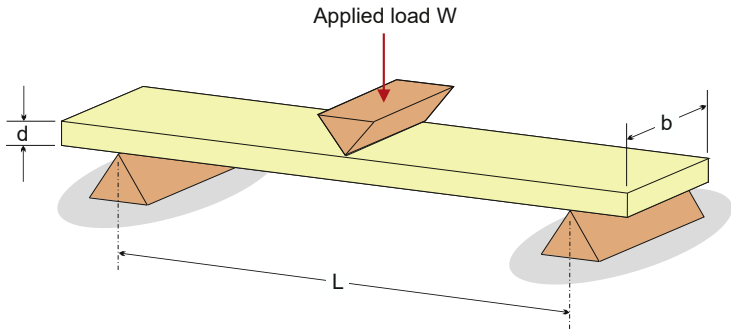


FIG. 2.3 Three-point bending.

examples later in this chapter and the reader is referred to Benham et al. for a greater variety of bending equations.

2.4 Long-term testing of plastics

Since the tensile test has disadvantages when used for plastics, creep tests have evolved as the best method of measuring the deformation behaviour of polymeric materials. In these tests a constant load is applied to the material and the variation of strain with time is recorded as shown in Fig. 2.4(a). Normally a logarithmic time scale is used as shown in Fig. 2.4(b) so that the time dependence after long periods can be included and as an aid to extrapolation. This figure shows that on the application of a stress (σ_1 in the figure) there is typically an almost instantaneous strain followed by a gradual increase. If a material is linearly viscoelastic then at

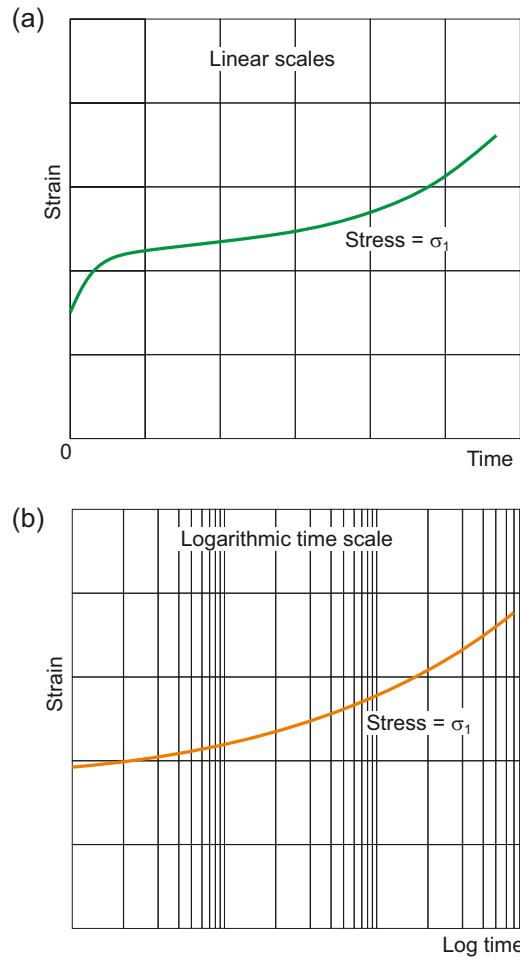


FIG. 2.4 Typical creep curves.

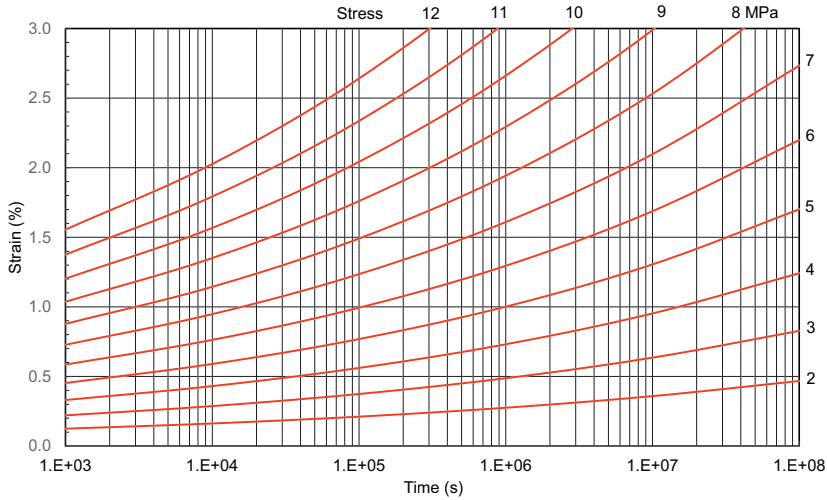


FIG. 2.5 Creep curves for polypropylene at 20°C (density 909 kg/m^3).

any selected time each line in a family of creep curves should be offset along the strain axis by the same amount. Although this type of behaviour may be observed for plastics at low strains and short times, in the majority of cases the response is non-linear as indicated in Fig. 2.5.

Occasionally creep curves are plotted as log (strain) against log (time). This is convenient because quite often this results in straight line plots suggesting that the creep behaviour can be described by an equation of the type

$$\varepsilon(t) = At^n \tag{2.8}$$

where 'n' is a material constant and 'A' is a constant which depends on the stress level.

To be strictly accurate, the right hand side should have the form $(A_0 + At^n)$ to allow for the instantaneous strain at zero time. However, for long creep times, sufficient accuracy can be obtained by ignoring A_0.

A variety of other creep-strain equations have been proposed. These take the form.

1.	$\varepsilon = a + bt^c$	Parabolic
2.	$\varepsilon = a + bt^{1/3} + ct$	Power
3.	$\varepsilon = \frac{at}{1+bt}$	Hyperbolic

4.	$\varepsilon = \frac{1}{1+at^b}$	Hyperbolic
5.	$\varepsilon = a + \ln(b+t)$	Logarithmic
6.	$\varepsilon = \frac{a(b+\ln t)}{c+d\ln t}$	Logarithmic
7.	$\varepsilon = a + b(1-e^{-ct})$	Exponential
8.	$\varepsilon = \sinh at$	Hyperbolic sine
9.	$\varepsilon = a + b\sinh ct$	Hyperbolic sine
10.	$\varepsilon = a + b\sinh ct^{1/3}$	Hyperbolic sine
11.	$\varepsilon = a(1 + bt^{1/3})e^{-ct}$	Power/exponential

Knowledge of the mechanisms of creep in polymers continues to advance through research and some aspects have been explained based on the structures described in Appendix A. For example, in a glassy plastic a particular atom is restricted from changing its position as a result of attractions and repulsions between it and (a) atoms in the same chain, (b) atoms in adjacent chains. It is generally considered that for an atom to change its position it must overcome an energy barrier and the probability of it achieving the necessary energy is improved when a stress is applied. In a semi-crystalline plastic there is an important structural difference in that the crystalline regions are set in an amorphous matrix. Movement of atoms can occur in both regions but in the majority of cases atom mobility is favoured in the non-crystalline material between the spherulites.

Plastics also have the ability to recover when the applied stress is removed and to a first approximation this can often be considered as a reversal of creep. This was illustrated in Fig. 1.12 and will be studied again in Section 2.7. At present it is proposed to consider the design methods for plastics subjected to steady forces.

2.5 Design methods for plastics using deformation data

2.5.1 Isochronous and isometric graphs

The usual method of displaying the interdependence of stress, strain and time is by means of creep curves. However, it should be realised that these represent a two-dimensional view of (or slices through) the three-dimensional stress–strain–time behaviour of plastics shown in Fig. 2.6. It would be equally sensible to consider the other two-dimensional views which could be taken of Fig. 2.6. These are the stress–strain plot (often called the **isochronous curve** because it represents a constant time section) and the stress–time plot

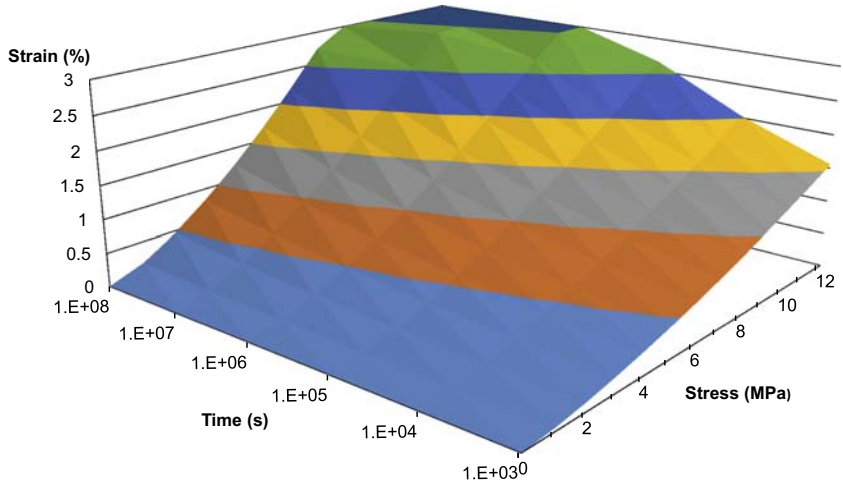


FIG. 2.6 Stress–strain–time curves for polypropylene.

(sometimes called the **isometric curve** because it represents a constant strain section). These two 'views' are shown in Figs. 2.7 and 2.8.

In practice, of course, it is most common to have the creep curves (strain–time curve) since these can be obtained relatively simply by experiment. The other two curves can then be derived from it. For example, the isometric graph is obtained by taking a constant strain section through the creep curves and re-plotting as stress versus time (see Fig. 2.10(a) for a strain of 1.6%). This is termed an **isometric graph** and is an indication of the

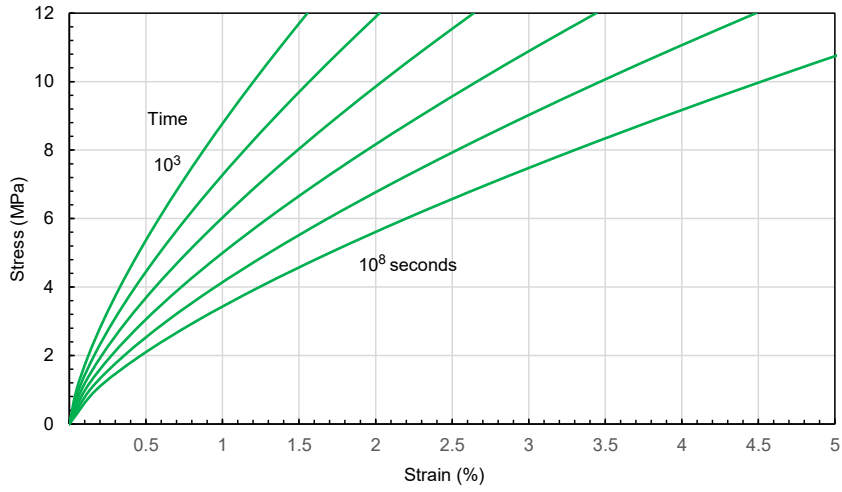


FIG. 2.7 Stress–strain curves for polypropylene.

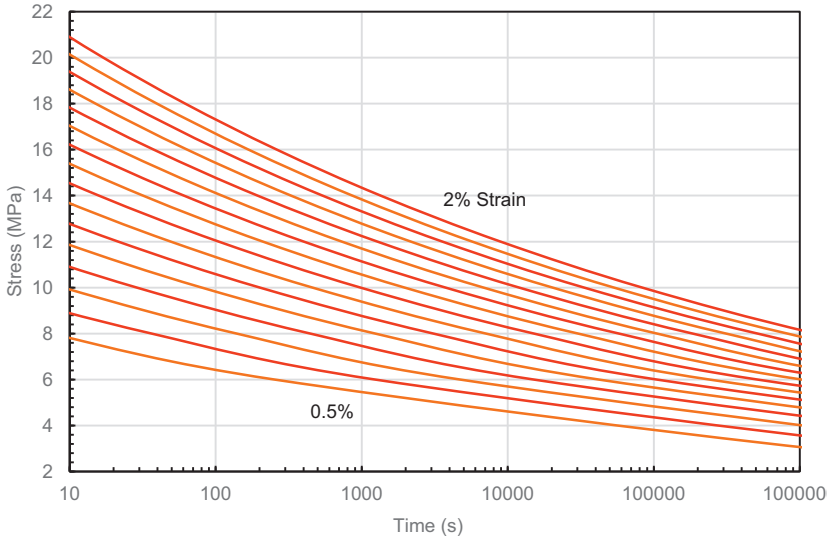


FIG. 2.8 Stress–time curves for polypropylene.

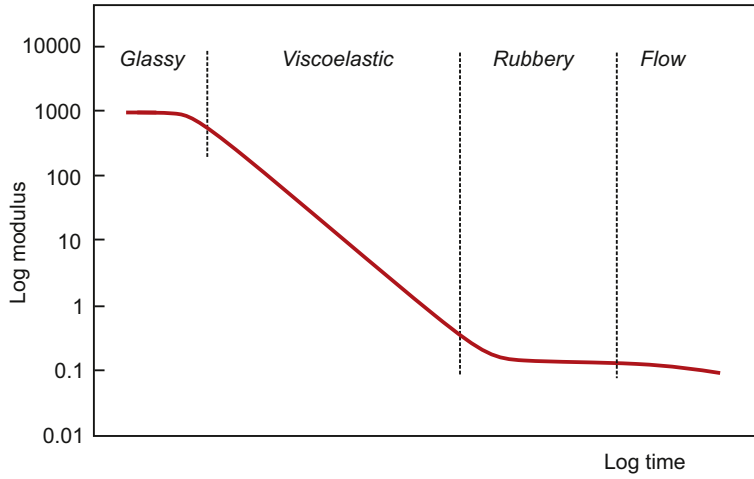


FIG. 2.9 Typical variation of creep or relaxation moduli with time.

relaxation of stress in the material when the strain is kept constant. This data is often used as a good approximation of stress relaxation in a plastic since the latter is a less common experimental procedure than creep testing. In addition, if the vertical axis (stress) is divided by the strain, ε, then we obtain a graph of modulus against time (Fig. 2.10(b)). This is a good illustration of the time dependent variation of modulus which was referred to earlier. It should be

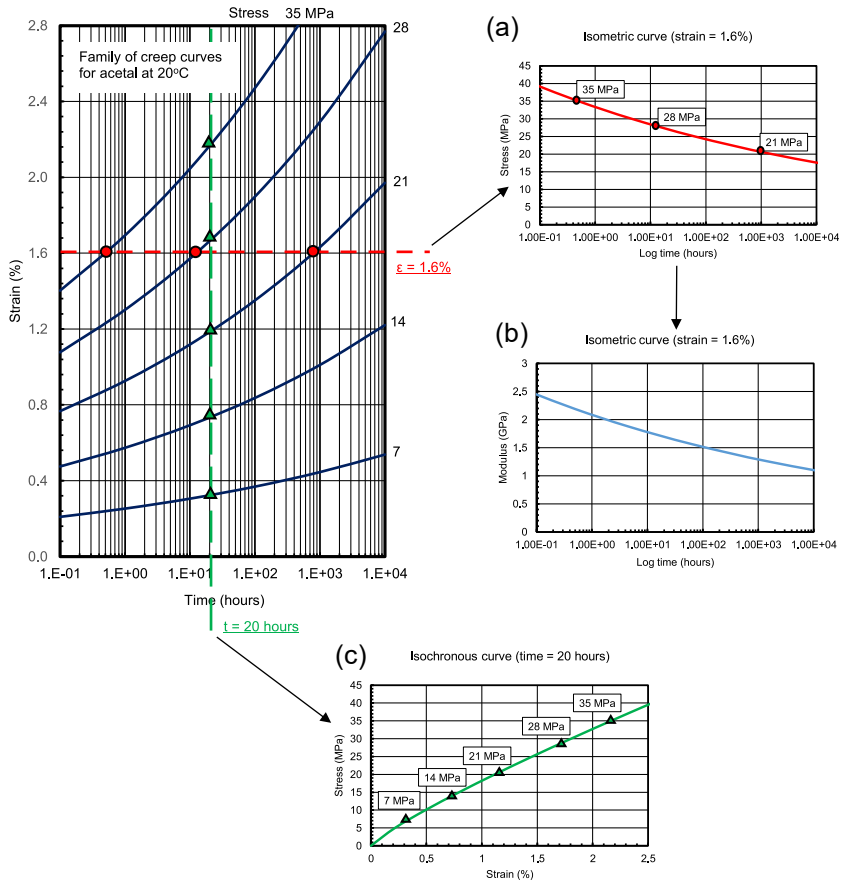


FIG. 2.10 Construction of isometric and isochronous graphs.

noted that this is a *Relaxation Modulus* since it relates to a constant strain situation. It will be slightly different from *the Creep Modulus* which could be obtained by dividing the constant creep stress by the strain at various times. Thus

$$\text{creep modulus, } E(t) = \frac{\sigma}{\varepsilon(t)} \tag{2.9}$$

The creep modulus will vary with time, i.e. decrease as time increases, in a manner similar to that shown for the relaxation modulus. The classical variation of these moduli is illustrated in Fig. 2.9. On log−log scales it is observed that there is a high value of creep or relaxation modulus at short times. This is referred to as the *Unrelaxed Modulus* and is independent of time. Similarly at long times there is a low value *Relaxed Modulus* which is also independent of time.

Occasionally in creep analysis it is convenient to use a *Creep Compliance* instead of the creep modulus. This is simply given by

$$\text{Creep compliance, } C(t) = \frac{1}{E(t)} = \frac{\varepsilon(t)}{\sigma} \tag{2.10}$$

An alternative to the isometric graph may be obtained by taking a constant time section through the creep curves and plotting stress versus strain as shown in Fig. 2.10(c). This **Isochronous Graph** can also be obtained experimentally by performing a series of mini-creep and recovery tests on a plastic. In this experiment a stress is applied to a plastic test-piece and the strain is recorded after a time, t (typically 100 s). The stress is then removed and the plastic allowed to recover, normally for a period of $4t$. A larger stress is then applied to the same specimen and after recording the strain at time t, this stress is removed and the material allowed to recover. This procedure is repeated until sufficient points have been obtained for the isochronous graph to be plotted.

These latter curves are particularly important when they are obtained experimentally because they are less time consuming and require less specimen preparation than creep curves. Isochronous graphs at several time intervals can also be used to build up creep curves and indicate areas where the main experimental creep programme could be most profitably concentrated. They are also popular as evaluations of deformational behaviour because the data presentation is similar to the conventional tensile test data referred to in Section 2.3. It is interesting to note that the isochronous test method only differs from that of a conventional incremental loading tensile test in that (a) the presence of creep is recognised, and (b) the memory which the material has for its stress history is accounted for by the recovery periods.

Quite often isochronous data is presented on log–log scales. One of the reasons for this is that on linear scales any slight, but possibly important, non-linearity between stress and strain may go unnoticed whereas the use of log–log scales will usually give a straight-line graph, the slope of which is an indication of the linearity of the material. If it is perfectly linear the slope will be 45°. If the material is non-linear the slope will be less than this.

As indicated above, the stress–strain presentation of the data in isochronous curves is a format which is very familiar to engineers. Hence in design situations it is quite common to use these curves and obtain a secant modulus (see Section 1.4.1, Fig. 1.10) at an appropriate strain. Strictly speaking this will be different from the creep modulus or the relaxation modulus referred to above since the secant modulus relates to a situation where both stress and strain are changing. In practice the values are quite similar and as will be shown in the following sections, the values will coincide at equivalent values of strain and time. That is, a 2% secant modulus taken from a 1 year isochronous curve will be the same as a 1 year relaxation modulus taken from a 2% isometric curve.

2.5.2 Pseudo-elastic design method for plastics

Throughout this chapter the viscoelastic behaviour of plastics has been described and it has been shown that deformations are dependent on such factors as the time under load and the temperature. Therefore, when structural components are to be designed using plastics, it must be remembered that the classical equations which are available for the design of springs, beams, plates, cylinders, etc., have all been derived under the assumptions that:

(i) the strains are small
(ii) the modulus is constant
(iii) the strains are independent of loading rate or history and are immediately reversible
(iv) the material is isotropic
(v) the material behaves in the same way in tension and compression

Since these assumptions are not always justified for plastics, the classical equations cannot be used indiscriminately. Each case must be considered' on its merits and account taken of such factors as mode of deformation, service temperature, fabrication method, environment and so on. In particular, it should be noted that the classical equations are derived using the relation.

$$\text{stress} = \text{modulus} \times \text{strain}$$

where the modulus is a constant. From the foregoing sections it should be clear that the modulus of a plastic is not a constant. Several approaches have been used to allow for this and some give very accurate results. The drawback is that the methods can be quite complex, involving Laplace transforms or numerical methods and they are certainly not attractive to designers. However, one method that has been widely accepted is the so called **Pseudo Elastic Design Method**. In this method, appropriate values of time dependent properties, such as modulus, are selected and substituted into the classical equations. It has been found that this approach gives sufficient accuracy in most cases provided that the value chosen for the modulus takes into account the service life of the component and the limiting strain of the plastic. This of course assumes that the limiting strain for the material is known. Unfortunately this is not just a straightforward value which applies for all plastics or even for one plastic in all applications. It is often arbitrarily chosen although several methods have been suggested for arriving at a suitable value. One method is to plot a secant modulus which is 0.85 of the initial tangent modulus (see Fig. 1.10) and note the strain at which this intersects the stress−strain characteristic. However, for many plastics (particularly crystalline ones) this is too restrictive and so in most practical situations the limiting strain is decided in consultations between the designer and the material manufacturers.

Once the limiting strain is known, design methods based on the creep curves are quite straightforward and the approach is illustrated in the following

examples. When using this pseudo-elastic design approach it should be remembered that the creep curves used to derive modulus values have normally been obtained on test pieces which are essentially isotropic. In practice the manufacture of the end-product by injection moulding or extrusion, etc. will have resulted in some degree of anisotropy. This may make the predictions inaccurate because the creep data for the material is no longer appropriate for the structural morphology introduced by the moulding method. Similar comments could, of course, also be made about metals in that the test data may have been obtained on specimens of the material which do not accurately reflect the nature of the material in the end-product. Therefore, pseudo-elastic design is a valid analytical procedure but one should always be cautious about the way in which the manufacturing method has affected the behaviour of the material.

Example 2.1. A ball-point pen made from polypropylene has the clip design shown in Fig. 2.11. When the pen is inserted into a pocket, the clip is subjected to a deflection of 2 mm at point A. If the limiting strain in the material is to be 0.5% calculate (i) a suitable thickness, *d,* for the clip (ii) the initial stress in the clip when it is first inserted into the pocket and (iii) the stress in the clip when it has been in the pocket for 1 week. The creep curves in Fig. 2.5 may be used and the short-term modulus of polypropylene is 1.6 GPa.

Solution Strain, ε, is given by the ratio of stress, σ, to modulus, E. In the case of the pen clip, it is effectively a cantilever of length 40 mm.

$$\text{Bending stress, } \sigma = \frac{My}{I}$$

where M = bending moment (WL)
y = half beam depth ($d/2$)
I = second moment of area ($= bd^3/12$)

$$\text{(i) Hence strain, } \varepsilon = \frac{WLd}{2EI} \tag{2.11}$$

Also, the classical elastic equation for the end deflection of a cantilever is:

$$\text{deflection, } \delta = \frac{WL^3}{3EI} \tag{2.12}$$

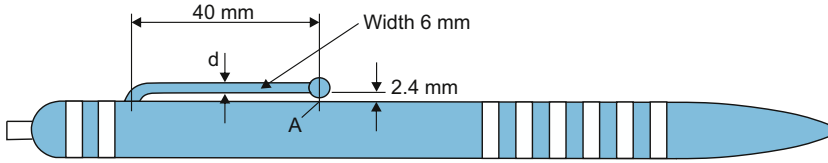


FIG. 2.11 Ball-point pen clip design.

Combining (2.11) and (2.12) gives

$$\text{strain, } \varepsilon = \frac{3\delta d}{2L^2} \tag{2.13}$$

So

$$d = \frac{2(40)^2 \times 0.005}{3 \times 2} = 2.7 \text{ mm}$$

(ii) The short-term stress in the material is obtained from the short-term modulus which is given in this question (or could be obtained from the creep/isometric curves, i.e. at 10 s, $E = 8 \times 10^6/0.5\% = 1.6$ GPa or from the appropriate isometric curve).

$$\text{stress, } \sigma = E\varepsilon = 1.6 \times 10^9 \times 0.005 = 8 \text{ M}Pa$$

(iii) After 1 week (6.05×10^5 s), the isometric curves (Fig. 2.8) derived from the creep curves show that at a strain of 0.5% the stress would have decayed to about 3.2 MPa.

Example 2.2. A polypropylene beam is 100 mm long, simply supported at each end and is subjected to a load W at its mid-span. If the maximum permissible strain in the material is to be 1.5%, calculate the largest load which may be applied so that the deflection of the beam does not exceed 5 mm in a service life of 1 year. For the beam $I = 28$ mm^4 and the creep curves in Fig. 2.5 should be used.

Solution. The central deflection in a beam loaded as shown in Fig. 2.12 is given by

$$\delta = \frac{WL^3}{48EI}$$

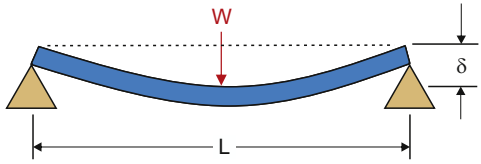


FIG. 2.12 Simply supported beam with central load.

$$W = \frac{48EI\delta}{L^3}$$

The only unknown on the right hand side is a value for modulus E. For the plastic this is time-dependent but a suitable value may be obtained by reference to the creep curves in Fig. 2.5. A section across these curves at the service life of 1 year gives the isochronous graph shown in Fig. 2.13. The maximum strain is recommended as 1.5% so a secant modulus may be taken at this value and is found to be 335 MPa. This is then used in the above equation.

So

$$W = \frac{48 \times 335 \times 28 \times 5}{(100)^3} = 2.25 \text{ N}$$

As before, a similar result could have been achieved by taking a section across the creep curves at 1.5% strain, plotting an isometric graph (or a 1.5% modulus/time graph) and obtaining a value for modulus at 1 year (see Fig. 2.8)

In this example it has been assumed that the service temperature is 20°C. If this is not the case, then curves for the appropriate temperature should be used. If these are not available then a linear extrapolation between temperatures which are available is usually sufficiently accurate for most purposes. If the beam in the above example had been built-in at both ends at 20°C, and subjected to service conditions at some other temperature, then allowance would need to be made for the *thermal strains* set up in the beam. These could be obtained from a knowledge of the coefficient of thermal expansion of the beam material. This type of situation is illustrated later.

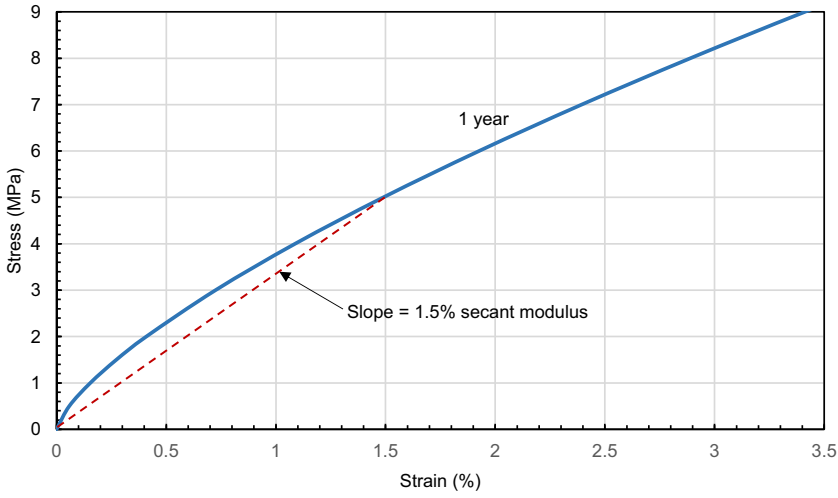


FIG. 2.13 Isochronous curve for polypropylene (1 year).

For some plastics, particularly nylon, the moisture content can have a significant effect on the creep behaviour. For such plastics, creep curves are normally available in the wet and dry states and a knowledge of the service conditions enables the appropriate data to be used.

For convenience so far we have referred generally to *creep curves* in the above examples. It has been assumed that one will be using the correct curves for the particular loading configuration. In practice, creep curves obtained under tensile and flexural loading conditions are quite widely available. Obviously it is important to use the creep curves which are appropriate to the particular loading situation. Occasionally it is possible to obtain creep curves for compressive or shear loading but these are less common.

If only one type of data is available (e.g. tensile creep curves) then it is possible to make conversions to the other test modes. It should always be remembered, however, that these may not always be absolutely accurate for plastics under all situations.

Some published experimental values of tensile and compressive moduli for selected polymers are shown in Table 2.1. Figures for tensile modulus are

TABLE 2.1 Tensile and compressive moduli for selected polymers.

Material (selected grades)	Tensile modulus (E_T) (GPa)	Compressive modulus (E_C) (GPa)	$M_R = E_C/E_T$
ABS	2.21	2.07	0.94
Acrylic (PMMA)	2.76	2.96	1.08
Polyethylene (LD)	0.39	0.37	0.95
Nylon 12	1.59	1.54	0.97
PC	2.34	2.38	1.01
PEEK	3.60	3.79	1.05
PEEK (30% glass)	9.65	6.89	0.71
PET	3.17	2.90	0.91
POM	3.10	3.10	1.00
PP	1.65	1.55	0.94
PSU	2.48	2.59	1.04
PTFE	0.55	0.48	0.88
PVC (rigid)	2.83	3.10	1.10

readily available but compressive modulus is measured less often and is rarely quoted in tables of mechanical properties. An explanation for this is that modulus values in tension and compression are quite often assumed to be the same, and generally this is a valid first approximation. Most of those shown in Table 2.1 are within 10% of each other. However, it should be pointed out that there are large variations in modulus values across different grades of the same polymer and the values are very sensitive to material composition and testing conditions. For some polymers (such as Acrylic, PEEK and PVC) there is a stiffening effect in compression compared to tension. In many others (such as LDPE, PP and PET) this effect is reversed and the polymer is stiffer in tension than in compression. Addition of short fibres generally enhances the modulus of a polymer and in the case of PEEK (shown in Table 2.1), addition of 30% glass fibres substantially raises the tensile modulus beyond the compressive modulus. However, one needs to be careful when comparing the experimental data because normally no account is taken of the changes in cross-sectional area during testing. In tension, the area will decrease so that the true stress will increase whereas in compression the opposite effect will occur.

The classical relationship between moduli in tension, compression and flexure is

$$E_{\text{flex}} = E_{\text{T}} \left[\frac{2\sqrt{M_{\text{R}}}}{1 + \sqrt{M_{\text{R}}}} \right]^2 \tag{2.14}$$

where

$$M_{\text{R}} = E_{\text{c}} / E_{\text{T}}$$

It may be seen that if $E_c = E_{\text{T}}$ then $E_{\text{flex}} = E_{\text{T}}$. However, if $E_{\text{c}} = 1.1E_{\text{T}}$ (for example), then $E_{\text{flex}} = 1.05E_{\text{T}}$.

The classical relationship between the *shear modulus G,* and the tensile modulus, *E,* for an isotropic material is

$$G = \frac{E}{2(1 + v)} \tag{2.15}$$

where $v =$ Poisson's ratio.

Finally, although it is less commonly used for plastics, the *bulk modulus, K,* is given by

$$K = \frac{E}{3(1 - 2v)} \tag{2.16}$$

The bulk modulus is appropriate for situations where the material is subjected to hydrostatic stresses. The proof of Eqs. (2.15) and (2.16) is given by Benham et al.

Example 2.3. A cylindrical polypropylene tank with a mean diameter of 1 m is to be subjected to an internal pressure of 0.2 MPa. If the maximum

strain in the tank is not to exceed 2% in a period of 1 year, estimate a suitable value for its wall thickness. What is the ratio of the hoop strain to the axial strain in the tank. The creep curves in Fig. 2.5 may be used.

Solution The maximum strain in a cylinder which is subjected to an internal pressure, *P,* is the hoop strain and the classical elastic equation for this is

$$\varepsilon_\theta = \frac{PR}{2hE}(2-v)$$

where E is the modulus, R is the cylinder radius and h *is* the wall thickness (See Appendix C).

The modulus term in this equation can be obtained in the same way as in the previous example. However, the difference in this case is the term *v.* For elastic materials this is called **Poisson's Ratio** and is the ratio of the transverse strain to the axial strain (See Appendix C). For any particular metal this is a constant, generally in the range 0.28−0.35. For plastics v is not a constant. It is dependent on time, temperature, stress, etc. and so it is often given the alternative names of **Creep Contraction Ratio** or **Lateral Strain Ratio**. There is very little published information on the creep contraction ratio for plastics but generally it varies from about 0.32 for hard plastics (such as acrylic) to almost 0.5 for elastomers. Some typical values are given in Table 2.2 but do remember that these may change in specific loading situations.

Using the value of 0.4 for polypropylene,

$$h = \frac{PR}{2\varepsilon E}(2-v)$$

from Fig. 2.7, $E = \frac{6.2}{0.02} = 310$ MPa

$$\therefore h = \frac{0.2 \times 0.5 \times 10^3 \times 1.6}{2 \times 0.02 \times 310} = 12.9 \text{ mm}$$

For a cylindrical tank the axial strain is given by

$$\varepsilon_x = \frac{PR}{2hE}(1-2v)$$

So

$$\frac{\varepsilon_\theta}{\varepsilon_x} = \left(\frac{2-v}{1-2v}\right) = \frac{1.6}{0.2} = 8$$

Note that the ratio of the ratio of the hoop stress (*PR/h)* to the axial stress (*PR/2h*) is only 2. From the data in this question the hoop stress will be 7.75 MPa. A plastic cylinder or pipe is an interesting situation in that it is an example of creep under biaxial stresses. The material is being stretched in the hoop direction by a stress of 7.75 MPa but the strain in this direction is restricted by the perpendicular axial stress of 0.5 (7.75) MPa. Reference to any solid mechanics text will show that this situation is normally dealt with by calculating an equivalent stress, σ_e. For a cylinder under pressure σ_e is given

TABLE 2.2 Typical tensile and shear moduli for a range of polymers.

Material	Density (kg/m^3)	Tensile modulus (E)[a]. (GPa)	Shear modulus (G) (GPa)	Poisson's ratio (v)
Polystyrene (PS)	1050	2.65	0.99	0.33
Polymethyl methacrylate (PMMA)	1180	3.10	1.16	0.33
Polyvinyl chloride (PVC) (unplasticised)	1480	3.15	1.13	0.39
Nylon 66 (at 65% RH)	1140	0.99	0.34	0.44
Acetal homopolymer (POM)	1410	3.24	1.15	0.41
Acetal copolymer (POM)	1410	2.52	0.93	0.39
Polyethylene – High density (HDPE)	955	1.05	0.39	0.34
Polyethylene – Low density (LDPE)	920	0.32	0.11	0.45
Polypropylene homopolymer (PP)	910	1.51	0.55	0.36
Polypropylene copolymer (PP)	902	1.13	0.40	0.40
Polylactic acid (PLA)	1252	3.50	1.29	0.36
Polycaprolactam	1146	4.00	1.43	0.40
Polycarbonate (PC)	1194	2.77	0.99	0.40
Polyethersulphone	1390	2.76	0.98	0.41
Polyphenylene oxide (PPO)	1073	2.94	1.07	0.37
Polytetrafluoroethylene (PTFE)	2180	3.06	1.16	0.32
Phenolic	1220	5.79	2.13	0.36
Epoxy	1184	5.05	1.83	0.38

[a]100 s modulus at 20°C for small strains (<0.2%).

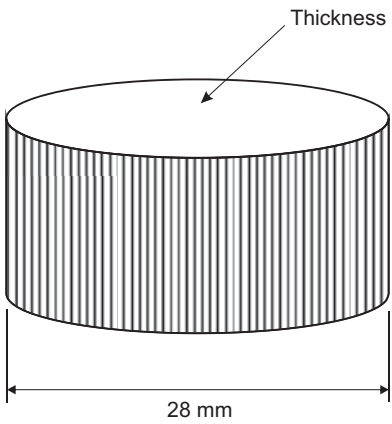


FIG. 2.14 Acetal bottle cap.

by $0.5\sigma_\theta\sqrt{3}$ where σ_θ is the hoop stress. This would permit the above question to be solved using the method outlined earlier.

Example 2.4. A glass bottle of sparkling water has an acetal cap as shown in Fig. 2.14. If the carbonation pressure is 375 kPa, estimate the deflection at the centre of the cap after 1 month. The value of Poisson's ratio for acetal may be taken as 0.33.

Solution The top of the bottle cap is effectively a plate with clamped edges. The central deflection in such a situation is given by Benham et al. as

$$\delta = \frac{PR^4}{64D} \quad \text{where } D = \frac{Eh^3}{12(1-v^2)}$$

To calculate δ after 1 month it is necessary to know the 1 month creep modulus. The stresses at the centre of the cap are biaxial (radial and circumferential) both given by

$$\sigma = \frac{3PR^2(1+v)}{8h^2} = \frac{2 \times 0.375 \times (14-1.2)^2(1.33)}{8(1.2)^2}$$

$$\sigma = 21.3MPa$$

After 1 month (2.6×10^6 s) at this stress, the strain is obtained from Fig. 2.15 as 2.1%. Hence $E = 21.3 \times 10^6/0.021 = 1$ GPa.

So,

$$\delta = \frac{PR^4}{64D} = \frac{0.375(12.8)^4 12\left(1-0.33^2\right)}{64 \times 1000 \times (1.2)^3}$$

$$\delta = 1 \text{ mm}$$

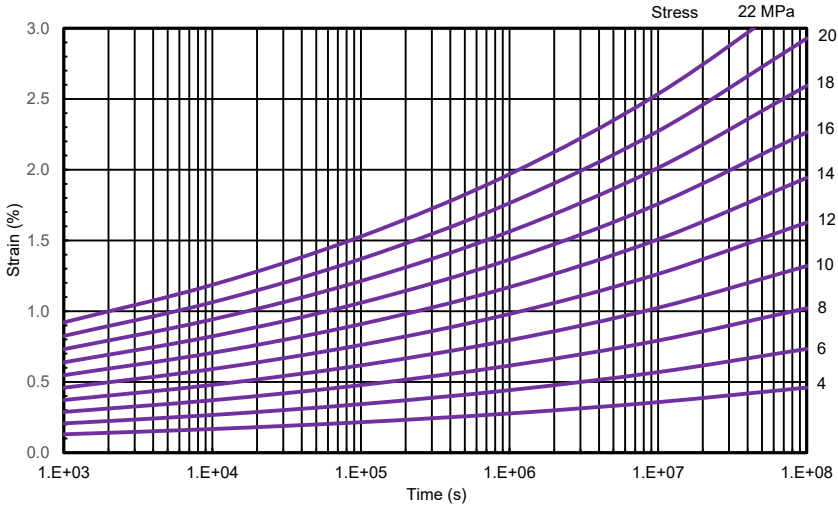


FIG. 2.15 Creep curves for acetal (20°C).

Example 2.5. In a small polypropylene pump the flange on the cover plate is 2 mm thick. When the rigid clamping screws are tightened, the flange is reduced in thickness by 0.03 mm. Estimate the initial stress in the plastic and the stress after 1 week

Solution The strain in the material is given by

$$\varepsilon = \frac{0.03}{2} \times 100 = 1.5\%$$

This is a stress relaxation problem and strictly speaking stress relaxation data should be used. However, for most purposes isometric curves obtained from the creep curves are sufficiently accurate. By considering the 1.5% isometric curve shown in Fig. 2.8 it may be seen that the initial stress is 17 MPa and the stress after 1 week is 7 MPa.

Accurately performed relaxation tests in which the strain in the material was maintained and the decaying stress monitored, would give slightly lower values than those values obtained from the isometric data.

It should also be noted that in this case the material was loaded in compression whereas the tensile creep curves were used. The vast majority of creep data which is available is for tensile loading mainly because this is the simplest and most convenient test method. However, it should not be forgotten that the material will behave differently under other modes of deformation. In compression the material deforms less than in tension although the effect is small for strains up to 0.5%. If no compression data is available then the use of tensile data is permissible because the lower modulus in the latter case will provide a conservative design.

2.6 Thermal stresses and strains

It is quite common in modern engineering designs, for plastics to be used in conjunction with other materials, particularly metals. In such cases it is wise to consider the possibility of thermal stresses being set up due to the differences in the thermal expansion (or contraction) in each material.

The change in shape of a material when it is subjected to a change in temperature is determined by the coefficient of thermal expansion, α_T. Normally for isotropic materials the value of α_T will be the same in all directions. For convenience this is often taken to be the case in plastics but one always needs to bear in mind that the manufacturing method may have introduced anisotropy which will result in different thermal responses in different directions in the material.

The coefficient of thermal expansion, α_T, is given by

$$\alpha_T = \frac{\delta L}{L(\Delta T)} \tag{2.17}$$

where δL is the change in length in the material.

L is the original length
ΔT is the change in temperature.

There are standard procedures for determining α_T (e.g. ASTM D696) and typical values for plastics are given in Table 1.8. It may be observed that the coefficients of thermal expansion for plastics are higher than those for metals. Thus if 50 mm lengths of polypropylene and stainless steel are each heated up by 60°C the changes in length would be.

(a) polypropylene, $\delta l = 100 \times 10^{-6} \times 50 \times 60 = 0.3$ mm
(b) stainless steel, $\delta l = 10 \times 10^{-6} \times 50 \times 60 = 0.03$ mm

If these changes in length take place freely then we will have a thermally induced strain in the material ($= 0.3/50 \times 100 = 0.6\%$ in the polypropylene) but no stress. However, if the polypropylene was constrained in some way so that the 0.3 mm expansion could not happen when it is heated by 60°C, then there would be a thermally induced stress in the material, i.e.,

$$\text{stress} = \text{modulus} \times \text{strain}$$

If the modulus of the material is 1.2 GPa at the final temperature, then the stress in the material would be given by

$$\text{stress} = 1.2 \times 10^9 \left(\frac{-0.6}{100}\right) = -7.2 \text{ MPa}$$

Note that the stress is compressive because the material is effectively compressed by 0.3 mm.

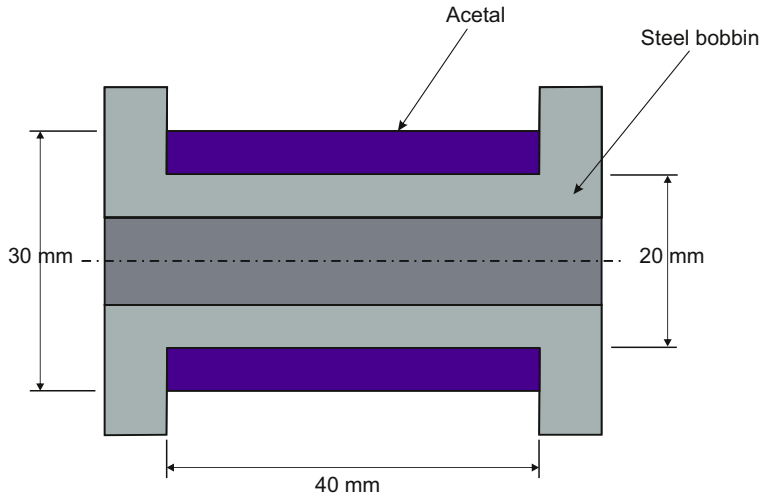


FIG. 2.16 Metal bobbin with plastic sleeve.

Example 2.6. The bobbin shown in Fig. 2.16 has been manufactured by sliding the acetal ring on to the steel inner and then placing the end-plate in position. At 20°C there are no stresses in the acetal and the distance between the metal end-plates is equal to the length of the acetal ring. If the whole assembly is heated to 100°C, calculate the axial stress in the acetal. It may be assumed that there is no friction between the acetal and the steel. The coefficients of thermal expansion for the acetal and the steel are $80 \times 10^{-6\circ}\mathrm{C}^{-1}$ and $11 \times 10^{-6\circ}\mathrm{C}^{-1}$ respectively. The modulus of the acetal at 100°C is 1.5 GPa.

Solution Under free conditions, the acetal would expand more than the steel but in the configuration shown they will both expand to the same extent. Hence, the acetal will effectively be put in compression by an amount given by Eq. (2.17)

$$\begin{aligned}\delta &= (\alpha_a - \alpha_s)L \cdot \Delta T \\ &= (80 - 11)10^{-6}(40)(80) \\ &= 0.22 \text{ mm}\end{aligned}$$

$$\text{strain} = -\frac{0.22}{40} \times 100 = -0.55\%$$

$$\begin{aligned}\text{stress} = E\varepsilon &= -1.5 \times 10^9 \times \frac{0.55}{100} \\ &= -8.3 \text{ MPa}\end{aligned}$$

Thus, there will be a compressive stress of 8.3 MPa in the acetal. It should be noted that the above analysis ignores the effect of the constraining effect which the acetal has on the thermal expansion of the steel. However, as the modulus of the steel is over 100 times greater than the acetal, this constraining effect will be very small. Thus, the above analysis is perfectly acceptable for engineering design purposes.

Example 2.7. A nylon ring with a nominal inside diameter of 30 mm, an outer diameter of 50 mm and a width of 5 mm is to be made an interference fit on a metal shaft of 30 mm diameter as shown in Fig. 2.17. The design condition is that the initial separation force is to be 1 kN. Calculate (a) the interference on the radius needed between the ring and the shaft and (b) the temperature to which the nylon must be heated to facilitate easy assembly. What will be the maximum stress in the nylon when it is in position on the shaft? The coefficient of friction between nylon and steel is 0.25. The short-term modulus of the nylon is 1 GPa, its Poisson's ratio is 0.4 and its coefficient of thermal expansion is $100 \times 10^{-6\circ}C^{-1}$.

Solution.

(a) Force, $F = \mu N$

where $N = PA$

$= P\pi DW$

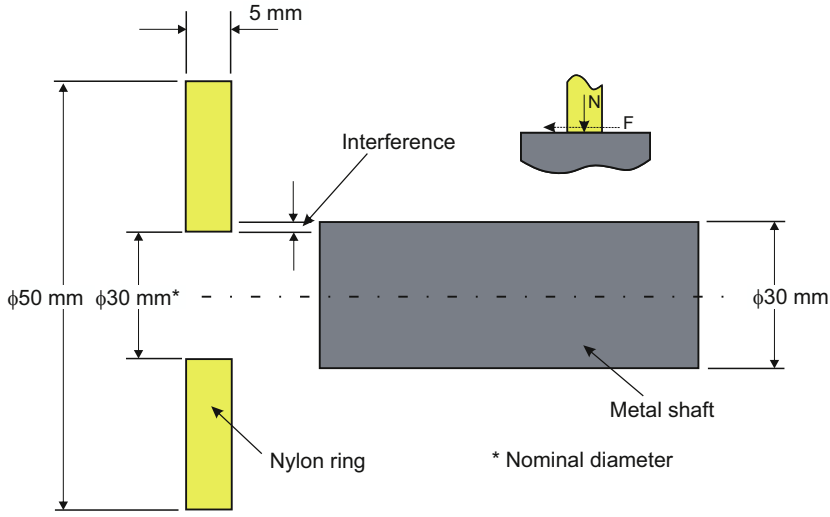


FIG. 2.17 Interference fit of nylon ring on metal shaft.

So, $F = \pi\mu pDW$

Therefore

$$P = \frac{1 \times 10^3}{\pi(0.25)(30)(5)} = 8.5\ MPa$$

The nylon ring may be considered as a thick wall cylinder subjected to this internal pressure (see Appendix D). At the inner surface of the ring there will be a hoop stress, σ_θ, and a radial stress, σ_r. Benham et al. shows these to be

$$\text{Hoop stress, } \sigma_\theta = P\left\{\frac{k^2+1}{k^2-1}\right\}$$

$$\text{Radial stress, } \sigma_r = -P$$

where k = ratio of outer to inner radius.

Hence the hoop strain, ε_θ, at the bore of the ring is given by

$$\varepsilon_\theta = \frac{\delta r}{r} = \frac{\sigma_\theta}{E} - \frac{v\sigma_r}{E}$$

so

$$\delta r = \frac{Pr}{E}\left\{\left(\frac{k^2+1}{k^2-1}\right) + v\right\}$$

$$= \frac{8.5(15)}{1 \times 10^3}\left\{\left(\frac{\left(50/30\right)^2 + 1}{\left(50/30\right)^2 - 1}\right) + 0.4\right\}$$

$$\delta r = 0.32\ \text{mm}$$

This is the interference needed on the radius to give the desired separation force.

(b) To facilitate easy assembly, the nylon should be heated so that the inner radius expands by this amount. As shown in the previous section

$$\delta r = \alpha \cdot r \cdot \Delta T$$

$$\Delta T = \frac{0.32}{100 \times 10^{-6} \times 15} = 214^\circ C$$

(c) The maximum stress in the nylon ring when it is on the shaft will be the hoop stress at the bore. This is given by

$$\sigma_\theta = P\left\{\frac{k^2+1}{k^2-1}\right\} = 8.5\left\{\frac{1.67^2+1}{1.67^2-1}\right\}$$

$$\sigma_\theta = 18 \text{ MPa}$$

As a practical point, it should be noted that the separation force will change with time. This is because the modulus, *E,* will decrease with time. Suppose that in Example 2.7, the assembly is to be maintained in position for 1 year and that during this time the modulus decreases to half its initial value (the 1 year modulus would be obtained from the creep curves in the normal way). The above analysis shows that the interface pressure would then be half its initial value (because δr is fixed) and this in turn means that the separation force would become 500 N instead of 1 kN.

2.7 Multi-layer mouldings

It is now common practice for the cross-section of a plastic moulding to be made up of several different materials. This may be desirable for many different reasons including design, economics or functionality. For example, a product may require a colorful or printable surface, whereas its centre is entirely hidden and may either be hollow, foamed or filled with a lower cost alternative polymer. Nowadays there are increasing pressures to reuse or recycle plastics and this has led industry to create multi-layer mouldings that can both conceal lower quality recycled materials and provide economic gain by reducing overall material costs. To perform stress analysis in such cases, it is often convenient to convert the cross-section into an equivalent section consisting of only one material. This new section will behave in exactly the same way as the multi-layer material when the loads are applied. A very common example of this type of situation is where a solid skin and a foamed core are moulded to provide a very efficient stiffness/weight ratio. This type of situation may be analysed as follows:

Example 2.8. A polypropylene sandwich moulding is 12 mm thick and consists of a foamed core sandwiched between solid skin layers 2 mm thick. A beam 12 mm wide is cut from the moulding and is subjected to a point load, *W,* at mid-span when it is simply supported over a length of 200 mm. Estimate the depth of a solid beam of the same width which would have the same stiffness when loaded in the same way. Calculate also the weight saving by using the foam moulding. The density of the solid polypropylene is 909 kg/m^3 and the density of the foamed core is 600 kg/m^3.

Solution The first step in analysing the foamed sandwich type structure is to calculate the second moment of area of the cross-section. This is done by converting the cross section to an equivalent section of solid plastic. This is shown in Fig. 2.18.

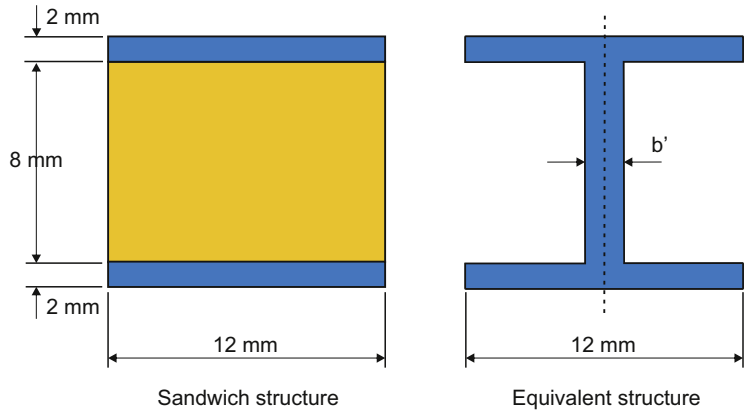


FIG. 2.18 Equivalent section for sandwich moulding.

The equivalent width of the flange in the I section is given by

$$b' = \frac{E_c}{E_s}(b_c) \tag{2.18}$$

where E_c and E_s refer to the modulus values for the core (c) and solid (s) material. Although it is possible to obtain modulus values for foams directly from literature, a number of empirical relationships are available. In general, the compressive strength and modulus of low density rigid cellular foams may be expressed as a power law relationship with foam density:

$$\sigma, E = A\rho_c^n$$

where A and n are constants. Tensile properties are reported to vary in a similar manner (Klempner et al.). For structural foams that are usually produced as fabricated articles by injection moulding or extrusion process the foam densities are relatively high (more than 320 kg/m^3) and in such cases the modulus (E) may be related to density (ρ) using the following equation:

$$\frac{E_c}{E_s} = \left(\frac{\rho_c}{\rho_s}\right)^2 \tag{2.19}$$

From the equivalent section the second moment of area can then be calculated as

$$I = \frac{12(12)^3}{12} - \frac{12(8)^3}{12} + 12\left(\frac{600}{909}\right)^2\frac{(8)^3}{12}$$

$$= 1439 \text{ mm}^4$$

The solid polypropylene beam which would have the same stiffness when loaded in the same way would need to have the same second moment of area. So if its depth is d then

$$\frac{12(d)^3}{12} = 1439mm^4$$
$$d = 11.3\text{mm}$$

The weight per unit length (1 m) of the solid beam would be

$$W_s = 12 \times 11.3 \times 10^{-6} \times 909 \times 10^3 = 123\text{g}$$

The weight per unit length of the foamed beam is

$$W_f = \left(909 \times 2 \times 12 \times 2 \times 10^{-3}\right) + \left(600 \times 12 \times 8 \times 10^{-3}\right)$$
$$= 101.2\text{g}$$

Hence the weight saving is 17.7%

Once the foamed plastic moulding has been converted to an equivalent section of solid plastic then the long term design procedures illustrated in the previous questions can be used. For example, to determine the 1 year deflection of the beam in this question, the appropriate 1 year modulus from the polypropylene creep curves could be used.

The relationship between foam modulus and density can be generalised to other properties such as shear modulus, fatigue strength and creep properties. . Thus if X is the general material property then

$$\frac{X_c}{X_s} = \left(\frac{\rho_c}{\rho_s}\right)^2 \tag{2.20}$$

However, many of these relationships are regarded as rules of thumb since they are not supported by sufficient experimental evidence (Kempler et al.).

Example 2.9. A solid polyethylene beam is 10 mm thick and 15 mm wide. If it is to be replaced with a sandwich section with solid polyethylene (density = 935 kg/m^3) in the two outer skins and polyethylene foam (density = 200 kg/m^3) in the centre, calculate the dimensions of the sandwich beam if it is to have optimum stiffness at the same weight as the solid beam. If the foam material costs 20% more than the solid material, calculate the increase or decrease in the cost of the sandwich beam.

Solution The weight per unit length, W, for the solid beam is

$$W = 935 \times 10^3 \times 15 \times 10 \times 10^{-6} = 140\text{ g/m}$$

For the sandwich section (shown in Fig. 2.19)

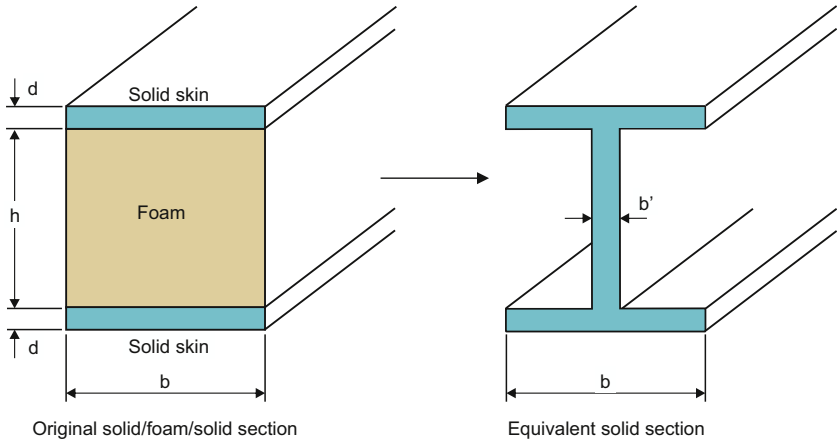


FIG. 2.19 Equivalent solid and solid/foam/solid section.

$$W = \rho_c bh + \rho_s 2bd$$

$$h = \frac{W - 2bd\rho}{\rho_c b} = \frac{W}{b\rho_s D} - \frac{2d}{D}$$

where $D =$ density ratio (ρ_c/ρ_s).

The flexural stiffness of the beam will be proportional to *EI*. So converting the section to an equivalent 'I' beam as in the previous example

$$E_s I = E_s \left[\frac{b(2d+h)^3}{12} - \frac{bh^3}{12} + \left(\frac{\rho_c}{\rho_s}\right)^2 \frac{bh^3}{12} \right]$$

Substituting for h from above, the stiffness may be optimised for constant *W,* by differentiating this expression and equating to zero. This gives the optimum beam depth as

$$d = \frac{1}{2\left(24 + \frac{72}{D^2} - \frac{96}{D}\right)} \left[\frac{48W}{b\rho_s D^2} - \frac{48W}{b\rho_s D} - \frac{24W\sqrt{(D^2-1)(D-1)}}{b\rho_s D^2} \right]$$

Using the information given

$$D = 200/935 = 0.214, \qquad \rho_s = 935 \times 10^{-6} \text{g/mm}^3, \qquad W = 0.14 \text{ g/mm}$$

So

$$d = 1.61 \text{ mm}$$

Using the expression for h from above, the thickness of the foam is given by

$$h = 31.7\text{mm}$$

The cost per unit length of the solid beam is given by

$$(\text{Cost})_{solid} = \rho_s t_s b C_s = 935 \times 10 \times 15 \times 10^{-6} \times C_s = 0.14 C_s$$

The cost per unit length of the sandwich beam is given by

$$(\text{Cost})_F = \rho_c bh C_c + \rho_s 2bd C_s = 0.159\ C_s$$

Hence

$$\text{the additional cost } = \frac{0.159 - 0.14}{0.14} = 13.5\%$$

It is interesting to generalise this solution for any core: skin density ratio. Fig. 2.20 shows how the optimum skin thickness varies with D. This is independent of the solid material density or modulus but is based on a weight per unit length of 140 g/m (equivalent to a solid thickness of 10 mm). If a different solid thickness is of interest then the optimum skin thickness would need to be scaled accordingly. For example, for a 5 mm thick solid beam which is to be converted to a foam sandwich beam of the same weight per unit length, the optimum skin thickness would be half of the value shown in Fig. 2.20. The optimum skin/core thickness ratios are shown in Fig. 2.21.

The stiffness ratios (i.e. stiffness of the foam sandwich beam relative to the original solid beam) are also given in Fig. 2.21. In both cases the values given are independent of the original solid material or its dimensions, so this provides a good design chart. The design of solid/foam sandwich structures is also considered in Chapter 3 in the laminate analysis.

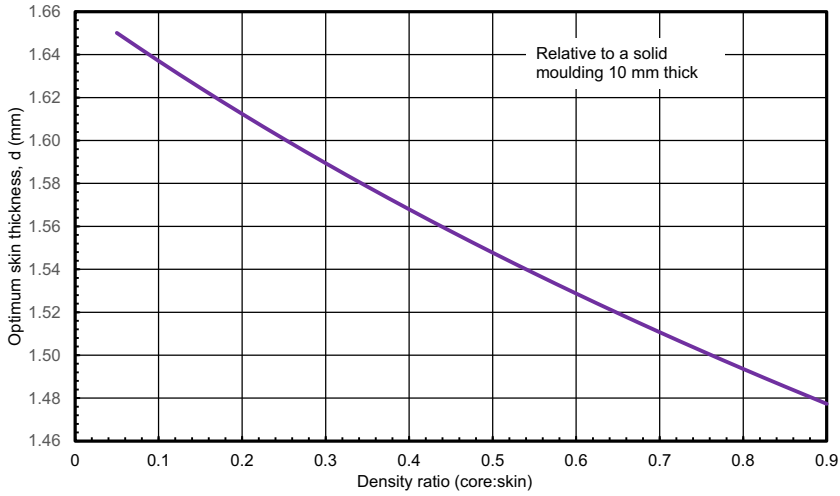


FIG. 2.20 Variation of optimum skin thickness with core: skin density ratio.

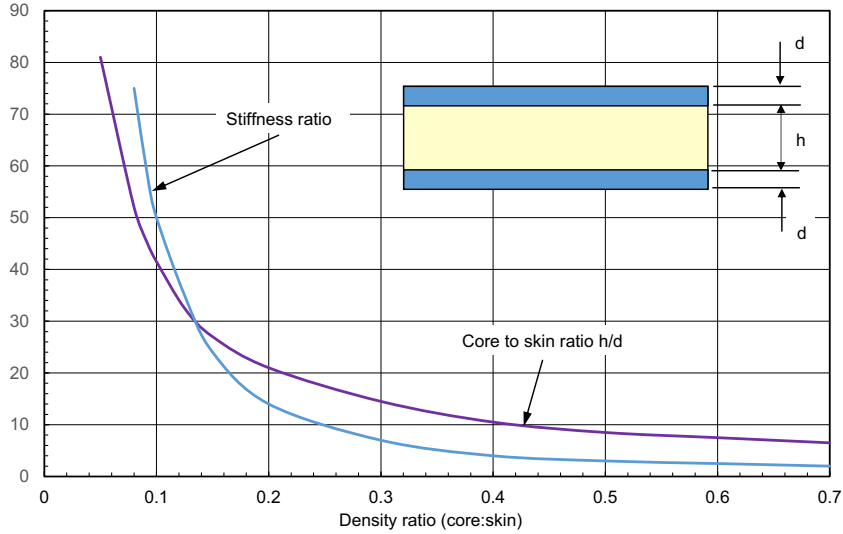


FIG. 2.21 Optimum skin to core ratio for constant weight.

2.8 Design of snap fits

A major attraction of plastics to designers is the ease with which fast assembly mechanisms can be incorporated into the end-product. A very good example of this is the snap fit. A typical design is shown in Fig. 2.22 although there are many variations. Snap fits exploit the fact that thin plastic sections can undergo relatively large flexural deflections for a short period of time and exhibit complete recovery. The design of snap fits is straightforward and does not involve creep curves since the time-scale of the deflection/stress is small. The point that will be illustrated here is that in a real design situation it is necessary to choose combinations of dimensions which provide the necessary function but which do not overstress the plastic. In the following example a set of design curves are developed to show how the different combinations of dimensions might be selected.

Example 2.10. The polypropylene snap fit shown in Fig. 2.22 is to have a length of 10−30 mm. The taper angle of the hook (α) is 45^{o} and the deflection required for assembly (δ) is 2 mm. If the insertion force is not to exceed 4 N and the yield stress of the plastic is 30 MPa, calculate suitable cross-sectional dimensions for the snap fit. The short-term modulus of the polypropylene is 900 MPa and the coefficient of friction is 0.3. The safety factor on stress is to be 2.

Solution.

Resolving vertical forces gives

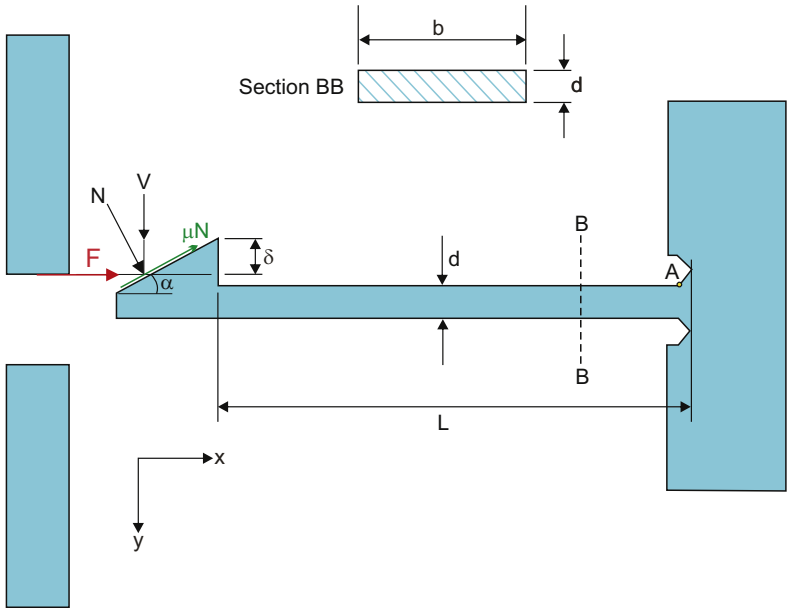


FIG. 2.22 Snap fit for Example 2.10.

$$V = N\cos\alpha - \mu N\sin\alpha$$

$$= N(\cos\alpha - \mu\sin\alpha)$$

Resolving vertical forces gives

$$V = N\cos\alpha - \mu N\sin\alpha$$

$$= N(\cos\alpha - \mu\sin\alpha)$$

Eliminating N from the above equations gives

$$V = F\left\{\frac{1-\mu\tan\alpha}{\mu+\tan\alpha}\right\}$$

The ratio of forces on the snap fit may therefore be represented by

$$\frac{F}{V} = \frac{\mu+\tan\alpha}{1-\mu\tan\alpha}$$

The variation of this parameter with the angle of inclination (α) and the coefficient of friction (μ) is shown in Fig. 2.23. Coefficients of friction between plastics and metals, such as steel, typically vary between about 0.12 for PTFE to 0.6 for PMMA or ABS. Values for plastic-plastic contact are generally higher and are up to 2× larger than those for metal-plastic contact.

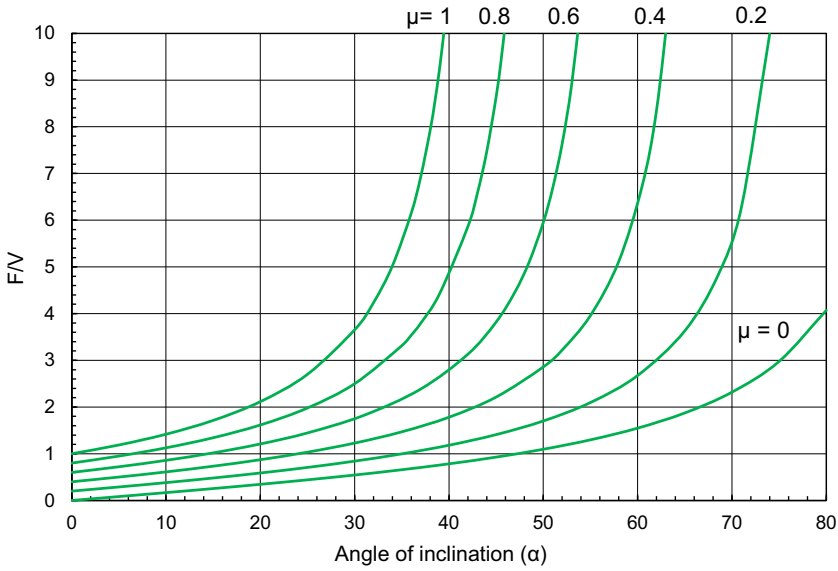


FIG. 2.23 Variation of ratio of forces (F/V) with angle of inclination and coefficient of friction.

The snap fit in this problem may be regarded as a cantilever and for this situation, the vertical deflection, δ, is given by

$$\delta = \frac{VL^3}{3EI} \text{ where } I = \frac{bd^3}{12}$$

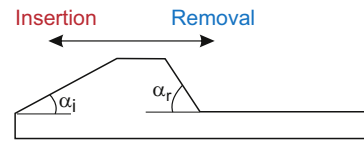
$$\delta = \frac{FL^3}{3EI}\left\{\frac{1 - \mu\tan\alpha}{\mu + \tan\alpha}\right\}$$

Insertion force

$$F = \frac{Eb\delta}{4}\frac{1}{(L/d)^3}\left\{\frac{1 - \mu\tan\alpha}{\mu + \tan\alpha}\right\} \tag{2.21}$$

Note that in some snap fits the hook may also have a reversed taper on its closed side as shown in Fig. 2.24. This permits the removal of the snap fit fastener and generally the angle of inclination is larger than on the insertion side so that the fixture requires a larger force for disassembly. Eq. (2.21) may

FIG. 2.24 Snap fit design with reverse taper.



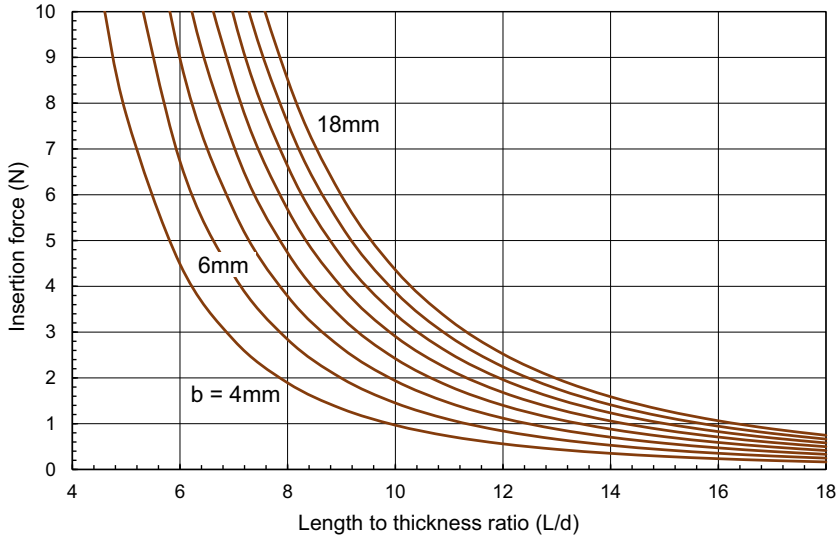


FIG. 2.25 Variation of insertion force with beam dimensions.

also be used to calculate removal force for such fasteners by substituting the angle of inclination on the insertion side (α_i) with that on the removal side (α_r).

For polypropylene in the situation given, Fig. 2.25 shows a set of design curves linking *F, b* and (*L/d*). For a limiting insertion force of 4 N and a typical maximum thickness, *d,* of 2 mm (to avoid excessive moulding times – Chapter 5), a length of 20 mm would give an *L/d* ratio of 10 which gives $b = 16$ mm.

It is also necessary to check that the stress in the snap fit does not exceed the yield strength for the material (30 MPa). Allowing for a safety factor of 2, the maximum permissible stress will be 15 MPa.

The stress in a cantilever beam of this type will be maximum at point A (Fig. 2.22) and is given by

$$\text{stress, } \sigma_A = \frac{My}{I}$$

where

M = bending moment (= VL)
y = half depth of beam (= $d/2$)
I = second moment of area (= $bd^3/12$)

$$\sigma_A = \frac{VLd}{2I} = \frac{FLd}{2I}\left\{\frac{1 - \mu \tan \alpha}{\mu + \tan \alpha}\right\}$$
$$\sigma_A = \frac{3E\delta d}{2L^2} \tag{2.22}$$

For the conditions given, $\sigma_A = 13.5$ MPa which is less than the permitted maximum of 15 MPa and so the chosen dimensions are acceptable. Note that the stress is independent of the width, *b*. Fig. 2.26 gives a set of design curves for the situation considered so that it may be seen that other combinations of *L*, *d* and *b* could be chosen to meet the design specification. For example, $L = 22$ mm, $d = 2.5$ mm and $b = 11$ mm gives an insertion force of 4 N and a maximum stress of 14 MPa which is again acceptable.

2.9 Design of ribbed sections

It will be shown later (Chapters 4 and 5) that it is normally good practice to design plastic products with cross-sections which are as thin as possible. This is because thick sections cool very slowly and hence the moulding cycle times are long resulting in uneconomic production rates. Also, thick sections tend to shrink more and can lead to warpage and distortion. Of course thin sections tend to have low stiffness and so engineers usually adopt geometrical configurations which will enhance stiffness whilst retaining the required thinness in the wall section.

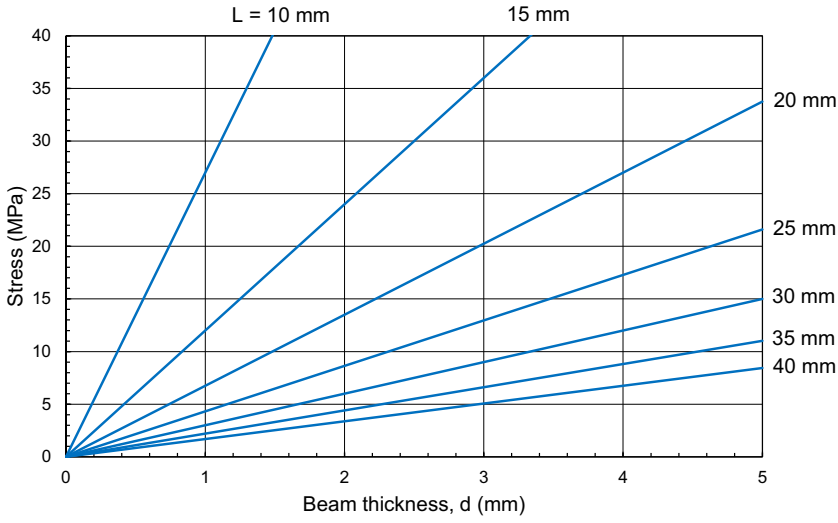


FIG. 2.26 Variation of stress with beam dimensions.

In any particular material, the flexural stiffness will be defined by the second moment of area, *I,* for the cross-section. As with a property such as area, the second moment of area is independent of the material – it is purely a function of geometry. If we consider a variety of cross-sections as follows, we can easily see the benefits of choosing carefully the cross-sectional geometry of a moulded plastic component.

All the sections have the same cross-sectional area (and hence the same weight).

(a) – Solid Rectangle	($B = 10D$)
(b) – Solid rectangle	($B = 4D$)
(c) – Solid rectangle	($B = 2D$)
(d) – Square	($B = D$)
(e) – Hollow rectangular box	($B = 2D$, $B = 10h$)
(f) – Solid circular section	
(g) – Thin wall tube	($D = 10h$)
(h) – Thick wall tube	($D = 4h$)
(i) – T-section	($B = 8h$, $D = B$)

Fig. 2.27 illustrates the various cross-sections and Fig. 2.28 compares their flexural stiffnesses. Note that the values quoted are based on cross-sections with an equivalent area to that of a 25 mm diameter round bar made from an aluminium alloy (E = 70 GPa). An important conclusion from this is that 'T' sections (or indeed 'L' or 'U' sections) are very efficient at providing excellent stiffness per unit weight. The following example illustrates how such sections can be designed into plastic products.

Example 2.11. An aluminium cantilever beam is 50 mm wide, 80 mm long and 2 mm deep. The loading is 200 N spread uniformly over the cantilever. If the beam is to be replaced by one made from acetal and the design criteria is that the end deflections should be the same in each beam after one month, calculate the dimensions of (a) a solid acetal beam and (b) an acetal beam with unidirectional ribs. The modulus of the aluminium is 70 GPa.

Solution.

(a) In order that the two beams (aluminium and acetal) will have the same stiffness it is necessary that

$$(EI)_{Al} = (EI)_{acetal} \tag{2.23}$$

In order to get the 1 month modulus for acetal, the strain in the beam must be known.

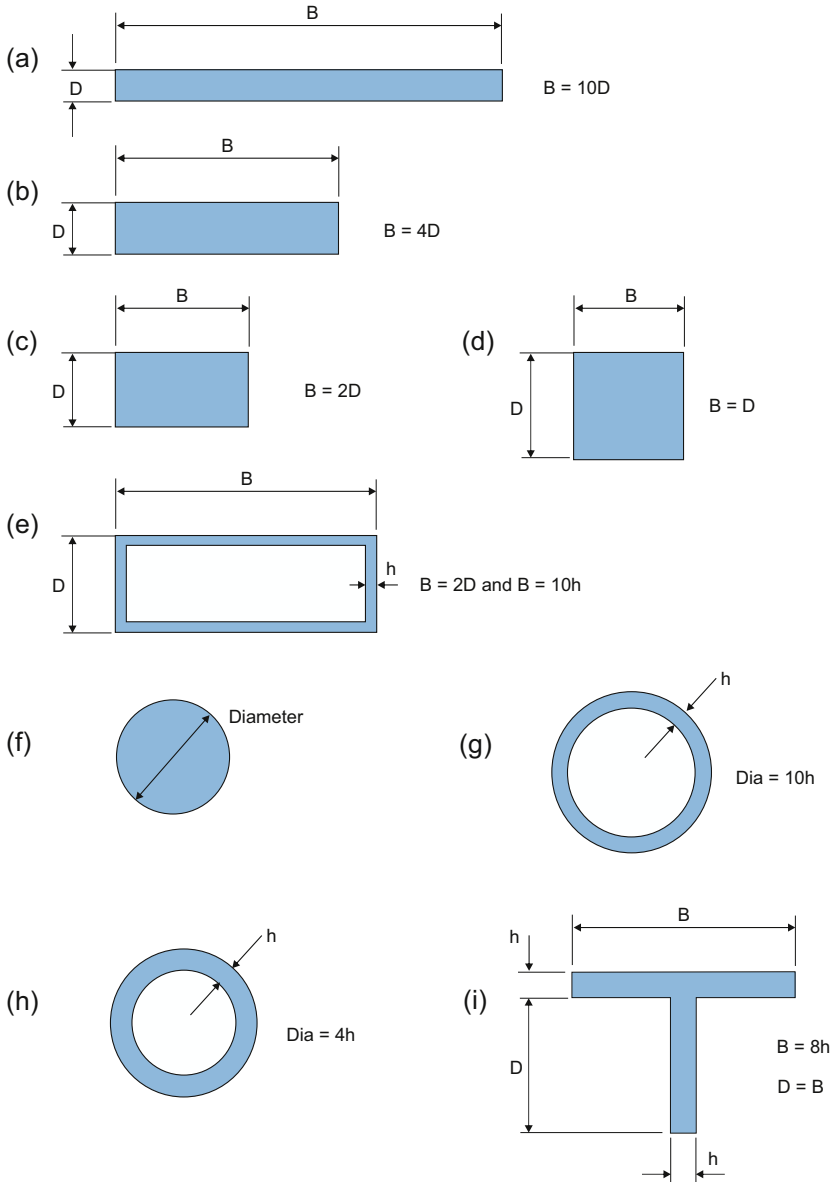


FIG. 2.27 Various cross-sections.

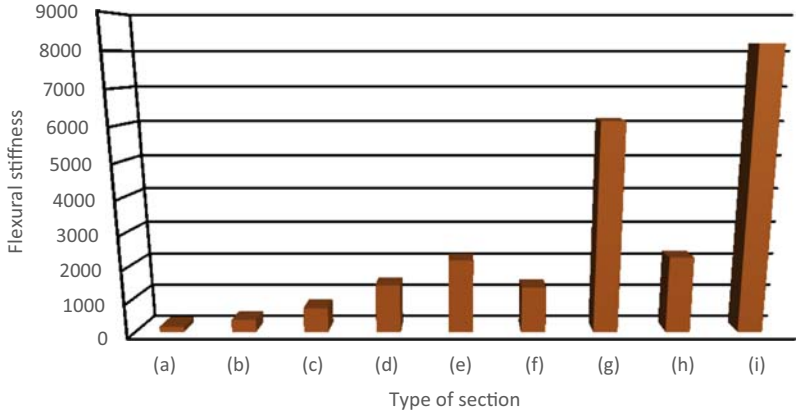


FIG. 2.28 Effect of geometry of flexural stiffness.

$$\text{Strain,} \qquad \varepsilon = \frac{\sigma}{E} = \frac{My}{EI} = \frac{W(L/2)(d_{al}/2)}{EI} = \frac{WLd_{al}}{4EI}$$

where $W =$ total load (200 N) and $d_{al} =$ depth of beam.

Also, deflection

$$\delta = \frac{WL^3}{8EI}$$

So, strain,

$$\varepsilon = \frac{2\delta d_{al}}{L^2}$$

Using the information for the aluminium

$$\delta = \frac{200 \times 80^2 \times 12}{8 \times 70 \times 10^3 \times 50 \times 2^3} = 5.5 \text{ mm}$$

Therefore,

$$\varepsilon = \frac{2 \times 5.5 \times 2}{80^2} = 0.34\%$$

From the creep curves for acetal (Fig. 2.15), at 1 month (2.6×10^6 s) and 0.34% strain, the modulus (σ/ε) is approximately 1.3 GPa.

Therefore, using (2.23) and ignoring (W/12) on each side

$$70 \times 2^3 = 1.3 \times D^3$$

$$D = 7.6 \text{ mm}$$

Hence an acetal beam 7.6 mm deep and of the same width and length as the aluminium beam will perform in exactly the same way when the load of 200 N is applied.

However, as will be shown in Chapters 4 and 5, it would not be good design practice to use a plastic beam Section 7.6 mm thick. Such a section would take a long time to mould and would probably have sink marks on its surface. It would be preferable to use thinner wall sections and introduce ribs to provide the desired stiffness. This is illustrated below.

(b) Consider the flat beam to be replaced by a ribbed section as shown in Fig. 2.29. It is necessary for the second moment of area, I, to be the same for both sections. Clearly there are many permutations for the dimensions of the ribbed section which would meet this requirement. One practical consideration is that the thickness of the rib should be less than the thickness of the top plate (h) in order that there will be no evidence (sink mark) to show the presence of the rib on the underside of the plate. A typical ratio (β) of rib thickness to plate thickness is 0.6.

In order to assist with the design of the ribbed plate, Fig. 2.30 shows a chart to enable permissible combinations of dimensions to be chosen. For example, suppose that we wish the plate thickness to be 2 mm and there are to be five ribs ($= N$) across the plate.

Then

$$W / ND = \frac{50}{5 \times 7.6} = 0.66 \text{ and } h/D = \frac{2}{7.6} = 0.26$$

From Fig. 2.30, $d/D = 1.3$.

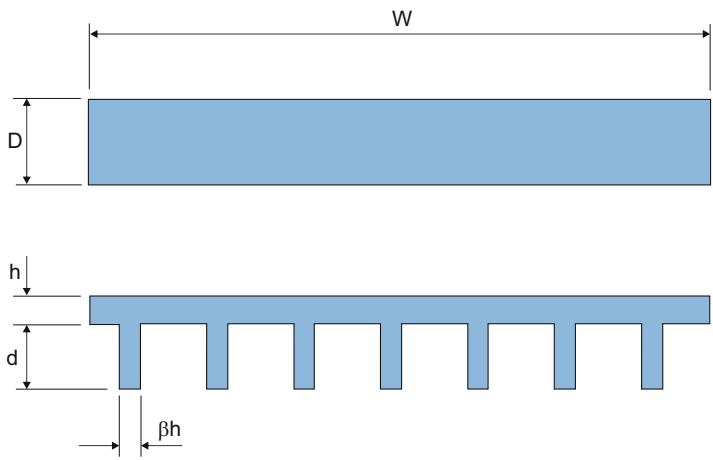


FIG. 2.29 Flat beam and ribbed section, Example 2.11.

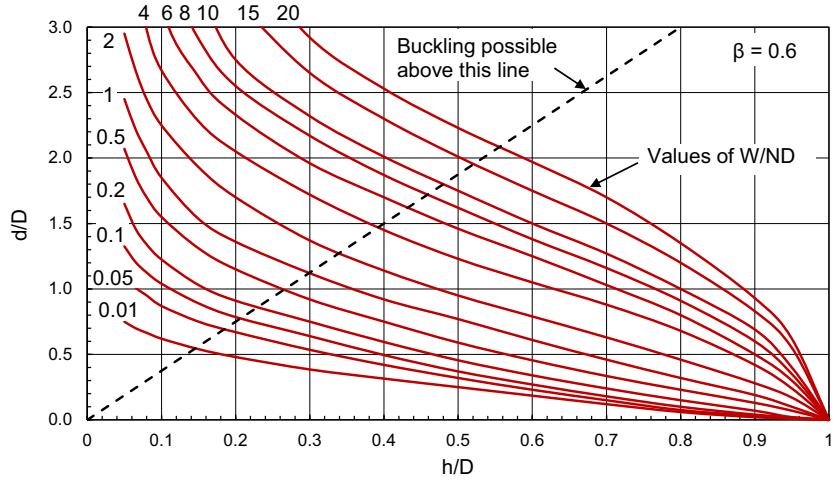


FIG. 2.30 Design of ribbed plates.

So the depth of the 5 ribs would be $1.3 \times 7.6 = 9.9$ mm and their width would be $0.6 \times 2 = 1.2$ mm.

Such a ribbed beam would perform in exactly the same way as the original aluminium beam or the flat acetal beam. However, an additional consideration is buckling of the ribs. If the ribs are thin and deep there is a possibility that they will buckle along the lower unsupported edge if they are loaded in compression (i.e. downward deflection of the cantilever in this Example).

Buckling is complex to analyse but if we consider the rib as a flat plate, clamped along one edge then Roark gives the formula for the critical buckling stress as

$$\sigma_c = \frac{1.2E}{(1-\nu^2)}\left(\frac{\beta h}{d}\right)^2 \tag{2.24}$$

or

$$\left(\frac{h}{d}\right) = \sqrt{\left(\frac{1-\nu^2}{1.2\beta^2}\right)\frac{\sigma_c}{E}}$$

If we take the critical stress as the yield stress then for many plastics, the ratio of σ_c/E is approximately 35×10^{-3}. Using Poisson's ratio, $\nu = 0.35$ and taking $\beta = 0.6$, as before, then

$$\frac{h}{d} = \frac{h}{D}\cdot\frac{D}{d} = 0.267$$

or

$$\frac{d}{D} = 3.75\frac{h}{D}$$

This line may be superimposed on the rib design data as shown in Fig. 2.30. Combinations of dimensions above this line are likely to provide ribs which are too slender and so are liable to buckling. Combinations below the line are likely to be acceptable but do remember the assumptions made in the determination of the buckling line – in particular, the ratio of σ_y/E will increase with time due to creep and this will cause the buckling line to move downwards.

Returning to the example, it is apparent that the dimensions chosen lie above the buckling line. It is necessary therefore, to choose other dimensions. For example, $h = 2.5$ mm gives

$$\frac{h}{D} = 0.33, \quad \frac{W}{ND} = 0.66 \quad \text{(as before)}$$

So $d/D = 1.15$ which gives $d = 11.15\ (7.6) = 8.7$ mm.

These dimensions lie below the buckling line and so are acceptable. The solution would therefore be a ribbed beam with five ribs, plate thickness = 2.5 mm, rib thickness = 1.5 mm and rib depth = 8.7 mm.

It should be noted that ribbed sections play an extremely important part in the design of plastic products. Not only do they reduce manufacturing times (because they utilise thinner sections), but they also save material. It may easily be shown in this case that the volume of the ribbed beam is half the volume of the flat acetal beam and this will result in a substantial cost saving.

Fig. 2.31 shows a design chart for slightly thicker ribs ($\beta = 0.8$) so as to reduce the likelihood of rib buckling.

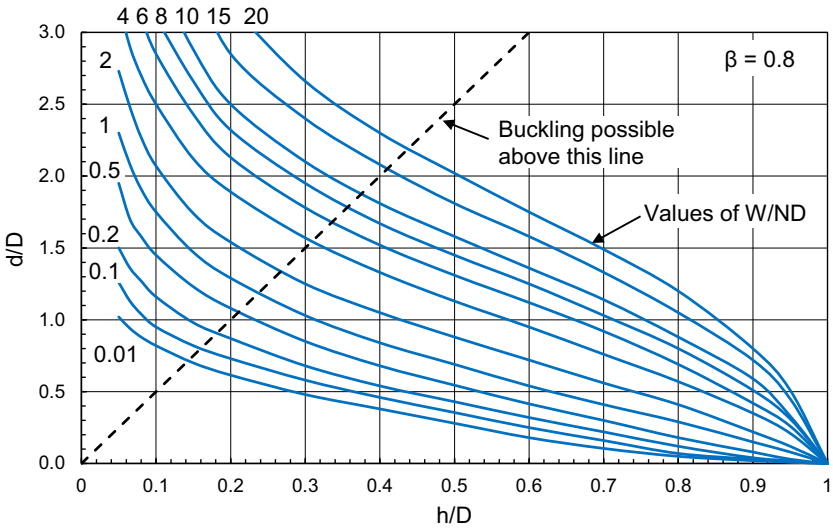


FIG. 2.31 Design of ribbed beams.

2.10 Stiffening mechanisms in other moulding situations

In some moulding methods such as blow moulding, thermoforming and rotational moulding, it is difficult if not impossible to produce stiffening ribs. Hence other stiffening configurations such as corrugations have to be used. Fig. 2.32 illustrates a typical repeat unit in such a corrugation. The second moment of area, I, will quantify the stiffening effect of the cross-section and if this is related to the I value for the flat sheet of the same length and thickness then it is possible to define a stiffness enhancement factor, q, *as*

$$q = \frac{1}{L}\left\{ mh + \frac{12m}{h}\left(\overline{y} - \frac{h}{2}\right)^2 + ph + \frac{12p}{h}\left(\overline{y} - \left(nh + \frac{h}{2}\right)\right)^2 + \frac{2nh}{\sin\alpha} + \frac{24n}{h\sin\alpha}\left(\overline{y} - \frac{nh}{2}\right)^2 \right\} \tag{2.25}$$

where $\overline{y}$ = distance to centre of area from the base of the cross-section, i.e.

$$\overline{y} = h\left\{ \frac{0.5m + pn + 0.5p + \dfrac{n^2}{\sin\alpha}}{\left(p + m + \dfrac{2n}{\tan\alpha}\right)} \right\}$$

and

$$m = \frac{b}{h}, \qquad p = \frac{B}{h}, \qquad n = \frac{D}{h}$$

Clearly there are many permutations of D, b, h, α, etc. and Fig. 2.33 shows how the stiffness enhancement factor, q, changes with various values of these parameters. In each case the angle α has been fixed at 85° and the corrugation dimensions have been expressed as a function of the wall thickness, h.

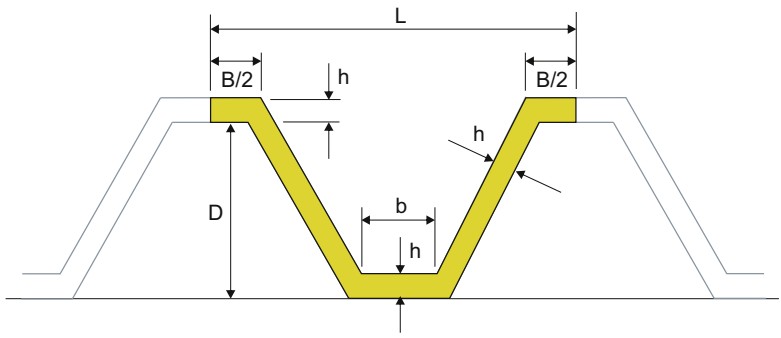


FIG. 2.32 Corrugation profile.

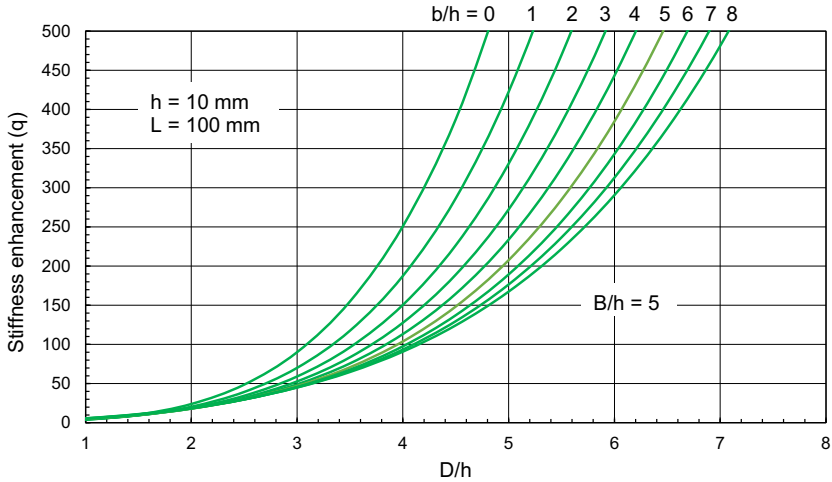


FIG. 2.33 Stiffness of corrugations as function of dimensions.

The obvious question is 'Is there an optimum design for the corrugations?' Unfortunately the answer is 'No' because if one wishes to increase transverse stiffness then the obvious thing to do is to increase D up to the point where buckling problems start to be a concern. Usually this is when $D/h = 10$, for short-term loading and less than this for long term loading because of the decrease in modulus of viscoelastic materials.

Another approach is to recognise that initially for a flat sheet, the axial stiffness is high but the transverse stiffness is relatively low. As the corrugation depth increases then the transverse stiffness increases but at the expense of the axial stiffness. It is readily shown that the axial deflection per unit load for the corrugations for the new geometry compared with the flat sheet is given by

$$\text{Axial stiffness ratio} = \frac{4n^3 h}{L \sin^2 \alpha} \tag{2.26}$$

If this is then divided into the previous enhancement ratio, q, it is possible to observe the way in which one stiffness increases at the expense of the other. Fig. 2.34 shows this transverse/axial stiffness ratio as a function of the depth of the corrugations. It may be seen that when the depth is less than four times the wall thickness then the axial stiffness ratio is better than the transverse stiffness ratio. However, when the depth is greater than four times the wall thickness then the transverse stiffness ratio dominates.

This would suggest that $D/h = 4$ offers the best balance of transverse and axial properties. In fact the 'optimum' ratio is essentially independent of the thickness, h, but it depends on B and b. Fig. 2.35 shows this relationship and reflects the combinations of B, b, D and h which will give the best design of corrugations. Generally it is desirable to have B and b approximately equal and

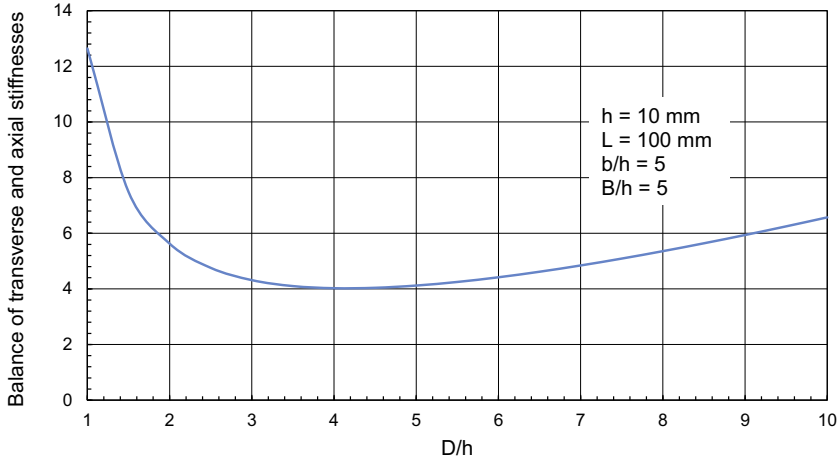


FIG. 2.34 Optimisation of corrugation depth.

it is also good design practice to keep D/h well below 10 (to avoid buckling). Hence values of B, h and D in the shaded area tend to be best. A combination of $D/h = 4$, $b/h = 5$ and $B/h = 4$ is known to give good results for rotationally moulded products where shape must be used very effectively to ensure good performance.

2.11 Mathematical models of viscoelastic behaviour

Over the years there have been many attempts to simulate the behaviour of viscoelastic materials. This has been aimed at (i) facilitating analysis of the behaviour of plastic products, (ii) promoting the development of computer-based simulations of manufacturing processes for plastics, (iii) assisting with extrapolation and interpolation of experimental data and (iv) reducing the need for extensive, time-consuming creep tests. The most well known of the mathematical models have been based on spring and dashpot elements to represent, respectively, the elastic and viscous responses of plastic materials. Although there are no discrete molecular structures which behave like the individual elements of the models, nevertheless they do aid in the understanding and analysis of the behaviour of viscoelastic materials. Some of the more important models will now be considered.

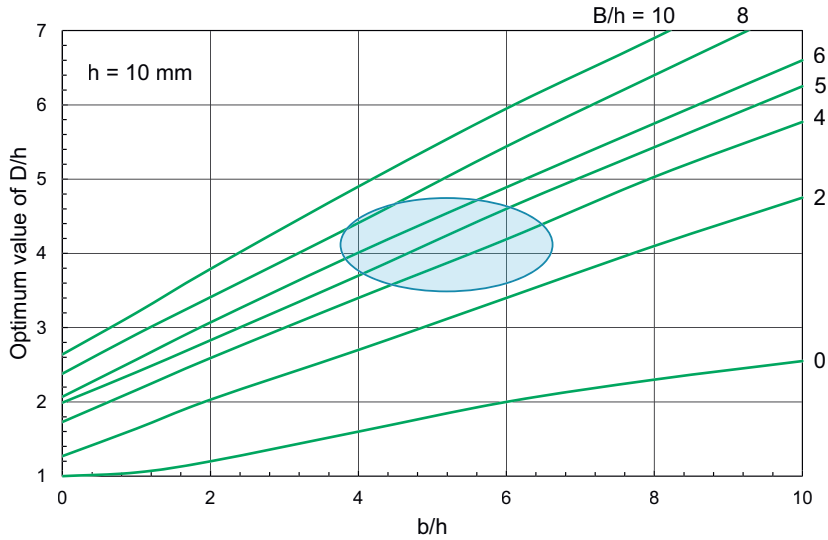


FIG. 2.35 Variation of optimum D/h with b/h.

2.11.1 Maxwell model

The Maxwell Model consists of a spring and dashpot in series at shown in Fig. 2.36. This model may be analysed as follows.

Stress–Strain Relations

The spring is the elastic component of the response and obeys the relation

$$\sigma_1 = \xi \cdot \varepsilon_1 \tag{2.27}$$

where σ_1 and ε_1 are the stress and strain respectively and ξ is a constant.

The dashpot is the viscous component of the response and in this case the stress σ_2 is proportional to the rate of strain $\dot{\varepsilon}_2$, i.e.

$$\sigma_2 = \eta \cdot \dot{\varepsilon}_2 \tag{2.28}$$

where η is a material constant.

Equilibrium Equation

For equilibrium of forces, assuming constant area

$$\text{Applied stress, } \sigma = \sigma_1 = \sigma_2 \tag{2.29}$$

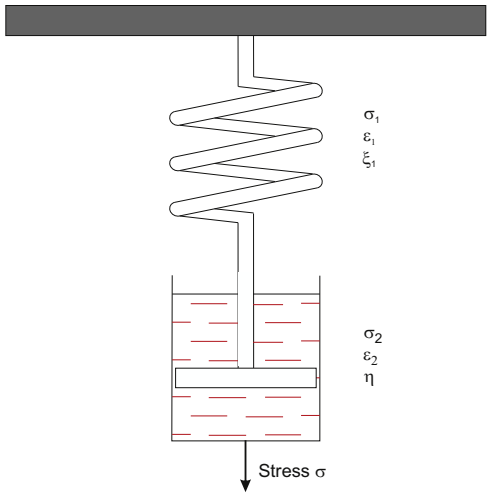


FIG. 2.36 The Maxwell model.

Geometry of Deformation Equation

The total strain, ε is equal to the sum of the strains in the two elements. So

$$\varepsilon = \varepsilon_1 + \varepsilon_2 \tag{2.30}$$

From Eqs. (2.27), (2.28) and (2.30)

$$\dot{\varepsilon} = \frac{1}{\xi}\dot{\sigma}_1 + \frac{1}{\eta}\sigma_2$$

$$\dot{\varepsilon} = \frac{1}{\xi}\cdot\dot{\sigma} + \frac{1}{\eta}\cdot\sigma \tag{2.31}$$

This is the governing equation of the Maxwell Model. It is interesting to consider the response that this model predicts under three common time-dependent modes of deformation.

(i) Creep

If a constant stress, σ_o, is applied then Eq. (2.31) becomes

$$\dot{\varepsilon} = \frac{1}{\eta}\cdot\sigma_o \tag{2.32}$$

which indicates a constant rate of increase of strain with time.

From Fig. 2.37 it may be seen that for the Maxwell model, the strain at any time, t, after the application of a constant stress, σ_o, is given by

$$\varepsilon(t) = \frac{\sigma_o}{\xi} + \frac{\sigma_o}{\eta} t$$

Hence, the creep modulus, $E(t)$, is given by

$$E(t) = \frac{\sigma_o}{\varepsilon(t)} = \frac{\xi\eta}{\eta + \xi t} \tag{2.33}$$

(ii) Relaxation

If the strain is held constant then Eq. (2.31) becomes

$$0 = \frac{1}{\xi} \cdot \dot{\sigma} + \frac{1}{\eta} \cdot \sigma$$

Solving this differential equation (see Appendix B) with the initial condition $\sigma = \sigma_o$ at $t = t_o$ then,

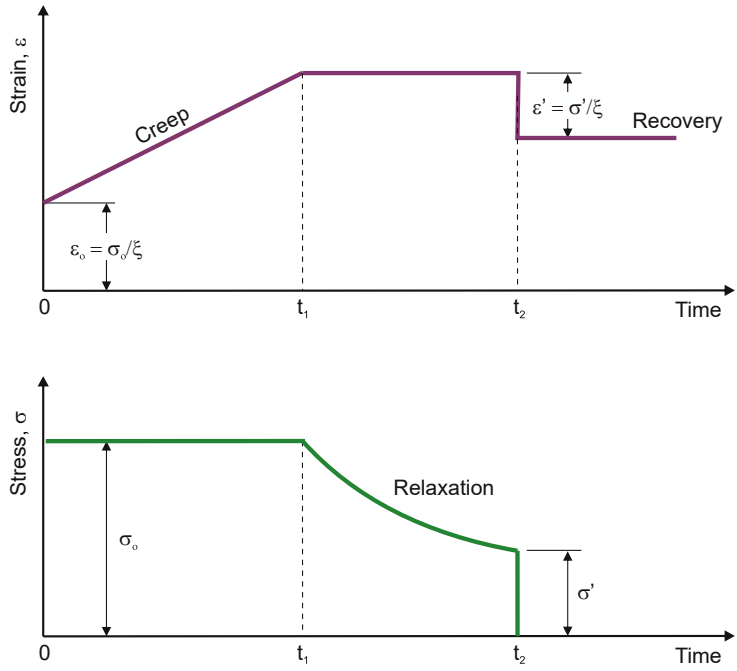


FIG. 2.37 Response of Maxwell model.

$$\sigma(t) = \sigma_o e^{-\frac{\xi}{\eta}t} \tag{2.34}$$

$$\sigma(t) = \sigma_o e^{-t/T_R} \tag{2.35}$$

where $T_R = \eta/\xi$ is referred to as the *relaxation time.*

This indicates that the stress decays exponentially with a time constant of η/ξ (see Fig. 2.37).

(iii) Recovery

When the stress is removed there is an instantaneous recovery of the elastic strain, ε^1, and then, as shown by Eq. (2.31), the strain rate is zero so that there is no further recovery (see Fig. 2.37).

It can be seen therefore that although the relaxation behaviour of this model is acceptable as a first approximation to the actual material's response, it is inadequate in its prediction for creep and recovery behaviour.

2.11.2 Kelvin or Voigt model

In this model the spring and dashpot elements are connected in parallel as shown in Fig. 2.38.

Stress–Strain Relations

These are the same as the Maxwell Model and are given by Eqs. (2.27) and (2.28).

Equilibrium Equation

For equilibrium of forces it can be seen that the applied load is supported jointly by the spring and the dashpot, so

$$\sigma = \sigma_1 + \sigma_2 \tag{2.36}$$

Geometry of Deformation Equation

In this case the total strain is equal to the strain in each of the elements, i.e.

$$\varepsilon = \varepsilon_1 = \varepsilon_2 \tag{2.37}$$

From Eqs. (2.27), (2.28) and (2.36)

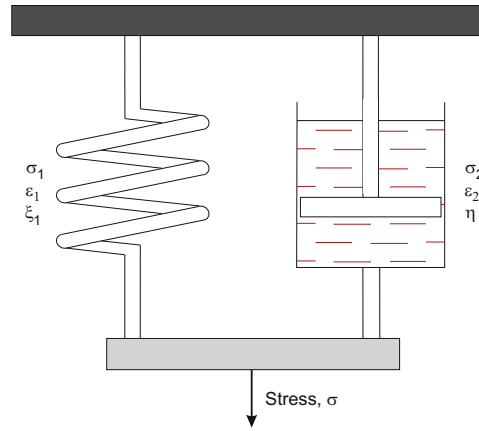


FIG. 2.38 The Kelvin or Voigt model.

$$\sigma = \xi \cdot \varepsilon_1 + \eta \cdot \dot{\varepsilon}_2$$

or using Eq. (2.37)

$$\sigma = \xi \cdot \varepsilon + \eta \cdot \dot{\varepsilon} \tag{2.38}$$

This is the governing equation for the Kelvin (or Voigt) Model and it is interesting to consider its predictions for the common time dependent deformations.

(i) Creep

If a constant stress, σ_o, is applied then Eq. (2.38) becomes

$$\sigma_o = \xi \cdot \varepsilon + \eta \cdot \dot{\varepsilon}$$

and this differential equation may be solved for the total strain, ε, to give

$$\varepsilon(t) = \frac{\sigma_o}{\xi}\left[1 - e^{-\frac{\xi}{\eta}t}\right]$$

where the ratio η/ξ is referred to as the *retardation time, T_R.*

This indicates an exponential increase in strain from zero up to the value, σ_o/ξ that the spring would have reached if the dashpot had not been present. This is shown in Fig. 2.39. As for the Maxwell Model, the creep modulus may be determined as

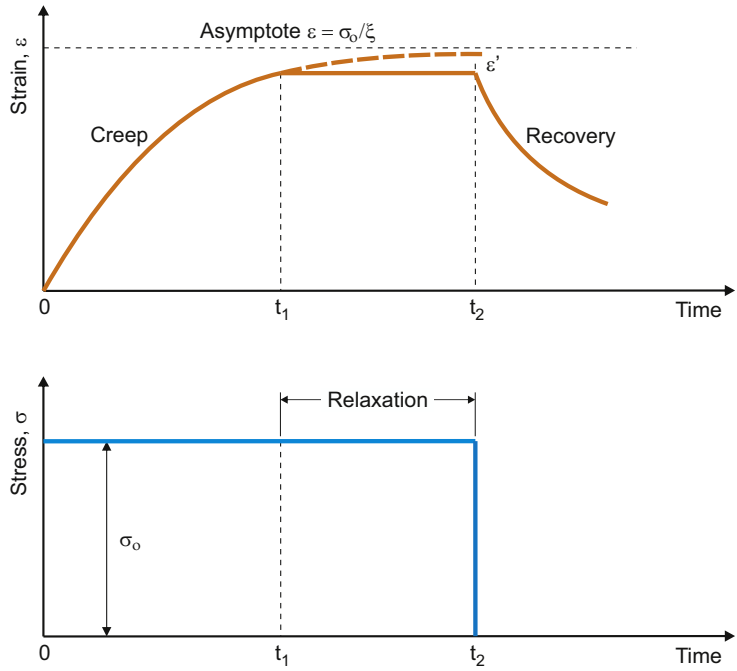


FIG. 2.39 Response of Kelvin/Voigt model.

$$E(t) = \frac{\sigma_o}{\varepsilon(t)} = \xi\left[1 - e^{-\frac{t}{T_R}}\right]^{-1} \tag{2.39}$$

(ii) Relaxation

If the strain is held constant then Eq. (2.38) becomes

$$\sigma = \xi \cdot \varepsilon$$

That is, the stress is constant and supported by the spring element so that the predicted response is that of an elastic material, i.e. no relaxation (see Fig. 2.37)

(iii) Recovery

If the stress is removed, then Eq. (2.38) becomes

$$0 = \xi \cdot \varepsilon + \eta \cdot \dot{\varepsilon}$$

Solving this differential equation with the initial condition $\varepsilon = \varepsilon'$ at the time of stress removal, then

$$\varepsilon(t) = \varepsilon' e^{-\frac{\xi t}{\eta}} \tag{2.40}$$

This represents an exponential recovery of strain which is a reversal of the predicted creep.

2.11.3 More complex models

It may be seen that the simple Kelvin model gives an acceptable first approximation to creep and recovery behaviour but does not account for relaxation. The Maxwell model can account for relaxation but was poor in relation to creep and recovery. It is clear therefore that some compromise may be achieved by combining the two models. Such a set-up is shown in Fig. 2.40.

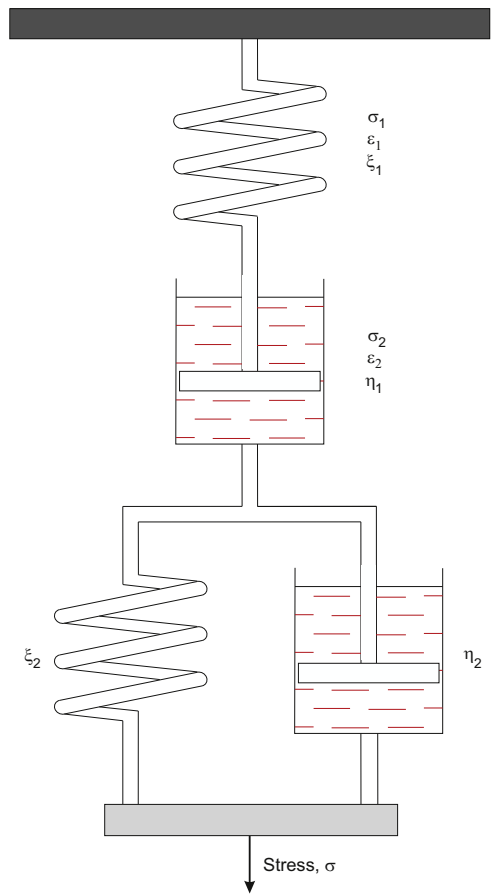


FIG. 2.40 Maxwell and Kelvin models in series.

In this case the stress–strain relations are again given by Eqs. (2.27) and (2.28). The geometry of deformation yields.

$$\text{Total strain, } \varepsilon = \varepsilon_1 + \varepsilon_2 + \varepsilon_k \tag{2.41}$$

where ε_k is the strain response of the Kelvin Model. From Eqs. (2.27), (2.28) and (2.41).

$$\varepsilon(t) = \frac{\sigma_0}{\xi_1} + \frac{\sigma_o t}{\eta_1} + \frac{\sigma_o}{\xi_2}\left[1 - e^{-\frac{\xi_2 t}{\eta_2}}\right] \tag{2.42}$$

From this the strain rate may be obtained as

$$\dot{\varepsilon} = \frac{\sigma_o}{\eta_1} + \frac{\sigma_o}{\eta_2} e^{-\frac{\xi_2}{\eta_2} t} \tag{2.43}$$

The response of this model to creep, relaxation and recovery situations is the sum of the effects described for the previous two models and is illustrated in Fig. 2.41. It can be seen that although the exponential responses predicted in these models are not a true representation of the complex viscoelastic response of polymeric materials, the overall picture is, for many purposes, an acceptable approximation to the actual behaviour. As more and more elements are added to the model then the simulation becomes better but the mathematics become complex.

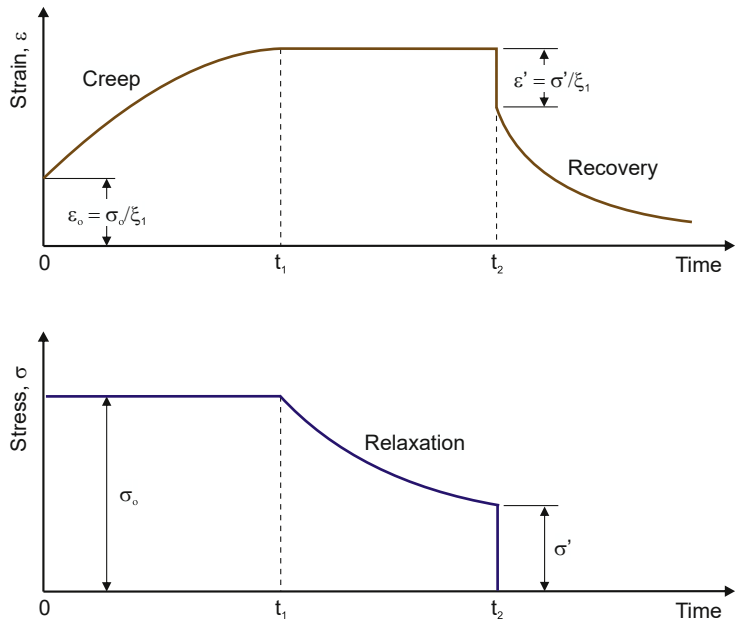


FIG. 2.41 Response of combined Maxwell and Kelvin models.

Example 2.12. An acrylic moulding material is to have its creep behaviour simulated by a four element model of the type shown in Fig. 2.40. If the creep curve for the acrylic at 14 MPa is as shown in Fig. 2.42, determine the values of the four constants in the model.

Solution The spring element constant, ξ_1, for the Maxwell model may be obtained from the instantaneous strain, ε_1. Thus

$$\xi_1 = \frac{\sigma_o}{\varepsilon_1} = \frac{14}{0.005} = 2800 \text{ MPa}$$

The dashpot constant, η_1, for the Maxwell element is obtained from the slope of the creep curve in the steady state region (see Eq. 2.32).

$$\eta_1 = \frac{\sigma_o}{\dot{\varepsilon}} = \frac{14}{1.167 \times 10^{-6}} = 1.2 \times 10^7 \text{MPa.hr}$$
$$= 4.32 \times 10^{10} \text{MPa.s}$$

The spring constant, ξ_2, for the Kelvin–Voigt element is obtained from the maximum retarded strain, ε_2, in Fig. 2.42.

$$\xi_2 = \frac{\sigma_o}{\varepsilon_2} = \frac{14}{(0.7 - 0.5) \times 10^{-2}} = 7000 \text{ M}Pa$$

The dashpot constant, η_2, for the Kelvin–Voigt element may be determined by selecting a time and corresponding strain from the creep curve in a region where the retarded elasticity dominates (i.e. the knee of the curve in Fig. 2.42) and substituting into Eq. (2.42). If this is done then $\eta_2 = 3.7 \times 10^8$ MPa·s.

Having thus determined the constants for the model the strain may be predicted for any selected time or stress level assuming of course these are within the region where the model is applicable.

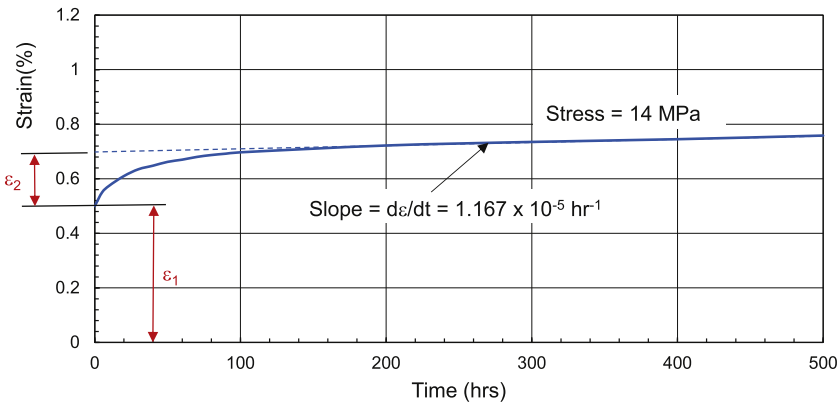


FIG. 2.42 Creep curve for acrylic at 20°C.

2.11.4 Standard linear solid

Another model consisting of elements in series and parallel is that attributed to Zener. It is known as the Standard Linear Solid and is illustrated in Fig. 2.43. The governing equation may be derived as follows.

Stress–Strain Relations

As shown earlier the stress–strain relations are

$$\sigma_1 = \xi_1 \varepsilon_1 \tag{2.44}$$

$$\sigma_2 = \xi_2 \varepsilon_2 \tag{2.45}$$

$$\sigma_3 = \eta_3 \dot{\varepsilon}_3 \tag{2.46}$$

Equilibrium Equation

In a similar manner to the previous models, equilibrium of forces yields.

$$\begin{aligned} \sigma_1 &= \sigma_3 \\ \sigma &= \sigma_1 + \sigma_2 \end{aligned} \tag{2.47}$$

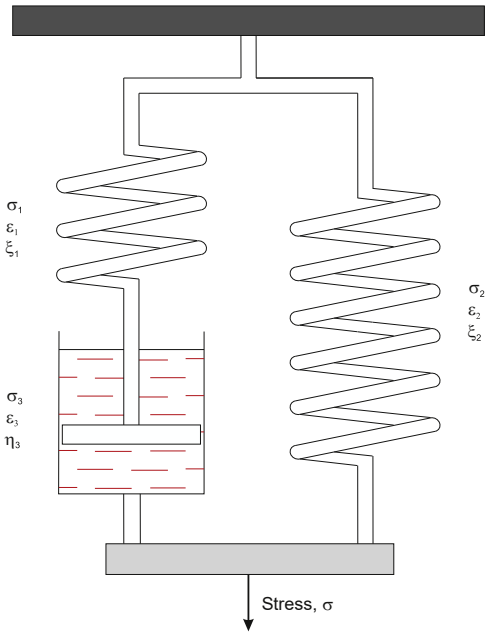


FIG. 2.43 The standard linear solid.

Geometry of Deformation Equation

In this case the total deformation, ε, is given by

$$\varepsilon = \varepsilon_2 = \varepsilon_1 + \varepsilon_3 \tag{2.48}$$

From Eq. (2.48)

$$\dot{\varepsilon} = \dot{\varepsilon}_1 + \dot{\varepsilon}_3$$

but from Eq. (2.47)

$$\dot{\sigma}_1 = \dot{\sigma} - \dot{\sigma}_2$$

and $\sigma_3 = \sigma - \sigma_2$

$$\dot{\varepsilon} = \frac{\dot{\sigma} - \xi_2\dot{\varepsilon}}{\xi_1} + \frac{\sigma - \xi_2\varepsilon}{\eta_3}$$

Rearranging gives

$$\eta_3\dot{\sigma} + \xi_1\sigma = \eta_3(\xi_1 + \xi_2)\dot{\varepsilon} + \xi_2\xi_1\varepsilon \tag{2.49}$$

This is the governing equation for this model.

The behaviour of this model can be examined as before.

(i) Creep

If a constant stress, σ_o, is applied then the governing equation becomes

$$\dot{\varepsilon}\{\eta_3(\xi_1 + \xi_2)\} + \xi_1\xi_2\varepsilon - \xi_1\sigma_o = 0$$

The solution of this differential equation may be obtained using the boundary condition $\varepsilon = \sigma_o/(\xi_1 + \xi_2)$ at $t = 0$. So

$$\text{strain, } \varepsilon(t) = \frac{\sigma_o}{\xi_2} - \frac{\sigma_o\xi_1}{(\xi_1 + \xi_2)\xi_2}e^{\frac{-\xi_1\xi_2 t}{\eta_3(\xi_1 + \xi_2)}} \tag{2.50}$$

It may be seen in Fig. 2.44 that this predicts the initial strain when the stress is first applied as well as an exponential increase in strain subsequently.

(ii) Relaxation

If the strain is held constant at ε', then the governing equation becomes

$$\eta_3\dot{\sigma} + \xi_1\sigma - \xi_1\xi_2\varepsilon' = 0$$

This differential equation may be solved with the boundary condition that

$$\text{stress, } \sigma(t) = \frac{\sigma_o}{\xi_1 + \xi_2}\left\{\xi_2 + \xi_1 e^{\frac{-\xi_1 t}{\eta_3}}\right\} \tag{2.51}$$

This predicts an exponential decay of stress as shown in Fig. 2.44.

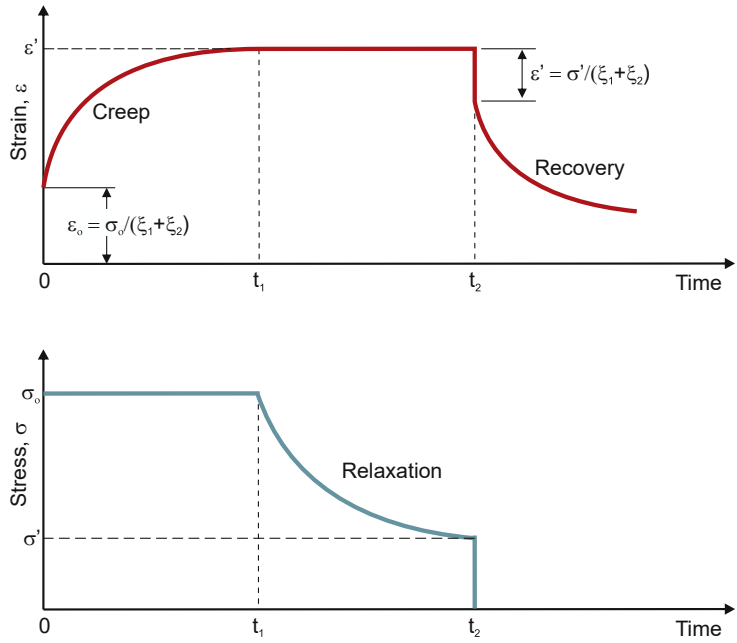


FIG. 2.44 Response of standard linear solid.

(iii) Recovery

If the stress is at a value of σ' and then completely removed, the governing equation becomes

$$\eta_3(\xi_1 + \xi_2)\dot{\varepsilon} + \xi_1\xi_2\varepsilon = 0$$

The solution of this differential equation may be obtained using the boundary condition that when the stress is removed, the strain is given by

$$\varepsilon' = \sigma'/(\xi_1 + \xi_2)$$

$$\text{strain}, \varepsilon(t) = \left\{\varepsilon' - \frac{\sigma'}{(\xi_1 + \xi_2)}\right\} e^{\frac{-\xi_1\xi_2 t}{\eta_3(\xi_1+\xi_2)}} \tag{2.52}$$

This predicts an instantaneous recovery of strain followed by an exponential decay.

It may be observed that the governing equation of the standard linear solid has the form

$$a_1\dot{\sigma} + a_o\sigma = b_1\dot{\varepsilon} + b_o\varepsilon$$

where a_1, a_o, b_1 and b_o are all material constants. In the more modern theories

of viscoelasticity this type of equation or the more general form given in Eq. (2.53) is favoured.

$$a_n\frac{\partial^n\sigma}{\partial t^n}+a_{n-1}\frac{\partial^{n-1}\sigma}{\partial t^n}+\ldots+a_o\sigma=b_m\frac{\partial^m\varepsilon}{\partial t^m}\ldots+b_o\varepsilon \tag{2.53}$$

The models described earlier are special cases of this equation.

2.12 Intermittent loading

The creep behaviour of plastics considered to date has assumed that the level of the applied stress is constant. However, in service the material may be subjected to a complex pattern of loading and unloading cycles. This can cause design problems in that clearly it would not be feasible to obtain experimental data to cover all possible loading situations and yet to design on the basis of constant loading at the maximum stress would not make efficient use of material or be economical. In these cases it is useful to have methods of predicting the extent of the recovered strain which occurs during the rest periods of conversely the accumulated strain after N cycles of load changes.

There are several approaches that can be used to tackle this problem and two of these will be considered now.

2.12.1 Superposition principle

The simplest theoretical model proposed to predict the strain response to a complex stress history is the *Boltzmann Superposition Principle*. Basically this principle proposes that for a linear viscoelastic material, the strain response to a complex loading history is simply the algebraic sum of the strains due to each step in load. Implied in this principle is the idea that the behaviour of a plastic is a function of its entire loading history. There are two situations to consider.

(a) Step Changes of Stress

When a linear viscoelastic material is subjected to a constant stress, σ_1, at time, t_1, then the creep strain, $\varepsilon(t)$, at any subsequent time, t, may be expressed as

$$\varepsilon(t)=\frac{1}{E(t-t_1)}\cdot\sigma_1 \tag{2.54}$$

where $E(t-t_1)$ is the time-dependent modulus for the elapsed time $(t-t_1)$.

Then suppose that instead of this stress σ_1, another stress, σ_2 is applied at some arbitrary time, t_2, then at any subsequent time, t, the stress will have been applied for a time $(t-t_2)$ so that the strain will be given by

$$\varepsilon(t) = \frac{1}{E(t-t_2)} \cdot \sigma_1$$

Now consider the situation in which the stress, σ_1, was applied at time, t_1, and an additional stress, σ_2, applied at time, t_2, then Boltzmanns' Superposition Principle states that the total strain at time, t, is the algebraic sum of the two independent responses.

$$\varepsilon(t) = \frac{1}{E(t-t_1)}\sigma_o + \frac{1}{E(t-t_2)} \cdot \sigma_1$$

This equation can then be generalised, for any series of N step changes of stress, to the form

$$\varepsilon(t) = \sum_{i=1}^{i=N} \sigma_i \left[\frac{1}{E(t-t_i)}\right] \tag{2.55}$$

where σ_i is the step change of stress which occurs at time, t_i.

To illustrate the use of this expression, consider the following example.

Example 2.13. A plastic which can have its creep behaviour described by a Maxwell model is to be subjected to the stress history shown in Fig. 2.45(a). If the spring and dashpot constants for this model are 20 GPa and 1000 GPa s respectively then predict the strains in the material after 150 s, 250 s, 350 s and 450 s.

Solution From Section 2.11 for the Maxwell model, the strain up to 100s is given by

$$\varepsilon(t) = \frac{\sigma}{\xi} + \frac{\sigma t}{\eta}$$

Also the time dependent modulus $E(t)$ is given by

$$E(t) = \frac{\sigma}{\varepsilon(t)} = \frac{\xi\eta}{\eta + \xi t} \tag{2.56}$$

Then using Eq. (2.54) the strains may be calculated as follows:

(i) at $t = 150$ s; $\sigma_i = 10$ MPa at $t_1 = 0$, $\sigma_2 = -10$ MPa at $t_2 = 100$ s

$$\varepsilon(150) = \sigma_1\left[\frac{\eta + \xi\cdot(t-t_1)}{\xi\eta}\right] + (\sigma_2)\left[\frac{\eta + \xi\cdot(t-t_2)}{\xi\eta}\right]$$
$$= 0.002 - 0.001 = 0.1\%$$

(ii) at 250 s; σ_1, σ_2 as above, $\sigma_3 = 5$ MPa at $t_3 = 200$ s

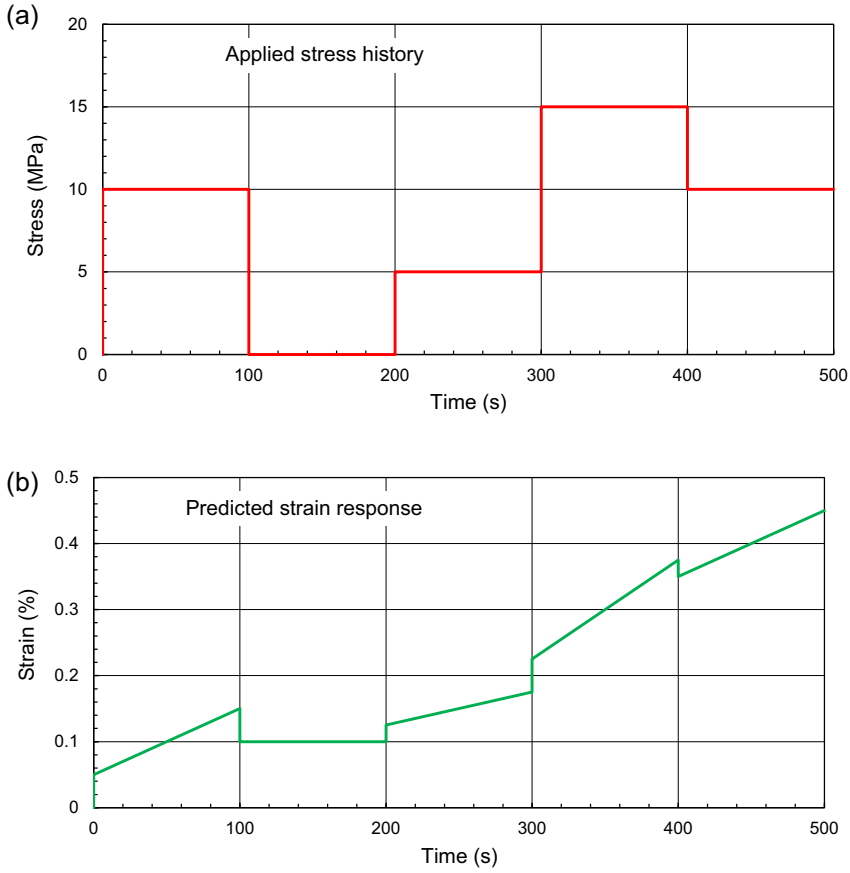


FIG. 2.45 Strain predictions using superposition theory.

$$\varepsilon(250) = 10\left[\frac{\eta + \xi\cdot(250-0)}{\xi\eta}\right] + (-10)\left[\frac{\eta + \xi\cdot(250-100)}{\xi\eta}\right] + 5\left[\frac{\eta + \xi\bullet(250-200)}{\xi\eta}\right]$$
$$= 0.003 - 0.002 + 0.0005 = 0.15\%$$

(iii) at 350 s; σ_1, σ_2, σ_3 as above, $\sigma_4 = 10$ MPa at $t_4 = 300$ s

So,

$$\varepsilon(350) = 0.003 = 0.3\%$$

(iv) and in the same way

$$\varepsilon(450) = 0.004 = 0.4\%$$

The predicted strain variation is shown in Fig. 2.45(b). The constant strain rates predicted in this diagram are a result of the Maxwell model used in this example to illustrate the use of the superposition principle. Of course superposition is not restricted to this simple model. It can be applied to any type of model or directly to the creep curves. The method also lends itself to a graphical solution as follows. If a stress σ_1 is applied at zero time, then the creep curve will be the time dependent strain response predicted by Eq. (2.54). When a second stress, σ_2 is added then the new creep curve will be obtained by adding the creep due to σ_2 to the anticipated creep if stress σ_1 had remained alone. This is illustrated in Fig. 2.46(a). Then if all the stress is removed this is equivalent to removing the creep strain due to σ_1 and σ_2 independently as shown in Fig. 2.46(b). The procedure is repeated in a similar way for any other stress changes.

(b) Continuous Changes of Stress

If the change in stress is continuous rather than a step function then Eq. (2.55) may be generalised further to take into account a continuous loading cycle. So

$$\varepsilon(t) = \int_{-\infty}^{t} \frac{1}{E(t-t_1)} \cdot \frac{\mathrm{d}\sigma(t)}{\mathrm{d}t} \cdot \mathrm{d}t \tag{2.57}$$

where $\sigma(t)$ is the expression for the stress variation that begins at time, t_1. The

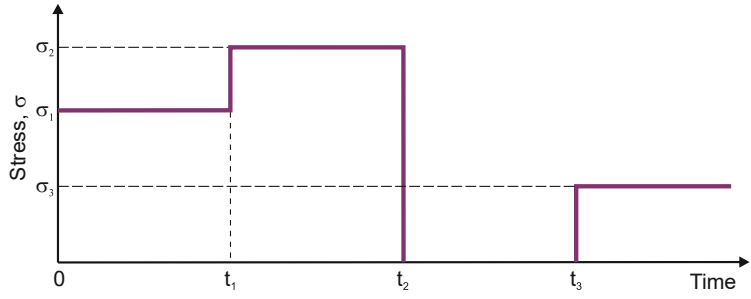


FIG. 2.46(a) Stress history.

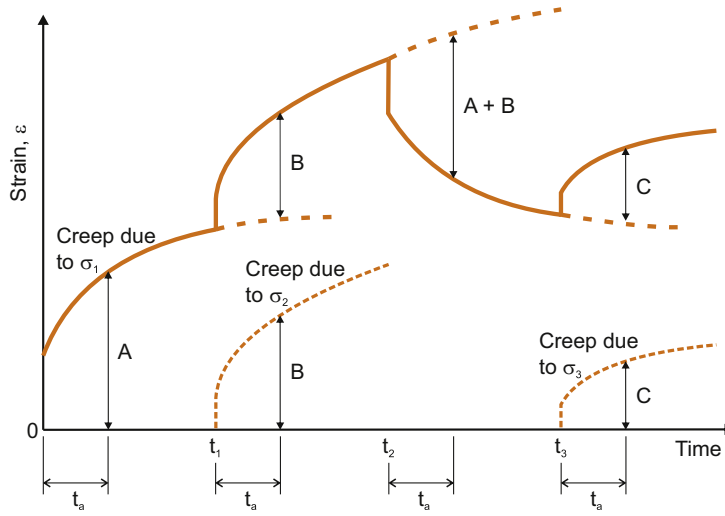


FIG. 2.46(b) Predicted strain response using Boltzmann's superposition principle.

lower limit is taken as minus infinity since it is a consequence of the Superposition Principle that the entire stress history of the material contributes to the subsequent response.

It is worth noting that in exactly the same way, a material subjected to a continuous variation of strain may have its stress at any time predicted by

$$\sigma(t) = \int_{-\infty}^{t} E(t - t_1) \cdot \frac{\mathrm{d}\varepsilon(t)}{\mathrm{d}t} \mathrm{d}t \tag{2.58}$$

To illustrate the use of Eq. (2.57) consider the following example.

Example 2.14. A plastic is subjected to the stress history shown in Fig. 2.47. The behaviour of the material may be assumed to be described by the Maxwell model in which the elastic component $\xi = 20$ GPa and the viscous component $\eta = 1000$ GPA.s. Determine the strain in the material (a) after u_1 seconds (b) after u_2 seconds and (c) after u_3 seconds.

Solution As shown in the previous example, the modulus for a Maxwell element may be expressed as

$$E(t) = \frac{\xi\eta}{\eta + \xi t}$$

(a) The stress history can be defined as

$$-\infty < t < 0, \sigma(t) = 0 \rightarrow d\sigma(t)/dt = 0$$
$$0 < t < T, \ \sigma(t) = K_1 t \rightarrow d\sigma(t)/dt = K_1$$

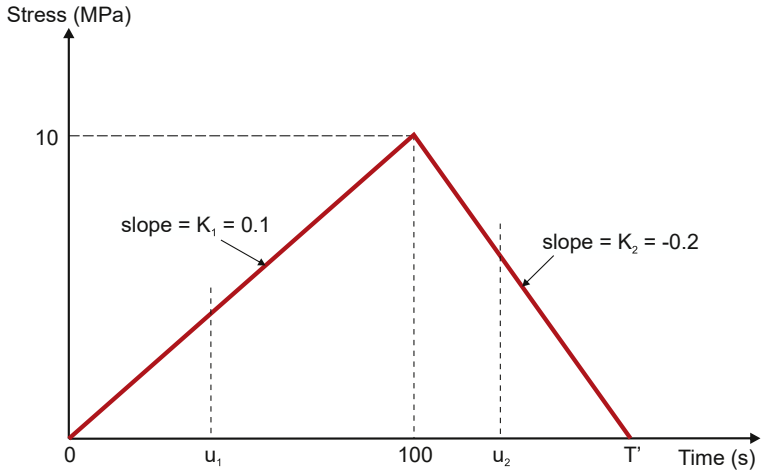


FIG. 2.47 Stress history to be analysed.

Substituting into Eq. (2.57)

$$\varepsilon(u_1) = \int_{-\infty}^{0} \frac{1}{E(t)} \cdot 0 \cdot du + \int_{0}^{u_1} \frac{(\eta + \xi t - \xi t_1)}{\xi \eta} K_1 \cdot dt$$

$$\varepsilon(u_1) = \frac{K_1}{\xi \eta} \cdot \left[\eta t + \frac{\xi t^2}{2} - \xi t_1 t \right]_0^{u_1} \text{ where } t = 0$$

$$\varepsilon(u_1) = K_1 u_1 \left(\frac{1}{\xi} + \frac{u_1}{2\eta} \right)$$

then for $u_1 = 50$ s and $K_1 = 0.1$ MPa/s

$$\varepsilon(50) = 0.1(50) \left(\frac{1}{20 \times 10^3} + \frac{20}{2 \times 10^6} \right) = 0.037\%$$

$$\varepsilon(100) = 0.1(100) \left(\frac{1}{20 \times 10^3} + \frac{100}{2 \times 10^6} \right) = 0.1\%$$

It is interesting to note that if K_1 was large (say $K_1 = 10$ in which case $T = 1$ s) then the strain predicted after application of the total stress (10 MPa) would be $\varepsilon(1) = 0.0505\%$. This agrees with the result in the previous example (Example 2.13) in which the application of stress was regarded as a step function. The reader may wish to check that if at time $T = 1$ s, the stress was held constant at 10 MPa then after 100 s the predicted strain using the integral expression would be $\varepsilon(100) = 0.1495\%$ which again agrees with the previous example.

(b) After the time T, the *change* in stress is given by

Change in stress, $\sigma(t) = -K_1(t-T) + K_2(t-T)$

$$\frac{d\sigma(t)}{dt} = -K_1 + K_2$$

Hence,

$$\varepsilon(u_2) = \int_{t_1}^{u_2} \frac{\eta + \xi t - \xi t_1}{\xi\eta} \cdot K_1 \cdot dt + \int_{t_2}^{u_2} \frac{\eta + \xi t - \xi t_2}{\xi\eta}(-K_1 + K_2)dt$$

where $t_1 = 0$ and $t_2 = T = 100$ s.

$$\varepsilon(u_2) = K_1 u_2 \left[\frac{1}{\xi} + \frac{u_2}{2\eta}\right] + (K_1 - K_2)T\left[\frac{1}{\xi} - \frac{T}{2\eta}\right]$$
$$-(K_1 - K_2)u_2\left[\frac{1}{\xi} + \frac{u_2}{2\eta} - \frac{T}{\eta}\right]$$

then for $K_2 = -0.2$ MPa/s, $T = 100$ s and $u_2 = 125$ s

$$\varepsilon(125) = 0.094\%$$

(c) After the time T^1, the change in stress is given by

Change in stress, $\sigma(t) = K_2(t-T^1)$

$$\frac{d\sigma(t)}{dt} = K_2$$

Hence,

$$\varepsilon(u_3) = \int_{t_1}^{u_3} \frac{\eta + \xi t - \xi_1}{\xi\eta} \cdot K_1 dt + \int_{t_2}^{u_3} \frac{\eta + \xi t - \xi t_2}{\xi\eta}(-K_1 + K_2)dt$$
$$+ \int_{T'}^{u_3} \frac{\eta + \xi t - \xi T^1}{\xi\eta} K_2 dt$$

and from this, for $u_3 = 200$ s and $K_2 = -0.2$ MPa/s

$$\varepsilon(200) = 0.075\%$$

This will in fact be constant for all values of u_3 because the Maxwell Model cannot predict changes in strain if there is no stress. The overall variation in strain is shown in Fig. 2.48.

Example 2.15. In the previous example, what would be the strain after 125 s if (a) the stress remained constant at 10 MPa after 100 s and (b) the stress was reduced to zero after 100 s?

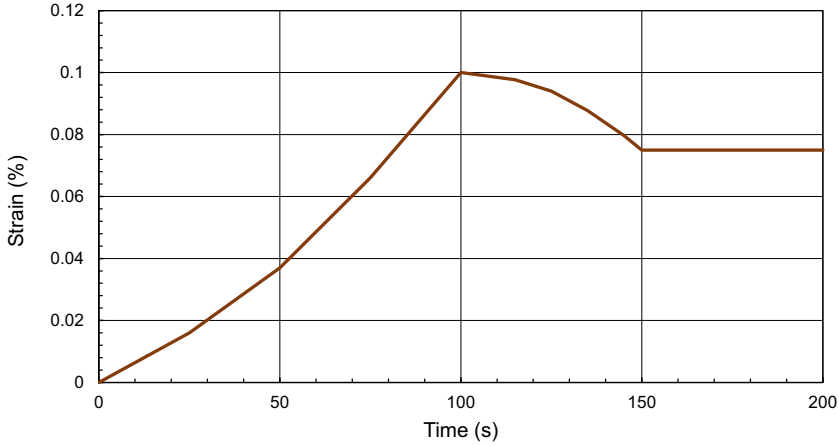


FIG. 2.48 Variation of strain with time.

Solution.

(a) If the stress was kept constant at 10 MPa after 100 s as shown in Fig. 2.49 then the effective change in stress would be given by

$$\text{change in stress}, \sigma(t) = -K_1(t - T)$$

$$\frac{d\sigma(t)}{dt} = -K_1$$

So

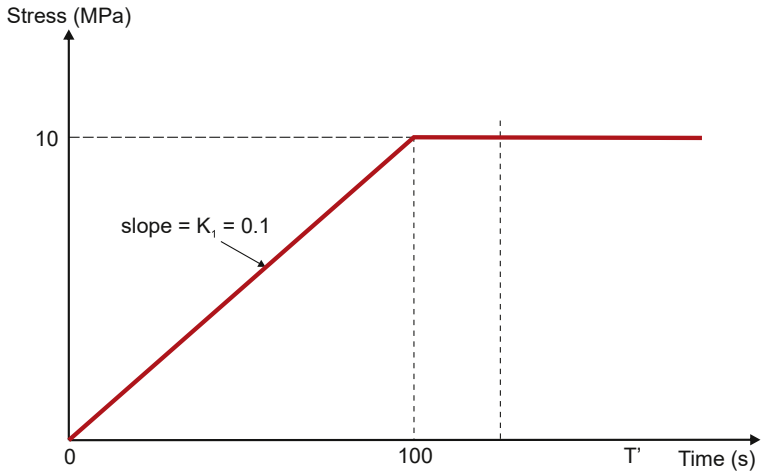


FIG. 2.49 Stress history: Example 2.15(a).

$$\varepsilon(u_2) = \int_{t_1}^{u_2} \frac{\eta + \xi t - \xi t_1}{\xi\eta} K_1 dt + \int_{t_2}^{u_2} \frac{\mu + \xi t - \xi t_2}{\xi\eta} (-K_1) dt$$

$$\varepsilon(u_2) = \frac{K_1 u_2 T}{\eta} + \frac{K_1 T}{\xi} - \frac{K_1 T^2}{2\eta}$$

$$\varepsilon(125) = 0.125\%$$

(b) If the stress was completely removed after 100 s as shown in Fig. 2.50 then the effective change in stress would be given by

$$\text{change in stress, } \sigma(t) = -K_1(t - T) - \Delta\sigma$$

$$\frac{d\sigma(t)}{dt} = -K_1$$

So

$$\varepsilon(u_3) = \int_{t_1}^{u_2} \frac{\eta + \xi t - \xi t_1}{\xi\eta} K_1 dt + \int_{t_2}^{u_2} \frac{\eta + \xi t - \xi t_2}{\xi\eta} (-K_1) dt - \frac{\Delta\sigma}{E(u_2 - T)}$$

$$\varepsilon(u_3) = \frac{K_1 T^2}{2\eta}$$

$$\varepsilon(125) = 0.05\%$$

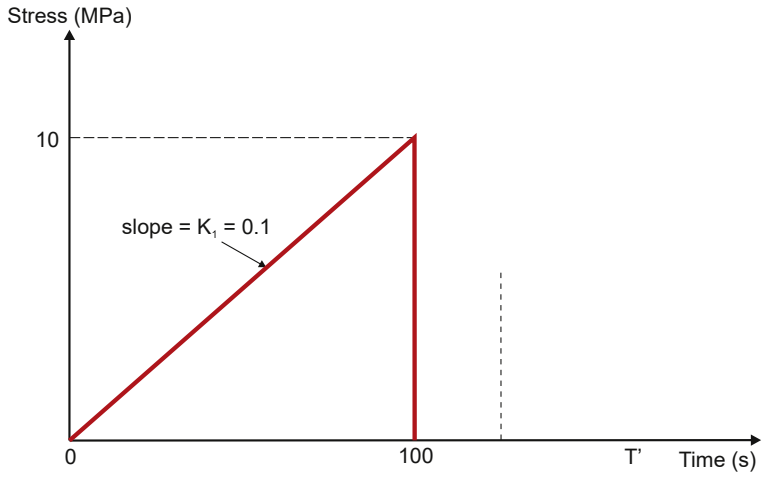


FIG. 2.50 Stress history: Example 2.15(b).

It is apparent therefore that the Superposition Principle is a convenient method of analysing complex stress systems. However, it should not be forgotten that the principle is based on the assumption of linear viscoelasticity which is quite inapplicable at the higher stress levels and the accuracy of the predictions will reflect the accuracy with which the equation for modulus (Eq. 2.33) fits the experimental creep data for the material. In Examples (2.13) and (2.14) a simple equation for modulus was selected in order to illustrate the method of solution. More accurate predictions could have been made if the modulus equation for the combined Maxwell/Kelvin model or the Standard Linear Solid had been used.

2.12.2 Empirical approach

As mentioned earlier, it is not feasible to generate test data for all possible combinations of load variations. However, there have been a number of experimental investigations of the problem and these have resulted in some very useful design aids. From the experimental point of view the most straightforward situation to analyse and one that has considerable practical relevance is the load/no-load cycle. In this case a constant load is applied for a period and then completely removed for a period. The background to this approach is as follows.

For a linear viscoelastic material in which the strain recovery may be regarded as the reversal of creep then the material behaviour may be represented by Fig. 2.51. Thus the time-dependent residual strain, $\varepsilon_r(t)$, may be expressed as

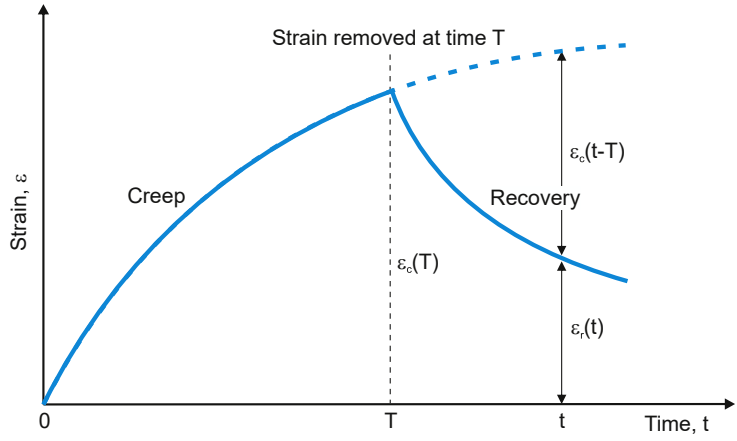


FIG. 2.51 Typical creep and recovery behaviour of a plastic.

$$\varepsilon_t(t) = \varepsilon_c(t) - \varepsilon_c(t-T) \tag{2.59}$$

where ε_c is the creep strain during the specified period denoted by (t) or $(t - T)$.

Since there can be an infinite number of combinations of creep and recovery periods it has been found convenient to express this behaviour in terms of two dimensionless variables. The first is called the **Fractional Recovery**, F_r, defined as

$$F_r = \frac{\text{Strain recovered}}{\text{Max. creep strain}} = \frac{\varepsilon_c(T) - \varepsilon(t)}{\varepsilon_c(T)} \tag{2.60}$$

where $\varepsilon_c(T)$ is the creep strain at the end of creep period and $\varepsilon_r(t)$ is the residual strain at any selected time during the recovery period.

The second dimensionless variable is called the **Reduced Time**, t_R, defined as

$$t_R = \frac{\text{Recovery time}}{\text{Creep time}} = \left(\frac{t-T}{T}\right) \tag{2.61}$$

Extensive tests have shown that if the final creep strain is not large then a graph of Fractional Recovery against Reduced Time is a master curve which describes recovery behaviour with acceptable accuracy (see Fig. 2.52). The relationship between F_r and t_R may be derived in the following way.

When creep curves are plotted on logarithmic strain and time scales they are approximately straight lines so that the creep strain, $\varepsilon_c(t)$ may be expressed as

$$\varepsilon_c(t) = At^n \tag{2.62}$$

and using this relationship in Eq. (2.59)

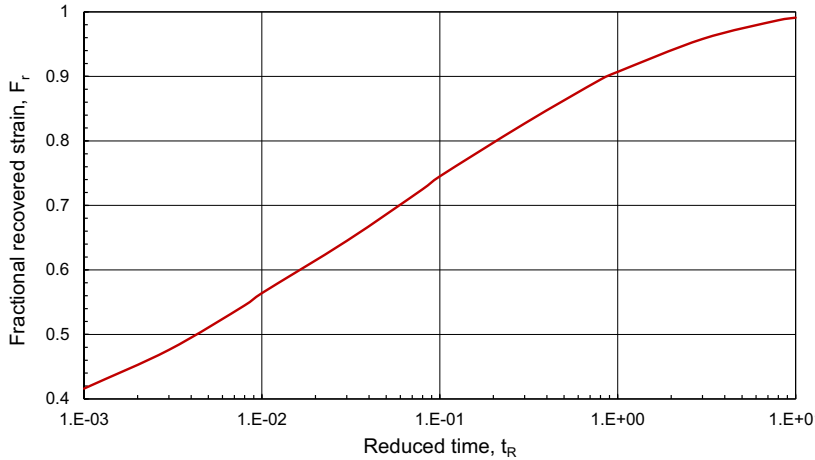


FIG. 2.52 Typical recovery behaviour of a plastic.

$$\varepsilon_r(t) = At^n - A(t-T)^n$$

and so the Fractional Recovery may be written as

$$\begin{aligned} F_r &= \frac{AT^n - [At^n - A(t-T)^n]}{AT^n} \\ &= 1 - \left(\frac{t}{T}\right)^n + \left(\frac{t}{T} - 1\right)^n \\ F_r &= 1 + t_R^n - (t_R + 1)^n \end{aligned} \tag{2.63}$$

In practice this relationship is only approximately correct because most plastics are not linearly viscoelastic, nor do they obey completely the power law expressed by Eq. (2.62). However, this does not detract from the considerable value of this simple relationship in expressing the approximate solution to a complex problem. For the purposes of engineering design the expression provides results which are sufficiently accurate for most purposes. In addition, Eq. (2.63) permits the problem of intermittent loading to be analysed in a relatively straightforward manner thus avoiding uneconomical overdesign which would result if the recovery during the rest periods was ignored.

From Eq. (2.63) and the definition of Fractional Recovery, F_r, the residual strain is given by

$$\begin{aligned} \varepsilon_r(t) &= \varepsilon_c(T) - F_r \cdot \varepsilon_c(T) \\ &= \varepsilon_c(T)\left[\left(\frac{t}{T}\right)^n - \left(\frac{t}{T} - 1\right)^n\right] \end{aligned}$$

If there have been N cycles of creep and recovery the accumulated residual strain would be

$$\varepsilon_r(t) = \varepsilon_c(T) \sum_{x=1}^{x=N} \left[\left(\frac{t_p x}{T}\right)^n - \left(\frac{t_p x}{T} - 1\right)^n\right] \tag{2.64}$$

where t_p is the period of each cycle and thus the time for which the total accumulated strain is being calculated is $t = t_p N$.

Note also that the total accumulated strain after the load application for the $(N+1)^{\text{th}}$ time will be the creep strain for the load-on period i.e. $\varepsilon_c(T)$ plus the residual strain $\varepsilon_r(t)$.

$$\text{i.e. } (\varepsilon_{N+1})_{\max} = \varepsilon_c(T)\left\{1 + \sum_{x=1}^{x=N}\left[\left(\frac{t_p x}{T}\right)^n - \left(\frac{t_p x}{T} - 1\right)^n\right]\right\} \tag{2.65}$$

Tests have shown that when total strain is plotted against the logarithm of the total creep time (i.e. NT or total experimental time minus the recovery time) there is a linear relationship. This straight line includes the strain at the

end of the first creep period and thus one calculation, for say the 10th cycle allows the line to be drawn. The total creep strain under intermittent loading can then be estimated for any combinations of loading/unloading times.

In many design calculations it is necessary to have the creep modulus in order to estimate deflections etc. from standard formulae. In the steady loading situation this is straightforward and the method is illustrated in the Examples (2.1)−(2.5). For the intermittent loading case the modulus of the material is effectively increased due to the apparent stiffening of the material caused by the recovery during the rest periods. For example, if a constant stress of 17.5 MPa was applied to acetal (see Fig. 2.53) for 9600 h then the total creep strain after this time would be 2%. This would give a 2% secant modulus of 17.5/0.02 = 875 MPa. If, however, this stress was applied intermittently for 6 h on and 18 h off, then the total creep strain after 400 cycles (equivalent to a total time of 9600 h) would only be 1.27%. This would be equivalent to a

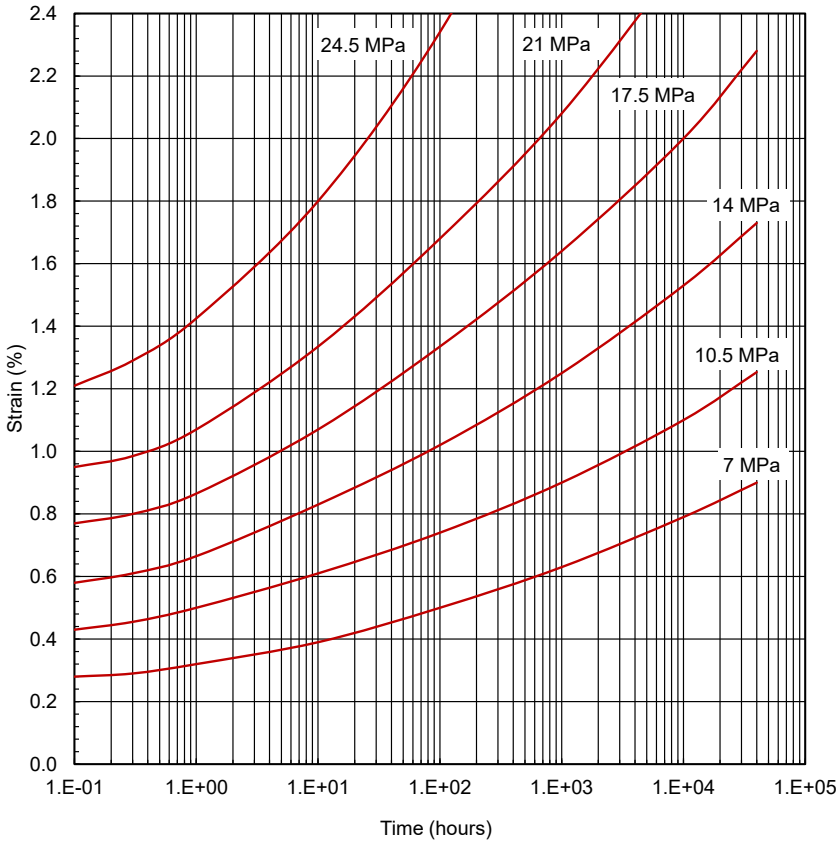


FIG. 2.53 Creep curves for acetal.

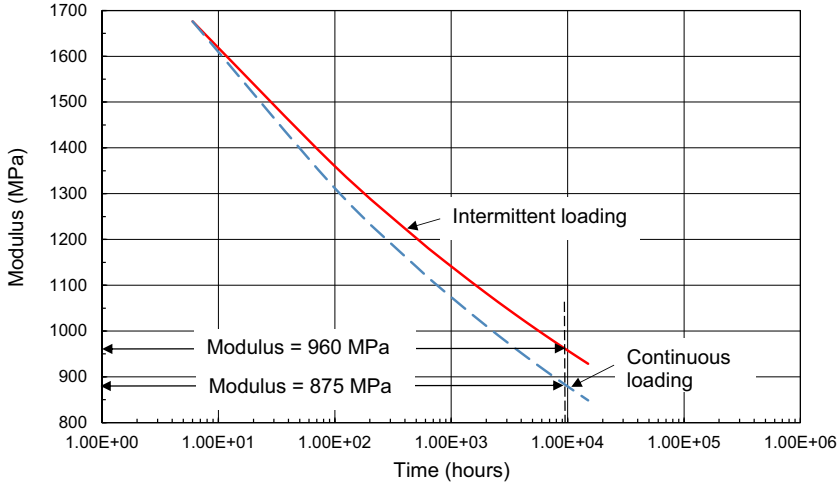


FIG. 2.54 Variation of modulus for continuous and intermittent loading.

stress of 12.2 MPa being applied continuously for 9600 h and so the *effective creep modulus* would be 12.2/0.0127 = 960 MPa.

The effective increase in modulus due to intermittent loading is shown in Fig. 2.54. This illustrates that considerable material savings can be made if intermittent loading of the plastic can be ensured.

Example 2.16. Analysis of the creep curves given in Fig. 2.53 shows that they can be represented by an equation of the form $\varepsilon(t) = A\sigma^{\alpha}t^{n}$ where the constants $n = 0.087$, $\alpha = 1.142$ and $A = 0.034$. A component made from this material is subjected to a loading pattern in which a stress of 10.5 MPa is applied for 100 h and then completely removed. Estimate (a) the residual strain in the material 100 h after the stress has been removed, (b) the total creep strain after the fifth loading cycle in which the stress has been applied for 100 h and removed for 100 h in each cycle and (c) the residual strain after 1000 cycles of the type described in (b).

Solution.

(a) The strain $\varepsilon_c(T)$ after 100 h at 10.5 MPa may be obtained from the creep curves in Fig. 2.53 or by calculation from the equation $\varepsilon_c(T) = A\sigma^{\alpha}T^{n}$.

So

$$\begin{aligned}\varepsilon_c(100) &= 0.034(10.5)^{1.142}(100)^{0.087}\\ &= 0.499(100)^{0.087} = 0.744\%\end{aligned}$$

Now from Eq. (2.60) the Fractional Recovery is given by

$$F_r = \frac{\varepsilon_c(100) - \varepsilon_r(t)}{\varepsilon_c(100)} = 1 - \frac{\varepsilon_r(t)}{0.744}.$$

Also, the Reduced Time is given by

$$t_R = \frac{t - T}{T} = \frac{200 - 100}{100} = 1$$

Then from Eq. (2.63)

$$F_r = 1 + t_R^n - (t_R + 1)^n$$

$$1 - \frac{\varepsilon_r(t)}{0.744} = 1 + 1 - (2)^{0.087}$$

$$\varepsilon_r(t) = 0.046\%$$

Alternatively, since recovery may be regarded as the reverse of creep this part of the problem may be solved as follows.

The projected creep strain after 200 h at 10.5 MPa is

$$\varepsilon_c(200) = 0.499(200)^{0.087} = 0.791\%$$

(see Fig. 2.53 to confirm this value of strain).

However, since the stress was removed after 100 h the recovered strain after a further 100 h will be the same as $\varepsilon_c(T)$, i.e. 0.744%. Thus the residual strain after the recovery period may be determined by superposition.

$$\varepsilon_r(t) = 0.791 - 0.744 = 0.047\%$$

This is simpler than the first solution but this approach is only convenient for the simple loading sequence of stress on − stress off. If this sequence is repeated many times then this superposition approach becomes rather complex. In these cases the analytical solution shown below is recommended but it should be remembered that the equations used were derived on the basis of the superposition approach illustrated above.

(b) If the stress is applied for 100 h and removed for 100 h then in Eq. (2.64), $T = 100$ h and $t_p = 200$ h. Therefore after four cycles i.e. $t = 800$ h.

$$\varepsilon_r(800) = \varepsilon_c(100) \sum_{x=1}^{x=4} \left[\left(\frac{t_p x}{T} \right)^n - \left(\frac{t_p x}{T} - 1 \right)^n \right]$$

$$= 0.744 \sum_{x=1}^{x=4} \left[\left(\frac{200x}{100} \right)^{0.087} - \left(\frac{200x}{100} - 1 \right)^{0.087} \right]$$

$$= 0.744(0.0622 + 0.0279 + 0.0184 + 0.0138)$$

$$= 0.091\%$$

Thus the total creep strain after the fifth load application for 100 h would be $0.091 + 0.744 = 0.835\%$.

(c) The residual strain after the 1000th cycle may be calculated as shown in (b) with the limits $x = 1$ to $x = 1000$. Clearly this repetitive calculation is particularly suitable for analysis using a computer. Thus for a time, t, of 1000×200 h.

$$\varepsilon_r\left(2 \times 10^5\right) = \varepsilon_c(100)\left\{\sum_{x=1}^{x=1000}\left[\left(\frac{200x}{100}\right)^{0.087} - \left(\frac{200x}{100} - 1\right)^{0.087}\right]\right\}$$

$$= 0.363\%.$$

However, in the absence of a computer the problem may be solved as follows. If the residual strain is calculated for, say 10 cycles then the value obtained is

$$\varepsilon\left(10^3\right) = 0.127\%$$

The total creep strain after the stress of 10.5 MPa has been applied for the 11^{th} time would be $0.127 + 0.744 = 0.868\%$. Now tests have shown that a plot of total creep strain plotted against the logarithm of the total creep time (i.e. ignoring the recovery times) is a straight line which includes the point $\varepsilon_c(T)$. Therefore after the 11^{th} cycle the total creep time is $11 \times 100 = 1.1 \times 10^3$ h. If the total strain at this time is plotted on Fig. 2.53 then a straight line can be drawn through this point and the point $\varepsilon_c(T)$, and this line may be extrapolated to any desired number of cycles. For the case in question the line must be extrapolated to (1001×100) hours at which point the total strain may be obtained as 1.11%. Thus the accumulated residual strain after 1000 cycles would be $1.11 - 0.744 = 0.366\%$ as calculated on the computer.

Of course it should always be remembered that the solutions obtained in this way are only approximate since the assumptions regarding linearity of relationships in the derivation of Eq. (2.64) are inapplicable as the stress levels increase. Also in most cases recovery occurs more quickly than is predicted by assuming it is a reversal of creep. Nevertheless this approach does give a useful approximation to the strains resulting from complex stress systems and as stated earlier the results are sufficiently accurate for most practical purposes.

2.13 Dynamic loading of plastics

So far the deformation behaviour of plastics has been considered for situations where (i) the stress (or strain) is constant (ii) the stress (or strain) is changing relatively slowly or (iii) the stress (or strain) is changed intermittently but the

frequency of the changes is small. In practice it is possible to have situations where the stress and strain are changing quite rapidly in a regular manner. This can lead to fatigue fracture which will be discussed in detail in later. However, it is also interesting to consider the stress/strain relationships when polymers are subjected to dynamic loading.

The simplest dynamic system to analyse is one in which the stress and strain are changing in a sinusoidal fashion. Fortunately, this is probably the most common type of loading which occurs in practice and it is also the basic deformation mode used in dynamic mechanical testing of plastics.

When a sinusoidally varying stress is applied to a material it can be represented by a rotating vector as shown in Fig. 2.55. Thus, the stress at any moment in time is given by

$$\sigma = \sigma_0 \sin \omega t \tag{2.66}$$

where ω is the angular velocity of the vector ($= 2\pi f = 2\pi/T$, where f is the cyclic frequency in hertz (H_z) and T is the period of the sinusoidal oscillations).

If the material being subjected to the sinusoidal stress is elastic then there will be a sinusoidal variation of strain which is in phase with the stress, i.e.

$$\varepsilon = \varepsilon_0 \sin \omega t$$

However, for a viscoelastic material the strain will lag behind the stress. The strain is thus given by

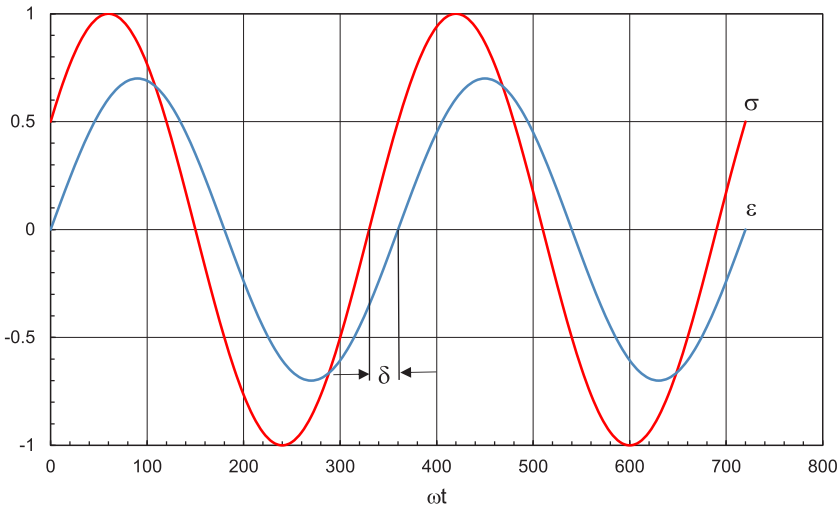


FIG. 2.55 Sinusoidal variation of stress and strain in viscoelastic material.

$$\varepsilon = \varepsilon_0 \sin(\omega t - \delta) \tag{2.67}$$

where δ is the phase lag.

It is more usual to write these equations in a form which shows the stress leading the strain, i.e.

$$\varepsilon = \varepsilon_0 \sin \omega t \tag{2.68}$$

$$\sigma = \sigma_0 \sin(\omega t + \delta) \tag{2.69}$$

The latter equation may be expanded to give

$$\sigma = \sigma_0 \sin \omega t \cos \delta + \sigma_0 \cos \omega t \sin \delta \tag{2.70}$$

Thus, the stress can be considered to have two components:

(i) $\sigma_0 \cos \delta$ which is in phase with the strain and

(ii) $\sigma_0 \sin \delta$ which is 90° out of phase with the strain.

This leads to the definition of two dynamic moduli, E_1 and E_2:

(i) $E_1 = (\sigma_0 \cos \delta)/\varepsilon_0$ in phase with the strain

(ii) $E_2 = (\sigma_0 \sin \delta)/\varepsilon_0$ 90° out of phase with strain

We could thus represent these two moduli on a phasor diagram as shown in Fig. 2.56. E_1 leads E_2 by 90° ($\pi/2$ radians) and from this diagram it is possible to define a *complex modulus, E** where

$$E^* = \frac{\sigma}{\varepsilon} = \sqrt{E_1^2 + E_2^2} = E_1 + iE_2 \tag{2.71}$$

where $i = \sqrt{-1}$.

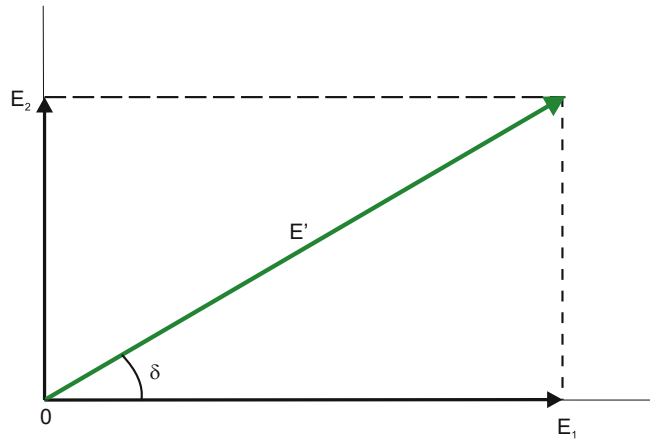


FIG. 2.56 Phasor diagram showing complex modulus (E^*) relative to loss (E_2) and storage (E_1) moduli.

This presentation format leads to the terminology.

E_1 = real modulus or storage modulus
E_2 = imaginary modulus or loss modulus.

Also, from Fig. 2.56 it is possible to relate E_1 and E_2 to the lag or phase angle, δ

$$\tan \delta = \frac{E_2}{E_1} \tag{2.72}$$

In dynamic mechanical analysis of plastics, the material is subjected to a sinusoidal variation of stress and the strain is recorded so that E_1, E_2 and δ can be determined. The classical variation of these parameters is illustrated in Fig. 2.57.

At very low frequencies the polymer is rubber-like and has a low modulus (E_1 typically 0.1 MPa). At very high frequencies, the material behaves like a stiff, glassy solid with a high modulus (typically about 10^3 MPa). It may be seen that this E_1 plot is the inverse of that shown in Fig. 2.9 since $\omega \propto 1/t$. The loss modulus, E_2, will be zero at low and high frequencies but will rise to a maximum close to the region where E_1 is increasing most rapidly. The loss factor, $\tan \delta$ ($=E_2/E_1$), will also have a maximum in the viscoelastic region but this will occur at a lower frequency than the peak in the E_2 curve.

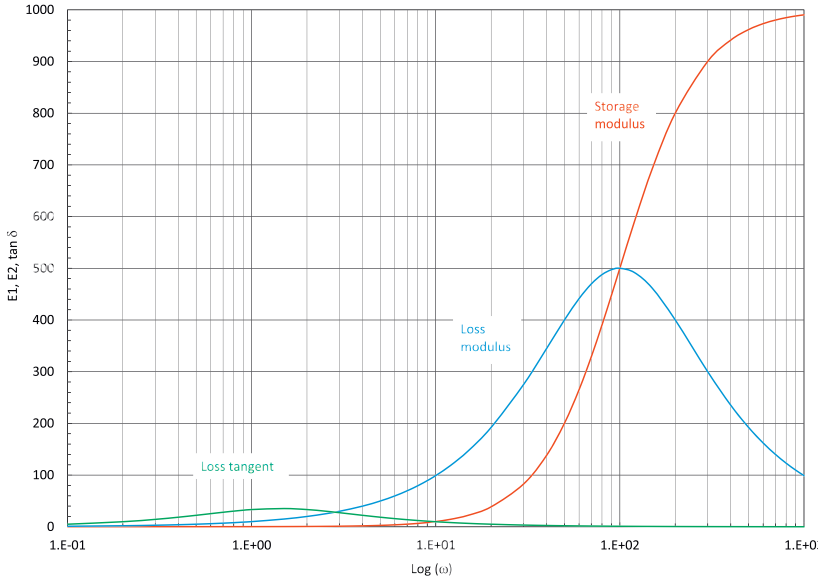


FIG. 2.57 Typical variation of E_1, E_2 and loss tangent for a viscoelastic material.

Example 2.17. Establish and plot the variation with frequency of the storage and loss moduli for materials which can have their viscoelastic behaviour described by the following models

(i) A Maxwell model with $\xi = 1$ GPa and $\eta = 0.1$ GPa.s.

(ii) A Standard Linear Solid with $\xi_1 = 2$ GPa, $\xi_2 = 0.1$ GPa, $\eta = 1$ GPa.s.

Solution As illustrated above, the stress and strain will be given by

$$\sigma = \sigma_0 \sin(\omega t + \delta)$$
$$\varepsilon = \varepsilon_0 \sin \omega t$$

However, in this type of question it is preferable to utilise complex numbers and so the transformations will be used so that

$$\sigma = \sigma_0 e^{i(\omega t + \delta)} \tag{2.73}$$

$$\varepsilon = \varepsilon_0 e^{i\omega t} \tag{2.74}$$

(i) As shown earlier in this chapter, the governing equation for the Maxwell model is given by

$$\dot{\varepsilon} = \frac{1}{\xi}\dot{\sigma} + \frac{1}{\eta}\sigma$$

Then from Eqs. (2.73) and (2.74)

$$\varepsilon_0 i\omega e^{i\omega t} = \frac{1}{\xi}\sigma_0 i\omega e^{i(\omega t+\delta)} + \frac{1}{\eta}\sigma_0 e^{i(\omega t+\delta)}$$

$$i\omega = \frac{i\omega}{\xi}\cdot\frac{\sigma_0 e^{i(\omega t+\delta)}}{\varepsilon_0 e^{i\omega t}} + \frac{1}{\eta}\cdot\frac{\sigma_0 e^{i(\omega t+\delta)}}{\varepsilon_0 e^{i\omega t}}$$

$$i\omega = \frac{i\omega}{\xi}\cdot E^* + \frac{1}{\eta}E^*$$

where E^* is the complex modulus. Rearranging gives

$$E^* = \frac{i\omega\eta\xi}{\xi + \omega\eta i}$$

Using the fact that $(a + bi)(a - bi) = a^2 + b^2$

$$E^* = \frac{i\omega\eta\xi}{(\xi + \omega\eta i)} \cdot \frac{(\xi - \omega\eta i)}{(\xi - \omega\eta i)} = \frac{\omega^2\eta^2\xi + \omega\eta\xi^2 i}{\omega^2\eta^2 + \xi^2}$$

and since $E^* = E_1 + iE_2$
then storage modulus,

$$E_1 = \frac{\omega^2\eta^2\xi}{\omega^2\eta^2 + \xi^2}$$

loss modulus,

$$E_2 = \frac{\omega\eta\xi^2}{\omega^2\eta^2 + \xi^2}$$

and loss tangent,

$$\tan\delta = \frac{E_2}{E_1} = \frac{\xi}{\omega\eta}$$

The variations of E_1, E_2 and tanδ with ω are shown in Fig. 2.58. It may be seen that the variations of E_1 and E_2 are of the general shape that would be expected. The tanδ curve does not go through a maximum and so this is a further shortcoming of this simple model.

(ii) For the Standard Linear Solid, the governing equation was derived earlier as

$$\eta\dot{\sigma} + \xi_1\sigma = \eta(\xi_1 + \xi_2)\dot{\varepsilon} + \xi_2\xi_1\varepsilon$$

substituting from Eqs. (2.73) and (2.74) once again

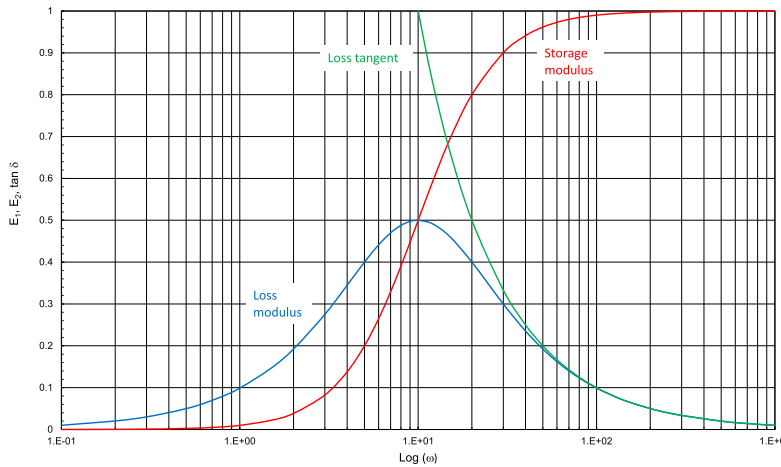


FIG. 2.58 Variation of E_1, E_2 and loss tangent for Maxwell model.

$$\eta\sigma_0 i\omega e^{i(\omega t+\delta)} + \xi_1\sigma_0 e^{i(\omega t+\delta)} = \eta(\xi_1+\xi_2)i\omega\varepsilon_0 e^{i\omega t} + \xi_1\xi_2\varepsilon_0 e^{i\omega t}$$

Dividing across by $\varepsilon_0 e^{i}\omega^{t}$ and letting $E^* = \sigma_0 e^{i(\omega t+\delta)}/\varepsilon_0 e^{i\omega t}$

$$\text{then, } E^* = \frac{\eta(\xi_1+\xi_2)i\omega + \xi_1\xi_2}{\xi_1 + \eta\omega i}$$

Multiplying top and bottom by the conjugate of the denominator, we get

$$E^* = \frac{\left\{\xi_1^2\xi_2 + \eta^2(\xi_1+\xi_2)\omega^2\right\} + \left\{\xi^2\eta\omega\right\}i}{\xi_1^2 + \omega^2\eta^2}$$

and since $E^* = E_1 + iE_2$,

$$\text{storage modulus, } E_1 = \frac{\xi_1^2\xi_2 + \eta^2(\xi_1+\xi_2)\omega^2}{\xi_1^2 + \omega^2\eta^2}$$

$$\text{loss modulus, } E_2 = \frac{\xi_1^2\eta\omega}{\xi_1^2 + \omega^2\eta^2}$$

$$\text{loss tangent, } \tan\delta = \frac{E_2}{E_1} = \frac{\xi_1^2\eta\omega}{\xi_1^2\xi_2 + \eta^2(\xi_1+\xi_2)\omega^2}$$

It may be seen in Fig. 2.59 that the variations of E_1, E_2 and tan δ follow the classical pattern referred to earlier in this section.

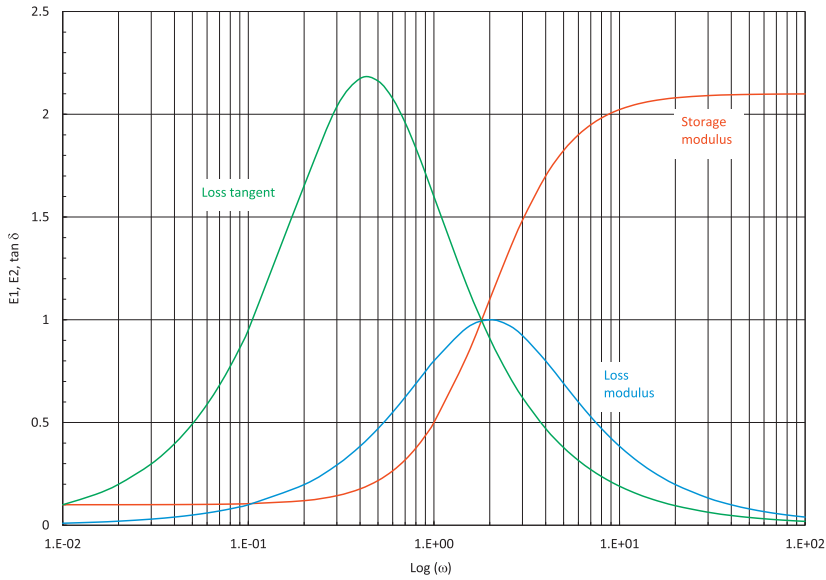


FIG. 2.59 Variation of E_1, E_2 and loss tangent for standard linear solid.

2.14 Time–temperature superposition

It has been shown throughout this chapter that the properties of plastics are dependent on time. In Chapter 1 the dependence of properties on temperature was also highlighted. The latter is more important for plastics than it would be for metals because even modest temperature changes below 100°C can have a significant effect on properties. Clearly it is not reasonable to expect creep curves and other physical property data to be available at all temperatures. If information is available over an appropriate range of temperatures then it may be possible to attempt some type of interpolation. For example, if creep curves are available at 20°C and 60°C whereas the service temperature is 40°C then a linear interpolation would provide acceptable design data.

If creep curves are available at only one temperature, then the situation is a little more difficult. It is known that properties such as modulus will decrease with temperature, but by how much? Fortunately, it is possible to use a time–temperature superposition approach as follows:

It was shown earlier that the variation of creep or relaxation moduli with time are as illustrated in Fig. 2.9. If we now introduce temperature as a variable, then a series of such curves will be obtained as shown in Fig. 2.60. In general, the relaxed and unrelaxed modulus terms are independent of temperature. The remainder of the moduli curves are essentially parallel and so this led to the thought that a shift factor, a_T, could be applied to move from one curve to another.

It may be seen from Fig. 2.61 that the two modulus curves for temperatures T_1 and T_2 are separated by a uniform distance (log a_T). Thus, if the material behaviour is known at T_1, in order to get the modulus at time, t, and

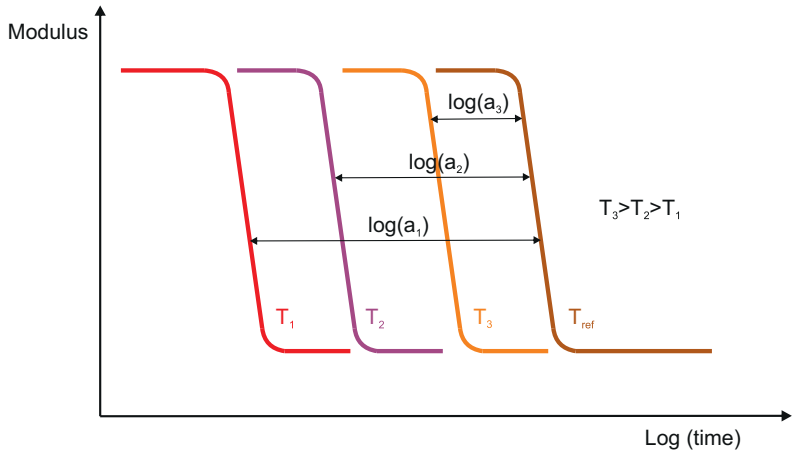


FIG. 2.60 Modulus–time curves for a range of temperatures.

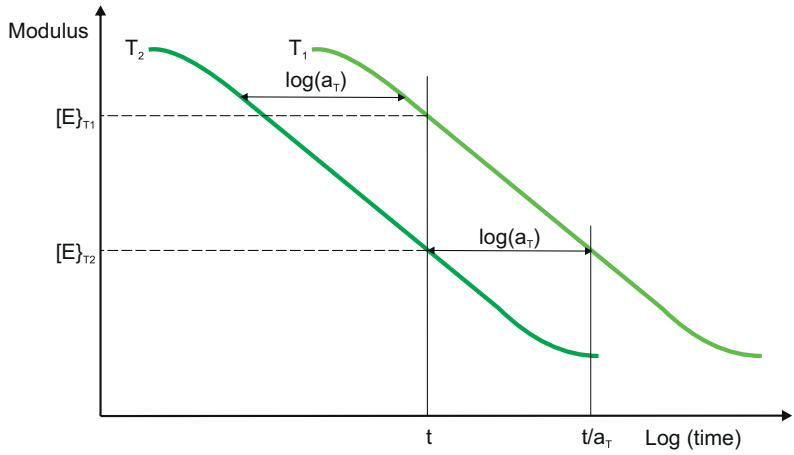


FIG. 2.61 Modulus curves at temperatures T_1 and T_2.

temperature T_2, it would be necessary to use a time (t/a_T) as shown in Fig. 2.61, in relation to the T_1 data. This means that

$$[E(t)]_{T_2} = \left[E\left(\frac{t}{a_T}\right)\right]_{T_1} \tag{2.75}$$

where $T_2 > T_1$. Log (a_T) is negative and so $a_T < 1$.

Williams, Landel and Ferry developed an empirical relationship for this type of shift factor. This has the form

$$\log a_T = \frac{C_1(T - T_{ref})}{C_2 + (T - T_{ref})} \tag{2.76}$$

where C_1 and C_2 are constants and T_{ref} is a reference temperature.

For many polymers, it has been found that C_1 and C_2 are constants and T_{ref} is taken as T_g, the glass transition temperature for the polymer (values are given in Table 1.8). The WLF equation then takes the form

$$\log a_T = \frac{-17.4(T - T_g)}{51.6 + (T - T_g)} \tag{2.77}$$

Thus, all the different temperature related data in Fig. 2.60 could be shifted to a single master curve at the reference temperature (T_g). Alternatively, if the properties are known at T_{ref} then it is possible to determine the property at any desired temperature. It is important to note that the shift factor cannot be applied to a single value of modulus. This is because the shift factor is on the horizontal time-scale, not the vertical, modulus scale. If a single value of modulus E_{T1} is known as well as the shift factor a_T it is not possible to determine E_{T2} without knowing how the modulus varies with time. This is

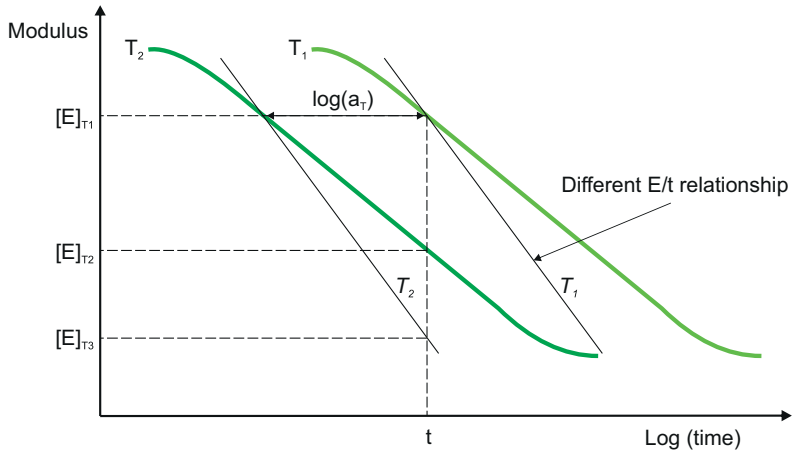


FIG. 2.62 Various modulus−time curves.

illustrated in Fig. 2.62 where it is readily seen that a knowledge of E_{T1} and a_T do not lead to a single value of E_{T2} unless the $E(t)$ relationship is known.

Example 2.18. A particular grade of polypropylene can have its relaxation modulus described by the equation

$$E(t) = 1.8t^{-0.1}$$

where $E(t)$ is in GPa when 't' is in seconds. The temperature of the material is 20°C. Use the WLF equation to determine the 1 year modulus of the material at 60°C. The glass transition temperature for the polypropylene is −10°C.

Solution To use Eq. (2.76) it would be necessary to know the properties at −10°C. In this example, the properties are known at 20°C which becomes the reference temperature (T_1). The approach taken will be to get the shift factor at T_2 (=60°C) and the shift factor at T_1 (= 20°C) and then subtract these to get the shift factor from T_1 to T_2.

$$\begin{aligned}\log a_T &= \frac{17.4(T_1 - T_g)}{51.6 + (T_1 - T_g)} - \frac{17.4(T_2 - T_g)}{51.6 + (T_2 - T_g)} \\ &= \frac{17.4(20 + 10)}{51.6 + (20 + 10)} - \frac{17.4(60 + 10)}{51.6 + (60 + 10)} \\ &= -3.62 \\ a_T &= 2.4 \times 10^{-4}\end{aligned} \tag{2.78}$$

Therefore, using Eq. (2.75)

$$[E(t)]_{T_2} = \left[E\left(\frac{t}{a_T}\right)\right]_{T_1}$$

$$= 1.8\left(\frac{t}{2.4 \times 10^{-4}}\right)^{-0.1}$$

$$[E(t)]_{T_2} = 0.78t^{-0.1}$$

The modulus at T_2(=60°C) can now be calculated at any desired time. For example, at 1 year ($t = 3.15 \times 10^6$ s)

$$[E(t)]_{60} = 0.78\left(3.15 \times 10^6\right)^{-0.1}$$

$$= 0.14 \text{ GPa}$$

The two modulus curves at 20°C and 60°C are illustrated in Fig. 2.63 along with the shift factor.

2.15 Fracture behaviour of unreinforced plastics

If a plastic moulding fails in the performance of its normal function it is usually caused by one of two factors — excessive deformation or fracture. In the previous sections it was pointed out that, for plastics, more often than not it will be excessive creep deformation which is the limiting factor. However, fracture, if it occurs, can have more catastrophic results. Therefore, it is essential that designers recognise the factors which are likely to initiate fracture in plastics so that steps can be taken to avoid this.

Fractures are usually classified as brittle or ductile. Although any type of fracture is serious, brittle fractures are potentially more dangerous because

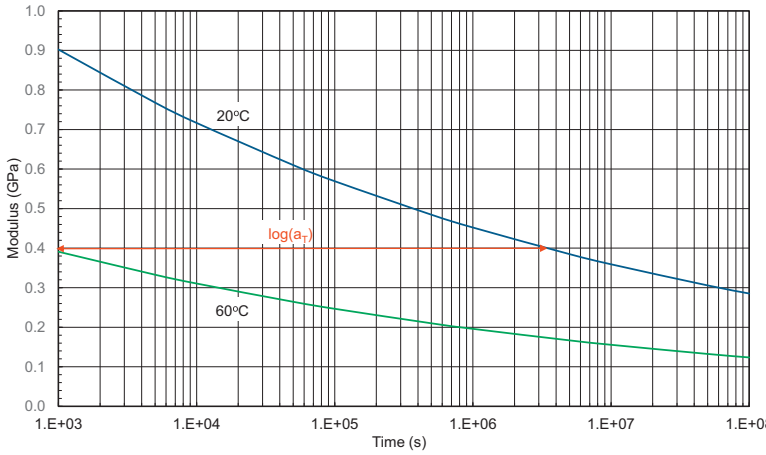


FIG. 2.63 Variation of modulus with time and temperature for polypropylene.

there is no observable deformation of the material prior to or during breakage. When a material fails in a ductile fashion, large non-recoverable deformations are evident and these serve as a warning that all is not well. In polymeric materials, fracture may be ductile or brittle depending on such variables as the nature of the additives, the processing conditions, the strain rate, the temperature and the stress system. The principal external causes of fracture are the application of a stress in a very short period of time (impact), the prolonged action of a steady stress (creep rupture) or the continuous application of a cyclically varying stress (fatigue). In all cases the fracture processes will be accelerated if the plastic is in an aggressive environment.

Basically there are two approaches to the fracture of a material. These are usually described as the microscopic and the continuum approaches. The former approach utilises the fact that the macroscopic fracture of the material must involve the rupture of atomic or molecular bonds. A study of the forces necessary to break these bonds should, therefore, lead to an estimate of the fracture strength of the material. In fact such an estimate is usually many times greater than the measured strength of the material. This is because any real solid contains multitudes of very small inherent flaws and microcracks which give rise to local stresses far in excess of the average stress on the material. Therefore, although the stress calculated on the basis of the cross-sectional area might appear quite modest, in fact the localised stress at particular defects in the material could quite possibly have reached the fracture stress level. When this occurs the failure process will be initiated and cracks will propagate through the material. As there is no way of knowing the value of the localised stress, the strength is quoted as the average stress on the section and this is often surprisingly small in comparison with the theoretical strength.

The second approach to fracture is different in that it treats the material as a continuum rather than as an assembly of molecules. In this case it is recognised that failure initiates at microscopic defects and the strength predictions are then made on the basis of the stress system and the energy release processes around developing cracks. From the measured strength values it is possible to estimate the size of the inherent flaws which would have caused failure at this stress level. In some cases the flaw size prediction is unrealistically large but in many cases the predicted value agrees well with the size of the defects observed, or suspected to exist in the material.

In the following sections of this chapter the various approaches to the fracture of plastics are described and specific causes such as impact loading, creep and fatigue are described in detail.

2.16 The concept of stress concentration

Any material which contains a geometrical discontinuity will experience an increase in stress in the vicinity of the discontinuity. This stress concentration effect is caused by the re-distribution of the lines of force transmission through

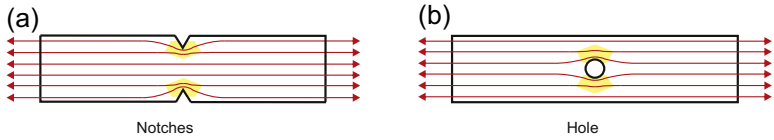


FIG. 2.64 Stress concentration.

the material when they encounter the discontinuity. Causes of stress concentration include holes, notches, keyways, corners, etc. as illustrated in Fig. 2.64.

The classical equation for calculating the magnitude of the stress concentration at a defect in the form of a hole as shown in Fig. 2.64(b) is

$$\sigma_c = \sigma\left(1 + 2\sqrt{a/r}\right) \tag{2.79}$$

where σ_c is the local stress, σ is the nominal stress on the material, $2a$ is the defect size and r is the radius of the defect at the area in question.

The parameter $(1 + 2\sqrt{a/r})$ is commonly termed the *stress concentration factor* (K_t) and for a hole where $a = r$ then $K_t = 3$, i.e. the stresses around the periphery of the hole are three times as great as the nominal stress in the material.

It should be noted, however, that for a crack-like defect in which $r \rightarrow 0$ then $K_t \rightarrow \infty$. Obviously, this does not occur in practice. It would mean that a material containing a crack could not withstand any stress applied to it. Therefore, it is apparent that the stress concentration approach is not suitable for allowing for the effects of cracks. This has given rise to the use of *Fracture Mechanics* to deal with this type of situation.

2.17 Energy approach to fracture

When a force is applied to a material there is work done in the sense that a force moves through a distance (the deformation of the material). This work is converted to elastic (recoverable) energy absorbed in the material and surface energy absorbed in the creation of new surfaces at cracks in the material. The original work on Fracture Mechanics was undertaken by Griffith and he proposed that unstable crack growth (fracture) would occur if the incremental change in the nett energy (work done − elastic energy) exceeded the energy which could be absorbed in the creation of the new surface. In mathematical terms this may be expressed as

$$\frac{\partial}{\partial a}(W - U) > \gamma \frac{\partial A}{\partial a} \tag{2.80}$$

where γ is the surface energy per unit area.

Note that for a situation where the applied force does no work (i.e. there is no overall change in length of the material) then $W = 0$ and Eq. (2.80) becomes

$$\frac{\partial U}{\partial a} > \gamma \frac{\partial A}{\partial a} \tag{2.81}$$

Now, for a through crack propagating in a sheet of material of thickness, B, we may write

$$\partial A = 2B\partial a$$

So Eq. (2.80) becomes

$$\frac{\partial}{\partial a}(W - U) > 2\gamma B \tag{2.83}$$

In the context of fracture mechanics the term 2γ is replaced by the G_c so that the condition for fracture is written as

$$\frac{1}{B}\frac{\partial}{\partial a}(W - U) > G_c \tag{2.84}$$

G_c is a material property which is referred to as the **toughness, critical strain energy release rate or crack extension force**. It is effectively the energy required to increase the crack length by unit length in a piece of material of unit width. It has units of J/m^2.

Eq. (2.84) may be converted into a more practical form as follows. Consider a piece of material of thickness, B, subjected to a force, F, as shown in Fig. 2.65(a). The load-deflection graph is shown as line (i) in Fig. 2.65(b). From this the elastic stored energy, U_1, may be expressed as

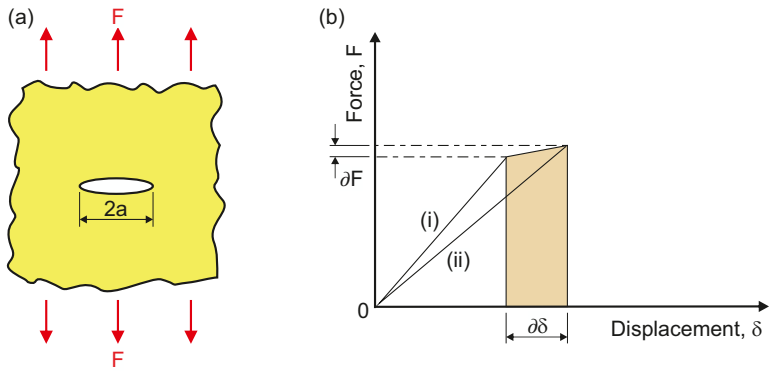


FIG. 2.65 Force displacement behaviour of an elastic cracked plate.

$$U_1 = \frac{1}{2} F\delta \tag{2.85}$$

If the crack extends by a small amount ∂a then the stiffness of the material changes and there will be a small change in both load, ∂F, and deflection, $\partial\delta$. This is shown as line (ii) in Fig. 2.65(b). The elastic stored energy would then be

$$U_2 = \frac{1}{2}(F + \partial F)(\delta + \partial\delta) \tag{2.86}$$

From Eqs. (2.85) and (2.86) the change in stored energy as a result of the change in crack length ∂a would be given by

$$\partial U = U_2 - U_1 = \frac{1}{2}(F\,\partial\delta + \delta\partial F + \partial F\,\partial\delta) \tag{2.87}$$

The work done, ∂W, as a result of the change in crack length ∂a is shown shaded in Fig. 2.65(b). This will be given by,

$$\partial W = F\partial\delta + \frac{1}{2}\partial F\partial\delta \tag{2.88}$$

Now using Eqs. (2.87) and (2.88) in Eq. (2.84)

$$\frac{1}{2B}\left\{\frac{F\partial\delta}{\partial a} - \frac{\delta\partial F}{\partial a}\right\} = G_c \tag{2.89}$$

This equation may be simplified very conveniently if we consider the *Compliance, C,* of the material. This is the reciprocal of stiffness and is given by

$$C = \frac{\delta}{F} \tag{2.90}$$

From this equation we may write

$$\partial\delta = F\partial C + C\partial F$$

and using this in Eq. (2.89) we get

$$G_c = \frac{F_c^2}{2B}\frac{\partial C}{\partial a} \tag{2.91}$$

where F_c is the applied force at fracture.

This is a very important relationship in that it permits the fundamental material property G_c to be calculated from the fracture force, F_c, and the variation of compliance with crack length.

Example 2.19. During tensile tests on 4 mm thick acrylic sheets of the type shown in Fig. 2.65(a), the force-displacement characteristics shown in Fig. 2.66(a) were recorded when the crack lengths were as indicated. If the

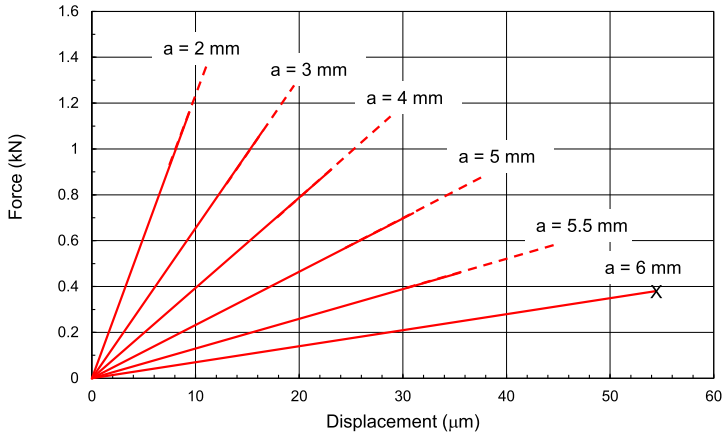


FIG. 2.66(a) Force-displacement characteristics for cracked plate.

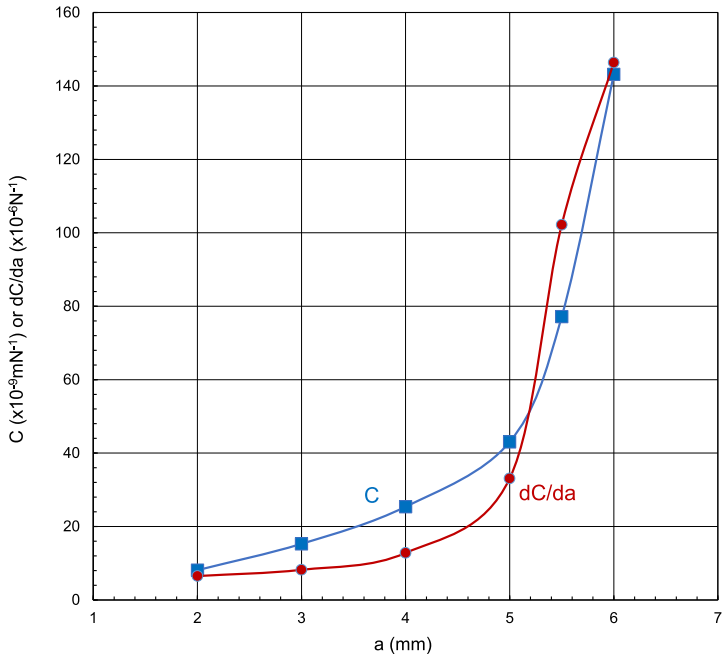


FIG. 2.66(b) Compliance and rate of change of compliance for various crack lengths.

sheet containing a 12 mm long crack fractured at a force of 330 N, determine the fracture toughness of the acrylic and calculate the applied force necessary to fracture the sheets containing the other crack sizes.

Solution The compliance (δ/F) of each sheet may be determined from the slope of the graph in Fig. 2.66(a). A plot of compliance, C, against crack

dimension, a, is shown in Fig. 2.66(b) and from this the parameter *dC/da* may be obtained. This is also shown plotted on Fig. 2.66(b). Using this, for a = 6 mm, it may be seen that $dC/da = 146 \times 10^{-6}\ \mathrm{N}^{-1}$.

Thus, from Eq. (2.91)

$$G_c = \frac{F_c^2}{2B}\frac{\partial C}{\partial a} = \frac{330^2\left(146 \times 10^{-6}\right)}{2(0.004)} = 2\ \mathrm{kJ/m^2}.$$

As this is a material constant, it may be used to calculate F_c for the other crack sizes. For example, for a = 2 mm, $dC/da = 6.5 \times 10^{-6}\ \mathrm{N}^{-1}$ so

$$F_c = \sqrt{\frac{2(0.004).2 \times 10^3}{6.5 \times 10^{-6}}} = 1.57\ \mathrm{kN}.$$

Similarly for $a = 3$, 4, 5 and 5.5 mm the fracture loads would be 1.4 kN, 1.12 kN, 0.7 kN and 0.4 kN respectively.

An alternative energy approach to the fracture of polymers has also been developed on the basis of non-linear elasticity. This assumes that a material without any cracks will have a uniform strain energy density (strain energy per unit volume). Let this be U_0. When there is a crack in the material this strain energy density will reduce to zero over an area as shown shaded in Fig. 2.67. This area will be given by ka^2 where k is a proportionality constant. Thus, the loss of elastic energy due to the presence of the crack is given by

$$-U = ka^2BU_0 \tag{2.92}$$

and

$$-\left(\frac{\partial U}{\partial a}\right) = 2kaBU_0 \tag{2.93}$$

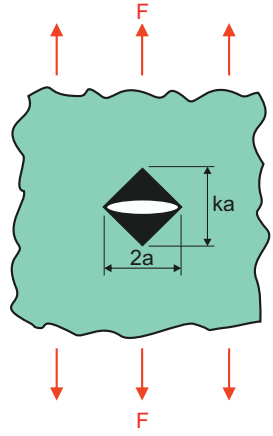


FIG. 2.67 Loading of cracked plate.

Comparing this with Eq. (2.84) and assuming that the external work is zero then it is apparent that

$$G_c = 2kaU_c \tag{2.94}$$

where U_c is the value of strain energy density at which fracture occurs.

Now, for the special case of a *linear* elastic material this is readily expressed in terms of the stress, σ_c, on the material and its modulus, E.

$$U_c = \frac{1}{2}\sigma_c\varepsilon_c = \frac{1}{2}\frac{\sigma_c^2}{E} \tag{2.95}$$

So, combining Eqs. (2.94) and (2.95)

$$G_c = \frac{k\sigma^2 a}{E}$$

and in practice it is found that k $\simeq \pi$, so

$$G_c = \frac{\pi\sigma_c^2 a}{E} \tag{2.96}$$

This is an alternative form of Eq. (2.91) and expresses the fundamental material parameter G_c in terms the applied stress and crack size. From a knowledge of G_c it is therefore possible to specify the maximum permissible applied stress for a given crack size, or vice versa. It should be noted that, strictly speaking, Eq. (2.96) only applies for the situation of plane stress. For plane strain it may be shown that material toughness is related to the stress system by the following equation.

$$G_{1c} = \frac{\pi\sigma_c^2 a}{E}\left(1 - v^2\right) \tag{2.97}$$

where v is the lateral contraction ratio (Poisson's ratio).

Note that the symbol G_{1c} is used for the plane strain condition and since this represents the least value of toughness in the material, it is this value which is usually quoted. Table 2.2 gives values for G_{1c} for a range of plastics.

2.18 Stress intensity factor approach to fracture

Although Griffith put forward the original concept of linear elastic fracture mechanics (LEFM), it was Irwin who developed the technique for engineering materials. He examined the equations that had been developed for the stresses in the vicinity of an elliptical crack in a large plate as illustrated in Fig. 2.68. The equations for the elastic stress distribution at the crack tip are as follows.

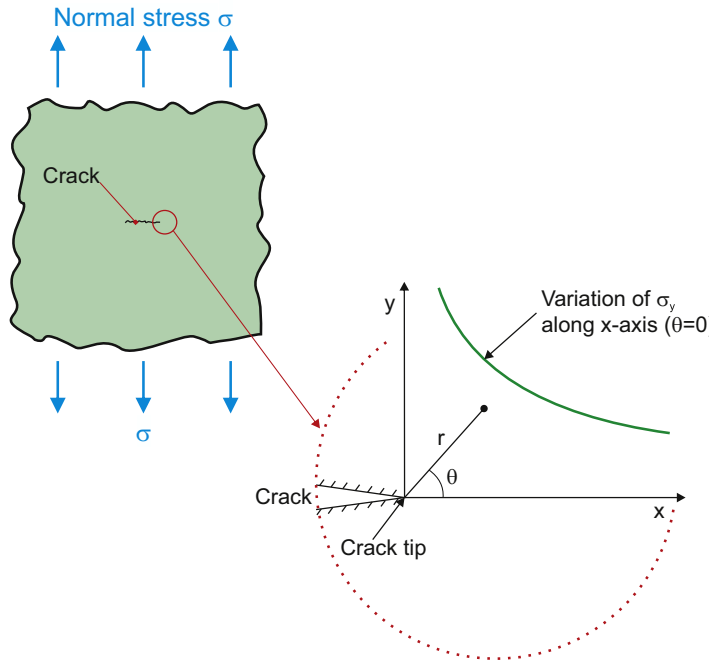


FIG. 2.68 Stress distribution in vicinity of a crack.

$$\left.\begin{aligned}\sigma_x &= \frac{K}{(2\pi r)^{1/2}}\cos\left(\frac{\theta}{2}\right)\left\{1-\sin\left(\frac{\theta}{2}\right)\sin\left(\frac{3\theta}{2}\right)\right\}\\ \sigma_y &= \frac{K}{(2\pi r)^{1/2}}\cos\left(\frac{\theta}{2}\right)\left\{1+\sin\left(\frac{\theta}{2}\right)\sin\left(\frac{3\theta}{2}\right)\right\}\\ \tau_{xy} &= \frac{K}{(2\pi r)^{1/2}}\sin\left(\frac{\theta}{2}\right)\cos\left(\frac{\theta}{2}\right)\cos\left(\frac{3\theta}{2}\right)\end{aligned}\right\} \tag{2.98}$$

and for plane strain

$$\sigma_z = \frac{2K}{(2\pi r)^{1/2}}\cos\left(\frac{\theta}{2}\right)$$

or for plane stress, $\sigma_z = 0$.

Irwin observed that the stresses are proportional to $(\pi a)^{1/2}$ where *'a'* is the half length of the crack. On this basis, a **Stress Intensity Factor, K**, was defined as

$$K = \sigma(\pi a)^{1/2} \tag{2.99}$$

The stress intensity factor is a means of characterising the elastic stress distribution near the crack tip but in itself has no physical reality. It has units of MN $m^{-3/2}$ and should not be confused with the elastic stress concentration factor (K_t) referred to earlier.

In order to extend the applicability of LEFM beyond the case of a central crack in an infinite plate, K is usually expressed in the more general form

$$K = Y\sigma(\pi a)^{1/2} \tag{2.100}$$

where Y is a geometry factor and *'a'* is the half length of a central crack or the full length of an edge crack.

Fig. 2.69 shows some crack configurations of practical interest and expressions for K are as follows.

(a) Central crack of length $2a$ in a sheet of finite width

$$K = \sigma(\pi a)^{1/2}\left\{\frac{W}{\pi a}\cdot\tan\left(\frac{\pi a}{W}\right)\right\}^{1/2} \tag{2.101}$$

(b) Edge cracks in a plate of finite width

$$K = \sigma(\pi a)^{1/2}\left\{\frac{W}{\pi a}\tan\left(\frac{\pi a}{W}\right) + \frac{0.2W}{\pi a}\sin\left(\frac{\pi a}{W}\right)\right\}^{1/2} \tag{2.102}$$

(c) Single edge cracks in a plate of finite width

$$K = \sigma(\pi a)^{1/2}\left\{1.12 - 0.23\left(\frac{a}{W}\right) + 10.6\left(\frac{a}{W}\right)^2 - 21.7\left(\frac{a}{W}\right)^3 + 30.4 = \left(\frac{a}{W}\right)^4\right\} \tag{2.103}$$

Note: in most cases $\left(\frac{a}{W}\right)$ is very small so $Y = 1.12$.

(d) Penny shaped internal crack

$$K = \sigma(\pi a)^{1/2}\left(\frac{2}{\pi}\right) \tag{2.104}$$

assuming $a \ll D$.

(e) Semi-elliptical surface flaw

$$K = \sigma(\pi a)^{1/2}\left(\frac{1.12}{\phi^{1/2}}\right) \tag{2.105}$$

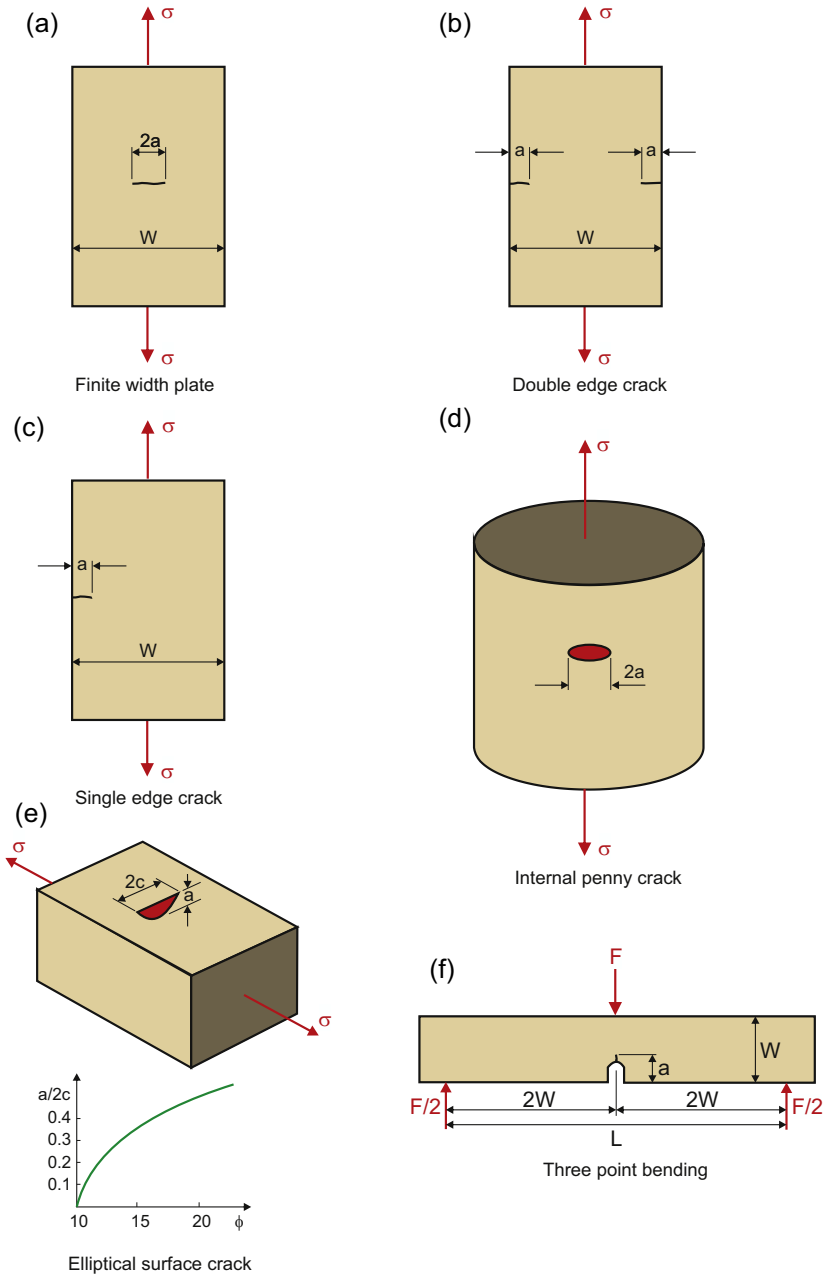


FIG. 2.69 Typical crack configurations.

(f) Three point bending

$$K = \frac{3FL}{2BW^{3/2}}\left\{1.93\left(\frac{a}{W}\right)^{1/2} - 3.07\left(\frac{a}{W}\right)^{3/2} + 14.53\left(\frac{a}{W}\right)^{5/2} - 25.11\left(\frac{a}{W}\right)^{7/2} + 25.8\left(\frac{a}{W}\right)^{9/2}\right\} \tag{2.106}$$

or

$$K = \frac{F}{BW^{1/2}} \cdot f_1\left(\frac{a}{W}\right) \tag{2.107}$$

Thus, the basis of the LEFM design approach is that:

(a) all materials contain cracks or flaws
(b) The stress intensity value, K, may be calculated for the particular loading and crack configuration
(c) failure is predicted if K exceeds the critical value for the material.

The **critical stress intensity factor** is sometimes referred to as the **fracture toughness** and will be designated K_c. By comparing Eqs. (2.96) and (2.99) it may be seen that K_c is related to G_c by the following equation

$$(EG_c)^{1/2} = K_c \tag{2.108}$$

This is for plane stress and so for the plane strain situation

$$\left(\frac{EG_{1c}}{1-\nu^2}\right)^{1/2} = K_{1c} \tag{2.109}$$

Table 2.2 gives typical values of K_{1c} for a range of plastics.

Example 2.20. A cylindrical vessel with an outside radius of 20 mm and an inside radius of 12 mm has a radial crack 3.5 mm deep on the outside surface. If the vessel is made from polystyrene which has a critical stress intensity factor of 1.0 MN $m^{-3/2}$ calculate the maximum permissible pressure in this vessel.

Solution The stress intensity factor for this configuration is

$$K = 3.05\left(\frac{PR_1^2(\pi a)^{1/2}}{(R_2 - R_1)(R_2 + R_1)}\right)$$

The information given in the question may be substituted directly into this equation to give the bursting pressure, P_B, as

$$P_B = \frac{1.0(8 \times 10^{-3})(32 \times 10^{-3})}{3.05(12 \times 10^{-3})^2(\pi \times 3.5 \times 10^{-3})^{1/2}} = 5.6 \text{ MPa}$$

2.19 General fracture behaviour of plastics

If the defect or crack in the plastic is very blunt then the stress intensification effect will be small and although failure will originate from the crack, the failure stress based on the net section will correspond to the failure stress in the uncracked material. If the stress on the material is based on the gross area then what will be observed is a reduction in the failure stress which is directly proportional to the size of the crack. This is shown as line A in Fig. 2.70.

If, however, the defect or crack is sharp then the picture can change significantly. Although ABS and MDPE are special cases, where the materials are insensitive to notch condition, other thermoplastics will exhibit brittle failure if they contain sharp cracks of significant dimensions.

Polycarbonate is perhaps the most notoriously notch-sensitive of all thermoplastics, although nylons are also susceptible to ductile/brittle transitions in failure behaviour caused by notch sharpening. Other plastics such as acrylic, polystyrene and thermosets are always brittle − whatever the crack condition.

For brittle failures we may use the fracture mechanics analysis introduced in the previous sections. From Eqs. (2.96) and (2.99) we may write

$$G_c = \frac{K_c^2}{E} = \frac{\pi \sigma_f^2 a}{E} = \text{constant} \tag{2.110}$$

From this therefore it is evident that the failure stress, σ_f, is proportional to $a^{-1/2}$. This relationship is plotted as line B on Fig. 2.70. This diagram is now very useful because it illustrates the type of ductile/brittle transitions which may be observed in plastics. According to line B, as the flaw size decreases the failure stress tends towards infinity. Clearly this is not the case and in practice what happens is that at some defect size (a_0) the material fails by yielding (line A) rather than brittle fracture.

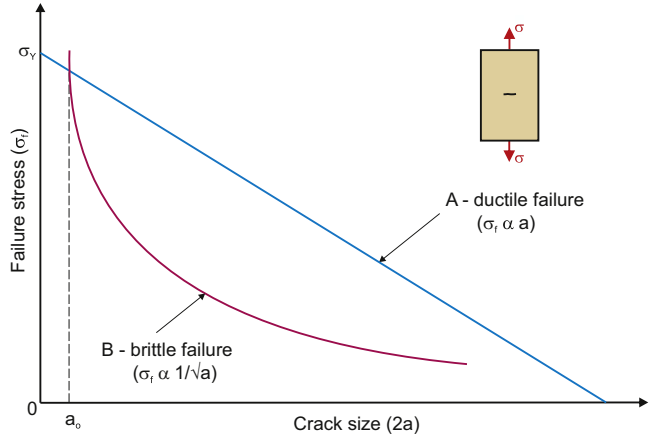


FIG. 2.70 Brittle and ductile failure characteristics for plastics.

This diagram also helps to illustrate why the inherent fracture toughness of a material is not the whole story in relation to brittle fracture. For example, Table 2.3 shows that polystyrene, which is known to be a brittle material, has a K value of about 1 MN $m^{-3/2}$. However, LDPE which has a very high resistance to crack growth also has a K value of about 1 MN $m^{-3/2}$. The explanation is that polyethylene resists crack growth not because it is tough but because it has a low yield strength. If a material has a low yield stress then its yield locus (line A in Fig. 2.70) will be pulled down, possibly below the brittle locus as happens for polyethylene. Fig. 2.71 illustrates some of the variations which are possible in order to alter the ductile/brittle characteristics of plastics. The brittle failure line can be shifted by

TABLE 2.3 Typical fracture toughness parameters for a range of materials (at 20°C).

Material	G_{1c} (kJ/m^2)	K_{1c} (MN/$m^{3/2}$)	$\left(\frac{K_{1c}}{\sigma_y}\right)$	Ductility factor (in mm) $\left(\frac{K_{1c}}{\sigma_y}\right)^{1/2}$
ABS	5	2–4	0.13	17
Acetal	1.2–2	4	0.08	6
Acrylic	0.35 –1.6	0.9–1.6	0.014 –0.023	0.2–0.5
Epoxy	0.1–0.3	0.3–0.5	0.005 –0.008	0.02–0.06
Glass reinforced polyester	5–7	5–7	0.12	14
LDPE	6.5	1	0.125	16
MDPE/HDPE	3.5–6.5	0.5–5	0.025 –0.25	5–100
Nylon 66	0.25–4	3	0.06	3.6
Polycarbonate	0.4–5	1–2.6	0.02 –0.5	0.4–2.7
Polypropylene copolymer	8	3–4.5	0.15 –0.2	22–40
Polystyrene	0.3–0.8	0.7–1.1	0.02	0.4
uPVC	1.3–1.4	1–4	0.03 –0.13	1.1–18
Glass	0.01 –0.02	0.75	0.01	0.1
Mild steel	100	140	0.5	250

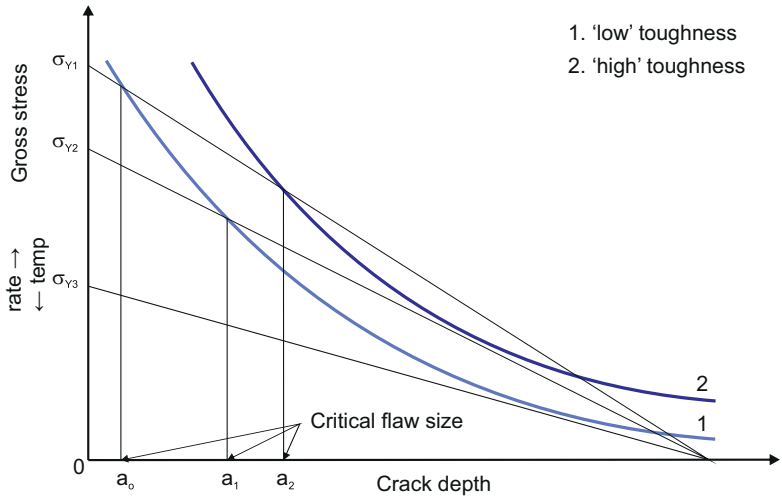


FIG. 2.71 Effect of varying stress field on flaw size for ductile/brittle transition (K = constant).

changes in chemical structure, use of alloying techniques, changes in processing conditions, etc. The yield locus line can be shifted by the use of additives or changes in the ambient temperature or straining rate.

It is apparent therefore that a material's resistance to crack growth is defined not just by its inherent toughness but by its ratio of toughness to yield stress. Some typical values of K_{1c}/σ_y are given in Table 2.3.

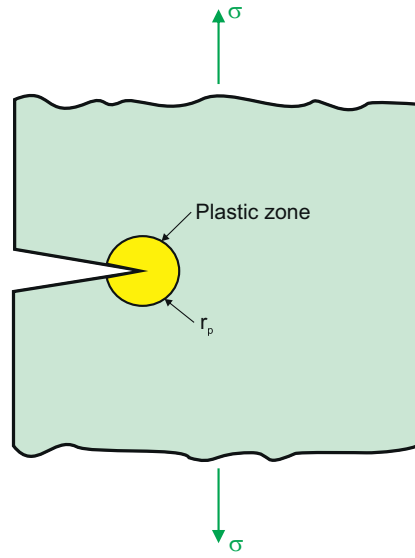
Another approach to the question of resistance to crack growth is to consider the extent to which yielding occurs prior to fracture. In a ductile material it has been found that yielding occurs at the crack tip and this has the effect of blunting the crack. The extent of the plastic zone (see Fig. 2.72) is given by

$$r_p = \frac{1}{2\pi}\left(\frac{K}{\sigma_y}\right)^2 \tag{2.111}$$

for plane stress. The plane strain value is about one-third of this.

The size of the plastic zone can be a useful parameter in assessing toughness and so the ratio $(K_{1c}/\sigma_y)^2$ has been defined as a *ductility factor*. Table 2.3 gives typical values of this for a range of plastics. Note that although the ratio used in the ductility factor is conceptually related to plastic zone size, it utilises K_{1c}. This is to simplify the definition and to remove any ambiguity in relation to the stress field conditions when related to the plastic zone size. It is important that consistent strain rates are used to determine K_{1c} and σ_y, particularly when materials are being compared. For this reason the values in Table 2.3 should not be regarded as definitive. They are given simply to illustrate typical orders of magnitude.

FIG. 2.72 Extent of plastic zone at crack tip.



2.20 Creep failure of plastics

When a constant stress is applied to a plastic it will gradually change in size due to the creep effect which was described earlier. Clearly the material cannot continue indefinitely to get larger and eventually fracture will occur. This behaviour is referred to as **Creep Rupture** although occasionally the less acceptable (to engineers) term of **Static Fatigue** is used. The time taken for the material to fracture will depend on the stress level, the ambient temperature, the type of environment, the component geometry, the molecular structure, the fabrication method, etc. At some stresses the creep rate may be sufficiently low that for most practical purposes the endurance of the material may be regarded as infinite. On the other hand, at high stresses the material is likely to fail shortly after the stress is applied.

The mechanism of time-dependent failure in polymeric materials remains an important area of ongoing research. In the simplest terms it may be considered that as the material creeps, the stress at some point in the material becomes sufficiently high to cause a microcrack to develop but not propagate catastrophically. The stress in the remaining unbroken section of the material will then be incremented by a small amount. This causes a further stable growth of the microcrack so that over a period of time the combined effects of creep and stable crack growth cause a build up of true stress in the material. Eventually a stage is reached when the localised stress at the crack reaches a value which the remaining cross-section of the material is unable to sustain. At this point the crack propagates rapidly across the whole cross-section of the material.

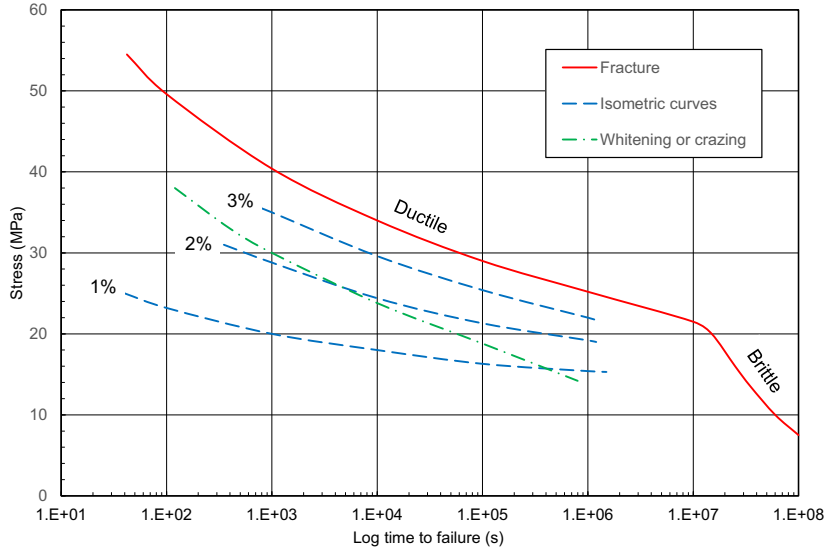


FIG. 2.73 Typical creep rupture behaviour of plastics.

Creep rupture data is usually presented as applied static stress, σ, against the logarithm of time to fracture, t, as shown in Fig. 2.73. If fracture is preceded by phenomena such as crazing (see Section 2.20.2), whitening and/or necking, then it is usual to indicate on the creep rupture characteristics the stage at which these were first observed. It may be seen from Fig. 2.73 that the appearance of crazing or whitening is not necessarily a sign the fracture is imminent. In many cases the material can continue to sustain the applied load for weeks, months or even years after these phenomena are observed. However, there is no doubt that when a load bearing component starts to craze or whiten, it can be disconcerting and so it is very likely that it would be taken out of service at this point. For this reason it is sometimes preferable to use the term **Creep Failure** rather than creep rupture because the material may have been deemed to have failed before it fractures.

Isometric data from the creep curves may also be superimposed on the creep rupture data in order to give an indication of the magnitudes of the strains involved. Most plastics behave in a ductile manner under the action of a steady load. The most notable exceptions are polystyrene, injection moulding grade acrylic and glass-filled nylon. However, even those materials which are ductile at short times tend to become embrittled at long times. This can cause difficulties in the extrapolation of short-term tests, as shown in Fig. 2.73. Other factors which promote brittleness are geometrical discontinuities (stress concentrations) and aggressive environments which are likely to cause ESC (see Section 1.4.2). The absorption of fluids into plastics (e.g. water into nylon) can

also affect their creep rupture characteristics, so advice should be sought where it is envisaged that this may occur.

It may be seen from Fig. 2.73 that in most cases where the failure is ductile the isometric curves are approximately parallel to the fracture curve, suggesting that this type of failure is primarily strain dominated. However, the brittle fracture line cuts across the isometric lines. It may also be seen that whitening or crazing occur at lower strains when the stress is low.

Many attempts have been made to obtain mathematical expressions which describe the time dependence of the strength of plastics. Since for many plastics a plot of stress, σ, against the logarithm of time to failure, t_f, is approximately a straight line, one of the most common expressions used is of the form

$$t_f = Ae^{-B\sigma} \tag{2.112}$$

where A and B are nominally constants although in reality they depend on such things as the structure of the material and on the temperature. Some typical values for A and B at 20°C are given below. It is recommended that the material manufacturers should be consulted to obtain values for particular grades of their materials.

	Acrylic		Polypropylene	
	Sheet	Moulded	Homopolymer	Copolymer
A(s)	1.33×10^{14}	4.73×10^{12}	1.4×10^{13}	1.03×10^{14}
B(m^2/MN)	0.404	0.42	0.88	1.19

One of the most successful attempts to include the effects of temperature in a relatively simple expression similar to the one above, has been made by Zhurkov and Bueche using an equation of the form

$$t_f = t_0 e^{((U_0 - \gamma\sigma)/RT)} \tag{2.113}$$

where

t_0 is a constant which is approximately 10^{-12} s for most plastics
U_0 is the activation energy of the fracture process
γ is a coefficient which depends on the structure of the material
R is the molar gas constant (= 8.314 J/mol° K)
and T is the absolute temperature.

If the values for U_0 and γ for the material are not known then a series of creep rupture tests at a fixed temperature would permit these values to be

determined from the above expression. The times to failure at other stresses and temperatures could then be predicted.

2.20.1 Fracture mechanics approach to creep fracture

Fracture mechanics has also been used to predict failure under static stresses. The basis of this is that observed crack growth rates have been found to be related to the stress intensity factor K by the following equation

$$\frac{da}{dt} = C_1 K^m \tag{2.114}$$

where C_1 and m are material constants.

Now using Eq. (2.100) we may write

$$\frac{da}{dt} = C_1 (Y\sigma)^m (\pi a)^{m/2}$$

If the material contains defects of size $(2a_i)$ and failure occurs when these reach a size $(2a_c)$ then the time to failure, t_f, may be obtained by integrating the above equation.

$$t_f = \frac{2}{C_1 (Y\sigma)^m \pi^{m/2} (m-2)} \left[a_i^{1-m/2} - a_c^{1-m/2} \right] \tag{2.115}$$

Although Eqs. (2.112), (2.113) and (2.115) can be useful they must not be used indiscriminately. For example, they are seldom accurate at short times but this is not a major worry since such short-time failures are usually not of practical interest. At long times they can also be inaccurate due to the embrittlement problem referred to earlier. In practice therefore it is generally advisable to use the equations in combination with safety factors as recommended by the appropriate national and international standards.

2.20.2 Crazing in plastics

When a tensile stress is applied to an amorphous (glassy) plastic, such as polystyrene, crazes may be observed to occur before fracture. Crazes are like cracks in the sense that they are wedge shaped and form perpendicular to the applied stress. However, they may be differentiated from cracks by the fact that they contain polymeric material which is stretched in a highly oriented manner perpendicular to the plane of the craze, i.e. parallel to the applied stress direction. Another major distinguishing feature is that unlike cracks, they are able to bear stress. Under static loading, the strain at which crazes start to form, decreases as the applied stress decreases. In constant strain rate testing the crazes always start to form at a well defined stress level. Of course, as with all aspects of the behaviour of plastics other factors such as temperature will influence the levels of stress and strain involved. Even a relatively

low stress may induce crazing after a period of time, although in some glassy plastics there is a lower stress limit below which crazes will never occur. This is clearly an important stress for design considerations. However, the presence of certain liquids (organic solvents) can initiate crazing at stresses far below this lower stress limit. This phenomenon of solvent crazing has been the cause of many service failures because it is usually impossible to foresee every environment in which a plastic article will be used.

There is considerable evidence to show that there is a close connection between crazing and crack formation in amorphous plastics. At certain stress levels, crazes will form and studies have shown that cracks can nucleate in the crazes and then propagate through the preformed craze matter. In polystyrene, crazes are known to form at relatively low stresses and this has a significant effect on crack growth mechanisms in the material. In particular, during fracture toughness testing, unless great care is taken the material can appear to have a greater toughness than acrylic to which it is known to be inferior in practice. The reason is that the polystyrene can very easily form bundles of crazes at the crack tip and these tend to blunt the crack.

If a plastic article has been machined then it is likely that crazes will form at the surface. In moulded components, internal nucleation is common due to the presence of localised residual stresses.

2.21 Fatigue of plastics

The failure of a material under the action of a fluctuating load, namely **fatigue**, has been recognised as one of the major causes of fracture in metals. Although plastics are susceptible to a wider range of failure mechanisms it is likely that fatigue still has an important part to play. For metals the fatigue process is generally well understood, being attributed to stable crack propagation from existing crack-like defects or crack initiation and propagation from structural microflaws known as dislocations. The cyclic action of the load causes the crack to grow until it is so large that the remainder of the cross-section cannot support the load. At this stage there is a catastrophic propagation of the crack across the material in a single cycle. Fatigue failures in metals are always brittle and are particularly serious because there is no visual warning that failure is imminent. The knowledge of dislocations in metals stems from a thorough understanding of crystal structure, and dislocation theory for metals is at an advanced stage. Unfortunately the same cannot be said for polymer fatigue. In this case the completely different molecular structure means that there is unlikely to be a similar type of crack initiation process although it is possible that once a crack has been initiated, the subsequent propagation phase may be similar.

If a plastic article has been machined then it is likely that this will introduce surface flaws capable of propagation, and the initiation phase of failure will be negligible. If the article has been moulded this tends to produce a

protective skin layer which inhibits fatigue crack initiation/propagation. In such cases it is more probable that fatigue cracks will develop from within the bulk of the material. In this case the initiation of cracks capable of propagation may occur through slip of molecules if the polymer is crystalline. There is also evidence to suggest that the boundaries of spherulites are areas of weakness which may develop cracks during straining as well as acting as a crack propagation path. In amorphous polymers it is possible that cracks may develop in the voids which are formed during viscous flow.

Moulded plastics will also have crack initiation sites created by moulding defects such as weld lines, gates, etc. and by filler particles such as pigments, stabilisers, etc. and, of course, stress concentrations caused by sharp geometrical discontinuities will be a major source of fatigue cracks. Fig. 2.74 shows a typical fatigue fracture in which the crack has propagated from a surface flaw.

There are a number of additional features which make polymer fatigue a complex subject and not one which lends itself to simple analysis. The very nature of the loading means that stress, strain and time are all varying simultaneously. The viscoelastic behaviour of the material means that strain rate (or frequency) is an important factor. There are also special variables peculiar to this type of testing such as the type of control (whether controlled load or controlled deformation), the level of the mean load or mean deformation and the shape of the cyclic waveform. To add to the complexity, the inherent damping and low thermal conductivity of plastics causes a temperature rise during fatigue. This may bring about a deterioration in the mechanical properties of the material or cause it to soften so much that it becomes useless in any load bearing application.

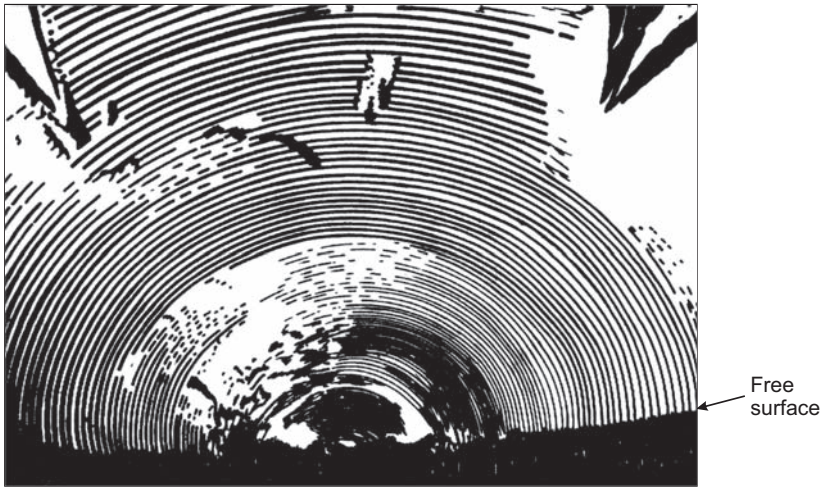


FIG. 2.74 Typical fatigue fracture surface.

Another important aspect of the fatigue of all materials is the statistical nature of the failure process and the scatter which this can cause in the results. In a particular sample of plastic there is a random distribution of microcracks, internal flaws and localised residual stresses. These defects may arise due to structural imperfections (for example, molecular weight variations) or as a result of the fabrication method used for the material. There is no doubt that failure processes initiate at these defects and so the development and propagation of a crack will depend on a series of random events. Since the distribution and size of the flaws are likely to be quite different, even in outwardly identical samples, then the breaking strength of the plastic is a function of the probability of a sufficiently large defect being correctly oriented in a highly stressed region of the material. Since there is a greater probability of a suitable defect existing in a large piece of material there may be a size effect. The most important point to be realised is that the breaking strength of a material is not a unique value which can be reproduced at will. At best there may be a narrow distribution of strength values but in all cases it is essential to satisfy oneself about the statistical significance of a single data point. The design procedures which are most successful at avoiding fracture usually involve the selection of a factor of safety which will reduce the probability of failure to an acceptably low value.

2.21.1 Effect of cyclic frequency

Consider a sample of plastic which is subjected to a fixed cyclic stress amplitude of $\pm\sigma_1$. The high damping and low thermal conductivity of the material means that some of the input energy will be dissipated in each cycle and will appear as heat. The temperature of the material will rise therefore, as shown in Fig. 2.75. Eventually a stage will be reached when the heat transfer to the surroundings equals the energy dissipation. At this point the temperature of the material stabilises until a conventional brittle fatigue failure occurs. This failure may be plotted on a graph of stress amplitude against the logarithm of the number of cycles to fracture as shown in Fig. 2.76. If, in the next test, the stress amplitude is increased to σ_2 then the material temperature will rise again and stabilise at a higher value as shown in Fig. 2.75. Continued cycling then leads to a fatigue failure as shown in Fig. 2.76. Higher stress amplitudes in subsequent tests will repeat this pattern until a point is reached when the temperature rise no longer stabilises. Instead the temperature continues to rise and results in a short term thermal softening failure in the material. Stress amplitudes above this crossover stress level will cause thermal failures in an even shorter time. The nett result of this is that the fatigue curve in Fig. 2.76 has two distinct regimes. One for the relatively short-term thermal failures and one for the long-term conventional fatigue failures.

If the frequency of cycling is reduced then stress amplitudes which would have produced thermal softening failures at the previous frequency, now result

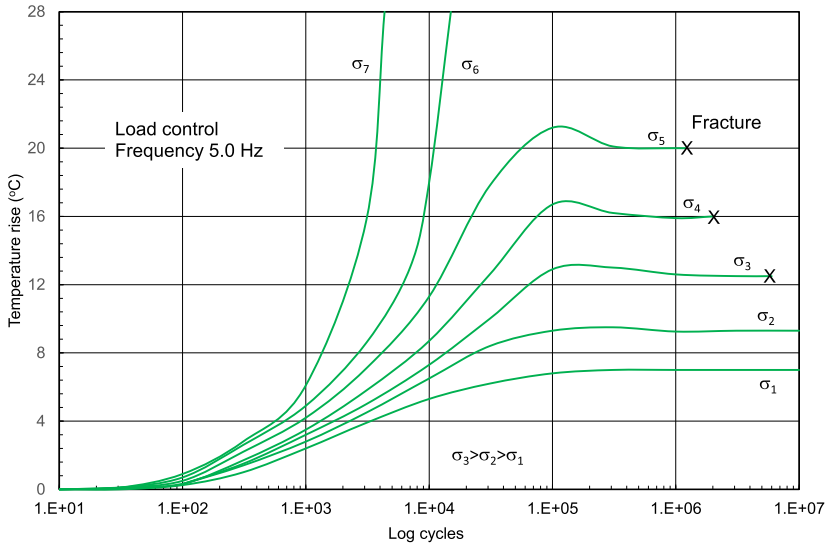


FIG. 2.75 Temperature rise during cyclic loading.

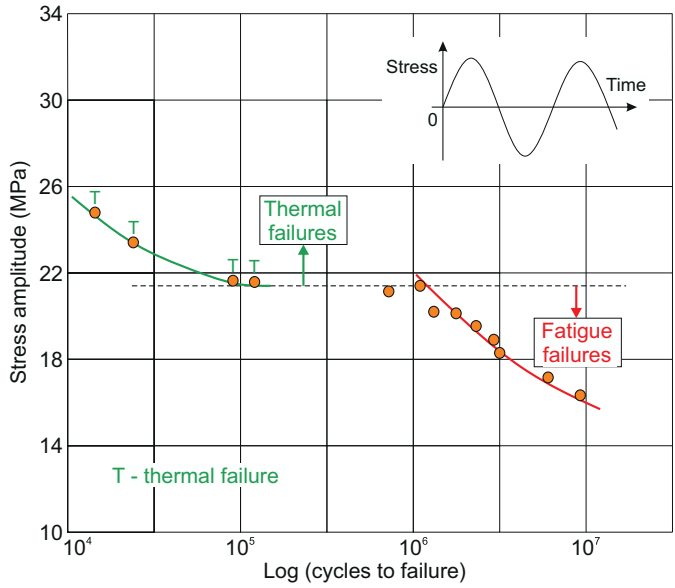


FIG. 2.76 Typical fatigue behaviour of acetal at 5 Hz.

in stable temperature rises and eventually fatigue failures. Normally it is found that these fatigue failures fall on the extrapolated curve from the fatigue failures at the previous frequency. Even at the lower frequency, however, thermal softening failures will occur at high stress levels. If fatigue failures are

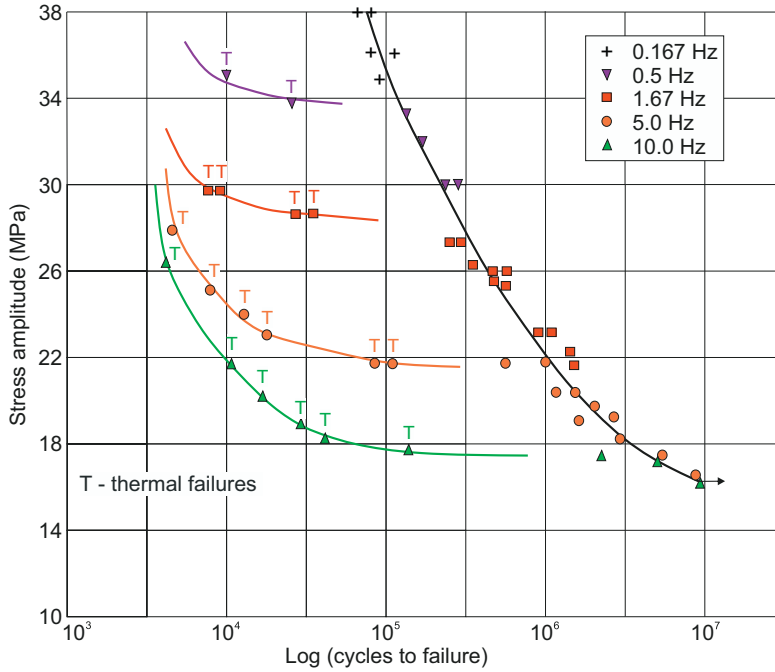


FIG. 2.77 Typical fatigue behaviour of acetal at several frequencies.

to occur at these high stresses, then the frequency must be reduced still further. The overall picture which develops therefore is shown in Fig. 2.77. In some plastics the fatigue failure curve becomes almost horizontal at large values of N. The stress level at which this occurs is clearly important for design purposes and is known as the *fatigue limit.* For plastics in which fatigue failures continue to occur even at relatively low stress levels it is necessary to define an *endurance limit* i.e. the stress level which would not cause fatigue failure until an acceptably large number of stress cycles.

The occurrence of thermal failures in a plastic depends not only on the cyclic frequency and applied stress level but also on the thermal and damping characteristics of the material. For example, polycarbonate has very little tendency towards thermal failures whereas with polypropylene there is a marked propensity in this direction. Thermosets, of course, are very thermally stable and only exhibit brittle fatigue failures.

2.21.2 Effect of waveform

Assuming that the cyclic waveform used in the previous section was sinusoidal then the effect of using a square wave is to reduce, at any frequency, the level of stress amplitude at which thermal softening failures start to occur. This is

because there is a greater energy dissipation per cycle when a square wave is used. If a ramp waveform is applied, then there is less energy dissipation per cycle and so higher stresses are possible before thermal runaway occurs.

2.21.3 Effect of testing control mode

During cyclic loading of a material the energy dissipated is proportional to the product of the stress and strain. If the loading on a plastic is such that the stress amplitude is maintained constant, then any temperature rise in the material will lead to an increase in strain since the modulus decreases with temperature. The increase in strain means that more energy is dissipated, leading to a further drop in modulus and a further increase in strain. It is this type of chain reaction which leads to the thermal softening failures if the heat transfer to the surroundings is insufficient.

The alternative mode of testing is to control the strain amplitude. In this case an increase in temperature again causes a drop in modulus but this leads to a drop in stress amplitude. There is therefore a drop in energy dissipation and hence temperature. In this case it is found that this self-stabilising mechanism prevents the occurrence of thermal softening failures. The nett result is that under this mode of control the temperature rise always stabilises and only fatigue type failures are observed.

2.21.4 Effect of mean stress

For convenience, in the previous sections it has been arranged so that the mean stress is zero. However, in many cases of practical interest the fluctuating stresses may be always in tension (or at least biased towards tension) so that the mean stress is not zero. The result is that the stress system is effectively a constant mean stress, σ_m superimposed on a fluctuating stress σ_a. Since the plastic will creep under the action of the steady mean stress, this adds to the complexity because if the mean stress is large then a creep rupture failure may occur before any fatigue failure. The interaction of mean stress and stress amplitude is usually presented as a graph of (σ_a vs σ_m) as shown in Fig. 2.78. This represents the locus of all the combinations of σ_a and σ_m which cause fatigue failure in a particular number of cycles, N. For plastics the picture is slightly different from that observed in metals. Over the region WX the behaviour is similar in that as the mean stress increases, the stress amplitude must be decreased to cause failure in the same number of cycles. Over the region YZ, however, the mean stress is so large that creep rupture failures are dominant. Point Z may be obtained from creep rupture data at a time equal to that necessary to give N cycles at the test frequency. It should be realised that, depending on the level of mean stress, different phenomena may be the cause of failure.

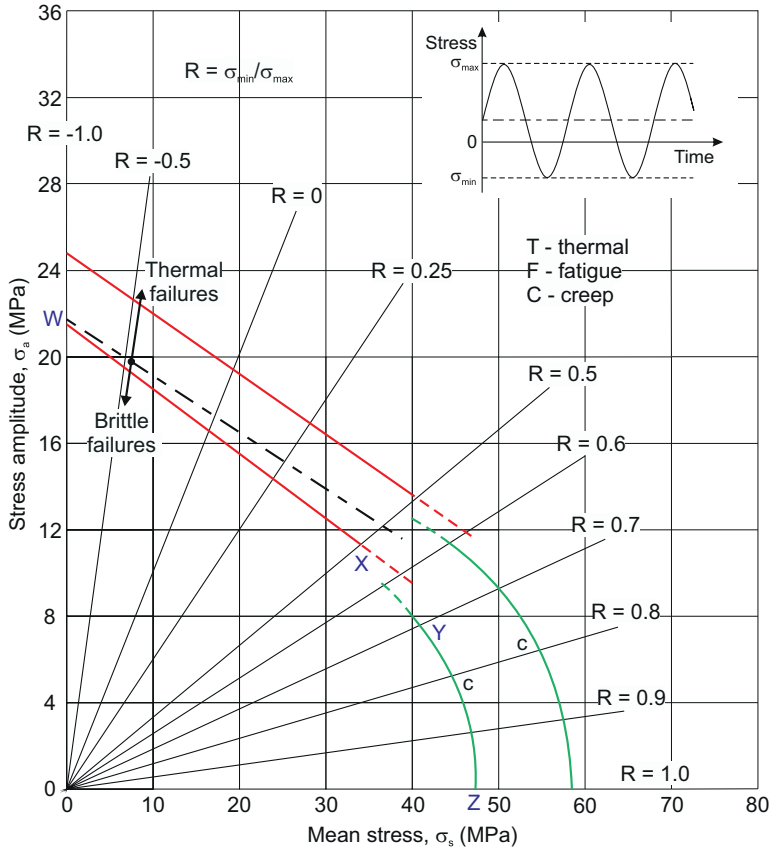


FIG. 2.78 Relationships between stress amplitude and mean stress.

The level of mean stress also has an effect on the occurrence of thermal failures. Typically, for any particular stress amplitude the stable temperature rise will increase as the mean stress increases. This may be to the extent that a stress amplitude which causes a stable temperature rise when the mean stress is zero, can result in a thermal runaway failure if a mean stress is superimposed.

For design purposes it is useful to have a relationship between σ_a and σ_m, similar to those used for metals (e.g. the Soderberg and Goodman relationships). It is suggested that the equation of a straight line joining points W and Z in Fig. 2.78 would be best because it is simple and will give suitably conservative estimates for the permissible combinations of σ_a and σ_m to produce failure in a pre-selected number of cycles. Such an equation would have the form

$$\sigma_a = \sigma_f \left(1 - \frac{\sigma_m}{\sigma_c}\right) \tag{2.116}$$

where σ_f is the fatigue endurance at N cycles., σ_c is the creep rupture strength at a time equivalent to N cycles.

Example 2.21. A rod of plastic is subjected to a steady axial pull of 50 N and superimposed on this is an alternating axial load of ± 100 N. If the fatigue limit for the material is 13 MPa and the creep rupture strength at the equivalent time is 40 MPa, estimate a suitable diameter for the rod. Thermal effects may be ignored and a fatigue strength reduction factor of 1.5 with a safety factor of 2.5 should be used.

Solution The alternating stress, σ_a is given by

$$\sigma_a = \frac{\text{Alternating load}}{\text{area}} = \frac{4 \times 100}{\pi d^2} (\text{MPa})$$

Also the mean stress, σ_m, is given by

$$\sigma_m = \frac{\text{Steady load}}{\text{area}} = \frac{4 \times 50}{\pi d^2} (\text{MPa})$$

Then using Eq. (2.116)

$$\sigma_a = \sigma_f \left(1 - \frac{\sigma_m}{\sigma_c}\right)$$

So applying the fatigue strength reduction factor and the factor of safety

$$\frac{2.5 \times 4 \times 100}{\pi d^2} = \frac{13}{1.5} \left(1 - \frac{4 \times 50 \times 2.5}{\pi d^2 \times 40}\right)$$

This may be solved to give $d = 6.4$ mm.

2.21.5 Effect of stress system

In the previous sections the stress system has been assumed to be cyclic uniaxial loading since this is the simplest to analyse. If, however, the material is subjected to bending, then this will alter the stress system and hence the fatigue behaviour. In general it is found that a sample subjected to fluctuating bending stresses will have a longer fatigue endurance than a sample of the same material subjected to a cyclic uniaxial stress. This is because of the stress gradient across the material in the bending situation. Fatigue cracks are initiated by the high stress at the surface but the rate of crack propagation is reduced due to the lower stresses in the bulk of the material. In addition, the crack initiation phase may have to be lengthened. This is because mouldings have a characteristic skin which appears to resist the formation of fatigue

cracks. Under uniaxial loading the whole cross-section is subjected to the same stress and cracks will be initiated at the weakest region.

The stress gradient also means that the occurrence of thermal softening failures is delayed. At any particular frequency of stressing, thermal softening failures will not occur until higher stresses if the stress system is bending rather than uniaxial.

2.21.6 Fracture mechanics approach to fatigue

During fatigue the stress amplitude usually remains constant and brittle failure occurs as a result of crack growth from a sub-critical to a critical size. Clearly the rate at which these cracks grow is the determining factor in the life of the component. It has been shown quite conclusively for many polymeric materials that the rate at which cracks grow is related to the stress intensity factor by a relation of the form

$$\frac{da}{dN} = C_2(\Delta K)^n \tag{2.117}$$

where $\frac{da}{dN}$ is the crack growth rate.

ΔK is the alternating stress intensity factor corresponding to the stress range $\Delta\sigma$ (i.e. $\Delta K = K_{\max} - K_{\min}$) and C_2 and n are constants.

Hence a graph of $\log(da/dN)$ against $\log(\Delta K)$ will be a straight line of slope n as shown Fig. 2.79. Now, in Section 3.4 it was shown that the range of stress intensity factor could be represented by a general equation of the form

$$K = Y\sigma(\pi a)^{1/2} \text{ or } \Delta K = Y(\Delta\sigma)(\pi a)^{1/2} \tag{2.118}$$

where Y is a geometry function.

Thus, combining Eqs. (2.117) and (2.118) gives

$$\frac{da}{dN} = C_2\left(Y(\Delta\sigma)(\pi a)^{1/2}\right)^n$$

Assuming that the geometry function, Y, does not change as the crack grows then this equation may be integrated to give the number of cycles, N_f, which are necessary for the crack to grow from its initial size ($2a_i$) to its critical size at fracture ($2a_c$).

$$\int_{a_i}^{a_c} \frac{1}{YC_2(\Delta\sigma)n\pi^{n/2}} \cdot \frac{da}{a^{n/2}} = \int_0^{N_f} dN$$

Assuming $n \neq 2$

$$\frac{2}{YC_2(\Delta\sigma)^n\pi^{n/2}(2-n)}\left\{a_c^{(1-n/2)} - a_i^{(1-n/2)}\right\} = N_f \tag{2.119}$$

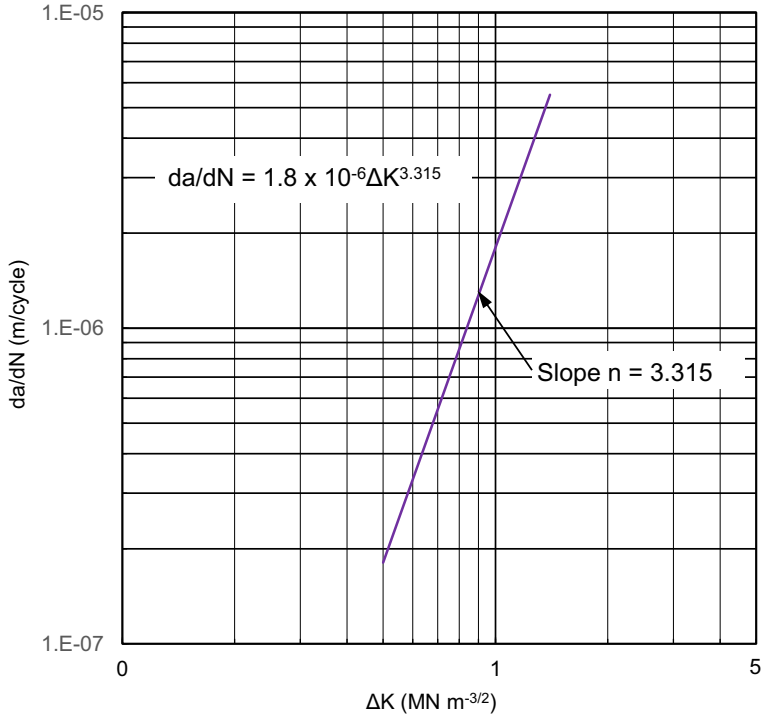


FIG. 2.79 Crack growth rate as a function of stress intensity factor.

The way in which this sort of approach may be used to design articles subjected to fatigue loading is illustrated in the following example.

Example 2.22. A certain grade of acrylic has a K_c value of 1.6 MN $m^{-3/2}$ and the fatigue crack growth data as shown in Fig. 2.79. If a moulding in this material is subjected to a stress cycle which varies from 0 to 15 MPa, estimate the maximum internal flaw size which can be tolerated if the fatigue endurance is to be at least 10^5 cycles.

Solution The first step is to calculate the critical flaw size which will cause brittle failure to occur in one cycle. This may be obtained from Eq. (2.100) assuming $Y = 1$.

$$K = \sigma(\pi a)^{1/2}$$

or

$$a_c = \left(\frac{K_c}{\sigma}\right)^2 \frac{1}{\pi} = \left(\frac{1.6}{15}\right)^2 \frac{1}{\pi} = 3.62 \times 10^{-3}\text{m}$$

During cyclic loading, any cracks in the material will propagate until they reach this critical size. If the article is to have an endurance of at least 10^5 cycles then Eq. (2.119) may be used to determine the size of the smallest flaw which can be present in the material before cycling commences.

$$a_c^{(2-n)/2} - a_i^{(2-n)/2} = \frac{C_2}{2} N(\Delta\sigma)^n \pi^{n/2}(2-n)$$

Using $C_2 = 1.8 \times 10^{-6}$ and $n = 3.315$ from Fig. 2.79 then $a_i = 1.67\ \mu$m. Therefore the inspection procedures must ensure that there are no defects larger than $(2 \times 1.67) = 3.34\ \mu$m in the material before the cyclic stress is applied.

2.22 Impact behaviour of plastics

The resistance to impact is one of the key properties of materials. The ability of a material to withstand accidental knocks can decide its success or failure in a particular application. It is ironical therefore that for plastics this is one of the least well defined properties. Although impact test data is widely quoted in the literature, most of it is of little value because impact strength is not an inherent material property and hence it is not possible to specify a unique universal value for the impact strength of any plastic. Impact strength depends on a range of variables including temperature, straining rate, stress system, anisotropy, geometry of the article, fabrication conditions, environment and so on. As a result of this there is often a poor correlation (a) between laboratory test data and product performance and (b) between test results from different laboratories. The first of these problems is the more serious because it can raise doubts in the mind of the designer about the use of plastics.

Fortunately the situation in practice is not quite as complex as it might seem. In general, very acceptable designs are achieved by using impact data obtained under conditions which relate as closely as possible to the service conditions. Impact strength values available in the literature may be used for the initial selection of a material on the basis of a desired level of toughness. Then, wherever possible this should be backed up by tests on the plastic article, or a specimen cut from it, to ensure that the material, as moulded, is in a satisfactory state to perform its function.

As always, of course, to alleviate fracture problems it is essential to avoid the factors which are likely to cause brittleness. These include stress concentrations and low temperatures and the effects of these will be considered in the following sections.

2.22.1 Effect of stress concentrations

During service the impact behaviour of a plastic article will be influenced by the combined effects of the applied stress system and the geometry of the

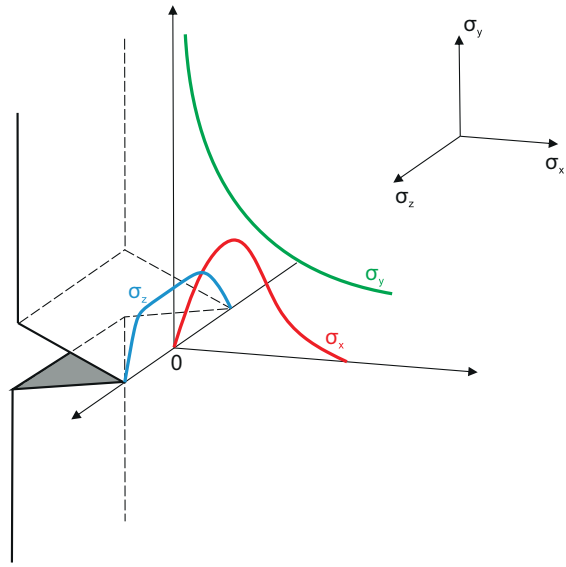


FIG. 2.80 Triaxial stress distribution at a notch.

article. Although the applied stress system may appear simple (for example, uniaxial) it may become triaxial in local areas due to a geometrical discontinuity. Fig. 2.80 shows the triaxial stresses which exist at the tip of a notch. It is this triaxiality which promotes brittleness in the material. Therefore, in practice one should avoid abrupt changes in section, holes, notches, keyways etc. at critical, highly stressed areas in a moulding.

In the laboratory the impact behaviour of a material could be examined by testing plain samples, but since brittle failures are of particular interest it is more useful to ensure that the stress system is triaxial. This may be achieved most conveniently by means of a notch in the sample. The choice of notch depth and tip radius will affect the impact strengths observed. A sharp notch is usually taken as 0.25 mm radius and a blunt notch as 2 mm radius.

Fig. 2.81 shows the typical variation of impact strength with notch tip radius for several thermoplastics. The first important fact to be noted from this graph is that the use of a sharp notch will rank the plastics materials in a different order to that obtained using a blunt notch. This may be explained by considering the total impact strength as consisting of both crack initiation and crack propagation energy. When the very sharp notch (0.25 mm radius) is used it may be assumed that the energy necessary to initiate the crack is small and the main contribution to the impact strength is propagation energy. On this basis, Fig. 2.81 shows that high density polyethylene and ABS have relatively high crack propagation energies whereas materials such as PVC, nylon and acrylic have low values. The significant improvement in impact strength for

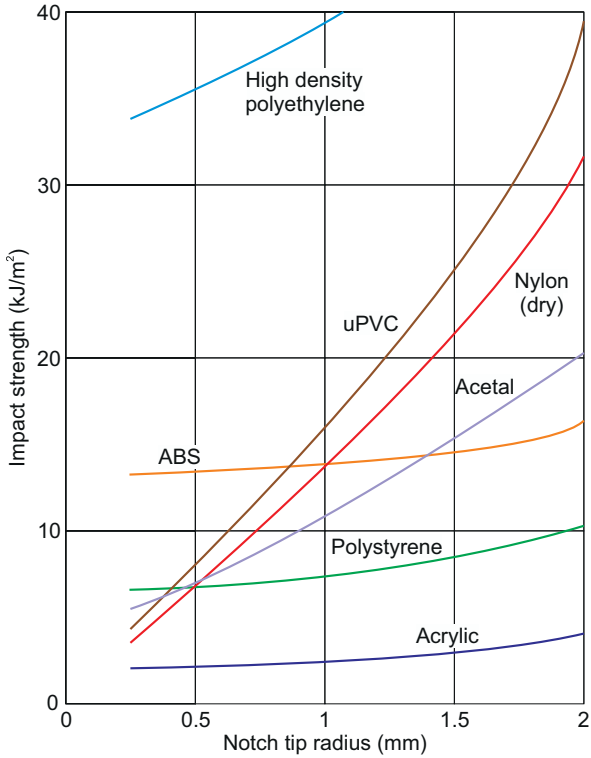


FIG. 2.81 Variation of impact strength with notch radius for several thermoplastics.

PVC and nylon when a blunt notch is used would suggest that their crack initiation energies are high. However, the smaller improvement in the impact behaviour of ABS with a blunt notch indicates that the contribution from crack initiation energy is low.

Graphs such as Fig. 2.81 also give a convenient representation of the notch sensitivity of materials. For example it may be seen that sharp notches are clearly detrimental to all the materials tested and should be avoided in any good design. However, it is also apparent that the benefit derived from using generously rounded corners is much less for ABS than it is for materials such as nylon or PVC.

Impact strength also increases as the notch depth is decreased. The variation of impact strength with notch depth and radius may be rationalised for some materials by use of the linear elastic stress concentration expression.

$$K_t = 1 + 2(a/r)^{1/2} \tag{2.120}$$

where 'r' is the notch radius and 'a' is the notch depth.

It has been shown that for acrylic, glass-filled nylon and polymethylpentene there is reasonable correlation between the reciprocal of the stress concentration factor, K_t, and impact strength. However, for PVC good correlation could only be achieved if the finite dimensions of the sample were taken into account in the calculation of stress concentration factor.

2.22.2 Effect of temperature

In most cases thermoplastic components are designed for use at room temperature. It might appear, therefore, that data on the impact properties at this temperature (approximately 20°C) would provide sufficient information for design. However, this approach would be rather naive since even indoors, temperatures may vary by an amount which can have a significant effect on impact behaviour. For components used outdoors of course, the situation can be much worse with conditions varying from sub-zero to tropical. In common with metals, many plastics exhibit a transition from ductile behaviour to brittle as the temperature is reduced.

Fig. 2.82 is typical of the effects which may be observed with several common plastics materials. Quite apart from the changes in impact strength

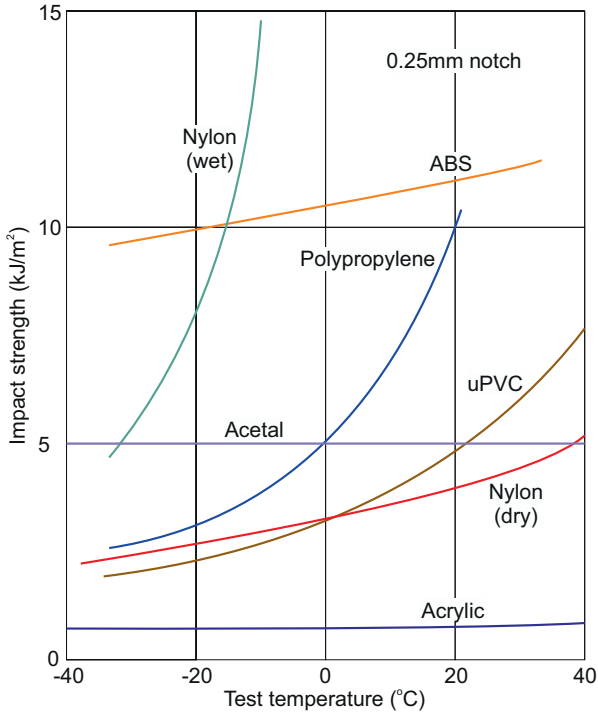


FIG. 2.82 Variation of impact strength with temperature for several thermoplastics.

with temperature an important lesson which should be learned from this diagram is that the ranking of the materials is once again influenced by the test conditions. For example, at 20°C polypropylene is superior to acetal whereas at −20°C it exhibits a considerable drop in impact strength to give it a poorer performance than acetal.

It may be seen from Fig. 2.82 that some plastics experience the change from ductile to brittle behaviour over a relatively narrow temperature range. This permits a tough/brittle transition temperature to be quoted. In other plastics this transition is much more gradual so that it is not possible to attribute it to a single value of temperature. In these circumstances it is common to quote a *Brittleness Temperature*, $T_B(1/4)$. This temperature is defined as the value at which the impact strength of the material with a sharp notch (1/4 mm tip radius) equals 10 kJ/m^2. This temperature, when quoted, gives an indication of the temperature above which there should be no problems with impact failures. It does not mean that the material should never be used below $T_B(1/4)$ because by definition it refers only to the sharp notch case. When the material has a blunt notch or is unnotched its behaviour may still be satisfactory well below $T_B(1/4)$.

2.22.3 Miscellaneous factors affecting impact

Other factors which can affect impact behaviour are fabrication defects such as internal voids, inclusions and additives such as pigments, all of which can cause stress concentrations within the material. In addition, internal welds caused by the fusion of partially cooled melt fronts usually turn out to be areas of weakness. The environment may also affect impact behaviour. Plastics exposed to sunlight and weathering for prolonged periods tend to become embrittled due to degradation. Alternatively if the plastic is in the vicinity of a fluid which attacks it, then the crack initiation energy may be reduced. Some plastics are affected by very simple fluids e.g. domestic heating oils act as plasticisers for polyethylene. The effect which water can have on the impact behaviour of nylon is also spectacular as illustrated in Fig. 2.82.

The surface finish of the specimen may also affect impact behaviour. Machined surfaces usually have tool marks which act as stress concentrations whereas moulded surfaces have a characteristic skin which can offer some protection against crack initiation. If the moulded surface is scratched, then this protection no longer exists. In addition, mouldings occasionally have an embossed surface for decorative effect and tests have shown that this can cause a considerable reduction in impact strength compared to a plain surface.

2.22.4 Impact test methods

The main causes of brittleness in materials are known to be.

(1) triaxiality of stress

(2) high strain rates, and
(3) low temperatures.

In order to provide information on the impact behaviour of materials, metallurgists developed tests methods which involved striking a notched bar with a pendulum. This conveniently subjected the material to triaxiality of stress (at the notch tip) and a high strain rate so as to encourage brittle failures. The standard test methods are the Izod and Charpy tests which use the test procedures illustrated in Fig. 2.83(a) and (b). The specimens have a standard notch machined in them and the impact energy absorbed in breaking the specimen is recorded. With the ever-increasing use of plastics in engineering applications it seemed appropriate that these well established test methods should be adopted. However, even the metallurgists recognised that the tests do have certain short-comings. The main problem is that the test conditions are arbitrary. The speed of impact, method of stressing and specimen geometry are fixed and experience has shown that it was too much to expect the results to be representative of material behaviour under different conditions.

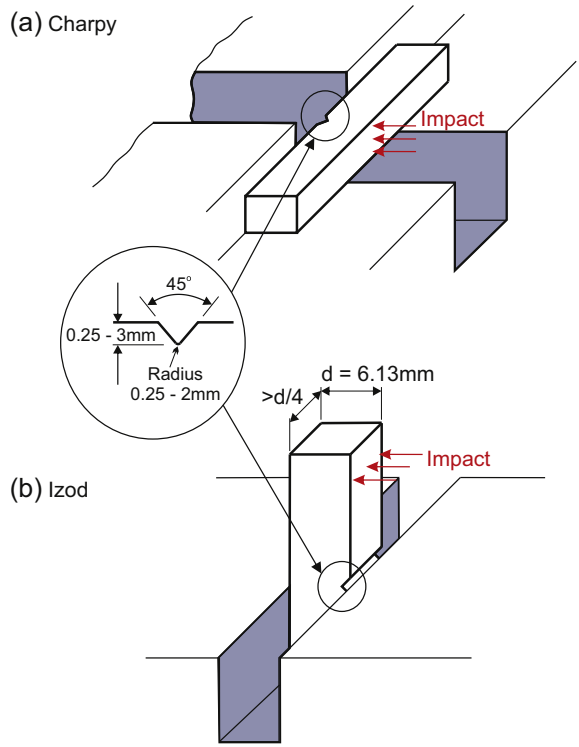


FIG. 2.83 Pendulum impact tests.

In particular, standard specimens contain a sharp notch so that it is propagation energy rather than initiation energy which is the dominant factor. In general the standard tests are useful for quality control and specification purposes but not for the prediction of end-product performance. The complex interaction of the variables does not permit component designs to be based on the data. A material which appears bad in the standard tests will not necessarily be bad in service.

Although the Izod and Charpy tests are widely used for plastics, other types of test are also popular. These include tensile impact tests and flexural plate (falling weight) tests. The latter is particularly useful in situations where the effects of flow anisotropy are being assessed. In addition, arbitrary end-product tests are widely used to provide reassurance that unforeseen factors have not emerged to reduce the impact performance of the product.

The results of impact tests are often scattered even with the most careful test procedures. In these circumstances it is normal practice to quote the median strength rather than the average. This is because the median will be more representative of the bulk of the results if there are odd very high or very low results. An unbroken sample can also be allowed for in median analysis but not when the average is used.

Impact strength are normally quoted as

$$\text{Impact Strength} = \frac{\text{Energy to break}}{\text{area at notch section}} \left(\text{J}/\text{m}^2\right)$$

Occasionally the less satisfactory term of energy to break per unit width may be quoted in units of J/m.

In some applications impact performance may not be critical and only a general knowledge of a materials behaviour is needed. In these circumstances it would be unrealistic to expect the designer to sift through all the combination of multi-point data. Therefore diagrams such as Fig. 2.84 can be useful for providing an overall indication of the general impact performance to be expected from different plastics. However, this type of general guide should be used with caution because it oversimplifies in at least two important respects. It ignores the plane stress/plane strain toughness transition which causes the order of merit to depend on the material thickness. Also it ignores the effect of molecular orientation except insofar as this particular diagram refers to specimens cut from one sort of moulding.

2.22.5 Fracture mechanics approach to impact

In recent years impact testing of plastics has been rationalised to a certain extent by the use of fracture mechanics. The most successful results have been achieved by assuming that LEFM assumptions (bulk linear elastic behaviour and presence of sharp notch) apply during the Izod and Charpy testing of a plastic.

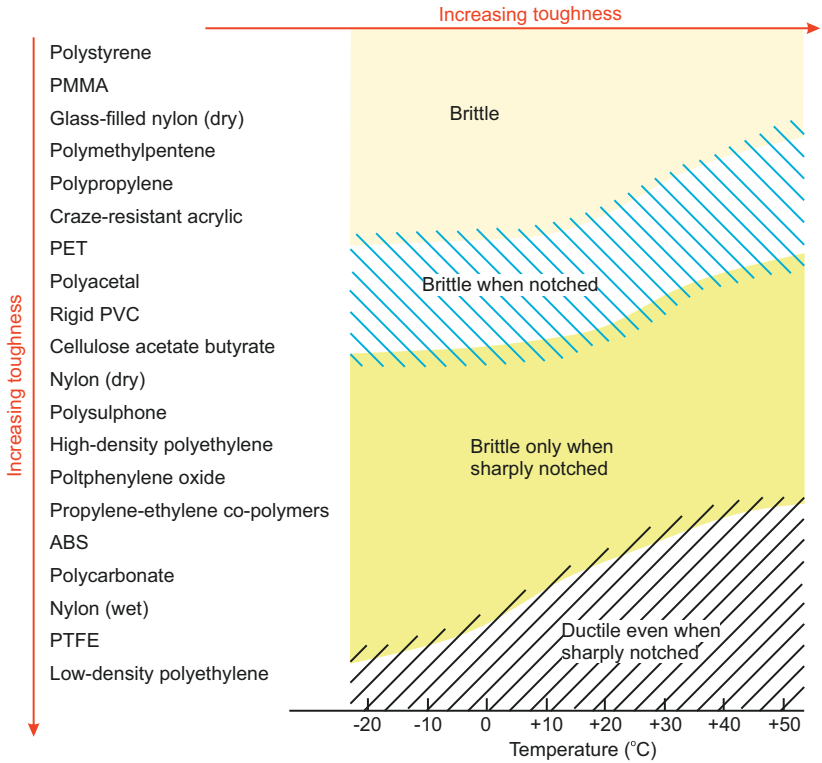


FIG. 2.84 Comparison of impact strengths as measured by Charpy test.

During these types of test it is the energy absorbed at fracture, U_c, which is recorded. In terms of the applied force, F_c, and sample deformation, δ, this will be given by

$$U_c = \frac{1}{2} F_c \delta \tag{2.121}$$

or expressing this in terms of the compliance, from Eq. (2.90)

$$U_c = \frac{1}{2} F_c^2 C \tag{2.122}$$

Now, from Eq. (2.91) we have the expression for the toughness, G_c, of the material

$$G_c = \frac{F_c^2}{2B} \frac{\partial C}{\partial a}$$

So using Eq. (2.122) and introducing the material width, D

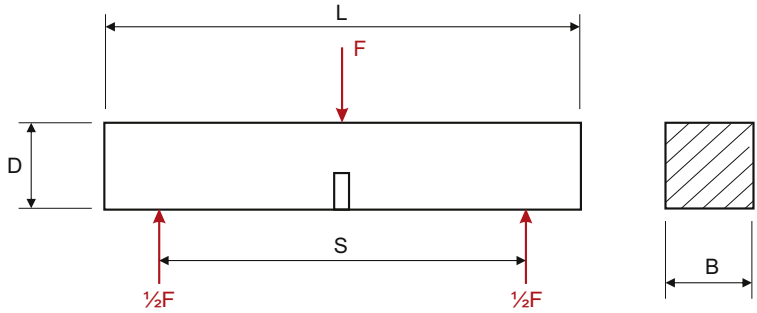


FIG. 2.85 Charpy test piece.

$$G_c = \frac{U_c}{BD\phi} \tag{2.123}$$

where $\phi = ((1/C)(\partial C/\partial a))^{-1}$. This is a geometrical function which can be evaluated for any geometry (usually by finite element analysis). Fig. 2.85 shows the preferred test geometry for a Charpy-type test and Table 2.4 gives the values of ϕ for this test configuration. Other values of ϕ may be determined by interpolation.

It is apparent from Eq. (2.123) that a graph of $BD\phi$ against fracture energy U_c (using different crack depths to vary ϕ) will be a straight line, the slope of which is the material toughness, G_c.

TABLE 2.4 Charpy calibration factor (ϕ).

	ϕ values		
a/D	S/D = 4	S/D = 6	S/D = 8
0.06	1.183	1.715	2.220
0.10	0.781	1.112	1.423
0.20	0.468	0.631	0.781
0.30	0.354	0.450	0.538
0.40	0.287	0.345	0.398
0.50	0.233	0.267	0.298
0.60	0.187	0.205	0.222

Example 2.23. A series of Charpy impact tests on uPVC specimens with a range of crack depths gave the following results

Crack length (mm)	1	2	3	4	5
Fracture energy (mJ)	100	62	46.5	37	31

If the sample section is 10 mm × 10 mm, and the support width is 40 mm calculate the fracture toughness of the uPVC. The modulus of the uPVC is 2 GPa.

Solution Since $B = D = 10$ mm and using the values of ϕ from Table 2.4 we may obtain the following information.

a(mm)	*a/D*	ϕ	$BD\phi$	*U(mJ)*
1	0.1	0.781	78.1×10^{-6}	100
2	0.2	0.468	46.8×10^{-6}	62
3	0.3	0.354	35.4×10^{-6}	46.5
4	0.4	0.287	28.7×10^{-6}	37
5	0.5	0.233	23.3×10^{-6}	31

A graph of U against $BD\phi$ is given in Fig. 2.86. The slope of this gives $G_c = 1.33$ kJ/m^2.

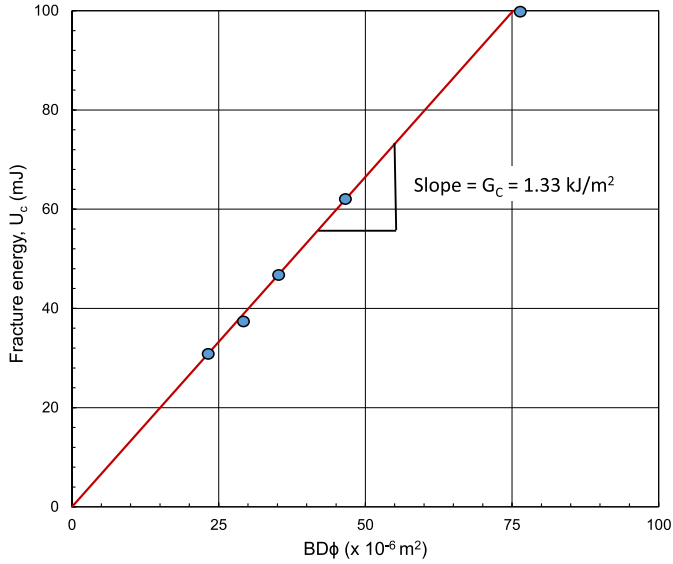


FIG. 2.86 Plot of U_c against $BD\phi$.

Then from Eq. (2.108) the fracture toughness is given by

$$K_c = \sqrt{EG_c} = \sqrt{2 \times 10^9 \times 1.33 \times 10^3} = 1.63 \text{ MN m}^{-3/2}$$

Questions

Where appropriate the creep curves in Fig. 2.5 should be used.

2.1 A plastic beam is to be subjected to load for a period of 1500 h. Use the 1500 h modulus values given below and the data in Table 1.5 to decide which of the materials listed would provide the most cost effective design (on a stiffness basis).

Material	PP	uPVC	ABS	Nylon 66	Polycarb.	Acetal	Polysulphone
1500 h modulus (GPa)	0.3	2.1	1.2	1.2	2.0	1.0	2.1

2.2 An extruded T-section beam in polypropylene has a cross-sectional area of 225 mm and a second moment of area, I, of 12.3×10^3 mm^4. If it is to be built-in at both ends and its maximum deflection is not to exceed 4 mm after 1 week, estimate a suitable length for the beam. The central deflection, δ, is given by

$$\delta = WL^3/384EI$$

where W is the weight of the beam. Use a limiting strain of 2%.

2.3 In the previous question the use of the 2% limiting strain will produce a conservative estimate for the beam length because the actual strain in the beam will be less than 2%. If the T-section is 25 mm wide and 25 mm deep with a general wall thickness of 5 mm, what is the % error incurred by using the 2% modulus? Calculate the likely beam deflection after 1 week. The central bending moment on the beam is given by WL/24.

2.4 A polypropylene pipe with an outside diameter of 80 mm is required to withstand a constant pressure of 0.5 MPa for at least 3 years. If the density of the material is 909 kg/m^3 and the maximum allowable strain is 1.5% estimate a suitable value for the wall thickness of the pipe. If a lower density grade of polypropylene ($\rho = 905$ kg/m^3) was used under the same design conditions, would there be any weight saving per unit length of pipe?

2.5 Show that for a simply supported beam of length, L, subjected to a point load, W, at mid-span the maximum strain, ε, in the material is given by

$$\varepsilon = \frac{6\delta d}{L^2}$$

where d is the beam depth and δ is the central deflection.

2.6 A piece of thin wall polypropylene pipe with a diameter of 300 mm is rotated about its longitudinal axis at a speed of 3000 rev/min. Calculate how long it would take for the diameter of the pipe to increase by 1.2 mm. The density of the polypropylene is 909 kg/m^3.

2.7 The maximum strain in a vertical liquid storage tank is given by $\varepsilon = \rho gHR/2Eh$ where H *is* the level above the base of the liquid of density ρ, and h is the wall thickness of the tank.

If a polypropylene tank of radius, $R = 0.625$ m, and height 3 m is to be filled with water for a period of one year, calculate the thickness of the tank material so that the change in its diameter will not exceed 12.5 mm. The density of the polypropylene is 904 kg/m^3.

2.8 The value of the external pressure, P_c, which would cause a thin wall sphere of radius, R, to collapse is given by

$$P_c = 0.365E\,(h/R)^2$$

where h is the wall thickness.

An underground polypropylene storage tank is a sphere of diameter 1.4 m. If it is to be designed to resist an external pressure of 20 kPa for at least 3 years, estimate a suitable value for the wall thickness. Tensile creep data may be used and the density of the polypropylene 904 kg/m^3.

2.9 A polypropylene bar with a square section (10 mm $\times$ 10 mm) is 225 mm long. It is pinned at both ends and an axial compressive load of 140 N is applied. How long would it be before buckling would occur. The relationship between the buckling load, F_c, and the bar geometry is

$$F_c = \pi^2 EI/L^2$$

where L is the length of the bar and I is the second moment of area of the cross-section.

2.10 Show that a ratio of depth to thickness equal to 10 is the normal limit if buckling is to be avoided during short-term loading of plastics. What is likely to happen to this ratio for long-term loading? You should consider the situation of buckling of a strut fixed at both ends for which the critical buckling load is given by

$$P_c = \frac{4\pi^2 EI}{L^2}$$

2.11 Show that the critical buckling strain in a strut with pinned ends is dependent only on the geometry of the strut.

A polypropylene rod, 150 mm long is to be designed so that it will buckle at a critical strain of 0.5%. Calculate a suitable diameter for the

rod and the compressive load which it could transmit for at least one year.

2.12 A circular polypropylene plate, 150 mm in diameter is simply supported around its edge and is subjected to a uniform pressure of 40 kPa. If the stress in the material is not to exceed 6 MPa, estimate a suitable thickness for the plate and the deflection, δ, after one year. The stress in the plate is given by

$$\sigma = 3(1+v)PR^2/8h^2$$

and

$$\delta = [3(1-v)(5+v)PR^4]/16Eh^3$$

2.13 A cylindrical polypropylene bottle is used to store a liquid under pressure. It is designed with a 4 mm skirt around the base so that it will continue to stand upright when the base bulges under pressure. If the diameter of the bottle is 64 mm and it has a uniform wall thickness of 2.5 mm, estimate the maximum internal pressure which can be used if the container must not rock on its base after one year. Calculate also the diameter change which would occur in the bottle after one year under pressure.

2.14 A rectangular section polypropylene beam has a length, L of 200 mm and a width of 12 mm. It is subjected to a load, W, of 150 N uniformly distributed over its length, L, and it is simply supported at each end. If the maximum deflection of the beam is not to exceed 6 mm after a period of 1 year, estimate a suitable depth for the beam. The central deflection of the beam is given by

$$\delta = 5WL/384EI$$

2.15 In a particular application a 1 m length of 80 mm diameter polypropylene pipe is subjected to two diametrically opposite point loads. If the wall thickness of the pipe is 3 mm, what is the maximum value of the load which can be applied if the change in diameter between the loads is not to exceed 3 mm in one year.

The deflection of the pipe under the load is given by

$$\delta = \frac{W}{Eh}\left[0.48(L/R)^{0.5}(R/h)^{1.22}\right]$$

and the stress is given by $\sigma = 2.4\ W/h^2$ where W is the applied load and h is the wall thickness of the pipe.

2.16 The stiffness of a closed coil spring is given by the expressions:

$$\text{Stiffness} = Gd^4/64R^3N$$

where d is the diameter of the spring material, R is the radius of the coils and N is the number of coils.

In a small mechanism, a polypropylene spring is subjected to a fixed extension of 10 mm. What is the initial force in the spring and what pull will it exert after one week. The length of the spring is 30 mm, its diameter is 10 mm and there are 10 coils. The design strain and creep contraction ratio for the polypropylene may be taken as 2% and 0.4 respectively.

2.17 A closed coil spring made from polypropylene is to have a steady force, W, of 3 N applied to it for 1 day. If there are 10 coils and the spring diameter is 15 mm, estimate the minimum diameter for the spring material if it is to recover completely when the force is released.

If the spring is subjected to a 50% overload for 1 day, estimate the percentage increase in the extension over the normal 1 day extension. The shear stress in the material is given by 16 WR/d^3. Use the creep curves supplied and assume a value of 0.4 for the lateral contraction ratio.

2.18 A rod of polypropylene, 10 mm in diameter, is clamped between two rigid fixed supports so that there is no stress in the rod at 20°C. If the assembly is then heated quickly to 60°C estimate the initial force on the supports and the force after 1 year. The tensile creep curves should be used and the effect of temperature may be allowed for by making a 56% shift in the creep curves at short times and a 40% shift at long times. The coefficient of thermal expansion for polypropylene is $1.35 \times 10^{-4}\ ^\circ\text{C}^{-1}$ in this temperature range.

2.19 When a pipe fitting is tightened up to a 12 mm diameter polypropylene pipe at 20°C the diameter of the pipe is reduced by 0.05 mm. Calculate the stress in the wall of the pipe after 1 year and if the inside diameter of the pipe is 9 mm, comment on whether or not you would expect the pipe to leak after this time. State the minimum temperature at which the fitting could be used. Use the tensile creep curves and take the coefficient of thermal expansion of the polypropylene to be $9.0 \times 10^{-5}\ ^\circ\text{C}^{-1}$.

2.20 A polypropylene pipe of inside diameter 10 mm and outside diameter 12 mm is pushed on to a rigid metal tube of outside diameter 10.16 mm. If the polypropylene pipe is in contact with the metal tube over a distance of 15 mm, calculate the axial force necessary to separate the two pipes (a) immediately after they are connected; (b) 1 year after connection. The

coefficient of friction between the two materials is 0.3 and the creep data in Fig. 2.5 may be used.

2.21 A nylon bush is to be inserted into a metal housing as illustrated in Fig. 2.87 The housing has a diameter of 40 mm and the inside diameter of the bush is 35 mm. If the length of the bush is 10 mm and the initial extraction force is to be 1.2 kN, calculate (a) the necessary interference on radius between the bush and the housing; (b) the temperature to which the bush must be cooled to facilitate easy assembly; (c) the internal diameter of the bush when it is in the housing; and (d) the long term extraction force for the bush. The short term modulus of the nylon is 2 GPa, its coefficient of friction is 0.24 and its coefficient of thermal expansion is $100 \times 10^{-6}\ ^{\circ}C^{-1}$. Poisson's Ratio for the Nylon is 0.4 and its long term modulus may be taken as 1 GPa.

2.22 If the bobbin illustrated in Example 2.6 (Fig. 2.16) is cooled from 20°C to −40°C, estimate the maximum hoop stress set up in the acetal. The **modulus** of the acetal at −40°C is 3 GPa and Poisson's ratio is 0.33. The coefficients of thermal expansion for acetal and steel are $80 \times 10^{-6\circ}C^{-1}$ and $11 \times 10^{-6\circ}C^{-1}$, respectively.

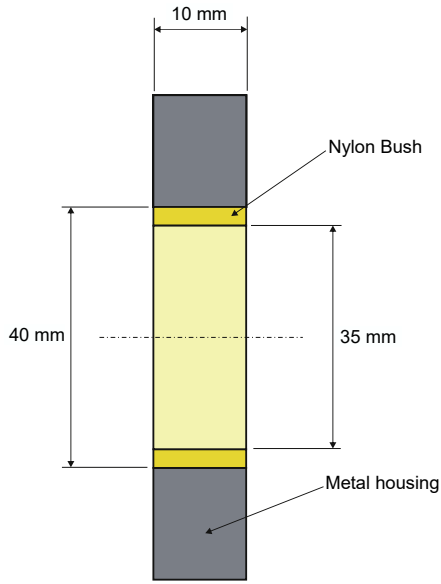


FIG. 2.87 Nylon bush in metal housing.

2.23 From the creep curves for a particular plastic the following values of creep rate at various stress levels were recorded for times between 10^6 and 10^7 s:

Stress (MPa)	1.5	3.0	4.5	6.0	7.5	9.0	12.0
Strain rate (s^{-1})	4.1×10^{-11}	7×10^{-11}	9.5×10^{-11}	1.2×10^{-10}	1.4×10^{-10}	1.6×10^{-10}	2×10^{-10}

Confirm whether or not this data obeys a law of the form

$$\dot{\varepsilon} = A\sigma^n$$

and if so, determine the constants A and n. When a stress of 5 MPa is applied to this material the strain after 10^6 s is 0.95%. Predict the value of the strain after 9×10^6 s at this stress.

2.24 For the grade of polypropylene whose creep curves are given in Fig. 2.5, confirm that the strain may be predicted by a relation of the form

$$\varepsilon(t) = At^n$$

where A and n are constants for any particular stress level. A small component made from this material is subjected to a constant stress of 5.6 MPa for 3 days at which time the stress is completely removed. Estimate the strain in the material after a further 3 days.

2.25 A small beam with a cross-section 15 mm square is foam moulded in polypropylene. The skin has a thickness of 2.25 mm and the length of the beam is 250 mm. It is to be built in at both ends and subjected to a uniformly distributed load, *w,* over its entire length. Estimate the dimensions of a square section solid polypropylene beam which would have the same stiffness when loaded in this way and calculate the percentage weight saving by using the foam moulding.

(Density of skin = 909 kg/m^3, density of core = 450 kg/m^3).

2.26 If the stress in the composite beam in the previous question is not to exceed 7 MPa estimate the maximum uniformly distributed load which it could carry over its whole length. Calculate also the central deflection after 1 week under this load. The bending moment at the centre of the beam is *WL*/24.

2.27 A rectangular section beam of solid polypropylene is 12 mm wide, 8 mm deep and 300 mm long. If a foamed core polypropylene beam, with a 2 mm solid skin on the upper and lower surfaces only, is to be made the same width, length and weight estimate the depth of the composite beam and state the ratio of the stiffness of the two beams. ($\rho = 909$ kg/m^3, $\rho = 500$ kg/m^3).

2.28 Compare the flexural stiffness to weight ratios for the following three plastic beams. (a) a solid beam of depth 12 mm, (b) a beam of foamed material 12 mm thick, and (c) a composite beam consisting of an 8 mm thick foamed core sandwiched between two solid skin layers 2 mm thick. The ratio of densities of the solid and foamed material is 1.5. (hint: consider unit width and unit length of beam).

2.29 For a sandwich beam with solid skins and a foamed core, show that (a) the weight of the core should be twice the weight of the skin if the beam is to be designed for maximum stiffness at minimum overall weight, and (b) the weight of the core should equal the weight of the skin if the beam is to be designed to provide maximum strength for minimum weight.

2.30 The viscoelastic behaviour of a certain plastic is to be represented by spring and dashpot elements having constants of 2 GPa and 90 GPa·s respectively. If a stress of 12 MPa is applied for 100 s and then completely removed, compare the values of strain predicted by the Maxwell and Kelvin−Voigt models after (a) 50 s; (b) 150 s.

2.31 Maxwell and Kelvin−Voigt models are to be set up to simulate the creep behaviour of a plastic. The elastic and viscous constants for the Kelvin−Voigt models are 2 GPa and 100 GPa·s respectively and the viscous constant for the Maxwell model is 200 GPa·s. Estimate a suitable value for the elastic constant for the Maxwell model if both models are to predict the same creep strain after 50 s.

2.32 During a test on a polymer which is to have its viscoelastic behaviour described by the Kelvin model the following creep data was obtained when a stress of 2 MPa was applied to it.

Time(s)	0	0.5×10^3	1×10^3	3×10^3	5×10^3	7×10^3	10×10^4	15×10^4
Strain	0	3.1×10^{-3}	5.2×10^{-3}	8.9×10^{-3}	9.75×10^{-3}	9.94×10^{-3}	9.99×10^{-3}	9.99×10^{-3}

Use this information to predict the strain after 1500 s at a stress of 4.5 MPa. State the relaxation time for the polymer.

2.33 A *Standard Model* for the viscoelastic behaviour of plastics consists of a spring element in series with a Voigt model as shown in Fig. 2.88. Derive the governing equation for this model and from this obtain the expression for creep strain. Show that the Unrelaxed Modulus for this model is ξ_1 and the Relaxed Modulus is $\xi_1\xi_2/(\xi_1+\xi_2)$.

2.34 The grade of polypropylene whose creep curves are given in Fig. 2.5 is to have its viscoelastic behaviour fitted to a Maxwell model for stresses up to 6 MPa and times up to 1000 s. Determine the two constants for the model and use these to determine the stress in the material after 900 s if the material is subjected to a constant strain of 0.4% throughout the 900 s.

2.35 The creep curve for polypropylene at 4.2 MPa (Fig. 2.5) is to be represented for times up to 2×10^6 s by a 4-element model consisting of a Maxwell unit and a Kelvin − Voigt unit in series. Determine the constants for each of the elements and use the model to predict the strain in this material after a stress of 5.6 MPa has been applied for 3×10^5 s.

2.36 Show that for a viscoelastic material in which the modulus is given by $E(t) = At^{-n}$, there will be a non-linear strain response to a linear increase in stress with time.

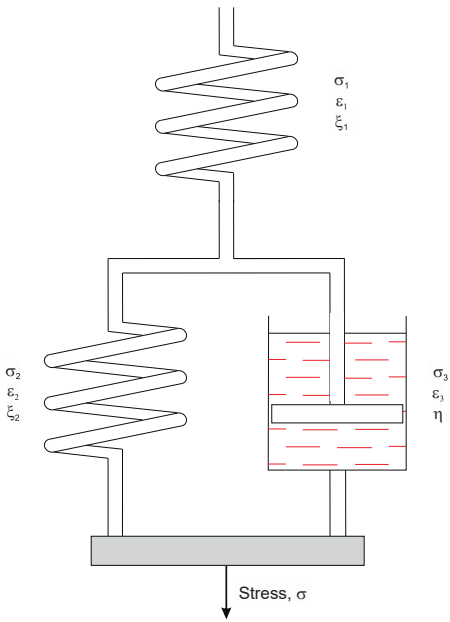


FIG. 2.88 Standard model for viscoelastic material.

2.37 In a tensile test on a plastic, the material is subjected to a constant strain rate of 10^{-5} s. If this material may have its behaviour modelled by a Maxwell element with the elastic component $\xi = 20$ GPa and the viscous element $\eta = 1000$ GPa·s, then derive an expression for the stress in the material at any instant. Plot the stress−strain curve which would be predicted by this equation for strains up to 0.1% and calculate the initial tangent modulus and 0.1% secant modulus from this graph.

2.38 A plastic is stressed at a constant rate up to 30 MPa in 60 s and the stress then decreases to zero at a linear rate in a further 30 s. If the time dependent creep modulus for the plastic can be expressed in the form

$$E(t) = \frac{\xi\eta}{\eta + \xi t}$$

use Boltzmann's Superposition Principle to calculate the strain in the material after (i) 40 s; (ii) 70 s; and (iii) 120 s. The elastic component of modulus in 3 GPa and the viscous component is 45×10^9 Pa·s.

2.39 A plastic with a time dependent creep modulus as in the previous example is stressed at a linear rate to 40 MPa in 100 s. At this time the stress in reduced to 30 MPa and kept constant at this level. If the elastic and viscous components of the modulus are 3.5 GPa and 50×10^9 Pa·s, use Boltzmann's Superposition Principle to calculate the strain after (a) 60 s and (b) 130 s.

2.40 A plastic has a time-dependent modulus given by

$$E(t) = 10^3 t^{-0.05}$$

where $E(t)$ is in MPa when 't' is in seconds. If this material is subjected to a stress which increases steadily from 0 to 20 MPa in 800 s and is then kept constant, calculate the strain in the material after (a) 500 s and (b) 1000 s.

2.41 A plastic which behaves like a Kelvin−Voigt model is subjected to the stress history shown in Fig. 2.89. Use the Boltzmann's Superposition Principle to calculate the strain in the material after (a) 90 s; (b) 150 s. The spring constant is 12 GPa and the dashpot constant is 360 GPa·s.

2.42 A plastic component was subjected to a series of step changes in stress as follows. An initial constant stress of 10 MPa was applied for 1000 s at which time the stress level was increased to a constant level of 20 MPa. After a further 1000 s the stress level was decreased to 5 MPa which was maintained for 1000 s before the stress was increased to 25 MPa for 1000 s after which the stress was completely removed. If the material may be represented by a Maxwell model in which the elastic constant $\xi = 1$ GPa and the viscous constant $\eta = 4000$ GPa·s, calculate the strain 4500 s after the first stress was applied.

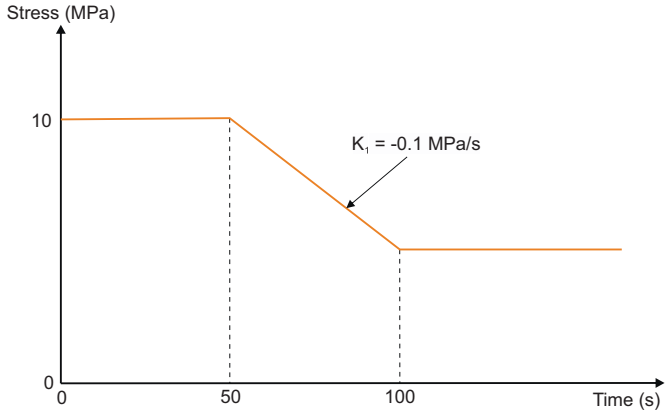


FIG. 2.89 Stress history of a plastic.

2.43 In tests on a particular plastic it is found that when a stress of 10 MPa is applied for 100 s and then completely removed, the strain at the instant of stress removal is 0.8% and 100 s later it is 0.058%. In a subsequent tests on the same material the stress of 10 MPa is applied for 2400 s and completely removed for 7200 s and this sequence is repeated 10 times. Assuming that the creep curves for this material may be represented by an equation of the form $\varepsilon(t) = At^n$ where A and n are constants, then determine the total accumulated residual strain in the material at the end of the 10^{th} cycle.

2.44 In a small polypropylene component a tensile stress of 5.6 MPa is applied for 1000 s and removed for 500 s. Estimate how many of these stress cycles could be permitted before the component reached a limiting strain of 1%. What is the equivalent modulus of the material at this number of cycles? The creep curves in Fig. 2.5 may be used.

2.45 A cylindrical polypropylene pressure vessel of 150 mm outside diameter is to be pressurised to 0.5 MPa for 6 h each day for a projected service life of 1 year. If the material can be described by an equation of the form $\varepsilon(t) = At^n$ where A and n are constants and the maximum strain in the material is not to exceed 1.5% estimate a suitable wall thickness for the vessel on the assumption that it is loaded for 6 h and unloaded for 18 h each day. Estimate the material saved compared with a design in which it is assumed that the pressure is constant at 0.5 MPa throughout the service life. The creep curves in Fig. 2.5 may be used.

2.46 For the type of Standard Linear Solid described in Q 2.33, derive equations for the storage modulus, the loss modulus and tan δ when the material is subjected to a sinusoidally varying stress. Confirm that for $\eta = 1$ GPa·s, $\xi_1 = 2$ GPa and $\xi_2 = 0.1$ GPa, your equations predict the classical variation of E_1, E_2 and tan δ for values of ω in the range $0.01-100\ s^{-1}$.

2.47 Creep rupture tests on a particular grade of uPVC at 20°C gave the following results for applied stress, σ, and time to failure, t.

Stress (MPa)	60	55	52	48	45	43
time(s)	800	7×10^3	3.25×10^4	2.15×10^5	8.9×10^6	2.4×10^6

Confirm that this data obeys a law of the form

$$t = Ae^{-B\sigma}$$

and determine the values of the constants A and B.

2.48 For the material in the previous question, use the Zhurkov-Beuche equation to calculate the time to failure under a steady stress of 44 MPa if the material temperature is 40°C. The activation energy, U_0, may be taken as 150 kJ/mol.

2.49 A 200 mm diameter plastic pipe is to be subjected to an internal pressure of 0.5 MPa for 3 years. If the creep rupture behaviour of the material is as shown in Fig. 2.73, calculate a suitable wall thickness for the pipe. You should use a safety factor of 1.5.

2.50 Fracture Mechanics tests on a grade of ABS indicate that its K value is 2 MN $m^{-3/2}$ and that under static loading its growth rate is described by the equation.

$$da / dt = 3 \times 10^{-11} K^{3.2}$$

where K has units MN $m^{-3/2}$. If, in service, the material is subjected to a steady stress of 20 MPa estimate the maximum defect size which could be tolerated in the material if it is to last for at least 1 year.

2.51 Use the data in Table 2.3 to compare crack tip plastic zone sizes in acrylic, ABS and polypropylene.

2.52 In a tensile test on an un-notched sample of acrylic the fracture stress is recorded as 57 MPa. Estimate the likely size of the intrinsic defects in the material.

2.53 In a small timing mechanism an acetal copolymer beam is loaded as shown in Fig. 2.90. The end load varies from 0 to F at a frequency of 5 Hz. If the beam is required to withstand at least 10 million cycles, calculate the permissible value of F assuming a fatigue strength reduction factor of 2. The surface stress (in MPa) in the beam at the support is given by $FL/60$ where F is in Newtons and L is the beam length in mm.

Fatigue and creep fracture data for the acetal copolymer are given in Figs. 2.91 and 2.92.

2.54 A plastic shaft of circular cross-section is subjected to a steady bending moment of 1 Nm and simultaneously to an alternating bending moment of 0.75 Nm. Calculate the necessary shaft diameter so as to avoid fatigue failure (the factor of safety is to be 2.5). The fatigue limit for the material in reversed bending is 25 MPa and the creep rupture strength at the equivalent time may be taken as 35 MPa. Calculate also the shaft diameter if the fatigue strength reduction factor is to be taken as 2.

2.55 A 10 mm diameter uPVC shaft is subjected to a steady tensile load of 500 N. If the fatigue strength reduction factor is 1.8 and the factor of safety is to be 2 calculate the largest alternating bending moment which could be applied at a frequency of 5 Hz if fatigue failure is not to occur inside 10^7 cycles. The creep rupture characteristic for the material is given in question 2.47 and the reversed bending fatigue behaviour is described by the $\sigma = (43.4 - 3.8 \log N)$ (where N is the number of cycles to failure and σ is the stress in MPa). It may be assumed that at 5 Hz, thermal softening will not occur.

2.56 A uPVC rod of diameter 12 mm is subjected to an eccentric axial force at a distance of 3 mm from the centre of the cross-section. If the force varies: sinusoidally from $-F$ to F at a frequency of 10 Hz, calculate the value of F so that fatigue failure will not occur in 10 cycles. Assume a safety factor of 2.5 and use the creep rupture and fatigue characteristics described in the previous question. Thermal softening effects may be ignored at the stress levels involved.

2.57 For the purposes of performing an impact test on a material it is proposed to use an elastic stress concentration factor of 3.5. If the notch tip radius is to be 0.25 mm estimate a suitable notch depth.

2.58 On an impact testing machine for plastics the weight of the pendulum is 4.5 kgf. When the pendulum is raised to a height of 0.3 m and allowed to swing (a) with no specimen in position and (b) with a plain sample

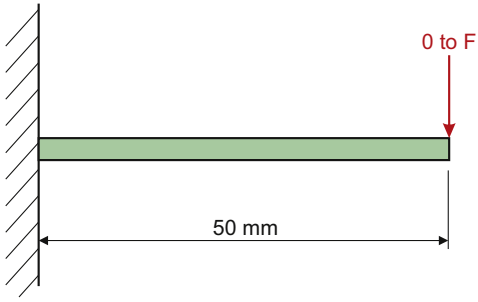


FIG. 2.90 Beam in timing mechanism.

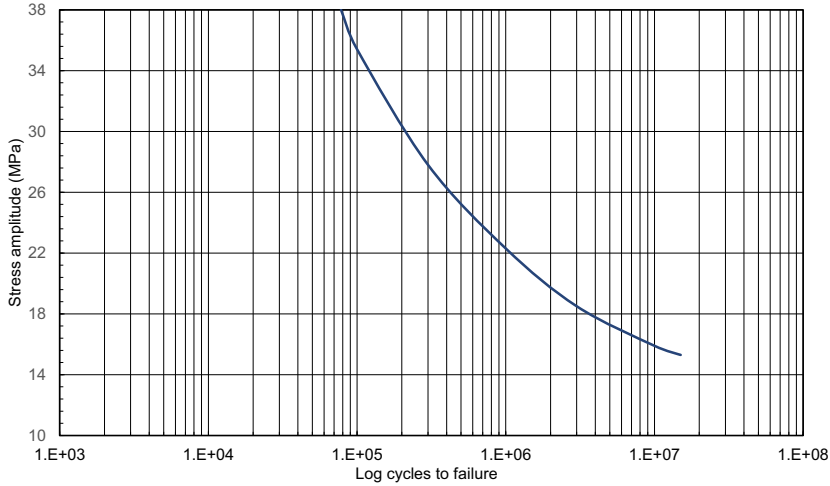


FIG. 2.91 Fatigue behaviour of acetal.

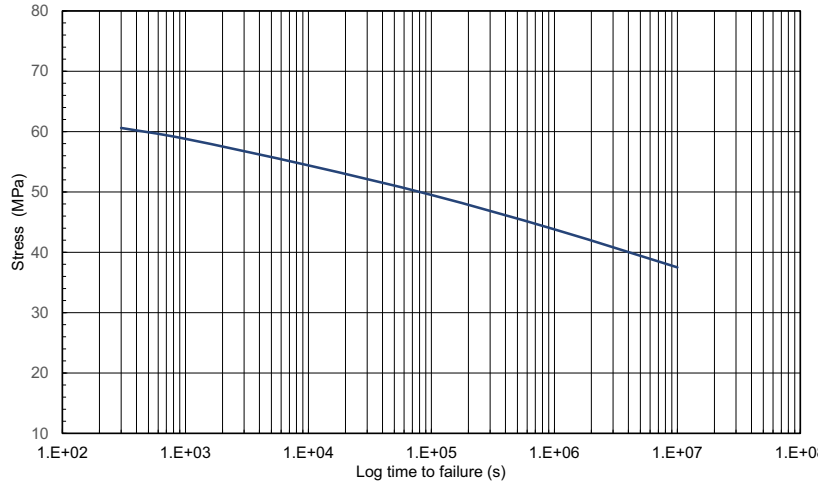


FIG. 2.92 Creep fracture of acetal.

(4×12 mm cross-section) in position, the pendulum swings to heights of 0.29 and 0.2 m respectively. Estimate (i) the friction and windage losses in the machine; (ii) the impact energy of the specimen; (iii) the height the pendulum will swing to if it is released from a height of 0.25 m and breaks a sample of exactly the same impact strength as in (ii). (Assume that the losses remain the same and that the impact strength is independent of strike velocity).

2.59 A sheet of polystyrene 100 mm wide, 5 mm thick and 200 mm long contains a sharp single edge crack 10 mm long, 100 mm from one end. If the critical stress intensity factor is 1.75 MN $m^{-3/2}$, what is the maximum axial force which could be applied without causing brittle fracture.

2.60 A certain grade of PMMA has a K value of 1.6 MN $m^{-3/2}$ and it is known that under cyclic stresses, cracks grow at a rate given by (2×10^{-6} $\Delta K^{3.32}$). If the intrinsic defects in the material are 50 mm long, how many hours will the material last if it is subjected to a stress cycle of 0−10 MPa at a frequency of 1 Hz.

2.61 A series of fatigue crack growth tests on a moulding grade of polymethyl methacrylate gave the following results

da/dN (m/cycle)	2.25×10^{-7}	4.0×10^{-7}	6.2×10^{-7}	11×10^{-7}	17×10^{-7}	29×10^{-7}
ΔK(MN $m^{-3/2}$)	0.42	0.53	0.63	0.79	0.94	1.17

If the material has a critical stress intensity factor of 1.8 MN $m^{-3/2}$ and it is known that the moulding process produces defects 40 m long, estimate the maximum repeated tensile stress which could be applied to this material for at least 10^6 cycles without causing fatigue failure.

2.62 A series of uniaxial fatigue tests on unnotched plastic sheets show that the fatigue limit for the material is 10 MPa. If a pressure vessel with a diameter of 120 mm and a wall thickness of 4 mm is to be made from this material, estimate the maximum value of fluctuating internal pressure which would be recommended. The stress intensity factor for the pressure vessel is given by $K = 2\sigma_\theta(2a)^{1/2}$ where σ_θ is the hoop stress and *'a'* is the half length of an internal defect.

Bibliography

Ashby MF, Jones DRH: *Engineering materials 1 − an introduction to properties, applications and design*, ed 4, Butterworth-Heinemann.

Benham PP, Crawford RJ, Armstrong CG: *Mechanics of engineering materials*, ed 2, Longmans.

Blackman BRK, Pavan A, Williams JG, editors: *Fracture of polymers, composites and adhesives II*, Oxford, 2003, Elsevier.

Brinson HF, Brinson LC: *Polymer engineering science and viscoelasticity − an introduction*, ed 2, New York, 2015, Springer.

Characterization and failure analysis of plastics ASM international, 2003.

Crawford RJ: *Plastics and rubber − engineering design and applications*, London, 1985, MEP Ltd.

Crompton TR: *Polymer reference book*, Shrewsbury, 2006, Rapra Technology Ltd.
Erhard G: *Designing with plastics*, Munich, 2006, Hanser.
Ezrin M: *Plastics failure guide − cause and prevention*, ed 2, Munich, 2013, Hanser.
Gerdeen JC, Rorrer RAL: *Engineering design with polymers and composites*, ed 2, Boca Raton, 2012, CRC Press.
Gibson LJ, Ashby MF: *Cellular solids: structure and properties*, ed 2, Cambridge University Press.
Grellmann W, Seidler S, editors: *Deformation and fracture behaviour of polymers*, New York, 2001, Springer.
Kausch HH: *Polymer fracture*, Berlin, 1978, Springer-Verlag.
Kinloch AJ, Young RJ: *Fracture behaviour of polymers*, London, 1983, Applied Science.
Klempner D, Sendijarevic V: *Handbook of polymeric foams and foam technology*, ed 2, Munich, 2004, Hanser.
Mark HF: *Encyclopedia of polymer science and technology*, ed 4, Wiley.
McKeen LW: *Fatigue and tribological properties of plastics and elastomers*, ed 3, Oxford, 2016, Elsevier.
Moore DR, Pavan A, Williams JG, editors: *Fracture mechanics testing methods for polymers, adhesives and composites*, Oxford, 2001, Elsevier.
Ogorkiewicz RM: *Engineering properties of plastics*, London, 1970, Wiley Interscience.
Powell PC, Housz AJI: *Engineering with polymers*, Cheltenham, 1998, Stanley Thornes.
Shah V: *Handbook of plastics testing and failure analysis*, ed 3, Hoboken, 2007, Wiley.
Swallowe GM: *Mechanical properties and testing of polymers: an A−Z reference*, Springer.
Williams ML, Landel RF, Ferry JD: *Journal of the American Chemical Society* 77:3701, 1955.
Wright D: *Failure of Plastics and rubber products − causes, Effects and case studies involving degradation*, Shrewsbury, 2001, Rapra.
Young WC, Budynas RG, Sadegh AM: *Roark's formulas for stress and strain*, ed 8, McGraw-Hill.

Chapter 3

Mechanical behaviour of composites

3.1 Deformation behaviour of reinforced plastics

It was mentioned earlier that the stiffness and strength of plastics can be increased significantly by the addition of a reinforcing filler. A reinforced plastic consists of two main components; a matrix which may be either thermoplastic or thermosetting and a reinforcing filler which for engineering applications usually takes the form of fibres. A wide variety of combinations are possible as shown in Fig. 3.1. Single layer fibre composites can employ either continuous or discontinuous fibres, which may be randomly distributed or oriented in a specific direction. Discontinuous fibres are generally shorter than continuous fibres, which are most often woven to align them in certain directions. Continuous fibre mats may be unidirectional, bidirectional and multidirectional. Single layer composites of various types and designs may then be combined layer by layer to produce multilayer laminates of numerous designs. Very often alternate layers are orientated in different directions to create laminates with enhanced properties in multiple directions. Single layers may also be used to sandwich other structures, such as honeycomb sections, to create thick section composite panels with very high stiffness or strength to weight ratios. Hybrid composites may also be produced by employing fibres of multiple materials in both single layer and multilayer composites. In general, the matrix has a low strength in comparison to the reinforcement which is also stiffer and brittle. To gain maximum benefit from the reinforcement, the fibres should bear as much as possible of the applied stress. The function of the matrix is to support the fibres and transmit the external loading to them by shear at the fibre/matrix interface. Since the fibre and matrix are quite different in structure and properties it is convenient to consider them separately.

3.2 Types of reinforcement

The reinforcing filler usually takes the form of fibres but particles (for example glass spheres) are also used, and increasingly a diverse selection of nanoscale reinforcements are being added to polymers to create new nanocomposite

Plastics Engineering. https://doi.org/10.1016/B978-0-08-100709-9.00003-0
Copyright © 2020 Elsevier Ltd. All rights reserved.

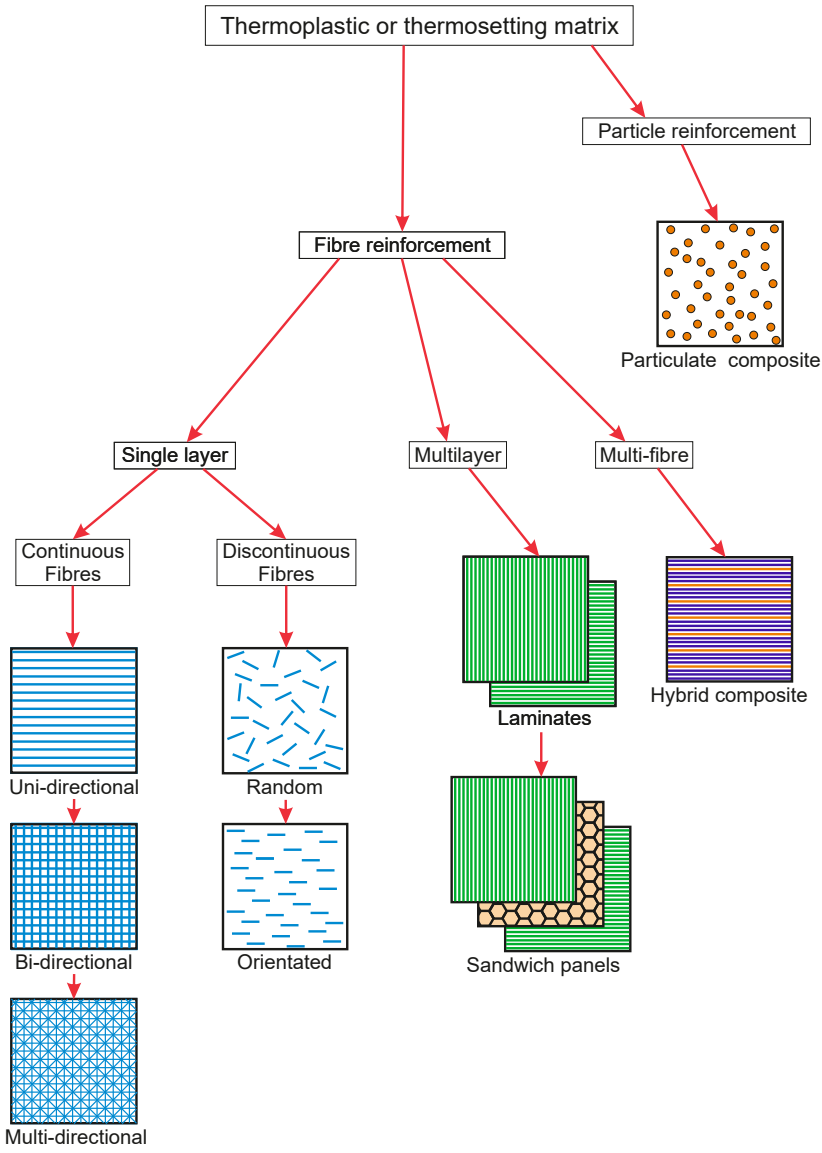


FIG. 3.1 Various types of composite.

materials A wide range of amorphous and crystalline materials can be used as reinforcing fibres. These include glass, carbon, boron, and basalt. Fibres have also been produced from synthetic polymers—for example, **Kevlar**® (or Aramid) fibres (from aromatic polyamides), **Dyneema**® fibres (from Ultra high molecular weight polyethylene (UHMWPE)) and highly drawn fibres of commercial

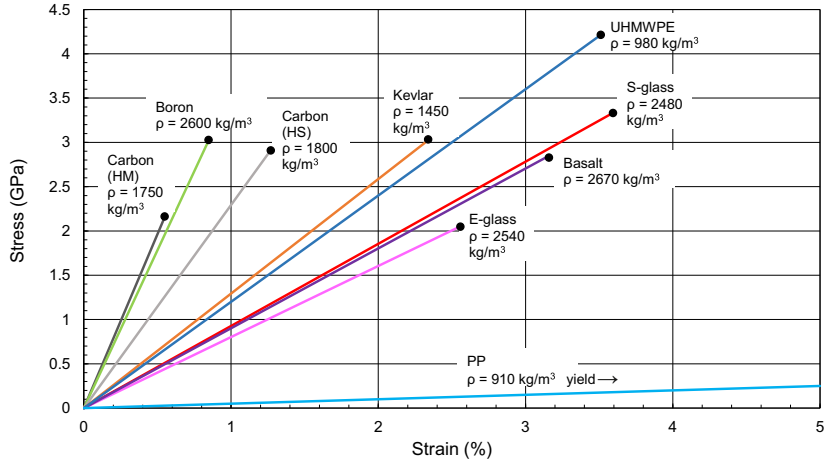


FIG. 3.2 Typical tensile behaviour of fibres.

thermoplastics such as PET and polypropylene. There is also increasing interest in the exploitation of natural fibres particularly when used with naturally derived polymers to create new classes of materials that are wholley biodegradable. This includes many forms of plant fibres derived from wood, stems (e.g. flax, jude and hemp), leaves (e.g. banana, sisal and palm), and seeds (e.g. cotton and coconut). The stress–strain behaviour of some typical fibres used in structural engineering composites is shown in Fig. 3.2. Note that carbon fibres may be classified as being of high modulus (HM) and high strength (HS).

Glass in the form of fibres is relatively inexpensive and is the principal form of reinforcement used in plastics. The fibres are produced by drawing off continuous strands of glass from an orifice in the base of an electrically heated platinum crucible which contains the molten glass. The earliest successful glass reinforcement had a calcium-alumina borosilicate composition developed specifically for electrical insulation systems (E glass). Although other glasses were subsequently developed for applications where electrical properties are not critical, no commercial composition has been found to provide a better overall combination of properties than that of E-glass. However, certain special glasses for extra high strength or modulus have been produced for applications in areas such as marine or aerospace technologies (e.g. S-glass (where S = 'strength'), C-glass (where C = 'chemical resistance'), or R-glass (where R = 'reinforcement')).

During production the fibres are treated with a fluid which performs several functions.

(a) it facilitates the production of strands from individual fibres
(b) it reduces damage to fibres during mechanical handling and
(c) it acts as a process aid during moulding.

This treatment is known as *sizing*. As mentioned earlier, the joint between the matrix and the fibre is critical if the reinforcement is to be effective and so the surface film on the glass ensures that the adhesion will be good.

3.3 Types of matrix

The matrix in a reinforced plastic may be either thermosetting or thermoplastic.

(a) Thermosets

In the early days nearly all thermosetting moulding materials were composites in that they contained fillers such as woodflour, mica, cellulose, etc. to increase their strength. However, these were not generally regarded as reinforced materials in the sense that they did not contain fibres.

Nowadays the major thermosetting resins used in conjunction with glass fibre reinforcement are unsaturated polyester resins and to a lesser extent epoxy resins. The most important advantages which these materials can offer are that they do not liberate volatiles during cross-linking and they can be moulded using low pressures at room temperature. Table 3.1 shows typical properties of fibre reinforced epoxy.

(b) Thermoplastics

A wide variety of thermoplastics have been used as the base for reinforced plastics and over the past decade there has been rising interest in the use of thermoplastics instead of thermosets. This has been driven largely by a desire

TABLE 3.1 Typical properties of bi-directional fibre composites.

Material	Volume fraction (V_f)	Density (kg/m^3)	Tensile strength (GPa)	Tensile modulus (GPa)
Epoxy	–	1200	0.07	6
Epoxy/E-glass	0.57	1970	0.57	22
Epoxy/Kevlar	0.60	1400	0.65	40
Epoxy/Carbon	0.58	1540	0.38	80
Epoxy/Boron	0.60	2000	0.38	106

to exploit the more adaptable and automated moulding processes associated with thermoplastics combined with rising pressures for plastic materials in many applications to be more reusable and recyclable. Some of the thermoplastics used include typical commodity plastics such as polypropylene, nylon, styrene-based materials, thermoplastic polyesters, acetal, polycarbonate, and polysulphone. However, in industries such as aerospace high performance thermoplastics such as polyphenylene sulphide (PPS) and polyether ether ketone (PEEK) are finding increasing applications within composite structures. The choice of a reinforced thermoplastic depends on a wide range of factors which includes the nature of the application, the service environment and costs. In many cases conventional thermoplastic processing techniques can be used to produce moulded articles (see Chapter 4). Some typical properties of fibre reinforced nylon are given in Table 3.2.

3.4 Forms of fibre reinforcement in composites

In traditional engineering composites reinforcing fibres typically have diameters varying from 7 μm to 100 μm. They may be continuous or in the form of chopped strands (lengths 3 mm−50 mm). When chopped strands are used, the length to diameter ratio is called the **Aspect Ratio.** The properties of a short-fibre composite are very dependent on the aspect ratio − the greater the aspect ratio the greater will be the strength and stiffness of the composite.

The amount of fibres in a composite is often expressed in terms of the **volume fraction,** V_f. This is the ratio of the volume of the fibres, v_f, to the volume of the composite, v_c. The weight fraction of fibres, W_f, may be related to the volume fraction as follows.

TABLE 3.2 Typical properties of fibre reinforced nylon 66.

Material	Weight fraction (W_f)	Density (kg/m^3)	Tensile strength (GPa)	Flexural modulus (GPa)
Nylon 66	–	1140	0.07	2.8
Nylon 66/ glass	0.40	1460	0.2	11.2
Nylon 66/ carbon	0.40	1340	0.28	24.0
Nylon 66/ glass/carbon	0.20C/0.20G	1400	0.24	20.0
Nylon 66/ glass beads	0.40	1440	0.09	5.6

TABLE 3.3 Effect of fibre content on properties of glass reinforced nylon 66.

	Weight fraction, W_f						
Property	**0**	**0.10**	**0.20**	**0.30**	**0.40**	**0.50**	**0.60**
Density	1140	1210	1280	1370	1460	1570	1700
Tensile strength (GPa)	0.07	0.09	0.13	0.18	0.21	0.23	0.24
% Elongation at break	60	3.5	3.5	3.0	2.5	2.5	1.5
Flexural modulus (GPa)	2.8	4.2	6.3	9.1	11.2	15.4	19.6
Thermal expansion μm/m/°C	90	37	32	30	29	25	22
Water absorption (24 h)	1.6	1.1	0.9	0.9	0.6	0.5	0.4

$$W_f = \frac{w_f}{w_c} = \frac{\rho_f v_f}{\rho_c v_c} = \frac{\rho_f}{\rho_c} V_f \tag{3.1}$$

where ρ is the density and the subscripts f and c refer to fibres and composite respectively.

Table 3.3 indicates the extent to which the properties of plastics are influenced by the level of fibre content. Full details of the forms in which reinforcing fibres are available for inclusion in plastics are given in Chapter 4.

3.5 Analysis of continuous fibre composites

The greatest improvement in the strength and stiffness of a plastic is achieved when it is reinforced with uni-directional continuous fibres. The analysis of such systems is relatively straightforward.

(i) Longitudinal properties

Consider a composite with continuous aligned fibres as shown in Fig. 3.3. If the moduli of the matrix and fibres are E_m and E_f respectively then the modulus of the composite may be determined as follows.

Equilibrium equation

The applied force on the composite will be shared by the fibres and the matrix. Hence

$$F_1 = F_f + F_m \tag{3.2}$$

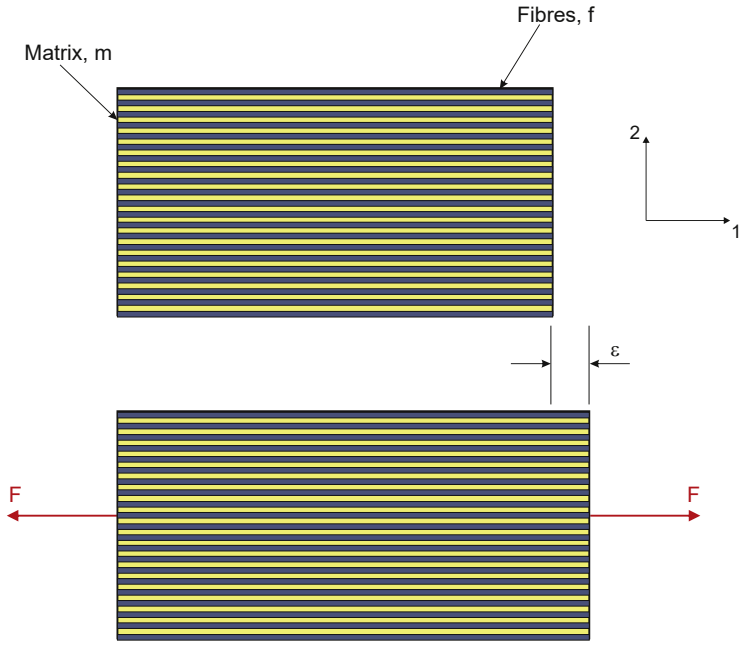


FIG. 3.3 Loading parallel to fibres.

Geometry of deformation equation

The strain, ε, is the same in the fibres and matrix and is equal to the strain in the composite.

$$\varepsilon_1 = \varepsilon_f = \varepsilon_m \tag{3.3}$$

Stress–strain relationships

$$\sigma_1 = E_1\varepsilon_{cL}, \quad \sigma_f = E_f\varepsilon_f, \quad \sigma_m = E_m\varepsilon_m \tag{3.4}$$

where subscript cL refers to composite in logitudinal direction

Combining Eqs. (3.3) and (3.4)

$$E_1\varepsilon_{cL}\mathrm{A}_c = E_f\varepsilon_f\mathrm{A}_f + E_m\varepsilon_m\mathrm{A}_\mathrm{m}$$

and using Eq. (3.2)

$$E_1 = E_f\left(\frac{A_f}{A_c}\right) + E_m\left(\frac{A_m}{A_c}\right)$$

If the fibres have a uniform cross-section, then the area fraction will equal the volume fraction, so

$$E_1 = E_f V_f + E_m V_m \tag{3.5}$$

This is an important relationship. It states that the modulus of a unidirectional fibre composite is proportional to the volume fractions of the materials in the composite. This is known as the **Rule of Mixtures.** It may also be used to determine the density of a composite as well as other properties such as the Poisson's ratio, strength, thermal conductivity and electrical conductivity in the fibre direction.

Example 3.1. The density of a composite made from unidirectional glass fibres in an epoxy matrix is 1950 kg/m^3. If the densities of the glass and epoxy are known to be 2540 kg/m^3 and 1300 kg/m^3, calculate the weight fraction of fibres in the composite.

Solution From the rule of mixtures

$$\rho_c = \rho_f V_f + \rho_m V_m = \rho_f V_f + \rho_m (1 - V_f)$$
$$1950 = 2540 \cdot V_f + 1300 \cdot (1 - V_f)$$
$$V_f = 0.52$$

Using Eq. (3.1). $W_f = \frac{\rho_f}{\rho_c} V_f = \frac{2540}{1950}(0.52) = 0.68$

Example 3.2. PEEK is to be reinforced with 30% by volume of unidirectional carbon fibres and the properties of the individual materials are given below. Calculate the density, modulus and strength of the composite in the fibre direction.

Material	Density (kg/m^3)	Tensile strength (GPa)	Modulus (GPa)
PEEK	1300	0.058[†]	3.8
Carbon fibre (HM)	1800	2.1	400

[†] Note that as shown below, this must be the matrix stress at the fibre fracture strain.

Solution From the rule of mixtures

$$\rho_c = \rho_f V_f + \rho_m V_m = 0.13(1800) + 0.7(1300) = 1450 \text{ kg/m}^3$$
$$\sigma_{cu} = \sigma_{fu} V_f + \sigma_m V_m = 0.3(2.1) + 0.7(0.058) = 0.67 \text{ GPa}$$
$$E_{cL} = E_f V_f + E_m V_m = 0.3(400) + 0.7(3.8) = 122.7 \text{ GPa}$$

Example 3.3. Calculate the fraction of the applied force which will be taken by the fibres in the composite referred to in Example 3.2

Solution From Eqs. (3.2), (3.3) and (3.4), the force in the fibres is given by

$$F_f = \sigma_f A_f = E_f \varepsilon_f V_f \nu_c$$

Similarly, the force in the composite is given by

$$F_1 = E_f \varepsilon_f V_f \nu_c + E_m \varepsilon_m V_m \nu_c$$

Hence,

$$\frac{F_f}{F_1} + \frac{E_f V_f}{E_f V_f + E_m V_m} + 0.978$$

It may be seen that a very large percentage of the applied force is carried by the fibres. Note also that the ratio of stresses in the fibre may be determined in a similar way.

From the rule of mixtures, the stresses are related as follows.

$$\sigma_1 = \sigma_f V_f + \sigma_m V_m$$

$$\frac{\sigma_1}{\sigma_f} = V_f + \frac{\sigma_m}{\sigma_f}(1 - V_f)$$

As the strains are the same in the matrix and fibres $\frac{\sigma_m}{\sigma_f} = \frac{E_m}{E_f}$

$$\frac{\sigma_1}{\sigma_f} = V_f + \frac{E_m}{E_f}(1 - V_f) = 0.3 + \frac{3.8}{400}(0.7) = 0.307$$

Thus,

$$\frac{\sigma_f}{\sigma_1} = 3.26$$

As shown in Fig. 3.4 stress–strain tests on uniaxially aligned fibre composites show that their behaviour lies somewhere between that of the fibres and that of the matrix. With regard to the strength of the composite, σ_{cu}, the rule of mixtures has to be modified to relate to the matrix stress, σ'_m at the fracture strain of the fibres rather than the ultimate tensile strength, σ_{mu} for the matrix. This is because, with brittle fibres, failure of the composite will occur when the fibres reach their fracture strain. At this point the matrix is subjected to the full applied load, which it is unable to sustain.

Thus, as shown earlier, the ultimate strength of the composite may be predicted by the rule of mixtures.

$$\sigma_{cu} = \sigma_{fu} V_f + \sigma'_m V_m \tag{3.6}$$

However, as shown in Fig. 3.5, this equation only applies when the volume fraction is greater than a certain critical value, V_{crit}. From Fig. 3.5 this will be defined by

$$\sigma_{mu}(1 - V_{\text{crit}}) = \sigma_{fu} V_{\text{crit}} + \sigma'_m(1 - V_{\text{crit}})$$

$$V_{\text{crit}} = \frac{\sigma_{mu} - \sigma'_m}{\sigma_{fu} + \sigma_{mu} + \sigma'_m} \tag{3.7}$$

In addition, it may be seen that the strengthening effect of the fibres is only observed (i.e. $\sigma_{cu} > \sigma_{mu}$) when the volume fraction is greater than a certain value V_1. From Fig. 3.5 the value of V_1 *is* obtained from

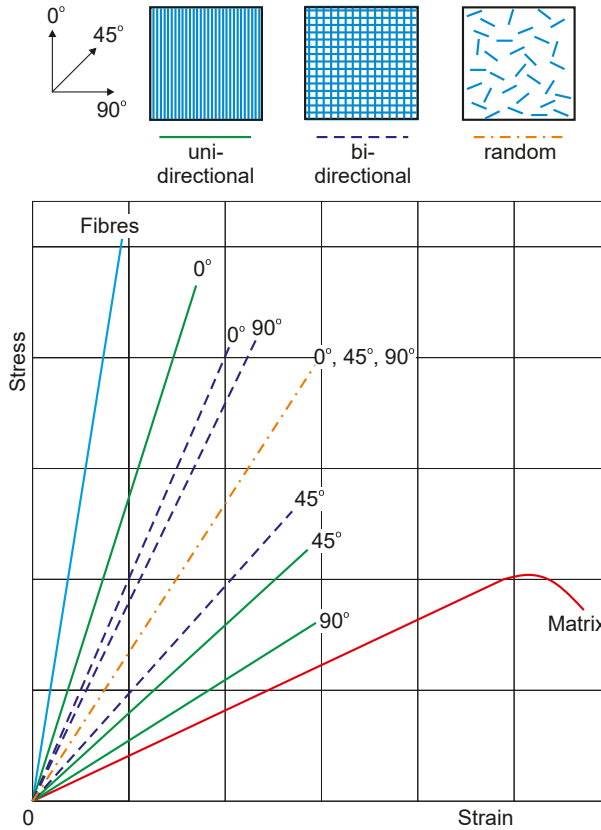


FIG. 3.4 Stress–strain behaviour for several types of fibre reinforcement.

$$\sigma_{mu} = \sigma_{fu} V_1 + \sigma'_m (1 - V_1)$$

$$V_1 = \frac{\sigma_{mu} - \sigma'_m}{\sigma_{fu} - \sigma_m} \tag{3.8}$$

In practice the maximum volume fraction, $V_{\max}$, which can be achieved in unidirectional fibre composites is about 0.8. Designers must therefore arrange for volume fractions to be in the range $V_1 \rightarrow V_{\max}$. It should also be noted that in commercial production it is not always possible to achieve the high standards of manufacture necessary to obtain full benefit from the fibres. It is generally found that although the stiffness is predicted quite accurately by Eq. (3.5), the strength is usually only about 65% of the value calculated by the rule of mixtures. For fibre reinforcement systems other than unidirectional fibres, these values can be reduced even more. To allow for this a constant 'k' is sometimes included in the fibre contribution to Eq. (3.6).

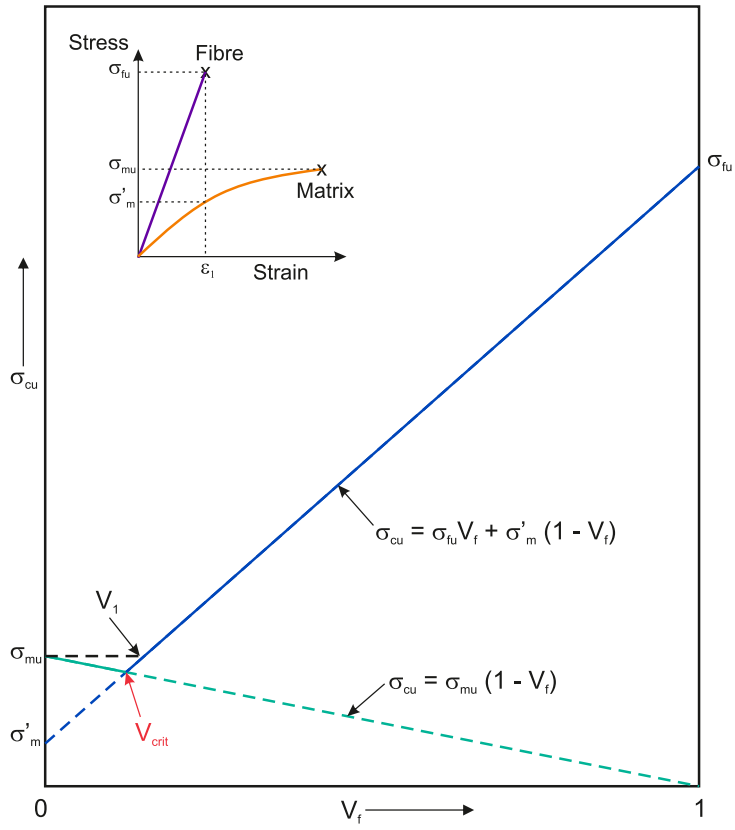


FIG. 3.5 Effect of volume fraction on strength.

Example 3.4. For the PEEK/carbon fibre composite referred to in Example 3.2 calculate the values of V_1 and V_{crit} if it is known that the ultimate tensile strength of PEEK is 62 MPa.

Solution From Eq. (3.7)

$$V_{crit} = \frac{\sigma_{mu} - \sigma'_m}{\sigma_{fu} + \sigma_{mu} - \sigma'_m} = \frac{0.062 - 0.058}{2.1 + 0.062 - 0.058} = 0.19\%$$

and from Eq. (2.46)

$$V_1 = \frac{\sigma_{mu} - \sigma'_m}{\sigma_{fu} - \sigma'_m} = \frac{0.062 - 0.058}{2.1 - 0.058} = 0.2\%$$

(ii) Properties perpendicular to longitudinal axis

The properties of a unidirectional fibre will not be nearly so good in the transverse direction compared with the longitudinal direction. As a material in service is likely to be subjected to stresses and strains in all directions it is important to be aware of the properties in all directions. The transverse direction will, of course, be the weakest direction and so it is necessary to pay particular attention to this.

The transverse modulus, E_{cT}, may be determined in a manner similar to that described earlier for the longitudinal modulus. Consider a unidirectional fibre composite subjected to a transverse force, F_{cT}, in the direction perpendicular to the fibre axis.

Equilibrium condition

Referring to Fig. 3.6. The force in the fibres will be the same as the force in the matrix:

$$F_2 = F_f = F_m$$

Assuming that the width and thickness (into the page) is the same for both the matrix and the fibres, then

$$\sigma_2 = \sigma_f = \sigma_m \tag{3.9}$$

Geometry of deformation equation

The total transverse deformation will be the sum of the deformations in the matrix and the fibres

$$\delta_2 = \delta_f + \delta_m$$

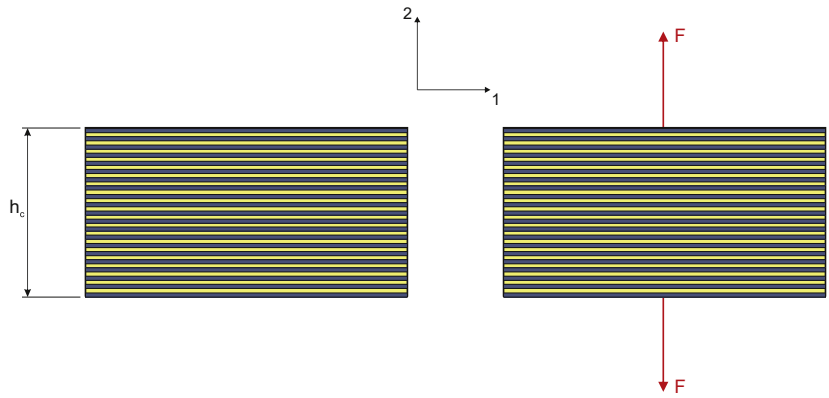


FIG. 3.6 Loading perpendicular to fibres.

$$\varepsilon_2 h_c = \varepsilon_f h_f + \varepsilon_m h_m \tag{3.10}$$

where h is the thickness of the relevant component.

Stress–strain relations

$$\sigma_2 = E_{cT}\varepsilon_{cT}, \sigma_f = E_f\varepsilon_f, \sigma_m = E_m\varepsilon_m \tag{3.11}$$

Then, from (3.10) and (3.11) we may write

$$\frac{\sigma_2}{E_2} = \frac{\sigma_f}{E_f}\frac{h_f}{h_c} + \frac{\sigma_m}{E_m}\frac{h_m}{h_c}$$

Using Eq. (3.9) and the fact that the thickness ratios will be equal to the corresponding volume fractions

$$\frac{1}{E_2} = \frac{V_f}{E_f} + \frac{V_m}{E_m} \tag{3.12}$$

$$E_2 = \frac{E_f E_m}{V_f E_m + V_m E_f} \tag{3.13}$$

Fig. 3.7 shows how the longitudinal and transverse moduli vary with volume fraction for a unidirectional fibre composite.

In practical terms the above analysis is too simplistic, particularly in regard to the assumption that the stresses in the fibre and matrix are equal. Generally the fibres are dispersed at random on any cross-section of the composite (see Fig. 3.8) and so the applied force will be shared by the fibres and matrix but not necessarily equally. Other inaccuracies also arise due to the mis-match of the Poisson's ratios for the fibres and matrix. Several other empirical equations

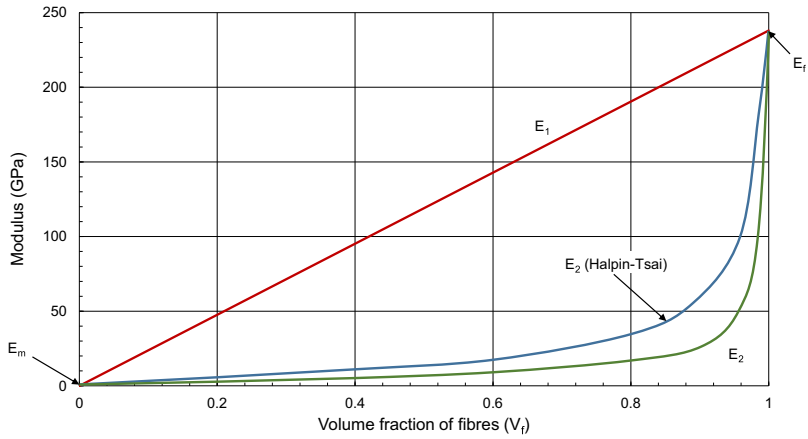


FIG. 3.7 Variation of longitudinal and transverse modulus in unidirectional composites.

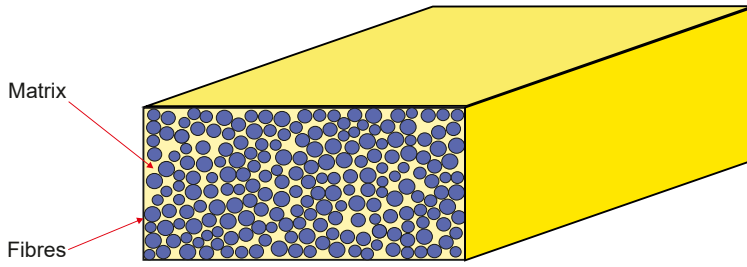


FIG. 3.8 Dispersion of fibres in cross-section of unidirectional composite.

have been suggested to take these factors into account. One of these is the Halpin−Tsai equation which has the following form

$$E_2 = E_m\left(\frac{1+2\beta V_f}{1-\beta V_f}\right) \tag{3.14}$$

where

$$\beta = \frac{(E_f/E_m)-1}{(E_f/E_m)+2}$$

The predictions from this equation are shown in Fig. 3.7.

Another alternative is the Brintrup equation which gives E_2 as

$$E_2 = \frac{E'_m E_f}{E_f(1-V_f)+V_f E'_m} \tag{3.15}$$

where

$$E'_m = E_m/\left(1-\nu_m^2\right)$$

A simplistic mechanics of materials analysis of the shear modulus G_{12} gives

$$\frac{1}{G_{12}} = \frac{V_f}{G_f} + \frac{V_m}{G_m}$$

or

$$G_{12} = \frac{G_f G_m}{V_f G_m + V_m G_f}$$

where the shear modulus of the fibres is the G_{12f} but it has been written as G_f for simplicity.

As in the case of the transverse tensile modulus, E_2, the above analysis tends to underestimate the in-plane shear modulus. Therefore, once again it is

common to resort to empirical relationships and the most popular is the Halpin–Tsai equation

$$G_{12} = G_m \left\{ \frac{(G_f + G_m) + V_f(G_f - G_m)}{(G_f + G_m) - V_f(G_f - G_m)} \right\} \tag{3.16}$$

Example 3.5. Calculate the transverse modulus of the PEEK/carbon fibre composite referred to in Example 3.2, using both the simplified solid mechanics approach and the empirical approach. For PEEK $v_m = 0.36$.
Solution From Eq. (3.13)

$$E_2 = \frac{3.8(400)}{0.3(3.8) + 0.7(400)} = 5.4 \text{ GPa}$$

Using the Halpin–Tsai equation

$$\beta = \frac{(E_f/E_m) - 1}{(E_f/E_m) + 2} = \frac{(400/3.8) - 1}{(400/3.8) + 2} = 0.97$$

$$E_2 = 3.8 \left[\frac{1 + 2(0.3)(0.97)}{1 - (0.3)(0.97)} \right] = 8.5 \text{ GPa}$$

Using the Brintrup equation

$$E'_m = 3.8/\left(1 - 0.36^2\right) = 4.37 \text{ GPa}$$

$$E_2 = \frac{(4.37)400}{400(1 - 0.3) + 0.3(4.37)} = 6.2 \text{ GPa}$$

Some typical elastic properties for unidirectional fibre composites are given in Table 3.4.

3.6 Deformation behaviour of a single ply or lamina

The previous section illustrated how to obtain the elastic properties of a unidirectional lamina. In practice considerably more information may be required about the behavioural characteristics of a single lamina. To obtain details of the stresses and strains at various orientations in a single ply the following type of analysis is required.

(i) Loading on fibre axis

Consider the situation of a thin unidirectional lamina under a state of plane stress as shown in Fig. 3.9. The properties of the lamina are anisotropic so it will have modulus values of E_1 and E_2 in the fibre and transverse directions,

TABLE 3.4 Typical elastic properties of unidirectional fibre reinforced plastics.

Material	Fibre volume fraction, V_f	E_1 (GPa)	E_2 (GPa)	G_{12} (GPa)	V_{12}
GFRP (E glass/ epoxy)	0.6	40	9	4	0.31
GFRP (E glass/ polyester)	0.42	32	7	3.1	0.35
KFRP (Kevlar 49/ epoxy)	0.6	79	4.1	1.5	0.43
CFRP (carbon/ epoxy)	0.6	125	9	4.4	0.34
CFRP (carbon HM/ epoxy)	0.62	497	5.3	5.6	0.31

CFRP, carbon fibre reinforced plastic; *GFRP*, glass fibre reinforced plastic; *KFRP*, Kevlar fibre reinforced plastic.

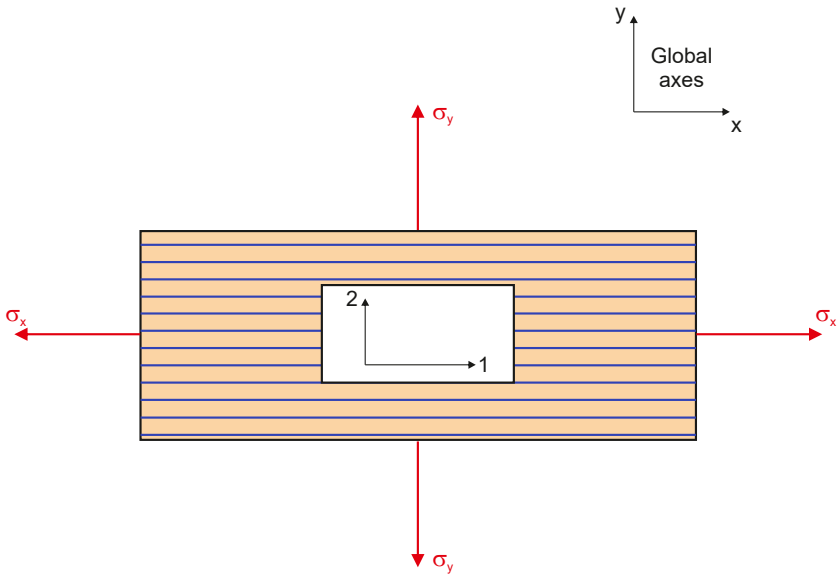


FIG. 3.9 Single thin lamina under plane stress.

respectively. The values of these parameters may be determined as illustrated above.

The direct strains in the global X and Y directions will be given by (see Appendix C for details)

$$\varepsilon_x = \frac{\sigma_x}{E_1} - \nu_{21}\frac{\sigma_y}{E_2} \tag{3.17}$$

$$\varepsilon_y = \frac{\sigma_y}{E_2} - \nu_{12}\frac{\sigma_x}{E_1} \tag{3.18}$$

and the shear strain γ_{xy} is related to the shear stress, τ_{xy}, and the shear modulus, G_{12}, by

$$\gamma_{xy} = \frac{\tau_{xy}}{G_{12}} \tag{3.19}$$

The convention normally used is that direct stresses and strains have one suffix to indicate the direction of the stress or strain. Shear stresses and strains have two suffices. The first suffix indicates the direction of the normal to the plane on which the stress acts and the second suffix indicates the direction of the stress (or strain). Poisson's Ratio has two suffices. Thus, ν_{12} is the negative ratio of the strain in the 2-direction to the strain in the 1-direction for a stress applied in the 1-direction ($\nu_{12} = -\varepsilon_2/\varepsilon_1$ for an applied σ_1). ν_{12} is sometimes referred to as the major Poisson's Ratio and ν_{21} is the minor Poisson's Ratio. In an isotropic material where $\nu_{21} = \nu_{21}$, then the suffices are not needed and normally are not used.

In the analysis of composites it is convenient to use matrix notation because this simplifies the computations very considerably. Thus, we may write the above equations as (see Appendix E)

$$\begin{Bmatrix} \varepsilon_x \\ \varepsilon_y \\ \gamma_{xy} \end{Bmatrix} = \begin{bmatrix} \dfrac{1}{E_1} & \dfrac{\nu_{21}}{E_2} & 0 \\ \dfrac{-\nu_{12}}{E_1} & \dfrac{1}{E_2} & 0 \\ 0 & 0 & \dfrac{1}{G_{12}} \end{bmatrix} \begin{Bmatrix} \sigma_x \\ \sigma_y \\ \tau_{xy} \end{Bmatrix}$$

or in abbreviated form

$$\{\varepsilon\} = [S]\{\sigma\} \tag{3.20}$$

where $[S]$ is called the *compliance* matrix.

In order to describe completely the state of triaxial (as opposed to biaxial) stress in an anisotropic material, the compliance matrix will have 36 terms. The reader is referred to the more advanced composites texts listed in the Bibliography if these more complex states of stress are of interest. It is

conventional to be consistent and use the terminology of the more general analysis even when one is considering the simpler plane stress situation. Hence, the compliance matrix [*S*] has the terms

$$[S] = \begin{bmatrix} S_{11} & S_{12} & S_{16} \\ S_{21} & S_{22} & S_{26} \\ S_{61} & S_{62} & S_{66} \end{bmatrix}$$

where

$$S_{11} = \frac{1}{E_1}, \quad S_{22} = \frac{1}{E_2}, \quad S_{66} = \frac{1}{G_{12}}$$

$$S_{12} = S_{21} = -\frac{\nu_{12}}{E_1} = -\frac{\nu_{21}}{E_2}$$

$$S_{16} = S_{61} = S_{26} = S_{62} = 0$$

Using matrix notation, Eq. (3.20) may be transposed to give the stresses as a function of the strains

$$\{\sigma\} = [S]^{-1}\{\varepsilon\}$$

This may also be written as

$$\{\sigma\} = [Q]\{\varepsilon\} \tag{3.21}$$

where [Q] is the stiffness matrix and its terms will be

$$Q_{11} = \frac{E_1}{1 - \nu_{12}\nu_{21}}, Q_{22} = \frac{E_2}{1 - \nu_{21}\nu_{12}}, Q_{66} = G_{12}$$

$$Q_{12} = Q_{21} = \frac{\nu_{12}E_2}{(1 - \nu_{12}\nu_{21})} = \frac{\nu_{21}E_1}{(1 - \nu_{21}\nu_{12})}$$

$$Q_{16} = Q_{61} = Q_{26} = Q_{62} = 0$$

(ii) Loading off the fibre axis

The previous analysis is a preparation for the more interesting and practical situation where the applied loading axis does not coincide with the fibre axis. This is illustrated in Fig. 3.10.

The first step in the analysis of this situation is the transformation of the applied stresses on to the fibre axis. Referring to Fig. 3.10 it may be seen that σ_x and σ_y may be resolved into the *x, y* axes as follows (the reader may wish to

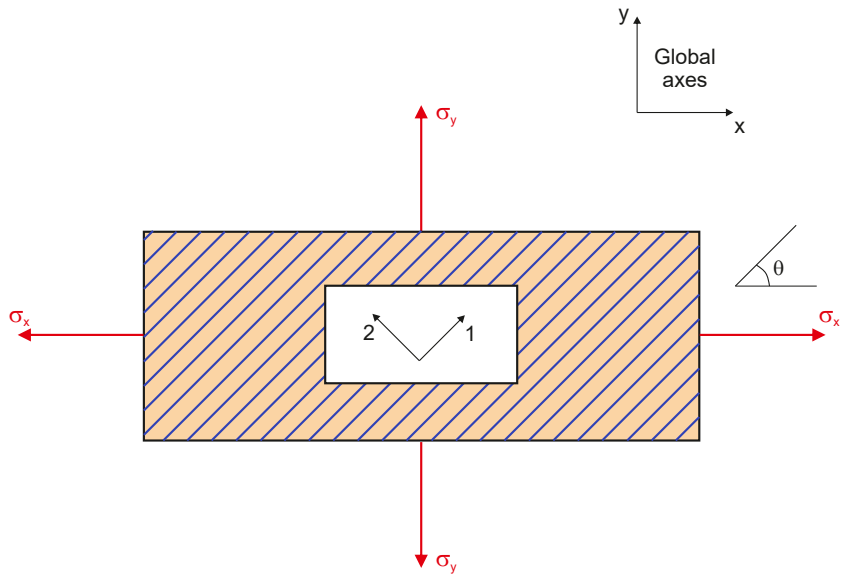


FIG. 3.10 Single thin lamina under plane stress.

refer to any standard Mechanics of Materials text such as Benham, Crawford and Armstrong for more details of this stress transformation):

$$\sigma_1 = \sigma_x \cos^2\theta + \sigma_y \sin^2\theta + 2\tau_{xy}\sin\theta\cos\theta$$
$$\sigma_2 = \sigma_x \sin^2\theta + \sigma_y \cos^2\theta - 2\tau_{xy}\sin\theta\cos\theta$$
$$\tau_{12} = -\sigma_x \sin\theta\cos\theta + \sigma_y \sin\theta\cos\theta + \tau_{xy}\left(\cos^2\theta - \sin^2\theta\right)$$

Using matrix notation

$$\begin{Bmatrix} \sigma_1 \\ \sigma_2 \\ \sigma_{12} \end{Bmatrix} = \begin{bmatrix} c^2 & s^2 & 2sc \\ s^2 & c^2 & -2sc \\ -sc & sc & (c^2 - s^2) \end{bmatrix} \begin{Bmatrix} \sigma_x \\ \sigma_y \\ \tau_{xy} \end{Bmatrix} \tag{3.22}$$

where $c = \cos\theta$ and $s = \sin\theta$.

In shorthand form, this matrix equation may be written as

$$\{\sigma\}_{12} = [T_\sigma]\{\sigma\}_{xy}$$

where $[T_\sigma]$ is called the **Stress Transformation** matrix.

Similar transformations may be made for the strains so that

$$\begin{Bmatrix} \varepsilon_1 \\ \varepsilon_2 \\ \frac{1}{2}\gamma_{12} \end{Bmatrix} = [T_\sigma] \begin{Bmatrix} \varepsilon_x \\ \varepsilon y \\ \frac{1}{2}\gamma_{xy} \end{Bmatrix} \tag{3.23}$$

In each case the stresses in the global directions *x, y* may also be expressed in terms of the local stresses or strains. For example,

$$\begin{Bmatrix} \sigma_x \\ \sigma_y \\ \tau_{xy} \end{Bmatrix} = [T_\sigma]^{-1} \begin{Bmatrix} \sigma_1 \\ \sigma_2 \\ \tau_{12} \end{Bmatrix}$$

where

$$[T_\sigma]^{-1} = \begin{bmatrix} c^2 & s^2 & -2sc \\ s^2 & c^2 & 2sc \\ sc & -sc & (c^2 - s^2) \end{bmatrix}$$

Now, in order to determine the stiffness in the global *(x, y)* directions for a lamina in which the fibres are aligned at an angle θ to the global x direction, it is necessary to go through the following three steps:

1. Determine the strains in the local (1,2) directions by transforming the applied strains through θ from the global (x,y) directions.
2. Calculate the stresses in the local directions using the on-axis stiffness matrix $[Q]$ derived earlier.
3. Transform the stresses back to the global directions through an angle of $-\theta^{\circ}$.

Using matrix notation, these three steps are carried out as follows:

Step 1

$$\begin{Bmatrix} \varepsilon_1 \\ \varepsilon_2 \\ \gamma_{12} \end{Bmatrix} = \begin{bmatrix} c^2 & s^2 & sc \\ s^2 & c^2 & -sc \\ -2_{sc} & 2_{sc} & (c^2 - s^2) \end{bmatrix} \begin{Bmatrix} \varepsilon_x \\ \varepsilon_y \\ \gamma_{xy} \end{Bmatrix}$$

Note the modification to $[T_\sigma]$ to give the **Strain Transformation** matrix T_ε so that we can use γ_{12} instead of $\frac{1}{2}\gamma_{12}$.

Step 2

$$\begin{Bmatrix} \sigma_1 \\ \sigma_2 \\ \sigma_{12} \end{Bmatrix} = \begin{bmatrix} Q_{11} & Q_{12} & 0 \\ Q_{21} & Q_{22} & 0 \\ 0 & 0 & Q_{66} \end{bmatrix} \begin{Bmatrix} \varepsilon_1 \\ \varepsilon_2 \\ \gamma_{12} \end{Bmatrix}$$

Step 3

$$\begin{Bmatrix} \sigma_x \\ \sigma_y \\ \tau_{xy} \end{Bmatrix} = \begin{bmatrix} c^2 & s^2 & -2sc \\ s^2 & c^2 & 2sc \\ sc & -sc & (c^2 - s^2) \end{bmatrix} \begin{Bmatrix} \sigma_1 \\ \sigma_2 \\ \tau_{12} \end{Bmatrix}$$

Linking these steps together to obtain the global stresses in terms of the global strains

$$\begin{Bmatrix} \sigma_x \\ \sigma_y \\ \tau_{xy} \end{Bmatrix} = \begin{bmatrix} c^2 & s^2 & -2sc \\ s^2 & c^2 & 2sc \\ sc & -sc & (c^2 - s^2) \end{bmatrix} \begin{bmatrix} Q_{11} & Q_{12} & 0 \\ Q_{21} & Q_{22} & 0 \\ 0 & 0 & Q_{66} \end{bmatrix} \times \begin{bmatrix} c^2 & s^2 & sc \\ s^2 & c^2 & -sc \\ -2sc & 2sc & (c^2 - s^2) \end{bmatrix} \begin{Bmatrix} \varepsilon_x \\ \varepsilon_\gamma \\ \gamma_{xy} \end{Bmatrix}$$

which provides an overall stiffness matrix $[\overline{Q}]$

$$\begin{Bmatrix} \sigma_x \\ \sigma_\gamma \\ \tau_{xy} \end{Bmatrix} = [\overline{Q}] \begin{Bmatrix} \varepsilon_x \\ \varepsilon_\gamma \\ \tau_{xy} \end{Bmatrix} \tag{3.24}$$

where

$$\overline{Q}_{11} = \frac{1}{\lambda}\left[E_1\cos^4\theta + E_2\sin^4\theta + (2\nu_{12}E_2 + 4\lambda G_{12})\cos^2\theta\sin^2\theta\right]$$

$$\overline{Q}_{21} = \overline{Q}_{12} = \frac{1}{\lambda}\left[\nu_{12}E_2\left(\cos^4\theta + \sin^4\theta\right) + (E_1 + E_2 - 4\lambda G_{12})\cos^2\theta\sin^2\theta\right]$$

$$\overline{Q}_{61} = \overline{Q}_{16} = \frac{1}{\lambda}\left[\cos^3\theta\sin\theta(E_1 - \nu_{12}E_2 - 2\lambda G_{12}) - \cos\theta\sin^3\theta (E_2 - \nu_{12}E_2 - 2\lambda G_{12})\right]$$

$$\overline{Q}_{22} = \frac{1}{\lambda}\left[E_2\cos^4\theta + E_1\sin^4\theta + \sin^2\theta\cos^2\theta(2\nu_{12}E_2 + 4\lambda G_{12})\right]$$

$$\overline{Q}_{62} = \overline{Q}_{26} = \frac{1}{\lambda}\left[\cos\theta\sin^3\theta(E_1 - \nu_{12}E_2 - 2\lambda G_{12}) - \cos^3\theta\sin\theta (E_2 - \nu_{12}E_2 - 2\lambda G_{12})\right]$$

$$\overline{Q}_{66} = \frac{1}{\lambda}\left[\sin^2\theta\cos^2\theta(E_1 + E_2 - 2\nu_{12}E_2 - 2\lambda G_{12}) + \lambda G_{12}\left(\cos^4\theta s + \sin^4\theta\right)\right]$$

in which $\lambda = (1 - \nu_{12}\nu_{21})$ and $\nu_{12}E_2 = \nu_{21}E_1$.

By a similar analysis it may be shown that, for applied stresses (rather than applied strains) in the global directions, the overall compliance matrix $[\overline{S}]$ has the form

$$\begin{Bmatrix} \varepsilon_x \\ \varepsilon_y \\ \gamma_{xy} \end{Bmatrix} = \begin{bmatrix} \overline{S}_{11} & \overline{S}_{12} & \overline{S}_{16} \\ \overline{S}_{21} & \overline{S}_{22} & \overline{S}_{26} \\ \overline{S}_{61} & \overline{S}_{62} & \overline{S}_{66} \end{bmatrix} \begin{Bmatrix} \sigma_x \\ \sigma_y \\ \tau_{xy} \end{Bmatrix} \tag{3.25}$$

where $[\overline{S}] = [\overline{Q}]^{-1}$ and the individual terms are

$$\overline{S}_{11} = S_{11}\cos^4\theta + S_{22}\sin^4\theta + (2S_{12} + S_{66})\cos^2\theta\sin^2\theta$$

$$\overline{S}_{21} = \overline{S}_{12} = (S_{11} + S_{22} - S_{66})\cos^2\theta\sin^2\theta + S_{12}\left(\cos^4\theta + \sin^4\theta\right)$$

$$\overline{S}_{61} = \overline{S}_{16} = (2S_{11} - 2S_{12} - S_{66})\cos^3\theta\sin\theta - (2S_{22} - 2S_{12} - S_{66})\sin^3\theta\cos\theta$$

$$\overline{S}_{22} = S_{11}\sin^4\theta + S_{22}\cos^4\theta + (2S_{12} + S_{66})\cos^2\theta\sin^2\theta$$

$$\overline{S}_{62} = \overline{S}_{26} = (2S_{11} - 2S_{12} - S_{66})\cos\theta\sin^3\theta - (2S_{22} - 2S_{12} - S_{66})\sin\theta\cos^3\theta$$

$$\overline{S}_{66} = 4(S_{11} - 2S_{12} - S_{66})\cos^2\theta\sin^2\theta + S_{66}\left(\cos^2\theta - \sin^2\theta\right)^2$$

from which, using the earlier terms from the on-axis lamina stiffness matrix [*S*],

$$\frac{1}{E_x} = \overline{S}_{11} = \frac{c^2}{E_1}\left(c^2 - s^2\nu_{12}\right) + \frac{s^2}{E_2}\left(s^2 - c^2\nu_{21}\right) + \frac{c^2s^2}{G_{12}}$$

$$\frac{1}{E_y} = \overline{S}_{22} = \frac{s^2}{E_1}\left(s^2 - c^2\nu_{12}\right) + \frac{c^2}{E_2}\left(c^2 - s^2\nu_{21}\right) + \frac{c^2s^2}{G_{12}}$$

$$\frac{1}{G_{xy}} = \overline{S}_{66} = \frac{4c^2s^2}{E_1}(1 + \nu_{12}) + \frac{4c^2s^2}{E_2}(1 + \nu_{21}) + \frac{(c^2 - s^2)^2}{G_{12}}$$

$$\frac{\nu_{xy}}{E_x} = \frac{\nu_{yx}}{E_y} = -\overline{S}_{21} = \frac{c^2}{E_1}\left(c^2\nu_{12} - s^2\right) + \frac{s^2}{E_2}\left(s^2\nu_{21} - c^2\right) + \frac{c^2s^2}{G_{12}}$$

Thus, one may use the above expressions to calculate the stiffness of a unidirectional lamina when it is loaded at any angle θ to the fibre direction. If computer facilities are available for the matrix manipulation, then it is not necessary to work out the individual terms as above – the required information can be determined directly from the matrices. For example, as indicated above

$$E_x = \frac{1}{\overline{S}_{11}}, E_y = \frac{1}{S_{22}}, G_{xy} = \frac{1}{S_{66}} \tag{3.26}$$

3.7 Summary of approach to analysis of unidirectional composites

1. The strains and stresses in the local (1−2) axis are related by

$$[\varepsilon]_{12} = [S][\sigma]_{12}$$

or

$$[\sigma]_{12} = [Q][\varepsilon]_{12}$$

$$\textit{where} \quad [Q] = [S]^{-1}$$

2. The global *(x−y)* stresses and strains may be related to the local (1−2) stresses and strains by

$$[\sigma]_{12} = [T_\sigma][\sigma]_{xy}$$
$$[\varepsilon]_{12} = [T_\varepsilon][\varepsilon]_{xy}$$

3. The global stresses and strains are related by

$$[\varepsilon]_{xy} = [\overline{S}][\sigma]_{xy}$$
$$[\sigma]_{xy} = [\overline{Q}][\varepsilon]_{xy}$$

where

$$[\overline{Q}] = [T_\sigma]^{-1}[Q][T_\varepsilon] \quad \text{and} \quad [\overline{S}] = [\overline{Q}]^{-1}$$

In each case $[\sigma]_{12}$ and $[\varepsilon]_{12}$ are written as shorthand for

$$\begin{bmatrix} \sigma_1 \\ \sigma_2 \\ \tau_{12} \end{bmatrix} \quad \text{and} \quad \begin{bmatrix} \varepsilon_1 \\ \varepsilon_2 \\ \gamma_{12} \end{bmatrix}$$

The following Examples illustrate the use of these equations.

Example 3.6. A unidirectional composite consisting of carbon fibres in a PEEK matrix has the fibres aligned at 25° to the loading axis. If the fibres and matrix have the properties indicated below, calculate E_x, E_y, G_{xy}, v_{xy}, and v_{yx}.

$$E_f = 240 \text{ GPa} \qquad E_m = 3 \text{ GPa}$$
$$\nu_f = 0.23 \qquad \nu_m = 0.35$$
$$V_f = 0.6$$
$$\rho_f = 1700 \text{ kg/m}^3 \qquad \rho_m = 1300 \text{ kg/m}^3$$
$$G_f = 80 \text{ GPa} \qquad G_m = 1.1 \text{ GPa}$$

Solution The lamina properties in the local (1−2) directions are calculated as follows:

$$E_1 = E_f \nu_f + E_m \cdot (1 - V_f), \qquad E_1 = 145.2 \text{ GPa}$$
$$E_2 = \frac{E_m \cdot (1 + 2 \cdot \beta \cdot V_f)}{(1 - \beta \cdot V_f)}, \qquad E_2 = 15.33 \text{ GPa}$$

Halpin-Tsai Equation

$$G_{12} = G_m \cdot \frac{(G_f + G_m) + V_f (G_f - G_m)}{(G_f + G_m) - V_f (G_f - G_m)},$$

$G_{12} = 4.185$ GPa Halpin-Tsai Equation

$$\nu_{12} = \nu_f \cdot V_f + \nu_m \cdot (1 - V_f), \qquad \nu_{12} = 0.278$$
$$\nu_{21} = \nu_{12} \cdot \left(\frac{E_2}{E_1}\right), \qquad \nu_{21} = 0.029$$

The behaviour of the lamina when subjected to loading at θ degrees off the fibre axis is determined using matrix manipulation as follows:

Loading On − Axis Compliance Matrix *Stiffness Matrix*

$$S = \begin{bmatrix} \frac{1}{E_1} & -\frac{\nu_{21}}{E_2} & 0 \\ -\frac{\nu_{12}}{E_1} & \frac{1}{E_2} & 0 \\ 0 & 0 & \frac{1}{G_{12}} \end{bmatrix} \qquad Q = S^{-1}$$

Stress Transformation Matrix *Overall Compliance Matrix*

$$S = \begin{bmatrix} c^2 & s^2 & 2.s.c \\ s^2 & c^2 & -2.s.c \\ -s.c & s.c & (c^2 - s^2) \end{bmatrix} \qquad \overline{S} = \overline{Q}^{-1}$$

The lamina properties are then obtained as:

$$\overline{S}_{11} = 0.041, \qquad E_x = \frac{1}{S_{11}} \qquad E_x = 24.26 \text{ GPa}$$

$$\overline{S}_{22} = 0.079, \qquad E_y = \frac{1}{S_{22}} \qquad E_y = 12.7 \text{ GPa}$$

$$\overline{S}_{66} = 0.143, \qquad G_{xy} = \frac{1}{\overline{S}_{66}} \qquad G_{xy} = 6.9 \text{ GPa}$$

$$\overline{S}_{21} = 0.026, \quad v_{xy} = -E_x \bullet \overline{S}_{21}, \quad v_{yx} = -E_y \cdot \overline{S}_{12},$$

$$v_{xy} = 0.627, \quad v_{yx} = -0.328$$

Alternatively the lamina properties can be calculated from the equations given above.

$$\overline{S}_{11} = \frac{c^2}{E_1} \cdot \left(c^2 - s^2 \cdot v_{12}\right) + \frac{s^2}{E_2} \cdot \left(s^2 - c^2 \cdot v_{21}\right) + \frac{c^2 \cdot s^2}{G_{12}} = 0.041,$$

$$E_x = \frac{1}{S_{11}} = 24.26$$

$$\overline{S}_{22} = \frac{s^2}{E_1} \cdot \left(s^2 - c^2 \cdot v_{12}\right) + \frac{c^2}{E_2} \cdot \left(c^2 - s^2 \cdot v_{21}\right) + \frac{c^2 \cdot s^2}{G_{21}} = 0.079,$$

$$E_y = \frac{1}{\overline{S}_{22}} = 12.702$$

$$\overline{S}_{66} = \frac{4 \cdot c^2 \cdot s^2}{E_1} \cdot (1 + v_{12}) + \frac{4 \cdot c^2 \cdot s^2}{E_2} \cdot (1 + v_{21}) + \frac{\left(c^2 \cdot s^2\right)^2}{G_{12}} = 0.143,$$

$$G_{xy} = \frac{1}{\overline{S}_{66}} = 6.9$$

$$\overline{S}_{12} = \frac{c^2}{E_1} \cdot \left(c^2 - v_1 - s^2\right) + \frac{s^2}{E_2} \cdot \left(s^2 \cdot v^2 - c^2\right) + \frac{c^2 \cdot s^2}{G_{12}}$$

$$v_{xy} = -\overline{S}_{21} \cdot E_x, v_{xy} = 0.627$$

$$v_{yx} = -\overline{S}_{12} \cdot E_y, v_{yx} = 0.328$$

In this Example the angle, θ, was set at 25°. Fig. 3.11 shows the variation of the moduli and Poisson's Ratio values for all angles between 0° and 90°. This gives an interesting overview of the performance of unidirectional composites when subjected to off-axis loading.

Example 3.7. A thin unidirectional Kevlar fibre/epoxy composite has the properties listed below. If the fibres are aligned at θ to the x-axis, show how the strains in the global XY directions vary with θ when a stress σ is applied as shown in Fig. 3.12.

$$E_1 = 80,000 \text{ MPa}, E_2 = 4000 \text{ MPa}, G_{12} = 1500 \text{ MPa}, v_{12} = 0.43$$

Solution Let $\theta = 25°$ and $\sigma_x = 10$ MPa to illustrate the method of solution.

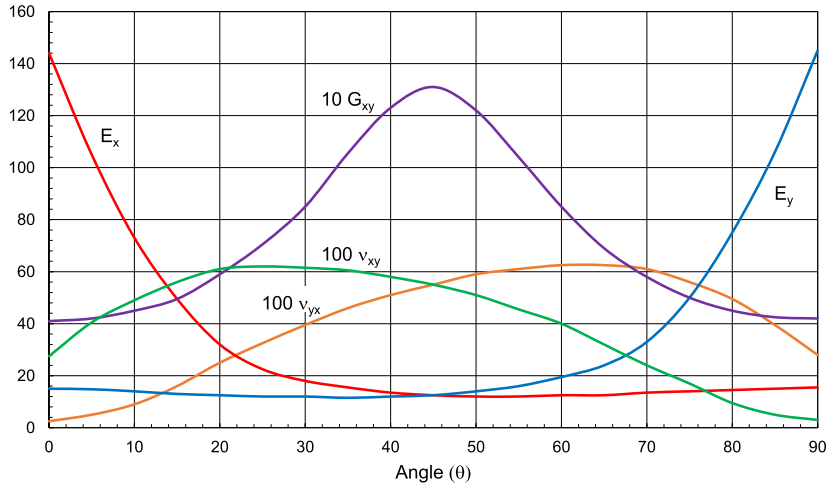


FIG. 3.11 Variation of properties in unidirectional composite as a function of fibre angle.

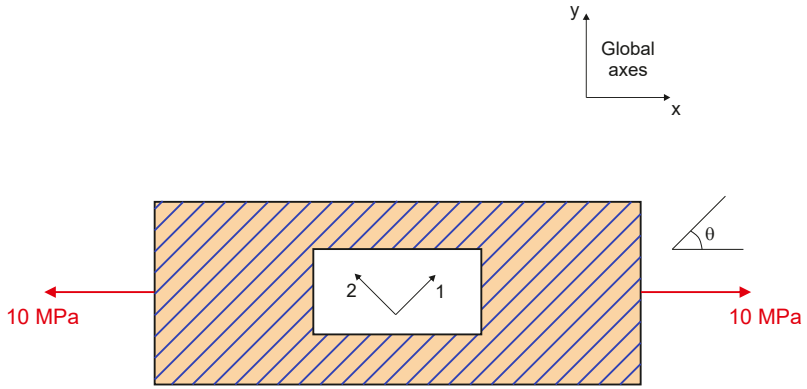


FIG. 3.12 Unidirectional Kevlar/epoxy composite (single ply).

The stress transformation matrix is

$$T_\sigma = \begin{bmatrix} c^2 & s^2 & 2sc \\ s^2 & c^2 & -2sc \\ -sc & sc & (c^2 - s^2) \end{bmatrix} \quad \text{or} \quad T_\sigma = \begin{pmatrix} 0.821 & 0.179 & 0.766 \\ 0.179 & 0.821 & -0.766 \\ -0.383 & 0.383 & 0.643 \end{pmatrix}$$

In order to get the strains in the global directions it is necessary to determine the overall compliance matrix $[\overline{S}]$. This is obtained as indicated above, i.e.

$$[\overline{S}] = [\overline{Q}]^{-1} \quad \text{where} \quad [\overline{Q}] = [T_\sigma]^{-1}[Q]\cdot[T_\varepsilon]$$

The local compliance matrix is

$$s = \begin{bmatrix} \frac{1}{E_1} & \frac{-v12}{E_1} & 0 \\ \frac{-v_{12}}{E_1} & \frac{1}{E_2} & 0 \\ 0 & 0 & \frac{1}{G_{12}} \end{bmatrix} \quad \text{and} \quad Q = S^{-1}$$

The Strain Transformation matrix is

$$T_\varepsilon = \begin{bmatrix} c^2 & s^2 & sc \\ s^2 & c^2 & -sc \\ -2sc & 2sc & (c^2 - s^2) \end{bmatrix}$$

So,

$$\overline{Q} = T_\sigma^{-1}\cdot Q\cdot T_\varepsilon \quad \text{and} \quad \overline{S} = \overline{Q}^{-1}$$

Then

$$\begin{bmatrix} \varepsilon_x \\ \varepsilon_y \\ \gamma_{xy} \end{bmatrix} = \overline{S}\begin{bmatrix} \sigma_x \\ \sigma_y \\ \tau_{xy} \end{bmatrix} \overline{S} = \begin{bmatrix} 1.12\cdot10^{-4} & -6.3\cdot10^{-5} & -1.87\cdot10^{-4} \\ -6.3\cdot10^{-5} & 2.65\cdot10^{-4} & 5.89\cdot10^{-6} \\ -1.87\cdot10^{-4} & 5.89\cdot10^{-6} & 4.35\cdot10^{-4} \end{bmatrix}$$

Directly by matrix manipulation

$$\varepsilon_x = 1.126\cdot10^{-3} \quad \varepsilon_y = -6.309\cdot10^{-4} \quad \gamma_{xy} = -1.878\cdot10^{-3}$$

or by multiplying out the terms

$$\varepsilon_x = \left[\left(\overline{S}_{11}\right)\cdot(\sigma_x) + \left(\overline{S}_{12}\right)\cdot(\sigma_y)\right] + \left(\overline{S}_{16}\right)\cdot(\tau_{xy}) \quad \varepsilon_x = 1.126\cdot10^{-3}$$

and similarly for the other two strains. Fig. 3.13 illustrates how the strains vary for different values of θ.

Example 3.8. A thin unidirectional carbon fibre composite is loaded as shown in Fig. 3.14 and has the properties listed below. If the fibres are aligned at 35° to the x-axis, calculate the stresses parallel and perpendicular to the fibres when the stresses σ_x, σ_y and τ_{xy} are applied. Calculate also the strains in the global XY directions.

$$E_1 = 125,000 \text{ MPa}, \quad E_2 = 7800 \text{ MPa}, \quad G_{12} = 4400 \text{ MPa},$$

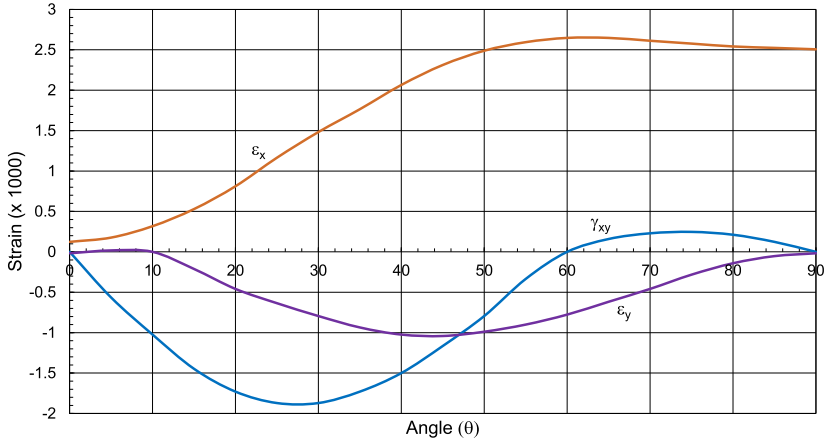


FIG. 3.13 Variation in direct and shear strains for unidirectional composite loaded axially.

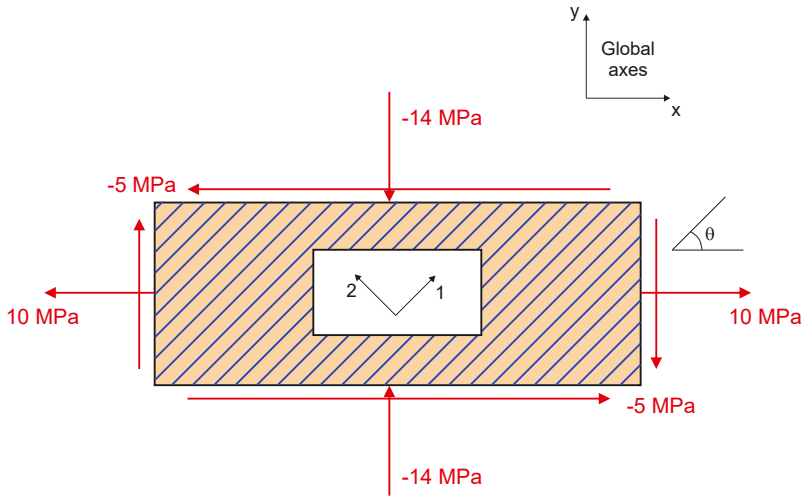


FIG. 3.14 Unidirectional carbon fibre single ply composite.

$$v_{12} = 0.34 \quad \sigma_x = 10 \text{ MPa}, \quad \sigma_y = -14 \text{ MPa}, \quad \tau_{xy} = -5 \text{ MPa}$$

Solution The stress transformation matrix is

$$T_\sigma = \begin{bmatrix} c^2 & s^2 & 2sc \\ s^2 & c^2 & -2sc \\ -sc & sc & (c^2 - s^2) \end{bmatrix} \quad \text{or} \quad T_\sigma = \begin{pmatrix} 0.671 & 0.329 & 0.94 \\ 0.329 & 0.671 & -0.94 \\ -0.47 & 0.47 & 0.342 \end{pmatrix}$$

The stresses parallel and perpendicular to the fibres are then given by

$$\begin{bmatrix} \sigma_1 \\ \sigma_2 \\ \tau_{12} \end{bmatrix} = T_\sigma \bullet \begin{bmatrix} \sigma_x \\ \sigma_y \\ \tau_{xy} \end{bmatrix}$$

So,

$$\sigma_1 = -2.59 \text{ MPa } \sigma_2 = -14 \text{ MPa } \tau_{12} = -12.98 \text{ MPa}$$

In order to get the strains in the global directions it is necessary to determine the overall compliance matrix $[\overline{S}]$. This is obtained as indicated above, i.e.

$$[\overline{S}] = [\overline{Q}]^{-1} \quad \textit{where} \quad [\overline{Q}] = [T_\sigma]^{-1} \cdot [Q] \cdot [T_\varepsilon]$$

The local compliance matrix is

$$D = \begin{bmatrix} \dfrac{1}{E_1} & \dfrac{-v_{12}}{E_1} & 0 \\ \dfrac{-v_{12}}{E_1} & \dfrac{1}{E_2} & 0 \\ 0 & 0 & \dfrac{1}{G_{12}} \end{bmatrix} \quad \textit{and} \quad Q = S^{-1}$$

The strain transformation matrix is

$$T_\varepsilon = \begin{bmatrix} c^2 & s^2 & sc \\ s^2 & c^2 & -sc \\ -2sc & 2sc & (c^2 - s^2) \end{bmatrix}$$

So,

$$\overline{Q} = T_\sigma^{-1} \cdot Q \cdot T_\varepsilon \quad \textit{and} \quad \overline{S} = \overline{Q}^{-1}$$

Then

$$\begin{bmatrix} \varepsilon_x \\ \varepsilon_y \\ \gamma_{xy} \end{bmatrix} = \overline{S} \cdot \begin{bmatrix} \sigma_x \\ \sigma_y \\ \tau_{xy} \end{bmatrix} \quad \overline{S} = \begin{pmatrix} 6.64 \times 10^{-5} & -2.16 \times 10^{-5} & -7.02 \times 10^{-5} \\ -2.16 \times 10^{-5} & 1.07 \times 10^{-4} & -4.27 \times 10^{-5} \\ -7.02 \times 10^{5} & -4.27 \times 10^{-5} & 1.51 \times 10^{-4} \end{pmatrix}$$

Directly by matrix manipulation

$$\varepsilon_x = 1.318 \times 10^{-3} \quad \varepsilon_y = -1.509 \times 10^{-3} \quad \gamma_{xy} = 8.626 \times 10^{-4}$$

or by multiplying out the terms

$$\varepsilon_x = \left[\left(\overline{S}_{11}\right)\cdot(\sigma_x) + \left(\overline{S}_{12}\right)\cdot(\sigma_y)\right] + \left(\overline{S}_{16}\right)\cdot(\tau_{xy}) \quad \varepsilon_x = 1.318 \times 10^{-3}$$

and similarly for the other two strains.

3.8 General deformation behaviour of a single ply

The previous section has considered the in-plane deformations of a single ply. In practice, real engineering components are likely to be subjected to this type of loading plus (or as an alternative) bending deformations. It is convenient at this stage to consider the flexural loading of a single ply because this will develop the method of solution for multi-ply laminates.

(i) Loading on fibre axis

Consider a unidirectional sheet of material with the fibres aligned in the x-direction and subjected to a stress, σ_x. if the sheet has thickness, h, as shown in Fig. 3.15 and we consider unit width, then the normal axial force N_x given by

$$N_x = \int_{-\frac{h}{2}}^{\frac{h}{2}} \sigma_x dz$$

Or more generally for all the force components N_x, N_y *and* N_{xy}

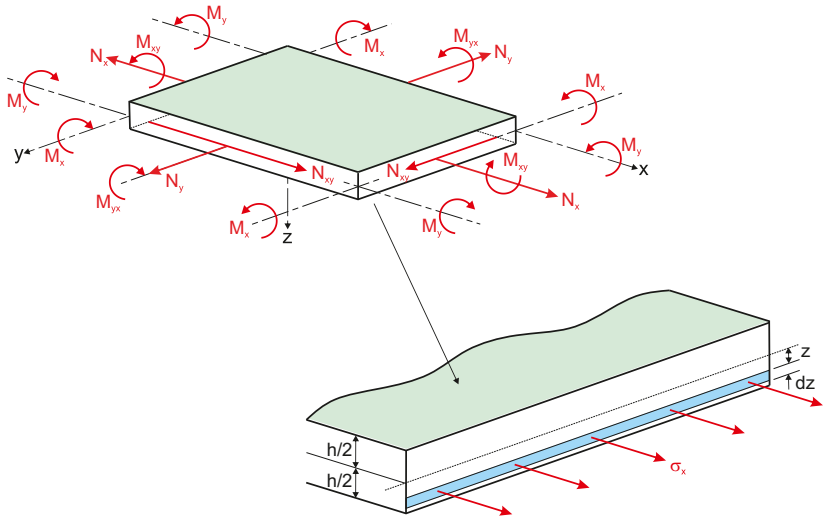


FIG. 3.15 General forces and moments acting on a single ply.

$$[N] = \int_{-\frac{h}{2}}^{\frac{h}{2}} [\sigma] dz \tag{3.27}$$

Similarly the bending moment, M_1, per unit width is given by

$$M_x = \int_{-\frac{h}{2}}^{\frac{h}{2}} \sigma_x \bullet z \bullet dz$$

Once again, all the moments M_x, M_y and M_{xy}, can be expressed as

$$[M] = \int_{-\frac{h}{2}}^{\frac{h}{2}} [\sigma] z \ dz \tag{3.28}$$

Now in order to determine $[\sigma]$ *as* a function of z, consider the strain $\varepsilon(z)$ at any depth across the section. It will be made up of an in-plane component (ε) plus a bending component (z/R) which is normally written as $z.\kappa$, where κ the curvature of bending.

Hence,

$$\varepsilon(z) = \varepsilon + z.\kappa$$

The stresses will then be given by

$$\sigma(z) = [Q] \bullet [\varepsilon] + [Q] \bullet z.[\kappa]$$

where $[Q]$ is the stiffness matrix as defined earlier.

Now, from Eq. (3.27), the forces $[N]$ are given by

$$[N] = \int_{\frac{-h}{2}}^{\frac{h}{2}} [Q] \cdot [\varepsilon] \cdot dz + \int_{\frac{-h}{2}}^{\frac{h}{2}} [Q] \cdot [\kappa] \cdot z dz$$

$$= [Q][\varepsilon]\mathrm{h} + [Q]\frac{1}{2}\left(\frac{h^2}{4} - \frac{h^2}{4}\right)[\kappa]$$

$$[N] = [A][\varepsilon] + [B][\kappa] \tag{3.29}$$

where $[A]$ is the *Extensional Stiffness* matrix ($= [Q]h$) and $[B]$ is a *Coupling Matrix*. It may be observed that in the above analysis $[B]$ is in fact zero for this simple single ply situation. However, its identity has been retained as it has relevance in laminate analysis, to be studied later.

Returning to Eq. (3.28), the moments may be written as

$$[M] = [Q][\varepsilon] \int_{\frac{-h}{2}}^{\frac{h}{2}} z dz + [Q][\kappa] \int_{\frac{-h}{2}}^{\frac{h}{2}} z^2 dz$$

$$= [B][\varepsilon] + [Q][\kappa] \cdot \frac{h^3}{12}$$

$$[M] = [B][\varepsilon] + [D][\kappa] \tag{3.30}$$

where $[D]$ is the Bending Stiffness Matrix ($= [Q]h^3/12$).

Eqs. (3.29) and (3.30) may be grouped into the following form

$$\begin{bmatrix} N \\ M \end{bmatrix} = \begin{bmatrix} A & B \\ B & D \end{bmatrix} \begin{bmatrix} \varepsilon \\ \kappa \end{bmatrix} \tag{3.31}$$

and these are known as the *Plate Constitutive Equations.*

For this special case of a single ply, $[B] = 0$ and so the forces are related to the strains by

$$[N] = [A][\varepsilon] \tag{3.32}$$

(which is effectively $[\sigma] = [Q][\varepsilon]$ as shown previously) or the strains are related to the forces by

$$[\varepsilon] = [a][N] \quad \text{where} \quad [a] = [A]^{-1}$$

(which is effectively $[\varepsilon] = [S][\sigma]$ as shown previously).

Also, for the single ply situation, the moments are related to the curvature by

$$[M] = [D][\kappa] \tag{3.33}$$

or the curvature is related to the moments by

$$[\kappa] = [d][M] \quad \text{where} \quad [d] = [D]^{-1}$$

It should be noted that it is only possible to utilise $[a] = [A]^{-1}$ and $[d] = [D]^{-1}$ for the special case where $[B] = 0$. In other cases, the terms in the $[a]$ and $[d]$ matrices have to be determined from

$$\begin{bmatrix} a & b \\ \beta & d \end{bmatrix} = \begin{bmatrix} A & B \\ B & D \end{bmatrix}^{-1} \tag{3.34}$$

(ii) Loading off fibre axis

For the situation where the loading is applied off the fibre axis, then the above approach involving the Plate Constitutive Equations can be used but it is necessary to use the *transformed* stiffness matrix terms $\overline{Q}$.

Hence, in the above analysis

$$[A] = [\overline{Q}] \cdot h$$
$$[D] = [\overline{Q}] \cdot h^3/12$$

The use of the Plate Constitutive Equations is illustrated in the following examples.

Example 3.9. For the 2 mm thick unidirectional carbon fibre/PEEK composite described in Example 3.6, calculate the values of the moduli, Poisson's Ratio and strains in the global direction when a stress of $\sigma_x = 50$ MPa is applied. You should use

(i) the lamina stiffness and compliance matrix approach and

(ii) the Plate Constitutive Equation approach.

Solution

(i) As shown in Example 3.6, for the loading in Fig. 3.16

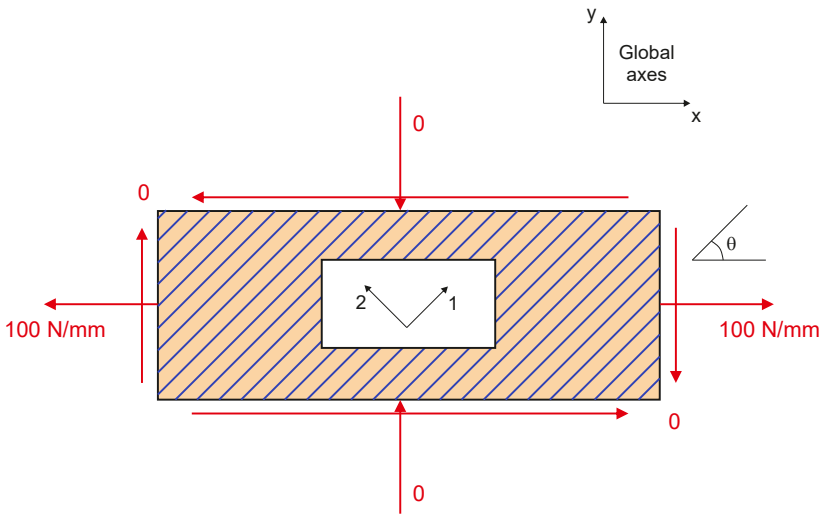


FIG. 3.16 Single ply composite subjected to plane stress.

$$\overline{S} = \begin{bmatrix} 4.12 \times 10^{-5} & -2.58 \times 10^{-5} & -6.24 \times 10^{-5} \\ -2.58 \times 10^{-5} & 7.87 \times 10^{-5} & 1.77 \times 10^{-5} \\ -6.24 \times 10^{-5} & 1.77 \times 10^{-5} & 1.43 \times 10^{-4} \end{bmatrix} \text{m}^2/\text{MN}$$

and

$$E_x = \frac{1}{\overline{S}_{11}} = 24.26 \text{ GPa}, \quad E_y = \frac{1}{\overline{S}_{22}} = 12.7 \text{ GPa}$$

$$G_{xy} = \frac{1}{\overline{S}_{66}} = 6.9 \text{ GPa}, \quad v_{xy} = -E_x \overline{S}_{21} = 0.627$$

$$v_{yx} = -E_y \overline{S}_{12} = 0.328$$

Also,

$$\begin{bmatrix} \varepsilon_x \\ \varepsilon_y \\ \gamma_{xy} \end{bmatrix} = \overline{S} \begin{bmatrix} \sigma_x \\ \sigma_y \\ \tau_{xy} \end{bmatrix}$$

So,

$$\varepsilon_x = 2.06 \times 10^{-3}, \quad \varepsilon_y = -1.29 \times 10^{-3}, \quad \gamma_{xy} = -3.12 \times 10^{-3}$$

Note that

$$\varepsilon_x = \frac{\sigma_x}{E_x} - v_{yx}\frac{\sigma_y}{E_y}$$

$$\varepsilon_y = \frac{\sigma_y}{E_y} - v_{xy}\frac{\sigma_x}{E_x}$$

As $\sigma_y = 0$ in this example

$$v_{xy} = -\frac{\varepsilon_y}{\varepsilon_x} = 0.627 \text{ as above}$$

(ii) Alternatively using the Plate Constitutive Equation Approach.

$$N_x = \sigma_x \cdot h = 100 \text{ N/mm}, \; N_y = 0, \; N_{xy} = 0$$

$$A = \overline{Q} \cdot h \text{ and } D = \overline{Q} \cdot \frac{h^s}{12}$$

$$A = \begin{bmatrix} 2.06 \times 10^5 & 4.86 \times 10^4 & 8.37 \times 10^4 \\ 4.86 \times 10^4 & 3.76 \times 10^4 & 1.65 \times 10^4 \\ 8.37 \times 10^4 & 1.65 \times 10^4 & 4.84 \times 10^4 \end{bmatrix} \text{N/mm}$$

$$D = \begin{bmatrix} 6.86 \times 10^4 & 1.62 \times 10^4 & 2.79 \times 10^4 \\ 1.52 \times 10^4 & 1.25 \times 10^4 & 5.51 \times 10^4 \\ 2.79 \times 10^4 & 5.51 \times 10^3 & 1.61 \times 10^4 \end{bmatrix} \text{N/mm}$$

$$a = A^{-1} \quad \textit{and} \quad d = D^{-1} (\textit{since } B = 0)$$

$$a = \begin{bmatrix} 2.06 \times 10^{-5} & -1.29 \times 10^{-5} & -3.12 \times 10^{-5} \\ -1.29 \times 10^{-5} & 3.93 \times 10^{-5} & 8.89 \times 10^{-6} \\ -3.12 \times 10^{-5} & 8.89 \times 10^{-6} & 7.16 \times 10^{-5} \end{bmatrix} \text{mm/N}$$

$$d = \begin{bmatrix} 6.18 \times 10^{-5} & -3.87 \times 10^{-5} & 9.37 \times 10^{-5} \\ -3.87 \times 10^{-5} & 1.18 \times 10^{-4} & 2.66 \times 10^{-5} \\ -9.37 \times 10^{-5} & 2.66 \times 10^{-6} & 2.14 \times 10^{-4} \end{bmatrix} \text{mm/N}$$

$$E_x = \frac{1}{a_{11} \times h}, \quad E_y \frac{1}{a_{22} \times h}, \quad G_{xy} \frac{1}{a_{66} \times h}, \quad \nu_{xy} \frac{-a_{12}}{a_{11}}, \quad \nu_{yx} \frac{-a_{12}}{a_{22}}$$

$$E_x = 24.26 \text{ GPa}, \quad E_y = 12.7 \text{ GPa}$$

$$G_{xy} = 6.98 \text{ GPa}, \quad \nu_{xy} = 0.627, \quad \nu_{yx} = 0.328$$

These values agree with those calculated above. Also, for the applied force $N_x = 50 \times 2 = 100$ N/mm.

$$\begin{bmatrix} \varepsilon_x \\ \varepsilon_y \\ \gamma_{xy} \end{bmatrix} = a \cdot \begin{bmatrix} N_x \\ N_y \\ N_{xy} \end{bmatrix} \left(= a \begin{bmatrix} \sigma_x \\ \sigma_y \\ \tau_{xy} \end{bmatrix} \cdot h \right)$$

$$\varepsilon_x = 2.061 \times 10^{-3} \quad \varepsilon_y = -1.291 \times 10^{-3} \quad \gamma_{xy} = -3.124 \times 10^{-3}$$

It is interesting to observe that as well as the expected axial and transverse strains arising from the applied axial stress, σ_x, we have also a shear strain. This is because in composites we can often get *coupling* between the different modes of deformation. This will also be seen later where coupling between axial and flexural deformations can occur in unsymmetric laminates. Fig. 3.17 illustrates why the shear strains arise in the uniaxially stressed single ply in this example.

Example 3.10. If a moment of $M_y = 100$ Nm/m is applied to the unidirectional composite described in the previous example, calculate the curvatures

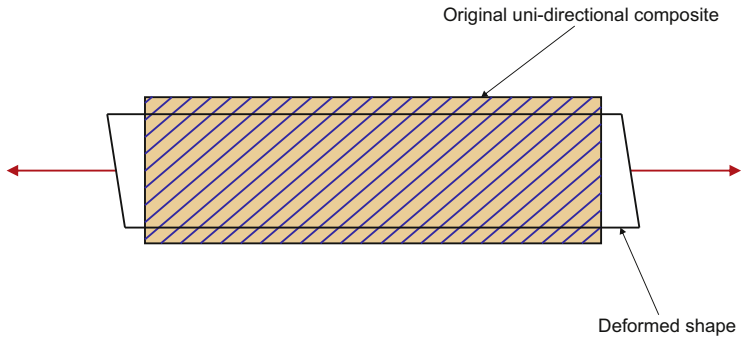


FIG. 3.17 Coupling effects between extension and shear.

which will occur. Determine also the stress and strain distributions in the global ($x-y$) and local ($1-2$) directions.

Solution Using the D and d matrices from the previous example, then for the applied moment $M_y = 100$ N:

$$\begin{bmatrix} \kappa_x \\ \kappa_y \\ \kappa_{xy} \end{bmatrix} = d \cdot \begin{bmatrix} M_x \\ M_y \\ M_{xy} \end{bmatrix} \quad v_{yx} = \frac{-\kappa_x}{\kappa_y} \quad v_{xy} = \frac{-\kappa_y}{\kappa_x}$$

This enables the curvatures to be determined as

$$\kappa_x = -3.87 \text{ m}^{-1}, \kappa_y = 12 \text{ m}^{-1}, \kappa_{xy} = 2.67 \text{ m}^{-1},$$
$$v_{yx} = 0.328, v_{xy} = 3.05$$

The bending strains in the global directions are given generally by

$$\varepsilon = \kappa . z$$

Hence

$$(\varepsilon_x)_{max} = \pm \kappa_x \left(\frac{h}{2}\right) = \pm 3.87 \times 10^{-3}$$

$$(\varepsilon_y)_{max} = \pm \kappa_y \left(\frac{h}{2}\right) = \pm 0.012$$

$$(\gamma_{xy})_{max} = \pm \kappa_{xy} \left(\frac{h}{2}\right) = \pm 2.67 \times 10^{-3}$$

The stresses are then obtained from

$$\begin{bmatrix} \sigma_x \\ \sigma_y \\ \tau_{xy} \end{bmatrix} = \overline{Q} \cdot \begin{bmatrix} \varepsilon_x \\ \varepsilon_y \\ \gamma_{xy} \end{bmatrix}$$

So

$$\sigma_x = 0, \quad \sigma_y = 150 \text{ MPa}, \quad \tau_{xy} = 0$$

For the local directions, the strain and stress transformation matrices can be used:

$$\begin{bmatrix} \sigma_1 \\ \sigma_2 \\ \tau_{12} \end{bmatrix} = T_\sigma \cdot \begin{bmatrix} \varepsilon_x \\ \varepsilon_y \\ \tau_{xy} \end{bmatrix}$$

So

$$\sigma_1 = 26.8 \text{ MPa}, \sigma_2 = 123.2 \text{ MPa}, \tau_{xy} = 57.5 \text{ MPa}$$

$$\begin{bmatrix} \varepsilon_1 \\ \varepsilon_2 \\ \gamma_{12} \end{bmatrix} = T_\varepsilon \cdot \begin{bmatrix} \varepsilon_x \\ \varepsilon_y \\ \gamma_{xy} \end{bmatrix}$$

So

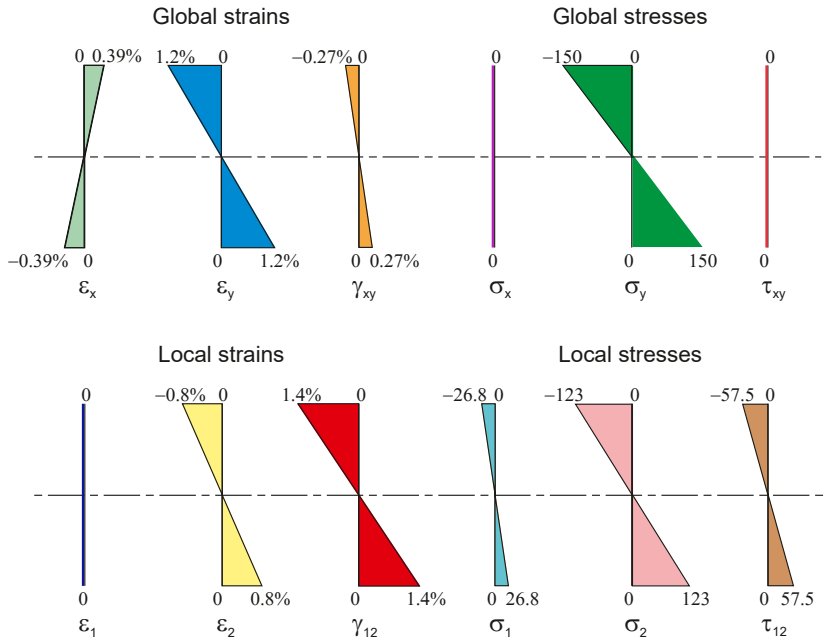


FIG. 3.18 Stresses and strains, Example 3.10.

$$\varepsilon_1 = -5.14 \times 10^{-5}, \varepsilon_2 = 8 \times 10^{-3}, \gamma_{12} = 0.014$$

These stresses and strains are illustrated in Fig. 3.18.

Note that if both plane stresses and moments are applied then the total stresses will be the algebraic sum of the individual stresses.

3.9 Deformation behaviour of laminates

(i) Laminates made from unidirectional plies

The previous analysis has shown that the properties of unidirectional fibre composites are highly anisotropic. To alleviate this problem, it is common to build up laminates consisting of stacks of unidirectional lamina arranged at different orientations. Clearly many permutations are possible in terms of the numbers of layers (or plies) and the relative orientation of the fibres in each layer. At first glance it might appear that the best means of achieving a more isotropic behaviour would be to have two layers with the unidirectional fibres arranged perpendicular to each other. For example, two layers arranged at 0° and 90° to the global x-direction or at +45° and −45° to the x-direction might appear to offer more balanced properties in all directions. In fact, the lack of symmetry about the centre plane of the laminate causes very complex behaviour in such cases.

In general, it is best to aim for symmetry about the centre plane. A laminate in which the layers above the centre plane are a mirror image of those below it is described as symmetric. Thus, a four-stack laminate with fibres oriented at 0°, 90°, 90° and 0° is symmetric. The convention is to denote this as $[0°/90°/90°/0°]_T$ or $[0°, 90°_2, 0°]_T$ or $[0°/90°]_s$.1n general terms any laminate of the type $[\theta, -\theta, -\theta, \theta]_T$ is symmetric and there may of course be any even number of layers or plies. They do not all have to be the same thickness, but symmetry must be maintained. In the case of a symmetric laminate where the central ply is not repeated, this can be denoted by the use of an overbar. Thus the laminate $[45/-45/0/90/0/-45/45]_T$ can be written as $\left[\pm 45, 0, \overline{90}\right]_s$.

In-plane behaviour of a symmetric laminate

The in-plane stiffness behaviour of symmetric laminates may be analysed as follows. The plies in a laminate are all securely bonded together so that when the laminate is subjected to a force in the plane of the laminate, all the plies deform by the same amount. Hence, the strain is the same in every ply but because the modulus of each ply is different, the stresses are not the same. This is illustrated in Fig. 3.19.

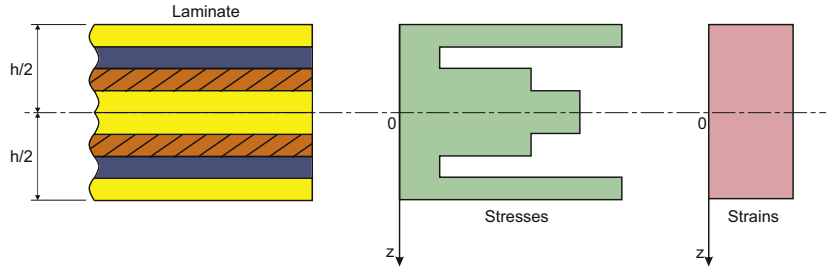


FIG. 3.19 Stresses and strains in a symmetric laminate.

When external forces are applied in the global $x-y$ direction, they will equate to the summation of all the forces in the individual plies. Thus, for unit width of laminate this may be expressed in terms of the stresses or forces as

$$\overline{\sigma}_x = \frac{1}{h}\int_{-h/2}^{h/2} (\sigma_x)_f dz \left(or \;\; N_x = \int_{-h/2}^{h/2} (\sigma_x)_f dz \right)$$

$$\overline{\sigma}_y = \frac{1}{h}\int_{-h/2}^{h/2} (\sigma_y)_f dz \left(or \;\; N_y = \int_{-h/2}^{h/2} (\sigma_y)_f dz \right)$$

$$\overline{\tau}_{xy} = \frac{1}{h}\int_{-h/2}^{h/2} (\tau_{xy})_f dz \left(or \;\; N_{xy} = \int_{-h/2}^{h/2} (\tau_{xy})_f dz \right)$$

where h is the thickness of the laminate. σ_x, N_x are the overall stresses or forces and $(\sigma)_f$ is the stress in the ply 'f' (see Fig. 3.20).

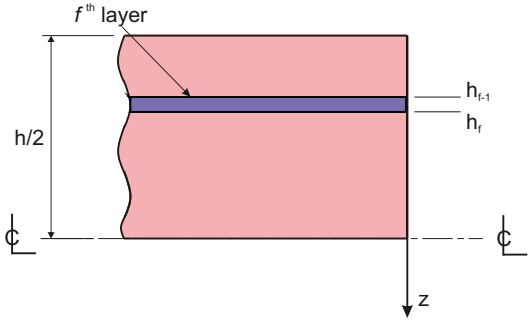


FIG. 3.20 Ply f in the laminate.

In matrix form we can write

$$\begin{Bmatrix} \overline{\sigma}_x \\ \overline{\sigma}_y \\ \overline{\tau}_{xy} \end{Bmatrix} = \frac{1}{h} \int_{-h/2}^{h/2} \begin{Bmatrix} \sigma_x \\ \sigma_y \\ \tau_{xy} \end{Bmatrix}_f dz$$

$$= \frac{1}{h} \int_{-h/2}^{h/2} \begin{bmatrix} \overline{Q}_{11} & \overline{Q}_{12} & \overline{Q}_{16} \\ & \overline{Q}_{22} & \overline{Q}_{26} \\ sym. & & \overline{Q}_{66} \end{bmatrix}_f dz \begin{Bmatrix} \varepsilon_x \\ \varepsilon_y \\ \gamma_{xy} \end{Bmatrix}_f dz$$

As the strains are independent of z they can be taken outside the integral:

$$\begin{Bmatrix} \overline{\sigma}_x \\ \overline{\sigma}_y \\ \overline{\tau}_{xy} \end{Bmatrix} = \frac{1}{h} \int_{-h/2}^{h/2} \begin{bmatrix} \overline{Q}_{11} & \overline{Q}_{12} & \overline{Q}_{16} \\ & \overline{Q}_{22} & \overline{Q}_{26} \\ sym. & & \overline{Q}_{66} \end{bmatrix} dz \begin{Bmatrix} \varepsilon_x \\ \varepsilon_y \\ \gamma_{xy} \end{Bmatrix}_f$$

$$\begin{Bmatrix} \overline{\sigma}_x \\ \overline{\sigma}_y \\ \overline{\tau}_{xy} \end{Bmatrix} = [A] \begin{Bmatrix} \varepsilon_x \\ \varepsilon_y \\ \gamma_{xy} \end{Bmatrix}_f \frac{1}{h} \qquad \left(or\ [N]_{xy} = [A][\varepsilon]_{xy} \right)$$

where, for example,

$$A_{11} = \int_{-h/2}^{h/2} \overline{Q}_{11} dz = 2. \int_{0}^{h/2} \overline{Q}_{11} dz$$

$[A]$ is the **Extensional Stiffness Matrix** although it should be noted that it also contains shear terms.

Within a single ply, such as the f th, the $\overline{Q}$ terms are constant so,

$$A_{11}^f = \sum \overline{Q}_{11}^f h_f$$

In overall terms

$$[A] = \sum_{f=1}^{p} \overline{Q} h_f \tag{3.35}$$

Thus, the stiffness matrix for a symmetric laminate may be obtained by adding, in proportion to the ply thickness, the corresponding terms in the stiffness matrix for each of the plies.

Having obtained all the terms for the extensional stiffness matrix $[A]$, this may then be inverted to give the compliance matrix $[a]$.

$$[a] = [A]^{-1}$$

The laminate properties may then be obtained as above from inspection of the compliance matrix.

$$E_x = \frac{1}{a_{11}h} \quad E_y = \frac{1}{a_{22}h} \quad G = \frac{1}{a_{66}h}$$

where h is the thickness of the laminate.

$$v_{xy} = \frac{-a_{12}}{a_{11}} \quad v_{yx} = \frac{-a_{12}}{a_{22}}$$

3.10 Summary of steps to predict stiffness of symmetric laminates

1. The Stiffness matrix $[\overline{Q}]$ is obtained as earlier each individual ply in the laminate.
2. The Stiffness matrix $[A]$ for the laminate is determined by adding the product of thickness and $[\overline{Q}]$ for each ply.
3. The Compliance matrix $[a]$ for the laminate is determined by inverting $[A]$ i.e. $[a] = [A]^{-1}$.
4. The stresses and strains in the laminate are then determined from

$$\begin{Bmatrix} \varepsilon_x \\ \varepsilon_y \\ \gamma_{xy} \end{Bmatrix} = [a] \cdot \begin{Bmatrix} \sigma_x \\ \sigma_y \\ \tau_{xy} \end{Bmatrix} h$$

Example 3.11. A series of individual plies with the properties listed below are laid in the following sequence to make a laminate

$$[0/35_2/-35_2]_s$$

Determine the moduli for the laminate in the global $x - y$ directions and the strains in the laminate when stresses of $\sigma_x = 10$ MPa, $\sigma_y = -14$ MPa and $\tau_{xy} = -5$ MPa are applied. The thickness of each is 1 mm.

$$E_1 = 125,000 \text{ MPa} \quad E_2 = 7800 \text{ MPa} \quad G_{12} = 4400 \text{ MPa}$$
$$v_{12} = 0.34$$

Solution The behaviour of each ply when subjected to loading at θ degrees off the fibre axis is determined using Matrix manipulation as follows:

Compliance Matrix *Stiffness Matrix*

$$S = \begin{bmatrix} \frac{1}{E_1} & -\frac{v_{12}}{E_1} & 0 \\ \frac{v_{12}}{E_1} & \frac{1}{E_2} & 0 \\ 0 & 0 & \frac{1}{G_{12}} \end{bmatrix} \qquad Q = S^{-1}$$

Stress Transformation Matrix *Strain Transformation Matrix*

$$[T]_\sigma = \begin{bmatrix} c^2 & s^2 & 2sc \\ s^2 & c^2 & -2sc \\ -sc & sc & (c^2 - s^2) \end{bmatrix} \quad [T]_\varepsilon = \begin{bmatrix} c^2 & s^2 & sc \\ s^2 & c^2 & -sc \\ -2sc & 2sc & (c^2 - s^2) \end{bmatrix}$$

Overall Stiffness Matrix *Overall compliance Matrix*

$$\overline{Q}(\theta) = T_\sigma^{-1} \cdot Q \cdot T_\varepsilon \qquad \overline{S}(\theta) = \overline{Q}(\theta)^{-1}$$

$$\overline{Q}(35) = \begin{bmatrix} 6.27 \times 10^4 & 2.71 \times 10^4 & 3.66 \times 10^4 \\ 2.71 \times 10^4 & 2.21 \times 10^4 & 1.87 \times 10^4 \\ 3.66 \times 10^4 & 1.87 \times 10^4 & 2.88 \times 10^4 \end{bmatrix}$$

Hence, the extension stiffness matrix is given by

$$A = 2.\overline{Q}(0) + 4.\overline{Q}(35) + 4.\overline{Q}(-35)$$

$$A = \begin{bmatrix} 7.53 \times 10^5 & 2.22 \times 10^5 & 0 \\ 2.22 \times 10^5 & 1.93 \times 10^5 & 0 \\ 0 & 0 & 2.39 \times 10^5 \end{bmatrix} \text{ N mm}$$

The compliance matrix is obtained by inverting [*A*]

$$a = A^{-1}$$

$$a = \begin{bmatrix} 2.0 \times 10^{-6} & -2.31 \times 10^{-6} & 0 \\ -2.31 \times 10^{-6} & 7.84 \times 10^{-6} & 0 \\ 0 & 0 & 4.17 \times 10^{-6} \end{bmatrix} \left(\text{N mm}^{-1}\right)$$

The stiffness terms in the global directions may be obtained from:

$$E_x = \frac{1}{a_{11} \times 10}, \quad E_x = 49.7 \text{ GPa}$$

$$E_y = \frac{1}{a_{22} \times 10}, \quad E_y = 12.8 \text{ GPa} \text{ and } G_{xy} = \frac{1}{a_{66} \times 10} = 24 \text{ GPa}$$

$$\nu_{xy} = \frac{a_{12}}{a_{11}} \quad \nu_{xy} = 1.151$$

(note the high value of Poisson's Ratio which can be obtained in composite laminates)

$$\nu_{yx} = \frac{a_{12}}{a_{22}} \quad \nu_{yx} = 0.295$$

and the strains may be obtained as

$$\begin{bmatrix} \varepsilon_x \\ \varepsilon_y \\ \gamma_{xy} \end{bmatrix} = a \cdot \begin{bmatrix} \sigma_x \\ \sigma_y \\ \tau_{xy} \end{bmatrix} \cdot 10$$

$$\varepsilon_x = 5.24 \times 10^{-4}, \quad \varepsilon_y = 1.33 \times 10^{-3} \quad \gamma_{xy} = -2.08 \times 10^{-4}$$
$$\varepsilon_x = 0.052\%, \quad \varepsilon_y = -0.133\%, \quad \gamma_{xy} = -0.021\%$$

It may be seen from the above analysis that for cross-ply $(0/90)_s$ and symmetric angle ply $[-0/\theta]_s$ laminates, $A_{16} = A_{61} = 0$ and $A_{26} = A_{62} = 0$ (also $a_{16} = a_{61} = a_{62} = 0$). For other types of laminates this will not be the case.

3.11 General deformation behaviour of laminates

The previous section has illustrated a simple convenient means of analysing in-plane loading of symmetric laminates. Many laminates are of this type and so this approach is justified. However, there are also many situations where other types of loading (including bending) are applied to laminates which may be symmetric or non-symmetric. In order to deal with these situations, it is necessary to adopt a more general type of analysis.

Convention for defining thicknesses and positions of plies

In this more general analysis, it is essential to be able to define the position and thickness of each ply within a laminate. The convention is that the geometrical mid-plane is taken as the datum. The top and bottom of each ply are then defined relative to this. Those above the mid-plane will have negative co-ordinates and those below will be positive. The bottom surface of the f^{th} ply has address h_f and the top surface of this ply has address h_{f-1}. Hence the thickness of the f^{th} ply is given by

$$h(f) = h_f - h_{f-1}$$

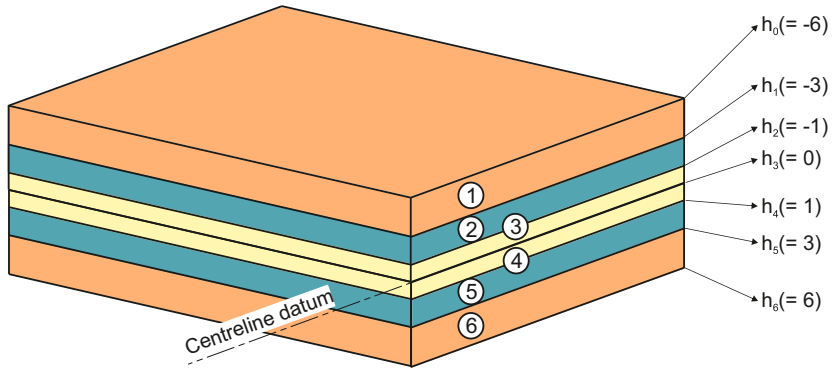


FIG. 3.21 Six ply laminate.

For the 6-ply laminate shown in Fig. 3.21, the thickness of ply 5 is given by

$$h(5) = h_5 - h_4 = 3 - 1 = 2 \text{ mm}$$

The thickness of ply 1 is given by

$$h(1) = h_1 - h_0 = (-3) - (-6) = 3 \text{ mm}$$

Analysis of laminates

The general deformation analysis of a laminate is very similar to the general deformation analysis for a single ply.

(i) Force Equilibrium: If there are F plies, then the force resultant, N_L, for the laminate is given by the sum of the forces for each ply.

$$[N]_L = \sum_{f=1}^{F} [N]_f = \sum_{f=1}^{F} \int_{h_{f-1}}^{h_f} [\sigma]_f dz$$

and using the definition for $[\sigma]$ from the analysis of a single ply,

$$[N]_L = \sum_{f=1}^{F} \left([\overline{Q}] \cdot [\varepsilon] + [\overline{Q}] \cdot z \cdot [\kappa] \right)_f dz$$

$$= \sum_{f=1}^{F} \left\{ [\overline{Q}] \cdot [\varepsilon] \int_{h_{f-1}}^{h_f} dz + [\overline{Q}] \cdot [\kappa] \int_{h_{f-1}}^{h_f} z \cdot dz \right\}_f$$

$$[N]_L = [A][\varepsilon]_L + [B][\kappa]_L \tag{3.36}$$

where

$$[A] = \sum_{f=1}^{F} [\overline{Q}]_f (h_f - h_{f-1}) \tag{3.37}$$

This is called the *Extensional Stiffness Matrix* and the similarity with that derived earlier for the single ply should be noted.

Also, the *Coupling Matrix,* $[B]$ *is* given by

$$[B] = \frac{1}{2} \sum_{f=1}^{F} [\overline{Q}]_f \left(h_f^2 - h_{f-1}^2 \right) \tag{3.38}$$

The coupling matrix will be zero for a symmetrical laminate.

(ii) Moment Equilibrium: As in the case of the forces, the moments may be summed across F plies to give

$$[M]_L = \sum_{f=1}^{F} [M]_f = \sum_{f=1}^{F} \int_{h_{f-1}}^{h_f} [\sigma]_f dz$$

and once again using the expressions from the analysis of a single ply,

$$[M]_L = \sum_{f=1}^{F} \int_{h_{f-1}}^{h_f} \left([\overline{Q}][\varepsilon] z + [\overline{Q}][\kappa] z^2 \right) dz$$

$$= \sum_{f=1}^{F} \left\{ [\overline{Q}][\varepsilon] \int_{h_{f-1}}^{h_f} z dz + [\overline{Q}][\kappa] \int_{h_{f-1}}^{h_f} z^2 dz \right\}_f$$

$$[M]_L = [B][\varepsilon]_L + [D][\kappa]_L \tag{3.39}$$

where $[B]$ is as defined above and

$$[D] = \frac{1}{3} \sum_{f=1}^{F} [\overline{Q}]_f \left(h_f^3 - h_{f-1}^3 \right) \tag{3.40}$$

As earlier we may group Eqs. (3.36) and (3.39) to give the *Plate Constitutive Equation* as

$$\begin{bmatrix} N \\ M \end{bmatrix} = \begin{bmatrix} A & B \\ B & D \end{bmatrix} \begin{bmatrix} \varepsilon \\ \kappa \end{bmatrix} \tag{3.41}$$

This equation may be utilised to give elastic properties, strains, curvatures, etc. It is much more general than the approach in the previous section and can accommodate bending as well as plane stresses. Its use is illustrated in the following Examples.

Example 3.12. For the laminate $[0/35_2/-35_2]s$ determine the elastic constants in the global directions using the Plate Constitutive Equation. When stresses of $\sigma_x = 10$ MPa, $\sigma_y = -14$ MPa and $\tau_{xy} = -5$ MPa are applied, calculate the stresses and strains in each ply in the local and global directions. If a moment of $M_x = 1000$ Nm/m is added, determine the new stresses, strains and curvatures in the laminate. The plies are each 1 mm thick.

$$E_1 = 125 \text{ GPa}, \quad E_2 = 7.8 \text{ GPa}, \quad G_{12} = 4.4 \text{ GPa}, \quad \nu_{12} = 0.34$$

Solution The locations of each ply are illustrated in Fig. 3.22.

Using the definitions given above, and the $\overline{Q}$ values for each ply, we may determine the matrices A, B and D from

$$A = \sum_{f=1}^{10} \overline{Q}_f (h_f - h_{f-1}),$$

$$B = \frac{1}{2} \sum_{f=1}^{10} \overline{Q}_f \left[\left((h_f)^2 - (h_{f-1})^2 \right], \quad D = \frac{1}{3} \sum_{f=1}^{10} \overline{Q}_f \left[(h_f)^3 - (h_{f-1})^3 \right] \right.$$

Then

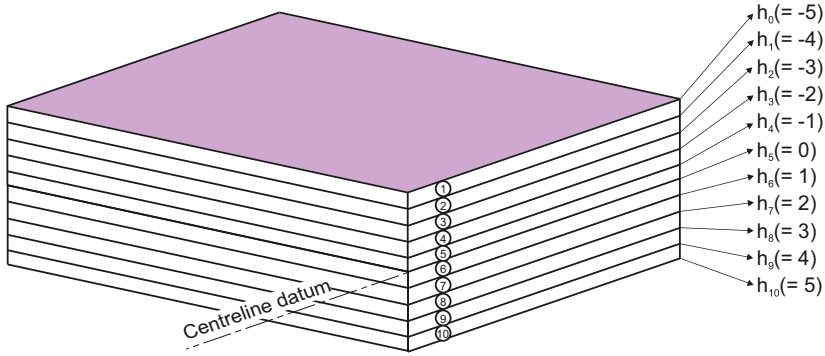


FIG. 3.22 Ten ply laminate.

$$\begin{bmatrix} \varepsilon_x \\ \varepsilon_y \\ \varepsilon_{xy} \end{bmatrix} = a \cdot \begin{bmatrix} N_x \\ N_y \\ N_{xy} \end{bmatrix} = a \cdot \begin{bmatrix} \sigma_x \\ \sigma_y \\ \tau_{xy} \end{bmatrix} \cdot h$$

where $h =$ full laminate thickness $= 10$ mm, and $a = A^{-1}$ since $[B] = 0$. This matrix equation gives the global strains as

$$\varepsilon_x = 5.24 \times 10^{-4}, \ \ \varepsilon_y = 1.33 \times 10^{-3}, \ \ \varepsilon_{xy} = 2.08 \times 10^{-4}$$

Also,

$$E_x = \frac{1}{a_{11} \cdot h}, \ \ E_y = \frac{1}{a_{22} \cdot h}, \ \ G_{xy} = \frac{1}{a_{66} \cdot h}$$

$$v_{xy} = \frac{-a_{12}}{a_{11}}, \quad v_{yx} = \frac{-a_{12}}{a_{22}}$$

$$E_x = 49.7 \ \text{GPa}, \ \ E_y = 12.8 \ \text{GPa}, \ \ G_{xy} = 24 \ \text{GPa}$$

$$v_{xy} = 1.149 \quad v_{yx} = 0.296$$

It may be seen that these values agree with those calculated in the previous example. To get the stresses in the global (xy) directions for the 'f^{th}' ply

$$\begin{bmatrix} \sigma_x \\ \sigma_y \\ \tau_{xy} \end{bmatrix} = \overline{Q}_f \begin{bmatrix} \varepsilon_x \\ \varepsilon_y \\ \gamma_{xy} \end{bmatrix}$$

when $f = 1, f = 2, f = 9$ and $f = 10$

$$\sigma_x = 4.5 \ \text{MPa}, \ \ \sigma_y = -11.3 \ \text{MPa}, \ \ \tau_{xy} = -0.28 \ \text{MPa}$$

when $f = 3, f = 4, f = 7$ and $f = 8$

$$\sigma_x = -10.8 \ \text{MPa}, \ \ \sigma_y = -19.2 \ \text{MPa}, \ \ \tau_{xy} = -11.8 \ \text{MPa}$$

when $f = 5$ and 6

$$\sigma_x = 62.6 \ \text{MPa}, \ \ \sigma_y = -9 \ \text{MPa}, \ \ \tau_{xy} = -0.9 \ \text{MPa}.$$

Note that in the original question, the applied force per unit width in the x-direction was 100 N/mm (i.e. $\sigma_x \cdot (10)$). As each ply is 1 mm thick, then the above stresses are also equal to the forces per unit width for each ply. If we add the above values for all 10 plies, then it will be seen that the answer is 100 N/mm as it should be for equilibrium. Similarly, if we add N_y and N_{xy} for each ply, these come to -140 N/mm and -50 N/mm which also agree with the applied forces in these directions.

In the local (1−2) directions we can obtain the stresses and strains by using the transformation matrices. Hence, for the 'f^{th}' ply

$$\begin{bmatrix} \sigma_1 \\ \sigma_2 \\ \tau_{12} \end{bmatrix} = T_{\sigma_f} \begin{bmatrix} \sigma_x \\ \sigma_y \\ \tau_{xy} \end{bmatrix}$$

$$\begin{bmatrix} \varepsilon_1 \\ \varepsilon_2 \\ \gamma_{12} \end{bmatrix} = T_{\varepsilon_f} \begin{bmatrix} \varepsilon_x \\ \varepsilon_y \\ \gamma_{xy} \end{bmatrix}$$

So that for $f = 1$, 2, 9 and 10

$$\sigma_1 = -0.44 \text{ MPa}, \quad \sigma_2 = -6.4 \text{ MPa}, \quad \tau_{xy} = 7.3 \text{ MPa}$$
$$\varepsilon_1 = 1.38 \times 10^{-5}, \quad \varepsilon_2 = -8.15 \times 10^{-4}, \quad \gamma_{12} = 1.67 \times 10^{-3}$$

For $f = 3$, 4, 7 and 8

$$\sigma_1 = -0.96 \text{ MPa}, \quad \sigma_2 = -5.8 \text{ MPa}, \quad \tau_{12} = -7.5 \text{ MPa}$$
$$\varepsilon_1 = 1.82 \times 10^{-4}, \quad \varepsilon_2 = -6.2 \times 10^{-4}, \quad \gamma_{12} = -1.8 \times 10^{-3}$$

For $f = 5$ and 6

$$\sigma_1 = 4.5 \text{ MPa}, \quad \sigma_2 = -11.3 \text{ MPa}, \quad \tau_{12} = -0.28 \text{ MPa}$$
$$\varepsilon_1 = 5.25 \times 10^{-4}, \quad \varepsilon_2 = -1.33 \times 10^{-3}, \quad \gamma_{12} = 2.09 \times 10^{-4}$$

When the moment $M_x = 1000$ Nm/m is added, the curvatures, κ, can be calculated from

$$\begin{bmatrix} \kappa_x \\ \kappa_y \\ \kappa_{xy} \end{bmatrix} = d \cdot \begin{bmatrix} M_x \\ M_y \\ M_{xy} \end{bmatrix} \quad v_{xy} = \frac{-\kappa_y}{\kappa_x} \quad v_{yx} = \frac{-\kappa_x}{\kappa_y}$$

where $d = \mathrm{D}^{-1}$ since $[B] = 0$.

$$\kappa_x = 0.435 \text{ m}^{-1}, \quad \kappa_y = -0.457 \text{ m}^{-1}, \quad \kappa_{xy} = -0.147 \text{ m}^{-1}$$
$$v_{xy} = 1.052 \quad v_{yx} = 0.95$$

When the bending moment is applied the global stresses and strains in each ply may be obtained as follows:

$$\varepsilon_x = \kappa_x \cdot z, \quad \varepsilon_y = \kappa_y \cdot z, \quad \gamma_{xy} = \kappa_{xy} \cdot z$$

At the top surface, $z = -5$ mm

$$\varepsilon_x = -2.17 \times 10^{-3}, \quad \varepsilon_y = 2.28 \times 10^{-3}, \quad \gamma_{xy} = -7.34 \times 10^{-4}$$

and the stresses are given by

$$\begin{bmatrix} \sigma_x \\ \sigma_y \\ \tau_{xy} \end{bmatrix} = \overline{Q}_1 \begin{bmatrix} \varepsilon_x \\ \varepsilon_y \\ \gamma_{xy} \end{bmatrix}$$

So that

$$\sigma_x = -47 \text{ MPa}, \quad \sigma_y = 5.7 \text{ MPa}, \quad \tau_{xy} = 15.4 \text{ MPa}.$$

The local stresses and strains are then obtained from the stress and strain transformations

$$\begin{bmatrix} \sigma_1 \\ \sigma_2 \\ \tau_{12} \end{bmatrix} = T_{\sigma_1} \begin{bmatrix} \sigma_x \\ \sigma_y \\ \tau_{xy} \end{bmatrix} \quad \text{and} \quad \begin{bmatrix} \varepsilon_1 \\ \varepsilon_2 \\ \gamma_{12} \end{bmatrix} = T_{\varepsilon_1} \begin{bmatrix} \varepsilon_x \\ \varepsilon_y \\ \gamma_{xy} \end{bmatrix}$$

$$\sigma_1 = -44.1 \text{ MPa}, \quad \sigma_2 = 2.8 \text{ MPa}, \quad \tau_{12} = -19.5 \text{ MPa}$$

$$\varepsilon_1 = -3.6 \times 10^{-4}, \quad \varepsilon_2 = 4.7 \times 10^{-4}, \quad \gamma_{12} = -4.44 \times 10^{-3}$$

For the next interface, $z = -4$ mm, the new values of ε_x, ε_y and γ_{xy} can be calculated and hence the stresses in the global and local co-ordinates. $f = 1$ and $f = 2$ need to be analysed for this interface but there will be continuity across the interface because the orientation of the plies is the same in both cases. However, at $z = -3$ mm there will be a discontinuity of stresses in the global direction and discontinuity of stresses and strains in the local directions due to the difference in fibre orientation in plies 2 and 3.

The overall distribution of stresses and strains in the local and global directions is shown in Fig. 3.23. If both the normal stress and the bending are applied together then it is necessary to add the effects of each separate condition. That is, direct superposition can be used to determine the overall stresses.

Note, to assist the reader the values of the terms in the matrices are

$$A = \begin{bmatrix} 7.52 \times 10^5 & 2.22 \times 10^5 & 0 \\ 2.22 \times 10^5 & 1.93 \times 10^5 & 0 \\ 0 & 0 & 2.39 \times 10^5 \end{bmatrix} \text{N/mm} \quad B = \begin{bmatrix} 0 & 0 & 0 \\ 0 & 0 & 0 \\ 0 & 0 & 0 \end{bmatrix}$$

$$a = \begin{bmatrix} 2.01 \times 10^6 & -2.31 \times 10^{-6} & 0 \\ -2.31 \times 10^{-6} & 7.82 \times 10^{-6} & 0 \\ 0 & 0 & 4.17 \times 10^{-6} \end{bmatrix} (\text{N/mm})^{-1}$$

$$D = \begin{bmatrix} 5.25 \times 10^6 & 2.24 \times 10^6 & -1.75 \times 10^6 \\ 2.24 \times 10^6 & 1.84 \times 10^6 & -9.04 \times 10^5 \\ -1.75 \times 10^6 & -9.04 \times 10^5 & 2.38 \times 10^6 \end{bmatrix} \text{N mm}$$

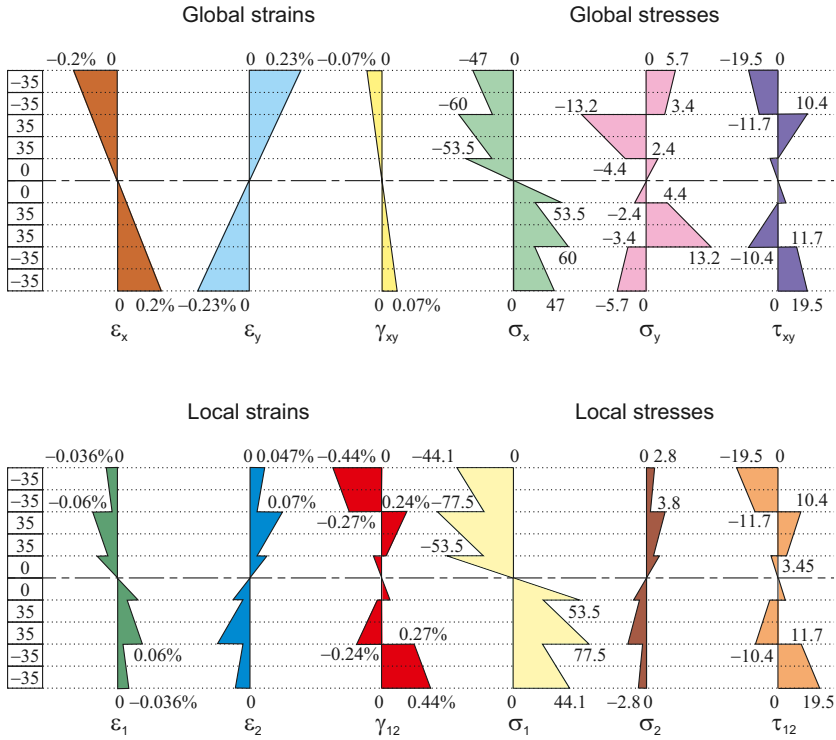


FIG. 3.23 Stresses and strains, Example 3.12: (A) global; (B) local.

$$d = \begin{bmatrix} 4.34 \times 10^{-7} & -4.57 \times 10^{-7} & 1.46 \times 10^{-7} \\ -4.57 \times 10^{-7} & 1.14 \times 10^{-6} & 9.75 \times 10^{-8} \\ 1.46 \times 10^{-7} & 9.75 \times 10^{-8} & 5.63 \times 10^{-7} \end{bmatrix} (\text{N mm})^{-1}$$

The solution method using the Plate Constitutive Equation is therefore straightforward and very powerful. A computer can easily handle the matrix manipulation — although this is not difficult, it is quite time-consuming if it has to be done manually.

The following example compares the behaviour of a single ply and a laminate.

Example 3.13. A single ply of carbon fibre/epoxy composite has the following properties:

$$E_1 = 175 \text{ GPa}, \quad E_2 = 12 \text{ GPa}, \quad G_{12} = 5 \text{ GPa}, \quad \nu_{12} = 0.3$$

Plot the variations of E_x, E_y, G_{xy} and ν_{xy} for values of θ in the range 0–90° for (i) a single ply 0.4 mm thick and (ii) a laminate with the stacking sequence $[\pm\theta]_s$. This laminate has four plies, each 0.1 mm thick. Discuss the meaning of the results.

Solution

(i) *Single ply* The method of solution simply involves the determination of $[S]$, $[Q]$, $[\overline{Q}]$, $[\overline{S}]$ and $[a]$ as illustrated previously, i.e.

$$|S| = \begin{vmatrix} \frac{1}{E_1} & -\frac{\nu_{12}}{E_1} & 0 \\ -\frac{\nu_{12}}{E_1} & \frac{1}{E_2} & 0 \\ 0 & 0 & \frac{1}{G_{12}} \end{vmatrix} \quad \text{and} \quad |Q| = |S|^{-1}$$

Then

$$|\overline{Q}| = T_\sigma \cdot Q \cdot T_\varepsilon \quad \text{and} \quad |\overline{S}| = |\overline{Q}|^{-1}$$

$$|A| = |\overline{Q}| \cdot h \quad \text{and} \quad |a| = |A|^{-1}$$

Then for $\theta = 25°$ (for example)

$$E_x = \frac{1}{a_{11}h} = 28.3 \text{ GPa}$$

$$E_y = \frac{1}{a_{22}h} = 11.7 \text{ GPa}$$

$$G_{xy} = \frac{1}{a_{66}h} = 7.3 \text{ GPa}$$

$$\nu_{xy} = \frac{-a_{12}}{a_{11}} = 0.495 \quad \textit{and} \quad \nu_{yx} = \frac{-a_{12}}{a_{22}} = 0.205$$

Fig. 3.24 shows the variation of these elastic constants for all values of θ between 0 and 90°.

(ii) *Symmetric 4 Ply Laminate* The same procedure is used again except that this time the $|A|$ matrix has to be summed for all the plies, i.e.

$$|A| = \sum_{f=1}^{f=4} |\overline{Q}|_f (h_f - h_{f-1}) \quad \text{and} \quad |a| = |A|^{-1}$$

where $h_0 = -0.2$, $h_1 = -0.1$, $h_2 = 0$, $h_3 = 0.1$, $h_4 = 0.2$.

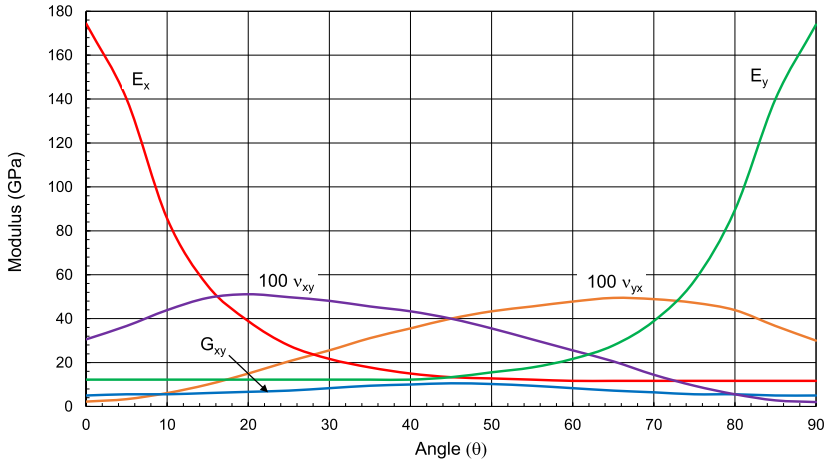


FIG. 3.24 Variation of elastic properties for a single ply of carbon/epoxy composite.

Once again, for $\theta = 50^\circ$ (for example)

$$E_x = \frac{1}{a_{11}h} = 14.6 \text{ GPa}$$

$$E_y = \frac{1}{a_{22}h} = 24.8 \text{ GPa}$$

$$G_{xy} = \frac{1}{a_{66}h} = 44 \text{ GPa}$$

$$\nu_{xy} = \frac{-a_{12}}{a_{11}} = 0.615 \quad \textit{and} \quad \nu_{yx} = \frac{-a_{12}}{a_{22}} = 1.045$$

Fig. 3.25 shows the variation of these elastic constants for values of θ in the range $0-90^\circ$.

It is interesting to compare the behaviour of the single ply and the laminate as shown in Figs 3.24 and 3.25. Firstly, it is immediately evident that the laminate offers a better balance of properties as well as improvements in absolute terms. The shear modulus in particular is much better in the laminate. Its peak value at 45° arises because shear is equivalent to a state of stress where equal tensile and compressive stresses are applied at 45° to the shear direction. Thus shear loading on a $[\pm 45]_s$ laminate is equivalent to tensile and compressive loading on a $[0/90]_s$ laminate. Thus, the fibres are effectively aligned in the direction of loading and this provides the large stiffness (or modulus) which is observed.

It is also worthy of note that large values of Poisson's Ratio can occur in a laminate. In this case a peak value of over 1.5 is observed – something which would be impossible in an isotropic material. Large values of Poisson's Ratio

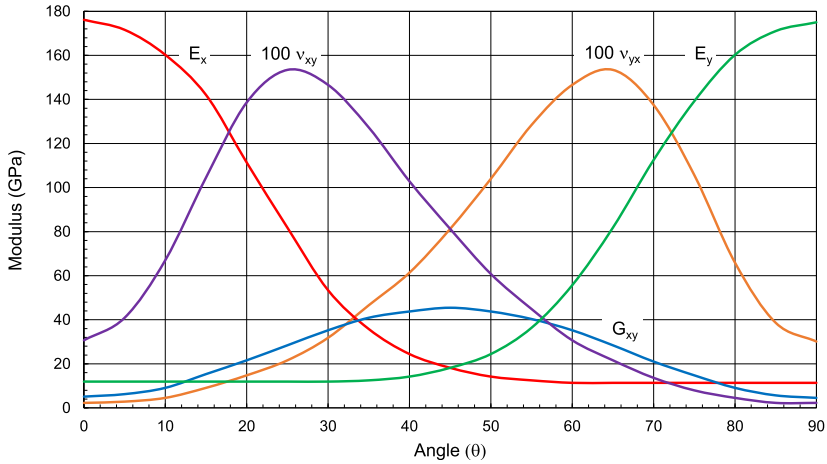


FIG. 3.25 Variation of elastic properties for a (+/−45) symmetric laminate of carbon/epoxy.

are a characteristic of unidirectional fibre composites and arise due to the coupling effects between extension and shear which were referred to earlier.

It is also important to note that although the laminae $[\pm 45]_s$ indicates that $E_x = E_y = 18.1$ GPa, this laminate is not isotropic or even quasi-isotropic. As shown in Chapter 2, in an isotropic material, the shear modulus is linked to the other elastic properties by the following equation

$$G_{xy} = \frac{E_x}{2(1 + v_{xy})}$$

For the $[\pm 45]_s$ laminate this would give

$$G_{xy} = \frac{18.1}{2(1 + 0.814)} = 5 \text{ GPa}$$

However, Fig. 3.25 shows that $G_{xy} = 45.2$ GPa for the $[\pm 45]_s$ laminate.

Some laminates do exhibit quasi-isotropic behaviour. The simplest one is $[0, \pm 60]_s$. For this laminate

$$E_x = E_y = 66.4 \text{ GPa} \quad \textit{and} \quad v_{xy} = v_{yx} = 0.321, \quad G_{xy} = 25.1 \text{ GPa}$$

(using the individual ply data in the above example).

If we check G_{xy} from the isotropic equation, we get

$$G_{xy} = \frac{E_x}{2(1 + v_{xy})} = \frac{66.4}{2(1 + 0.321)} = 25.1 \text{ GPa}$$

This agrees with the value calculated from the laminate theory.

In general any laminate with the lay-up

$$\left[0,\ \frac{\pi}{N},\ \frac{2\pi}{N},\ \cdots,\ \frac{N-1}{N}\pi\right]_s$$

or

$$\left[\frac{\pi}{N},\ \frac{2\pi}{N},\ \cdots,\ \pi\right]_s$$

is quasi-isotropic where N is an integer equal to 3 or greater. The angles for the plies are expressed in radians.

3.12 Analysis of multi-layer isotropic materials

The Plate Constitutive equations can be used for curved plates provided the radius of curvature is large relative to the thickness (typically $r/h > 50$). They can also be used to analyse laminates made up of materials other than unidirectional fibres, e.g. layers which are isotropic or made from woven fabrics can be analysed by inserting the relevant properties for the local 1−2 directions. Sandwich panels can also be analysed by using a thickness and appropriate properties for the core material. These types of situation are considered in the following examples.

Example 3.14. A blow moulded plastic bottle has its wall thickness made of three layers. The layers are:

$$\text{Outside and inside skin} - \text{Material A}$$

$$\text{thickness} = 0.4\text{ mm}, E_1 = E_2 = 3\text{ GPa},\ G_{12} = 1.1\text{ GPa},\ \nu_{12} = 0.364$$

$$\text{Core} - \text{Material B}$$

$$\text{thickness} = 0.4\text{ mm}, E_1 = E_2 = 0.8\text{ GPa},\ G_{12} = 0.285\text{ GPa},\ \nu_{12} = 0.404$$

If the diameter of the bottle is 160 mm, calculate the hoop and axial strains in the bottle wall when an internal pressure of 200 kPa is applied. Calculate also the stresses in the individual layers.

Solution Although the composite wall is curved, the (r/h) value is large and so it can be analysed using the method illustrated for laminates. In this case, each ply is isotropic and so the properties do not vary with θ. It is thus necessary to get $\overline{Q}$ for each ply relative to the centreline of the wall thickness

$$h_0 = 0.6, \quad h_1 = -0.2, \quad h_2 = 0, \quad h_3 = 0.2, \quad h_4 = 0.6$$

i.e. the wall section is treated as if it has four plies

$$[\text{material A}(0.4\text{ mm})/\text{material B}(0.2\text{ mm})]_s$$

Also

$$\textit{hoop stress},\ \sigma_y = \frac{Pr}{h} = \frac{0.2 \times 80}{1.2} = 13.33 \quad \text{MPa}$$

(or $N_y = \sigma_y h = 16$ N/mm)

$$\textit{axial stress},\ \sigma_x = \frac{Pr}{2h} = \frac{0.2 \times 80}{2 \times 1.2} = 6.67 \text{ MPa}$$

(or $N_R = \sigma_R h = 8$ N/mm)

$$\overline{Q}_1 = \begin{bmatrix} 3.444 \times 10^3 & 1.244 \times 10^3 & 0 \\ 1.244 \times 10^3 & 3.444 \times 10^3 & 0 \\ 0 & 0 & 1.103 \times 10^3 \end{bmatrix} \text{N/mm}^2,$$

$$\overline{Q}_1 = \begin{bmatrix} 956.5 & 376.7 & 0 \\ 376.7 & 956.5 & 0 \\ 0 & 0 & 285.8 \end{bmatrix} \text{N/mm}^2$$

Also,

$$\overline{Q}_1 = \overline{Q}_4 \quad \text{and} \quad \overline{Q}_2 = \overline{Q}_3$$

Then the Extensional Stiffness Matrix is given by

$$A = \sum_{f=1}^{4} Q_f (h_f - h_{f-1}), \quad a = A^{-1} \ (\textit{since}\ [B] = 0).$$

The strains are related to the forces (or stresses) by

$$\begin{bmatrix} \varepsilon_x \\ \varepsilon_y \\ \gamma_{xy} \end{bmatrix} = a \cdot \begin{bmatrix} N_x \\ N_y \\ N_{xy} \end{bmatrix}$$

Therefore, the axial and hoop strains are

$$\varepsilon_x = 7.932 \times 10^{-4}, \quad \varepsilon_y = 7.809 \times 10^{-3} \left(\gamma_{xy} = 0\right)$$

The effective elastic constants for the composite are:

$$E_x = \frac{1}{a_{11} \cdot h} \quad E_y = \frac{1}{a_{22} \cdot h} \quad G_{xy} = \frac{1}{a_{66} \cdot h}$$

$$v_{xy} = \frac{-a_{12}}{a_{11}} \quad v_{yx} = \frac{-a_{12}}{a_{22}}$$

So

$$E_x = 2.26 \times 10^3 \ \text{MPa} \quad E_y = 2.26 \times 10^3 \ \text{MPa} \quad G_{xy} = 830.6 \ \text{MPa}$$

and

$$v_{xy} = 0.36, \quad v_{yx} = 0.36$$

The stresses in the individual layers are obtained from

$$\begin{bmatrix} \sigma_{Ax} \\ \sigma_{Ay} \\ \tau_{Axy} \end{bmatrix} = \overline{Q}_1 \cdot \begin{bmatrix} \varepsilon_x \\ \varepsilon_y \\ \gamma_{xy} \end{bmatrix} \quad \begin{bmatrix} \sigma_{Bx} \\ \sigma_{By} \\ \tau_{Bxy} \end{bmatrix} = \overline{Q}_2 \cdot \begin{bmatrix} \varepsilon_x \\ \varepsilon_y \\ \gamma_{xy} \end{bmatrix}$$

So,

$$\sigma_{Ax} = 8.71 \text{ MPa} \quad \text{and} \quad \sigma_{Ay} = 17.55 \text{ MPa}$$
$$(\tau_{Axy} = 0 \text{ MPa})$$
$$\sigma_{Bx} = 2.5 \text{ MPa} \quad \text{and} \quad \sigma_{By} = 4.9 \text{ MPa}$$
$$(\tau_{Bxy} = 0 \text{ MPa})$$

The values of stress may be checked by simple equilibrium analysis.

(i) Force equilibrium: $N_A + N_B = N_x$

$$\sigma_{Ax} A_A + \sigma_{Bx} A_B = N_x$$

(ii) Geometry of deformation:

$$\varepsilon_A = \varepsilon_B = \varepsilon_x$$

So

$$\frac{\sigma_{Ax}}{E_A} = \frac{\sigma_{Bx}}{E_B} \quad or \quad \sigma_{Ax} = \left(\frac{E_A}{E_B}\right) \sigma_{Bx}$$

$$\left(\frac{E_A}{E_B E}\right) \sigma_B A_A + \sigma_B A_B = N_x$$

$$\sigma_{Bx} = N_x / \left(\left(\frac{E_A}{E_B}\right) A_A + A_B \right) = 2.4 \text{ N/mm}^2$$

$$\sigma_{Ax} = \left(\frac{3}{0.8}\right) 2.4 = 8.8 \text{ N/mm}^2$$

To assist the reader the values of the terms in the matrices are

$$A = \begin{bmatrix} 3.15 \times 10^3 & 1.16 \times 10^3 & 0 \\ 1.16 \times 10^3 & 3.158 \times 10^3 & 0 \\ 0 & 0 & 996.7 \end{bmatrix} \text{N/mm} \quad B = \begin{bmatrix} 0 & 0 & 0 \\ 0 & 0 & 0 \\ 0 & 0 & 0 \end{bmatrix}$$

$$a = \begin{bmatrix} 3.67 \times 10^{-4} & -1.35 \times 10^{-4} & 0 \\ -1.35 \times 10^{-4} & 3.67 \times 10^{-4} & 0 \\ 0 & 0 & 1.003 \times 10^{-3} \end{bmatrix} \text{mm/N}$$

This type of analysis could also be used for a sandwich structure with solid skins and a foamed core. It is simply a matter of using the appropriate values of E_1, G_{12}, E_2, v_{12} for the skin and core material. This is illustrated in the following example.

Example 3.15. A sandwich moulding is made up of solid skins with a foamed plastic core. The skins and core may be regarded as isotropic with the following the properties:

$$\text{Skin} - \text{Material A}, E_1 = E_2 = 3.5 \text{ GPa}, G_{12} = 1.25 \text{ GPa}, v_{12} = 0.4$$

$$\text{Foam Core} - \text{Material B}, E_1 = E_2 = 0.06 \text{ GPa}, G_{12} = 0.021 \text{ GPa}, v_{12} = 0.43$$

The skins are each 1 mm thick and the core is 20 mm thick.

If moments of $M_x = 400$ Nm/m and $M_y = 300$ Nm/m are applied to the moulding, calculate the resulting curvatures and the stresses and strains in the cross-section.

Solution As the skins and core are isotropic, we only need to get the $\overline{Q}$ values for each:

Skin

$$\overline{Q}_1 = \begin{bmatrix} 4.167 \times 10^3 & 1.667 \times 10^3 & 0 \\ 1.667 \times 10^3 & 4.167 \times 10^3 & 0 \\ 0 & 0 & 1.25 \times 10^3 \end{bmatrix}$$

$$\overline{Q}_4 = \overline{Q}_1,$$

Foamed Core

$$\overline{Q}_2 = \begin{bmatrix} 73.63 & 31.63 & 0 \\ 31.63 & 73.63 & 0 \\ 0 & 0 & 20.98 \end{bmatrix}$$

$$\overline{Q}_3 = \overline{Q}_2$$

Assuming as before that there are four layers with the centreline at the mid-plane of the cross-section, then

$$h_0 = -11, \quad h_1 = -10, \quad h_2 = 0, \quad h_3 = 10, \quad h_4 = 11 \text{ mm}$$

As these are only moments applied and the section is symmetric ($B = 0$) we only need the D and d matrices. These are given by

$$D = \frac{1}{3}\sum_{f=1}^{4} \overline{Q}_f \left[h_f^3 - h_{f-1}^3\right]$$

$$D = \begin{bmatrix} 9.69 \times 10^5 & 3.89 \times 10^5 & 0 \\ 3.89 \times 10^5 & 9.69 \times 10^5 & 0 \\ 0 & 0 & 2.89 \times 10^5 \end{bmatrix} \text{N mm}$$

$$d = \begin{bmatrix} 1.23 \times 10^{-6} & -4.94 \times 10^{-7} & 0 \\ -4.94 \times 10^{-6} & 1.23 \times 10^{-6} & 0 \\ 0 & 0 & 3.45 \times 10^{-6} \end{bmatrix}$$

Then the curvatures, κ, are given by

$$\begin{bmatrix} \kappa_x \\ \kappa_y \\ \kappa_{xy} \end{bmatrix} = d \begin{bmatrix} M_x \\ M_y \\ M_{xy} \end{bmatrix}$$

So,

$$\kappa_x = 3.44 \times 10^{-4} \text{ mm}^{-1}, \quad \kappa_y = 1.72 \times 10^{-4} \text{ mm}^{-1}, \quad \kappa_{xy} = 0$$

The strains will be directly proportional to the distance across the thickness, i.e.

$$\varepsilon = \kappa \cdot z$$

At top surface, $z = -11$ mm, so $\varepsilon_x = (3.44 \times 10^{-4})\ (-11) = -3.78 \times 10^{-3}$:

$$\text{stress, } \sigma_x = E_1 \varepsilon_x = 3500\left(3.78 \times 10^{-3}\right) = -13.25 \text{ MPa}$$

At interface (skin side), $z = -10$ mm, so $\varepsilon_x = (3.44 \times 10^{-4})\ (-10) = -3.44 \times 10^{-3}$:

$$\text{stress, } \sigma_x = E_1 \varepsilon_x = 3500\left(3.44 \times 10^{-3}\right) = -12.04 \text{ MPa}$$

At interface (core side), $\varepsilon_x = -3.44 \times 10^{-3}$:

$$\text{stress, } \sigma_x = 60\left(-3.44 \times 10^{-3}\right) = -0.21 \text{ MPa}$$

Similarly, in the y-direction.

At top surface

$$\varepsilon_y = -1.89 \times 10^{-3}, \quad \sigma_y = -6.6 \text{ MPa}$$

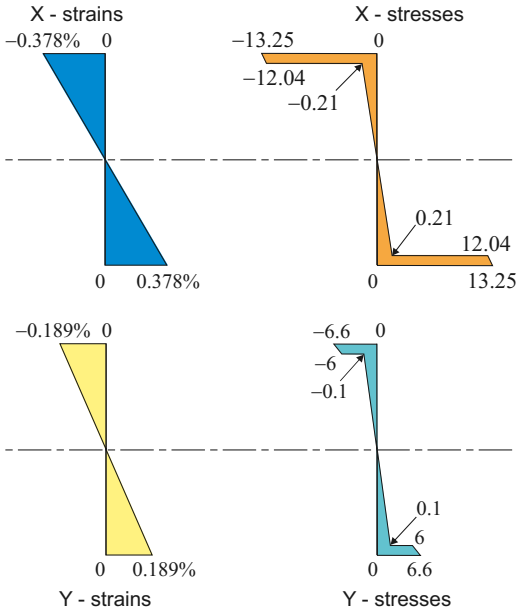


FIG. 3.26 Stresses and strains, Example 3.15.

At interface (skin)

$$\varepsilon_y = -1.72 \times 10^{-3}, \quad \sigma_y = -6 \text{ MPa}$$

At interface (core)

$$\varepsilon_y = -1.72 \times 10^{-3}, \quad \sigma_y = -0.1 \text{ MPa}$$

In both cases the stresses and strains will be mirrored on the bottom section of the beam (i.e. positive instead of negative). These are illustrated in Fig. 3.26.

3.13 Analysis of non-symmetric laminates

Example 3.16. A unidirectional carbon fibre/PEEK laminate has the stacking sequence $[0/35_2/-35_2]_T$. If it has an in-plane stress of $\sigma_x = 100$ MPa applied, calculate the strains and curvatures in the global directions. The properties of the individual plies are

$$E_1 = 145 \text{ GPa}, \quad E_2 = 15 \text{ GPa}, \quad G_{12} = 4 \text{ GPa}, \quad \nu_{12} = 0.278$$

Each ply has a thickness of 0.1 mm.

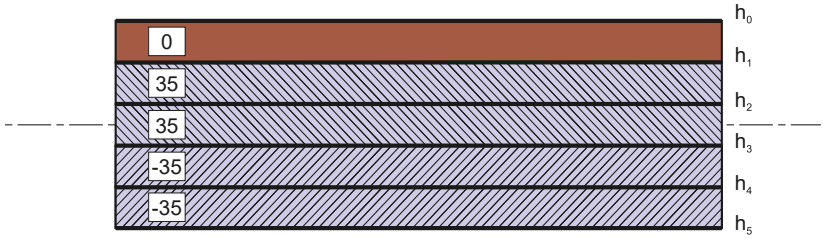


FIG. 3.27 Non-symmetric laminate.

Solution This stacking sequence is similar to that in *Example 3.11* except that in this case the laminate is not symmetrical. As shown in Fig. 3.27, the centreline of the laminate is in the middle of one of the plies and

$$h_0 = -0.25, \quad h_1 = -0.15, \quad h_2 = -0.05, \quad h_3 = 0.05, \quad h_4 = 0.15, \quad h_5 = 0.25$$

The approach is the same as before. $\overline{Q}$ must be determined for each layer as shown below and thus the values in the *A, B* and *D* matrices.

$$\overline{Q}_1 = \begin{bmatrix} 1.46 \times 10^5 & 4.20 \times 10^3 & 0 \\ 4.20 \times 10^3 & 1.51 \times 10^4 & 0 \\ 0 & 0 & 4 \times 10^3 \end{bmatrix}$$

$$\overline{Q}_2 = \begin{bmatrix} 7.28 \times 10^4 & 3.44 \times 10^4 & 4.17 \times 10^4 \\ 3.44 \times 10^4 & 2.80 \times 10^4 & 1.98 \times 10^4 \\ 4.17 \times 10^4 & 1.98 \times 10^4 & 3.42 \times 10^4 \end{bmatrix}$$

$$\overline{Q}_3 = \begin{bmatrix} 7.28 \times 10^4 & 3.44 \times 10^4 & 4.17 \times 10^4 \\ 3.44 \times 10^4 & 2.80 \times 10^4 & 1.98 \times 10^4 \\ 4.17 \times 10^4 & 1.98 \times 10^4 & 3.42 \times 10^4 \end{bmatrix}$$

$$\overline{Q}_4 = \begin{bmatrix} 7.28 \times 10^4 & 3.44 \times 10^4 & -4.17 \times 10^4 \\ 3.44 \times 10^4 & 2.80 \times 10^4 & -1.98 \times 10^4 \\ -4.17 \times 10^4 & -1.98 \times 10^4 & 3.42 \times 10^4 \end{bmatrix}$$

$$\overline{Q}_5 = \begin{bmatrix} 7.28 \times 10^4 & 3.44 \times 10^4 & -4.17 \times 10^4 \\ 3.44 \times 10^4 & 2.80 \times 10^4 & -1.98 \times 10^4 \\ -4.17 \times 10^4 & -1.98 \times 10^4 & 3.42 \times 10^4 \end{bmatrix}$$

$$A = \sum_{f=1}^{5} \overline{Q}_f (h_f - h_{f-1}) \quad B = \frac{1}{2} \sum_{f=1}^{5} \overline{Q}_f \left[(h_f)^2 - (h_{f-1})^2 \right]$$

$$D = \frac{1}{3} \sum_{f=1}^{5} \overline{Q}_f \left[(h_f)^3 - (h_{f-1})^3 \right]$$

In this case $[B] \neq 0$ and so $[a]$ and $[d]$ cannot be obtained by inverting the $[A]$ and $[D]$ matrices respectively. They must be obtained from

$$\begin{bmatrix} a & b \\ \beta & d \end{bmatrix} = \begin{bmatrix} A & B \\ B & D \end{bmatrix}^{-1}$$

The in-plane strains and the moments and curvatures are all linked in this non-symmetrical lamina and are obtained from

$$\begin{bmatrix} \varepsilon_x \\ \varepsilon_y \\ \gamma_{xy} \\ \kappa_x \\ \kappa_y \\ \kappa_{xy} \end{bmatrix} = \begin{bmatrix} a_{11} & a_{12} & a_{16} & b_{11} & b_{12} & b_{16} \\ a_{21} & a_{22} & a_{26} & b_{21} & b_{22} & b_{26} \\ a_{61} & a_{62} & a_{66} & b_{61} & b_{62} & b_{66} \\ \beta_{11} & \beta_{12} & \beta_{16} & d_{11} & d_{12} & d_{16} \\ \beta_{21} & \beta_{22} & \beta_{26} & d_{21} & d_{22} & d_{26} \\ \beta_{61} & \beta_{62} & \beta_{66} & d_{61} & d_{62} & d_{66} \end{bmatrix} \begin{bmatrix} N_x \\ N_y \\ N_{xy} \\ M_x \\ M_y \\ M_{xy} \end{bmatrix}$$

where

$$N = \sigma \cdot h (N_x = 50 \text{ N/mm})$$

which gives the strains and curvatures as

$$\varepsilon_x = 3.326 \times 10^{-3}, \quad \varepsilon_y = -2.868 \times 10^{-3}, \quad \gamma_{xy} = -3.405 \times 10^{-5}$$

$$\kappa_x = 0.012 \text{ mm}^{-1}, \quad \kappa_y = -0.01 \text{ mm}^{-1}, \quad \kappa_{xy} = 0.019 \text{ mm}^{-1}$$

The important point to note from this example is that in a non-symmetrical laminate the behaviour is very complex. It can be seen that the effect of a simple uniaxial stress, σ_x, is to produce strains and curvatures in all directions. This has relevance in a number of polymer processing situations because unbalanced cooling (for example) can result in layers which have different properties, across a moulding wall thickness. This is effectively a composite laminate structure which is likely to be non-symmetrical and complex behaviour can be expected when loading is applied.

The reader may wish to check the matrices in this example:

$$A = \begin{bmatrix} -4.37 \times 10^4 & 1.41 \times 10^4 & 0 \\ 1.41 \times 10^4 & 1.27 \times 10^4 & 0 \\ 0 & 0 & 1.4 \times 10^4 \end{bmatrix}$$

$$a = \begin{bmatrix} 6.65 \times 10^{-5} & -5.73 \times 10^{-5} & -6.81 \times 10^{-7} \\ -5.73 \times 10^{-5} & 1.53 \times 10^{-4} & -2.05 \times 10^{-5} \\ -6.81 \times 10^{-7} & -2.05 \times 10^{-5} & 1.02 \times 10^{-4} \end{bmatrix}$$

$$B = \begin{bmatrix} -1.46 \times 10^3 & 604.5 & -16.7 \times 10^3 \\ 604.5 & 258.2 & -792 \\ -16.7 \times 10^3 & -792 & 604.4 \end{bmatrix}$$

$$b = \begin{bmatrix} 2.30 \times 10^{-4} & -2.09 \times 10^{-4} & 3.77 \times 10^{-4} \\ -2.24 \times 10^{-4} & 1.49 \times 10^{-4} & 5.34 \times 10^{-5} \\ 9.55 \times 10^{-5} & 2.01 \times 10^{-4} & -2.03 \times 10^{-4} \end{bmatrix}$$

$$\beta = \begin{bmatrix} 2.30 \times 10^{-4} & -2.24 \times 10^{-4} & 9.55 \times 10^{-5} \\ -2.09 \times 10^{-4} & 1.49 \times 10^{-4} & 2.01 \times 10^{-4} \\ 3.77 \times 10^{-4} & 5.34 \times 10^{-5} & -2.03 \times 10^{-4} \end{bmatrix}$$

$$D = \begin{bmatrix} 1.05 \times 10^3 & 235.2 & -167.1 \\ 235.2 & 239.2 & -79.2 \\ -167.1 & -79.2 & 233.0 \end{bmatrix}$$

$$d = \begin{bmatrix} 2.15 \times 10^{-3} & -1.60 \times 10^{-3} & 1.64 \times 10^{-3} \\ -1.601 \times 10^{-3} & 6.65 \times 10^{-3} & -4.04 \times 10^{-4} \\ 1.64 \times 10^{-3} & -4.04 \times 10^{-3} & 8.74 \times 10^{-3} \end{bmatrix}$$

3.14 Analysis of short fibre composites

In order to understand the effect of discontinuous fibres in a polymer matrix it is important to understand the reinforcing mechanism of fibres. Fibres exert their effect by restraining the deformation of the matrix as shown in Fig. 3.28. The external loading applied through the matrix is transferred to the fibres by shear at the fibre/matrix interface. The resultant stress distributions in the fibre and matrix are complex. In short fibres the tensile stress increases from zero at the ends to a value $(\sigma_f)_{\max}$ which it would have if the fibre was continuous.

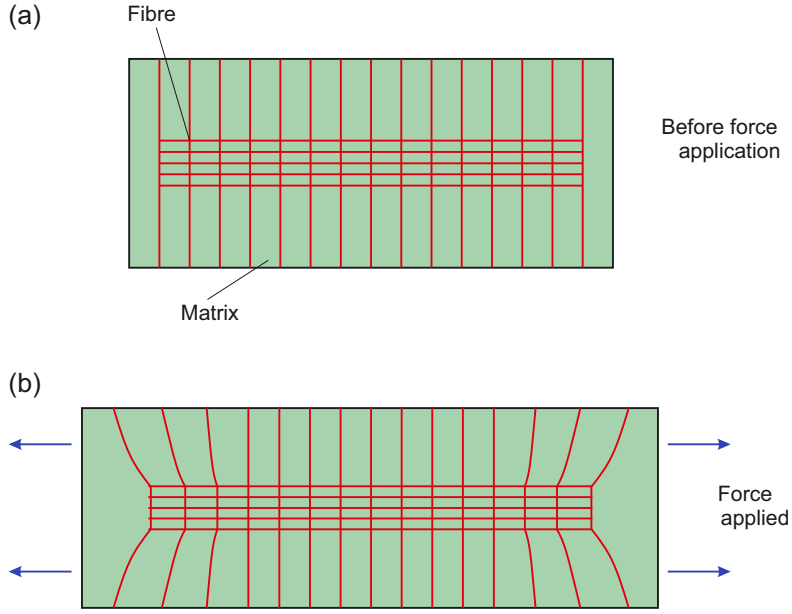


FIG. 3.28 Effect of fibre on deformation of matrix.

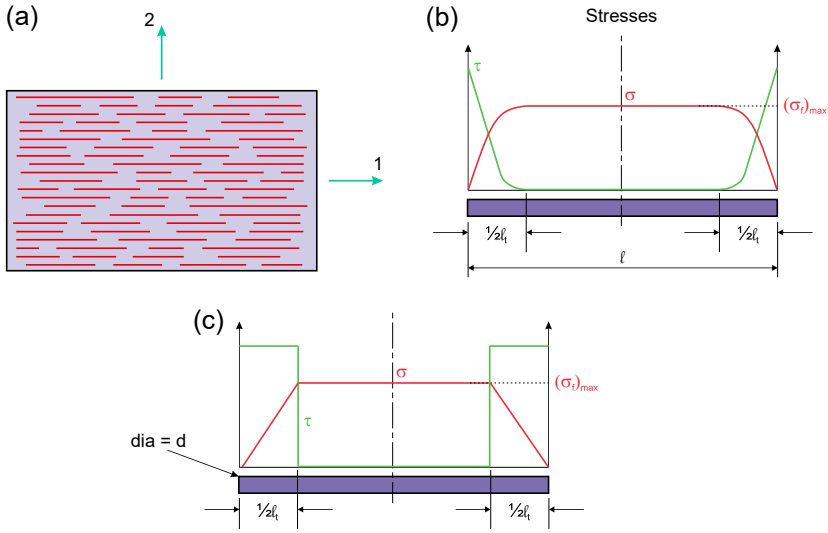


FIG. 3.29 Short fibre composites.

This is shown in Fig. 3.29. From the previous section it may be seen that $(\sigma_f)_{\max}$ may be determined from

$$\frac{(\sigma_f)_{max}}{E_f} = \frac{\sigma_c}{E_1} \tag{3.42}$$

where σ_c is the stress applied to the composite and E_1 may be determined from the rule of mixtures.

The stress distribution in short fibres is often simplified to the form shown in Fig. 3.29(c)

It is evident from Fig. 3.29 that there is a minimum fibre length which will permit the fibre to achieve its full load-carrying potential. The minimum fibre length in which the maximum fibre stress, $(\sigma_f)_{\max}$, can be achieved is called the **load transfer length**, ℓ_t. The value of ℓ_t may be determined from a simple force balance

Force transmitted by shear at interface $= \tau_y\ (\ell/2)\pi d$

Force exerted by fibre $= \sigma_f\ (\pi d^2/4)$.

hence,

$$\ell_t = \frac{(\sigma_f)_{max} d}{2\tau_y} \tag{3.43}$$

where, τ_y is the shear strength of the fibre/matrix interface.

The maximum value of ℓ_t will occur when $(\sigma_f)_{\max}$ reaches the tensile strength of the fibre, σ_{fu}, and this is defined as the **critical fibre length**, ℓ_c

$$\ell_c = \frac{\sigma_{fu} d}{2\tau_y} \tag{3.44}$$

Example 3.17. Short carbon fibres with a diameter of 10 μm are to be used to reinforce nylon 66. If the design stress for the composite is 300 MPa and the following data is available on the fibres and nylon, calculate the load transfer length for the fibres and also the critical fibre length. The volume fraction of the fibres is to be 0.3.

	Modulus (GPa)	Strength (GPa)
Carbon fibres	230	2.9
Nylon 66	2.8	–

The interfacial shear strength for carbon/nylon may be taken as 4 MPa.

Solution

$$E_1 = E_f V_f + E_m V_m$$
$$E_1 = 230(0.3) + 2.8(0.7) = 71\ GPa$$

Using (3.42)

$$(\sigma_f)_{max} = E_f\left(\frac{\sigma_c}{E_1}\right) = 230\left(\frac{300}{71}\right) = 972\ MPa$$

Using (3.43)

$$\ell_t = \frac{(\sigma_f)_{max}d}{2\tau_y} = \frac{972(10\times10^{-3})}{2\times4} = 1.2\ mm$$

Using (3.44)

$$\ell_c = \frac{\sigma_{fu}d}{2\tau_y} = \frac{2900(10\times10^{-3})}{2\times4} = 3.6\ mm$$

It may be seen from Fig. 3.29 that due to the ineffective end portions of short fibres, the average stress in the fibre will be less than in a continuous fibre. The exact value of the average stress will depend on the length of the fibres. Using the stress distributions shown in Fig. 3.29(b) the fibre stresses may be analysed as follows.

$$F_1 = \sigma_f\left(\pi d^2/4\right)$$

$$F_2 = \left[\sigma_f + \left(\frac{d\sigma_f}{dx}\right)dx\right]\ \frac{\pi d^2}{4}$$

$$F_3 = (\tau_y\pi d)dx$$

Now, for equilibrium of forces $F_1 = F_2 + F_3$

$$\sigma_f\left(\pi d^2/4\right) = \left(\sigma_f + \frac{d\sigma_f}{dx}dx\right)\left(\pi d^2/4\right) + (\tau\pi d)dx$$

$$(d/4)d\sigma_f = -\tau_y dx$$

Integrating this equation gives

$$(d/4)\int_0^{\sigma_f} d\sigma_f = -\int_{\frac{1}{2}\ell}^{x}\tau_y dx$$

$$\sigma_f = \frac{4\tau_y\left(\frac{1}{2}\ell - x\right)}{d} \tag{3.45}$$

This is the general equation for the stress in the fibres but there are 3 cases to consider, as shown in Fig. 3.30.

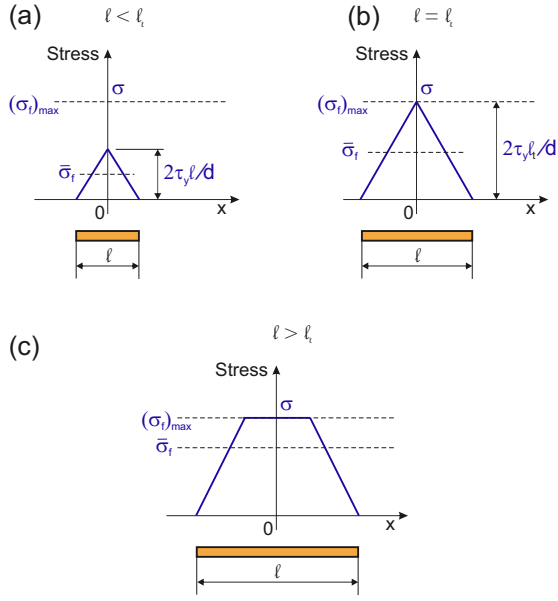


FIG. 3.30 Stress variations in short fibres.

(a) Fibre lengths less than ℓ_t

In this case the peak value of stress occurs at $x = 0$, so from Eq. (3.45)

$$\sigma_f = \frac{2\tau_y \ell}{d}$$

The average fibre stress, $\overline{\sigma}_f$, is obtained by dividing the area under the stress/fibre length graph by the fibre length.

$$\overline{\sigma}_f = \frac{\frac{1}{2}\ell\left(\frac{2\tau_y \ell}{d}\right)}{\ell} = \frac{\tau_y \ell}{d}$$

Now from (3.6)

$$\sigma_c = \left(\frac{\tau_y \ell}{d}\right) V_f + \sigma'_m(1 - V_f) \tag{3.46}$$

(b) Fibre length equal to ℓ_t

In this case the peak stress is equal to the maximum fibre stress.

So at $x = 0$

$$\sigma_f = (\sigma_f)_{max} = \frac{2\tau_y \ell_t}{d} \tag{3.47}$$

$$\text{Average fibre stress} = \overline{\sigma}_f = \frac{\frac{1}{2}\left(\frac{2\tau_y \ell_t}{d}\right)\ell_t}{\ell}$$

$$\overline{\sigma}_f = \frac{\tau_y \ell_t}{d}$$

So from (3.6)

$$\sigma_c = \left(\frac{\tau_y \ell_t}{d}\right) V_f + \sigma'_m(1 - V_f) \tag{3.48}$$

(c) Fibre length greater than ℓ_t

(i) For $\frac{1}{2}\ell > x > \frac{1}{2}(\ell - \ell_t)$

$$\sigma_f = \frac{4\tau_y}{d}\left(\frac{1}{2}\ell - x\right)$$

(ii) For $\frac{1}{2}(\ell - \ell_t) > x > 0$

$$\sigma_f = \text{constant} = (\sigma_f)_{max}$$

$$\sigma_f = \frac{2\tau_y \ell_t}{d}$$

Also, as before, the average fibre stress may be obtained from

$$\overline{\sigma}_f = \frac{\left[(\sigma_f)_{max}\right](\ell - \ell_t) + \left[(\sigma_f)_{max}\right]\frac{1}{2}\ell_t}{\ell} = \left[(\sigma_f)_{max}\right]\left(1 - \frac{\ell_t}{2\ell}\right)$$

So from (3.6)

$$\sigma_c = V_f(\sigma_f)_{max}\left(1 - \frac{\ell_t}{2\ell}\right) + \sigma'_m(1 - V_f) \tag{3.49}$$

Note that in order to get the average fibre stress as close as possible to the maximum fibre stress, the fibres need to be considerably longer than the critical length. At the critical length the average fibre stress is only half of the value achieved in continuous fibres.

Experiments show that equations such as (3.49) give satisfactory agreement with the measured values of strength and modulus for polyester sheets reinforced with chopped strands of glass fibre. Of course, these strengths and modulus values are only about 20−25% of those achieved with continuous fibre reinforcement. This is because with randomly oriented short fibres only a small percentage of the fibres are aligned along the line of action of the applied stress. Also, the packing efficiency is low and the generally accepted maximum value for V_f of about 0.4 is only half of that which can be achieved with continuous filaments.

In order to get the best out of fibre reinforcement it is not uncommon to try to control within close limits the fibre content which will provide maximum stiffness for a fixed weight of matrix and fibres. In flexure it has been found that optimum stiffness is achieved when the volume fraction is 0.2 for chopped strand mat (CSM) and 0.37 for continuous fibre reinforcement.

Example 3.18. Calculate the maximum and average fibre stresses for glass fibres which have a diameter of 15 μm and a length of 2.5 mm. The interfacial shear strength is 4 MPa and $\ell_t/\ell = 0.3$.

Solution Since $\ell > \ell_t$ then

$$(\sigma_f)_{max} = \frac{2\tau_y \ell}{d}\left(\frac{\ell_t}{\ell}\right) = \frac{2 \times 4 \times 2.5 \times 10^{-3} \times 0.3}{15 \times 10^{-6}}$$

$$(\sigma_f)_{max} = 400 \text{ MPa}$$

Also

$$\overline{\sigma}_f = (\sigma_f)_{max}\left(1 - \frac{\ell_t}{2\ell}\right) = 400\left(1 - \frac{0.3}{2}\right)$$

$$\overline{\sigma}_f = 340 \text{ MPa}$$

In practice it should be remembered that short fibres are more likely to be randomly oriented rather than aligned as illustrated in Fig. 3.4. The problem of analysing and predicting the performance of randomly oriented short fibres is complex. However, the stiffness of such systems may be predicted quite accurately using the following simple empirical relationship.

$$E_{\text{random}} = 3E_1/8 + 5E_2/8 \tag{3.50}$$

Clyne & Hull also proposed that the shear modulus and Poisson's Ratio for a random short fibre composite could be approximated by

$$G_{\text{random}} = \frac{1}{8}E_1 + \frac{1}{4}E_2 \tag{3.51}$$

$$\nu_{\text{random}} = \frac{E_r}{2G_r} - 1 \tag{3.52}$$

E_1 and E_2 refer to the longitudinal and transverse moduli for aligned fibre composites of the type shown in (Fig. 3.29). These values can be determined

experimentally or using specifically formulated empirical equations. However, if the fibres are relatively long then Eqs. (3.5) and (3.13) may be used. These give results which are sufficiently accurate for most practical purposes.

3.15 Creep behaviour of fibre reinforced plastics

The viscoelastic nature of the matrix in many fibre reinforced plastics causes their properties to be time and temperature dependent. Under a constant stress they exhibit creep which will be more pronounced as the temperature increases. However, since fibres exhibit negligible creep, the time dependence of the properties of fibre reinforced plastics is very much less than that for the unreinforced matrix.

3.16 Strength of fibre composites

Up to this stage we have considered the deformation behaviour of fibre composites. An equally important topic for the designer is avoidance of failure. If the definition of 'failure' is the attainment of a specified deformation, then the earlier analysis may be used. However, if the occurrence of yield or fracture is to be predicted as an extra safeguard then it is necessary to use another approach.

In an isotropic material subjected to a uniaxial stress, failure of the latter type is straightforward to predict. The tensile strength of the material $\widehat{\sigma}_T$ will be known from material data sheets and it is simply a question of ensuring that the applied uniaxial stress does not exceed this.

If an isotropic material is subjected to multi-axial stresses, then the situation is slightly more complex but there are well established procedures for predicting failure. If σ_x and σ_y are applied it is not simply a question of ensuring that neither of these exceed $\widehat{\sigma}_T$. At values of σ_x and σ_y below $\widehat{\sigma}_T$ there can be a plane within the material where the stress reaches $\widehat{\sigma}_T$ and this will initiate failure.

A variety of methods have been suggested to deal with the prediction of failure under multi-axial stresses and some of these have been applied to composites. The main methods are

(i) *Maximum Stress Criterion:* This criterion suggests that failure of the composite will occur if any one of five events happens

$$\sigma_1 \geq \widehat{\sigma}_{1T} \quad \text{or} \quad \sigma_1 \leq \widehat{\sigma}_{1C} \quad \text{or} \quad \sigma_2 \geq \widehat{\sigma}_{2T} \quad \text{or} \quad \sigma_2 \leq \widehat{\sigma}_{2C} \quad \text{or} \quad \tau_{12} \geq \widehat{\tau}_{12}$$

That is, if the local tensile, compressive or shear stresses exceed the materials tensile, compressive or shear strength then failure will occur. Some typical values for the strengths of uni-directional composites are given in Table 3.5.

TABLE 3.5 Typical strength properties of unidirectional fibre reinforced plastics.

Material	Fibre volume fraction, V_f	$\widehat{\sigma}_{1T}$ (GPa)	$\widehat{\sigma}_{2T}$ (GPa)	$\widehat{\tau}_{12}$ (GPa)	$\widehat{\sigma}_{1C}$ (GPa)	$\widehat{\sigma}_{2C}$ (GPa)
GFRP (E glass/ epoxy)	0.6	1.4	0.05	0.04	0.22	0.1
GFRP (E glass/ polyester)	0.42	0.52	0.034	–	–	–
KFRP (Kevlar 49/epoxy)	0.6	1.5	0.027	0.047	0.24	0.09
CFRP (carbon/ epoxy)	0.6	1.8	0.08	0.1	1.57	0.17
CFRP (carbon HM/epoxy)	0.62	1.24	0.02	0.04	0.29	0.03

CFRP, carbon fibre reinforced plastic; *GFRP*, glass fibre reinforced plastic; *KFRP*, Kevlar fibre reinforced plastic.

(ii) *Maximum Strain Criterion:* This criterion is similar to the above only it uses strain as the limiting condition rather than stress. Hence, failure is predicted to occur if

$$\varepsilon_1 \geq \widehat{\varepsilon}_{1T} \quad \text{or} \quad \varepsilon_1 \leq \widehat{\varepsilon}_{1C} \quad \text{or} \quad \varepsilon_2 \geq \widehat{\varepsilon}_{2T} \quad \text{or} \quad \varepsilon_2 \leq \widehat{\varepsilon}_{2C} \quad \text{or} \quad \gamma_{12} \geq \widehat{\gamma}_{12}$$

(iii) *Tsai–Hill Criterion:* This empirical criterion defines failure as occurring if

$$\left(\frac{\sigma_1}{\widehat{\sigma}_1}\right)^2 - \left(\frac{\sigma_1\sigma_2}{\widehat{\sigma}_1^2}\right) + \left(\frac{\sigma_2}{\widehat{\sigma}_2}\right)^2 + \left(\frac{\tau_{12}}{\widehat{\tau}_{12}}\right)^2 \geq 1 \tag{3.53}$$

The values in this equation are chosen so as to correspond with the nature of the loading. For example, if σ_1 is compressive, then $\widehat{\sigma}_{1C}$ is used and so on.

In practice the second term in the above equation is found to be small relative to the others and so it is often ignored and the reduced form of the Tsai–Hill Criterion becomes.

$$\left(\frac{\sigma_1}{\widehat{\sigma}_1}\right)^2 + \left(\frac{\sigma_2}{\widehat{\sigma}_2}\right)^2 + \left(\frac{\tau_{12}}{\widehat{\tau}_{12}}\right)^2 \geq 1 \tag{3.54}$$

3.16.1 Strength of single plies

These failure criteria can be applied to single ply composites as illustrated in the following examples.

Example 3.19. A single ply Kevlar 49/epoxy composite has the following properties.

$$E_1 = 79 \text{ GPa}, \quad E_2 = 4.1 \text{ GPa}, \quad G_{12} = 1.5 \text{ GPa}, \quad v_{12} = 0.43$$
$$\widehat{\sigma}_{1T} = 1.5 \text{ GPa}, \quad \widehat{\sigma}_{2T} = 0.027 \text{ GPa}, \quad \widehat{\tau}_{12} = 0.047 \text{ GPa}$$
$$\widehat{\sigma}_{1C} = 0.24 \text{ GPa}, \quad \widehat{\sigma}_{2C} = 0.09 \text{ GPa}.$$

If the fibres are aligned at 15° to the x-direction, calculate what tensile value of σ_x will cause failure according to (i) the Maximum Stress Criterion (ii) the Maximum Strain Criterion and (iii) the Tsai-Hill Criterion. The thickness of the composite is 1 mm.

Solution

(i) Maximum stress criterion

Consider the situation where $\sigma_x = 1$ MPa.

The stresses on the local (1−2) axes are given by

$$\begin{bmatrix} \sigma_1 \\ \sigma_2 \\ \tau_{12} \end{bmatrix} = T_\sigma \begin{bmatrix} \sigma_x \\ \sigma_y \\ \tau_{xy} \end{bmatrix}$$

Hence, $\sigma_1 = 0.93$ MPa, $\sigma_2 = 0.067$ MPa, $\tau_{12} = -0.25$ MPa.

So

$$\frac{\widehat{\sigma}_{1T}}{\sigma_1} = 1608, \quad \frac{\widehat{\sigma}_{2T}}{\sigma_2} = 402, \quad \frac{\widehat{\tau}_{12}}{\tau_{12}} = 188$$

Hence, a stress of $\sigma_x = 1608$ MPa would cause failure in the local 1-direction. A stress of $\sigma_x = 402$ MPa would cause failure in the local 2-direction and a stress of $\sigma_x = 188$ MPa would cause shear failure in the local 1−2 directions. Clearly the latter is the limiting condition since it will occur first.

(ii) Maximum strain criterion

Once again, let $\sigma_x = 1$ MPa. The limiting strains are given by

$$\widehat{\varepsilon}_{1T} = \frac{\widehat{\sigma}_{1T}}{E_1} = 0.019, \quad \widehat{\varepsilon}_{1C} = \frac{\widehat{\sigma}_{1C}}{E_1} = 3.04 \times 10^{-3}$$

$$\widehat{\varepsilon}_{2T} = \frac{\widehat{\sigma}_{2T}}{E_2} = 6.59 \times 10^{-3}, \quad \widehat{\varepsilon}_{2C} = \frac{\widehat{\sigma}_{2C}}{E_2} = 0.022$$

$$\widehat{\gamma}_{12} = \frac{\widehat{\tau}_{12}}{G} = 0.031$$

The strains in the local directions are obtained from

$$\begin{bmatrix} \varepsilon_1 \\ \varepsilon_2 \\ \gamma_{12} \end{bmatrix} = S. \begin{bmatrix} \sigma_1 \\ \sigma_2 \\ \tau_{12} \end{bmatrix}$$

$$\varepsilon_1 = 1.144 \times 10^{-5}, \;\; \varepsilon_2 = 1.128 \times 10^{-5}, \;\; \gamma_{12} = -1.688 \times 10^{-4}$$

$$\frac{\widehat{\varepsilon}_{1T}}{\varepsilon_1} = 1659, \;\; \frac{\widehat{\varepsilon}_{2T}}{\varepsilon_2} = 583, \;\; \frac{\widehat{\gamma}_{12}}{\gamma_{12}} = 188$$

Thus, once again, an applied stress of 188 MPa would cause shear failure in the local 1−2 direction.

(iii) Tsai − Hill criterion

For an applied stress of 1 MPa and letting X be the multiplier on this stress, we can determine the value of X to make the Tsai − Hill equation become equal to 1.

$$\left(\frac{X \bullet \sigma_1}{\widehat{\sigma}_{1T}}\right)^2 - \left(\frac{X^2 \bullet \sigma_1 \sigma_2}{\widehat{\sigma}_{1T}}\right) + \left(\frac{X \bullet \sigma_2}{\widehat{\sigma}_{2T}}\right)^2 + \left(\frac{X \bullet \tau_{12}}{\widehat{\tau}_{12}}\right)^2 = 1$$

Solving this gives $X = 169$. Hence a stress of $\sigma_x = 169$ MPa would cause failure. It is more difficult with the Tsai−Hill criterion to identify the nature of the failure i.e. tensile, compression or shear. Also, it is generally found that for fibre angles in the regions 5°−15° and 40°−90°, the Tsai − Hill criterion predictions are very close to the other predictions. For angles between 15° and 40° the Tsai−Hill tends to predict more conservative (lower) stresses to cause failure.

Example 3.20. The single ply in the previous example is subjected to the stress system

$$\sigma_x = 80 \;\text{MPa}, \;\; \sigma_y = -40 \;\text{MPa}, \;\; \tau_{xy} = -20 \;\text{MPa}$$

Determine whether failure would be expected to occur according to (a) the Maximum Stress (b) the Maximum Strain and (c) the Tsai-Hill criteria.

Solution

(a) *Maximum stress criterion*

The stresses in the 1−2 directions are

$$\begin{bmatrix} \sigma_1 \\ \sigma_2 \\ \tau_{12} \end{bmatrix} = T_\sigma \begin{bmatrix} \sigma_x \\ \sigma_y \\ \tau_{xy} \end{bmatrix}$$

$$\sigma_1 = 61.9 \text{ MPa}, \quad \sigma_2 = -21.9 \text{ MPa}, \quad \tau_{12} = -47.3 \text{ MPa}$$

$$\frac{\widehat{\sigma}_{1T}}{\sigma_1} = 24.2, \quad \frac{\widehat{\sigma}_x}{\sigma_2} = 4.1, \quad \frac{\widehat{\tau}_{12}}{\tau_{12}} = 0.99$$

There are thus no problems in the tensile or compressive directions, but the shear ratio has dropped below 1 and so failure is possible.

(b) *Maximum strain criterion*

The limiting strains are as calculated in the previous example.

The local strains are obtained from

$$\begin{bmatrix} \varepsilon_1 \\ \varepsilon_2 \\ \gamma_{12} \end{bmatrix} = S \cdot \begin{bmatrix} \sigma_1 \\ \sigma_2 \\ \tau_{12} \end{bmatrix}$$

$$\varepsilon_1 = 9.04 \times 10^{-4}, \quad \varepsilon_2 = -5.69 \times 10^{-3}, \quad \gamma_{12} = -0.032$$

$$\frac{\widehat{\varepsilon}_{1T}}{\varepsilon_1} = 21, \quad \frac{\widehat{\varepsilon}_{2C}}{\varepsilon_2} = 3.86, \quad \frac{\widehat{\gamma}_{12}}{\gamma_{12}} = 0.99$$

Once again failure is just possible in the shear direction.

(c) Tsai-Hill criterion

The Tsai−Hill equation gives

$$\left(\frac{\sigma_1}{\widehat{\sigma}_{1T}}\right)^2 - \left(\frac{\sigma_1\sigma_2}{\widehat{\sigma}_{1T}}\right)^2 + \left(\frac{\sigma_2}{\widehat{\sigma}_{2C}}\right)^2 + \left(\frac{\tau_{12}}{\widehat{\tau}_{12}}\right)^2 = 1.08$$

As these terms equate to > 1, failure is likely to occur.

3.16.2 Strength of laminates

When a composite is made up of many plies, it is unlikely that all plies will fail simultaneously. Therefore we should expect that failure will occur in one ply before it occurs in the others. To determine which ply will fail first it is simply a question of applying the above method to each ply in turn. Thus it is necessary to determine the stresses or strains in the local (1−2) directions for each ply and then check for the possibility of failure using any or all of the above criteria. This is illustrated in the following Example.

Example 3.21. A carbon-epoxy composite has the properties listed below. If the stacking sequence is $[0/\text{-}30/30]_s$ and stresses of $\sigma_x = 400$ MPa, $\sigma_y = 160$ MPa and $\tau_{xy} = -100$ MPa are applied, determine whether or not failure would be expected to occur according to (a) the Maximum Stress,

(b) the Maximum Strain, and (c) the Tsai-Hill criteria. The thickness of each ply is 0.2 mm.

$$E_1 = 125 \text{ GPa}, \quad E_2 = 9 \text{ GPa}, G_{12} = 4.4 \text{ GPa}, \nu_{12} = 0.34$$

$$\widehat{\sigma}_{1T} = 1.8 \text{ GPa}, \widehat{\sigma}_{2T} = 0.08 \text{ GPa}, \widehat{\sigma}_{1C} = 1.57 \text{ GPa}$$

$$\widehat{\sigma}_{2C} = 0.17 \text{ GPa}, \widehat{\tau}_{12} = 0.1 \text{ GPa}$$

Solution It is necessary to work out the global strains for the laminate (these will be the same for each ply) and then get the local strains and stresses. Thus, for the 30° ply

$$\begin{bmatrix} \varepsilon_x \\ \varepsilon_y \\ \gamma_{xy} \end{bmatrix} = a \begin{bmatrix} N_x \\ N_y \\ N_{xy} \end{bmatrix}$$

Using $h_0 = -0.6$, $h_1 = -0.4$, $h_2 = -0.2$, $h_3 = 0$, $h_4 = 0.2$, $h_5 = 0.4$ and $h_6 = 0.6$ ($h = 1.2$ mm) gives

$$\begin{bmatrix} \varepsilon_x \\ \varepsilon_y \\ \gamma_{xy} \end{bmatrix} = \begin{bmatrix} 2.94 \\ 7.51 \\ -5.46 \end{bmatrix} \times 10^{-3}$$

Thus

$$\begin{bmatrix} \varepsilon_1 \\ \varepsilon_2 \\ \gamma_{12} \end{bmatrix} = T_\varepsilon \begin{bmatrix} \varepsilon_x \\ \varepsilon_y \\ \gamma_{xy} \end{bmatrix} = \begin{bmatrix} 1.72 \\ 8.73 \\ 1.23 \end{bmatrix} \times 10^{-3}$$

$$\begin{bmatrix} \sigma_1 \\ \sigma_y \\ \tau_{xy} \end{bmatrix} = \overline{Q}_f \begin{bmatrix} \varepsilon_x \\ \varepsilon_y \\ \tau_{xy} \end{bmatrix} \text{ and } \begin{bmatrix} \sigma_1 \\ \sigma_2 \\ \tau_{12} \end{bmatrix} = T_\sigma \begin{bmatrix} \sigma_x \\ \sigma_y \\ \tau_{xy} \end{bmatrix}$$

So

$$\begin{bmatrix} \sigma_1 \\ \sigma_2 \\ \tau_{12} \end{bmatrix} = \begin{bmatrix} 243 \\ 84 \\ 5.4 \end{bmatrix} \text{MPa}$$

If this is repeated for each ply, then the data in Fig. 3.31 is obtained. It may be seen that failure can be expected to occur in the +30° plies in the 2-direction because the stress exceeds the boundary shown by the dotted line.

The Tsai−Hill criteria gives the following values

(i) 0° plies, 1.028
(ii) −30° plies, 0.776
(iii) 30° plies, 1.13

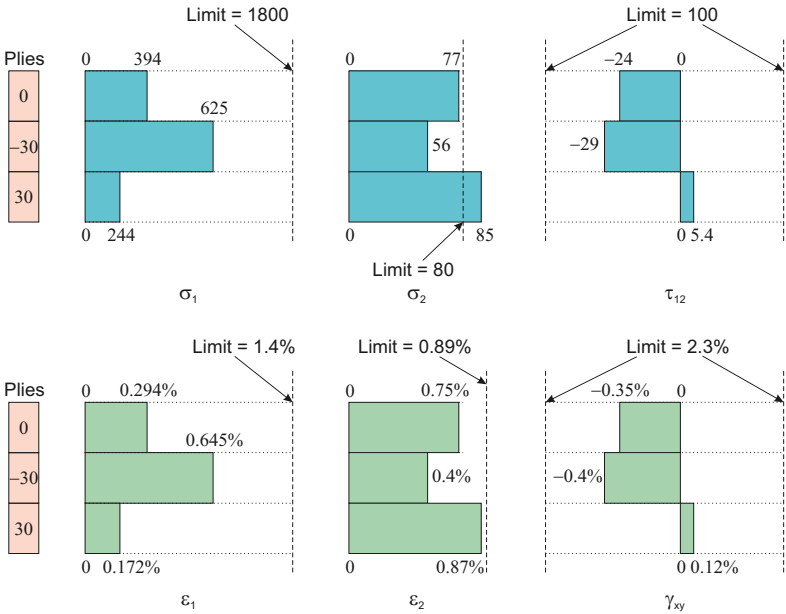


FIG. 3.31 Stress and strain in the plies, Example 3.21.

The failure in the 30° plies is thus confirmed. The Tsai−Hill criteria also predicts failure in the 0° plies and it may be seen in Fig. 3.31 that this is probably because the stress in the 2−direction is getting very close to the limiting value.

3.17 Fatigue behaviour of reinforced plastics

In common with metals and unreinforced plastics there is considerable evidence to show that reinforced plastics are susceptible to fatigue. If the matrix is thermoplastic then there is a possibility of thermal softening failures at high stresses or high cyclic frequencies as described in Section 2.21.1. However, in general, the presence of fibres reduces the hysteretic heating effect and there is a reduced tendency towards thermal softening failures. When conditions are chosen to avoid thermal softening, the normal fatigue process takes place in the form of a progressive weakening of the material due to crack initiation and propagation.

Plastics reinforced with carbon or boron are stiffer than glass reinforced plastics (GRP) and they are found to be less vulnerable to fatigue. In short-fibre GRP, cracks tend to develop relatively easily in the matrix and particularly at the interface close to the ends of the fibres. It is not uncommon for cracks to propagate through a thermosetting type matrix and destroy its integrity long before fracture of the moulded article occurs. With short-fibre

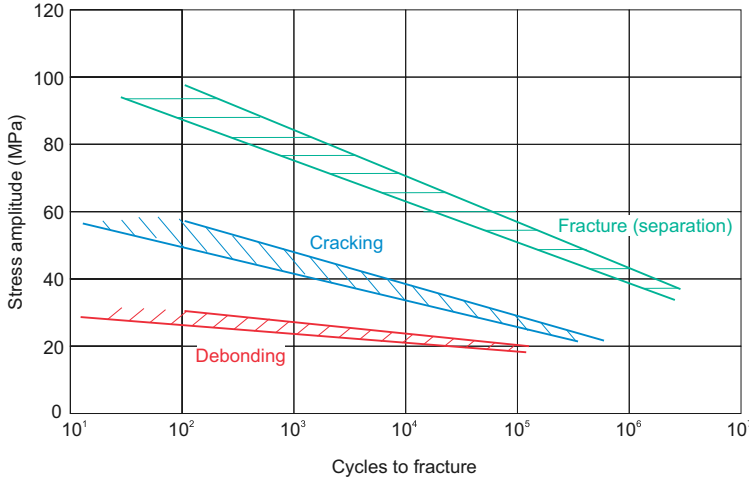


FIG. 3.32 Typical fatigue behaviour of glass reinforced polyester.

composites it has been found that fatigue life is prolonged if the aspect ratio of the fibres is large.

The general fatigue behaviour which is observed in glass fibre reinforced plastics is illustrated in Fig. 3.32. In most GRP materials, debonding occurs after a small number of cycles, even at modest stress levels. If the material is translucent then the build-up of fatigue damage may be observed. The first signs are that the material becomes opaque each time the load is applied. Subsequently, the opacity becomes permanent and more pronounced. Eventually resin cracks become visible but the article is still capable of bearing the applied load until localised intense damage causes separation of the component. However, the appearance of the initial resin cracks may cause sufficient concern, for safety or aesthetic reasons, to limit the useful life of the component. Unlike most other materials, therefore, glass reinforced plastics give a visual warning of fatigue failure.

Since GRP does not exhibit a fatigue limit it is necessary to design for a specific endurance and factors of safety in the region of 3−4 are commonly employed. Most fatigue data is for tensile loading with zero mean stress and so to allow for other values of mean stress it has been found that the empirical relationship described in Section 2.21.4 can be used. In other modes of loading (e.g. flexural or torsion) the fatigue behaviour of GRP is worse than in tension. This is generally thought to be caused by the setting up of shear stresses in sections of the matrix which are unprotected by properly aligned fibres.

There is no general rule as to whether or not glass reinforcement enhances the fatigue behaviour of the base material. In some cases the matrix exhibits longer fatigue endurances than the reinforced material whereas in other cases

the converse is true. In most cases the fatigue endurance of GRP is reduced by the presence of moisture.

Fracture mechanics techniques, of the type described in Section 2.21.6 have been used very successfully for fibre reinforced plastics. Typical values of K for reinforced plastics are in the range 5−50 MN $m^{-3/2}$, with carbon fibre reinforcement producing the higher values.

3.18 Impact behaviour of reinforced plastics

Reinforcing fibres are brittle and if they are used in conjunction with a brittle matrix (e.g. epoxy or polyester resins) then it might be expected that the composite would have a low fracture energy. In fact, this is not the case and the impact strength of most glass reinforced plastics is many times greater than the impact strengths of the fibres or the matrix. A typical impact strength for polyester resin is 2 kJ/m^2 whereas a CSM/polyester composite has impact strengths in the range 50−80 kJ/m^2. Woven roving laminates have impact strengths in the range 100−150 kJ/m^2. The much higher impact strengths of the composite in comparison to its component parts have been explained in terms of the energy required to cause debonding and work done against friction in pulling the fibres out of the matrix. Impact strengths are higher if the bond between the fibre and the matrix is relatively weak because if it is so strong that it cannot be broken, then cracks propagate across the matrix and fibres, with very little energy being absorbed. There is also evidence to suggest that in short-fibre reinforced plastics, maximum impact strength is achieved when the fibre length is at the critical value. There is a conflict therefore between the requirements for maximum tensile strength (long fibres and strong interfacial bond) and maximum impact strength. For this reason, it is imperative that full details of the service conditions for a particular component are given in the specifications so that the sagacious designer can tailor the structure of the material accordingly.

Questions

3.1 Compare the energy absorption capabilities of composites produced using carbon fibres, aramid fibres and glass fibres. Comment on the meaning of the answer. The data in Fig. 3.2 may be used.

3.2 A hybrid composite material is made up of 20% HS carbon fibres by weight and 30% E-glass fibres by weight in an epoxy matrix. If the density of the epoxy is 1300 kg/m^3 and the data in Fig. 3.2 may be used for the fibres, calculate the density of the composite.

3.3 What weight of carbon fibres (density = 1800 kg/m^3) must be added to 1 kg of epoxy (density = 1250 kg/m^3) to produce a composite with a density of 1600 kg/m^3.

3.4 A unidirectional glass fibre/epoxy composite has a fibre volume fraction of 60%. Given the data below, calculate the density, modulus and thermal conductivity of the composite in the fibre direction.

	(kg/m^3)	E (GPa)	K (W/m K)
Epoxy	1250	6.1	0.25
Glass fibre	2540	80.0	1.05

3.5 In a unidirectional Kevlar/epoxy composite the modular ratio is 20 and the epoxy occupies 60% of the volume. Calculate the modulus of the composite and the stresses in the fibres and the matrix when a stress of 50 MPa is applied to the composite. The modulus of the epoxy is 6 GPa.

3.6 In a unidirectional carbon fibre/epoxy composite, the modular ratio is 40 and the fibres take up 50% of the cross-section. What percentage of the applied force is taken by the fibres?

3.7 A reinforced plastic sheet is to be made from a matrix with a tensile strength of 60 MPa and continuous glass fibres with a modulus of 76 GPa. If the resin ratio by volume is 70% and the modular ratio of the composite is 25, estimate the tensile strength and modulus of the composite.

3.8 A single ply unidirectional carbon fibre reinforced PEEK material has a volume fraction of fibres of 0.58. Use the data given below to calculate the Poisson's Ratio for the composite in the fibre and transverse directions.

Material	Modulus (GPa)	Poisson's Ratio
Carbon fibres (HS)	230	0.23
PEEK	3.8	0.35

3.9 A single ply unidirectional glass fibre/epoxy composite has the fibres aligned at 40° to the global x-direction. If the ply is 1.5 mm thick and it is subjected to stresses of $\sigma_x = 30$ MPa and $\sigma_y = 15$ MPa, calculate the effective moduli for the ply in the $x-y$ directions and the values of ε_x and ε_y. The properties of the ply in the fibre and transverse directions are

$$E_1 = 35 \text{ GPa}, E_2 = 8 \text{ GPa}, G_{12} = 4 \text{ GPa and } \nu_{12} = 0.26$$

3.10 A single ply uni-directional carbon fibre/epoxy composite has the fibres aligned at 30° to the x-direction. If the ply is 2 mm thick and it is subjected to a moment of $M_x = 180$ Nm/m and to an axial stress of $\sigma_x = 80$ MPa, calculate the moduli, strains and curvatures in the $x-y$ directions. If an additional moment of $M_y = 250$ Nm/m is added, calculate the new curvatures.

3.11 State whether the following laminates are symmetric or non-symmetric.
(i) $[0/90/45/45/90/0]_T$
(ii) $[0/90_2/45/-45/45/90_2/0]_T$
(iii) $[0/90/45/-45_6/45/90/0]_T$

3.12 A plastic composite is made up of three layers of isotropic materials as follows:

Skin layers: *Material A*, $E = 3.5$ GPa, $G = 1.25$ GPa, $v = 0.4$
Core layer: *Material B*, $E = 0.6$ GPa, $G = 0.222$ GPa, $v = 0.35$.

The skins are each 0.5 mm thick and the core is 0.4 mm thick. If an axial stress of 20 MPa, a transverse stress of 30 MPa and a shear stress of 15 MPa are applied to the composite, calculate the axial and transverse stresses and strains in each layer.

3.13 A laminate is made up of plies having the following elastic constants

$$E_1 = 133 \text{ GPa}, \quad E_2 = 9 \text{ GPa}, \quad G_{12} = 5 \text{ GPa}, \quad v_{12} = 0.31$$

If the laminate is based on $(-60, -30, 0, 30, 60, 90)_s$ and the plies are each 0.2 mm thick, calculate E_x, E_y, G_{xy} and v_{xy}'. If a stress of 100 MPa is applied in the x direction, what will be the axial and lateral strains in the laminate?

3.14 A unidirectional carbon fibre/epoxy composite has the following lay-up

$$[40, \ -40, \ 40, \ -40]_s$$

The laminate is 8 mm thick and is subjected to stresses of $\sigma_x = 80$ MPa and $\sigma_y = 40$ MPa, determine the strains in the x and y directions. The properties of a single ply are

$$E_1 = 140 \text{ GPa}, \quad E_2 = 9 \text{ GPa}, \quad G_{12} = 7 \text{ GPa}, \quad \text{and} \quad v_{12} = 0.3$$

3.15 A filament wound composite cylindrical pressure vessel has a diameter of 1200 mm and a wall thickness of 3 mm. It is made up of 10 plies of continuous glass fibres in a polyester resin. The arrangement of the plies is $[0_3/60/-60]_s$, Calculate the axial and hoop strain in the cylinder when an internal pressure of 3 MPa is applied. The properties of the individual plies are

$$E_1 = 32 \text{ GPa}, \quad E_2 = 8 \text{ GPa}, \quad G_{12} = 3 \text{ GPa}, \quad v_{12} = 0.3$$

3.16 Compare the response of the following laminates to an axial force N_x of 40 N/mm. The plies are each 0.1 mm thick.
(a) $[30/-30/-30/30]_T$
(b) $[30/-30/30/-30]_T$
The properties of the individual plies are

$$E_1 = 145 \text{ GPa}, \quad E_2 = 15 \text{ GPa}, \quad G_{12} = 4 \text{ GPa}, \quad v_{12} = 0.278$$

3.17 A unidirectional carbon fibre/PEEK laminate has the stacking sequence $[0/35/-35]_T$. If the properties of the individual plies are

$$E_1 = 145 \text{ GPa}, \quad E_2 = 15 \text{ GPa}, \quad G_{12} = 4 \text{ GPa}, \quad v_{12} = 0.278$$

If the plies are each 0.1 mm thick, calculate the strains and curvatures if an in-plane stress of 100 MPa is applied.

3.18 A single ply of carbon/epoxy composite has the properties listed below and the fibres are aligned at 25° to the x-direction, If stresses of

$$\sigma_x = 80 \text{ MPa}, \quad \sigma_y = 20 \text{ MPa}, \quad \text{and} \quad \tau_{xy} = -10 \text{ MPa}$$

are applied, determine whether or not failure would be expected to occur according to the (a) Maximum Stress, (b) Maximum Strain and (c) Tsai-Hill criteria.

$$E_1 = 497 \text{ GPa}, \quad E_2 = 5.3 \text{ GPa}, \quad G_{12} = 5.6 \text{ GPa}, \quad \nu_{12} = 0.31$$

$$\widehat{\sigma}_{1T} = 1.24 \text{ GPa}, \quad \widehat{\sigma}_{2T} = 0.02 \text{ GPa}, \quad \widehat{\sigma}_{1C} = 0.029 \text{ GPa}$$

$$\widehat{\sigma}_{2C} = 0.03 \text{ GPa}, \quad \tau_{12} = 0.04 \text{ GPa}$$

3.19 A single ply glass/epoxy composite has the properties listed below. If the fibres are aligned at 30° to the x-direction, determine the value of in-plane stresses, σ_x, which would cause failure according to (a) the Maximum Stress criterion (b) the Maximum Strain criterion and (c) the Tsai−Hill criterion.

$$E_1 = 40,000 \text{ MPa}, \quad E_2 = 9000 \text{ MPa}, \quad G_{12} = 4000 \text{ MPa},$$

$$\nu_{12} = 0.31, \quad \widehat{\sigma}_{1T} = 1400 \text{ MPa}, \quad \widehat{\sigma}_{2T} = 50 \text{ MPa}$$

$$\widehat{\sigma}_{1C} = 220 \text{ MPa}, \quad \widehat{\sigma}_{2C} = 100 \text{ MPa}, \quad \widehat{\tau}_{12} = 40 \text{ MPa}$$

3.20 A carbon/epoxy composite with the stacking arrangement $[0/-30/30]_s$, has the properties listed below. Determine the value of in-plane stress σ_x

which would cause failure according to the (a) Maximum Strain (b) Maximum Stress and (c) Tsai − Hill criteria.

$$E_1 = 130 \text{ GPa}, \quad E_2 = 8.8 \text{ GPa}, \quad G_{12} = 6.9 \text{ GPa}, \quad \nu_{12} = 0.3$$

$$\widehat{\sigma}_{1T} = 1.9 \text{ GPa}, \quad \widehat{\sigma}_{2T} = 0.038 \text{ GPa}, \quad \widehat{\sigma}_{1C} = 1.7 \text{ GPa}$$

$$\widehat{\sigma}_x = 0.2 \text{ GPa}, \widehat{\tau}_{12} = 0.09 \text{ GPa}$$

The thickness of each ply is 0.2 mm.

3.21 A long sheet of carbon fibre reinforced epoxy is 30 mm wide, 5 mm thick and has a sharp crack 10 mm long placed centrally relative to its width and length. If the critical stress intensity factor for this material is 43 MN $m^{-3/2}$, calculate the axial tension which would cause the sheet to fracture.

3.22 A very wide sheet of GRP which is known to contain intrinsic defects 1 mm long, is subjected to a fluctuating stress which varies from 0 to 80 MPa. How many cycles would the sheet be expected to withstand if it is made from (a) chopped strand mat (CSM) and (b) woven roving (WR) reinforcement. The crack growth parameters C and n, and the critical stress intensity factors, K_c, for these materials are

	C	n	K_c (MN $m^{1/2}$)
CSM	3.3×10^{-18}	12.7	13.5
WR	2.7×10^{-14}	6.4	26.5

3.23 If the matrix in 3.7 was reinforced with the same volume fraction of glass but in the form of randomly oriented glass fibres rather than continuous filaments, what would be the tensile strength of the composite. The fibres are 15 mm long, have an aspect ratio of 1000 and produce a reinforcement efficiency of 0.25. The fibre strength is 2 GPa and the shear strength of the interface is 4 MPa.

3.24 A polyester matrix is reinforced with continuous glass fibres. A 15 mm wide beam made from this material is to be simply supported over a 300 mm length and have a point load at mid-span. For a fixed beam weight of 90 g/m investigate how the stiffness of the beam changes with the volume fraction of glass and state the optimum volume fraction. ($\rho_f = 2560$ kg/m^3, $\rho_m = 1210$ kg/m^3, $E_f = 76$ GPa, $E_m = 3$ GPa).

3.25 A sheet of chopped strand mat-reinforced polyester is 5 mm thick and 10 mm wide. If its modulus is 8 GPa calculate its flexural stiffness when subjected to a point load of 200 N midway along a simply supported span of 300 mm. Compare this with the stiffness of a composite beam made up of two 2.5 mm thick layers of this reinforced material separated by a 10 mm thick core of foamed plastic with a modulus of 40 MPa.

3.26 A composite of GFRP skin and foamed core is to have a fixed weight of 200 g/m. If its width is 15 mm investigate how the stiffness of the composite varies with skin thickness. The density of the skin material is 1450 kg/m^3 and the density of the core material is 450 kg/m^3. State the value of skin thickness which would be best and for this thickness calculate the ratio of the weight of the skin to the total composite weight.

3.27 In a short carbon fibre reinforced nylon moulding the volume fraction of the fibres is 0.2. Assuming the fibre length is much greater that the critical fibre length, calculate the modulus of the moulding, The modulus values for the fibres and nylon are 230 GPa and 2.8 GPa respectively.

Bibliography

Agarwal B, Broutman LJ, Chandrashekhara K: *Analysis and performance of fibre composites*, 4th ed., Hoboken NJ, 2018, Wiley.

Ashbee K: *Fundamental principles of* fiber reinforced composites, 2nd Ed., PA, 1993, Technomic Lancaster.

Clyne TW, Hull D: *An introduction to composite materials*, 3rd Ed., Cambridge, 2019, Cambridge University Press.

Daniel IM, Ishai O: *Engineering mechanics of composite materials*, 2nd ed., London, 2005, Oxford University Press.

Folkes MJ: *Short fibre reinforced thermoplastics*, CT, 1982, Research Studies Press.

Fu SY, Lauke B, Mai YW: *Science and engineering of short fibre reinforced polymer composites*, Oxford, 2009, Woodhead Publishing.

Hancox NL, Mayer RM: *Design data for reinforced plastics*, Chapman and Hall.

Kelly A, editor: *Concise encyclopedia of composite materials*, Oxford, 1994, Elsevier Science.

Kemmish DJ: *Practical guide to high performance engineering plastics*, Shrewsbury, 2011, iSmithers.

Mathews FL, Rawlings RD: *Composite materials: engineering and science*, Somerset, 1993, Chapman and Hall.

Mayer RM: *Design with reinforced plastics*, London, 1993, HMSO.

Piggott MR: *Load bearing fibre composites*, Pergamon.

Phillips LN, editor: *Design with advanced composite materials*, London, 1989, Design Council.

Powell PC: *Engineering with fibre-polymer laminates*, Chapman and Hall.

Richardson MOW: *Polymer engineering composites*, London, 1977, Applied Science.

Stellbrink KKU: *Micromechanics of composites*, Munich, 1996, Hanser.
Strong BA: *Fundamentals of composites manufacturing: materials, methods and applications*, Dearborn MI, 2008, SME.
Tsai SW, Hahn HT: *Introduction to composite materials*, London, 1980, Technomic Westport.
Vassilopoulos AP: *Fatigue of fiber-reinforced composites*, London, 2011, Springer.

Chapter 4

Processing of plastics

4.1 Introduction

One of the most outstanding features of plastics is the ease with which they can be quickly converted from either powdered solids (most thermoplastics) or liquids (many thermosets) into a wide variety of manufactured products. This simplicity and economy through which plastics can be shaped and formed is in very sharp contrast to the meticulous and labour-intensive manufacturing methods for wood, or the high temperature and energy-intensive production methods required for metals. In some cases semi-finished articles such as sheets or rods are produced from plastics, which are subsequently fabricated into the final shape using conventional methods such as machining, welding or other fabrication techniques. However, this approach is relatively uncommon and instead in the majority of cases the unique properties of plastics are exploited to create fully finished articles in a single operation. Typically processing techniques for plastics consist of three main stages:

(1) Heating: The plastic is heated to either soften it or melt it so that it can be easily pressed into a new shape (thermoplastics), or to catalyse its cross-linking reaction (thermosets).
(2) Forming: Force is applied in some way to transform the heated soft solid or liquid plastic into a new shape. Forming may involve a number of distinct stages requiring different levels and types of forces.
(3) Cooling: Heat must be rapidly drawn from the deformed plastic so that it retains its new shape and its mechanical properties revert to those of the material in its cold solid form. Heat transfer and its implications therefore dominate the processing of plastics.

The processing stages of heating, shaping and cooling may be continuous (e.g. production of pipe by extrusion) or a repeated cycle of events (e.g. production of a telephone housing by injection moulding), but in most cases the processes may be automated and so are particularly suitable for mass production. There is a wide range of processing methods which may be used for plastics. In most cases the choice of method is based on the shape of the component and whether it is thermoplastic or thermosetting. It is important therefore that throughout the design process, the designer must have a basic

Plastics Engineering. https://doi.org/10.1016/B978-0-08-100709-9.00004-2
Copyright © 2020 Elsevier Ltd. All rights reserved.

understanding of the range of processing methods for plastics since an ill-conceived shape or design detail may limit the choice of moulding methods.

In this chapter each of the principal processing methods for plastics is described and where appropriate a simple analysis of the process is developed. This includes processes where the plastic may be either thermoplastic or thermosetting, or in the form of a liquid, melt or soft solid. However, since industrial manufacturing of plastics is dominated by techniques employing thermoplastics and melt phase processing (e.g. extrusion and injection moulding), the chapter largely concentrates on these processes. For these an understanding of polymer melt flow theory is important and initially this is developed by treating the polymer melt flow as Newtonian. Although most polymer melt flows are in fact non-Newtonian, the simplified Newtonian analysis is useful at this stage because it illustrates the approach to the problem without concealing it by mathematical complexity. In practice the simplified analysis may provide sufficient accuracy for the engineer to make initial design decisions and at least it provides a quantitative aspect which assists in the understanding of the process. For those requiring more accurate models of plastics moulding, these are developed in Chapter 5 where the non-Newtonian aspects of polymer melt flow are considered.

4.2 Extrusion

Extrusion is one of the most important processing methods for plastics. It involves forcing a polymer melt through a die of a particular shape to create a plastic product of continuous length and constant cross-section. Notable products include items such as plastic sheet, film, fibres and pipes. However, extrusion is also employed for compounding where the pure polymer powder from the polymerisation reactor is mixed with various additives and converted into plastic pellets for subsequent use in extrusion and other processes. This is in fact the most important application of extrusion and the reason why its influence and significance must be considered in many of the other major processing techniques for plastics.

4.2.1 General features of single screw extrusion

The most common method of processing plastics by **Extrusion** uses a screw inside a barrel as illustrated in Fig. 4.1. This is known as 'Single Screw Extrusion'. The plastic, usually in the form of granules or powder, is fed from a hopper onto the screw. It is then conveyed along the barrel where it is heated by conduction from heater bands that are wrapped around the exterior of the barrel along its length and shear due to its movement along the screw flights. At the hopper end a cooling jacket controls the local temperature and prevents feed blockage due to stickiness or premature melting of the feedstock. The depth of the screw channel is reduced along the length of the screw to compact

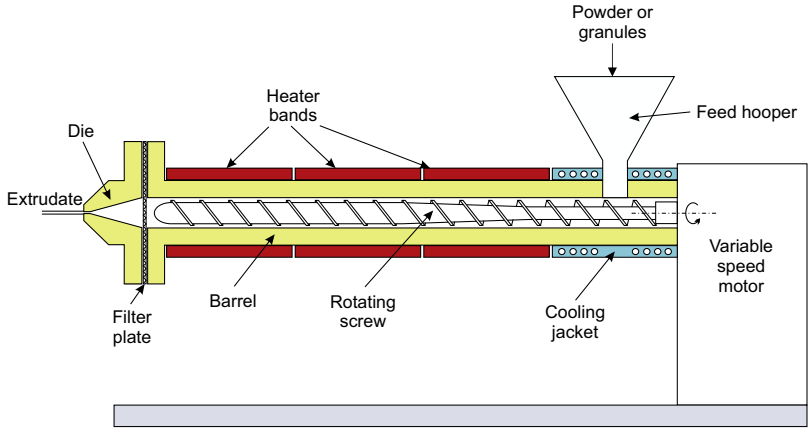


FIG. 4.1 Schematic view of a single screw extruder.

the material. At the end of the extruder the melt passes through a die to produce an extrudate of the desired shape. As will be seen later, the use of different dies and ancillary equipment means that the extruder screw/barrel is used as the basic unit of many melt phase processing techniques.

Basically an extruder screw has three different zones (as illustrated in Fig. 4.2):

(a) Feed zone

The function of this zone is to preheat the initially solid plastic and convey it to the subsequent zones. The design of this section is important since the constant screw depth must supply sufficient material to the metering zone so as not to starve it, but on the other hand not supply so much material that the metering zone is overrun. The optimum design is related to the nature and shape of the feedstock, the geometry of the screw and the frictional properties of the screw and barrel in relation to the plastic. The frictional behaviour of the feedstock material has a considerable influence on the rate of melting which can be achieved.

(b) Compression zone

In this zone the screw depth gradually decreases to compact the plastic. This compaction has the dual role of squeezing any trapped air pockets back into the feed zone and improving the heat transfer through the reduced thickness of material. Melting of the plastic may initially begin in the final section of the *Feed Zone* (beyond the cooling jacket around the hopper), but should largely be completed by the end of the *Compression Zone*. Gradually the solid bed of powder or granules is reduced as it gathers heat through a combination of

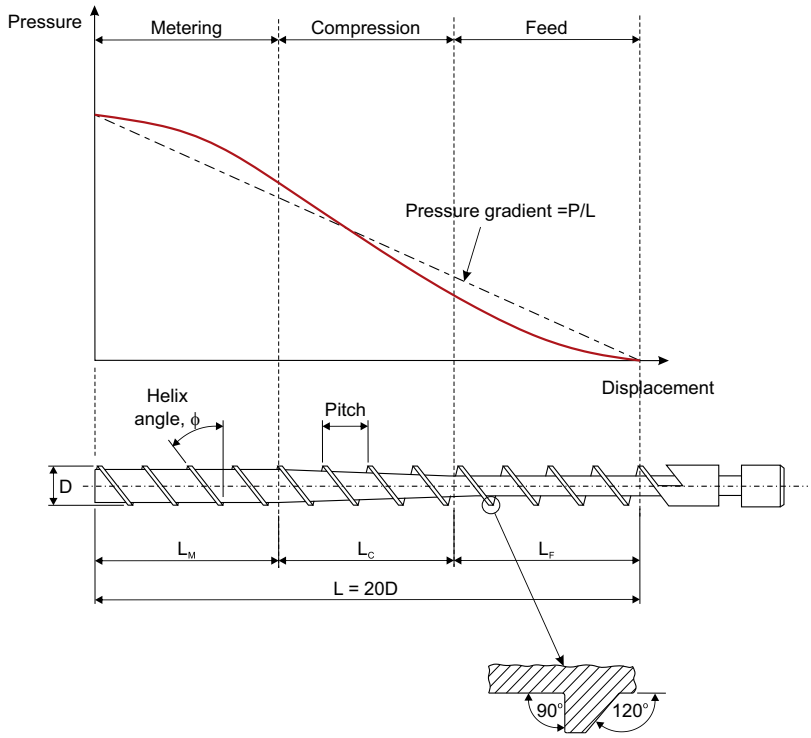


FIG. 4.2 Typical zones on an extruder screw.

friction, shearing and conduction at its edges that are in contact with the heated barrel wall. This process of compression and gradual melting of the solid bed across the compression zone is illustrated in Fig. 4.3.

(c) Metering zone

In this section the screw depth is again constant but it is much lower than in the feed zone, reflecting the fact that the plastic has been transformed from a loose solid powder or pellet form into a highly compressed molten state. In the *Metering Zone* the plastic should now be in the form of a homogenised melt and the purpose of the zone is to supply it to the die at a constant rate, and

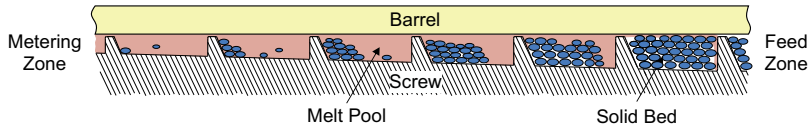


FIG. 4.3 The process of compression and melting in single screw extrusion.

uniform temperature and pressure. This zone is the most straight-forward to analyse since it involves a viscous melt flowing along a uniform channel.

The pressure build-up which occurs along a screw is illustrated in Fig. 4.2. The lengths of the zones on a particular screw depend on the material to be extruded. With nylon, for example, melting takes place quickly so that the compression of the melt can be performed in one pitch of the screw. PVC on the other hand is very heat sensitive and so a compression zone which covers the whole length of the screw is preferred.

As plastics can have quite different viscosities, they will tend to behave differently during extrusion. Fig. 4.4 shows some typical outputs possible with different plastics in single screw extruders with a variety of barrel diameters. This diagram is to provide a general idea of the ranking of materials – actual outputs may vary ±25% from those shown, depending on temperatures, screw speeds, etc.

In commercial extruders, additional zones may be included to improve the quality of the output. For example, there may be a mixing zone consisting of screw flights of reduced or reversed pitch. The purpose of this zone is to ensure uniformity of the melt and it is sited in the metering section. Fig. 4.5 shows some designs of mixing sections in extruder screws.

Some extruders also have a venting zone. This is principally because a number of plastics are hygroscopic i.e. they absorb moisture from the atmosphere. If these materials are extruded wet in conventional equipment the quality of the output is poor due to trapped water vapour in the melt. One possibility is to pre-dry the feedstock to the extruder but this is expensive and can lead to contamination. Vented barrels were developed to overcome these problems. As shown in Fig. 4.6, in the first part of the screw the granules are taken in and melted, compressed and homogenised in the usual way. The melt

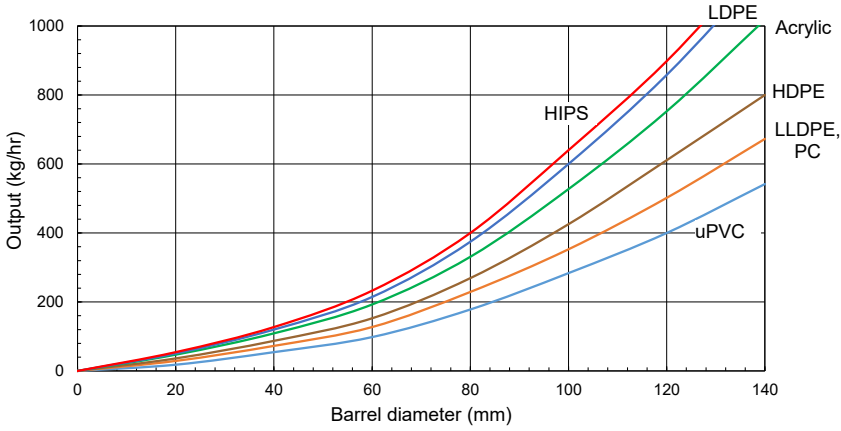


FIG. 4.4 Typical extruder outputs for different plastics.

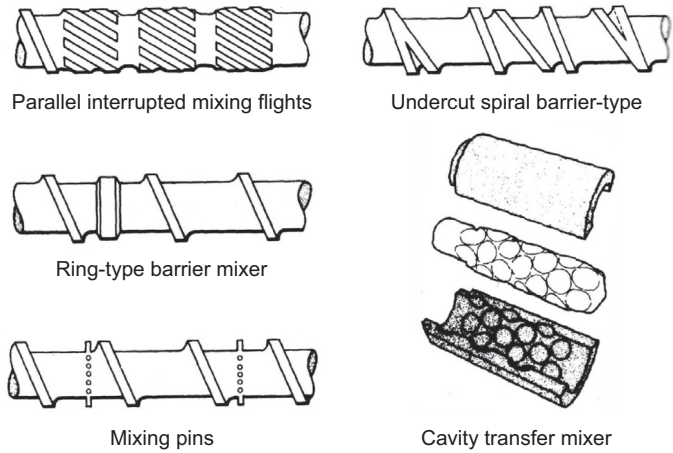


FIG. 4.5 Typical designs of mixing zones.

pressure is then reduced to atmospheric pressure in the decompression zone. This allows the volatiles to escape from the melt through a special port (or vent) in the barrel. The melt is then conveyed along the barrel to a second compression zone which prevents air pockets from being trapped, before it enters a final metering section for supply to the die.

The venting works because at a typical extrusion temperature of 250 °C the water in the plastic exists as a vapour at a pressure of about 4 MPa. At this

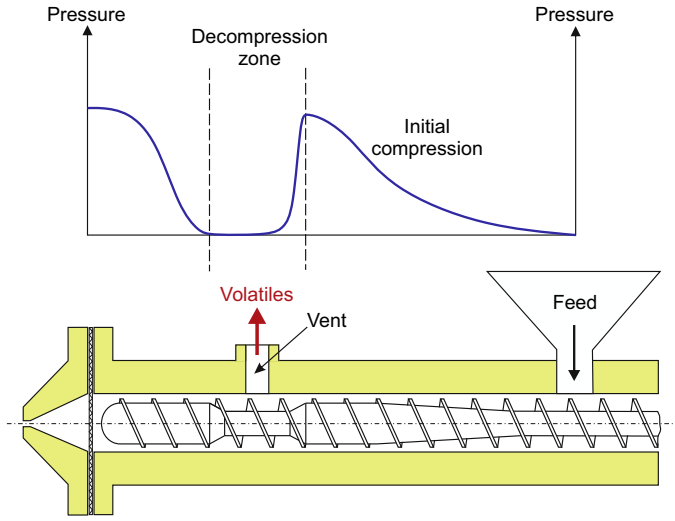


FIG. 4.6 Zones on a vented extruder.

pressure it will easily pass out of the melt and through the exit orifice. Note that since atmospheric pressure is about 0.1 MPa the application of a vacuum to the exit orifice will have little effect on the removal of volatiles.

Another feature of an extruder is the presence of a gauze filter after the screw and before the die. This effectively filters out any inhomogeneous material which might otherwise clog the die. These *screen packs* as they are called, will normally filter the melt to 120−150 μm, but a wide range of filter sizes are available for specific applications. In some cases problems may arise due to unmelted pellets or powder passing through the extruder, but more seriously the feedstock may be contaminated with foreign bodies. Metal objects such as small screws, nails or swarf may accidently enter the hopper in the factory environment and can be particularly damaging to the precision-machined surfaces of the screw, barrel and die. In some cases processors may employ metal detectors specifically to identify and remove such contaminants. Such precautions are increasingly important due to the rapid growth in plastics derived from recycling processes of various kinds, including the use of post-consumer waste streams. There is also evidence to show that even very small particles of contaminants can initiate cracks in some plastic extrudates e.g. polyethylene pipes that are designed to carry high pressures. In such cases it has been found that fine melt filtration ($\simeq$45 μm) can significantly improve the performance of the extruded plastic pipes.

Since the filters by their nature tend to be flimsy they are usually supported by a breaker plate. As shown in Fig. 4.7 this consists of a large number of

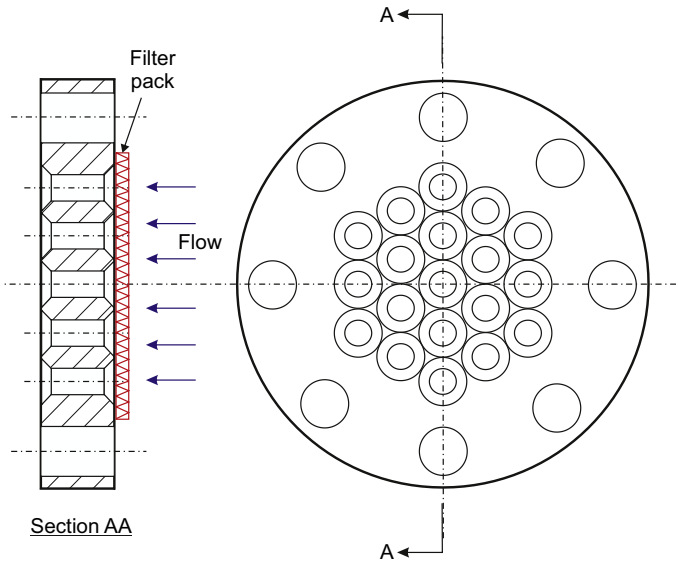


FIG. 4.7 Breaker plate with filter pack.

countersunk holes to allow passage of the melt whilst preventing dead spots where the flow slows and the melt can gather for extended periods. The breaker plate also conveniently straightens out the spiralling melt flow which emerges from the screw. Since the fine mesh on the filter will gradually become blocked it is periodically removed and replaced. In many modern extruders, and particularly with the fine filter systems referred to above, the filter is changed automatically so as not to interrupt continuous extrusion.

It should also be noted that although it is not their primary function, the breaker plate and filter also assist the build-up of back pressure which improves mixing along the screw. Since the pressure at the die is important, extruders also have a valve after the breaker plate to provide the necessary control.

4.2.2 Mechanism of flow

As the plastic moves along the screw, it melts by the following mechanism, which is illustrated in Fig. 4.3. Initially a thin film of molten material is formed at the barrel wall. As the screw rotates, it scrapes this film off and the molten plastic moves down the front face of the screw flight. When it reaches the core of the screw it sweeps up again, setting up a rotary movement in front of the leading edge of the screw flight. Initially solid granules (which form a solid bed) are squeezed between the screw flights and the screw and barrel walls but these tend to be swept into the molten pool by the rotary movement. As the screw rotates, the material passes further along the barrel and more and more solid material melts and is swept into the molten pool until eventually only a plastic melt exists between the screw flights.

As the screw rotates inside the barrel, the movement of the plastic along the screw is dependent on whether or not it adheres to the screw and barrel. In theory there are two extremes. In one case the material sticks to the screw only and therefore the screw and material rotate as a solid cylinder inside the barrel. This would result in zero output and is clearly undesirable. In the second case the material slips on the screw and has a high resistance to rotation inside the barrel. This results in a purely axial movement of the melt and is the ideal situation. In practice the behaviour is somewhere between these limits as the material adheres to both the screw and the barrel. The useful output from the extruder is the result of a drag flow due to the interaction of the rotating screw and stationary barrel. This is equivalent to the flow of a viscous liquid between two parallel plates when one plate is stationary and the other is moving. Superimposed on this is a flow due to the pressure gradient which is built up along the screw. Since the high pressure is at the end of the extruder, the pressure flow will reduce the output. In addition, the clearance between the screw flights and the barrel allows material to leak back along the screw and effectively reduces the output. This leakage will be worse when the screw becomes worn.

The external heating and cooling on the extruder also plays an important part in the melting process. In high output extruders the material passes along the barrel so quickly that sufficient heat for melting is generated by the shearing action and the barrel heaters are not required. In these circumstances it is the barrel cooling which is critical if excess heat is generated in the melt. In some cases the screw may also be cooled. This is not intended to influence the melt temperature but rather to reduce the frictional effect between the plastic and the screw. In all extruders, barrel cooling is essential around the feed hopper to ensure an unrestricted supply of feedstock.

The thermal state of the melt in the extruder is frequently compared with two ideal thermodynamic states. One is where the process may be regarded as **adiabatic**. This means that the system is fully insulated to prevent heat gain or loss from or to the surroundings. If this ideal state was to be reached in the extruder it would be necessary for the work done on the melt to produce just the right amount of heat without the need for heating or cooling. The second ideal case is referred to as **isothermal**. In the extruder this would mean that the temperature at all points is the same and would require immediate heating or cooling from the barrel to compensate for any loss or gain of heat in the melt. In practice the thermal processes in the extruder fall somewhere between these ideals. Extruders may be run without external heating or cooling but they are not truly adiabatic since heat losses will occur. Isothermal operation along the whole length of the extruder cannot be envisaged if it is to be supplied with relatively cold granules. However, particular sections may be near isothermal and the metering zone is often considered as such for analysis.

4.2.3 Analysis of flow in extruder

As discussed in the previous section, it is convenient to consider the output from the extruder as consisting of three components – drag flow, pressure flow and leakage. The derivation of the equation for output assumes that in the metering zone the melt has a constant viscosity and its flow is isothermal in a wide shallow channel. These conditions are most likely to be approached in the metering zone.

(a) Drag Flow Consider the flow of the melt between parallel plates as shown in Fig. 4.8(a).

For the small element of fluid ABCD the volume flow rate dQ is given by

$$dQ = V \cdot dy \cdot dx \tag{4.1}$$

Assuming the velocity gradient is linear, then

$$V = V_d \left[\frac{y}{H}\right]$$

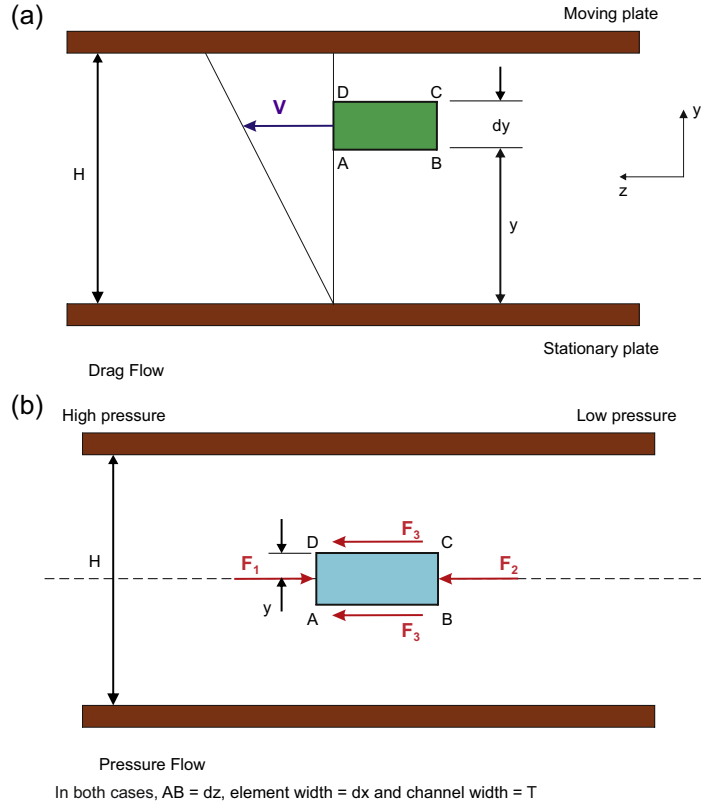


FIG. 4.8 Melt flow between parallel plates.

Substituting in (4.1) and integrating over the channel depth, H, then the total drag flow, Q_d, is given by

$$Q_d = \int_0^H \int_0^T \frac{V_d y}{H} \cdot dy \cdot dx$$

$$Q_d = \frac{1}{2} THV_d \tag{4.2}$$

This may be compared to the situation in the extruder where the fluid is being dragged along by the relative movement of the screw and barrel. Fig. 4.9 shows the position of the element of fluid and (4.2) may be modified to include terms relevant to the extruder dimensions.

For example,

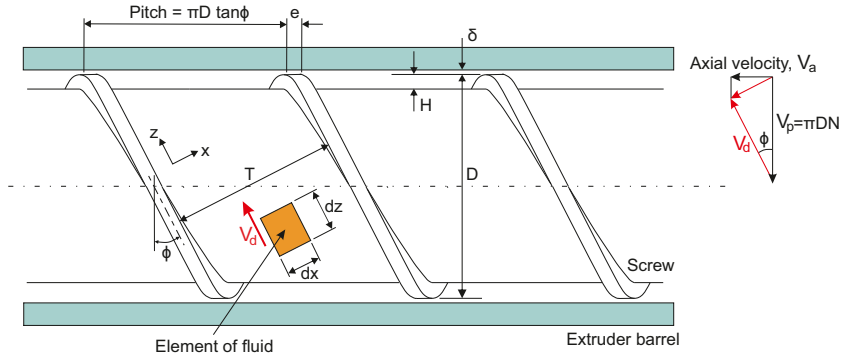


FIG. 4.9 Details of extruder screw.

$$V_d = \pi DN \cos \phi$$

where N is the screw speed (in revolutions per unit time).

$$T = (\pi D \tan \varphi - e)\cos \varphi$$

So

$$Q_d = \frac{1}{2}(\pi D \tan \phi - e)\left(\pi DN \cos^2 \phi\right)H$$

In most cases the term, e, is small in comparison with $(\pi D \tan \phi)$ so this expression is reduced to

$$Q_d = \frac{1}{2}\pi^2 D^2 NH \sin \phi \cos \phi \tag{4.3}$$

Note that the shear rate in the metering zone will be given by V_d/H.

(b) Pressure flow: Consider the element of fluid shown in Fig. 4.8(b). The forces are

$$F_1 = \left(P + \frac{\partial P}{\partial z} \cdot dz\right) dy\, dx \quad F_2 = P \cdot dy\, dx \quad F_3 = \tau_y dz\, dx$$

where P is pressure and $d\tau$ is the shear stress acting on the element. For steady flow these forces are in equilibrium so they may be equated as follows:

$$F_1 = F_2 + F_3$$

which reduces to

$$y\frac{dP}{dz} = \tau_y \tag{4.4}$$

Now for a Newtonian fluid, the shear stress, τ_y, is related to the viscosity, η, and the shear rate, $\dot{\gamma}$, by the equation

$$\tau_y = \eta\dot{\gamma} = \eta\frac{dV}{dy}$$

Using this in Eq. (4.4)

$$y\frac{dP}{dz} = \eta\frac{dV}{dy}$$

Integrating

$$\int_0^v dV = \frac{1}{\eta}\frac{dP}{dz}\int_{H/2}^{y} y\,dy$$

So

$$V = \frac{1}{\eta}\frac{dp}{dz}\left(\frac{y^2}{2} - \frac{H^2}{8}\right) \tag{4.5}$$

Also, for the element of fluid of depth, *dy,* at distance, *y,* from the centreline (and whose velocity is *V*) the elemental flow rate, *dQ,* is given by

$$dQ = VT\,dy$$

This may be integrated to give the pressure flow, Q_p

$$\begin{aligned} Q_p &= 2\int_0^{H/2}\frac{1}{\eta}\frac{dP}{dz}\cdot T\left(\frac{y^2}{2} - \frac{H^2}{8}\right)dy \\ Q_p &= -\frac{1}{12\eta}\frac{dP}{dz}\cdot TH^3 \end{aligned} \tag{4.6}$$

Referring to the element of fluid between the screw flights as shown in Fig. 4.9, this equation may be rearranged using the following substitutions. Assuming e is small, $T = \pi D \tan\phi \cdot \cos\phi$

Also,

$$\sin\phi = \frac{dL}{dz}$$

So

$$\frac{dP}{dz} = \frac{dP}{dL}\sin\phi$$

Thus, the expression for Q_p becomes

$$Q_p = -\frac{\pi D H^3 \sin^2 \phi}{12\eta} \cdot \frac{dP}{dL} \tag{4.7}$$

(c) Leakage: The leakage flow may be considered as flow through a wide slit which has a depth, δ, a length ($e \cos \phi$,) and a width of ($\pi D/\cos \phi$). Since this is a pressure flow, the derivation is similar to that described in (b). For convenience therefore the following substitutions may be made in (4.6) (see Fig. 4.10).

$$h = \delta$$

$$T = \pi D/\cos \phi$$

$$\text{Pressure gradient} = \frac{\Delta P}{e \cos \phi}$$

So the leakage flow, Q_L, is given by

$$Q_L = \frac{\pi^2 D^2 \delta^3}{12\eta e} \tan \phi \frac{dP}{dL} \tag{4.8}$$

A factor is often required in this equation to allow for eccentricity of the screw in the barrel. Typically this increases the leakage flow by about 20%.

The total output is the combination of drag flow, back pressure flow and leakage. So from (4.3), (4.7) and (4.8)

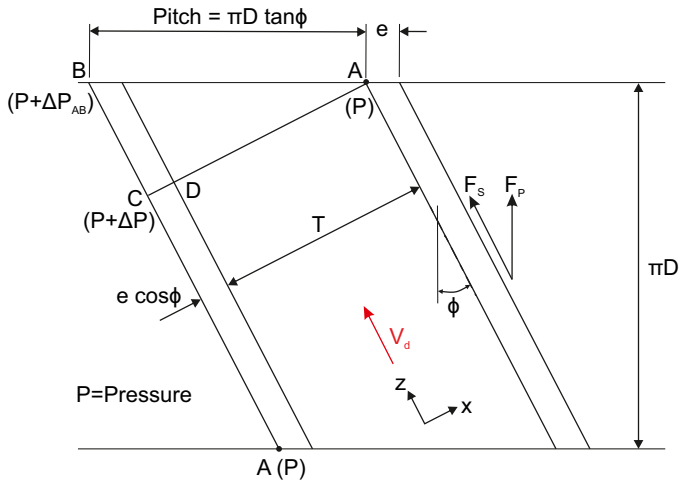


FIG. 4.10 Development of screw.

$$Q = \frac{1}{2}\pi^2 D^2 NH \sin\phi \cos\phi - \frac{\pi DH^3 \sin^2\phi}{12\eta}\frac{dP}{dL} - \frac{\pi^2 D^2 \delta^3}{12\eta e}\tan\phi\frac{dP}{dL} \qquad (4.9)$$

For many practical purposes sufficient accuracy is obtained by neglecting the leakage flow term. In addition, the pressure gradient is often considered as linear so

$$\frac{dP}{dL} = \frac{P}{L}$$

where 'L' is the length of the extruder. In practice the length of an extruder screw can vary between 17 and 30 times the diameter of the barrel. The shorter the screw the cooler the melt and the faster the moulding cycle. In the above analysis, it is the melt flow which is being considered and so the relevant pressure gradient will be that in the metering zone. However, as shown in Fig. 4.2 this is often approximated by P/L. If all other physical dimensions and conditions are constant then the variation of output with screw flight angle, φ, can be studied. As shown in Fig. 4.11 the maximum output would be obtained if the screw flight angle was about 35°. In practice a screw flight angle of 17.7° is frequently used because:

(i) this is the angle which occurs if the pitch of the screw is equal to the diameter and so it is convenient to manufacture,
(ii) for a considerable portion of the extruder length, the screw is acting as a solids conveying device and it is known that the optimum angle in such cases is 17°−20°.

It should also be noted that in some cases correction factors, F_d, and F_p are applied to the drag and pressure flow terms. They are to allow for edge effects and are solely dependent on the channel width, T, and channel depth, h, in the metering zone. Typical values are illustrated in Fig. 4.12.

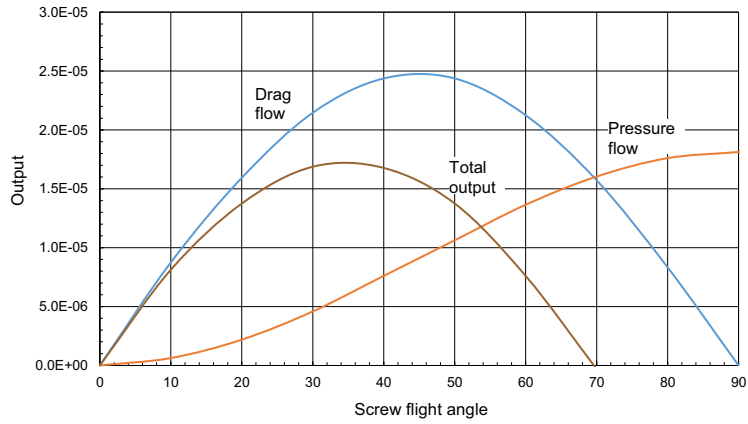


FIG. 4.11 Variation of drag flow and pressure flow.

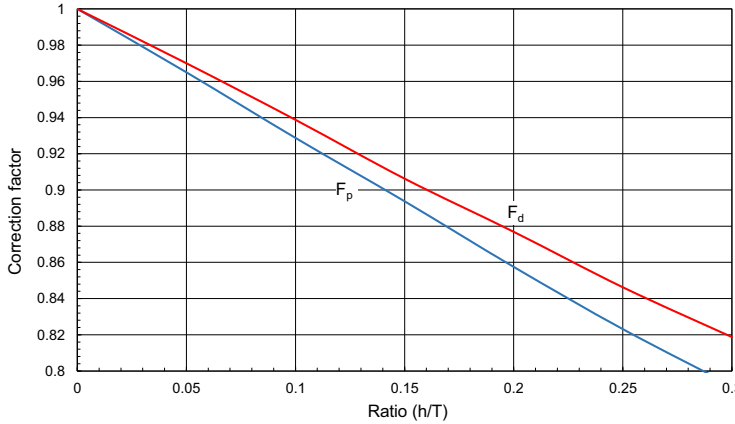


FIG. 4.12 Flow correction factors as a function of screw geometry.

4.2.4 Extruder/die characteristics

From Eq. (4.9) it may be seen that there are two interesting situations to consider. One is the case of free discharge where there is no pressure build up at the end of the extruder so

$$Q = Q_{\max} = \frac{1}{2}\pi^2 D^2 N H \sin\phi \cos\phi \tag{4.10}$$

The other case is where the pressure at the end of the extruder is large enough to stop the output. From (4.9) with $Q = 0$ and ignoring the leakage flow

$$P = P_{\max} = \frac{6\pi D L N \eta}{H^2 \tan\phi} \tag{4.11}$$

In Fig. 4.12 these points are shown as the limits of the screw characteristic. It is interesting to note that when a die is coupled to the extruder their requirements are conflicting. The extruder has a high output if the pressure at its outlet is low. However, the outlet from the extruder is the inlet to the die and the output of the latter increases with inlet pressure. As will be seen later the output, Q, of a Newtonian fluid from a die is given by a relation of the form

$$Q = KP \tag{4.12}$$

where $K = \frac{\pi R^4}{8\eta L_d}$ for a capillary die of radius R and length L_d.

Eq. (4.12) enables the die characteristics to be plotted on Fig. 4.13 and the intersection of the two characteristics is the operating point of the extruder. This plot is useful in that it shows the effect which changes in various parameters will have on output. For example, increasing screw speed, N, will move the extruder characteristic upward. Similarly an increase in the die

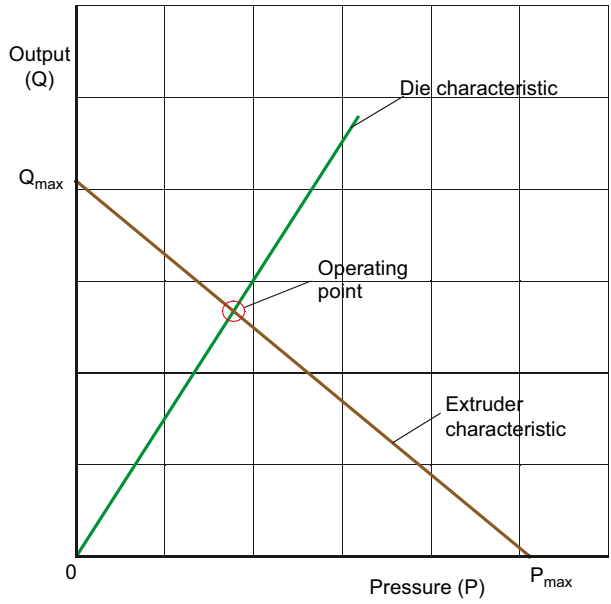


FIG. 4.13 Extruder and die characteristics.

radius, *R,* would increase the slope of the die characteristic and in both cases the extruder output would increase.

The operating point for an extruder/die combination may also be determined from Eqs (4.9) and (4.12) − ignoring leakage flow

$$Q = \frac{1}{2}\pi^2 D^2 NH \sin\phi \cos\phi - \frac{\pi DH^3 \sin^2\phi}{12\eta}\frac{P}{L} = \frac{\pi R^4}{8\eta L_d}\cdot P$$

So for a capillary die, the pressure at the operating point is given by

$$P_{op} = \left\{\frac{2\pi\eta D^2 NH \sin\phi \cos\phi}{(R^4/2L_d) + (DH^3 \sin^2\phi)/3L}\right\} \tag{4.13}$$

4.2.5 Other die geometries

For other die geometries it is necessary to use the appropriate form of Eq. (4.12). The equations for a capillary and a slit die are derived in Chapter 5. For other geometries it is possible to use the empirical equation which was developed by Boussinesq. This has the form

$$Q = \frac{Fbd^3}{12\eta L_d} \cdot P \tag{4.14}$$

where

b is the greatest dimension of the cross-section
d is the least dimension of the cross-section
F is a non-dimensional factor as given in Fig. 4.14

Using Eq. (4.14) it is possible to modify the expression for the operating pressure to the more general form

$$P_{op} = \left\{ \frac{2\pi\eta D^2 NH \sin\phi \cos\phi}{\frac{Fbd^3}{3\pi L_d} + (DH^3 \sin^2\phi / 3L)} \right\} \tag{4.15}$$

For a capillary die, one may obtain a value of F from Fig. 4.14 as 0.295 and substituting $b = d = 2R$, this equation reduces to the same form as Eq. (4.13).

Example 4.1 A single screw extruder is to be designed with the following characteristics:

L/D ratio = 24, screw flight angle = 17.7°
Max. screw speed = 100 rev/min, screw diameter = 40 mm
flight depth (metering zone) = 3 mm.

If the extruder is to be used to process polymer melts with a maximum melt viscosity of 500 Pa·s, calculate a suitable wall thickness for the extruder barrel based on the von Mises yield criterion. The tensile yield stress for the barrel metal is 925 MPa and a factor of safety of 2.5 should be used.

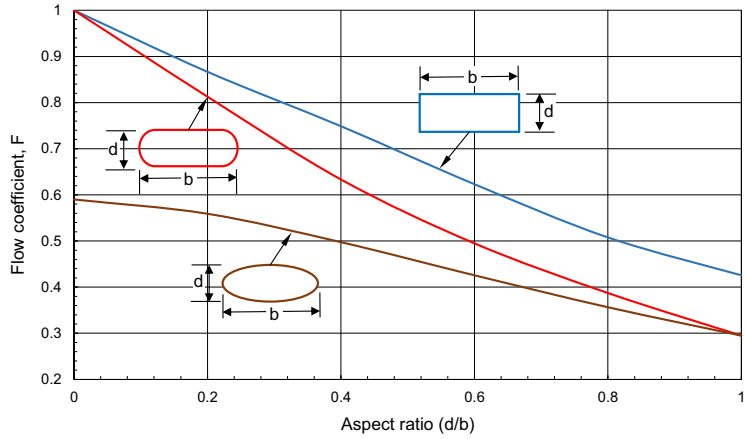


FIG. 4.14 Flow coefficient as a function of channel geometry.

Solution The maximum pressure which occurs in the extruder barrel is when there is no output. Therefore the design needs to consider this worst case blockage situation. As given by Eq. (4.11)

$$P_{\max} = \frac{6\pi DLN\eta}{H^2 \tan\phi} = \frac{6\pi \times 40 \times (24 \times 40) \times (100/60) \times 500}{(3)^2 \tan 17.7^0} = 210 \text{ MPa}$$

The von Mises criterion relates the tensile yield stress of a material to a state of multi-axial stress in a component made from the material. In a cylinder (the barrel of the extruder in this case), the principal stresses which exist as a result of an internal pressure are

$$\text{hoop stress, } \sigma_1 = \frac{P_{\max}}{2h}$$

$$\text{axial stress, } \sigma_2 = \frac{P_{\max}}{4h}$$

where $h =$ wall thickness of the barrel.

The von Mises criterion simply states that yielding (failure) will occur if

$$\left(\frac{\sigma_Y}{FS}\right)^2 \leq \sigma_1^2 + \sigma_2^2 - \sigma_1\sigma_2$$

where

$\sigma_Y =$ tensile yield stress of material
$FS =$ factor of safety.

In this case, therefore

$$\left(\frac{925}{2.5}\right)^2 = \left(\frac{(210)40}{2h}\right)^2 + \left(\frac{(210)40}{4h}\right)^2 - \frac{(210)^2(40)^2}{8h^2}$$

$$h = 9.8 \text{ mm}$$

Hence a barrel wall thickness of 10 mm would be appropriate.

Example 4.2 A single screw extruder is to be used to manufacture a nylon rod 5 mm in diameter at a production rate of 1.5 m/min. Using the following information, calculate the required screw speed.

Nylon	Extruder	Die
Viscosity = 420 Pa·s	Diameter = 30 mm	Length = 4 mm
Density (solid) = 1140 kg/m^3	Length = 750 mm	Diameter = 5 mm
Density (melt) = 790 kg/m^3	Screw flight angle = 17.7°	
	Metering channel depth = 2.5 min	

Die swelling effects may be ignored and the melt viscosity can be assumed to be constant.

Solution The output rate of solid rod = speed × cross-sectional area

$= 1.5 \times \pi\ (2.5 \times 10^{-3})^2/60$
$= 49.1 \times 10^{-6}\ \mathrm{m}^3/\mathrm{s}$

As the solid material is denser than the melt, the melt flow rate must be greater in the ratio of the solid/melt densities. Therefore melt flow rate through the die $= 49.1 \times 10^{-6}\left(\frac{1140}{790}\right) = 70.8 \times 10^{-6}\ \mathrm{m}^3/\mathrm{s}$

The pressure necessary to achieve this flow rate through the die is obtained from

$$Q = \frac{\pi P R^4}{8\eta L_d}$$

$$P = \frac{8 \times 420 \times 4 \times 10^{-3} \times 70.8 \times 10^{-6}}{\pi(2.5 \times 10^{-3})^4} = 7.8\ \mathrm{MPa}$$

At the operating point, the die output and the extruder output will be the same. Hence

$$Q = 70.8 \times 10^{-6} = \frac{1}{2}\pi^2(30 \times 10^{-3})^2 N(2.5 \times 10^{-3}) \sin 17.7 \cos 17.7 - \frac{\pi(30 \times 10^{-3})(2.5 \times 10^{-3})^3 \sin^2 17.7}{12 \times 420}\left(\frac{7.8 \times 10^6}{0.75}\right)$$

$N = 22\ \mathrm{rev/min}$

4.2.6 General features of twin screw extruders

The concept of employing multiple screws in extrusion has been around since the early days of the process, but it is only in the past few decades that the technology has been transformed into a mainstream production process. Twin screw extruders are now increasingly common in industry and their fields of application have grown sharply in recent years. More complex systems that employ more than two screws have been the subject of research and development over the years but to date very few of these have progressed much beyond the level of early stage designs and prototypes. Commercially there are a few triple screw systems, but these are largely confined to very specialised laboratory applications. In general twin screw extruders permit a wider range of possibilities in terms of output rates, mixing efficiency, heat

generation, etc. compared with a single screw extruder. They have become increasingly important in overcoming some of the inherent challenges in successful extrusion of materials requiring high degrees of mixing or temperature control (e.g. as found in polymer nanocomposites or medical/pharmaceutical polymers). The output of a twin screw extruder can be typically three times that of a single screw extruder of the same diameter and speed. Although the term 'twin-screw' is used almost universally for extruders having two screws, the screws are generally not identical. There are in fact a large variety of machine types and these may be classified by two main criteria:

(a) *Directions of rotation of the screws:* the screws are co-rotating if they rotate in the same direction, or counter-rotating if the rotate in opposite directions (see Fig. 4.15).
(b) *Positions of the screws in relation to each other:* the screws are intermeshing if the flights of one (or both) penetrates into the channel of the other, and non-intermeshing if the flights of each screw are either tangential or separated (see Figs 4.16 and 4.17). The conveying process in non-intermeshing twin screw extruders is similar to that of a single screw extruder. In addition, the screws may be conjugated or non-conjugated. A non-conjugated screw configuration is one in which the screw flights are a loose fit into one another so that there is ample space for material between the screw flights (see Fig. 4.18).

In a counter-rotating twin screw extruder the material is sheared and pressurised in a mechanism similar to calendering (see Section 4.5), i.e., the material is effectively squeezed between counter-rotating rolls. In a co-rotating system the material is transferred from one screw to the other following a figure of eight pattern around the two screws as may be seen in Fig. 4.15. This type of arrangement is particularly suitable for heat sensitive materials because the material is conveyed through the extruder quickly with little possibility of entrapment. The movement around the screws is slower if the screws are conjugated but the propulsive action is greater.

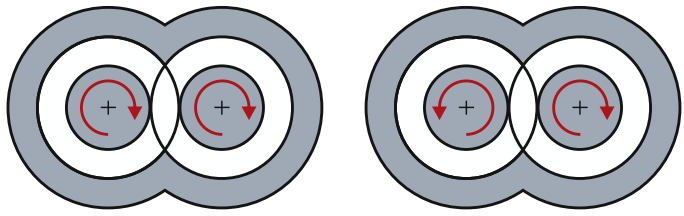


FIG. 4.15 Co-rotating and counter-rotating twin screw extruders.

TABLE 4.1 Comparison of single-screw, co-rotating and counter-rotating twin-screw extruders.

		Co-rotating screw		
Type	**Single screw**	**Low speed type**	**High speed type**	**Counter-rotating twin screw**
Principle	Friction between cylinder and materials and the same between material and screw	Mainly depend on the frictional action as in the case of single screw extruder		Forced mechanical conveyance based on gear pump principle
Conveying Efficiency	Low	Medium		High
Mixing efficiency	Low	Medium/High		High
Shearing action	High	Medium	High	Low
Self-cleaning effect	Slight	Medium/ High	High	Low
Energy efficiency	Low	Medium/High		High
Heat generation	High	Medium	High	Low
Temp distribution	Wide	Medium	Narrow	Narrow
Max. revolving speed (rpm)	100–300	25–35	250–300	35–45
Max. effective length of screw L/D	30–32	7–18	30–40	10–21

Table 4.1 compares the single screw extruder with the main types of twin screw extruders.

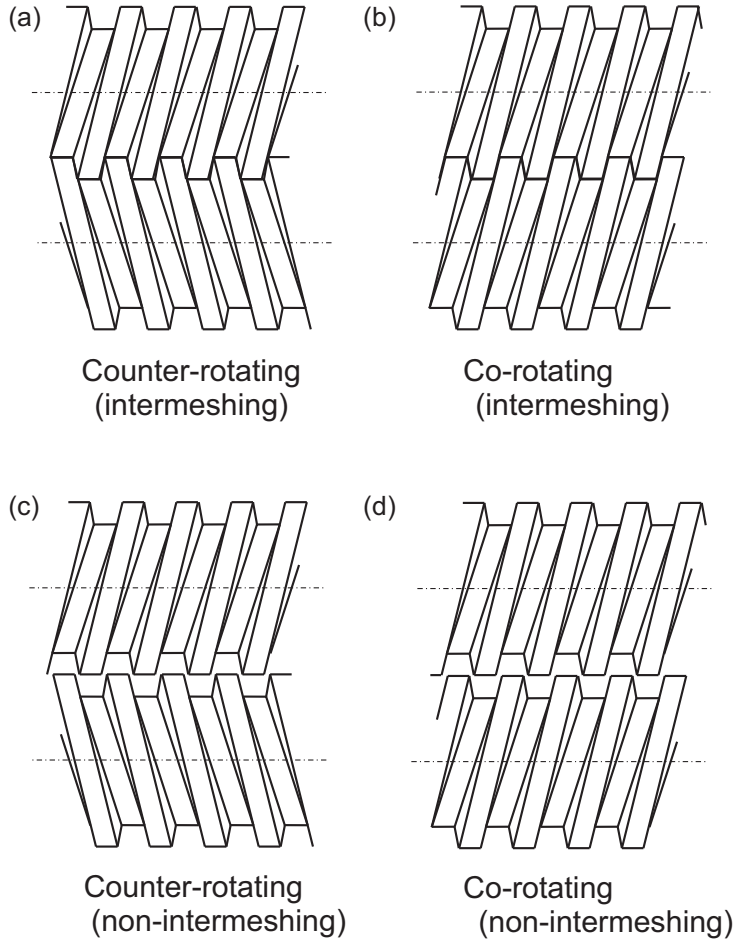


FIG. 4.16 Different screw arrangements in twin screw extruders.

4.2.7 Processing methods based on the extruder

Extrusion is an extremely versatile process in that it can be adapted, by the use of appropriate dies, to produce a wide range of products. Some of the more common of these production techniques are now described.

(a) Granule production/compounding

In the simplest case an extruder may be used to convert polymer formulations and additives into a form (usually granules) which is more convenient for use in other processing methods, such as injection moulding. In the extruder the feedstock is melted, homogenised and forced through a capillary shaped die. It emerges as a continuous lace which is cooled in a long water bath so that it may

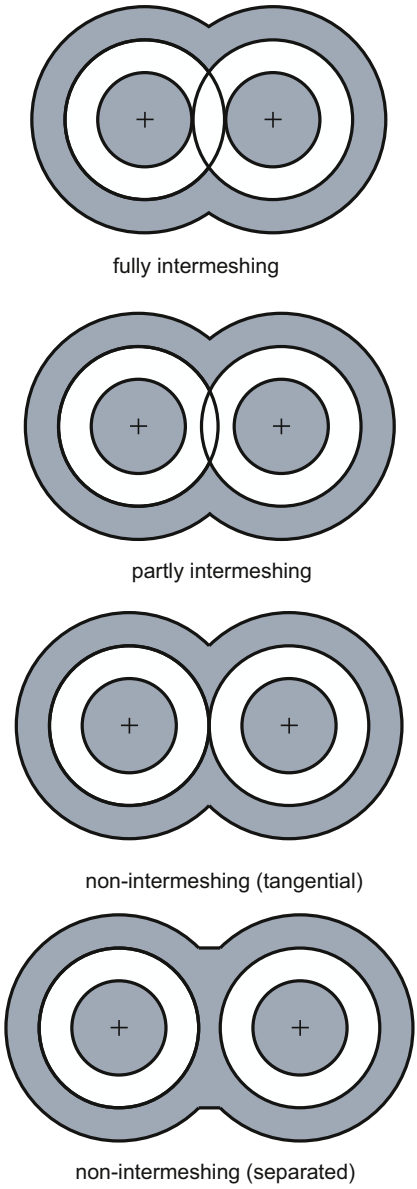


FIG. 4.17 Degrees of screw intermeshing in twin screw extrusion.

be chopped into short granules and packed into sacks. The haul-off apparatus shown in Fig. 4.19 is used to draw down the extrudate to the required dimensions. The granules are typically 3 mm diameter and about 4 mm long. In most cases a multi-hole die is used to increase the production rate.

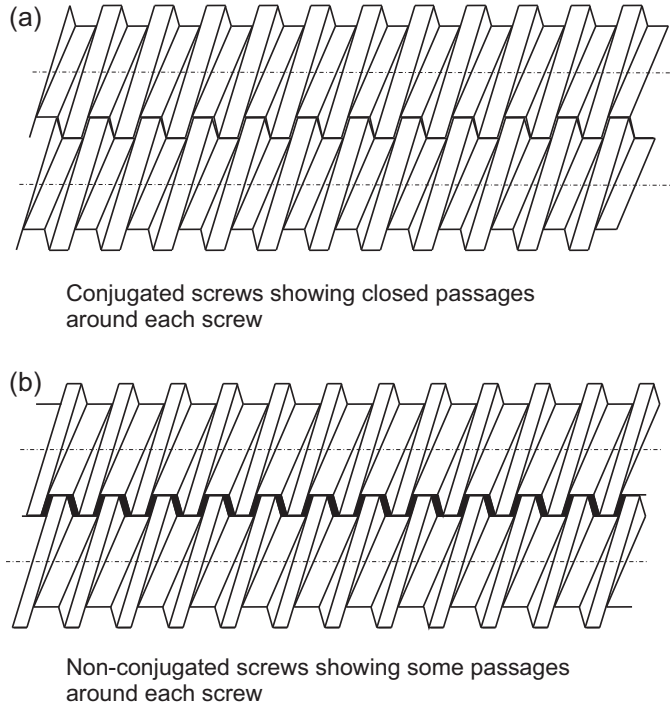


FIG. 4.18 Conjugated and non-conjugated twin screws.

(b) Profile production

Extrusion, by its nature, is ideally suited to the production of continuous lengths of plastic mouldings with a uniform cross-section. Therefore as well as producing the laces as described in the previous section, the simple operation of a die change can provide a wide range of profiled shapes such as pipes, sheets, rods, curtain track, edging strips, window frames, etc. (see Fig. 4.20).

The successful manufacture of profiled sections depends to a very large extent on good die design. Generally this is not straightforward, even for a simple cross-section such as a square, due to the interacting effects of post-extrusion swelling and the flow characteristics of complex viscoelastic fluids. Most dies are designed from experience to give approximately the correct shape and then *sizing* units are used to control precisely the desired shape. The extrudate is then cooled as quickly as possible. For many products, such as pipes or tubing, this is usually done in a water bath, the length of which depends on the section and the material being cooled (see Fig. 4.21(a)). For example, longer baths are needed for crystalline plastics since the recrystallisation process is exothermic. In the case of sheet extrusion, sizing and cooling of the product is carried out by passing it through a series of temperature controlled rollers (known as a roll-stack) (see Fig. 4.21(b)).

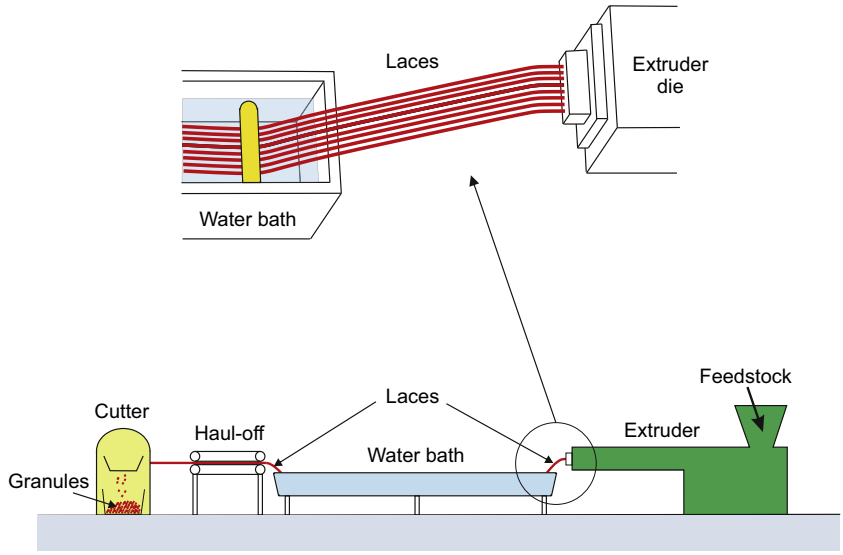


FIG. 4.19 Use of extruder to produce granules.

The storage facilities at the end of the profile production line depend on the type of product. The examples shown are for pipes/tubes (see Fig. 4.21(a)) and for sheet (see Fig. 4.21(b)). If the product is rigid then the cooled extrudate may be cut to size on a guillotine for stacking. If the extrudate is flexible then it can be collected by winding it onto drums. Most commercial systems are provided with twin storage facilities so that a full drum may be removed without stopping the process.

(c) Film extrusion

Although some forms of plastic sheeting and film may be produced using a slit die and a roll stack (as was shown in Fig. 4.21(b)), most fine plastic films are either produced by *Cast Film Extrusion* or *Blown Film Extrusion*.

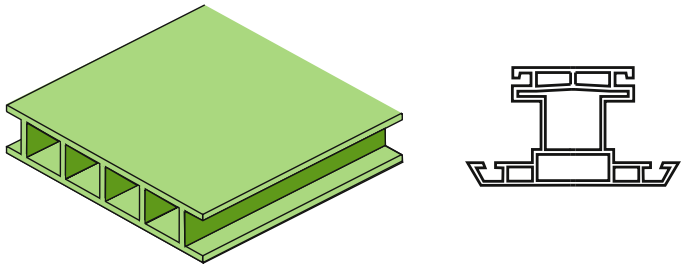


FIG. 4.20 (A) Extruded panel sections (B) Extruded window profile.

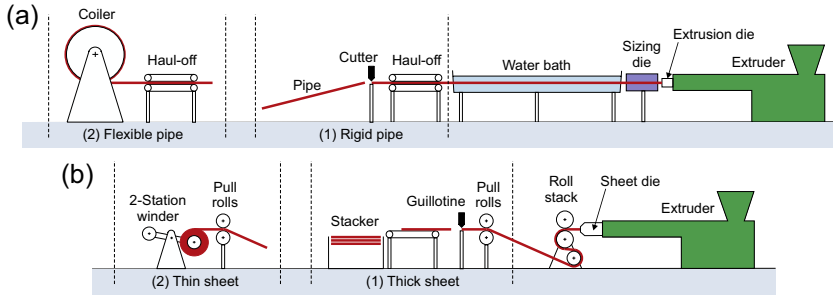


FIG. 4.21 (a) Pipe extrusion (1) rigid pipe (2) flexible pipe. (b) Sheet extrusion (1) thick sheet (2) thin sheet.

In Cast Film Extrusion a slit die is employed but instead of being mounted horizontally, it is positioned vertically so as to extrude a fine melt film onto a highly polished, high speed chill roll (see Fig. 4.22). The melt is pinned to the surface of the chill roll by either the pressure from an air knife or a vacuum box located close to the roll. This causes the fine film to be rapidly quenched, which improves its mechanical properties and clarity. The film then travels through a further series of chill, polishing and nip rolls, which help to draw the film down to the correct thickness, before its edges are trimmed and it is wound onto a drum for storage.

The most common method for large scale production of plastic films is the Blown Film Extrusion process, which is illustrated in Fig. 4.23. The molten plastic from the extruder passes through an annular die and emerges as a thin tube. A supply of air to the inside of the tube prevents it from collapsing and may be used to inflate it to a larger diameter. Initially the bubble consists of molten plastic but a jet of air around the outside of the tube (cooling ring) promotes cooling and at a certain distance from the die exit, a freeze line can be identified. Eventually the cooled film passes through collapsing guides and nip rolls before being taken off to storage drums or, for example, gussetted and cut to length for plastic bags.

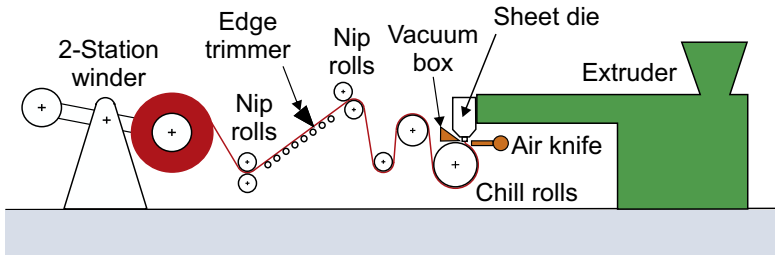


FIG. 4.22 Cast film extrusion.

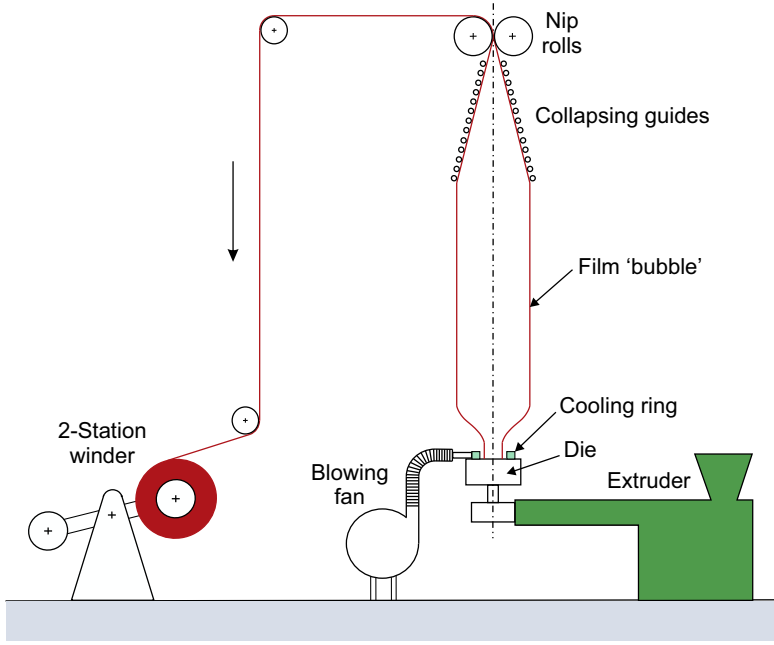


FIG. 4.23 Film blowing process.

The major advantage of film blowing is the ease with which biaxial orientation can be introduced into the film. The pressure of the air in the bubble determines the *blow-up* and this controls the circumferential orientation. In addition, axial orientation may be introduced by increasing the nip roll speed relative to the linear velocity of the bubble. This is referred to as *draw-down.*

It is possible to make a simple estimate of the orientation in blown film by considering only the effects due to the inflation of the bubble. Since the volume flow rate is the same for the plastic in the die and in the bubble, then for unit time

$$\pi D_d h_d L_d = \pi D_b h_b L_b$$

where D, h and L refer to diameter, thickness and length respectively and the subscript 'd' is for the die and 'b' is for the bubble.

So the orientation in the machine direction, O_{MD}, is given by

$$O_{MD} = \frac{L_b}{L_d} = \frac{D_d h_d}{h_b D_b} = \frac{h_d}{h_b B_R}$$

where B_R = blow-up ratio (D_b/D_d)

Also the orientation in the transverse direction, O_{TD}, is given by

$$O_{TD} = \frac{D_b}{D_d} = B_R$$

Therefore the ratio of the orientations may be expressed as

$$\frac{O_{MD}}{O_{TD}} = \frac{h_d}{h_b (B_R)^2} \tag{4.16}$$

Example 4.3 A plastic shrink wrapping with a thickness of 0.05 mm is to be produced using an annular die with a die gap of 0.8 mm. Assuming that the inflation of the bubble dominates the orientation in the film, determine the blow-up ratio required to give uniform biaxial orientation.

Solution Since $O_{MD} = O_{TD}$

$$\text{then the blow} - \text{up ratio, } B_R = \sqrt{\frac{h_d}{h_b}}$$

$$= \sqrt{\frac{0.8}{0.05}} = 4$$

Common blow-up ratios are in the range 1.5–4.5.

This example illustrates the simplified approach to film blowing. Unfortunately in practice the situation is more complex in that the film thickness is influenced by draw-down, relaxation of induced stresses/strains and melt flow phenomena such as die swell. In fact the situation is similar to that described for blow moulding (see below) and the type of analysis outlined in that section could be used to allow for the effects of die swell. However, since the most practical problems in film blowing require iterative type solutions involving melt flow characteristics, volume flow rates, swell ratios, etc. The study of these is addressed in Chapter 5 where a more rigorous approach to polymer flow is adopted.

(d) Blow moulding

This process evolved originally from glass blowing technology. It was developed as a method for producing hollow plastic articles (such as bottles and barrels) and although this is still the largest application area for the process, nowadays a wide range of technical mouldings can also be made by this method. e.g. automotive dashboards, ducting and spoilers. There is also a number of variations on the original process but we will start by considering the conventional extrusion blow moulding process.

Extrusion blow moulding

Initially a molten tube of plastic called the *Parison* is extruded through an annular die. A mould then closes round the parison and a jet of gas inflates it to take up the shape of the mould. This is illustrated in Fig. 4.24. Although this process is principally used for the production of bottles (for washing-up liquid,

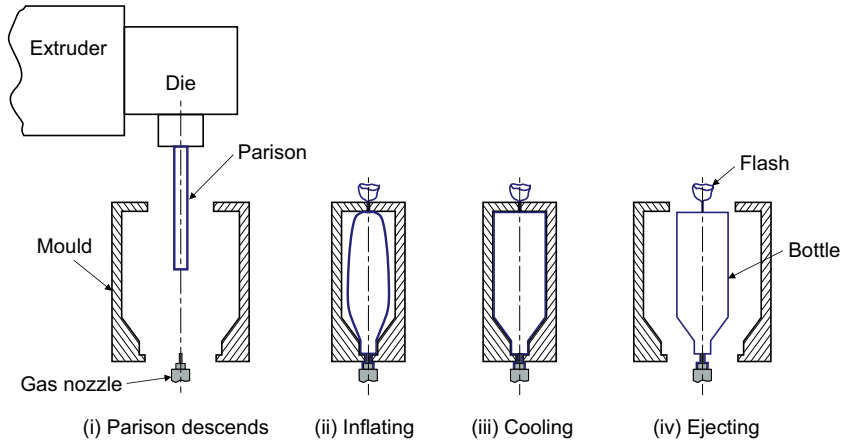


FIG. 4.24 Stages in blow moulding.

disinfectant, soft drinks, etc.) it is not restricted to small hollow articles. Domestic cold water storage tanks, large storage drums and 200 gallon containers have been blow-moulded. The main materials used are polyethylene, polypropylene, PVC and PET.

The conventional extrusion blow moulding process may be continuous or intermittent. In the former method the extruder continuously supplies molten polymer through the annular die. In most cases the mould assembly moves relative to the die. When the mould has closed around the parison, a hot knife separates the latter from the extruder and the mould moves away for inflation, cooling and ejection of the moulding. Meanwhile the next parison will have been produced and this mould may move back to collect it or, in multi-mould systems, this would have been picked up by another mould. Alternatively, in some machines the mould assembly is fixed and the required length of parison is cut off and transported to the mould by a robot arm.

In the intermittent processes, single or multiple parisons are extruded using a reciprocating screw or ram accumulator. In the former system the screw moves forward to extrude the parisons and then screws back to prepare the charge of molten plastic for the next shot. In the other system the screw extruder supplies a constant output to an accumulator. A ram then pushes melt from the accumulator to produce a parison as required.

Although it may appear straightforward, in fact the geometry of the parison is complex. In the first place its dimensions will be greater than those of the die due to the phenomenon of post extrusion swelling (see Chapter 5). Secondly there may be deformities (e.g. curtaining) due to flow defects. Thirdly, since most machines extrude the parison vertically downwards, during the delay between extrusion and inflation, the weight of the parison causes sagging or draw-down. This sagging limits the length of articles which can be produced

from a free hanging parison. The complex combination of swelling and thinning makes it difficult to produce articles with a uniform wall thickness. This is particularly true when the cylindrical parison is inflated into an irregularly shaped mould because the uneven drawing causes additional thinning. In most cases therefore to blow mould successfully it is necessary to program the output rate or die gap to produce a controlled non-uniform distribution of thickness in the parison which will give a uniform thickness in the inflated article.

During moulding, the inflation rate and pressure must be carefully selected so that the parison does not burst. Inflation of the parison is generally fast but the overall cycle time is dictated by the cooling of the melt when it touches the mould. Various methods have been tried in order to improve the cooling rate e.g. injection of liquid carbon dioxide, cold air or high pressure moist air. These usually provide a significant reduction in cycle times but since the cooling rate affects the mechanical properties and dimensional stability of the moulding it is necessary to try to optimise the cooling in terms of production rate and quality.

Extrusion blow moulding is continually developing to be capable of producing even more complex shapes. These include unsymmetrical geometries and double wall mouldings. Fig. 4.25 illustrates three stages in the blow moulding of a complex container. In this example the mould contains movable side cores that close and trap the partly inflated parison to create the final complex part geometry. In recent years there have also been considerable developments in the use of in-the-mould labelling (IML). This technology enables labels to be placed into the mould prior to inflation so that they are attached to bottles and containers as they are being moulded. Labels are typically made from either paper or plastics and are 15–40 μm thick. Although one of the main attractions of these labels is the high quality colour printing that is now possible, processors are increasingly exploiting their presence as a means of reducing the wall thickness required in the

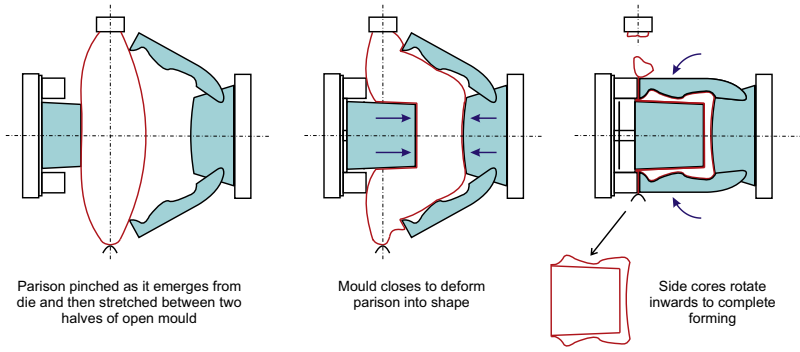


FIG. 4.25 Stages in blow moulding of complex hollow container.

parison. Similar IML technologies are available for other processes such as injection moulding and thermoforming. Many of the major applications of IML are in packaging but the technology is also being exploited in areas such as display and instrument panels in automobiles and consumer electronics.

Analysis of blow moulding

As mentioned previously, when the molten plastic emerges from the die it swells due to the recovery of elastic deformations in the melt. It will be shown later that the following relationship applies:

$$B_{SH} = B_{ST}^2 (\text{from Chapter 5})$$

where

B_{SH} = swelling of the thickness ($= h_1/h_d$)
B_{ST} = swelling of the diameter ($= D_1/D_d$)

therefore

$$\frac{h_1}{h_d} = \left(\frac{D_1}{D_d}\right)^2$$

$$h_1 = h_d (B_{ST})^2 \tag{4.17}$$

Now consider the situation where the parison is inflated to fill a cylindrical die of diameter, D_m. Assuming constancy of volume and neglecting draw-down effects, then from Fig. 4.26

$$\pi D_1 h_1 = \pi D_m h$$

$$h = \frac{D_1}{D_m} h_1$$

$$= \frac{D_1}{D_m} \left(h_d \cdot B_{ST}^2\right)$$

$$= \frac{B_{ST} \cdot D_d}{D_m} \left(h_d \cdot B_{ST}^2\right)$$

$$h = B_{ST}^3 h_d \left(\frac{D_d}{D_m}\right) \tag{4.18}$$

This expression therefore enables the thickness of the moulded article to be calculated from a knowledge of the die dimensions, the swelling ratio and the mould diameter. The following example illustrates the use of this analysis. A further example on blow moulding may be found towards the end of Chapter 5

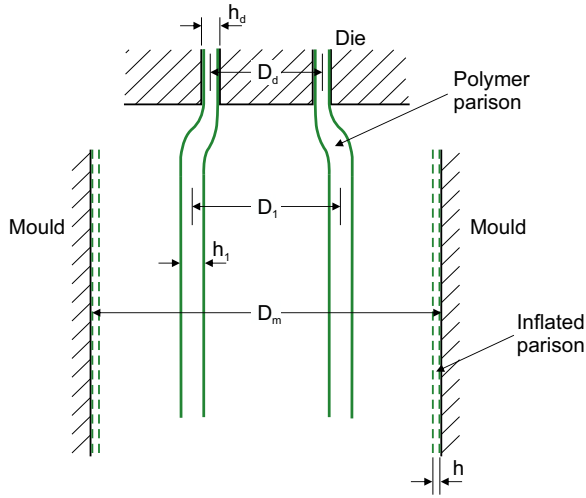


FIG. 4.26 Analysis of blow moulding.

where there is also an example to illustrate how the amount of sagging of the parison may be estimated.

Example 4.4 A blow moulding die has an outside diameter of 30 mm and an inside diameter of 27 mm. The parison is inflated with a pressure of 0.4 MPa to produce a plastic bottle of diameter 50 mm. If the extrusion rate used causes a thickness swelling ratio of 2, estimate the wall thickness of the bottle. Comment on the suitability of the production conditions if melt fracture occurs at a stress of 6 MPa.

Solution

From Eq. (4.18)

$$\text{wall thickness, } h = B_{ST}^3 h_d \left(\frac{D_d}{D_m}\right)$$

Now

$$h_d = \frac{1}{2}(30 - 27) = 1.5 \text{ mm}$$

$$B_{ST} = \sqrt{B_{SH}} = \sqrt{2} = 1.414$$

$$D_d = \frac{1}{2}(30 + 27) = 28.5 \text{ mm}$$

So

$$h = (1.414)^3(1.5)\left(\frac{28.5}{50}\right) = 2.42 \text{ mm}$$

The maximum stress in the inflated parison will be the hoop stress, σ_θ, which is given by

$$\sigma_\theta = \frac{PD_m}{2h} = \frac{0.4 \times 50}{2 \times 2.42}$$
$$= 4.13 \text{ MPa}$$

Since this is less than the melt fracture stress (6 MPa) these production conditions would be suitable. These are more worked examples on extrusion blow moulding towards the end of Chapter 5.

Extrusion stretch blow moulding

Molecular orientation has a very large effect on the properties of a moulded article. During conventional blow moulding the inflation of the parison causes molecular orientation in the hoop direction. However, biaxial stretching of the plastic before it starts to cool in the mould has been found to provide even more significant improvements in the quality of blow-moulded bottles. Advantages include improved mechanical properties, greater clarity and superior permeation characteristics. Cost savings can also be achieved through the use of lower material grades or thinner wall sections.

Biaxial orientation may be achieved in blow moulding by

(a) stretching the extruded parison longitudinally before it is clamped by the mould and inflated. This is based on the Neck Ring process developed as early as the 1950s. In this case, molten plastic is extruded into a ring mould which forms the neck of the bottle and the parison is then stretched.

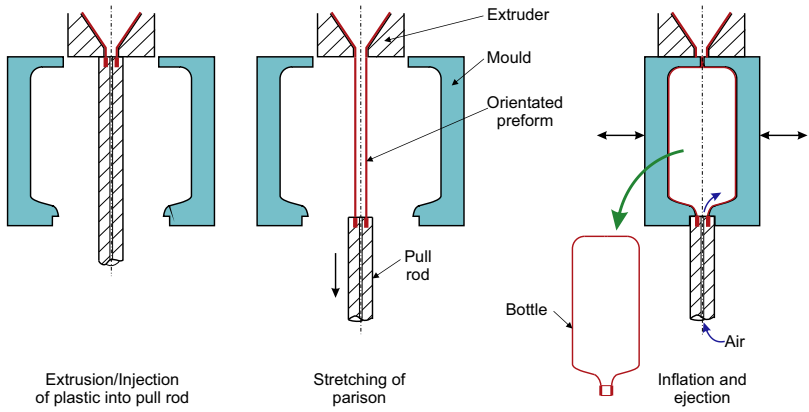


FIG. 4.27 Neck ring stretch blow moulding.

After the mould closes around the parison, inflation of the bottle occurs in the normal way. The principle is illustrated in Fig. 4.27.

(b) producing a small, thick-walled preform 'bottle' by extrusion blow moulding in one mould and then stretching this longitudinally using a 'stretch rod' prior to inflation in the full size bottle mould. This is illustrated in Fig. 4.28.

Injection stretch blow moulding

This is another method which is used to produce biaxially oriented blow moulded containers. It is very similar to the process illustrated in Fig. 4.28, except that the manufacture of the preform is carried out by injection moulding. The description of this process will be considered in more detail later (Section 4.3.8).

(e) Extrusion coating processes

There are many applications in which it is necessary to put a plastic coating onto fabric, paper or metal sheets and the extruder provides an ideal way of doing this. Some typical examples are waterproof wallpapers or fabric reinforced vinyl floor-coverings. Normally a thin film of plastic is extruded from a slit die and is immediately brought into contact with the medium to be coated.

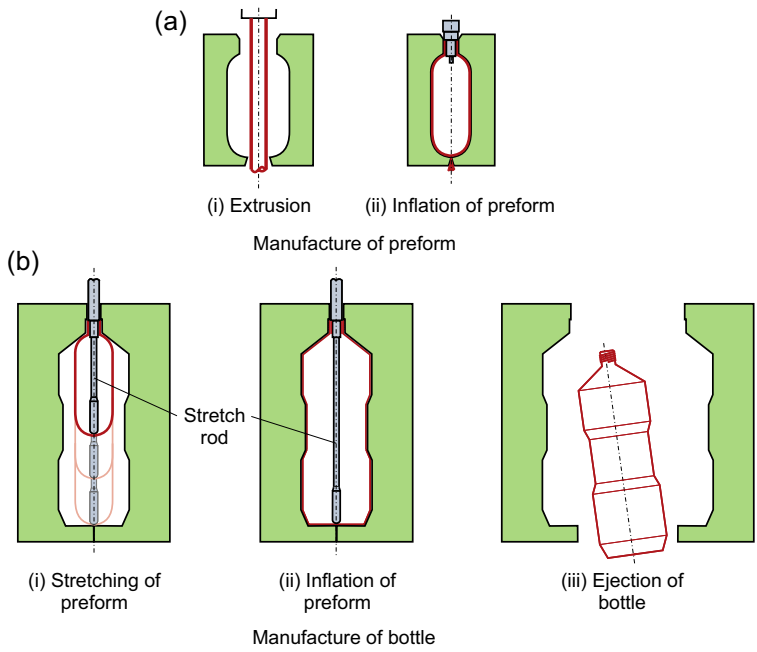


FIG. 4.28 Extrusion stretch blow moulding.

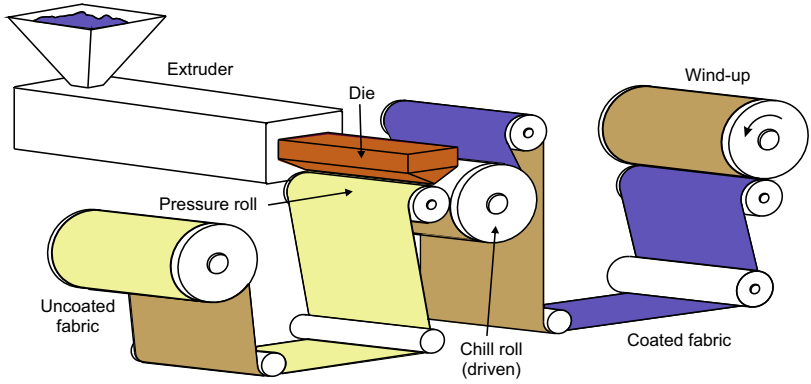


FIG. 4.29 Extrusion coating process.

The composite is then passed between rollers to ensure proper adhesion at the interface and to control the thickness of the coating (see Fig. 4.29). Rollers may be patterned to provide an embossed finish on the final product.

Another major type of coating process is *Wire Covering*. The tremendous demand for insulated cables in the electrical industry means that large tonnages of plastic are used in this application. Plastics are ideal for this application due to their natural electrical insulating properties, their flexibility, durability and the ease with which they can be coloured. Basically a bare wire, which may be heated or have its surface primed, is drawn through a special die attached to an extruder (see Fig. 4.30). The drawing speed may be anywhere between 1 m/min and 1000 m/min depending on the diameter of the wire. When the wire emerges from the die it has a coating of plastic, the thickness of which depends on the speed of the wire and the extrusion conditions. It then passes into a cooling

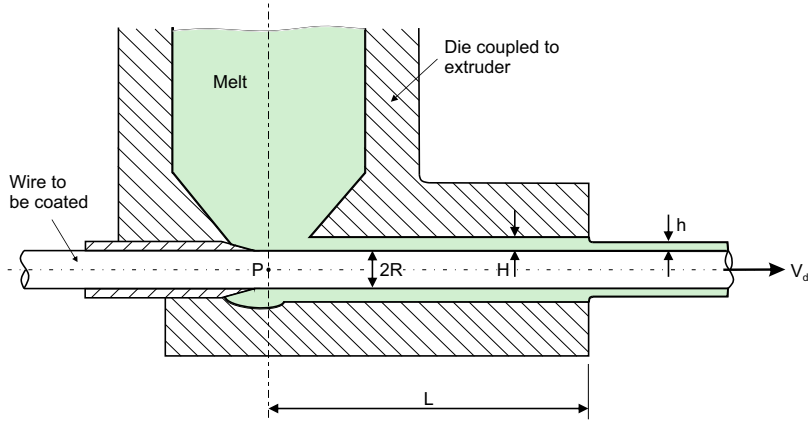


FIG. 4.30 Wire covering die.

trough which may extend for a linear distance of several hundred metres. The coated wire is then wound onto storage drums. The same process may be utilised to create the outer sheath of multi-core cables by feeding bundles of previously coated individual wires through a further wire covering die.

Wire covering can be analysed in a very similar manner to that described for extrusion. The coating on the wire arises from two effects:

(a) Drag Flow due to the movement of the wire
(b) Pressure Flow due to the pressure difference between the extruder exit and the die exit.

From (4.2) the drag flow, Q_d, is given by

$$Q_d = \frac{1}{2} THV_d \quad \text{where} \quad T = 2\pi\left(R + \frac{h}{2}\right)$$

From (4.6) the pressure flow, Q_p, is given by

$$Q_p = \frac{1}{12\eta}\frac{dP}{dz} \cdot TH^3$$

So combining these two equations, the total output, Q, is given by

$$Q = \frac{1}{2} THV_d + \frac{TH^3}{12\eta} \cdot \frac{P}{L} \tag{4.19}$$

This must be equal to the volume of coating on the wire so

$$Q = \pi V_d\left((R+h)^2 - R^2\right)$$

$$Q = \pi V_d h\ (2R + h) \tag{4.20}$$

Combining Eqs (4.19) and (4.20)

$$\pi V_d h\ (2R + h) = \frac{1}{2} THV_d + \frac{TH^3}{12\eta} \cdot \frac{P}{L}$$

from which

$$P = \frac{6\eta L V_d}{H^3}(2h - H) \tag{4.21}$$

This is an expression for the pressure necessary at the extruder exit and therefore enables the appropriate extrusion conditions to be set.

(f) Fibre spinning

Nowadays textiles made from plastics such nylon, acrylic and polyester are commonplace and over many decades these synthetic materials have replaced natural fibres such as wool, cotton and silk. Many types of synthetic fibres may be manufactured by melt extrusion and the basic manufacturing process is

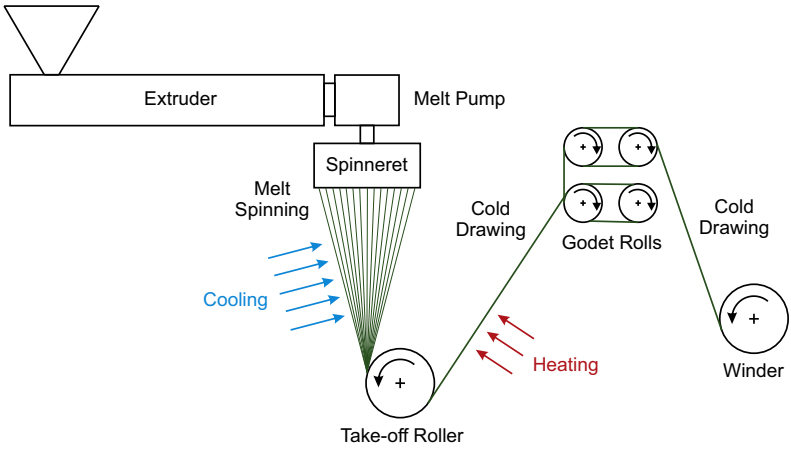


FIG. 4.31 Fibre extrusion.

illustrated in Fig. 4.31. It consists of a screw extruder attached to a multi-hole die called a *spinneret*, which produces multiple fine filaments or fibres. Some spinnerets can contain 1000 or more holes. Between the extruder and the die it is normal to have a very fine filter, or screen pack, and in many cases this is actually assembled within the spinneret to create what is termed a 'spin pack'. Most systems also employ a *gear (or melt) pump* to closely control the flow of the melt entering the die. The fine extruded fibres are drawn off by a take-off roller and in-between they are subjected to carefully controlled cooling in the form of a quench air stream. This ensures that optimal properties are retained in the plastic and the speed of the take-off roller may be used to both straighten and provide some orientation in the fibres. In the case of mono-filament yarns, water cooling is required. Some fibres may be subjected to heat treatment before they are drawn by passing them through a series of further rollers or godets that are running at different speeds. This drawing process creates very high levels of molecular orientation in the plastic, which in turn leads to substantial improvements in the mechanical properties of the fibres. The finished fibres are drawn onto a final winder roll for storage.

(g) Co-extrusion

As a result of the wide range of requirements which occur in practice it is not surprising that in many cases there is no individual plastic which has the correct combination of properties to satisfy a particular need. Therefore it is quite common in the manufacture of articles such as packaging film, yoghurt containers, refrigerator liners, gaskets and window frames that a multi-layer plastic composite is used. This is particularly true for extruded film and thermoforming sheets (see Section 4.4), but the same technology is now widely exploited in the manufacture of products as diverse as tubing or pipes

for automotive fuel or brake lines, or extended shelf-life bottles for beverages. Any form of extrusion can be adapted to create a multilayer structure, and in co-extrusion the output melt flows from two or more extruders are linked together through a special die to produce a multilayer product. Co-extruded films can either be produced by a blown film or a cast film process as illustrated in Fig. 4.32(a) and (b). The cast process using a slot die and chill roll to cool the film, produces a film with good clarity and high gloss. The film blowing process, however, produces a stronger film due to the transverse orientation which can be introduced, and this process offers more flexibility in terms of film thickness.

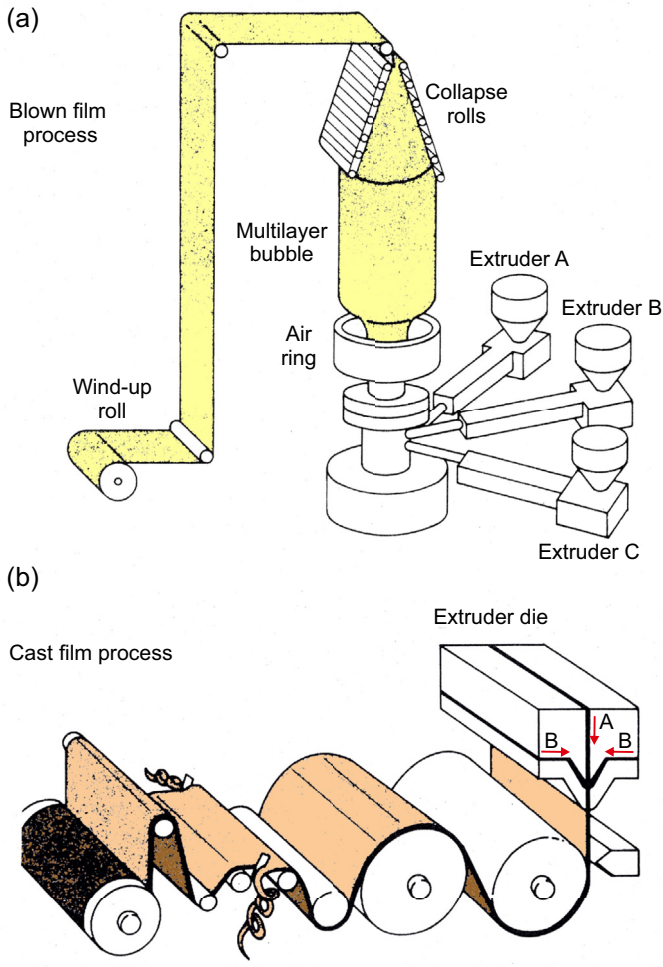


FIG. 4.32 Co-extrusion of plastic film.

In many cases chemical incompatibilities lead to insufficient adhesion between the layers of different polymers and so it is necessary to have a fine adhesive film between each of the layers. This is usually called a tie layer. Advances are continuing to be made that provide improvements in the chemical compatibility of polymers used in multilayer products. Alternatively, a promising area of research is in the use of nano-particles blended with a polymer matrix to create a polymer nanocomposite with specific property enhancements. By employing co-extrusion, multilayer sandwich structures may be readily produced with alternate layers of nanocomposite and the matrix polymer.

The main reason for producing multi-layer co-extruded films and sheet is to provide materials with better barrier properties – particularly in regard to gas permeation. This is of greatest importance to the food packaging industry where there is an ever growing need to secure, protect and extend the shelf life of foodstuffs. In most packaging applications plastics are almost ideally suited due to their combination of flexibility, durability, transparency, and the ease to which they can be manufactured, coloured and printed. However, most plastics, and typically those used in food packaging (e.g. PE and PP), exhibit quite poor gas barrier resistance and as a result can only preserve fresh foodstuffs for a maximum of 2–3 days. The typical gas transmittance rates for a range of common plastics used in food packaging are presented in Table 4.2. The most important gases are oxygen for fresh food packaging and moisture for dry foods packaging. In addition, transmission of carbon dioxide is an important consideration for bottling of fizzy drinks. Where longer shelf-life is desired, alternative materials may either be selected or introduced to the structure in the form of a co-extruded layer. A number of these materials and their effects on the transmittance rates of packaging films are shown in Table 4.3. Barrier layers can be formed from other plastics such as polyamide or ethylene vinyl alcohol (EVOH), which naturally offer much lower gas transmission rates. Foil laminates, where a fine metal foil (usually aluminium) is laminated within the coextruded structure, provides the most effective gas barrier. However, new metalised barrier films, where an extremely fine metallic layer is directly deposited onto the surface of the polymer using a physical vapour deposition process, are finding increasing applications. Examples of such barrier packaging includes PET/AL/LDPE for coffee and medical pouches, metallised PET/LDPE for snacks and biscuits, and PET/AL/PP for ready meals. Ongoing pressures to reduce the thicknesses of packaging films are continuing to drive new developments in these areas. Data on permeability of plastics are also given in Figs 1.17 and 1.18. An example of the layered structure in a co-extruded barrier sheet to be used in thermoformed food packaging is shown in Fig. 4.33. In this case barrier protection is provided by a thin layer of EVOH (around 4% of the sheet thickness), which is capped top and bottom by tie layers of an adhesive (around 3% of the sheet thickness). This is sandwiched within the polymer

TABLE 4.2 Transmission rates for a range of plastics.

			Transmission rates	
Polymer	Layer distribution (μm)	Density (kg/m^3)	Oxygen (cm^3/m^2 24 hr atm)	Water vapour (g/m^2 24 hr)
ABS	1000	1050	30	2
uPVC	1000	1390	5	0.75
Nylon 6	1000	1140	2	7
Polypropylene	1000	910	60	0.25
Polystyrene	1000	1040	162	5.2
PLA	1000	1240	12	8
PET	1000	1360	1	2
LDPE	1000	920	140	0.5
HDPE	1000	960	60	0.3
PS/EVOH[a]/PE	825/25/150	1050	5[b]	1.6
PS/PVdC/PE	825/50/125	1070	1	0.4
PP/EVOH/PP	300/40/660	930	1[b]	0.25

[a]*EVOH ethyl vinyl alcohol.*
[b]*Depends on humidity.*

bulk which is a blend of a homopolymer and a copolymer polypropylene. Also included within the core of the structure is a layer of factory regrind, which is the same polypropylene from various factory waste streams including scrap produced during set-up and skeletal waste from the sheet remaining after thermoforming. It is extremely important for economic reasons that this material is reused, but for many products such plastic waste cannot be used on an outer surface that may contact food. Therefore co-extrusion is essential. Altogether the sheet contains 6 layers and requires 4 separate extruders of various sizes to produce the structure shown.

(h) Biaxially orientated plastics

The direction of flow through the die will naturally lead to some level of molecular orientation in extrusion processes, but it is only through deliberate large strain biaxial stretching of the plastics that it is possible to achieve very substantial increases in the mechanical properties of the final product. This is readily obtainable with blown film extrusion and stretch blow moulding through a combination of mechanical drawing for axial orientation and

TABLE 4.3 Transmission rates of plastic packaging films.

		Transmission rates	
Film material	Layer distribution (μm)	Oxygen (cm^3/m^2 24 hr atm)	Water vapour (g/m^2 24 h)
Aluminium foil	7	0.15	0.2
Cast PP	30	4800	12
BOPP	20	2000	8
Metallised BOPP	20	100	0.8
PET	12	110	50
PVdC coated PET	12	8	8
Metallised PET	12	1.5	1.5
BOPA	15	30	180
LDPE	12	8000	18

inflation for transverse orientation. However, it is also possible to adapt other extrusion variants to create biaxially orientated plastics such as biaxially orientated forms of polypropylene (BOPP), polyethylene (BOPE), polyamide (BOPA), polylactic acid (BOPLA) and polyethylene terephthalate (BOPET). These materials are most often exploited in high strength, thin gauge co-extruded packaging and adhesive tapes. A good example of their impact is in the development of highly orientated grids. These net-like polymer grids have become a very common sight on construction sites where they are often employed as an extremely strong reinforcement to the soil or other loose building materials. They are also frequently used as temporary fencing. One of the best known of these products is the 'Tensar geogrid' system.

Biaxially orientated plastics in sheet or film form are generally manufactured by an extrusion process followed by biaxial stretching in two stages. The



FIG. 4.33 Structure of a co-extruded barrier sheet.

extruded plastic is firstly orientated in the machine direction by running it through a series of haul-off rollers, before it enters a section known as a 'tenter frame' that clamps and gradually extends the width of the film/sheet and orientates it in the transverse direction. The process is illustrated in Fig. 4.34, which shows the manufacturing process for a highly orientated grid. In this case an extruded sheet, which is produced to a very fine tolerance and with a controlled structure, is punched to create the initial unorientated grid preform. The hole shapes and pattern can be altered depending on the performance required of the finished product. The plastic may be reheated between the different stages. The perforated sheet is then stretched in one direction to give thin sections of highly orientated polymer with the tensile strength of mild steel. This type of grid can be used in applications where uniaxial strength is required. In other cases, where biaxial strength is necessary, the sheet is subjected to a second stretching operation in the transverse direction. The advantages of highly oriented grids are that they are light and very easy to handle. The advantage of obtaining a highly oriented molecular structure is also readily apparent when one compares the stiffness of a HDPE grid ($\simeq$10 GPa) with the stiffness of unoriented HDPE ($\simeq$ 1 GPa).

Biaxially orientated plastics in tubular form may be manufactured using a technique known as the 'double-bubble' orientation process. As the name implies, the first half of the production line resembles a standard blown-film

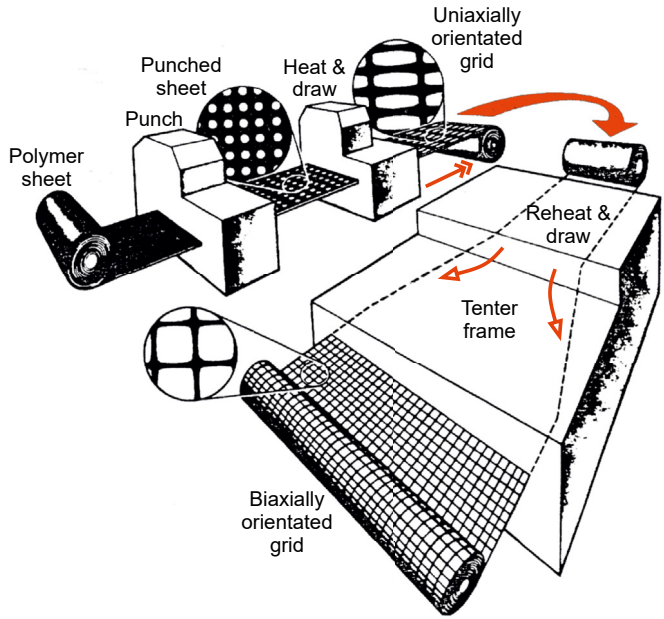


FIG. 4.34 Manufacturing process for highly orientated grids.

line, but after the first set of nip rolls, the tube is carefully reheated and reinflated with high air pressure, expanding the diameter while simultaneously being drawn axially by a second set of collapsing nip rolls operating at high speed. The completed film is then wound in the normal manner.

(i) Reactive extrusion

Reactive extrusion is a special process in which a chemical reaction to combine polymer components is carried out within the extruder. This has the advantage of enabling relatively small quantities of specialised polymers and polymer blends to be manufactured without the use of a full-size reactor. Nowadays the process is most often undertaken using twin screw extruders (usually co-rotating) because of their enhanced mixing capabilities. An example of its application is in the manufacture of thermoplastic polyurethanes (TPUs), where the liquid components are introduced to the extruder via highly accurate liquid feeders. The reaction to polyurethane takes place in the twin screw extruder under constant mixing and kneading. Surplus reaction heat is dissipated through the barrel wall. As well as polymerisation processes, reactive extruder systems may also be used for chemical modification of polymers such as grafting, crosslinking, functionalisation, depolymerisation etc. and for enzymatic reactions such as hydrolysis of biopolymers (starch and proteins).

4.3 Injection moulding

4.3.1 Introduction

By far the most common processing method for plastics is injection moulding. Nowadays almost every complex manufactured product is either largely made of plastics or is comprised of some or many plastic components. The vast majority of plastic products that are small, complex in shape and manufactured in large numbers will have been made by injection moulding. This extends to every part of our modern world from our homes, our offices, our transport systems and our factories. Familiar products include such things as toy dolls, electric drill casings, yoghurt cartons, television housings, hairbrushes, syringes, paint brush handles, crash helmets, gearwheels, keyboards, fascia panels, reflectors, mobile phones, trolley cases – the list is endless. In their early days plastics were simply used to replace more expensive materials such as wood or metals in many products, but today there are large numbers of products that are designed specifically to exploit the unique properties of plastics. Injection moulding in particular has been at the forefront of these advances due to its ability to accurately create highly complex shapes in a single manufacturing operation.

The original injection moulding machines were based on the pressure die casting technique for metals. The first machine is reported to have been patented in the United States in 1872, specifically for use with Celluloid. This was an important invention but probably before its time because in the

following years very few developments in injection moulding processes were reported and it was not until the 1920s, in Germany, that a renewed interest was taken in the process. The first German machines were very simple pieces of equipment and relied totally on manual operation. Levers were used to clamp the mould and inject the melted plastic with the result that the pressures which could be attained were not very high. Subsequent improvements led to the use of pneumatic cylinders for clamping the injection which not only lifted some of the burden from the operator but also meant that higher pressures could be used.

The next major development in injection moulding, i.e. the introduction of hydraulically operated machines, did not occur until the late 1930s when a wide range of thermoplastics started to become available. However, these machines still tended to be hybrids based on die casting technology and the design of injection moulding machines for plastics was not taken really seriously until the 1950s when a new generation of equipment was developed. These machines catered more closely for the particular properties of polymer melts and modern machines are of the same basic design although of course the control systems are very much more sophisticated nowadays.

In principle, injection moulding is a simple process. A thermoplastic, in the form of granules or powder, passes from a feed hopper into the barrel where it is heated so that it becomes soft. It is then forced through a nozzle into a relatively cold mould which is clamped tightly closed. When the plastic has had sufficient time to become solid the mould opens, the article is ejected and the cycle is repeated. The major advantages of the process include its versatility in moulding a wide range of products, the ease with which automation can be introduced, the possibility of high production rates and the manufacture of articles with close tolerances. The basic injection moulding concept can also be adapted for use with thermosetting materials.

4.3.2 Details of the process

The earliest injection moulding machines were of the plunger type as illustrated in Fig. 4.35, but for large scale production these have now been largely phased out in favour of the more reliable screw-based machines. However, some variants of the plunger system are still used for specialized applications. A predetermined quantity of moulding material drops from the feed hopper into the barrel. The plunger then conveys the material along the barrel where it is heated by conduction from the external heaters. The material is thus plasticised under pressure so that it may be forced through the nozzle into the mould cavity. In order to split up the mass of material in the barrel and improve the heat transfer, a torpedo is fitted in the barrel as shown.

Unfortunately, there are a number of inherent disadvantages with this type of machine which can make it difficult to produce consistent moulding. The main problems are:

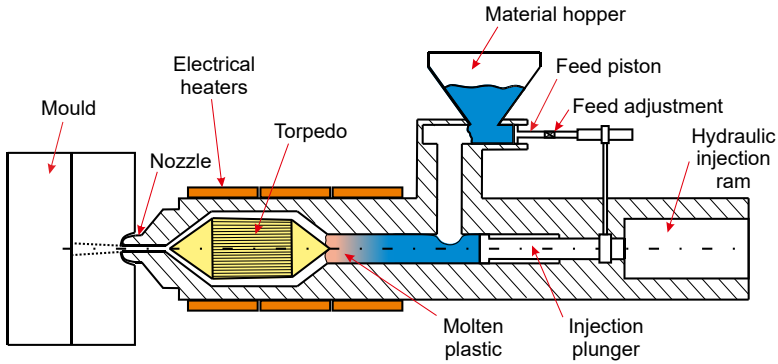


FIG. 4.35 Plunger type injection moulding machine.

(a) There is little mixing or homogenisation of the molten plastic.
(b) It is difficult to meter accurately the shot size. Since metering is on a volume basis, any variation in the density of the material will alter the shot weight.
(c) Since the plunger is compressing material which is in a variety of forms (varying from a solid granule to a viscous melt) the pressure at the nozzle can vary quite considerably from cycle to cycle.
(d) The presence of the torpedo causes a significant pressure loss.
(e) The flow properties of the melt are pressure sensitive and since the pressure is erratic, this amplifies the variability in mould filling.

Some of the disadvantages of the plunger machine may be overcome by using a pre-plasticising system. This type of machine has two barrels. Raw material is fed into the first barrel where an extruder screw or plunger plasticises the material and feeds it through a non-return valve into the other barrel. A plunger in the second barrel then forces the melt through a nozzle and into the mould. In this system there is much better homogenisation because the melt has to pass through the small opening connecting the two barrels. The shot size can also be metered more accurately since the volume of material fed to the second barrel can be controlled by a limit switch on its plunger. Another advantage is that there is no longer a need for the torpedo on the main injection cylinder. However, nowadays this type of machine is seldom used because it is considerably more complicated and more expensive than necessary. One area of application where it is still in use is for large mouldings because a large volume of plastic can be plasticised prior to injection using the primary cylinder plunger.

For normal injection moulding, however, the market is now almost entirely dominated by the reciprocating screw type of injection moulding machine. This was a major breakthrough in machine design and yet the principle is simple. An extruder type screw in a heated barrel performs a dual role. On the one hand it rotates in the normal way to transport, melt and pressurize the material in the

barrel but it is also capable, whilst not rotating, of moving forward like a plunger to inject melt into the mould. A typical injection moulding machine cycle is illustrated in Fig. 4.36. It involves the following stages:

(a) After the mould closes, the screw (not rotating) pushes forward to inject melt into the cooled mould. The air inside the mould will be pushed out through small vents at the furthest extremities of the melt flow path.
(b) When the cavity is filled, the screw continues to push forward to apply a holding pressure (see Fig. 4.36). This has the effect of squeezing extra melt into the cavity to compensate for the shrinkage of the plastic as it cools. This holding pressure is only effective as long as the gate(s) remain open.

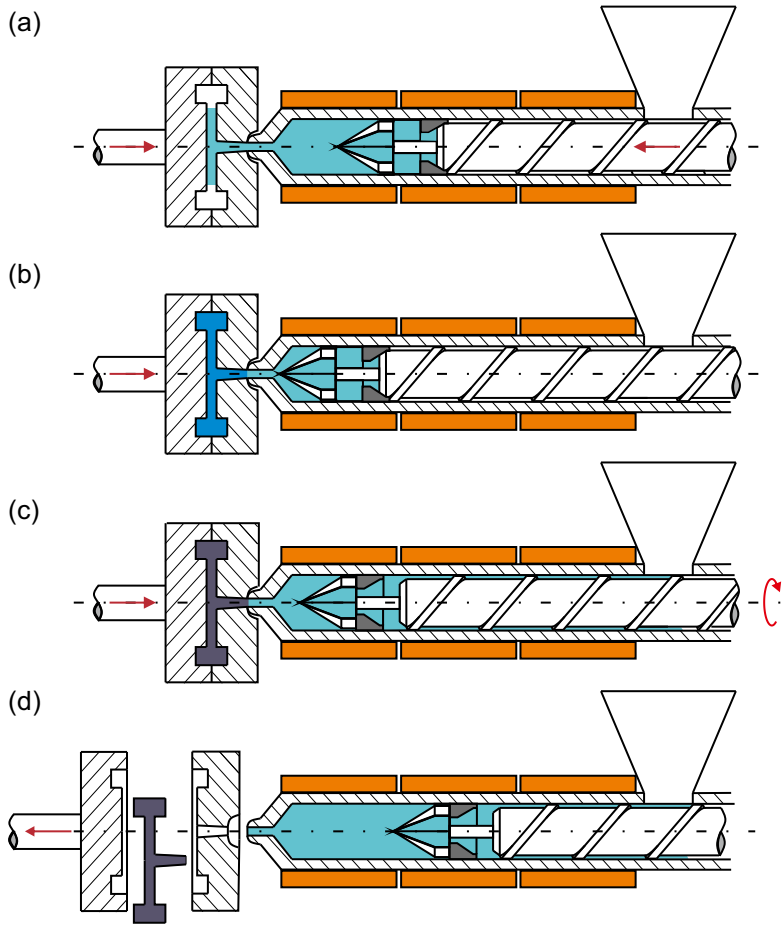


FIG. 4.36 Typical cycle in reciprocating screw injection moulding machine.

(c) Once the gate(s) freeze, no more melt can enter the mould and so screw-back commences. At this stage the screw starts to rotate and draw in new plastic from the hopper. This is conveyed to the front of the screw but as the mould cavity is filled with plastic, the effect is to push the screw backwards. This prepares the next shot by accumulating the desired amount of plastic in front of the screw. At a pre-set point in time, the screw stops rotating, and the machine sits waiting for the solidification of the moulding and runner system to be completed.
(d) When the moulding has cooled to a temperature where it is solid enough to retain its shape, the mould opens and the moulding is ejected. The mould then closes and the cycle is repeated.

The relative lengths of the stages in an injection moulding cycle are shown in Fig. 4.37. In most cases cooling dominates and is the largest contributor to cycle time. There are a number of important features in reciprocating screw injection moulding machines and these will now be considered in turn.

Screws. The screws used in these machines are basically the same as those described earlier for extrusion. The compression ratios are usually in the range 2.5:1 to 4:1 and the most common L/D ratios are in the range 15−20. Some screws are capable of injecting the plastic at pressures up to 200 MPa. One important difference from an extruder screw is the presence of a back-flow check valve at the end of the screw as illustrated in Fig. 4.38. The purpose of this valve is to stop any back flow across the flights of the screw when it is acting as a plunger.

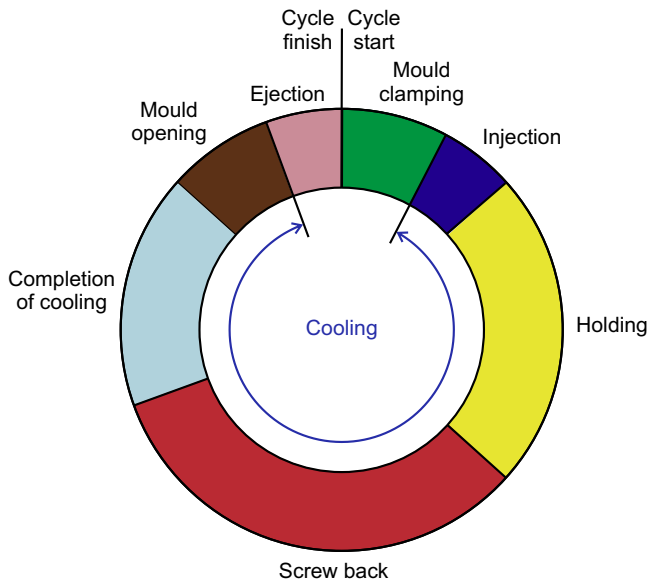


FIG. 4.37 Stages in injection moulding cycle.

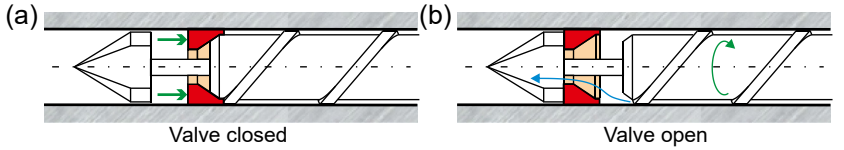


FIG. 4.38 Typical check valve.

When material is being conveyed forward by the rotation of the screw, the valve opens as shown. One exception is when injection moulding heat-sensitive materials such as PVC. In such cases there is no check valve because this would provide sites where material could become trapped and would degrade.

Barrels and Heaters. These are also similar to those in extruders. In recent years, vented barrels have become available to facilitate the moulding of water sensitive plastics without the need for pre-drying. Water sensitivity in plastics can take several forms. If the plastic absorbs water then dimensional changes will occur, just as with wood or paper. The plastic will also be plasticised by the water so that there will be property changes such as a reduction in modulus and an increase in toughness. All these effects produced by water absorption are reversible.

Another event which may occur is *hydrolysis*. This is a chemical reaction between the plastic and water. It occurs extremely slowly at room temperature but can be significant at moulding temperatures. Hydrolysis causes degradation, reduction in properties (such as impact strength) and it is irreversible. Table 4.4 indicates the sensitivity of plastics to moisture. Note that generally extrusion requires a lower moisture content than injection moulding to produce good quality products.

Nozzles. The nozzle is screwed into the end of the barrel and provides the means by which the melt can leave the barrel and enter the mould. It is also a region where the melt can be heated both by friction and conduction from a heater band before entering the relatively cold channels in the mould. Contact

TABLE 4.4 Water sensitivity of some common plastics.

Drying not required (materials do not hydrolyse)	Drying required	
	Absorbs only	Hydrolyses
Polyethylene	Acrylic (0.02/0.08)[a]	PET (0.002/0.002)
Polypropylene	ABS (0.02/0.08)	Polycarbonate (0.01/0.02)
Polystyrene	SAN (0.02/0.08)	Nylon 66 (0.08/0.15)
PVC		PLA (0.025/0.025)

[a]*Required maximum moisture content for extrusion/injection moulding (%).*

with the mould causes heat transfer from the nozzle and in cases where this is excessive it is advisable to withdraw the nozzle from the mould during the screw-back part of the moulding cycle. Otherwise the plastic may freeze off in the nozzle.

There are several types of nozzle. The simplest is an open nozzle as shown in Fig. 4.39(a). This is used whenever possible because pressure drops can be minimised and there are no hold up points where the melt can stagnate and decompose. However, if the melt viscosity is low then leakage will occur from this type of nozzle particularly if the barrel/nozzle assembly retracts from the mould each cycle. The solution is to use a shut-off nozzle of which there are many types. Fig. 4.39(b) shows a nozzle which is shut off by external means. Fig. 4.39(c) shows a nozzle with a spring loaded needle valve which opens when the melt pressure exceeds a certain value or alternatively when the nozzle is pressed up against the mould. Most of the shut-off nozzles have the disadvantage that they restrict the flow of the material and provide undesirable stagnation sites. For this reason they should not be used with heat sensitive materials such as PVC.

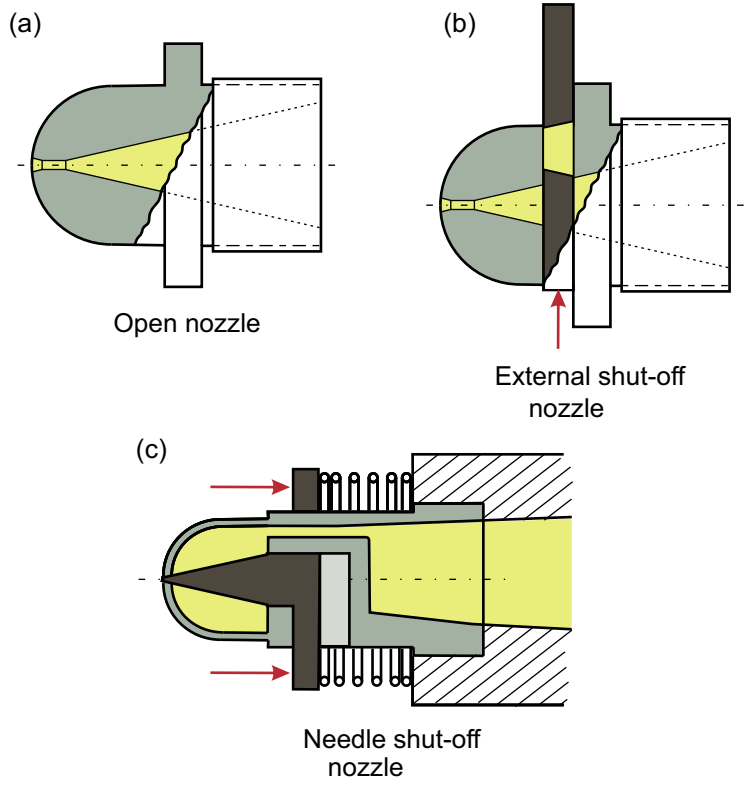


FIG. 4.39 Types of nozzle.

Clamping Systems. In order to keep the mould halves tightly closed when the melt is being injected under high pressures it is necessary to have a clamping system. This may be either (a) hydraulic or (b) mechanical (toggle) – or some combination of the two. The general arrangement of these systems are illustrated in Fig. 4.40.

In the hydraulic system (Fig. 4.40(b)), oil under pressure is introduced behind a piston connected to the moving platen of the machine. This causes the mould to close and the clamp force can be adjusted so that there is no leakage of molten plastic from the mould.

The toggle (Fig. 4.40(a)) is a mechanical device used to amplify force. Toggle mechanisms tend to be preferred for high speed machines and where the clamping force is relatively small. The two main advantages of the toggle system are that it is more economical to run the small hydraulic cylinder and since the toggle is self locking it is not necessary to maintain the hydraulic

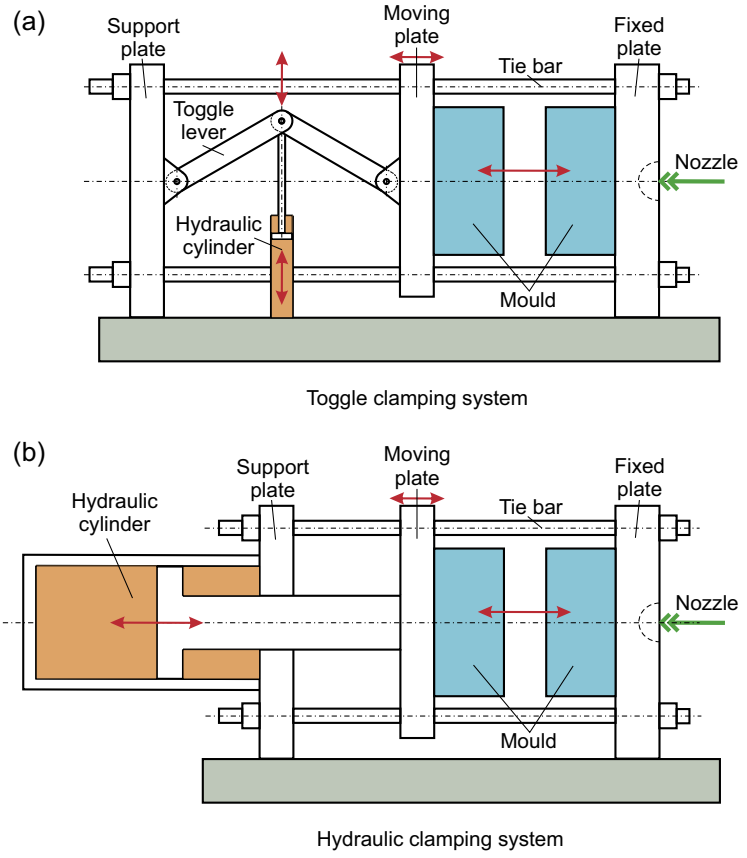


FIG. 4.40 Mould clamping systems.

pressure throughout the moulding cycle. On the other hand the toggle system has the disadvantages that there is no indication of the clamping force and the additional moving parts increase maintenance costs.

4.3.3 Moulds

In the simplest case an injection mould (or 'tool') consists of two-halves into which the impression of the part to be moulded is cut. The mating surfaces of the mould halves are accurately machined so that no leakage of plastic can occur at the split line. If leakage does occur the flash on the moulding is unsightly and expensive to remove. A typical injection mould is illustrated in Fig. 4.41. It may by seen that in order to facilitate mounting the mould in the machine and cooling and ejection of the moulding, several additions are made to the basic mould halves. Firstly, backing plates permit the mould to be bolted on to the machine platens. Secondly, channels are machined into the mould to allow the mould temperature to be controlled. Thirdly, ejector pins are included to that the moulded part can be freed from the mould. In most cases the ejector pins are operated by the shoulder screw hitting a stop when the

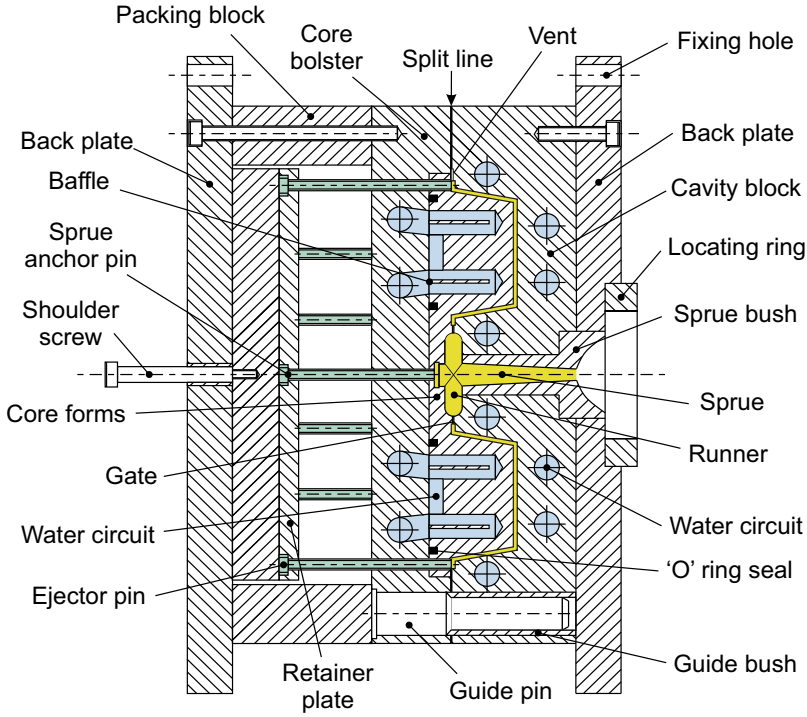


FIG. 4.41 Details of injection mould.

mould opens. The mould cavity is joined to the machine nozzle by means of the **sprue**. The sprue anchor pin then has the function of pulling the sprue away from the nozzle and ensuring that the moulded part remains on the moving half of the mould, when the mould opens (shown in Fig. 4.42(a)). Further movement of the mould half then activates the shoulder screw to lock the ejector bar so that the ejector pins emerge from the cavity block at key points on the moulding, causing it to be fully ejected from the mould (shown in

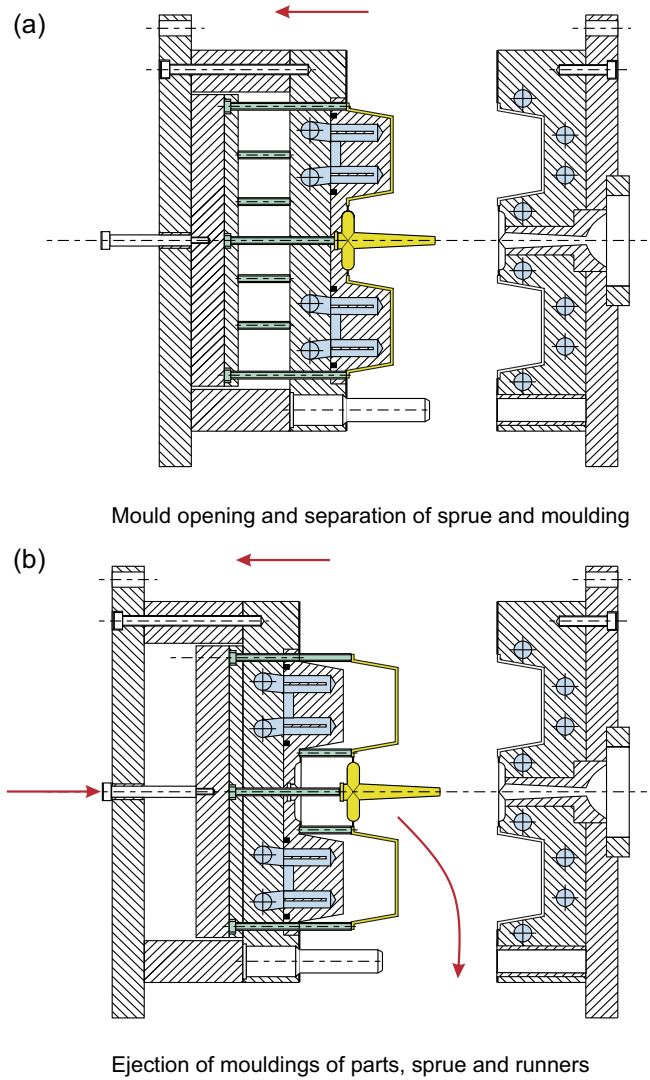


FIG. 4.42 Mould opening and part ejection.

Fig. 4.42(b)). For multi-cavity moulds the impressions are joined to the sprue by **runners** – channels cut in one or both halves of the mould through which the plastic will flow without restriction. A narrow constriction between the runner and the cavity allows the moulding to be easily separated from the runner and sprue. This constriction is called the **gate**.

A production injection mould is a piece of high precision engineering manufactured to very close tolerances by modern computer-controlled machining techniques. A typical mould can be considered to consist of (i) the cavity and core and (ii) the remainder of the mould (often referred to as the bolster). Of these two, the latter is the more straightforward because although it needs to be accurately made, in general, conventional machine tools can be used. The cavity and core, however, may be quite complex in shape and so they often need special techniques. These can include casting, electro-deposition, hobbing, pressure casting, water jet machining, and electro-discharge machining or spark erosion.

Finishing and polishing the mould surfaces is also extremely important because the melt will tend to reproduce every detail on the surface of the mould. Finally the mould will have to be hardened to make it stand up to the treatment it receives in service. As a result of all the time and effort which goes into mould manufacture, it is sometimes found that a very complex mould costs more than the moulding machine on which it is used. Several features of the mould are worthy of special mention.

(a) Gates

As mentioned earlier the gate is the small orifice which connects the runner to the cavity. It has a number of functions. Firstly, it provides a convenient weak link by which the moulding can be broken off from the runner system. In some moulds the degating may be automatic when the mould opens. The gate also acts like a valve in that it allows molten plastic to fill the mould but being small it usually freezes off first. The cavity is thus sealed off from the runner system which prevents material being sucked out of the cavity during screw-back. As a general rule, small gates are preferable because no finishing is required if the moulding is separated cleanly from the runner. So for the initial trials on a mould the gates are made as small as possible and are only opened up if there are mould filling problems.

In a multi-cavity mould it is not always possible to arrange for the runner length to each cavity to be the same. This means that cavities close to the sprue would be filled quickly whereas cavities remote from the sprue receive the melt later and at a reduced pressure. To alleviate this problem it is common to use small gates close to the sprue and progressively increase the dimensions of the gates further along the runners. This has the effect of balancing the fill of the cavities. If a single cavity mould is multi-gated then here again it may be beneficial to balance the flow by using various gate sizes.

Examples of gates which are in common use are shown in Fig. 4.43. Sprue gates (a) are used when the sprue bush can feed directly into the mould cavity as, for example, with single symmetrical moulding such as buckets. Pin gates (b) are particularly successful because they cause high shear rates which reduce the viscosity of the plastic and so the mould fills more easily. The side gate (c) is the most common type of gate and is a simple rectangular section feeding into the side of the cavity. A particular attraction of this type of gate is that mould filling can be improved by increasing the width of the gate but the freeze time is unaffected because the depth is unchanged. The fan gate (d) is wide and shallow, and it is effective in minimising defects around the gate. It is normally used for flat products.

(b) Runners

The runner is the flow path by which the molten plastic travels from the sprue (i.e. the moulding machine) to the gates (i.e. the cavity). To prevent the runner freezing off prematurely, its surface area should be small so as to minimise

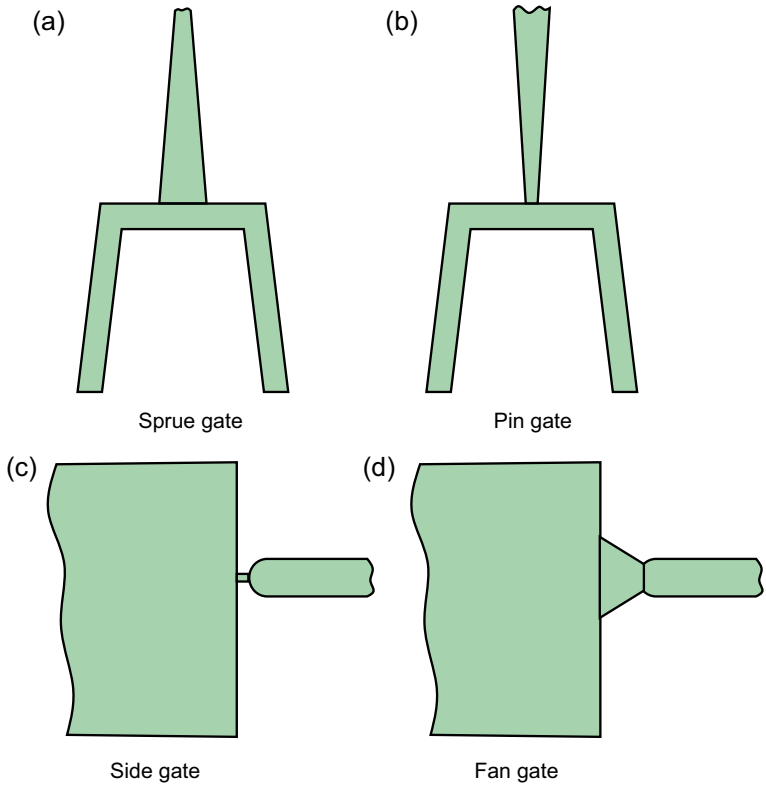


FIG. 4.43 Types of gate.

heat transfer to the mould. However, the cross sectional area of the runner should be large so that it presents little resistance to the flow of the plastic but not so large that the cycle time needs to be extended to allow the runner to solidify for ejection. A good indication of the efficiency of a runner is, therefore, the ratio of its cross-sectional area to its surface area. For example, a semi-circular channel cut into one-half of the mould is convenient to machine but it only has an area ratio of 0.153 D where D is the diameter of the semi-circle. A full round runner, on the other hand, has a ratio of 0.25 D. A square section also has this ratio but is seldom used because it is difficult to eject. A compromise is a trapezoidal section (cut into one-half of the mould) or a hexagonal section. These provide a sloped side which is very easy to eject.

(c) Sprues

The sprue is the channel along which the molten plastic first enters the mould. It delivers the melt from the nozzle to the runner system. The sprue is incorporated in a hardened steel bush which has a seat designed to provide a good seal with the nozzle. Since it is important that the sprue is pulled out when the mould opens it is tapered as shown in Fig. 4.41 and there is a sprue pulling device mounted directly opposite the sprue entry. This can take many forms but typically it would be an undercut or reversed taper to provide a key for the plastic on the moving half of the mould. Since the sprue, like the runner system, is effectively waste it should not be made excessively long.

(d) Venting

Before the plastic melt is injected, the cavity in the closed mould contains air. When the melt enters the mould, if the air cannot escape it becomes compressed. At worst this may affect the mould filling, but in any case the sudden compression of the air causes considerable heating. This may be sufficient to burn the plastic and the mould surface at local hot spots. To alleviate this problem, vents are machined into the mating surfaces of the mould to allow the air to escape. An example is shown at the edge of the upper cavity in Fig. 4.41. The vent channel must be small so that molten plastic will not flow along it and cause unsightly flash on the moulded article. Typically a vent is about 0.025 mm deep and several millimetres wide. Away from the cavity the depth of the vent can be increased so that there is minimum resistance to the flow of the gases out of the mould.

(e) Mould temperature control

For efficient moulding, the temperature of the mould should be controlled and this is normally done by passing a fluid through a suitably arranged channel in the mould. The rate at which the moulding cools affects the total cycle time as well as the surface finish, tolerances, distortion and internal stresses of the moulded article. High mould temperatures improve surface gloss and tend to

eliminate voids. However, the possibility of flashing is increased and sink marks are likely to occur. If the mould temperature is too low then the material may freeze in the cavity before it is filled. In most cases the mould temperatures used are a compromise based on experience. In Chapter 5 we will consider ways of estimating the time taken for a moulding to cool down in a mould.

Example 4.5 The runner lay-out for an eight cavity mould is illustrated in Fig. 4.44. If the mould is to be designed so that the pressure at the gate is the same in all cases, determine the radius of the runner in Section 2 as illustrated in Fig. 4.44. The flow may be assumed to be isothermal.

Solution Although this runner system is symmetrical, it is not balanced. If the runner had the same diameter throughout all sections, then the mouldings close to the sprue would fill first and would be over-packed before the outermost cavities were filled. In a good mould design, all the cavities fill simultaneously at the same pressure. In this case it is necessary to ensure that the pressure drop in Sections 1 and 3 is the same as the pressure drop in Section 2.

It will be shown in Chapter 5 that the pressure drop, ΔP for isothermal flow in a circular section channel is given by

$$\Delta P = \frac{8\eta LQ}{\pi R^4} \tag{4.22}$$

where

η = viscosity of the plastic
L = length of channel
Q = volume flow rate
R = radius of channel

If the volume flow rate towards point J is q (i.e. the input at the sprue is $2q$) then at J the flow will split as follows:

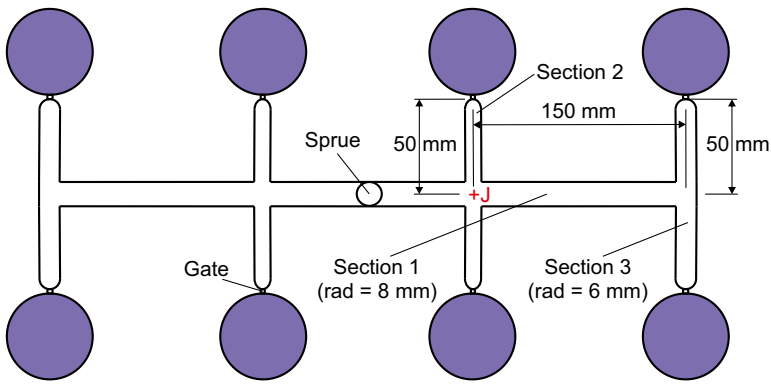


FIG. 4.44 Lay-out for eight cavity mould.

Flow along runner 1 = xq
Flow along runner 2 = $^1/_2\ (1 - x)q$
Flow along runner 3 = $^1/_2\ xq$

where

$$x = \frac{A_1}{A_1 + 2A_2} = \frac{R_1^2}{R_1^2 + 2R_2^2}$$

(A refers to the area of the relevant runner).

Using Eq. (4.22) we can write

$$\text{Pressure loss in runner 1} = \frac{8\eta L_1 xq}{\pi R_1^4}$$

$$\text{Pressure loss in runner 2} = \frac{8\eta L_2 (1 - x)q}{2\pi R_2^4}$$

$$\text{Pressure loss in runner 3} = \frac{8\eta L_3 xq}{2\pi R_3^4}$$

Thus, equating pressure losses after point J

$$\frac{8\eta L_2 (1 - x)q}{2\pi R_2^4} = \frac{8\eta L_1 xq}{\pi R_1^4} + \frac{8\eta L_3 xq}{2\pi R_3^4}$$

Substituting for x and rearranging to get R_2

$$R_2 = \frac{R_1 R_3^2 \sqrt{2L_2}}{\sqrt{2L_1 R_3^4 + L_3 R_1^4}}$$

For the dimensions given:

$$R_2 = 3.8 \text{ mm}$$

In practice there are a number of other factors to be taken into account. For example, the above analysis assumes that this plastic is Newtonian, i.e. that it has a constant viscosity, η. In reality the plastic melt is non-Newtonian so that the viscosity will change with the different shear rates in each of the three runner sections analysed. In addition, the melt flow into the mould will not be isothermal – the plastic melt immediately in contact with the mould will solidify. This will continuously reduce the effective runner cross-section for the melt coming along behind. The effects of non-Newtonian and non-isothermal behaviour are dealt with in Chapter 5.

Multi-daylight moulds

This type of mould, also often referred to as a three plate mould, is used when it is desired to have the runner system in a different plane from the parting line

of the moulding. This would be the case in a multi-cavity mould where it was desirable to have a central feed to each cavity (see Fig. 4.45). In this type of mould there is automatic degating and the runner system and sprue are ejected separately from the moulding.

Hot runner moulds

The runners and sprues are necessary in a mould but they are not part of the end-product. During the production of small or micro-scale injection moulded parts (e.g. in micro-injection moulding), the volume of plastic used in the runner/sprue system may be many times larger than that of the parts. This wasted material is an unfortunate biproduct of the conventional injection moulding process, but with many plastics it is relatively straightforward to collect this material, regrind it and reintroduce it into the process at the moulding stage. However, the collection and regrinding processes add to the overall manufacturing costs and with some plastics there is a danger that this factory 'regrind' will exhibit inferior properties when compared to the original plastic. Some plastics are susceptible to severe thermal degradation through repeated manufacturing cycles and many others will exhibit a small but steady loss of mechanical properties when reprocessed multiple times. For these reasons a number of systems have been developed to prevent the runners from freezing so that they can be automatically reused on every cycle. This is really a logical extension of three plate moulding and the main systems used are

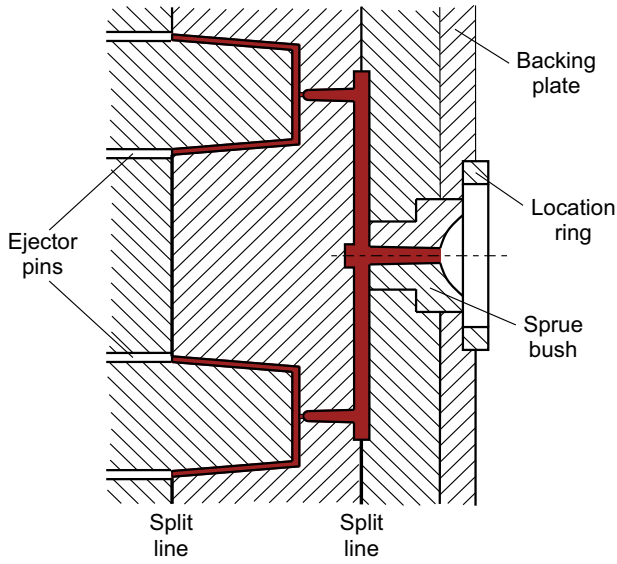


FIG. 4.45 Typical 3-plate mould.

either known as hot runner moulds or insulated runner moulds. In a hot runner mould, strategically placed heaters and insulation isolate a separate mould block containing the runner system from the main cavity block so that the plastic in the runner remains at the injection temperature. During each cycle therefore the component is ejected but the melt in the runner channel is retained and injected into the cavity during the next shot. A typical mould layout is shown in Fig. 4.46.

Additional advantages of hot runner moulds are (i) elimination of trimming and (ii) possibility of faster cycle times because the runner system does not have to freeze off. However, these have to be weighed against the disadvantages of the system. Since the hot runner mould is more complex than a conventional mould it will be more expensive. Also, there are many areas in the hot runner manifold where there is an increased risk of the melt flow stagnating and material can remain trapped from cycle to cycle. This means that problems can be experienced during colour or grade changes because it is difficult to remove all of the previous material. As a practical point it should also be realised that a hot runner system only works as long as the runner remains molten. If the runner system freezes off then the hot runner manifold needs to be dismantled to remove the runners. Note also that hot runner systems are not suitable for heat sensitive materials such as PVC.

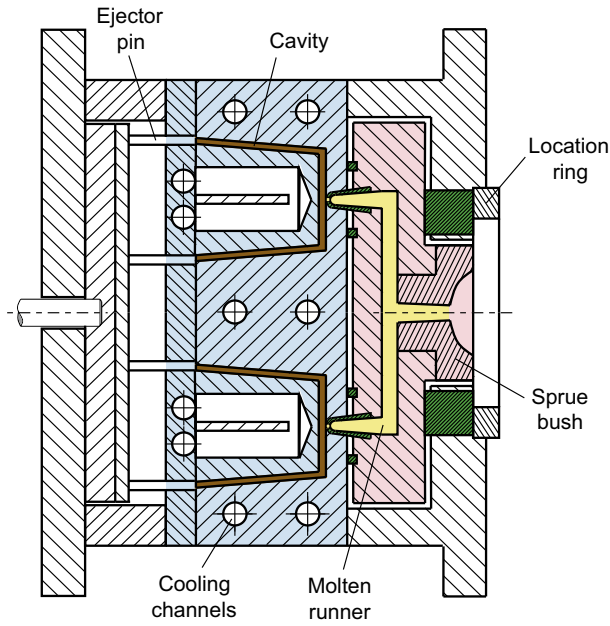


FIG. 4.46 Layout of hot runner mould.

Insulated runner moulds

This is similar in concept to the hot runner mould system. In this case, instead of having a specially heated manifold in the mould, large runners (13−25 mm diameter) are used. The relatively cold mould causes a frozen skin to form in the runner which then insulates its core so that this remains molten. As in the previous case the runner remains in the mould when the moulding is ejected and the molten part of the runner is then injected into the cavity for the next shot. If an undue delay causes the whole runner to freeze off then it may be ejected and when moulding is restarted the insulation layer soon forms again. At the gates heated inserts (often heated by electrical cartridge heaters) are used to prevent the narrow exit to the cavity from freezing over between cycles. This is illustrated in Fig. 4.47. The insulated runner system is widely used for moulding of fast cycling products such as flower pots and disposable goods. The main disadvantage of the system is that it is not suitable for polymers or pigments which have a low thermal stability or high viscosity, as some of the material may remain in a semi-molten form in the runner system for long periods of time. The performance of the system may be enhanced through the insertion of heating tubes along the centres of the runners, which creates what is termed a *distribution tube* runner system.

Mould clamping force

In order to prevent 'flashing', i.e. a thin film of plastic escaping out of the mould cavity at the parting line, it is necessary to keep the mould tightly

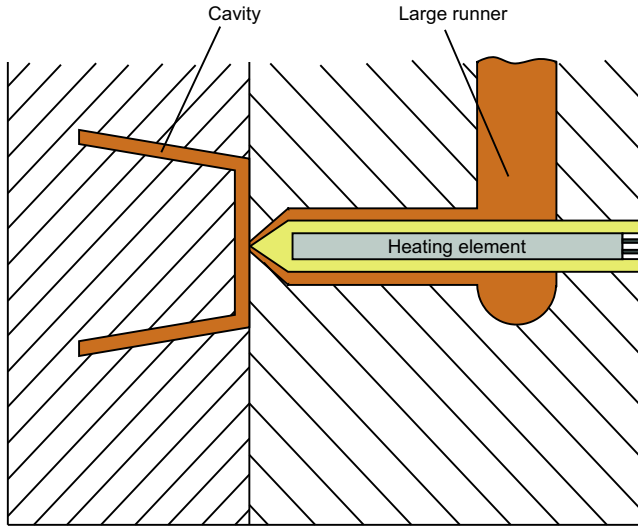


FIG. 4.47 Insulated and distributed runner systems.

closed during injection of the molten plastic. Before setting up a mould on a machine it is always worthwhile to check that there is sufficient clamping force available on the machine. To do this it is necessary to be able to estimate what clamping force will be needed. The relationship between mould area and clamp requirements has occupied the minds of moulders for many years. Practical experience suggests that the clamping pressure over the projected area of the moulding should be between 10 and 50 MPa depending on factors such as shape, thickness, and type of material. The mould clamping force may also be estimated in the following way. Consider the moulding of a disc which is centre gated as shown in Fig. 4.48(a). The force on the shaded element is given by

Force,

$$F = \int_0^R P_r 2\pi r \, dr \tag{4.23}$$

The cavity pressure will vary across the disc and it is necessary to make some assumption about this variation. Experimental studies have suggested that an empirical relation of the form

$$P_r = P_0\left(1 - \left(\frac{r}{R}\right)^m\right) \tag{4.24}$$

is most satisfactory. P_0 is the pressure at the gate and m is a constant which is usually between 0.3 and 0.75. It will be shown later (Chapter 5) that 'm' is in fact equal to $(1 - n)$ where 'n' is the index in the Power Law expression for polymer melt flow.

Substituting (4.24) in (4.23) then

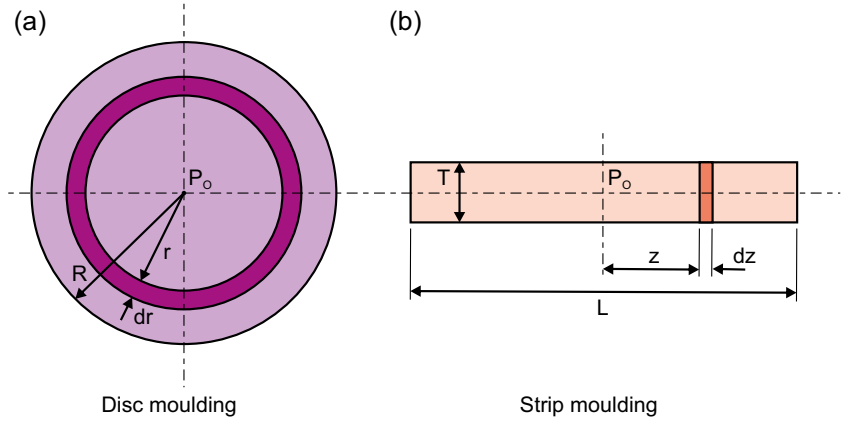


FIG. 4.48 Clamp force analysis.

$$F = \int_0^R P_0\left(1 - \left(\frac{r}{R}\right)^m\right) 2\pi r\, dr$$

$$F = \pi R^2 P_0\left(\frac{m}{m+2}\right) \tag{4.25}$$

This is a simple convenient expression for estimating the clamping force required for the disc. The same expression may also be used for more complex shapes where the projected area may be approximated as a circle. It will also give sufficiently accurate estimates for a square plate when the radius, *R*, in Fig. 4.48(a) is taken as half of the diagonal.

An alternative way of looking at this equation is that the clamping pressure, based on the projected area of the moulding, is given by

$$\text{Clamping pressure} = \left(\frac{m}{m+2}\right) \times \text{Injection pressure}$$

For any particular material the ratio $(m/(m+2))$ may be determined from the flow curves and it will be temperature and (to some extent) pressure dependent.

In practice the clamping pressure will also depend on the geometry of the cavity. In particular the flow ratio (flow length/channel lateral dimension) is important. Fig. 4.49 illustrates typical variations in the Mean Effective Pressure in the cavity for different thicknesses and flow ratios. The data used here is typical for easy flow materials such as polyethylene, polypropylene and polystyrene. To calculate the clamp force, simply multiply the appropriate Mean Effective Pressure by the projected area of the moulding. In practice it is

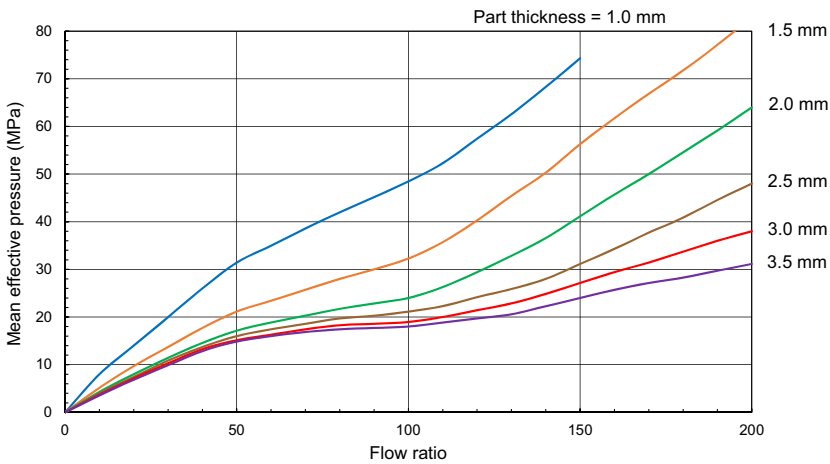


FIG. 4.49 Clamping pressures for different cavity geometries (typical values for easy flow materials).

prudent to increase this value by 10–20% due to the uncertainties associated with specific moulds.

For plastics other than the easy flow materials referred to above, it would be normal to apply a factor to allow for the higher viscosity. Typical viscosity factors are given below.

Material	Viscosity factor
Polyethylene, polypropylene, polystyrene	1
Nylon 66	1.2 → 1.4
ABS	1.3 → 1.4
Acrylic	1.5 → 1.7
PVC	1.6 → 1.8
Polycarbonate	1.7 → 2.0

Example 4.6 The mould shown in Fig. 4.41 produces four cup shaped ABS mouldings. The depth of the cups is 60 mm, the diameter at the is 90 mm and the wall thickness is 1.0 mm. The distance from the sprue to the cavity is 40 mm and the runner diameter is 6 mm. Calculate the clamp force necessary on the moulding machine and estimate how the clamp force would change if the mould was designed so as to feed the cups through a pin gate in the centre of the base (as illustrated in Fig. 4.43). The clamp pressure data in Fig. 4.49 should be used and the taper on the side of the cups may be ignored.

Solution

(a) Within the cavity, the maximum flow length for the plastic melt will be from the gate, along the side of the cup and across the base of the cup, i.e.

$$\text{Flow length} = 60 + 90 = 150 \text{ mm}$$

The thickness of the moulding is 1 mm, hence the flow ratio = 150/1 = 150. From Fig. 4.49 at this thickness and flow ratio, the mean effective pressure is 75 MPa.

Allowing an extra 15% for uncertainties and applying the viscosity factor of 1.4 for ABS, then the appropriate mean effective pressure is $75 \times 1.15 \times 1.4 = 120$ MPa. For each cavity, the projected area is $(\pi/4)(90)^2 = 6360 \text{ mm}^2 = 6.36 \times 10^{-3} \text{ m}^2$.

Hence clamp force per cavity $= 120 \times 6.36 \times 10^{-3} = 763$ kN.

The projected area of the runners is $4 \times 40 \times 6 = 960 \text{ mm}^2$.

Assuming that the mean effective pressure also applies to the runner system, then clamp force for runners $= 120 \times 0.96 \times 10^{-3} = 115$ kN

Hence total clamp force for 4 cavities and 1 runner system is given by

Total clamp force $= (4 \times 763) + 115 = 3167$ kN

The required clamp force is therefore 317 tonnes.

(b) If a pin gate in the middle of the base is used instead of an edge gate, then the flow ratio will be different. In this case

flow length = $^1/_2$ (90) + 60 = 105

This is also the flow ratio, so from Fig. 4.49 the mean effective pressure is 50 MPa. Applying the viscosity factor, etc as above, then

$$\text{Clamp force per cavity} = 50 \times 1.15 \times 1.4 \times \left(\frac{\pi}{4}\right) \cdot (90)^2 \times 10^{-6} = 512 \text{ kN}$$

In this case the runner system will be almost totally in the 'shadow' of the projected area of the cavities and so they can be ignored.

Hence, total clamp force = 4 × 512 = 2048 kN = 205 tonnes.

Another common shape which is moulded is a thin rectangular strip. Consider the centre gated strip as shown in Fig. 4.48(b). In the same way as before the clamping force, *F,* is given by

$$F = 2\int_0^{L/2} P_z T \, dz \tag{4.26}$$

$$F = 2\int_0^{L/2} P_0 \left(1 - \left(\frac{z}{L/2}\right)^m\right) T \, dz$$

i.e.

$$F = TP_0L\left(\frac{m}{m+1}\right) \tag{4.27}$$

The calculation of clamp force is considered in more detail in Chapter 5.

4.3.4 Structural foam injection moulding

Foamed thermoplastic articles have a cellular core with a relatively dense (solid) skin. The foam effect is achieved by the dispersion of inert gas throughout the molten resin directly before moulding. Introduction of the gas is usually carried out either by pre-blending the resin with a chemical blowing agent which releases gas when heated or by direct injection of the gas (usually nitrogen or carbon dioxide).

When the compressed gas/resin mixture is rapidly injected into the mould cavity, the gas expands explosively and forces the material into all parts of the mould.

The advantages of these types of foam moulding are:

(a) for a given weight they are many times more rigid than a solid moulding
(b) they are almost completely free from orientation effects and the shrinkage is uniform
(c) very thick sections can be moulded without sink marks.

Foamed plastic articles may be produced with good results using normal screw-type injection moulding machines (see Fig. 4.50(a)). However, the limitations on shot size, injection speed and platen area imposed by conventional injection equipment have led to the development of specialised foam moulding machines (see Fig. 4.50(b)). In these an injection screw system feeds a separate accumulator which enables greater control of the temperature, pressure and injection speed of the melt as it enters the cavity and the cellular structure is created.

Greater control of the process variables, which is linked to greater understanding of the physics of bubble nucleation, have led to the development of new forms of *microcellular plastics* that are designed to be lightweight alternatives to conventional plastics. In these materials cell structures are tightly controlled to produce billions of individual bubbles with diameters less than 50 μm. This can produce plastics with substantially reduced densities (between 5 and 99% of the original plastic) and enhanced mechanical properties that are much superior to conventional polymer foams. The most recent developments in these technologies are in the production of *nanocellular foams* where the individual bubble diameters are less than 100 nm.

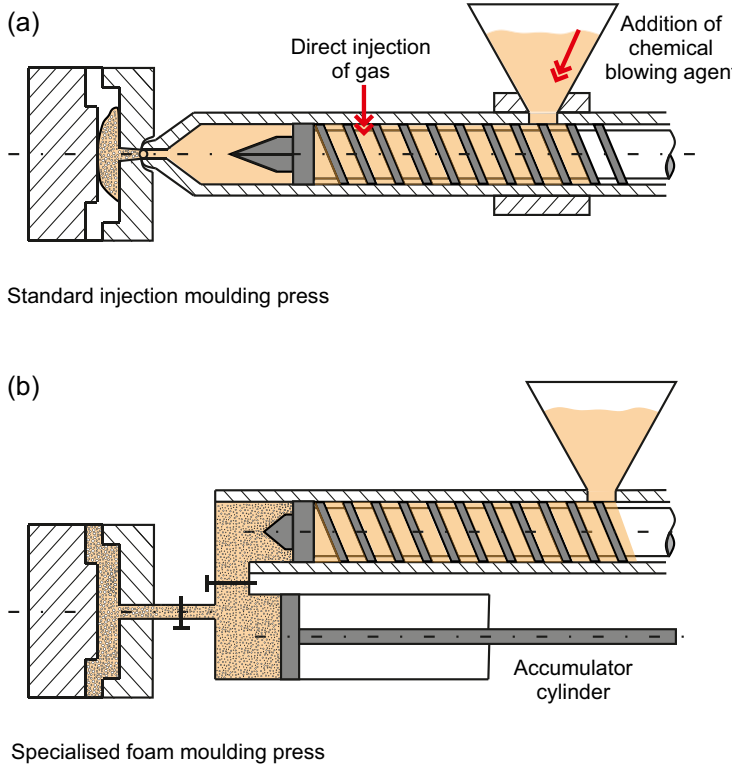


FIG. 4.50 Structural foam moulding equipment.

Wall sections in foam moulding are thicker than in solid material. Longer cycle times can therefore be expected due to both the wall thickness and the low thermal conductivity of the cellular material. In contrast, however, the injection pressures in foam moulding are low when compared with conventional injection moulding. This means that less clamping force is needed per unit area of moulding and tooling costs are less because lower strength mould materials may be used.

4.3.5 Sandwich moulding

This is an injection moulding method which permits material costs to be reduced in large mouldings. In most mouldings it is the outer surface of an article which is important in terms of performance in service. If an article has to be thick in order that it will have adequate flexural stiffness then the material within the core of the article is wasted because its only function is to keep the outer surfaces apart. The philosophy of sandwich moulding is that two different materials (or two forms of the same material) should be used for the core and skin. That is, an expensive high performance material is used for the skin and a low-cost commodity or recycled plastic is used for the core. The way that this can be achieved is illustrated in Fig. 4.51.

Initially the skin material is injected from one cylinder to partly fill the mould, while a second cylinder is being charged with core material (Fig. 4.51(a)). The core material is then injected, and it flows laminarly into the interior of the core (Fig. 4.51(b)). This continues until the cavity is filled as shown in Fig. 4.51(c). At the same time the first cylinder is recharged with skin material. Finally, the nozzle valve rotates so that the skin material is injected into the sprue thereby clearing the valve of core material in preparation for the next shot (Fig. 4.51(d)). In a number of cases the core material is foamed to produce a sandwich section with a thin solid skin and a cellular core.

In most applications of sandwich moulding, it is the skin material that provides the principal functionality of the moulded part (e.g. colour, surface finish, printability etc.) and the interior may be made from an inferior or lower cost material. However, there are applications such as covers or housings for electronics where the requirement to provide electromagnetic interference (EMI) shielding can be satisfied by using a plastic with a high loading of conductive filler (usually carbon black) in the core of the sandwich and an unloaded plastic on the exterior to ensure that a good quality surface/colour can be achieved on the final part.

4.3.6 Assisted injection moulding

The term ‘Assisted’ in relation to injection moulding refers to several process variants that are mostly employed to allow hollow injection moulded parts to be produced. In all cases the normal injection moulding process is assisted by

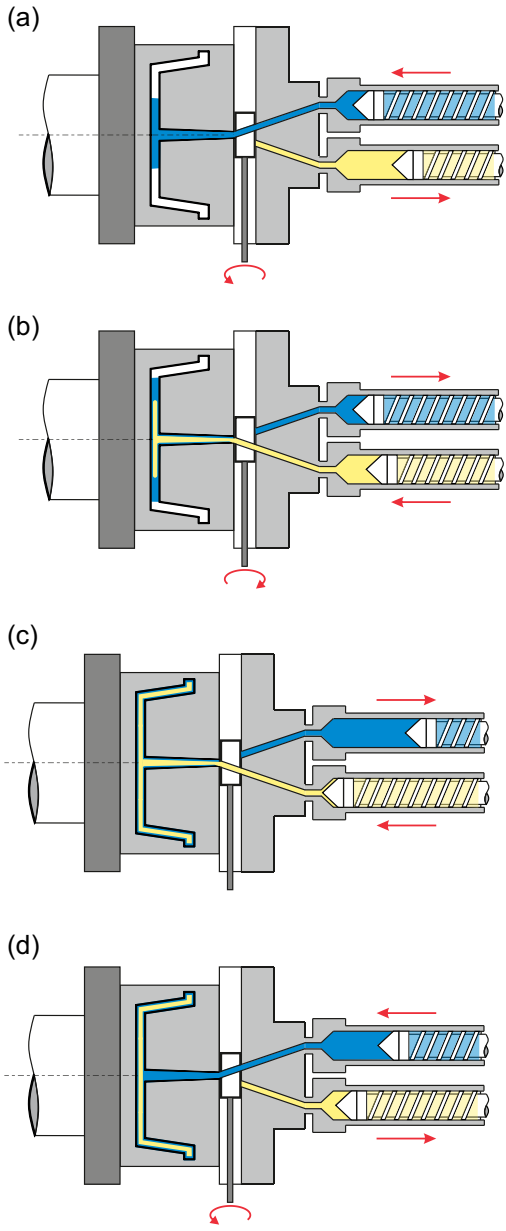


FIG. 4.51 Stages in sandwich moulding process.

the injection of a fluid during the cycle and the principal methods either employ a gas (*Gas-Assisted Injection Moulding* or *Gas Injection Moulding*) or water (*Water-Assisted Injection Moulding* or *Water Injection Moulding*). In the

main process variants, the injection of the fluid during the moulding process hollows out the core of the part with the advantages that the mouldings produced contain less plastic, are faster to cool, have greater stiffness/weight ratios and have reduced moulded-in stresses and distortion.

There are two major forms of Gas-Assisted Injection Moulding:

(1) *Internal Gas Injection* (Fig. 4.52) – This produces hollow injection-moulded parts and it is the most widely used process.
(2) *External Gas Injection* (Fig. 4.53) – This technique employs externally applied gas pressure to create parts with increased surface definition.

In Internal Gas-Assisted Injection Moulding the initial stage of the cycle is the flow of plastic melt into the mould cavity through a standard feed system (Fig. 4.52(a)). However, the plastic injected is only sufficient to partially fill the mould (Fig. 4.52(b)) and at this point pressurised air is introduced into the core of the moulding through a separate air channel (Fig. 2.52(c)). Throughout this process, the pressure at the sprue or gate remains high and, therefore, the gas chooses a natural path through the hotter and less viscous parts of the polymer melt towards the lower pressure areas. The flow of gas cores out a hollow centre extending from its point of entry towards the last point of fill. By controlling the amount of gas injected into the hollow core, the pressure on the cooling polymer is controlled and maintained until the moulding is packed. The final stage is the reversal of the gas flow, prior to mould opening, which allows the gas held in the hollow core to vent. The timing, pressure and speed of the gas injection is critical to the success of the process.

In External Gas-Assisted Injection Moulding the mould cavity is almost fully filled through a standard feed system (Fig. 4.53(a)), but on filling to around 98–99% with melt, air is introduced between the mould wall and moulding on one side of the cavity (Fig. 4.53(b)). This causes the soft moulding to be firmly pressed against the opposite face of the cavity and thereby enhances the level of surface definition achievable on this face.

The gas injection process overcomes many of the limitations of injection mouldings such as moulded-in stress and distortion. These limitations are caused by laminar flow and variation in pressure throughout the moulding. With the gas injection process, laminar flow is considerably reduced and a uniform pressure is maintained. The difficulty of transmitting a very high pressure uniformly throughout a moulding can also cause inconsistent volumetric shrinkage of the polymer, and this leads to isolated surface sink marks. Whilst cycle times are comparable with those of conventional injection moulding, clamping forces are much lower. Also, by using gas to core out the polymer instead of mixing with it, gas-injection overcomes a number of shortcomings of the structural foam process. In particular there are no surface imperfections (caused by escaping gas bubbles in structural foam moulding) and cycle times are lower because thinner sections are being cooled.

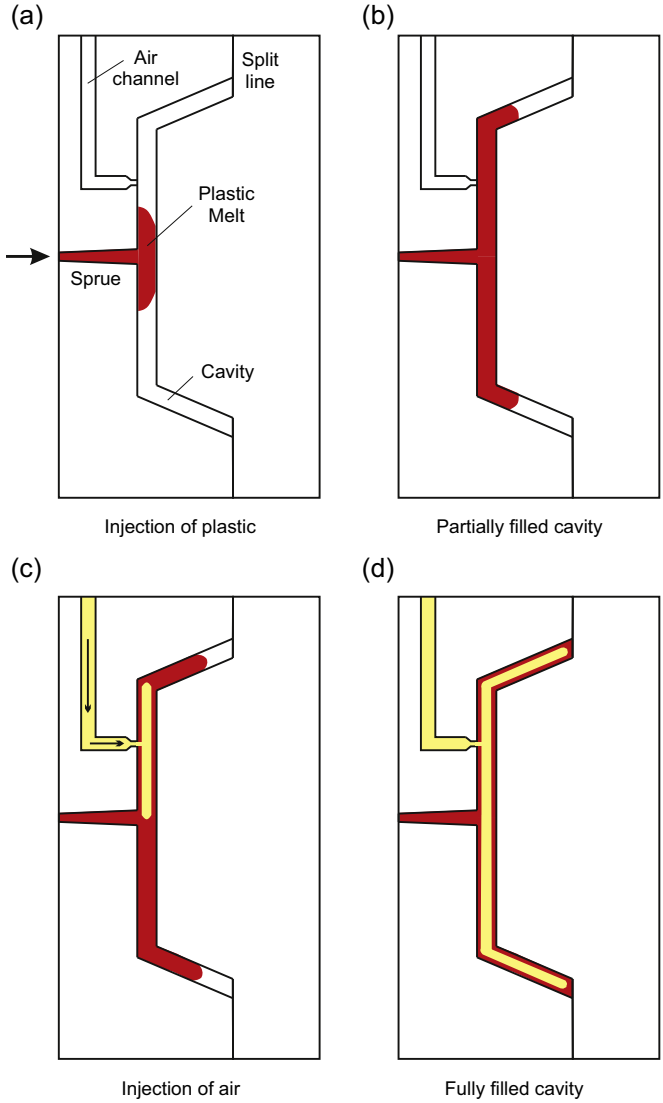


FIG. 4.52 Internal gas-assisted injection moulding.

Water-Assisted Injection Moulding is normally used to produce either hollow or partly hollow plastic parts. The manufacturing process resembles that of Internal Gas-Assisted Injection Moulding (shown in Fig. 4.52), with water replacing air as the internally injected fluid. However, since water is incompressible, the process is easier to control and thinner wall sections may be moulded with better surface definition and less part shrinkage. In addition,

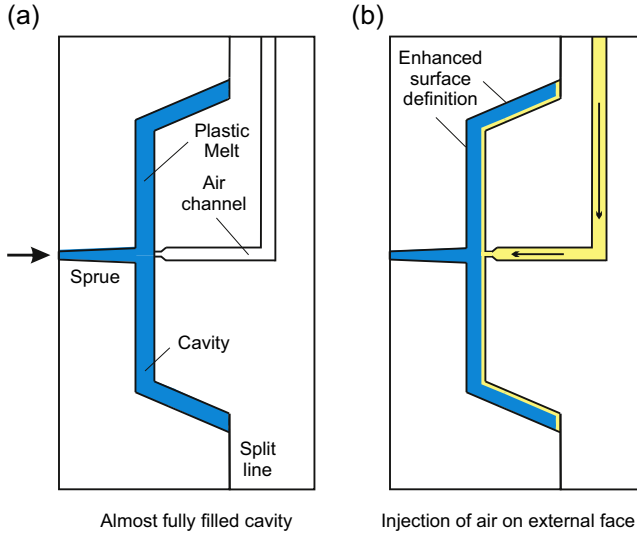


FIG. 4.53 External gas-assisted injection moulding.

water can be used to significantly enhance the internal cooling of the part since its thermal conductivity is around 25 times and its heat capacity around 4 times that of a gas. In all water injection moulding processes provision must be made for the removal of water from the core of the moulding. This can be as simple as employing gravity, but in some cases gas is used to purge water from the core, or it is used in combination with water during the moulding process.

4.3.7 Reaction injection moulding

Specific injection moulding processes have been developed for polymer materials available in the form of liquid reagents. One of the most common of these techniques is *Reaction Injection Moulding* (RIM), where liquid reactants are brought together just prior to being injected into the mould. In-mould polymerisation then takes place which forms the plastic at the same time as the moulding is being produced. In some cases reinforcing fillers are incorporated in one of the reactants and this is referred to as *Reinforced Reaction Injection Moulding* (RRIM).

The basic RIM process is illustrated in Fig. 4.54. A range of plastics lend themselves to the type of fast polymerisation reaction which is required in this process – polyesters, epoxies, nylons and vinyl monomers. However, by far the most commonly used material is polyurethane. The components A and B are an isocyanate and a polyol and these are kept circulating in their separate systems until an injection shot is required. At this point the two reactants are brought together in the mixing head and injected into the mould.

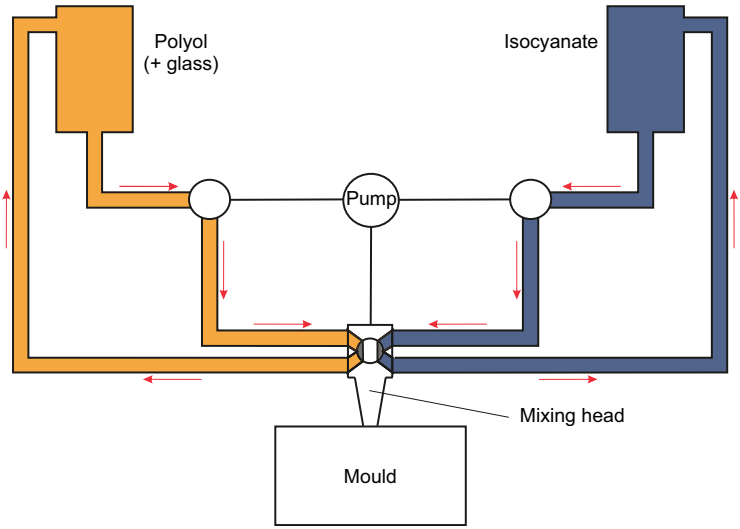


FIG. 4.54 Schematic view of reaction injection moulding.

Since the reactants have a low viscosity, the injection pressures are relatively low in the RIM process. Thus, comparing a conventional injection moulding machine with a RIM machine having the same clamp force, the RIM machine could produce a moulding with a much greater projected area (typically about 10 times greater). Therefore the RIM process is particularly suitable for large area mouldings such as car bumpers and body panels. Another consequence of the low injection pressures is that mould materials other than steel may be considered. Aluminium has been used successfully and this permits weight savings in large moulds. Moulds are also less expensive than injection moulds but they must not be regarded as cheap. RIM moulds require careful design and, in particular, a good surface finish because the expansion of the material in the mould during polymerisation causes every detail on the surface of the mould to be reproduced on the moulding.

4.3.8 Injection blow moulding

In Section 4.2.7 the process of extrusion blow moulding was described and it was mentioned that there are also variants of blow moulding that are derived from the injection moulding process. In both cases the blowing processes are very similar, but what distinguishes them is how the plastic is prepared and presented prior to blowing. In the case of *Extrusion Blow Moulding* (EBM), the plastic is in the form of an extruded (melt phase) preformed shape known as a *Parison* (Fig. 4.24), whereas in *Injection Blow Moulding* (IBM), it is in the form of a reheated (solid phase) injection-moulded part known as a *Preform* (Fig. 4.55). While injection-moulded preforms may simply be reheated and

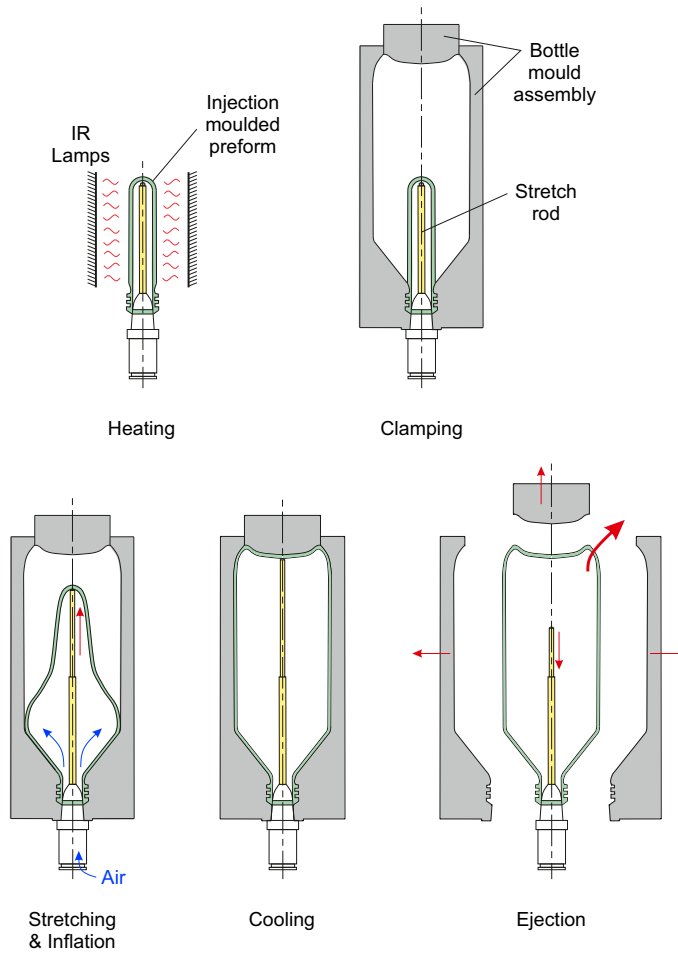


FIG. 4.55 Injection stretch blow moulding process.

inflated by the application of air pressure to form blow-moulded products, nowadays the predominate form of injection blow moulding exploits the capability of the process to induce biaxial orientation in the plastic, and thereby create products with substantially enhanced mechanical properties. This is most evident today in the *Injection Stretch Blow Moulding* (ISBM) of aPET to form a wide range of transparent plastic bottles for the packaging of water and carbonated soft drinks. Such products have now largely replaced glass as a packaging material and are finding ever diverse engineering applications. It is worth noting that aPET is particularly suitable for this form of blow moulding since its mechanical strength can be increased many times by large strain solid phase biaxial stretching. Normally strains greater than 200%

are required, but these are easily attained in processes such as blow moulding and thermoforming.

The main stages in the ISBM process for the manufacture of plastic bottles are illustrated in Fig. 4.55. What is not shown here is the injection moulding of the bottle preform, which is manufactured using a conventional injection moulding process. The preform resembles a standard sized glass test tube but with a threaded top. Injection moulding is particularly important in providing a high quality threaded bottle top at this stage and in the subsequent blowing process this area is deliberately unheated and protected from further deformation. The blowing process begins by reheating the preform to a temperature at which it is soft enough to blow easily in the solid phase. In the case of aPET this is around 110 °C, but with other materials the temperature used may be close to the crystalline melting point of the polymer. Reheating is normally accomplished by passing the preform through a series of infrared (IR) lamps (Fig. 4.55). Once the correct forming temperature is reached the heated preform is moved to the bottle mould where it is clamped. Forming is then completed through a combination of the movement of a mechanical stretch rod that pushes the base of the preform along its axis towards the base of the mould, and the application of air pressure that inflates the preform radially into the walls of the bottle mould. With careful timing of these two actions, the levels of strain and the degrees of biaxial orientation induced in the polymer can be carefully controlled. Once all areas of the inflated preform reach the mould walls, the pressure is maintained to allow the polymer to cool, before the mould is opened and the final bottle is ejected.

The advantages of injection blow moulding are that:

(i) the injection moulded parison may have a carefully controlled wall thickness profile to ensure a uniform wall thickness in the inflated bottle.
(ii) it is possible to have intricate detail in the bottle neck.
(iii) there is no trimming or flash (compared with extrusion blow moulding).

4.3.9 Injection moulding of thermosetting materials

In the early days of injection moulding processing of the thermosetting materials available at the time was deemed to be impractical due to their critical time-temperature relationship and the inherent difficulty of preventing the setting of the thermoset within the barrel. However, through developments in screw and barrel designs and in the stability of thermoset materials at elevated temperatures, many thermosetting materials may now be injection moulded using equipment that largely resembles that employed with thermoplastics. The key differences when comparing standard equipment for injection moulding of thermoplastics to that of thermosets is that the barrel/screw system is shorter and the mould assembly requires heating, rather than cooling, in order to cure the thermosetting resin in the mould. The injection moulding

of fibre reinforced thermosets, such as DMC (Section 4.11.2), is also increasingly common.

Granules or pellets of injection mouldable thermosets are readily available today and they consist of partially polymerised resin, fillers and additives. The formulation of the material is such that it will flow easily in the barrel with a slow rate of polymerisation. The curing is then completed rapidly in the mould. In most respects the process is similar to the injection moulding of thermoplastics and the sequence of operations in a single cycle is as described earlier. For thermosets a special barrel and screw are used. The screw is of approximately constant depth over its whole length and there is no check value which might cause material blockages (see Fig. 4.56). The barrel is only kept warm (80−110 °C) rather than very hot as with thermoplastics because the material must not cure in this section of the machine. Also, the increased viscosity of the thermosetting materials means that higher screw torques and injection pressures (up to 200 MPa are needed).

On the mould side of the machine the major difference is that the mould is maintained at a relatively high temperature (150−200 °C) rather than being cooled as is the case with thermoplastics. This is to accelerate the curing of the material once it has taken up the shape of the cavity. Another difference is that, as thermosetting materials are abrasive and require higher injection pressures, harder steels with extra wear resistance should be used for mould manufacture.

When moulding thermosetting articles, the problem of material wastage in sprues and runners is more severe because these cannot be reused. In many instances it is desirable therefore to keep the sprue and runner sections of the mould cool so that these do not cure with the moulding. They can then be retained in the mould during the ejection stage and then injected into the cavity to form the next moulding. This is analogous to the hot runner system described earlier for thermoplastics.

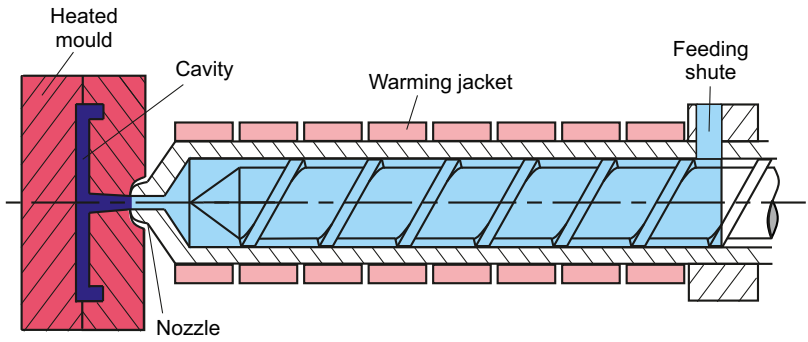


FIG. 4.56 Injection moulding of thermosets and rubbers.

The advantages of injection moulding thermosets are as follows:

(a) fast cyclic times (see Table 4.5)
(b) efficient metering of material
(c) efficient pre-heating of material
(d) thinner flash – easier finishing
(e) lower mould costs (fewer impressions).

4.3.10 Other advanced injection moulding technologies

Over the many decades of research and development in injection moulding, a large number of technological advances have been made that have either adapted the basic injection moulding process for new types of products or have led to significant improvements in the quality of the products produced. Some of the most important of these technologies are described in the following sections.

(a) Micromoulding

Micromoulding is a highly specialised form of injection moulding in which parts are manufactured with either major dimensions or key features that are in the micrometre range. The development of the process reflects the increasing trend towards miniaturisation in many areas of engineering. Micromoulding requires very high precision tooling and closely controlled miniaturised

TABLE 4.5 For the same part, injection moulding of thermosets can offer up to 25% production increase and lower part-costs than compression moulding.

Compression moulding	**Minutes**
Open mould, unload piece	0.105
Mould cleaning	0.140
Close machine, start pressure	0.100
Moulding cycle time	2.230
Total compression cycle	**2.575**
Injection moulding	
Unload piece, open/close machine	0.100
Moulding cycle time	1.900
Total injection cycle	**2.000**

injection systems. Screws of less than 10 mm diameter may be employed, with the plastic supplied in the form of micro-granules. Shot weights in some cases may be less than 0.05 g. However, within a mould block, it is typical that the dimensions of sprues and runners are many times larger than the cavities. In many applications, high performance engineering polymers are often specified, which magnifies the challenges in successful micromoulding.

(b) Overmoulding

Injection Overmoulding is a hybrid moulding process in which injection moulding is used to mould a plastic material around or over another material. It is most familiar in the manufacture of household items such as screwdrivers or saucepans with moulded plastic handles. Here, the metal part is inserted into the injection mould cavity and the plastic is moulded around it (Fig. 4.57). This variant of Overmoulding is known as *Insert Moulding*. However, the process is now finding increasing applications where the overmoulded component is either made from another plastic or from a polymer-based composite. In some cases, the initial part is simply a smaller component that is produced elsewhere by a separate process and then inserted into the mould for overmoulding by a plastic. In other cases, the overmoulded part is completed sequentially in two injection moulding stages. This is illustrated in Fig. 4.58. In this example, the first moulding is made in the conventional way using a two-piece mould. However, rather than ejecting it from the mould, the

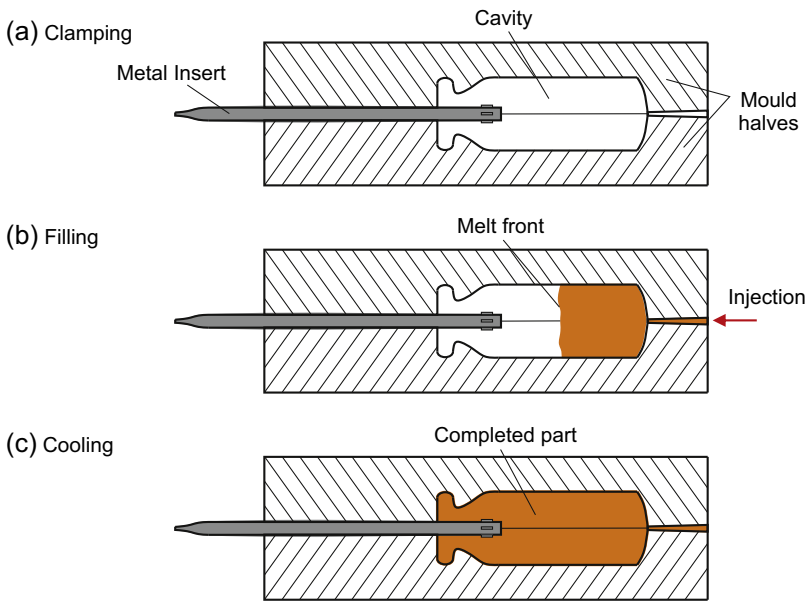


FIG. 4.57 Insert moulding.

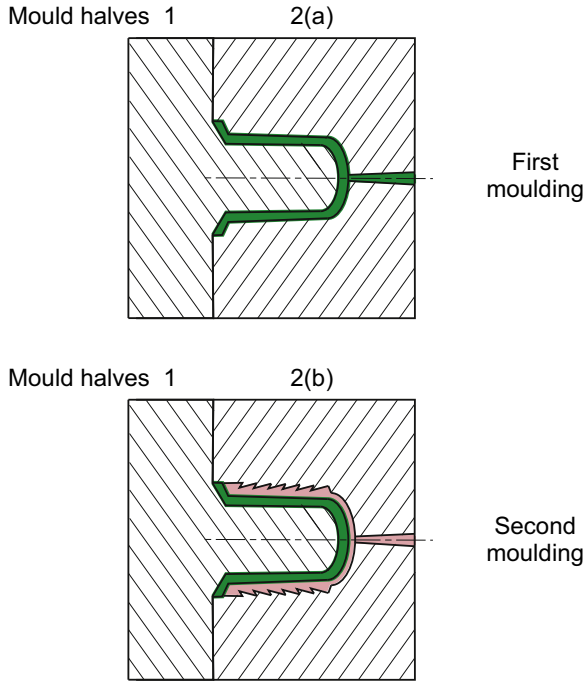


FIG. 4.58 Injection overmoulding.

moulding is retained on the left-hand section of the mould block, while the right-hand section is replaced with an identical block containing a larger cavity. A second injection unit is then used to fill this cavity with another plastic, which overmoulds the original moulding and creates a two plastic structure in the final product. Once cooled the overmoulded part may be ejected from the mould block in the normal way and the cycle repeated. Overmoulding of this type is often used to combine plastics of different colours or hardnesses (e.g. in providing a soft grip handle or an impact absorbing surface on the outside of a product).

(c) In-mould labelling

In-Mould Labelling (or IML) is a technique in which a pre-printed label is inserted into a mould immediately before moulding takes place. In this way fully printed parts may be produced at the end of the moulding process, without the need for a further difficult and expensive printing stage. Printing can be particularly difficult on complex parts and on some types of plastics. In the design of printed parts, it is often necessary to compromise on some design features to provide flat areas that can facilitate a subsequent printing operation. Printing is easiest when the subject surface is flat and therefore with flat labels

it is possible to create some of the highest quality printed images possible on a plastic. Labels may be made from a variety of materials such as paper or plastics that are designed to match those of the plastic being moulded, and vary in thickness from a few hundreds of microns upwards. Although injection moulding is the largest user of IML technologies, it also has major applications in thermoforming and blow moulding processes.

In injection moulding the technique involves inserting the label into the mould cavity immediately after ejection of the part and before the mould closes for the next cycle (Fig. 4.59). The label is designed to fold easily so that it can accurately take the shape of the internal surface of the cavity. Vacuum

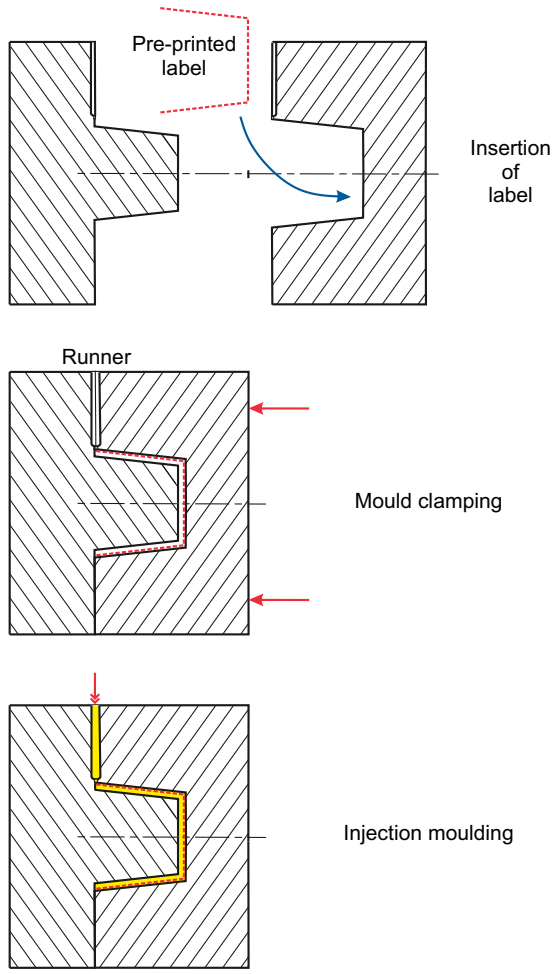


FIG. 4.59 In-mould labelling.

holes or electrostatic charge may sometimes be used to aid the positioning of the label. Although the IML technique is most often associated with food packaging, it is also widely used in technical products where there is a need to label or decorate the surface of a plastic part. In such applications the technique may be referred to as In-Mould Decoration (IMD).

(d) Microcellular injection moulding

Microcellular Injection Moulding is a technique for manufacturing lightweight parts by creating a very fine cellular structure in the injection moulded plastic. Typically foams are produced containing billions of tiny bubbles less than 50 μm in size, although recent research has demonstrated that nanocellular foams (with cell sizes below 100 nm) may also be successfully manufactured. The foam structure is created as a result of homogeneous nucleation that occurs when a single phase solution of polymer and gas is passed from the high pressure of the injection system through the gate into the low pressure environment of mould cavity. By precise control of melt temperature this very rapid pressure drop, ideal conditions are created for widespread, instantaneous bubble nucleation and growth. The gas used is most commonly nitrogen, but sometimes it may be carbon dioxide. This is injected in the form a supercritical fluid (SCF) directly into the polymer melt, where it initially goes into solution. The normal injection moulding system must be modified to accommodate the SCF delivery system and a specially designed mixing screw and gas shut-off nozzle are also required. In addition to manufacturing parts of low density, microcellular moulding requires reduced cavity pressures, and stresses in the mouldings are lower and more evenly distributed. This minimizes part shrinkage and warpage, and may eliminate sink marks. The microcellular technique may also be employed in extrusion and blow moulding processes.

(e) Shear controlled orientation in injection mould (SCORIM)

SCORIM is a technology that employs pulsed pressure through the gates to introduce and control the orientation of the structure (or fillers) in injection moulded products. A special manifold is attached to the machine nozzle as illustrated in Fig. 4.60 and separate pistons are then used to pulse the pressures of the melt entering the gates at either side of the cavity. This induces microscopic shearing stresses at the melt-solid interface during solidification of the polymer within the cavity. In this way the technique may be used to induce alignment within either the polymer or reinforcements, such as fibres, or it may eliminate potential defects such as internal weld lines.

4.4 Thermoforming

When a preformed thermoplastic material is heated it becomes soft and pliable and the techniques for shaping it further in this softened state are known as

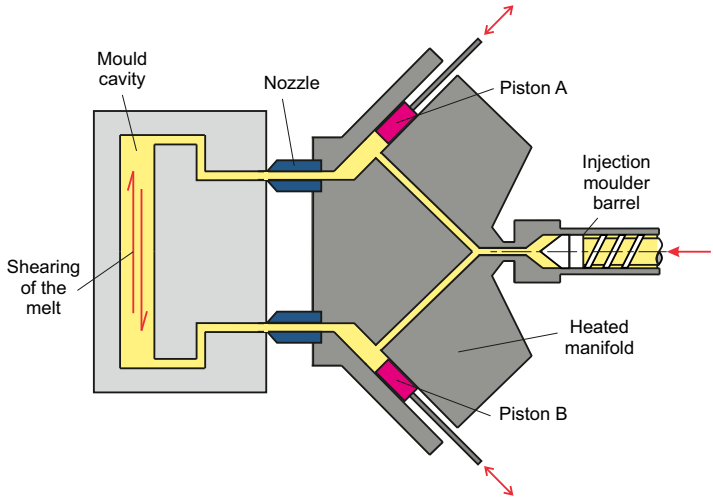


FIG. 4.60 Shear controlled orientation in injection moulding (SCORIM).

thermoforming. It is most often associated with the processing of extruded sheet into a wide variety products, but any starting shape can be thermoformed, provided it is made from a thermoplastic that can be softened by further heating. Thermoforming is therefore a secondary manufacturing process, which relies on a primary process such as extrusion to provide the initial preformed shape for furthering processing. It is also very important to note that most thermoforming processes are carried out whilst the material is in the solid phase. Materials are reheated, but only to a softening temperature, which lies below the melting temperature of the polymer. Temperature ranges (or processing windows) for a number of common polymers are shown in Table 4.6. In most cases the ideal thermoforming temperature range lies between the glass transition temperature (T_g) and the melting temperature (T_m). For amorphous polymers, such as polystyrene or PVC, softening begins once the glass transition temperature is reached and such materials can normally be successfully thermoformed over a broad temperature window above T_g. With semi - crystalline polymers, such as polypropylene, the polymer is only sufficiently soft for thermoforming when it approaches its crystalline melting point. This creates a very narrow thermoforming temperature window, and typically close temperature control is very important when thermoforming polypropylene and other semi-crystalline polymers. In the case of PET, the thermoforming temperature range is dictated by whether the polymer is amorphous (aPET) or semi-crystalline (cPET). With aPET the maximum thermoforming temperature is restricted to 120 °C, since above this temperature the polymer naturally reverts to the crystalline form through a mechanism known as *cold crystallization*.

TABLE 4.6 Thermoforming temperatures for common polymers.

	Temperatures (°C)		
Polymer	Glass transition (T_g)	Melting (T_m)	Ideal thermoforming range (T_{form})
ABS	105	200	140–150
PVC	87	210	110–140
PMMA	105	160	160–180
PS	100	239	135–150
PC	150	265	170–190
LDPE	−110	115	135–145
HDPE	−90	137	130–150
PP	−14	167	155–165
cPET	73	265	135–160
aPET	73	265	90–120
PLA	60	170	90–110

Although modern industrial thermoforming of plastics dates back to the 1950s, early processes suffered from limitations such as poor wall thickness distribution and large peripheral waste and this restricted its use to simple packaging applications. However, there have been major advances in machine design and control systems, and in the diversity of materials available with the result that although packaging is still the major market sector for the process, a wide range of other products are made by thermoforming. These include aerospace and automotive interior panels and displays, refrigerator liners, bath tubs, switch panels, car bumpers, motorbike fairings etc. In the vast majority of thermoforming processes, products are manufactured from a previously extruded sheet. This enables thermoforming to take advantage of extrusion processes such as co-extrusion to create multilayer thermoformed products exhibiting a wide variety of mechanical properties and surface finishes. For example, many thermoformed cups and trays for food packaging are made from multilayer barrier sheet so that the product shelf life may extended from a few days to many months, or even years.

There are a large variety of industrial thermoforming processes that are largely distinguishable by the method used to apply the change in shape to the heated and softened polymer sheet. Force is normally applied either by air pressure or through mechanical contact with a tool surface. These mechanisms

may be carried out either in tandem or in sequence to create more advanced forms of thermoforming. Processes are also categorised according to the starting thickness with those involving sheets thinner than 2.5 mm being known as thin-gauge thermoforming, and those involving sheets of 2.5 mm and above being known as thick-gauge thermoforming. The major variants of the thermoforming process are described in the following sections.

(a) Vacuum forming

This is probably the simplest and best-known variant of thermoforming. A thermoplastic sheet is heated and then shaped by reducing the air pressure between it and a mould, causing the sheet to stretch and contact the mould surface where it cools. The forming pressure is created by drawing a vacuum on the mould side of the sheet, hence giving the process its name. In the simplest type of vacuum forming, illustrated in Fig. 4.61, the heated sheet is drawn down into a female mould cavity and the process is referred to as negative forming. The process begins by heating the sheet (Fig. 4.61(a)). In the majority of thermoforming processes heating is carried by radiation, where banks of heating elements or lamps bathe the sheet in infrared radiation. This gradually raises the temperature of the sheet, but since most of the radiation is absorbed at the sheet's surface, time is needed to enable the heat to transfer evenly through its thickness by conduction. With thicker sheets or high-volume production processes, it is normal to heat the sheet on both sides at the same time by placing banks of heaters above and below the sheet. The heated sheet is then transferred to the forming station where it is placed above the mould and it is firmly clamped around its periphery. This seals the mould cavity so that when it is evacuated, atmospheric pressure presses down from above (Fig. 4.61(b)), pushing the sheet firmly into the surface of the mould where it cools (Fig. 4.61(c)). At the same time air that may become trapped between the bottom of the sheet and the mould surface can escape through carefully positioned vent holes within the mould block. Vent holes are typically less than 0.8 mm in diameter so that they are not visible on the surface of the product.

Wall thickness in vacuum forming is dictated by the proximity of the original sheet from its final position of the mould surface, with areas furthest away stretching and thinning the most in creating the final product. This means that with a normal female mould, vacuum formed parts are quite thin in the base and much thicker in the sidewalls (Fig. 4.61(c)). In practice this means that this form of vacuum forming is normally restricted to products with depths of draw less than 1/3−1/2 of the maximum width, since deeper products are simply too thin in the base to meet design requirements. For some products improvements in the wall thickness distribution may be obtained by changing the female mould to a male mould of the same design. This is shown in Fig. 4.62. In this process, which is known as Drape Vacuum Forming, the sheet

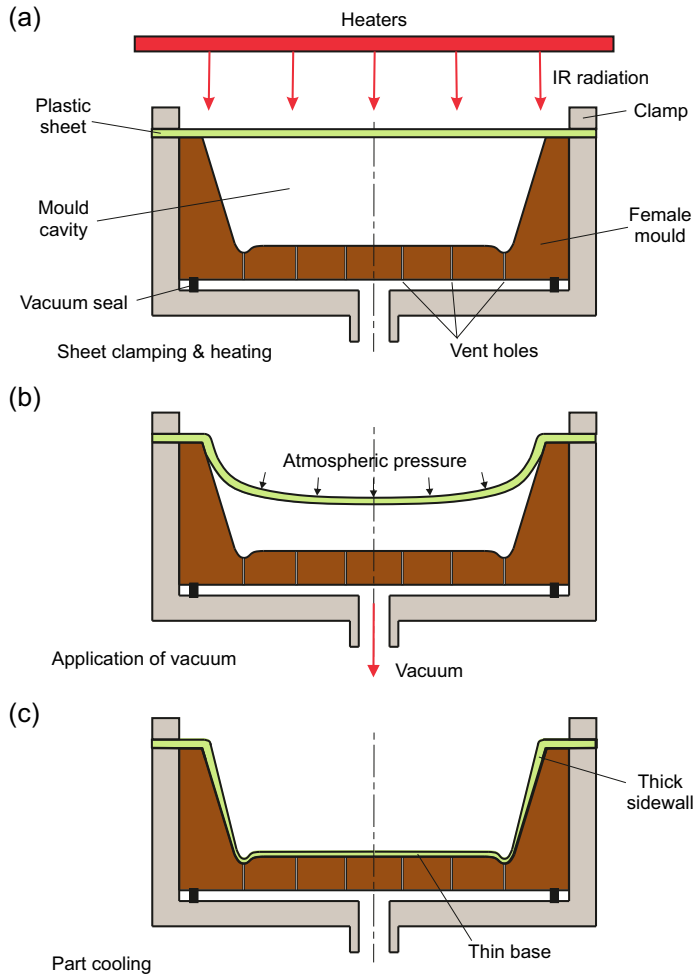


FIG. 4.61 Vacuum forming process.

is heated and clamped above the mould as before (Fig. 4.62(a)), but this time the mould is driven upwards into the sheet (Fig. 4.62(b)), before the vacuum is applied below causing the sheet to become firmly pressed against the surface of the mould (Fig. 4.62(c)). With this arrangement, which may be referred to as positive forming, a very different wall thickness distribution is produced. The middle of the sheet now touches the mould very quickly, and it has little need to stretch, which leaves the product with a thick base. In comparison, the ends of the sheet nearest the clamps must undergo much of the stretching, which creates thin sidewalls. This is almost the opposite the wall thickness distribution seen with the female mould and it illustrates the key role that

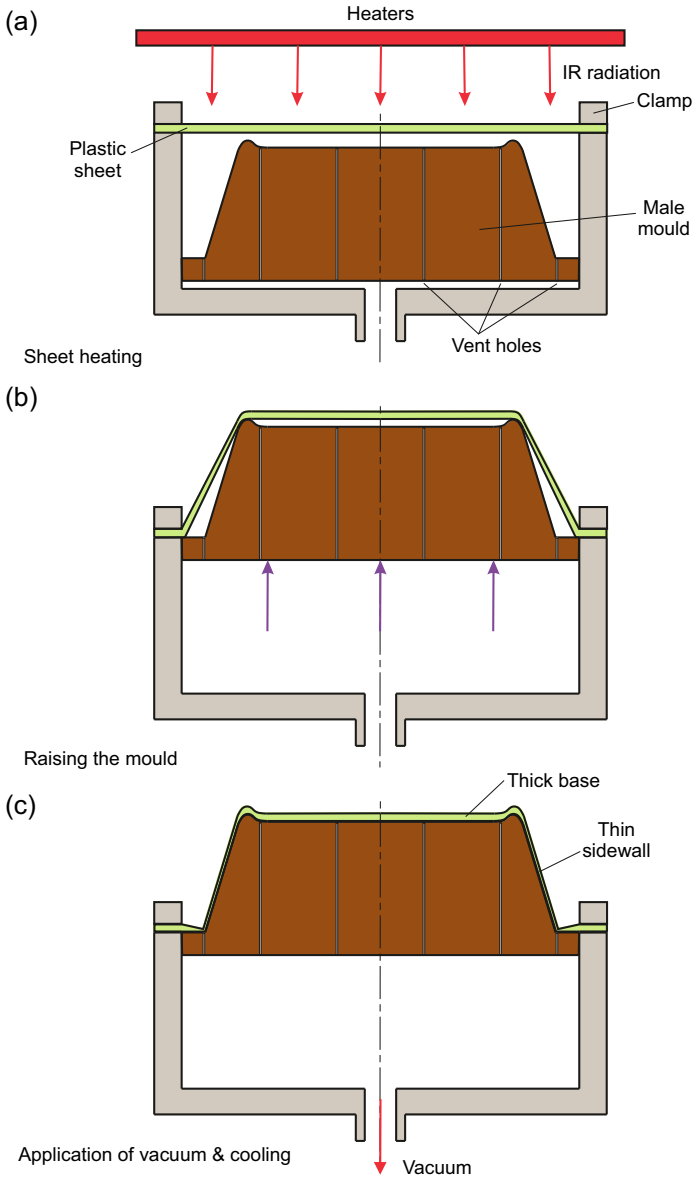


FIG. 4.62 Drape vacuum forming process.

process design plays in thermoforming. With drape forming products with depth to width ratios as high as 1:1 can be successfully produced.

Electrically heated ceramic elements and quartz lamps are the two most common types of infrared heaters used in thermoforming and typically they

have loadings of between 10 and 30 kW/m^2. Normally extra heat is concentrated at the clamped edges of the sheet to compensate for the additional heat losses in this region. The key to successful vacuum forming is achieving uniform heating over the sheet. One of the major attractions of vacuum forming is that since only atmospheric pressure is used to form the soft plastic, the moulds do not have to be very strong. Materials such as plaster, wood and thermosetting resins have all been used successfully, but, in long production runs or where cooling needs to be closely controlled, use of metal moulds becomes essential. Experience has shown that the most satisfactory metal is aluminium, since it is easily shaped, has good thermal conductivity, can be highly polished and has an almost unlimited life.

Materials which can be vacuum formed satisfactorily include polystyrene, ABS, PVC, acrylic, polycarbonate, polypropylene, high and low density polyethylene, aPET, cPET, and PLA. One of the major advantages of thermoforming is that co-extruded sheets of different plastics or different laminate structures may be manufactured. This can be very difficult to achieve with competing technologies such as injection moulding or blow moulding, and it is particularly important for applications such as barrier packaging. Rising demand for thermoplastic composites is also driving interest in thermoforming as a means of shaping these reinforced materials.

(b) Pressure forming

This is generally similar to vacuum forming except that elevated pressure is applied above the sheet rather than simply drawing a vacuum below it. The advantage of this is that higher forces can be used to form the sheet, and typically pressures up to 10 bar are commonly found. This is often necessary when forming thicker gauge sheets due to the extra force required to create clear surface definition, or as a means of reducing cycle times in high volume production of thin gauge products such as packaging. Carefully positioned vent holes are required to ensure that the air trapped below the sheet can escape through the mould, and sometimes the elevated pressure above is combined with a vacuum drawn below to prevent a cushion of air forming below the expanding sheet. A typical system is illustrated in Fig. 4.63 and the key difference from the vacuum forming system is the addition of an upper pressure chamber (or pressure bell) above the sheet, which is heated elsewhere before being brought to the mould assembly for clamping and forming. With higher pressures it is possible to successfully thermoform larger sheet thicknesses or polymers that are stiffer at forming temperatures. This has enabled thermoforming to be increasingly used in applications for larger structural parts such as baths, automotive bumpers and fairings, and a variety of sporting goods such as canoes or kayaks.

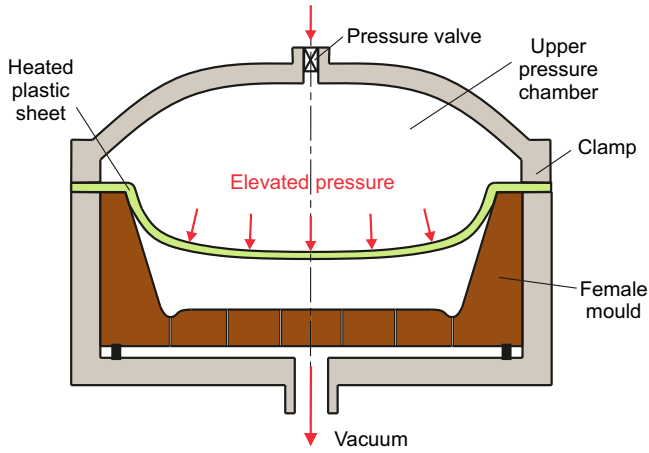


FIG. 4.63 Pressure forming process.

(c) Plug-assisted thermoforming

When the depth of draw of a thermoformed product exceeds its lateral dimensions, it becomes increasingly difficult to achieve an acceptable wall thickness distribution using a mould alone, and a two stage thermoforming process is required. This technique is called *Plug Assisted Forming* and a typical system is illustrated in Fig. 4.64. The process begins by positioning a heated sheet between the two-halves of the mould assembly, which consists of an upper block, containing a rounded, movable forming tool known as a plug, and a lower block containing a matching female mould cavity (Fig. 4.64(a)). The mould halves are then pushed together to clamp the sheet (Fig. 4.64(b)), before the plug is driven mechanically downwards into its surface (Fig. 4.64(c)). Forming is then completed by applying a positive air pressure to the upper cavity and/or a vacuum to the lower cavity, which strip the sheet from the surface of the plug and press it into the surface of the mould cavity (Fig. 4.64(d)). The sheet then cools, the formed part may be trimmed and ejected, and the cycle can be repeated.

The addition of a plug to a thermoforming process severely reduces the stretching capacity of the sheet in contact with its surface and therefore thickness changes largely shift to the remaining areas of free sheet. This has the effect of providing greater balance to the wall thickness distribution, but it is important to note that generally plugs are not designed to entirely capture the sheet in contact. Instead, their rounded shapes and their material properties are deliberately selected to allow the sheet to slide during the period of plug contact. The material properties of most importance are the coefficients of friction between the contacting surfaces and the thermal properties of the plug material (since friction is very temperature dependent). Usually this dictates

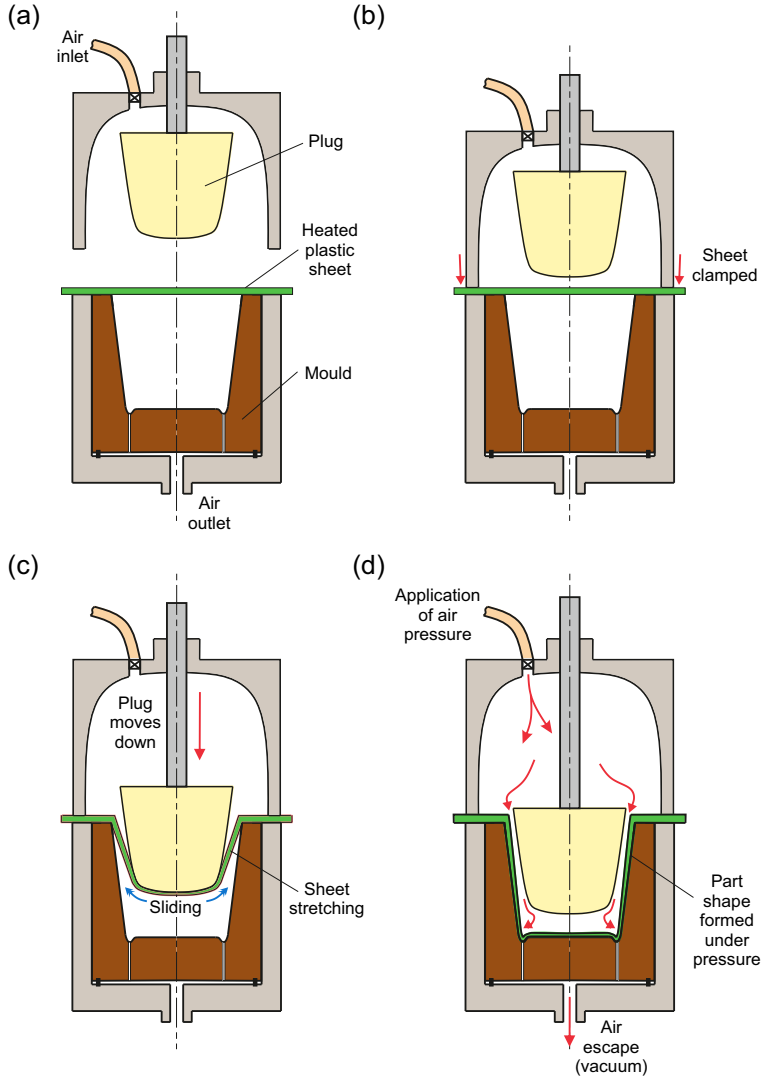


FIG. 4.64 Plug-assisted thermoforming process.

that an ideal plug for a given application is a poor conductor of heat and has a low coefficient of surface friction (i.e. it promotes sliding). In early thermoforming processes materials such as wood or felt were often employed as plugs, but nowadays most plugs are either made from other polymers such as nylon or POM, or from composites such as syntactic foams. The latter consist of either a thermosetting or thermoplastic polymer matrix containing

microspheres of glass or ceramic, and other additives such as PTFE, which are used to modify the thermal and frictional properties of the plug.

Today plug-assisted thermoforming is commonplace, particularly in the high-volume production of food packaging products such as yoghurt pots, fruit punnets or margarine tubs. As a result, over 90% of all thin-gauge thermoforming is plug-assisted and plugs are being increasingly exploited in thick-gauge thermoforming to meet the needs of ever more technically challenging applications. Note that both Positive Forming and Plug Assisted Forming effectively apply a pre-stretch to the plastic sheet which improves the mechanical performance of the material quite apart from the improved wall thickness distribution. Orientation can be very significant in many thermoforming processes since local strains are often well excess of 100% and vary substantially across the plane of the original sheet.

(d) Matched die forming

A variation of thermoforming which does not involve gas pressure or vacuum is matched die forming. The concept is very simple and is illustrated in Fig. 4.65. The plastic sheet is heated to a softened state as described previously and is then sandwiched between two-halves of a matched die set which is designed to fit together with sufficient space for the deformed sheet in between. Very precise detail can be reproduced using this thermoforming technique and importantly surface features are replicated on both sides of the sheet. However, local pressures are much higher with this type of thermoforming so the die sets need to be more robust than the moulds used for the more conventional processes involving gas pressure or vacuum.

(e) Twin-sheet thermoforming

Twin-Sheet (or Dual-Sheet) thermoforming, is a growing process that is essentially a hybrid of blow moulding and thermoforming. Two heated sheets are (a) placed between two mould halves and (b) clamped as shown in Fig. 4.66. Forming (c) takes place by introducing air pressure between the two clamped sheets, so that they are forced to move in opposite directions and into

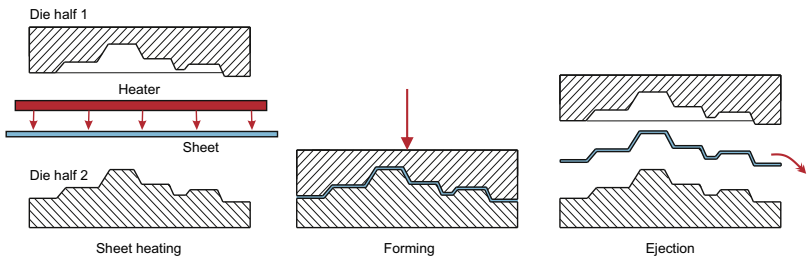


FIG. 4.65 Thermoforming between matched dies.

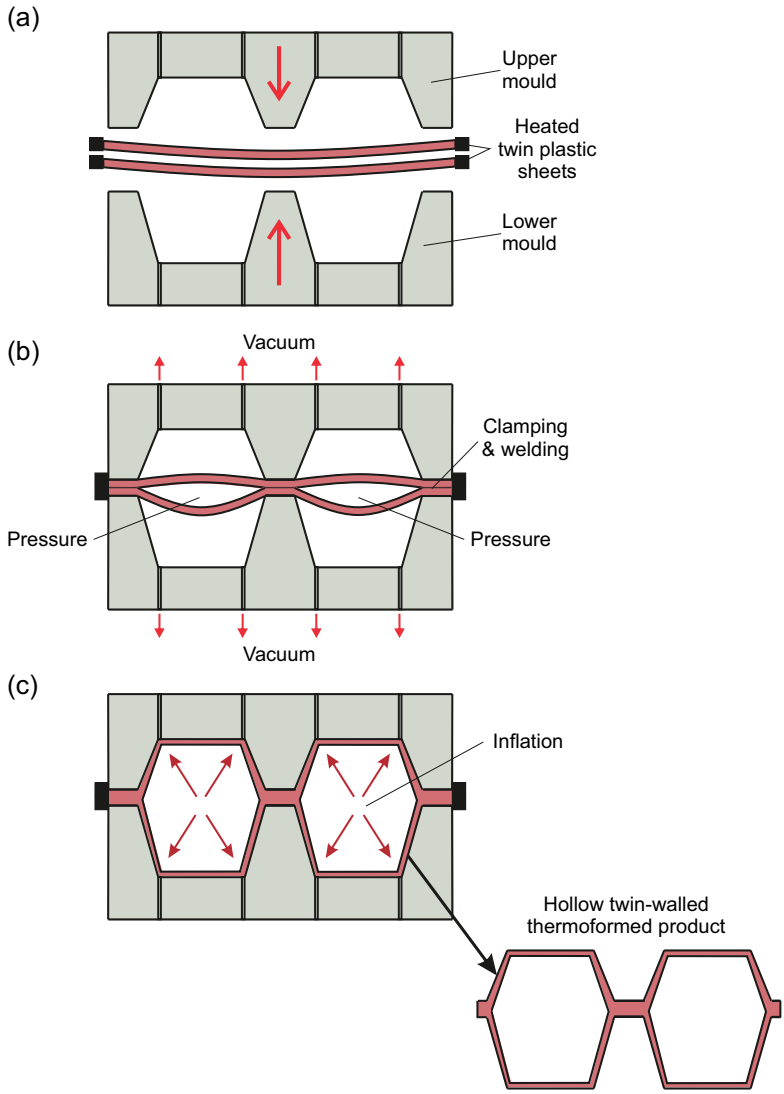


FIG. 4.66 Twin sheet forming.

the surfaces of their respective halves of the mould. This can be achieved by introducing high pressure air through an inflation tube at the parting line, or alternatively, or sometimes simultaneously, by drawing a vacuum between each plastic sheet and the mould in each half of the system. At the same time, the clamped areas of sheet are welded together under the applied clamping pressure. This technique has enabled thermoforming to compete more effectively with blow moulding, injection moulding and rotational moulding in a

number of market sectors. Products are typically double-walled and hollow, and applications include drinks bottles, air ducts, truck bed liners, carrying cases, fuel tanks, electrical enclosures, and pallets. Particular advantages of twin-sheet thermoforming are that the two mould halves can be of quite different shapes and the two plastic sheets can be of different materials. However, care must be taken to ensure that the plastics can produce high strength welds by hot compression.

4.4.1 Analysis of thermoforming

If a thermoplastic sheet is softened by heat and then pressure is applied to one of the sides so as to generate a freely blown surface, it will be found that the shape so formed has a uniform thickness. If this was the case during thermoforming, then a simple volume balance between the original sheet and the final shape could provide the wall thickness of the end product.

$$A_i h_i = A_f h_f \tag{4.28}$$

where A = surface area, and h = wall thickness (the subscripts 'i' and 'f' refer to initial and final conditions).

Example 4.7 A rectangular box 150 mm long, 100 mm wide and 60 mm deep is to be thermoformed from a flat sheet 150 mm × 100 mm × 2 mm. Estimate the average thickness of the walls of the final product if (a) conventional vacuum forming is used and (b) plug assisted thermoforming is used (the plug being 140 mm × 90 mm).

Solution

(a) The initial volume of the sheet is given by

$$A_i h_i = 150 \times 100 \times 2 = 3 \times 10^4 \text{ mm}^3$$

The surface area of the final product is

$$\begin{aligned} A_f &= (150 \times 100) + 2(100 \times 60) + 2(150 \times 60) \\ &= 4.5 \times 10^4 \text{ mm}^2 \end{aligned}$$

Therefore, from Eq. (4.28)

$$h_f = \frac{3 \times 10^4}{4.5 \times 10^4} = 0.67 \text{ mm}$$

(b) If plug assist is used then it could be assumed that over the area 140 mm × 90 mm, the wall thickness will remain at 2 mm. The volume of this part of the moulding will be

$$\text{Vol} = 140 \times 90 \times 2 = 2.52 \times 10^4 \text{ mm}^3$$

This would leave a volume of $(3 \times 10^4 - 2.52 \times 10^4)$ to form the walls. The area of the walls is

$$A_w = (2 \times 100 \times 60) + (2 \times 150 \times 60) = 3 \times 10^4 \text{ mm}^2$$

This ignores a small area in the base of the box, outside the edges of the plug. Hence, the thickness of the walls in this case would be

$$h_w = \frac{(3 \times 10^4) - (2.52 \times 10^4)}{3 \times 10^4} = 0.16 \text{ mm}$$

These calculations can give a useful first approximation of the average dimensions of a thermoformed part. However, they will not be strictly accurate because in a real situation, when the plastic sheet is being stretched down into the cold mould it will freeze off at whatever thickness it has reached when it touches the mould. In addition, in part (b) the solution assumes that there will be no sliding on the surface of the plug, which means that the plug in this case entirely captures the original thickness of the sheet during contact and delivers it to the base of the product. In reality, it is more likely that the plug will be designed to allow the sheet material to stretch across its surface to some degree and thus return some of the wall thickness to the sides of the product.

Consider the thermoforming of a plastic sheet of thickness, h_0, into a conical mould as shown in Fig. 4.67(a). At this moment in time, *t*, the plastic is in contact with the mould for a distance, *S*, and the remainder of the sheet is in the form of a spherical dome of radius, *R*, and thickness, *h*. From the geometry of the mould the radius is given by

$$R = \frac{H - S \sin \alpha}{\sin \alpha \tan \alpha} \tag{4.29}$$

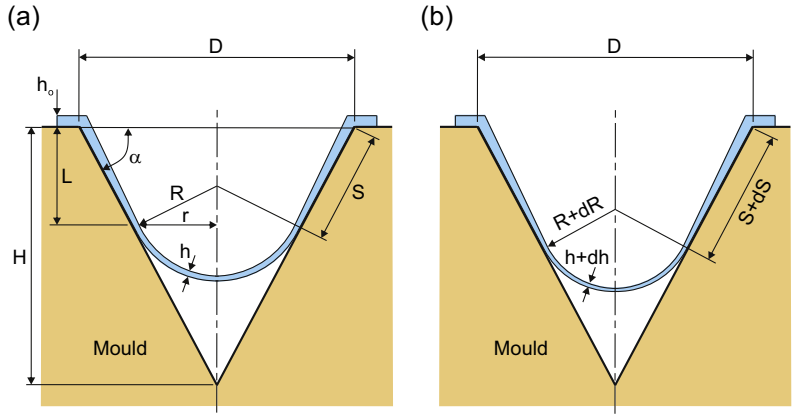


FIG. 4.67 Analysis of thermoforming.

Also the surface area, A, of the spherical bubble is given by

$$A = 2\pi R^2(1 - \cos\alpha) \tag{4.30}$$

At a subsequent time, $(t + dt)$, the sheet will be formed to the shape shown in Fig. 4.67(b). The change in thickness of the sheet in this period of time may be estimated by assuming that the volume remains constant.

$$2\pi R^2(1 - \cos\alpha)h = 2\pi(R + dR)^2(1 - \cos\alpha)(h + dh) + 2\pi r h dS \sin\alpha$$

Substituting for r ($r = R \sin\alpha$) and for R from (4.29) this equation may be reduced to the form

$$\frac{dh}{h} = \left[2 - \left(\frac{\sin^2\alpha \tan\alpha}{1 - \cos\alpha}\right)\right] \cdot \frac{\sin\alpha ds}{(H - S\sin\alpha)} \tag{4.31}$$

This equation may be integrated with the boundary condition that $h = h_1$ at $S = 0$. As a result, the thickness, h, at a distance, S, along the side of the conical mould is given by

$$h = h_1\left(\frac{H - S\sin\alpha}{H}\right)^{\sec\alpha - 1} \tag{4.32}$$

Now consider again the boundary condition referred to above. At the point when the softened sheet first enters the mould it forms part of a spherical bubble which does not touch the sides of the cone. The volume balance is therefore

$$\left(\frac{D^2}{4}\right)h_0 = \frac{2(D/2)^2(1 - \cos\alpha)h_1}{\sin^2\alpha}$$

So,

$$h_1 = \frac{\sin^2\alpha}{2(1 - \cos\alpha)} \cdot h_0$$

Making the substitution for h_1 in (4.32)

$$h = \frac{\sin^2\alpha}{2(1 - \cos\alpha)}\left[\frac{H - S \cdot \sin\alpha}{H}\right]^{\sec\alpha - 1} \cdot h_0 \tag{4.33}$$

or

$$h/h_0 = \left(\frac{1 + \cos\alpha}{2}\right)\left[\frac{H - L}{H}\right]^{\sec\alpha - 1}$$

This equation may also be used to calculate the wall thickness distribution in deep truncated cone shapes but note that its derivation is only valid up to the point when the spherical bubble touches the centre of the base. Thereafter the analysis involves a volume balance with freezing-off on the base and sides of the cone.

Example 4.8 A small flower pot as shown in Fig. 4.68 is to be thermoformed using negative forming from a flat plastic sheet 2.5 mm thick. If the diameter of the top of the pot is 70 mm, the diameter of the base is 45 mm and the depth is 67 mm estimate the wall thickness of the pot at a point 40 mm from the top. Calculate also the draw ratio for this moulding.

Solution

(a) $\alpha = \tan^{-1}\left(\dfrac{67}{12.5}\right) = 79.4°$

Using the terminology from Fig. 4.67(a)
$H = 35 \tan \alpha = 187.6$ mm
From Eq. (4.33)

$$h/h_0 = \left(\frac{1 + \cos 79.4°}{2}\right)\left(\frac{187.6 - 40}{187.6}\right)^{(\sec 79.4)-1} = 0.203$$

$$h = 0.203 \times 2.5 = 0.51 \text{ mm}$$

(b) The *draw-ratio* for a thermoformed moulding is the ratio of the area of the product to the initial area of the sheet. In this case therefore

$$\text{Draw ratio} = \frac{\pi\sqrt{\left[(R-r)^2 + h^2\right](R+r) + \pi r^2}}{\pi R^2}$$

$$= \frac{\pi\sqrt{\left[(35-22.5)^2 + 67^2\right](35+22.5) + \pi(22.5)^2}}{\pi(35)^2}$$

$$= 3.6$$

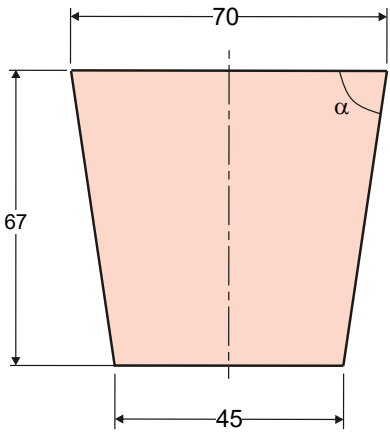


FIG. 4.68 Thermoformed flower pot.

4.5 Calendering

Calendering is a method of producing plastic film and sheet by squeezing the plastic through the gap (or 'nip') between two counter-rotating cylinders. The art of forming a sheet in this way can be traced to the paper, textile and metal industries. The first development of the technique for polymeric materials was in the middle 19th century when it was used for mixing additives into rubber. The subsequent application to plastics was not a complete success because the early machines did not have sufficient accuracy or control over such things as cylinder temperature and the gap between the rolls. Therefore, acceptance of the technique as a viable production method was slow until the 1930s when special equipment was developed specifically for the new plastic materials. As well as being able to maintain accurately roll temperature in the region of 200 °C these new machines had power assisted nip adjustment and the facility to adjust the rotational speed of each roll independently. These developments are still the main features of modern calendering equipment.

Calenders vary in respect of the number of rolls and of the arrangement of the rolls relative to one another. One typical arrangement is shown in Fig. 4.69 – the inverted L-type. Although the calendering operation as illustrated here looks very straightforward it is not quite as simple as that. In the production plant a lot of ancillary equipment is needed in order to prepare the plastic material for the calendar rolls and to handle the sheet after the calendering operation. A typical sheet production unit would start with premixing of the polymer, plasticiser, pigment, etc. in a ribbon mixer followed by gelation of the premix in a Banbury

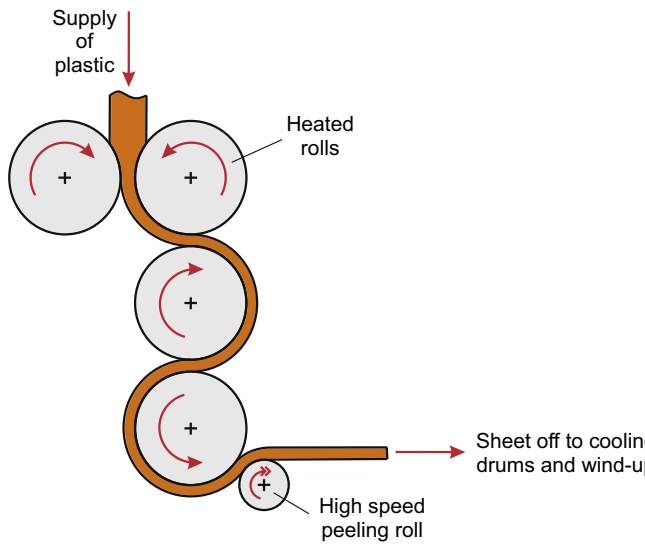


FIG. 4.69 Typical arrangement of calendar rolls.

Mixer and/or a short screw extruder. At various stages, strainers and metal detectors are used to remove any foreign matter. These preliminary operations result in a material with a dough-like consistency which is then supplied to the calendar rolls for shaping into sheets.

However, even then the process is not complete. Since the hot plastic tends to cling to the calendar rolls it is necessary to peel it off using a final high speed roll of smaller diameter located as shown in Fig. 4.69. When the sheet leaves the calendar it passes between embossing rolls and then on to cooling drums before being trimmed and stored on drums. For thin sheets the speed of the winding drum can be adjusted to control the drawdown. Outputs vary in the range 0.1−2 m/s depending on the sheet thickness.

Calendering can achieve surprising accuracy on the thickness of a sheet. Typically the tolerance is ±0.005 mm but to achieve this it is essential to have very close control over roll temperatures, speeds and proximity. In addition, the dimensions of the rolls must be very precise. The production of the rolls is akin to the manufacture of an injection moulding tool in the sense that very high machining skills are required. The particular features of a calendar roll are a uniform specified surface finish, minimal eccentricity and a special barrel profile ('crown') to compensate for roll deflection under the very high pressures developed between the rolls.

Since calendering is a method of producing sheet/film it must be considered to be in direct competition with extrusion-based processes. In general, film blowing and die extrusion methods are preferred for materials such as polyethylene, polypropylene and polystyrene but calendering has the major advantage of causing very little thermal degradation and so it is widely used for heat sensitive materials such as PVC.

4.5.1 Analysis of calendering

A detailed analysis of the flow of molten plastic between two rotating rolls is very complex but fortunately sufficient accuracy for many purposes can be achieved by using a simple Newtonian model. The assumptions made are that

(a) the flow is steady and laminar
(b) the flow is isothermal
(c) the fluid is incompressible
(d) there is no slip between the fluid and the rolls.

If the clearance between the rolls is small in relation to their radius then at any section x the problem may be analysed as the flow between parallel plates at a distance h apart. The velocity profile at any section is thus made up of a drag flow component and a pressure flow component.

For a fluid between two parallel plates, each moving at a velocity V_d, the drag flow velocity is equal to V_d. In the case of a calendar with rolls of radius, R, rotating at a speed, N, the drag velocity will thus be given by $2\pi RN$.

The velocity component due to pressure flow between two parallel plates has already been determined in Section 4.2.3(b).

$$V_p = \frac{1}{2\eta}\frac{dP}{dx}\left(y^2 - (h/2)^2\right)$$

Therefore, the total velocity at any section is given by

$$V = V_d + \frac{1}{2\eta}\frac{dP}{dx}\left[y^2 - (h/2)^2\right]$$

Considering unit width of the calendar rolls the total throughput, Q, is given by

$$\begin{aligned} Q &= 2\int_0^{h/2} V dy \\ &= 2\int_0^{h/2}\left[V_d + \frac{1}{2\eta}\frac{dP}{dx}\left(y^2 - (h/2)^2\right)\right]dy \\ &= h\left(V_d - \frac{h^2}{12\eta}\frac{dP}{dx}\right) \end{aligned} \tag{4.34}$$

Since the output is given by V_dH
then

$$V_dH = h\left(V_d - \frac{h^2}{12\eta}\frac{dP}{dx}\right) \tag{4.35}$$

From this it may be seen that $\frac{dP}{dx} = 0$ at $h = H$.

To determine the shape of the pressure profile it is necessary to express h as a function of x. From the equation of a circle it may be seen that

$$h = H_0 + 2\left(R - \left(R^2 - x^2\right)^{1/2}\right) \tag{4.36}$$

However, in the analysis of calendering this equation is found to be difficult to work with and a useful approximation is obtained by expanding $(R^2 - x^2)^{1/2}$ using the binomial series and retaining only the first two terms. This gives

$$h = H_0\left(1 + \frac{x^2}{H_0R}\right) \tag{4.37}$$

Therefore, as shown earlier dP/dx will be zero at

$$H = H_0\left(1 + \frac{x^2}{H_0R}\right)$$

$$x = \pm\sqrt{(H - H_0)R} \tag{4.38}$$

This gives a pressure profile of the general shape shown in Fig. 4.70. The value of the maximum pressure may be obtained by rearranging (4.35) and substituting for h from (4.37)

$$\frac{dP}{dx} = \frac{12\eta V_d\left(H_0 - H + \dfrac{x^2}{R}\right)}{\left(H_0 + \dfrac{x^2}{R}\right)^3} \tag{4.39}$$

If this equation is integrated and the value of x from (4.38) substituted, then the maximum pressure may be obtained as

$$P_{\max} = \frac{3\eta V_d}{H_0}\left(2\omega - \frac{(4H_0 - 3H)}{H_0}\left(\omega + \sqrt{\frac{R}{H_0}}\tan^{-1}\sqrt{\left(\frac{H - H_0}{H}\right)}\right)\right) \tag{4.40}$$

where

$$\omega = \frac{\sqrt{(H - H_0)R}}{H} \tag{4.41}$$

Example 4.9 A calender having rolls of diameter 0.4 m produces plastic sheet 2 m wide at the rate of 1300 kg/h. If the nip between rolls is 10 mm and the exit velocity of the sheet is 0.01 m/s estimate the position and magnitude of the

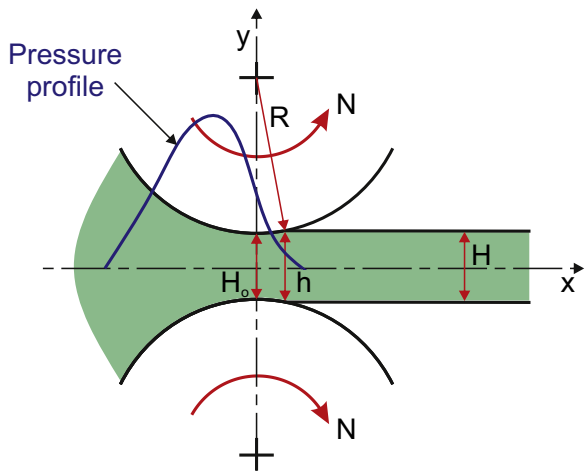


FIG. 4.70 Melt flow between calender rolls.

maximum pressure. The density of the material is 1400 kg/m^3 and its viscosity is 10^4 Pa·s.

Solution

Flow rate, $Q = 1300$ kg/h $= 0.258 \times 10^{-3}$ m^3/s

but $Q = HWV_d$, where $W =$ width of sheet

So

$$H = \frac{0.258 \times 10^{-3}}{2 \times 0.01} = 12.9 \text{ mm}$$

The distance upstream of the nip at which the pressure is a maximum is given by Eq. (4.38)

$$x = \sqrt{(12.9 - 10) \times 200} = 24.08 \text{ mm}$$

Also from (4.37)

$$P_{\max} = \frac{3 \times 10^4 \times 0.01}{10 \times 10^{-3}} \{(2 \times 1.865) - 0.13[1.865 + (4.45)(0.494)]\}$$
$$= 96 \text{ kPa}$$

4.6 Rotational moulding

Rotational moulding, like blow moulding, is used to produce hollow plastic articles. However, the principles in each method are quite different. In rotational moulding a carefully weighed charge of plastic powder is placed in one-half of a metal mould. The mould halves are then clamped together and heated in an oven. During the heating stage the mould is rotated about two perpendicular axes. After a time the plastic will be sufficiently softened to form a homogeneous layer on the surface of the mould. The latter is then cooled while still being rotated. The final stage is to take the moulded article from the mould.

The process was originally developed in the 1940s for use with vinyl plastisols in liquid form. It was not until the 1950s that polyethylene powders were successfully moulded in this way. Nowadays a range of materials such as nylon, polycarbonate, ABS, high impact polystyrene and polypropylene can be moulded but by far the most common material is polyethylene.

The process is attractive for a number of reasons. Firstly, since it is a low pressure process the moulds are generally simple and relatively inexpensive. Also, the moulded articles can have a very uniform thickness, can contain reinforcement, are virtually strain free and their surface can be textured if desired. The use of rotational moulding is now very firmly established in industry because although the cycle times are slow compared with injection or blow moulding, it can produce very large, thick walled articles which could not be produced economically by any other technique. Wall thicknesses of 10 mm are not a problem for rotationally moulded articles.

There is a variety of ways in which the cycle of events described above may be carried out. For example, in some cases (particularly for very large articles) the whole process takes place in one oven. However, a more common set-up is illustrated in Fig. 4.71. The mould is on the end of an arm which is initially charged with a pre-determined weight of polymer powder in the Charging area (1) before being carried into a heated oven (2). During heating the mould rotates about the arm (major) axis and also about its own (minor) axis (see Fig. 4.72). After a pre-set time in the oven the arm brings the mould into a cooling chamber (3). The rate of cooling is very important. Clearly, fast cooling is desirable for economic reasons but this may cause problems such as

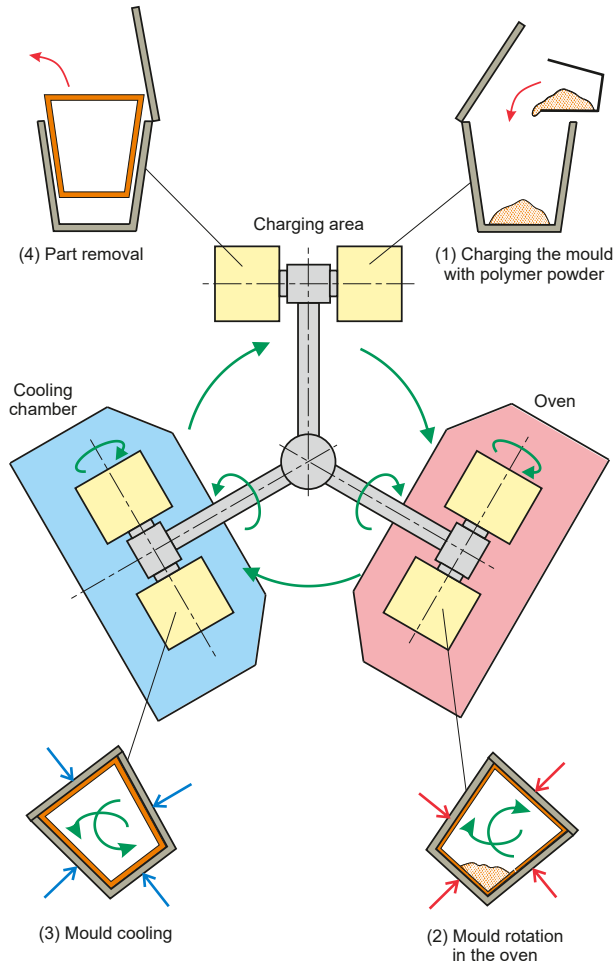


FIG. 4.71 Typical rotational moulding process.

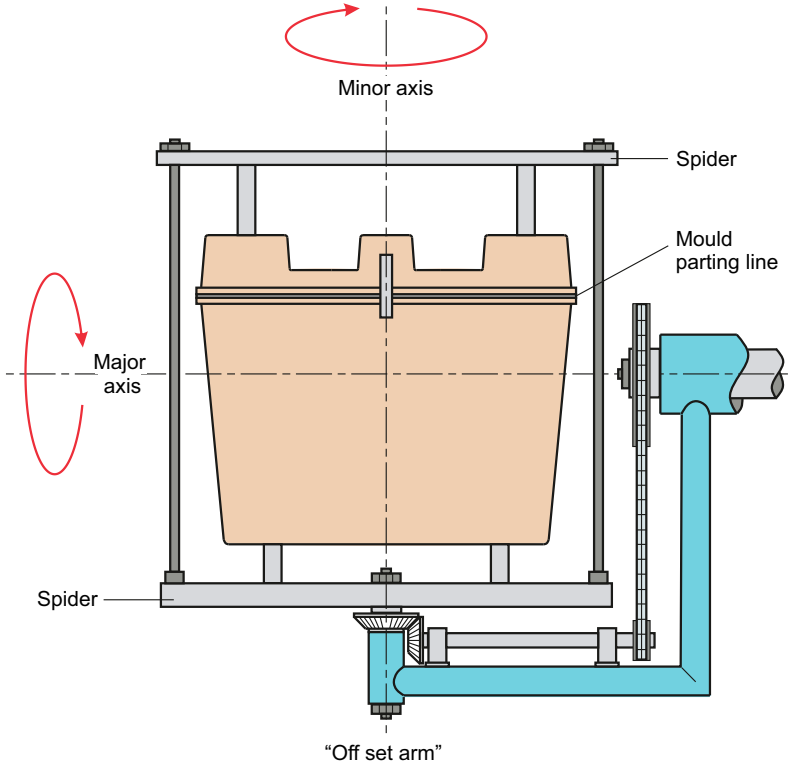


FIG. 4.72 Typical 'off-set arm' rotation.

warping. Normally therefore the mould is initially cooled using blown air and this is followed by a water spray. The rate of cooling has such a major effect on product quality that even the direction of the air jets on the mould during the initial gradual cooling stage can decide the success or otherwise of the process. On the completion of cooling the mould is returned to the Charging area, where it is opened, the moulded part is removed and the mould is recharged ready for the next cycle. As shown in Fig. 4.71 there are normally three arms (mould holders) in a complete system so that as one is being heated another is being cooled and so on. In many machines the arms are fixed rigidly together and so the slowest event (heating, cooling or charging/discharging) dictates when the moulds progress to the next station. In some modern machines, the arms are independent so that if cooling is completed then that arm can leave the cooling bay whilst the other arms remain in position.

It is important to realise that rotational moulding is not a centrifugal casting technique. The rotational speeds are generally below 20 rev/min with the ratio of speeds about the major and minor axes being typically 4 to 1. Also, since all mould surfaces are not equidistant from the centre of rotation any

centrifugal forces generated would tend to cause large variations in wall thickness. In fact, in order to ensure uniformity of wall thickness it is normal design practice to arrange that the point of intersection of the major and minor axis does not coincide with the centroid of the mould.

The heating of rotational moulds may be achieved using infra-red, hot liquid, open gas flame or hot-air convection. However, the latter method remains the most common. Nevertheless new techniques are also emerging that employ in-built electrical heaters within the mould, and these are gaining interest due to their high levels of programmability and control compared to the traditional heating methods.

In a typical rotational moulding process the oven temperature is usually in the range 250−450 °C and since the mould is cool when it enters the oven it takes a certain time to get up to a temperature which will melt the plastic. This time may be estimated as follows.

When the mould is placed in the heated oven, the heat input (or loss) per unit time must be equal to the change in internal energy of the material (in this case the mould).

$$hA(T_0 - T) = \rho C_p V \left(\frac{dT}{dt}\right) \tag{4.42}$$

where

h is the convective heat transfer coefficient
A is the surface area of mould
T_0 is the temperature of the oven
T_t is the temperature of the mould at time t
ρ is the density of the mould material
C_p is the specific heat of the mould material
V is the volume of the walls of the mould
and t is time

Rearranging this equation and integrating then

$$hA\int_0^t dt = \rho C_p V \int_{T_i}^{T_t} \frac{dT}{(T_0 - T)}$$

$$hAt = -\rho C_p V log_e \left(\frac{T_0 - T_t}{T_0 - T_i}\right)$$

$$\left(\frac{T_0 - T_t}{T_0 - T_i}\right) = e^{-\frac{h\beta t}{\rho C_p}} \tag{4.43}$$

where T_i is the initial temperature of the mould and β is the surface area to volume ratio (A/V).

This equation suggests that there is an exponential rise in mould temperature when it enters the oven, and in practice this is often found to be the case. Fig. 4.73 illustrates typical temperature profiles during the rotational moulding of polyethylene. With typical values of oven temperatures and data for an aluminium mould

$$T_0 = 300^\circ\text{C}, \quad T_i = 30^\circ\text{C}, \quad T_t = 20^\circ\text{C}$$

$$\text{h} = 22\ \text{W/m}^2\text{K} \quad C_p = 917\ \text{J/kg K}, \quad \rho = 2700\ \text{kg/m}^3$$

then for an aluminium cube mould 330 mm side and 6 mm thick, as was used to produce Fig. 4.73 then

$$t = \frac{-\rho C_p}{\beta h}\log_e\left\{\frac{T_o - T_t}{T_o - T_i}\right\} = \frac{-2700 \times 917}{1000 \times 22}\log_e\left\{\frac{330 - 220}{330 - 30}\right\} t = 1.9\ \text{min}$$

For a steel mould of the same dimensions and thickness, a quick calculation ($h = 11$ W/m^{2}K, $C_p = 480$ J/kg K and $p = 7850$ kg/m^3) shows that the steel mould would take three times longer to heat up. However, in practice, steel moulds are less than a third of the thickness of aluminium. Therefore, although aluminium has a better thermal conductivity, steel moulds tend to heat up more quickly because they are thinner.

It is important to note that the above calculation is an approximation for the time taken to heat the mould to any desired temperature. Fig. 4.73 shows that in practice it takes considerably longer for the mould temperature to get to 220 °C. This is because although initially the mould temperature is rising at the rate predicted in the above calculation, once the plastic starts to melt, it absorbs a significant amount of the thermal energy input.

Fig. 4.73 illustrates that the mould temperature is quite different from the set oven temperature (330 °C) or indeed the actual oven temperature,

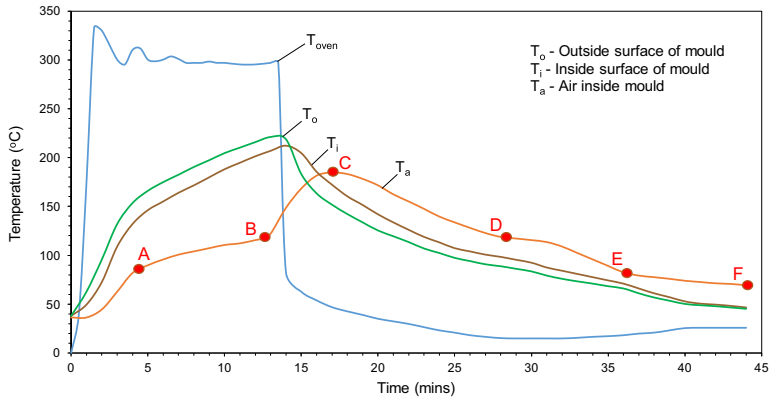


FIG. 4.73 Temperature profiles during rotational moulding.

throughout the moulding cycle. An even more important observation is that in order to control the rotational moulding process it is desirable to monitor the temperature of the air inside the mould. This is possible because there is normally a vent tube through the mould wall in order to ensure equal pressures inside and outside the mould. This vent tube provides an easy access for a thermocouple to measure the internal air temperature.

The internal air temperature characteristic has a unique shape which shows clearly what is happening at all stages throughout the process. Up to point A in Fig. 4.73 there is simply powder tumbling about inside the mould. At point A the mould has become sufficiently hot that plastic starts to melt and stick to the mould. The melting process absorbs energy and so over the region AB, the internal air temperature rises less quickly. It may also be seen that the temperature of the mould now starts to rise less quickly. At B all the plastic has melted and so a larger proportion of the thermal energy input goes to heating the inner air. This temperature rises more rapidly again, at a rate similar to that in the initial phase of the process.

Over the region BC the melt is effectively sintering because at B it is a powdery mass loosely bonded together whereas at C it has become a uniform melt. The value of temperature at C is very important because if the oven period is too short, then the material will not have sintered properly and there will be an excess of pin-holes. These are caused where the powder particles have fused together and trapped a pocket of air. If the oven period is too long then the pin-holes will all have disappeared but thermal/oxidative degradation will have started at the inner surface of the moulding. Extensive tests have shown that this is a source of brittleness in the mouldings and so the correct choice of temperature at C is a very important quality control parameter. For most grades of polyethylene the optimum temperature is in the region of 200 °C ± 5 °C.

Once the mould is removed from the oven the mould starts to cool at a rate determined by the type of cooling − blown air (slow) or water spray (fast). There may be an overshoot in the internal air temperature due to the thermal momentum of the melt. This overshoot will depend on the wall thickness of the plastic product. In Fig. 4.73 it may be seen that the inner air temperature continues to rise for several minutes after the mould has been taken out of the oven (at about 13.5 min).

During cooling, a point D is reached where the internal air temperature decreases less quickly for a period. This represents the solidification of the plastic and because this process is exothermic, the inner air cannot cool so quickly. Once solidification is complete, the inner air cools more rapidly again. Another kink (point E) may appear in this cooling curve and, if so, it represents the point where the moulding has separated from the mould wall. In practice this is an important point to keep consistent because it affects shrinkage, warpage, etc in the final product. Once the moulding separates from

the mould, it will cool more slowly and will tend to be more crystalline, have greater shrinkage and lower impact strength.

Developments in rotational moulding have continued gradually over the years but across the industry the basic processes involving biaxial rotation of a mould within a large convection oven, has remained largely the same. Compared to other polymer processes, rotational moulding has been relatively slow to embrace new technologies such as sensors, simulation and automation. Nevertheless, there have been a range of important new technologies developed that are leading to the ever-increasing use of features such as

(i) mould pressurisation (to consolidate the melt, remove pin-holes, reduce cycle times and provide more consistent mould release),
(ii) internal heating/cooling (to increase cycle times and reduce warpage effects),
(iii) internally heated moulds (using hot oil or electrical heaters) to eliminate the restrictions of the oven,
(iv) drop-boxes or material injectors to enable multilayer products (including foam layers or cores) to be manufactured.

In addition, research has led to the introduction of simulation packages for rotational moulding that can assist in part, mould and process design, and process optimisation. The best known of these packages is Rotosim®, which was originally developed at Queen's University Belfast. Automation is also starting to find its way into rotational moulding, where a new moulding system called Robomould® has been introduced to the market. This novel technology combines the use of an electrically heated mould with a robotic arm to create a flexible system with highly controlled heating and multi-axial rotation.

In overall terms the disadvantages of rotational moulding are its relative slowness (cycle times are typically well in excess of 30 min, depending on the part wall thickness) and the limited choice of plastics which are commercially available in powder form with the correct additive package. However, the advantages of rotational moulding in terms of stress-free moulding, low mould costs, fast lead times and easy control over wall thickness distribution (relative to blow moulding) means that rotational moulding remains one of the faster growing sectors of the plastics processing industry.

4.6.1 Slush moulding

This is a method for making hollow articles using liquid plastics, particularly PVC plastisols. A shell-like mould is heated to a pre-determined temperature (typically 130 °C for plastisols) and the liquid is then poured into the mould to completely fill it. A period of time is allowed to elapse until the required thickness of plastic gels. The excess liquid is then poured out and the plastic

skin remaining in the mould is cured in an oven. The moulding is then taken from the mould.

It should be noted that when the plastisol liquid gels it has sufficient strength to remain in position on the inside surface of the mould. However, it has insufficient tear strength to be useful and so it has to go through the higher temperature curing stage to provide the necessary toughness and strength in the end-product. The mould is not rotated during slush moulding.

4.7 Compression moulding

Compression moulding is one of the most common methods used to produce articles from thermosetting plastics. The process can also be used for thermoplastics but this is less common − the most familiar example is the production of vinyl LP records. The moulding operation as used for thermosets is illustrated in Fig. 4.74. A pre-weighed charge of partially polymerised thermoset is placed in the lower half of a heated mould and the upper half is then forced down. This causes the material to be squeezed out to take the shape of the mould. The application of the heat and pressure accelerates the polymerisation of the thermoset and once the crosslinking ('curing') is completed the article is solid and may be ejected while still very hot. Mould temperatures are usually in the range of 130−200 °C. Cycle times may be long (possibly several minutes) so it is desirable to have multi-cavity moulds to increase production rates. As a result, moulds usually have a large projected area so the closing force needed could be in the region of 100−500 tonnes to give the 7−25 MPa cavity pressure needed. It should also be noted that compression moulding is also used for Dough Moulding Compounds (DMC) − these will be considered in Section 4.11.2.

During compression moulding, the charge of material may be put into the mould either as a powder or a preformed 'cake'. In both cases the material is preheated to reduce the temperature difference between it and the mould. If the material is at a uniform temperature in the mould then the process may be analysed as follows.

Consider a 'cake' of moulding resin between the compression platens as shown in Fig. 4.75. When a constant force, *F,* is applied to the upper platen the resin flows as a result of a pressure gradient. If the flow is assumed to be Newtonian then the pressure flow equation derived in Section 4.2.3 may be used

$$\text{flow rate, } Q_p = \frac{1}{12\eta}\left(\frac{dP}{sz}\right)TH^3 \quad (4.6)$$

For the annular element of radius, *r,* in Fig. 4.75 it is more convenient to use cylindrical co-ordinates so this equation may be rewritten as

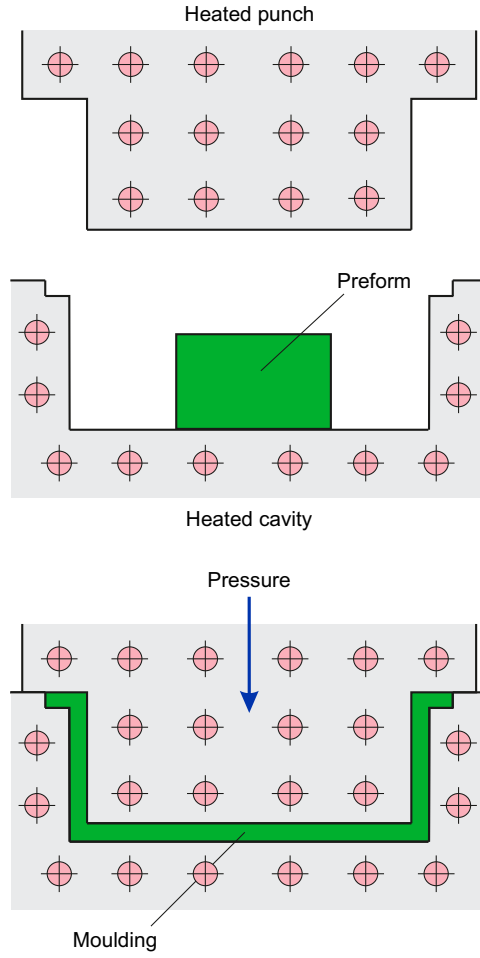


FIG. 4.74 Principle of compression moulding.

$$Q_p = \frac{1}{12\eta}\left(\frac{dP}{dr}\right)\cdot(2\pi r)H^3$$

Now if the top platen moves down by a distance, dH, the volume displaced is ($\pi r^2 dH$) and the volume flow rate is πr^2 (dH/dt).

Therefore

$$\pi r^2\left(\frac{dH}{dt}\right) = \frac{1}{12\eta}\left(\frac{dP}{dr}\right)\cdot(2\pi r)H^3$$

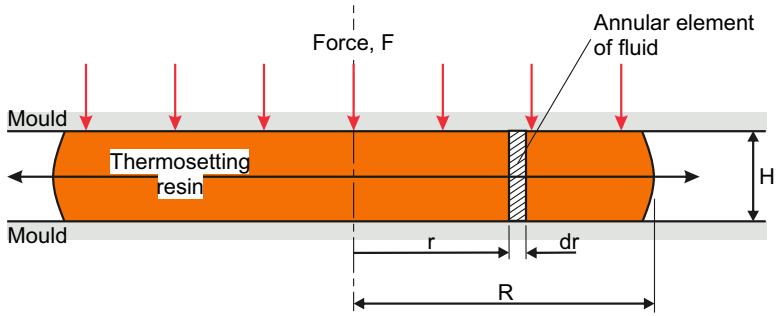


FIG. 4.75 Analysis of compression moulding.

$$\frac{12\eta}{H_3}\cdot\frac{dH}{dt}=\frac{2}{r}\frac{dP}{dr} \tag{4.44}$$

This simple differential equation is separable and so each side may be solved in turn.

Let

$$\frac{2}{r}\frac{dP}{dr}=A \quad \text{where } A=f(H)$$

so

$$\int_0^P dP=\frac{A}{2}\int_R^r rdr$$

or

$$P=\frac{A}{4}\left(r^2-R^2\right)$$

Now the force on the element is $2\pi rdr(P)$ so the total force, F, is given by integrating across the platen surface.

$$F=\int_0^R 2\pi r\left(\frac{A}{4}\right)\left(r^2-R^2\right)dr=-\frac{\pi AR^4}{8}$$

This may be rearranged to give

$$A=\frac{8F}{\pi R^4}=-\frac{8\pi FH^2}{V^2}$$

where $V=\pi R^2H$

Substituting for A in (4.44)

$$-\frac{8\pi FH^2}{V^2} = \frac{12\eta}{H^3}\frac{dH}{dt}$$

So

$$-\int_0^t \frac{2\pi F}{3\eta V^2}dt = \int_{H_0}^{H} \frac{dH}{H^5}$$

$$\frac{2\pi Ft}{3\eta V^2} = \frac{1}{4}\left(\frac{1}{H^4} - \frac{1}{H_0^4}\right)$$

Since $H_0 >> H$ then $(1/H_0^4)$ may be neglected. As a result the compaction force F, is given by

$$F = \frac{3\eta V^2}{8\pi tH^4} \tag{4.45}$$

where H *is* the platen separation at time, t.

Example 4.10 A circular plate with a diameter of 0.3 m is to be compression moulded from phenol formaldehyde. If the preform is cylindrical with a diameter of 50 mm and a depth of 36 mm estimate the platen force needed to produce the plate in 10 s. The viscosity of the phenol may be taken as 10^3 Pa·s.

Solution
Volume,

$$V = \pi\left(\frac{50}{2}\right)^2 \times 0 = \pi\left(\frac{300}{2}\right)^2 H$$

So

$$H = 1 \text{ mm}$$

From (4.45)

$$F = \frac{3\eta V^2}{8\pi tH^4} = \frac{3 \times 10^3 \times (\pi \times 625 \times 36)^2}{10^6 \times 8\pi \times 10 \times (1)^4} = 59.6 \text{ kN}$$

4.8 Transfer moulding

Transfer moulding is similar to compression moulding except that instead of the moulding material being pressurized in the cavity, it is pressurized in a separate chamber and then forced through an opening and into a closed mould.

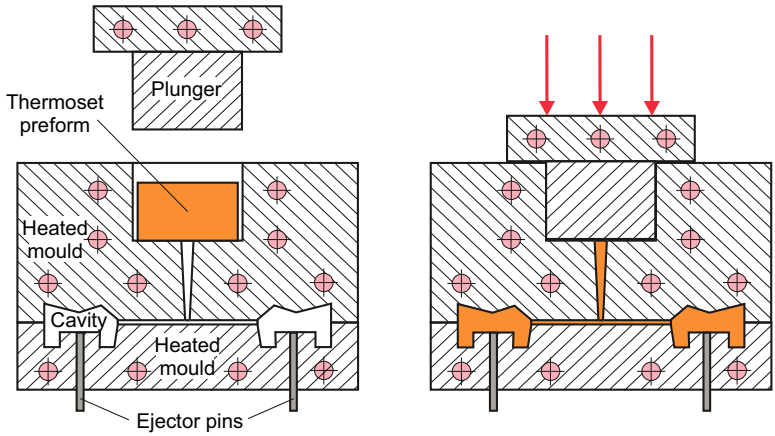


FIG. 4.76 Transfer moulding of thermosetting materials.

Transfer moulds usually have multi-cavities as shown in Fig. 4.76. The advantages of transfer moulding are that the preheating of the material and injection through a narrow orifice improves the temperature distribution in the material and accelerates the crosslinking reaction. As a result the cycle times are reduced and there is less distortion of the mouldings. The improved flow of the material also means that more intricate shapes can be produced.

The success of transfer moulding prompted further developments in this area and clearly it was only a relatively small step to an injection moulding process for thermosets as described in Section 4.3.9.

4.9 Additive manufacturing techniques

Since their early development in the mid-1980s, a range of new highly programmable manufacturing techniques have emerged for the rapid production of three-dimensional parts. These are collectively known as 'Additive manufacturing' processes since they involve the addition of materials to form a part rather than the removal or subtraction of materials that is characteristic of most conventional machining techniques. Early versions of these processes were originally called 'rapid prototyping techniques' due to their ability to enable manufacturers to create an accurate physical 3D model of a part design. Due to limitations in both the processes themselves and the ranges of materials that could be processed, these manufacturing processes were largely restricted either to part visualisation and prototyping, or the production of very specialised one-off components. However, as technology has advanced over the past decade, new process variants have emerged, and it is now possible to accurately create parts from a very wide range of materials that in the manufactured form can rival the properties achievable by machining from solid feedstock. Equally important is that the costs of many of the additive techniques have

fallen sharply in recent years and simplified variants of many of the processes are now available for home or hobbyist use. At the same time industry is beginning to embrace the technology for direct manufacturing of some of its components, and it is predicted that use of such techniques across many market sectors will grow rapidly in the coming years.

While additive manufacturing techniques are available for most materials, some of the most important are associated with the manufacture of plastic parts from both thermoplastics and thermosets. In some cases, it is possible to add reinforcement (in the form of powders, fibres or layers) to the polymers to additively create more sophisticated reinforced polymer composite structures. These days it is increasingly common for most of the new additive manufacturing techniques to be called '3D printing' rather than 'rapid prototyping'.

4.9.1 Stereolithography (SLA)

In stereolithography (shown in Fig. 4.77) a vat of liquid photopolymer is located beneath an ultraviolet laser that can be programmed to selectively cure regions within the liquid as it is traversed in two dimensions. A platform is placed just below the surface of the liquid, exposing a very thin layer in the third dimension. The operating principle of the process is quite simple in that where the computer-controlled laser strikes the liquid monomer it cures, becoming a solid thermosetting plastic, so that a fine solid layer is created representing a slice at that level through the 3D part design. Typical

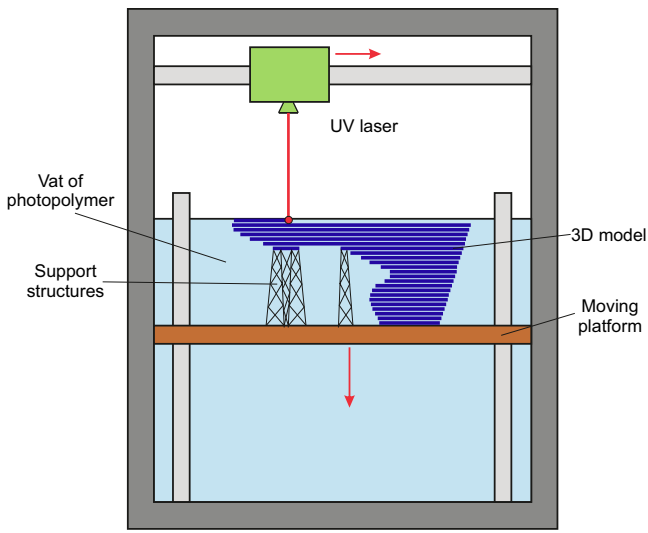


FIG. 4.77 Stereolithography.

photopolymers employed are acrylates, methacrylates and epoxies. When a layer is completed, the platform moves down, creating a fresh layer of liquid above the model ready for curing. In this way a complex 3-dimensional shape may be created layer by layer. With some part designs it may be necessary to print a temporary support structure for some features as the shape emerges. This may be subsequently removed during finishing after the printing process. Parts typically have a rough surface due to the stepped edge left by the layered structure. This may be improved by reducing the layer size and the size of the laser beam, but this can significantly increase the cost and time of production. Resolution in stereolithography is generally in the range 0.05−0.15 mm. For prototypes, manual surface sanding or polishing may be employed as an alternative. The main advantages of stereolithography are that relatively large, complex parts can be manufactured, relatively quickly. However, while a range of monomer blends are available to mimic the properties of common plastics, the number of these options are limited. Other disadvantages are the relatively high costs of the photopolymers and the laser systems, and the practical requirements for liquid handling, part cleaning and surface finishing.

4.9.2 Fused filament fabrication (FFF)

Fused Filament Fabrication (also known as Fused Deposition Modelling® (FDM)) is an additive manufacturing process in which a fine filament of polymer melt is gradually deposited by a programmable print head to create the structure of a 3D part layer by layer. In many ways the underlying process closely resembles that of stereolithography (see Section 4.9.1) apart from the deposition process. The print head moves in two dimensions, while the polymer is deposited, and when a layer is completed either the base platform or the print head is moved vertically to enable the next layer to be printed. The deposition process is illustrated in Fig. 4.78, and it is essentially a very simple extrusion process in which a thermoplastic is melted and then deposited as a fine filament. The process begins with a pre-extruded thermoplastic filament, which is supplied on a spool. This is fed by a pair of drive wheels to a print head containing a heater and a nozzle. As it is fed forward the filament begins to melt and the solid feedstock behind acts as a plunger, creating a very simple extruder that pushes the polymer melt through the nozzle and thereby generates the deposited filament that creates the layer of the 3D part (Fig. 4.78(b)). The most common diameters for the filament feedstock are 1.75 mm and 2.85 mm but nozzle diameters are typically in the range 0.1−1 mm, with 0.4 mm being very common. A wide range of thermoplastics may be printed in this way including acrylonitrile butadiene styrene (ABS), polylactic acid (PLA), polycarbonate (PC), polystyrene (PS), thermoplastic polyurethane (TPU) and polyamides (nylon), Many other thermoplastics and custom blended polymers and polymer composites may be printed using FFF systems. A major advantage of this form of 3D printing is that it is extremely adaptable

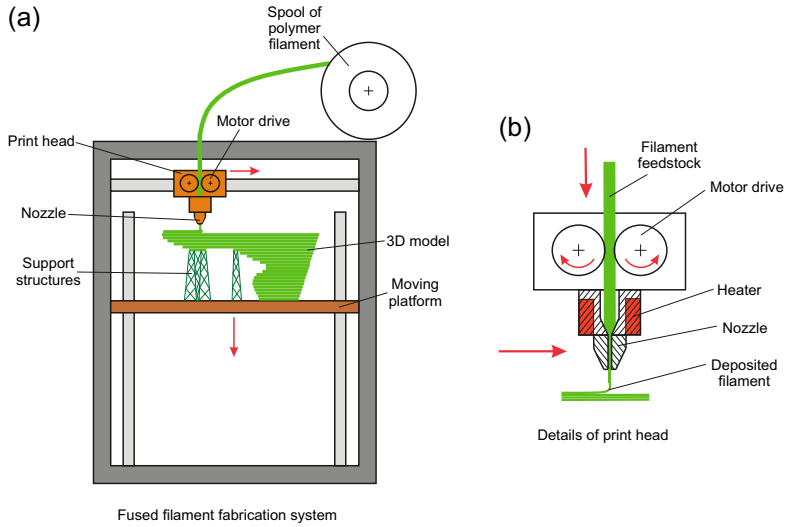


FIG. 4.78 Fused filament fabrication.

and any thermoplastic that is capable of being extruded at moderate temperatures can be printed in this way. Systems are also quite inexpensive since they are constructed from basic components that are readily available. This has led to an explosion in the popularity of such systems, with a particularly strong hobbyist market. More advanced systems permit printing with multiple print heads (different polymers and colours, or water-soluble support structures) and process technology is constantly advancing. Latest developments include printing in inert atmospheres to aid layer adhesion, and printing of high melting point temperature polymers such as PEEK. Researchers have also been exploiting FFF for the manufacture of next generation products in applications such as medical scaffolds, pharmacological membranes or smart sensors where specially blended polymer and/or polymer nanocomposites are deliberately being structurally designed to suit the application.

4.9.3 Selective laser sintering (SLS)

Selective laser sintering (SLS) involves the use of a high-power laser (usually a carbon dioxide laser) to selectively fuse small particles of a material into a mass that has a desired 3D shape. The process again resembles that of stereolithography (Section 4.9.1) in its operation, since the programmed movement of the laser is used to selectively fuse the particles within a powder bed that it strikes so that the full 3D shape is constructed layer-by-layer. SLS can be applied to any material that is fusible and therefore variants of SLS may be used to create parts from metals, plastics, and ceramics (including glass). With

metals the process has become very important across a range of industries as it is one of the most effective means of 3D printing metal structures. One of its most important applications is in the prototyping of metallic mould tools for polymer processes, where the use of metal prolongs tool life and provides comparable cycle times to that of full production tools.

Polymers may be very successfully manufactured by laser sintering, although much less laser power is required due to their much lower melting points. The layout of a typical SLS system for polymers is shown in Fig. 4.79. The equipment generally consists of 2 chambers with movable platforms as bases, which sit below the programmable laser that may be traversed in two dimensions. Initially the base of the build chamber sits just below its top surface, leaving a fine layer of polymer powder above it. A levelling roller is used to ensure that this powder layer is flat and consistent, and ready for sintering. The laser then traces out the required pattern for the layer and where it strikes the surface of the powder (Fig. 4.79(a)), the particles are fused together to create the first solid layer of the part. When the layer is completed the base of the build chamber indexes down to create space for the next layer, and the base of the powder delivery chamber is indexed upwards to provide the next layer of powder, which is pushed into position by the levelling roller as shown in Fig. 4.79(b). The process is repeated, and the next solid layer is traced out by the laser on top of the previous layer, and so on. To aid the sintering process the bed of powder may be preheated in some applications. The typical resolution achievable in SLS is similar to that of SLA and is around 0.1 mm. While polymers such as thermoplastic polyurethane (TPU), polystyrene (PS), polyester block amide (PEBA) and polyether ether ketone (PEEK) have been successfully laser sintered using the SLS process, the predominant plastics used to date in SLS are various grades and blends of polyamide (nylon), including glass-reinforced grades. The advantages of SLS are that it is one of the faster forms of 3D printing (with SLA) and since parts

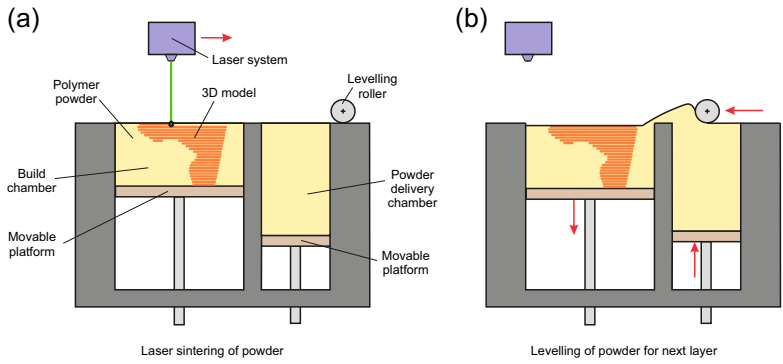


FIG. 4.79 Selective laser sintering.

are supported by the powder, support structures are not required. Multiple components may also be nested within the powder bed to speed production further. Its disadvantages are that it can be expensive (due to the cost of the laser), the range of thermoplastics available to make parts is limited, and parts often have a porous surface finish that may require post processing.

4.9.4 Other 3D printing techniques

The technologies for rapid prototyping or 3D printing are evolving very rapidly at present and there is a variety of other techniques that may be used to create parts in plastics and other materials. New techniques are also constantly emerging. *Digital light processing* (DLP) is similar to stereolithography except that conventional light sources are used to cure the photopolymer, rather than more expensive laser systems. In *Laminated object manufacturing* (LOM) layers of adhesive-coated paper, plastic, or metal films/foils are successively cut to shape with a laser cutter and then bonded together to produce a 3D part. Inkjet printing technology is also being exploited by replacing the ink with a binder so that when used on a bed of powder (similar to SLS, see Section 4.9.3), the print head can selectively bond the powder layer by layer to create a 3D part. This is known as *Binder jetting 3D printing*. In some cases, bonding is finalised by briefly exposing the printed structure to UV radiation. As this technique does not involve heat, it is of particular interest to researchers in the medical field for the printing of biological structures (bioprinting).

4.10 Processing reinforced thermoplastics

Particulate and short-fibre reinforced thermoplastics can be processed using most of the conventional thermoplastic processing methods described earlier. Extrusion, rotational moulding, blow moulding and thermoforming of reinforced thermoplastics are all possible, but the most important commercial technique is injection moulding. In most respects this process is similar to the moulding of un-reinforced thermoplastics but there are a number of important differences. For example, the melt viscosity of a reinforced plastic is generally higher than the unreinforced material. As a result, the injection pressures need to be higher, by up to 80% in some cases. In addition, the cycle times are generally lower because the greater stiffness of the material allows it to be ejected from the mould at a higher temperature than normal. However, the increased stiffness can also hamper ejection from the mould so it is important to have adequate taper on side walls of the cavity and a sufficient number of strategically placed ejector pins. Where possible a twin screw machine is preferred to a single screw machine because of the better mixing, homogenisation, metering and temperature control of the melt. However, particular attention needs to be paid to such things as screw speed and back pressure because these will tend to break up the fibres and thus affect the mechanical

properties of the mouldings. In the case of thermoplastic nanocomposites containing reinforcements such as nano-clays, nanotubes or graphene, the requirements are the opposite and greater shearing and mixing of the melt should be encouraged to improve dispersion and ultimately the properties of the composite. For this reason, twin screw extruders are used almost exclusively in the preparation of blended pellets of polymer nanocomposites and techniques such as ultrasonic mixing may be deployed to further enhance the level of dispersion. Achieving full dispersion or exfoliation of nanoparticles in viscous thermoplastic melts remains one of the most challenging aspects of ongoing research into polymer nanocomposites.

A practical difficulty which arises during the extrusion or injection moulding of reinforced plastics is the increased wear of the moulding machine and the die or mould due to the abrasive nature of the particles or fibres. However, if hardened tool steels are used in the manufacture of screws, barrels and mould cavities then the problem may be negligible.

When considering fibre-reinforced composites, an inherent problem with all of the conventional melt processing methods is that they must, by their nature, use short fibres (typically 0.2−0.4 mm long). As a result, the full potential of the reinforcing fibres is not always realised (see Section 3.5). However, it is possible to manufacture products of long-fibre or woven laminate thermoplastic composites using alternative methods. The most important of these is a hot press variant of compression moulding (see Section 4.7) where the fibres are consolidated with a thermoplastic under pressure between two-halves of a heated mould. The long fibres may be in a variety of forms including uniaxially oriented, woven (biaxially orientated) or randomly distributed, and the thermoplastic may be introduced over and between layers of the fibres as film (film stacking) or in the form of pre-consolidated tapes. Composite tapes may be produced by squeezing fibres onto a thermoplastic film with a heated roller. This process is known as *Tape Laying* and if unidirectional fibres are used then by changing the orientation of the tape in subsequent layers, the properties of the composite may be tailored to meet the application. Generally the direct pressing of thermoplastic powders and fibres is discouraged due to difficulties in distributing and consolidating the matrix. However, in some applications the thermoplastic may be sputtered onto the surface of the fibres prior to consolidation or fibres of thermoplastic may be co-mingled with the reinforcing fibres, only to melt on consolidation to form the matrix of the composite. A similar approach has been taken in the manufacture of self-reinforced composites, where the heating of the highly drawn thermoplastic fibres during consolidation is carefully controlled so that only the outer portion of each fibre is permitted to melt and thereby create a matrix for the remainder of the fibres. Completed parts may be manufactured directly from long fibre composites using a dedicated die set. Alternatively, laminate composite sheets may be produced for subsequent thermoforming or for overmoulding (see Section 4.3.10(b)). In the case of thermoforming (see

Section 4.4), the presence of the long fibres within the structures can severely restrict the degree to which the shape can be changed further, and much higher forces are normally required. It is usually difficult to thermoform such materials using air pressure and instead movable plug and mould tools are employed.

A further alternative technology is Long Fibre Reinforced Thermoplastics (LFRT) which are special injection moulding grades of thermoplastics containing long fibres. At the granule production stage the thermoplastic lace contains continuous fibres and to achieve this it is produced by pultrusion (see Section 4.11.3) rather than the conventional compounding extruder. The result is that the granules contain fibres of the same length as the granule ($\simeq 10$ mm). These long fibres give better product performance although injection moulding machine modifications may be necessary to prevent fibre damage and reduce undesirable fibre orientation effects in the mould.

4.11 Processing reinforced thermosets

There is a variety of ways in which fibre reinforcement may be introduced into thermosetting materials and as a result there is a range of different methods used to process these materials. In many cases the reinforcement is introduced during the fabrication process so that its extent and its orientation can be carefully controlled by the moulder. Processes for thermosets tend to be quite different from those used for reinforced thermoplastics for two main reasons: (i) the precursors of many thermosets are in the form of low viscosity liquids, which means that they are much easier to mix, consolidate and infuse into the structure of the reinforcement; (ii) thermosets cure rapidly from liquids or doughs to rigid solids and it is therefore very important that they are clear of processing equipment when this chemical reaction takes place.

Before looking at the possible manufacturing methods for fibre reinforced thermosetting articles it is worth considering the semantics of fibre technology. Because of their fibre form, reinforcing materials have borrowed some of their terminology from the textile industry.

Filament. This is a single fibre which is continuous or at least very long compared with its diameter.

Yarn or Roving. Continuous bundle of filaments generally fewer than 10,000 in number.

Tow. A large bundle of fibres generally 10,000 or more, not twisted.

Fabric, Cloth or Mat. Woven strands of filament. The weave pattern used depends on the flexibility and balance of strength properties required in the warp and fill directions. Fig. 4.80 shows a plain weave in which the strength is uniform in both directions. The warp direction refers to the direction parallel to the length of the fabric. Fabrics are usually designated in terms of the number of yarns of filament per unit length of warp and fill direction.

Chopped Fibres. These may be subdivided as follows

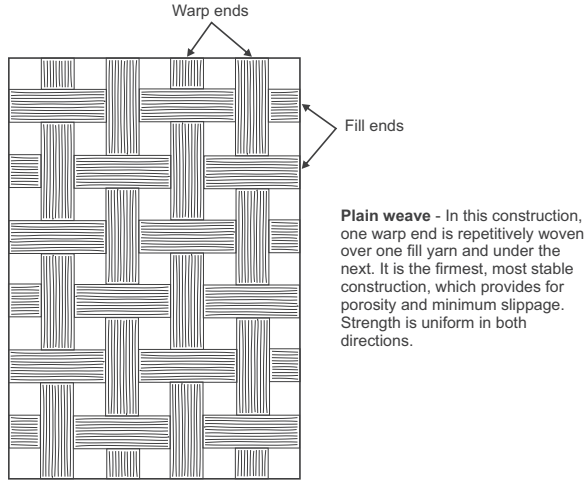


FIG. 4.80 Plain weave fibre fabric.

Milled Fibres: These are finely ground or milled fibres. Lengths range from 30 to 3000 μm and the fibre (L/D) ratio is typically about 30. Fibres in this form are popular for closed mould manufacturing methods such as injection moulding.

Short Chopped Fibres: These are fibres with lengths up to about 6 mm. The fibre (L/D) ratio is typically about 800. They are more expensive than milled fibres but provide better strength and stiffness enhancement.

Long Chopped Fibres: These are chopped fibres with lengths up to 50 mm. They are used mainly in the manufacture of Sheet Moulding Compounds (SMC) and Dough Moulding Compounds (DMC) (see Section 4.11.2).

Chopped Strand Mat. This consists of strands of long chopped fibres deposited randomly in the form of a mat. The strands are held together by a resinous binder.

Manufacturing Methods. The methods used for manufacturing articles using fibre reinforced thermosets are almost as varied as the number of material variations that exist. They can, however, be divided into three main categories. These are manual, semiautomatic and automatic.

The *Manual* processes cover methods such as hand lay-up, spray-up, pressure bag and autoclave moulding.

The *Semi-Automatic* processes include processes such as cold pressing, hot pressing, compression moulding of SMC and DMC, resin injection.

The *Automatic* processes are those such as pultrusion, filament winding, centrifugal casting and injection moulding.

4.11.1 Manual processing methods

(a) Hand lay-up

This method remains by far the most widely used processing method for fibre reinforced materials. Globally it has a market share of about 30%, but this is declining as a proportion of total output of fibre-reinforced plastics (FRP) due to the increasing use of automated processes in major industrial sectors such as aerospace and automotive and the expanding applications for thermoplastic composites. The major advantage of hand lay-up is that it is a very simple process so that very little special equipment is needed and the moulds may be made from plaster, wood, sheet metal or even FRP. The first step is to coat the mould with a release agent to prevent the moulding sticking to it. This is followed by a thin layer (approximately 0.3−0.4 mm) of pure resin (called a gelcoat) which has a number of functions. Firstly it conceals the irregular mesh pattern of the fibres and this improves the appearance of the product when it is taken from the mould. Secondly, and probably most important, it protects the reinforcement from attack by moisture which would tend to break down the fibre/resin interface. A tissue mat may be used on occasions to back up the gelcoat. This improves the impact resistance of the surface and also conceals the coarse texture of the reinforcement. However, it is relatively expensive and is only used if considered absolutely necessary.

When the gelcoat has been given time to partially cure the main reinforcement is applied. Initially a coat of resin (unsaturated polyester is the most common) is brushed on and this is followed by layers of tailored glass mat positioned by hand. As shown in Fig. 4.81(a) a roller is then used to consolidate the mat and remove any trapped air. The advantage of this technique is that the strength and stiffness of the composite can be controlled by building up the thickness with further layers of mat and resin as desired. Curing takes place at room temperature but heat is sometimes applied to accelerate this. Ideally any trimming should be carried out before the curing is complete because the material will still be sufficiently soft for knives or shears to be used. After curing, special cutting wheels may be needed.

Variations on this basic process are (i) *vacuum bag moulding* and (ii) *pressure bag moulding*. In the former process a flexible bag (frequently rubber) is clamped over the lay-up in the mould and a vacuum is applied between the moulding and the bag. This sucks the bag on to the moulding to consolidate the layers of reinforcement and resin. It also squeezes out trapped air and excess resin. The latter process is similar in principle except that pressure is applied above the bag instead of a vacuum below it. These techniques are illustrated in Fig. 4.81(b) and (c).

(b) Spray-up

In this process, the preparatory stages are similar to the previous method but instead of using glass mats the reinforcement is applied using a spray gun. Roving is fed to a chopper unit and the chopped strands are sprayed onto the

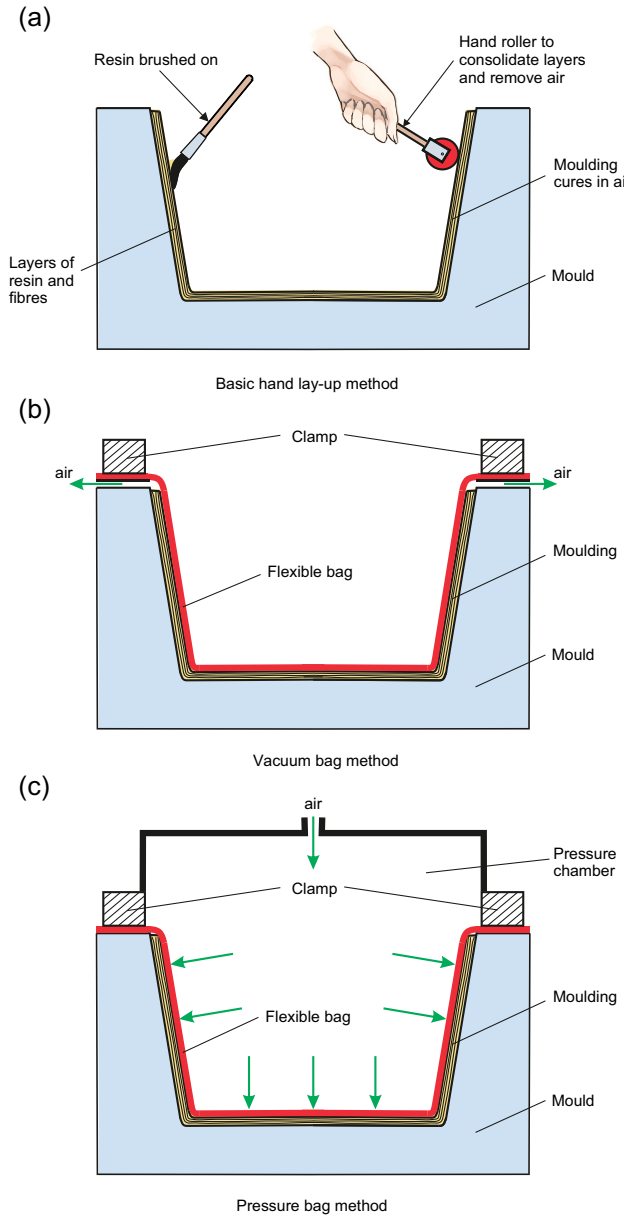


FIG. 4.81 Hand lay-up techniques.

mould simultaneously with the resin (see Fig. 4.82). The thickness of the moulding (and hence the strength) can easily be built up in sections likely to be highly stressed. However, the success of the method depends to a large extent

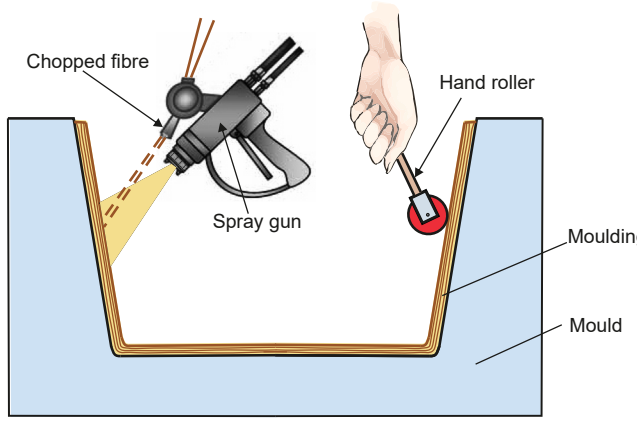


FIG. 4.82 Spray-up technique.

on the skill of the operator since he/she controls the overall thickness of the composite and also the glass/resin ratio.

(c) Autoclave moulding

In order to repetitively produce high quality, high precision mouldings for the aerospace and automotive industries, it is necessary to have strict control over fibre alignment and consolidation of the fibres in the matrix. To achieve this, fabric 'pre-pregs' (i.e. a fabric consisting of woven fibre yarns pre-impregnated with the matrix material) are carefully arranged in layers in an open mould. The arrangement of the layers will determine the degree of anisotropy in the moulded article. A typical layer arrangement is shown in Fig. 4.83(a). The pre-preg stack is then covered with a series of bleeder and breather sheets, as shown in Fig. 4.83(b) and finally with a flexible vacuum bag. When the air is extracted from between the flexible bag and the pre-preg stack, the latter will be squeezed tightly on to the mould. The whole assembly is then transferred to a very large oven (autoclave) for curing.

4.11.2 Semi-automatic processing methods

(a) Cold press moulding

The basis of this process is to utilise pressure applied to two unheated halves of a mould to disperse resin throughout a prepared fabric stack placed in the mould. The typical procedure is as follows. Release agent and gelcoat are applied to the mould surfaces and the fibre fabric is laid into the lower part of the open mould. The activated resin is then poured on top of the mat and when the mould is closed the resin spreads throughout the reinforcement. High pressures are not necessary as the process relies on squeezing the resin

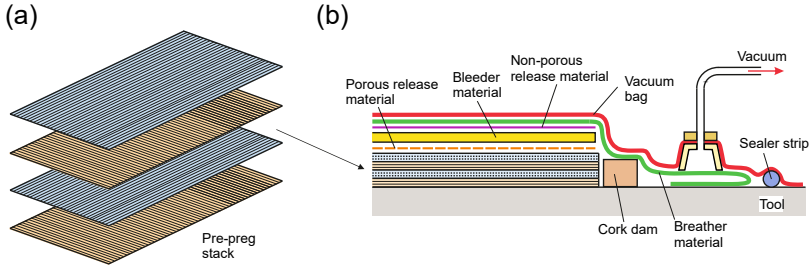


FIG. 4.83 Diagrammatic cross section of a bagged lay-up.

throughout the reinforcement rather than forcing the composite into shape. A typical value of cycle time is about 10−15 min compared with several hours for hand lay-up methods. The process is illustrated in Fig. 4.84.

(b) Hot press mouldings

In this type of moulding the curing of the reinforced plastic is accelerated by the use of heat ($\simeq$ 180 °C) and pressure ($\simeq$ 15 MPa). The general heading of Hot Press Moulding includes both preform moulding and compression moulding.

(i) *Pre-form Moulding*: This technique is particularly suitable for mass production and/or more complex shapes. There are two distinct stages. In the first a preform is made by, for example, spraying chopped fibres on to a perforated metal screen which has the general shape of the article to moulded. The fibres are held on the screen by suction applied behind it (see Fig. 4.85). A resin binder is then sprayed on the mat and the resulting preform is taken from the screen and cured in an oven at about 150 °C for several minutes. Other methods by which the preform can be made include

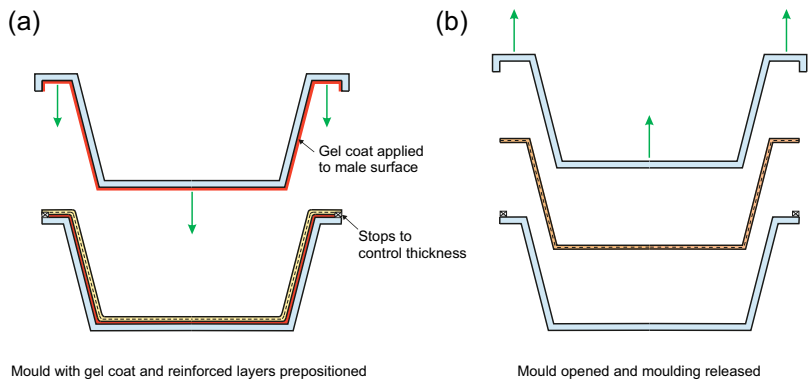


FIG. 4.84 Basic cold press moulding process.

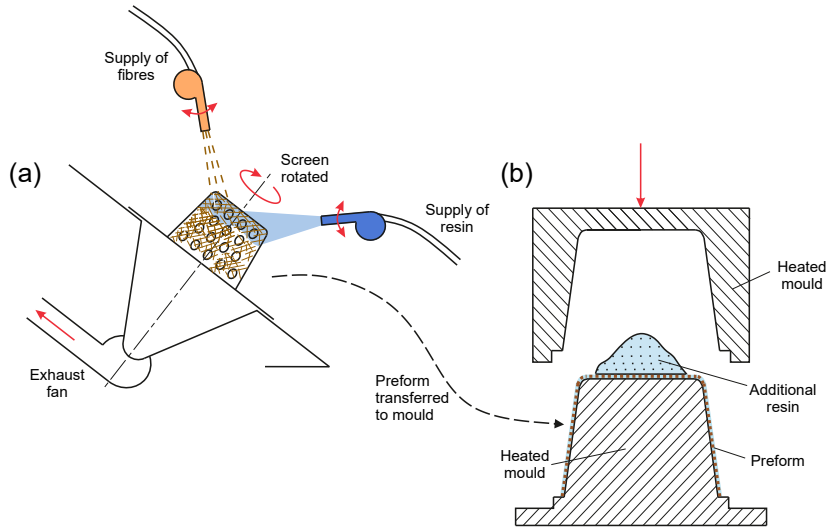


FIG. 4.85 Pre-form moulding of GFRP.

tailoring a continuous fibre fabric to shape and using tape to hold it together. The preform is then transferred to the lower half of the heated mould and the activated resin poured on top. The upper half of the mould is then brought into position to press the composite into shape. The cure time in the mould depends on the temperature, varying typically from 1 min at 150 °C to 10 min at 80 °C. If the mould was suitably prepared with release agent the moulding can then be ejected easily. This method would not normally be considered for short production runs because the mould costs are high.

(ii) *Compression Moulding* (see also Section 4.7): Sheet Moulding Compounds: SMC is supplied as a pliable sheet which consists of a mixture of chopped strand mat or chopped fibres (25% by weight) pre-impregnated with resin, fillers, catalyst and pigment. It is ready for moulding and so is simply placed between the halves of the heated mould. The application of pressure then forces the sheet to take up the contours of the mould. The beauty of the method is that the moulding is carried out 'dry' i.e. it is not necessary to pour on resins. Fig. 4.86 illustrates a typical method used to manufacture SMC material.

Dough Moulding Compounds: DMC (also known as BMC – Bulk Moulding Compound) is supplied as a dough or rope and is a mixture of chopped strands (20% by weight) with resin, catalyst and pigment. It flows readily and so may be formed into shape by compression or transfer moulding

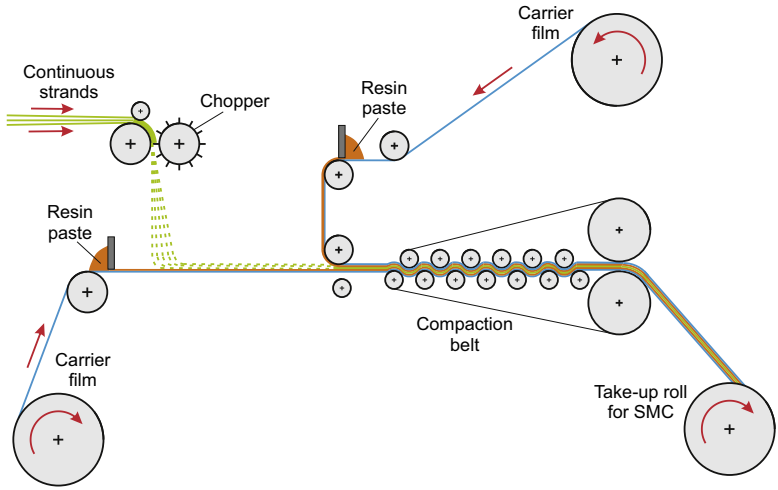


FIG. 4.86 Manufacture of SMC material.

techniques. In compression moulding the charge of dough may be placed in the lower half of the heated mould, in a similar fashion to that illustrated in Fig. 4.74 although it is generally wise to preform it to the approximate shape of the cavity. When the mould is closed, pressure is applied causing the DMC to flow in all sections of the cavity. Curing generally takes a couple of minutes for mould temperatures in the region of 120−160 °C although clearly this also depends on the section thickness.

In general, SMC moulds less well than DMC on intricate shapes but it is particularly suitable for large shell-like mouldings − automotive parts such as body panels and fascia panels are ideal application areas. DMC finds its applications in the more complicated shapes such as business machine housings, electric drill bodies, etc. Injection moulding of DMC is also an option for intricately shaped articles (see Section 4.3.9).

Other types of compression moulding and stamp forming used for continuous fibre reinforced composites are illustrated in Fig. 4.87. Initially compression moulding may be used to prepare the uncured laminates, which can either be compression moulded in a heated moulded, or the laminate may be heated separately and then formed in a cold mould. With continuous fibres, or woven mats, it is important to carefully control the level of clamping used so that a portion of the initially clamped laminate is able to enter the mould to aid in the prevention of wrinkling.

(c) Resin injection

This is a cold mould process using relatively low pressures (approximately 450 kPa). The mould surfaces are prepared with release agent and gelcoat

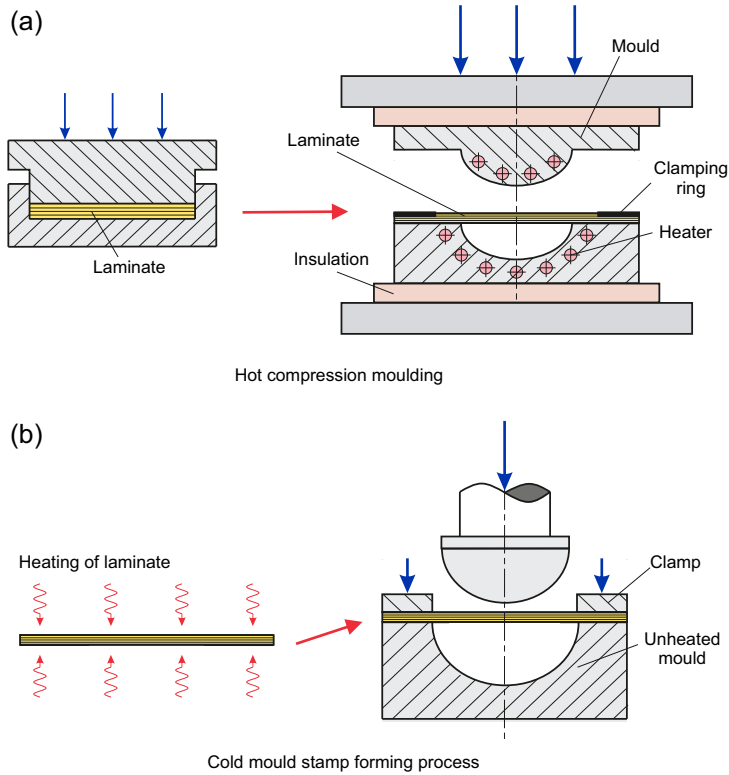


FIG. 4.87 Other types of compression moulding and stamp forming.

before the reinforcing mat is arranged in the lower half of the mould. The upper half is then clamped in position and the activated resin is injected under pressure into the mould cavity. The advantage of this type of production method is that it reduces the level of skill needed by the operator because the quality of the mould will determine the thickness distribution in the moulded article (see Fig. 4.88). In recent times there has been a growing use of pre-formed fabric shells in the resin injection process. The pre-form is produced using one of the methods described above and this is placed in the mould. This improves the quality and consistency of the product and reinforcements varying from chopped strand mat to close weave fabric in glass, aramid, carbon or hybrids of these may be used. It is possible, with care, to achieve reinforcement loadings in the order of 65%.

(d) Vacuum injection

This is a development of resin injection in which a vacuum is used to gently draw activated resin throughout the reinforcement. It overcomes the problem

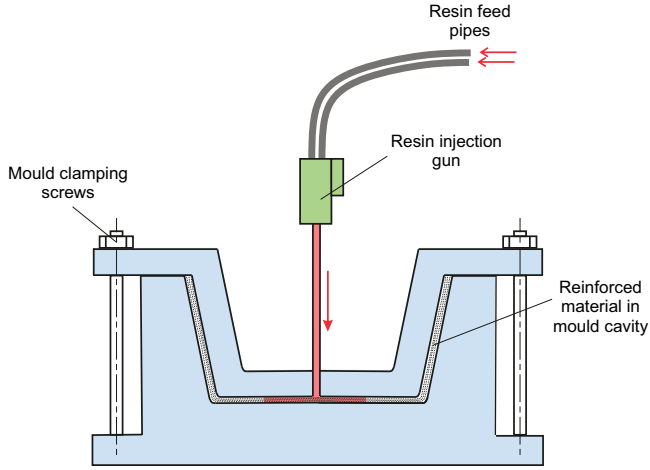


FIG. 4.88 Resin injection process.

of voids in the resin/fibre laminate and offers faster cycle times with greater uniformity of product.

4.11.3 Automatic processes

(a) Filament winding

In this method, continuous strands of reinforcement are used to gain maximum benefit from the fibre strength. In a typical process rovings or single strands are passed through a resin bath and then wound on to a rotating mandrel. By arranging for the fibres to traverse the mandrel at a controlled and/or programmed manner, as illustrated in Fig. 4.89, it is possible to lay down the reinforcement in any desired fashion. This enables very high strengths to be achieved and is particularly suited to pressure vessels where reinforcement in the highly stressed hoop direction is important. In the past a limitation on this process was that it tended to be restricted to shapes which were symmetrical about an axis of rotation and from which the mandrel could be easily extracted. However, through the use of collapsible or expendable cores and most importantly through the development of computer-controlled winding equipment, such limitations have been overcome. Modern machines typically have between 2 and 6 axes of motion and can exploit textiles technologies such as braiding to orientate combinations of fibres precisely where they are needed for the performance of the product. Applications of filament winding include pressure vessels, pipes, missile casings, aircraft fuselages, lamp posts, and a range of performance sporting goods such as golf clubs, oars, bicycle frames and yacht masts.

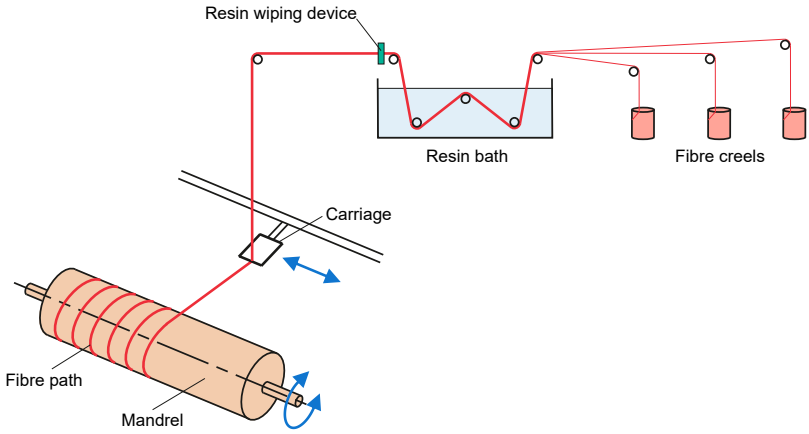


FIG. 4.89 Filament winding of fibre composites.

(b) Centrifugal casting

This method is used for cylindrical products which can be rotated about their longitudinal axis. Resin and fibres are introduced into the rotating mould/mandrel and are thrown out against the mould surface. The method is particularly suited to long tubular structures which can have a slight taper e.g. street light columns, telegraph poles, pylons, etc.

(c) Pultrusion

This is a continuous production method similar in concept to extrusion. Woven fibre mats and/or rovings are drawn through a resin bath and then through a die to form some desired shape (for example a 'plank' as illustrated in Fig. 4.90). The profiled shape emerges from the die and then passes through a tunnel oven to accelerate the curing of the resin. The pultruded composite is eventually cut to length for storage. A wide range of pultruded shapes may be produced—U channels, I beams, aerofoil shapes, etc.

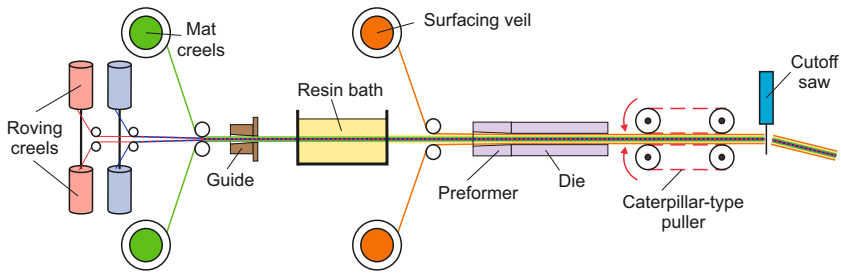


FIG. 4.90 Pultrusion process.

(d) Injection moulding

The injection moulding process can also be used for fibre reinforced thermoplastics and thermosets, for example DMC materials. This offers considerable advantages over compression moulding due to the higher production speeds, more accurate metering and lower product costs which can be achieved. The injection moulding process for thermosets has already been dealt with in Section 4.3.9. See also the section on Reaction Injection Moulding (RIM) (Section 4.3.7) since this offers the opportunity to incorporate fibres.

Questions

4.1 In a particular extruder screw the channel depth is 2.4 mm, the screw diameter is 50 mm, the screw speed is 100 rev/min, the flight angle is 17° 42′ and the pressure varies linearly over the screw length of 1000 mm from zero at entry to 20 MPa at the die entry. Estimate
(a) the drag flow
(b) the pressure flow
(c) the total flow.

The plastic has a viscosity of 200 Pa·s. Calculate also the shear rate in the metering zone.

4.2 Find the operating point for the above extruder when it is combined with a die of length 40 mm and diameter 3 mm. What would be the effect on pressure and output if a plastic with viscosity 400 Pa·s was used.

4.3 A single screw extruder has the following dimensions:
screw length = 500 mm
screw diameter = 25 mm
flight angle = 17°42′
channel depth = 2 mm
channel width = 22 mm

If the extruder is coupled to a die which is used to produce two laces for subsequent granulation, calculate the output from the extruder/die combination when the screw speed is 100 rev/min. Each of the holes in the lace die is 1.5 mm diameter and 10 mm long and the viscosity of the melt may be taken as 400 Pa·s.

4.4 An extruder is coupled to a die, the output of which is given by (KP/η) where P is the pressure drop across the die, η is the viscosity of the plastic and K is a constant. What are the optimum values of screw helix angle and channel depth to give maximum output from the extruder.

4.5 A circular plate of diameter 0.5 m is to be moulded using a sprue gate in its centre. If the melt pressure is 50 MPa and the pressure loss coefficient is 0.6 estimate the clamping force required.

4.6 The container shown Fig. 4.91 is injection moulded using a gate at point A. If the injection pressure at the nozzle is 140 MPa and the pressure loss coefficient, m, is 0.5, estimate (i) the flow ratio and (ii) the clamping force needed.

4.7 Compare the efficiencies of the runners shown on Fig. 4.92.

4.8 A calender having rolls of diameter 0.3 m produces plastic sheet 1 m wide at the rate of 2000 kg/h. If the roll speed is 5 rev/minute and the nip between the rolls is 4.5 mm, estimate the position and magnitude of the maximum pressure. The density of the material is 1400 kg/m^3 and its viscosity is 1.5×10^4 Pa·s.

4.9 A calender having rolls of 0.2 m diameter produces 2 mm thick plastic sheet at a linear velocity of 0.1 m/s. Investigate the effect of nips in the range 0.8−1.9 mm on the pressure profile. The viscosity is 10^3 Pa·s.

4.10 A hemispherical dome of 200 mm diameter has been vacuum formed from a flat sheet 4 mm thick. What is the thickness of the dome at the point furthest away from its diameter?

4.11 A disposable tumbler which has the shape of a frustum of a cone is to be vacuum formed from a flat plastic sheet 3 mm thick. If the diameter of the mouth of the tumbler is 60 mm, the diameter of the base is 40 mm

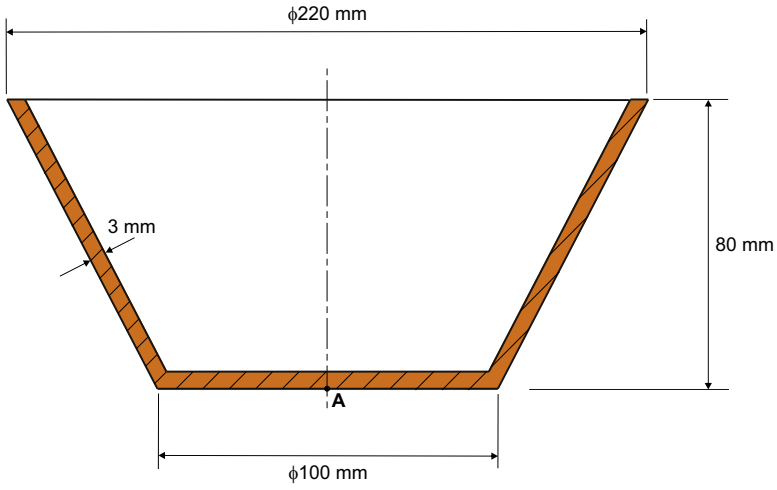


FIG. 4.91 Injection moulded part in cross-section.

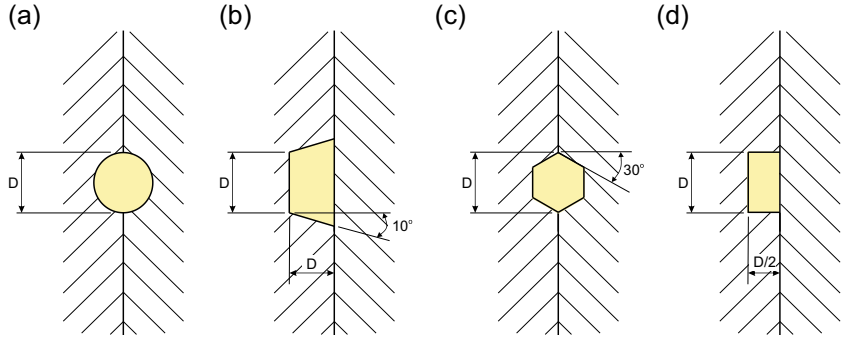


FIG. 4.92 Runner sections of different design.

and the depth is 60 mm estimate the wall thickness at (a) a point 35 mm from the top and (b) in the centre of the base.

4.12 A blow moulding die which has an outside diameter of 40 mm and a die gap of 2 mm is used to produce a plastic bottle with a diameter of 70 mm. If the swelling ratio of the melt in the thickness direction is 1.8 estimate
(a) the parison dimensions
(b) the thickness of the bottle
(c) a suitable inflation pressure if melt fracture occurs at a stress of 10 MPa.

4.13 A plastic film, 0.1 mm thick, is required to have its orientation in the transverse direction twice that in the machine direction. If the film blowing die has an outer diameter of 100 mm and an inner diameter of 98 mm estimate the blow-up ratio which will be required and the lay flat film width. Neglect extrusion induced effects and assume there is no draw-down.

4.14 A molten polymer is to-be coated on a cable at a speed of 0.5 m/s. The cable diameter is 15 mm and the coating thickness required is 0.3 mm. The die used has a length of 60 mm and an internal diameter of 16 mm. What pressure must be developed at the die entry if the viscosity of the polymer under these operating conditions is 100 Pa·s?

4.15 During a rotational moulding operation an aluminium mould with a uniform thickness of 3 mm is put into an oven at 300 °C. If the initial temperature of the mould is 23 °C, estimate the time taken for it to reach 250 °C. The natural convection heat transfer coefficient is 28.4 J/m^{2}s K and the thermal diffusivity and conductivity of aluminium may be taken as 8.6×10^{-5} m^2/s and 230.1 J/ms K respectively.

4.16 A billet of PVC weighing 150 g is to be compression moulded into a long-playing record of diameter 300 mm. If the maximum force which the press can apply is 100 kN estimate the time needed to fill the mould. The density and viscosity of the PVC may be taken as 1200 kg/m^3 and 10 Pa·s respectively.

Bibliography

Ashter SL: *Thermoforming of single and multilayer laminates: plastic films technologies, testing and applications*, Elsevier.

Avery J: *Injection molding alternatives: a guide for designers and product engineers*, Hanser.

Avery J: *Gas-assist injection molding: principles and applications*, Hanser.

Baird DG, Collias DI: *Polymer processing*, Newton, USA, 1995, Butterworth-Heinemann.

Balasubramanian M: *Composite materials and processing*, CRC Press.

Beaumont JP, Nagel R, Sherman R: *Successful injection molding: process, design and simulation*, Hanser.

Biron M: *Thermosets and composites: technical information for plastics users*, ed 2, Plastics Design Library.

Bouvier J-M: *Extrusion processing technology: food and non-food materials*, Wiley.

Brandau O: Stretch blow molding. *PDL handbook*, ed 3, New York, 2017, Elsevier.

Cantor K: *Blown film extrusion*, ed 2, Hanser.

Crawford RJ: *Rotational moulding of plastics*, ed 2, Research Studies Press.

Crawford RJ, Kearns MP: *Practical guide to rotational moulding*, ed 2, Smithers Rapra Technology.

Davé RS, Loos AC, editors: *Processing of composites*, Hanser.

Davis B, Gramann P, Rios A, Osswald T: *Compression molding*, Hanser.

Harper CA: *Handbook of plastic processes*, Wiley.

Harper CA, Petrie EM: *Plastics materials and processes: a concise encyclopedia*, Wiley.

Ibeh CC: *Thermoplastic materials: properties, manufacturing methods and applications*, CRC Press.

Kamal MR, Isayev A, Liu SJ, editors: *Injection molding: technology and fundamentals*, Hanser.

Lafleur PG, Vergnes B: *Polymer extrusion*, Wiley.

Lee N, editor: *Plastic blow moulding handbook*, New York, 1990, Van Nostrand Reinhold.

Michaeli W: *Polymer processing*, Munich, 1992, Hanser.

Mitchell P, editor: *Tool and manufacturing engineers handbook* (vol. 8). ed 4, Society of Manufacturing Engineers.

Nicolais L, Borzacchiello A, editors: *Encyclopedia of composites*, ed 2, Wiley.

Osswald TA: *Polymer processing fundamentals*, Hanser.

Rao NS: *Understanding plastics engineering calculations*, Hanser.

Rauwendaal C: *Polymer extrusion*, ed 5, Hanser.

Rosato AV, DiMattia DP, Rosato DV: *Blow molding handbook*, Hanser.

Rosato DV, Rosato DV: *Injection molding handbook*, ed 2, New York, 1995, Chapman and Hall.

Rosen SR: *Thermoforming: improving process performance*, Dearborn MI, USA, 2002, Society of Manufacturing Engineers.

Shoemaker J, editor: *Moldflow design guide: a resource for plastics engineers*, Hanser.

Stevens MJ, Covas JA: *Extruder principles and operation*, ed 2, London, 1995, Chapman and Hall.
Strong AB: *Plastics: materials and processing*, ed 3, Pearson/Prentice-Hall.
Strong AB: *Fundamentals of composites manufacturing: materials, methods and applications*, ed 2, Society of Manufacturing Engineers.
Thomas S, Yang W, editors: *Advances in polymer processing: from macro to nano scales*, Woodhead Publishing Ltd.
Throne JL: *Technology of thermoforming*, Munich, 1996, Hanser.
Wagner JR, Mount EM, Giles HF: *Extrusion: the definitive processing guide and handbook*, ed 2, Plastics Design Library.
White JL, Kim EK: *Twin screw extrusion: technology and principles*, Hanser.
Xu J: *Microcellular injection molding*, Wiley.

Chapter 5

Analysis of polymer melt flow

5.1 Introduction

In general, all polymer processing methods involve three stages – heating, shaping and cooling of a plastic. However, this apparent simplicity can be deceiving. Most plastic moulding methods are not straightforward, and the practical know-how can only be gained by experience, often using trial and error methods. In most cases plastics processing has developed from other technologies (e.g. metal and glass) as an art rather than as a science. This is principally because in the early days the flow of polymeric materials was not understood and the rate of increase in the usage of the materials was much greater than the advances in the associated technology.

Nowadays the position has changed because, as ever-increasing demands are being put on materials and moulding machines it is now essential to be able to make reliable quantitative predictions about performance. Today much of this is addressed through computer-aided simulation, which is an increasingly important feature of many polymer processing techniques. Nevertheless, it remains important for designers and engineers using plastics to develop an understanding of how melt flow theory may be used to predict and analyse the operation of major polymer processing techniques. In Chapter 4 it was shown that a simple Newtonian approach gives a useful first approximation to many of the processes but unfortunately the assumption of constant viscosity can lead to serious errors in some cases. For this reason, a more detailed analysis using a non-Newtonian model is often necessary and this will now be illustrated.

Most melt processing methods involve flow in capillary or rectangular sections, which may be uniform or tapered. Therefore, the approach taken here will be to develop first the theory for Newtonian flow in these channels and then when the non-Newtonian case is considered it may be seen that the steps in the analysis are identical although the mathematics is a little more complex. At the end of the chapter a selection of processing situations is analysed quantitatively to illustrate the use of the theory. It must be stressed however, that even the more complex analysis introduced in this chapter will not give precisely accurate solutions due to the highly complex nature of polymer melt flow. This chapter simply attempts to show how a quantitative approach may be taken to polymer processing and the methods illustrated are generally sufficiently accurate for

Plastics Engineering. https://doi.org/10.1016/B978-0-08-100709-9.00005-4
Copyright © 2020 Elsevier Ltd. All rights reserved.

most engineering design situations. Those wishing to take a more rigorous approach should refer to the work of Pearson, for example.

5.2 General behaviour of polymer melts

In a fluid under stress, the ratio of the shear stress, τ to the rate of strain, $\dot{\gamma}$ is called the shear viscosity, η, and is analogous to the modulus of a solid. In an ideal (Newtonian) fluid the viscosity is a material constant. However, for plastics the viscosity varies depending on the stress, strain rate, temperature etc. A typical relationship between shear stress and shear rate for a plastic is shown in Fig. 5.1.

As a starting point it is useful to plot the relationship between shear stress and shear rate as shown in Fig. 5.1 since this is similar to the stress—strain characteristics for a solid. However, in practice it is often more convenient to rearrange the variables and plot viscosity against strain rate as shown in Fig. 5.2. Logarithmic scales are common so that several decades of stress and viscosity can be included. Fig. 5.2 also illustrates the effect of temperature on the viscosity of polymer melts.

When a fluid is flowing along a channel which has a uniform cross-section then the fluid will be subjected to shear stresses only. To define the flow behaviour, we may express the fluid viscosity, η, as the ratio of shear stress, τ, to shear rate $\dot{\gamma}$,

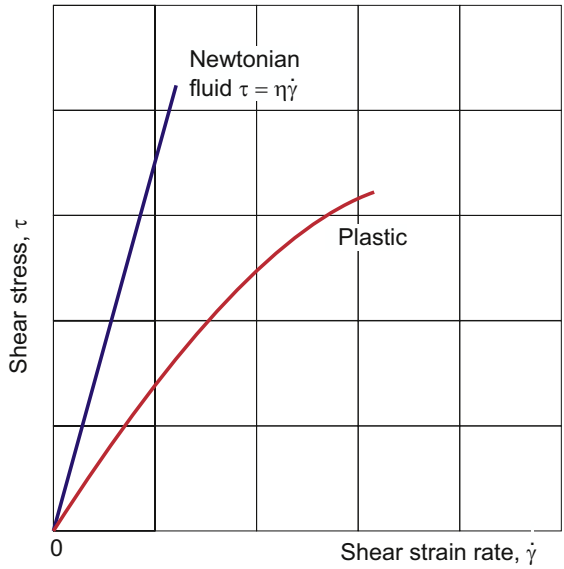


FIG. 5.1 Relations between shear stress and shear rate.

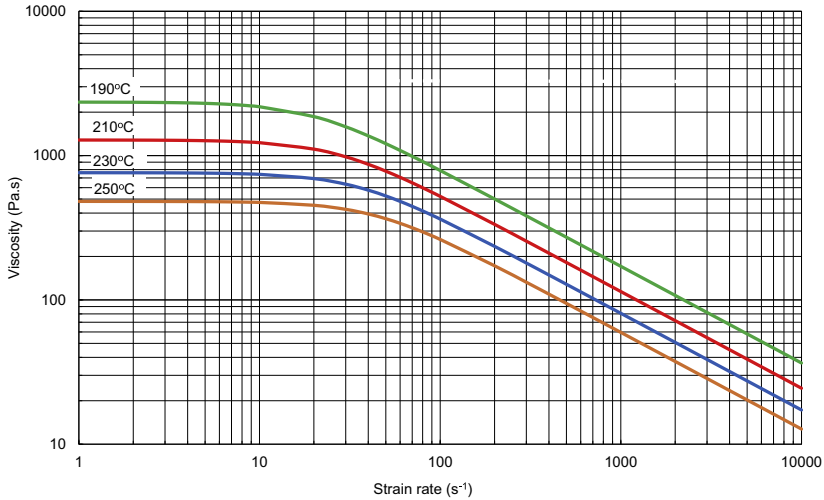


FIG. 5.2 Viscosity curves for polypropylene.

$$\eta = \frac{\tau}{\dot{\gamma}} \tag{5.1}$$

If, on the other hand, the channel section changes then tensile stresses will also be set up in the fluid and it is often necessary to determine the tensile viscosity, λ, for use in flow calculations. If the tensile stress is σ and the tensile strain rate is $\dot{\varepsilon}$ then

$$\lambda = \frac{\sigma}{\dot{\varepsilon}} \tag{5.2}$$

For many polymeric melts the tensile viscosity is fairly constant and at low stresses is approximately three times the shear viscosity.

To add to this picture, it should be realised that so far only the viscous component of behaviour has been referred to. Since plastics are viscoelastic there will also be an elastic component which will influence the behaviour of the fluid. This means that there will be a shear modulus, G, and, if the channel section is not uniform, a tensile modulus, E, to consider. If γ_R and ε_R are the recoverable shear and tensile strains respectively then

$$G = \frac{\tau}{\gamma_R} \tag{5.3}$$

$$E = \frac{\sigma}{\varepsilon_R} \tag{5.4}$$

These two moduli are not material constants and typical variations are shown in Fig. 5.3. As with the viscous components, the tensile modulus tends to be about three times the shear modulus at low stresses. Fig. 5.3 has been

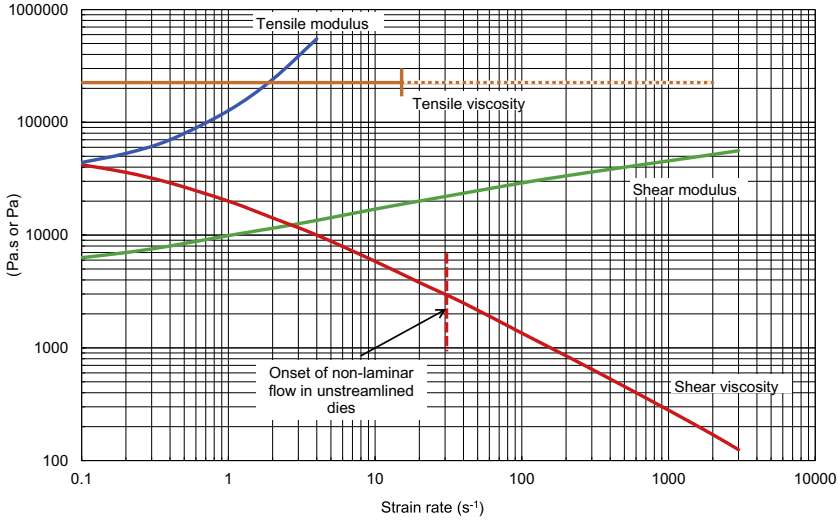


FIG. 5.3 Flow curves for polyethylene at 170 °C.

included here as an introduction to the type of behaviour which can be expected from a polymer melt as it flows. The methods used to obtain these data will be described later, when the effects of temperature and pressure will also be discussed.

5.3 Isothermal flow in channels: Newtonian fluids

In the analysis of flow in channels the following assumptions are made:

1. There is no slip at the wall.
2. The melt is incompressible.
3. The flow is steady, laminar and time independent.
4. Fluid viscosity is not affected by pressure changes along the channel.
5. End effects are negligible.

The steady isothermal flow of incompressible fluids through straight horizontal tubes is of importance in a number of cases of practical interest.

(a) Flow of Newtonian fluid along a channel of uniform circular cross-section

Consider the forces acting on an element of fluid as shown in Fig. 5.4.

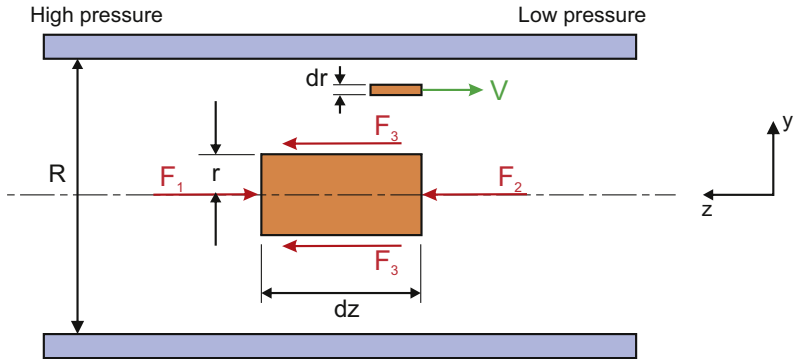


FIG. 5.4 Element of fluid in a capillary.

$$F_1 = \pi r^2 \left(P + \frac{\partial P}{\partial z} dz \right)$$

$$F_2 = \pi r^2 P$$

$$F_3 = 2\pi r dz \tau_r$$

Since the flow is steady $\Sigma F_z = O$

$$\pi r^2 P = \pi r^2 \left(P + \frac{\partial P}{\delta z} dz \right) - 2\pi dz \cdot \tau_r$$

$$\tau_r = \frac{r}{2} \left(\frac{dP}{dz} \right) \tag{5.5}$$

In many cases the pressure gradient is uniform, so that for a pressure drop, P, over a length, L, the maximum shear stress will be at the wall where $r = R$

$$\tau_w = \frac{PR}{2L} \tag{5.6}$$

Also since

$$\tau = \eta \dot{\gamma} = \eta \frac{\partial V}{\partial r}$$

So using Eq. (5.5)

$$\eta \cdot \frac{\partial V}{\partial r} = \frac{r}{2} \left(\frac{dP}{dz} \right)$$

Integrating this gives

$$\int_0^V dV = \int_R^r \frac{1}{2\eta}\frac{dP}{dz}\cdot r dr$$

$$V = \frac{1}{2\eta}\frac{dP}{dz}\left(\frac{r^2}{2} - \frac{R^2}{2}\right)$$

At $r = 0$, $V = V_0$

So

$$V_0 = -\frac{1}{4\eta}\cdot\frac{dP}{dz}\cdot R^2 \tag{5.7}$$

and

$$V = V_0\left(1 - \left(\frac{r}{R}\right)^2\right) \tag{5.8}$$

The volume flow rate, Q, may be obtained from

$$Q = \int_0^R 2\pi r V dr$$

This can be rearranged using (5.7) to the form

$$Q = \int_0^R 2\pi r V_0\left(1 - \left(\frac{r}{R}\right)^2\right)\cdot dr = \frac{1}{2}\pi V_0 R^2$$

$$Q = -\frac{\pi R^2}{8\eta}\cdot\frac{dP}{dz} \tag{5.9}$$

Once again if the pressure drop is uniform this may be expressed in the more common form

$$Q = \frac{\pi R^4 P}{8\eta L} \tag{5.10}$$

It is also convenient to derive an expression for the shear rate $\dot{\gamma}$.then

$$\dot{\gamma} = \frac{\partial V}{\partial r}$$

then

$$\dot{\gamma} = \frac{\partial}{\partial r}\left[V_0\left(1 - \left(\frac{r}{R}\right)^2\right)\right] \tag{5.11}$$

This may be rearranged using the relation between flow rate and V_0 to give the shear rate at $r = R$ as

$$\dot{\gamma}_w = \frac{-4Q}{\pi R^3} \tag{5.12}$$

The negative signs for velocity and flow rate indicate that these are in the opposite direction to the chosen z-direction.

(b) Flow of Newtonian fluid between parallel plates

Consider an element of fluid between parallel plates, T wide and spaced a distance H apart. For unit width of element the forces acting on it are:

$$F_1 = \left(P + \frac{\partial P}{\partial z} \cdot dz\right) 2y$$

$$F_2 = P \cdot 2y$$

$$F_3 = \tau_y dz$$

For steady flow there must be equilibrium of forces so

$$P.2y = \left(P + \frac{\partial P}{\partial z} \bullet dz\right) 2y - 2\tau_y dz$$

$$y \frac{\partial P}{\partial z} = \tau_y \tag{5.13}$$

In many cases the pressure gradient is uniform ($\partial P/\partial z = \Delta P/L$) so the maximum shear stress will be at the wall where $y = {}^1/_2\, H$

$$\tau_w = \frac{PH}{2L} \tag{5.14}$$

For a Newtonian fluid the shear stress, τ, is also given by

$$\tau = \eta\dot{\gamma} = \eta \frac{\partial V}{\partial y}$$

So using (5.13)

$$\eta \frac{\partial V}{\partial y} = y \frac{\partial P}{\partial z}$$

Integrating this gives

$$\int_0^V dV = \int_{H/2}^{y} \frac{1}{\eta}\frac{dP}{dz} \cdot y dy$$

$$V = \frac{1}{2\eta}\frac{dP}{dz}\left(y^2 - \left(\frac{H}{2}\right)^2\right)$$

Now at $y = 0$, $V = V_0$.

So

$$V_0 = -\frac{1}{2\eta}\frac{dP}{dz}\left(\frac{H}{2}\right)^2 \tag{5.15}$$

Substituting $\partial P/\partial z$ in the expression for V gives

$$V = V_0\left(1 - \left(\frac{2y}{H}\right)^2\right) \tag{5.16}$$

The volume flow rate, Q, is given by

$$Q = 2\int_0^{H/2} TV dy$$

Using Eq. (5.16) this may be expressed in the form

$$Q = 2\int_0^{H/2} TV_0\left(1 - \left(\frac{2y}{H}\right)^2\right) dy$$

$$= 2TV_0\left(\frac{H}{3}\right)$$

$$Q = -\frac{TH^3}{12\eta}\cdot\frac{dP}{dz} \tag{5.17}$$

which, for a uniform pressure gradient, reduces to

$$Q = \frac{TPH^3}{12\eta L} \tag{5.18}$$

An expression for the shear rate, $\dot{\gamma}$ may also be derived from

$$\dot{\gamma} = \frac{\delta V}{\delta y}$$

$$= \frac{\delta}{\delta y}\left[V_0\left(1-\left(\frac{2y}{H}\right)^2\right)\right]$$

$$\dot{\gamma} = -\frac{8V_0 y}{H^2} \tag{5.19}$$

but as shown above

$$V_0 = \frac{3Q}{2TH}$$

So

$$\dot{\gamma} = \frac{-12Qy}{TH^3}$$

At the wall

$$y = \frac{H}{2}$$

$$\dot{\gamma}_w = -\frac{6Q}{TH^2} \tag{5.20}$$

It is worth noting that the equations for flow between parallel plates may also be used with acceptable accuracy for flow along a circular annular slot. The relevant terms are illustrated in Fig. 5.6.

5.4 Rheological models for polymer melt flow

When log (viscosity) is plotted against log (shear rate) or log (shear stress) for the range of shear rates encountered in many polymer processing operations,

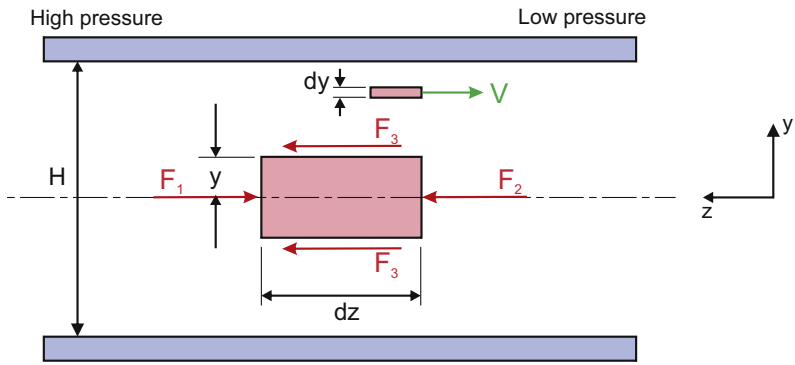


FIG. 5.5 Element of fluid between parallel plates.

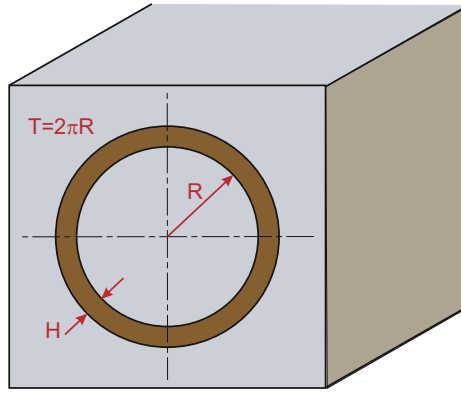


FIG. 5.6 Flow in an annular slot.

the result is a straight line. This suggests a simple power law relation of the type

$$\tau = \tau_0 \left[\frac{\dot{\gamma}_a}{\dot{\gamma}_o}\right]^n \tag{5.21}$$

where n is the Power Law index and τ_0 and γ_0 refer to the shear stress and shear rate at some reference state. This is often taken as $\dot{\gamma}_0 = 1s^{-1}$ and so the Power Law may be expressed as

$$\tau = \tau_0 \dot{\gamma}_a^n \tag{5.22}$$

It is common practice nowadays to express the apparent viscosity as a function of the shear rate, $\dot{\gamma}_a$. This may be obtained using the definition of apparent viscosity η_a as the ratio of shear stress to shear rate, i.e.

$$\frac{\tau}{\tau_0} = \frac{\eta_a}{\eta_0} \bullet \frac{\dot{\gamma}_a}{\dot{\gamma}_0}$$

So using

$$\frac{\eta_a}{\eta_0} \cdot \frac{\dot{\gamma}_a}{\dot{\gamma}_0} = \left[\frac{\dot{\gamma}_a}{\dot{\gamma}_0}\right]^n$$

$$\frac{\eta_a}{\eta_0} = \left[\frac{\dot{\gamma}_a}{\dot{\gamma}_0}\right]^{n-1} \tag{5.23}$$

or rearranging to use shear stress instead of shear rate

$$\frac{\eta_a}{\eta_0} = \left[\frac{\tau}{\tau_0}\right]^{\frac{n-1}{n}} \tag{5.24}$$

Eqs. (5.21)–(5.23) are useful for the high strain rates experienced in injection moulding or extrusion but unfortunately, they do not predict the low strain rate situation very well where plastic melts tend towards Newtonian behaviour (i.e. $n \rightarrow 1$). This is illustrated in Fig. 5.7.

Carreau proposed an alternative equation to overcome this problem. It has the form

$$\frac{\eta_a}{\eta_0} = \left[1 + (A_t\dot{\gamma}_a)^2\right]^{\frac{n-1}{2}} \tag{5.25}$$

where A_t is a material constant.

It may be seen that when $\dot{\gamma} >> 1$, this equation reduces to the Power Law (5.23) but as shown in Fig. 5.7, it also predicts the low shear rate situation very well.

In order to allow for the effect of temperature on viscosity a shift factor, a_T is often used. The Carreau equation then becomes

$$\frac{\eta_a}{\eta_0} = a_T\left[1 + a_T(A_t\dot{\gamma}_a)^2\right]^{\frac{n-1}{2}} \tag{5.26}$$

where typically the shift factor, a_T, may be obtained from

$$\log a_T = \frac{C_1(T_1 - T_0)}{C_2 + (T_1 - T_0)} - \frac{C_1(T_2 - T_0)}{C_2 + (T_2 - T_0)} \tag{5.27}$$

where C_1 and C_2 are material constants, T_1 (°C) is the temperature at which the

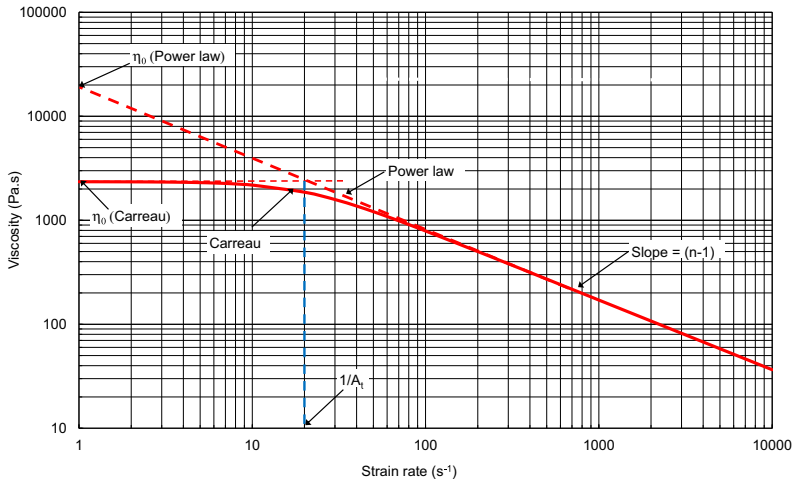


FIG. 5.7 Comparison of models for flow behaviour.

viscosity is known, T_2 (°C) is the temperature at which the viscosity is required and T_0 (°C) is a reference temperature.When $T_0 = T_g$ then $C_1 = 17.4$ and $C_2 = 51.6$.

With the widespread use of software packages to assist with computational fluid dynamics (CFD) of polymer flow situations, other types of viscosity relationships are also used. For example, the regression equation of Klien takes the form

$$\ln \eta_a = a_0 + a_1 \ln \gamma_a + a_{11}(ln\dot{\gamma})^2 + a_2 T + a_{22} T^2 + a_{12} \cdot T \cdot ln\dot{\gamma}_a \qquad (5.28)$$

where a_{ij} are material constants and T is the temperature of the melt (°C).

It should be noted that if a_{11} is small (which is often the case) then this equation also reduces to the Power Law.

Another equation is the polynomial of Muenstedt, which takes the form

$$\begin{aligned} \log \eta_a = \log a_T + A_0 + A_1 \log(a_T \dot{\gamma}_a) + A_2[\log(a_T \dot{\gamma})]^2 \\ + A_3[\log(a_T \dot{\gamma}_a)]^3 + A_4\Big[[\log(a_T \dot{\gamma})]^4 \end{aligned} \qquad (5.29)$$

However, for the high strain rates appropriate for the analysis of typical extrusion and injection moulding situations it is often found that the simple Power Law is perfectly adequate. Thus Eqs. (5.22), (5.23) and (5.27) are important for most design situations relating to polymer melt flow.

Example 5.1 Applying the Carreau model to polypropylene, the following constants are known at 190 °C.

$$\eta_0 = 2350\ Pa \cdot s, \quad A_T = 0.05, \quad n = 0.33$$

Estimate the viscosity of polypropylene at 230 °C and a shear rate of 1000 s^{-1}. The glass transition temperature for the polypropylene is −10 °C.

Solution The temperature shift factor from 190 °C to 230 °C may be obtained from

$$\log a_T = \frac{C_1(T_1 - T_g)}{C_2 + (T_1 - T_g)} - \frac{C_1(T_2 - T_g)}{C_2 + (T_2 - T_g)}$$

$$= \frac{17.4(190 + 10)}{51.6 + (190 + 10)} - \frac{17.4(230 + 10)}{51.6 + (230 + 10)}$$

$$a_T = 0.324$$

Using the Carreau model

$$\eta_a = \eta_0 a_T \left(1 + a_T \left(A_T \cdot \dot{\gamma}_a\right)^2\right)^{\frac{n-1}{2}}$$

$$= 2350(0.324)\left(1 + 0.324(0.05 \times 1000)^2\right)^{\frac{0.33-1}{2}}$$

So, $\eta_a = 80.7$ Pa·s at 230 °C and $\dot{\gamma} = 1000$ s^{-1}

5.5 Isothermal flow in channels: Non-Newtonian fluids

(a) Flow of power law fluid along a channel of uniform circular cross-section

Referring to Fig. 5.4 and remembering that equilibrium of forces was the only condition necessary to derive (5.5) then this equation may be used as the starting point for the analysis of any fluid.

$$\tau = \frac{r}{2}\left(\frac{\partial P}{\partial z}\right) \qquad (5.5)$$

Now $$\tau = \eta\dot{\gamma} = \eta\frac{\partial v}{\partial r}$$

So $$\frac{\partial V}{\partial R} = \frac{r}{2\eta}\left(\frac{\partial P}{\partial z}\right)$$

but from (5.23)

$$\eta = \eta_0\left[\frac{\dot{\gamma}}{\dot{\gamma}_0}\right]^{n-1} = \eta_0\left[\frac{\partial V/\partial r}{\dot{\gamma}_0}\right]^{n-1}$$

So from above

$$\frac{\partial V}{\partial r} = \frac{r}{2\eta_0\left[\frac{\partial V/\partial r}{\dot{\gamma}_0}\right]^{n-1}}\cdot\left(\frac{\partial P}{\partial z}\right)$$

$$\left(\frac{\partial V}{\partial r}\right)^n = \frac{r\left(\dot{\gamma}_0\right)^{n-1}}{2\eta_0}\cdot\left(\frac{\partial P}{\partial z}\right)$$

Integrating this between the limits

$$\text{Velocity} = V \text{ at radius} = r$$

$$\text{Velocity} = 0 \text{ at radius} = R$$

The equation for velocity at any radius may then be expressed as

$$V = \left(\frac{n}{n+1}\right)\dot{\gamma}_0^{(n-1)/n}\left[\frac{(\partial P)/(\partial z)}{2\eta_0}\right]^{1/n}\left[r^{(n+1)/n} - R^{(n+1)/n}\right]$$

$$\text{At } r = 0,\ V = V_0$$

$$V_0 = -\left(\frac{n}{n+1}\right)\dot{\gamma}_0^{(n+1)/n}\left[\frac{(\partial P)/(\partial z)}{2\eta_0}\right]^{1/n} R^{(n+1)/n} \tag{5.30}$$

$$V = V_0\left[1 - \left(\frac{r}{R}\right)^{(n+1)/n}\right] \tag{5.31}$$

The volume flow rate, Q, is given by

$$Q = \int_o^R 2\pi r V dr = 2\pi V_0 \int_0^R r\left(1 - \left(\frac{r}{R}\right)^{(n+1)/n}\right)dr$$

$$Q = \left(\frac{n+1}{3n+1}\right)\pi R^2 V_0 \tag{5.32}$$

Also Shear Rate,

$$\dot{\gamma} = \frac{\partial V}{\partial r} = \frac{\partial}{\partial r}\left[V_0\left(1 - \left(\frac{r}{R}\right)^{(n+1)/n}\right)\right]$$

$$\dot{\gamma} = -\frac{\left(\frac{n+1}{n}\right)V_0}{R} \cdot \left(\frac{r}{R}\right)^{1/n} \tag{5.33}$$

The shear rate at the wall is obtained by letting $r = R$ and the equation is more convenient if V_0 is replaced by Q from (5.33). In this case

$$\text{Shear Rate at wall} \quad \dot{\gamma}_w = -\left(\frac{3n+1}{4n}\right)\frac{4Q}{\pi R^3}$$

It is worth noting that since a Newtonian Fluid is a special case of the Power Law fluid when $n = 1$, then the above equations all reduce to those derived in Section 5.3(a) if this substitution is made.

(b) Flow of power law fluid between parallel plates

Referring to Fig. 5.5 and recognising that Eq. (5.13) is independent of the fluid then

$$\tau = y\frac{\partial P}{\partial z}$$

but
$$\tau = \eta\frac{\partial V}{\partial y} \text{ and } \eta = \eta_0\left[\frac{\dot{\gamma}}{\dot{\gamma}_0}\right]^{n-1}$$

So
$$\frac{\partial V}{\partial y} = \frac{y}{\eta_0\left[\frac{\partial V/\partial y}{\dot{\gamma}_0}\right]^{n-1}} \cdot \left(\frac{\partial P}{\partial z}\right)$$

$$\frac{\partial V}{\partial y} = \dot{\gamma}_0^{(n-1)/n} y^{1/n}\left(\frac{1}{\eta_0}\frac{\partial P}{\partial z}\right)^{1/n}$$

Integrating this equation between the limits

Velocity $= V$ at distance $= y$

Velocity $= 0$ at distance $= H/2$

$$V = \left(\frac{n}{n+1}\right)\dot{\gamma}_0\left(\frac{1}{\eta_0\dot{\gamma}_0}\frac{\partial P}{\partial z}\right)^{1/n}\left[y^{(n+1)/n} - \left(\frac{H}{2}\right)^{(n+1)/n}\right]$$

At $y = 0$, $V = \mathrm{V}_0$

$$V_0 = -\left(\frac{n}{n+1}\right)\dot{\gamma}_0\left(\frac{1}{\eta_0\dot{\gamma}_0}\frac{\partial P}{\partial z}\right)^{1/n}\left(\frac{H}{2}\right)^{(n+1)/n} \tag{5.34}$$

And using this to simplify the expression for V

$$V = V_0\left(1 - \left(\frac{2y}{H}\right)^{(n+1)/n}\right) \tag{5.35}$$

The flow rate, Q, may then be obtained from the expression

$$Q = 2T\int_0^{H/2} V dy$$

$$= 2T\int_0^{H/2} V_0\left(1 - \left(\frac{2y}{H}\right)^{(n+1)/n}\right)dy$$

$$Q = \left(\frac{n+1}{2n+1}\right) T V_0 H \tag{5.36}$$

And as before

$$\dot{\gamma} = \frac{\partial V}{\partial y} = \frac{\partial}{\partial y}\left[V_0\left(1 - \left(\frac{2y}{H}\right)^{(n+1)/n}\right)\right]$$

$$\dot{\gamma} = -V_0\left(\frac{2}{H}\right)^{(n+1)/n}\left(\frac{n+1}{n}\right) y^{1/n} \tag{5.37}$$

At the wall $y = H/2$ and substituting for V_0 from (5.36) then

$$\dot{\gamma}_w = -\left(\frac{2n+1}{n}\right)\frac{2Q}{TH^2}$$

It can be seen that in the special case of $n = 1$ these equations reduce to those for Newtonian Flow.

5.6 Isothermal flow in non-uniform channels

In many practical situations involving the flow of polymer melts through dies and along channels, the cross-sections are tapered. In these circumstances, tensile stresses will be set up in the fluid and their effects superimposed on the effects due to shear stresses as analysed above. Cogswell has analysed this problem for the flow of a power law fluid along coni-cylindrical and wedge channels. The flow in these sections is influenced by three factors:

(1) entry effects given suffix O
(2) shear effects given suffix S
(3) extensional effects given suffix E

Each of these will contribute to the behaviour of the fluid although since each results from a different deformation mode, one effect may dominate depending on the geometry of the situation. This will be seen more clearly later when specific design problems are tackled.

(a) Flow in coni-cylindrical dies

Consider the channel section shown in Fig. 5.8(a) from which the element shown in Fig. 5.8(b) may be taken.

(i) Pressure drop due to shear, P_s

Assuming that the different modes of deformation are separable then considering equilibrium of forces in regard to the shear stress only, gives

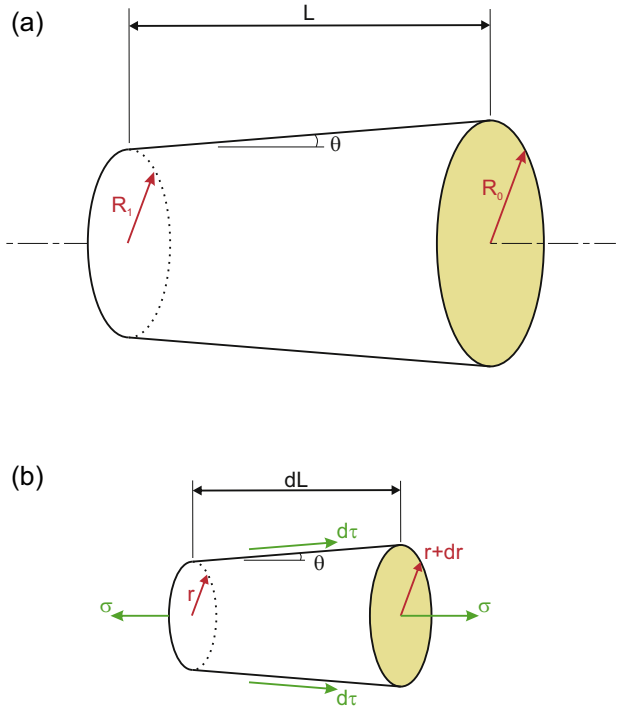


FIG. 5.8 Analysis of coni-cylindrical die.

$$dP_s \cdot \pi r^2 = 2\pi r dl \sec\theta \cdot \tau \cos\theta$$

$$dP_s = \frac{2\tau}{r} \cdot dl \tag{5.38}$$

but for a power law fluid

$$\tau = \tau_0 \dot{\gamma}^n \quad \text{and} \quad \dot{\gamma} = \left(\frac{3n+1}{n}\right) \frac{Q}{\pi r^3}$$

and using

$$dl = \frac{dr}{\tan\theta}$$

then (5.38) becomes

$$dP_s = \frac{2\tau_0}{\tan\theta} \left(\left(\frac{3n+1}{n}\right)\frac{Q}{\pi}\right)^n \frac{dr}{r^{1+3n}}$$

Integrating

$$P_s = \frac{2\tau_0}{\tan\theta}\left(\left(\frac{3n+1}{n}\right)\frac{Q}{\pi}\right)^n \int_{R_1}^{R_0} \frac{dr}{r^{1+3n}}$$

$$P_s = \frac{2\tau_0}{3n\tan\theta}\left(\left(\frac{3n+1}{n}\right)\frac{Q}{\pi R_1^3}\right)^n \left[1-\left(\frac{R_1}{R_0}\right)^{3n}\right]$$

$$P_s = \frac{2\tau_1}{3n\tan\theta}\left[1-\left(\frac{R_1}{R_0}\right)^{3n}\right] \tag{5.39}$$

(ii) Drop due to extensional flow P_E

$$dP_E \cdot \pi r^2 = \sigma\left[\pi(r+dr)^2 - \pi r^2\right]$$

$$dP_E = \frac{2\sigma dr}{r}$$

Integrating

$$P_E = \int_{R_1}^{R_0} \frac{2\sigma dr}{r} \tag{5.40}$$

In order to integrate the right hand side of this equation it is necessary to get an equation for σ in terms of r. This may be obtained as follows.

Consider a converging annulus of thickness, h, and radius, a, within the die. If the angle of convergence is ϕ then simple geometry indicates that for uniform convergence

$$\tan\phi = \frac{a}{r}\tan\theta \quad \text{and} \quad \frac{dh}{h} = \frac{da}{a}$$

Now if the simple tensile strain, ε, is given by

$$\varepsilon = \frac{dA}{A}$$

then the strain rate, $\dot{\varepsilon}_a$ will be given by

$$\dot{\varepsilon}_a = \frac{1}{area}\frac{d(area)}{dt} = \frac{1}{2\pi ah}\cdot\frac{d(2\pi ah)}{at} = \frac{2}{a}\frac{da}{dt}$$

but
$$\frac{da}{dt} = \tan\phi \cdot \frac{dl}{dt} = \frac{a}{r}\tan\theta \cdot V$$

where V is the velocity of the fluid parallel to the centre line of the annulus. From Eqs. (5.31) and (5.32) this velocity is given by

$$V = \left(\frac{3n+1}{n+1}\right)\ \frac{Q}{\pi r^3}\left[\left(\frac{a}{r}\right)^{(n+1)/n} - 1\right]$$

So

$$\dot{\varepsilon}_a = \frac{2}{r}\tan\theta\left(\frac{3n+1}{n+1}\right)\ \frac{Q}{\pi r^3}\left[\left(\frac{a}{r}\right)^{(n+1)/n} - 1\right]$$

The average extensional stress is obtained by integrating across the element so

$$\sigma\pi r^2 = \int_0^r \sigma_a 2\pi a da$$

and since by definition $\sigma_a = \lambda\dot{\varepsilon}_a$

$$\sigma\pi r^2 = \int_0^r \lambda\dot{\varepsilon}_a 2\pi a da = \int_0^r \lambda\cdot\frac{2}{r}\tan\theta\left(\frac{3n+1}{n+1}\right)\ \frac{Q}{\pi r^2}\left[\left(\frac{a}{r}\right)^{(n+1)/n} - 1\right]2\pi a da$$

$$\sigma = \lambda\left(\frac{2Q}{\pi r^3}\right)\tan\theta \tag{5.41}$$

So in (5.40)

$$P_E = \int_{R_1}^{R_0}\frac{2}{r}\lambda\left(\frac{2Q}{\pi r^3}\right)\tan\theta\cdot dr = \frac{\lambda\tan\theta}{2}\left(\frac{4Q}{\pi R_1^3}\right)\left[1 - \left(\frac{R_1}{R_0}\right)^3\right]$$

Using (5.41)

$$P_E = 2\sigma_1/3\left[1 - \left(\frac{R_1}{R_0}\right)^3\right] \tag{5.42}$$

(iii) Pressure drop at die entry, P_0

When the fluid enters the die from a reservoir it will conform to a streamline shape such that the pressure drop is a minimum. This will tend to be of a coni-cylindrical geometry and the pressure drop, P_0, may be estimated by considering an infinite number of very short frustrums of a cone.

Consider a coni-cylindrical die with outlet radius, R_0, and inlet radius, R_i, and an included angle $2\alpha_0$.

From (5.40)

$$P_S = \frac{2\tau_0}{3n \tan \alpha_0}[1 - x^n]$$

From (5.42)

$$P_E = \frac{\lambda \tan \theta}{3}\left(\frac{4Q}{\pi R_0^3}\right)[1 - x]$$

where $x = \left(\frac{R_0}{R_1}\right)^3$ for convenience.

The pressure drop, P_1, for such a die is

$$P_1 = P_S + P_E$$
$$= \frac{a}{\tan \alpha_0} + b \tan \alpha_0$$

where $$a = \frac{2\tau_0}{3n}[1 - x^n], b = \frac{\lambda}{3}\left(\frac{4Q}{\pi R_0^3}\right)[1 - x]$$

For minimum pressure drop the differential of pressure drop with respect to the angle α_0 should be zero

$$\frac{dP_1}{d(\tan\alpha_0)} = \frac{-a}{\tan^2\alpha_0} + b = 0$$

$$\tan\alpha_0 = \left(\frac{a}{b}\right)^{1/2}$$

So the minimum value of pressure is given by

$$P_1 = a^{1/2}b^{1/2} + a^{1/2}b^{1/2} = 2a^{1/2}b^{1/2}$$

If this procedure is repeated for other short coni-cylindrical dies then it is found that

$$P_2 = x^{(1+n)/2}P_1$$

$$P_3 = \left(x^{(1+n)/2}\right)^2 P_1$$

and so on.

So the total entry pressure loss, P_0, is given by

$$P_0 = \underset{x\to 1}{\text{Limit}} \sum_{i=1}^{i=\infty} P_i = \frac{2\sqrt{2}}{3}\left(\frac{4Q}{\pi R_0^3}\right)\left(\frac{\eta\lambda}{n}\right)^{1/2} \cdot \underset{x\to 1}{\text{Limit}}\, f(x)$$

where

$$f(x) = [(1-x^n)(1-x)]^{1/2} \cdot \left[1 + x^{(1+n/2)} + \left(x^{(1+n/2)}\right)^2 + \left(x^{(1+n/2)}\right)^3 + \ldots\right]$$

and η = viscosity corresponding to shear rate at die entry.

$$P_0 = \frac{4\sqrt{2}}{3(n+1)}\left(\frac{4Q}{\pi R_0^3}\right)(\eta\lambda)^{1/2} \tag{5.43}$$

Also $$\tan^2\alpha_0 = \frac{2\tau_0}{3n}\cdot\frac{3}{\lambda}\left(\frac{\pi R_0^3}{4Q}\right)\underset{x\to 1}{\text{Limit}}\left[\frac{1-x^n}{1-x}\right]$$

$$\tan\,\alpha_0 = \left(\frac{2\eta}{\lambda}\right)^{1/2}$$

So that from (5.44)

$$P_0 = \frac{8\sigma}{3(n+1)} \tag{5.44}$$

(b) Flow in wedge shaped die

Referring to the terminology in Fig. 5.9 and using analysis similar to that for the coni-cylindrical die, it may be shown that the shear, extensional and die entry pressure losses are given by

$$P_S = \frac{\tau_1}{2n\tan\phi}\left[1 - \left(\frac{H_1}{H_0}\right)^{2n}\right] \tag{5.45}$$

$$P_E = \frac{\sigma_1}{2}\left[1 - \left(\frac{H_1}{H_0}\right)^2\right] \tag{5.46}$$

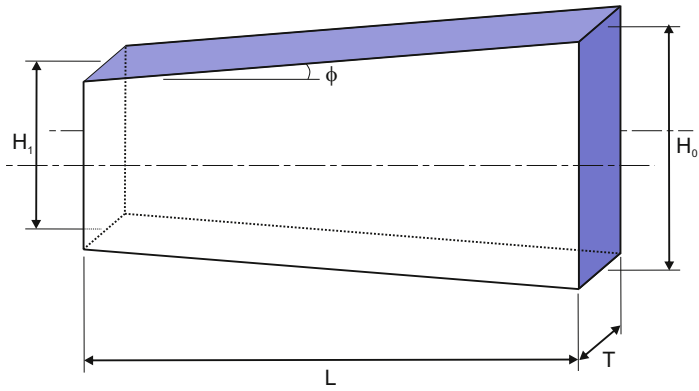


FIG. 5.9 Analysis of flow in tapered wedge.

$$P_0 = \frac{4}{(3n+1)}\left(\frac{6Q}{TH_0^2}\right)(\eta\lambda)^{1/2} \tag{5.47}$$

where η corresponds to shear rate at die entry.

Also
$$\dot{\gamma} = \left(\frac{2n+1}{n}\right)\left(\frac{2Q}{TH^2}\right) \tag{5.48}$$

$$\dot{\varepsilon} = (\dot{\gamma}/3)\tan\phi \tag{5.49}$$

And
$$\tan\beta_0 = \frac{3}{2}\left(\frac{\eta}{\lambda}\right)^{1/2} \tag{5.50}$$

where β_0 is the half angle of convergence to the die.

5.7 Elastic behaviour of polymer melts

As discussed earlier, polymer melts can also exhibit elasticity. During flow they have the capacity to store strain energy and when the stresses are removed, this strain is recoverable. A good example of elastic recovery is post extrusion swelling. After extrusion the dimensions of the extrudate are larger than those of the die, which may present problems if the dimensions of the extrudate are critical. In these circumstances some knowledge of the amount of swelling likely to occur is essential for die design. If the die is of a non-uniform section (tapered, for example) then there will be recoverable tensile and shear strains. If the die has a uniform cross-section and is long in relation to its transverse dimensions then any tensile stresses which were set up at the die entry for example, normally relax out so that only the shear component contributes to the

swelling at the die exit. If the die is very short (ideally of zero length) then no shear stresses will be set up and the swelling at the die exit will be the result of recoverable tensile strains only. In order to analyse the phenomenon of post extrusion swelling it is usual to define the swelling ratio, B, as

$$B = \frac{\text{dimension of extrudate}}{\text{dimension of die}}$$

5.7.1 Swelling ratios due to shear stresses

(a) Long capillary

Fig. 5.10 shows an annular element of fluid of radius r and thickness dr subjected to a shear stress in the capillary. When the element of fluid emerges from the die it will recover to the form shown by $ABCD$.

If the shear strain at radius r is γ_r then

$$\gamma_r = \tan\alpha = \frac{ED}{AE}$$

Also

$$\frac{\text{area of swollen annulus}}{\text{initial area of annulus}} = \frac{2\pi rdr'}{2\pi rdr} = \frac{AD}{AE}$$

$$= \frac{(AE^2 + ED^2)^{1/2}}{AE}$$

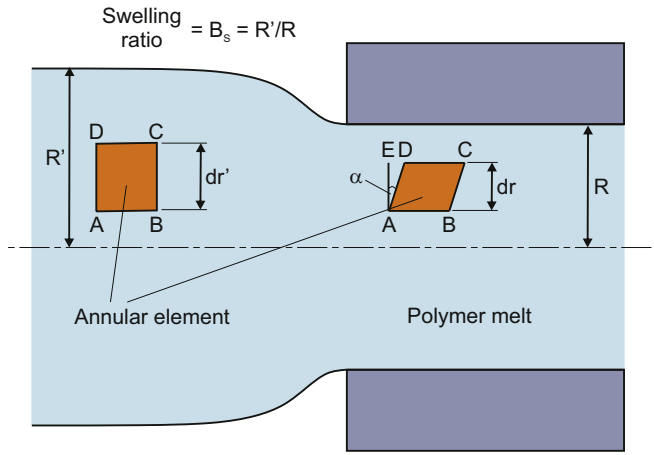


FIG. 5.10 Polymer melt emerging from a long die.

$$= \left(1 + \left(\frac{ED}{AE}\right)^2\right)^{1/2}$$

$$= \left(1 + \gamma_r^2\right)^{1/2}$$

So from the definition of swelling ratio and using the subscripts **S** and **R** to denote **S**hear swelling in the **R**adial direction then

$$B_{SR}^2 = \frac{\text{area of swollen extrudate}}{\text{area of capillary}} = \frac{\int_0^R \left(1 + \gamma_r^2\right)^{1/2} 2\pi r dr}{\int_0^R 2\pi r dr}$$

Assuming that the shear strain, γ_r, varies linearly with radius, r, then

$$\gamma_r = \frac{r}{R}\gamma_R$$

where γ_R is the shear strain at the wall.

So

$$B_{SR}^2 = \frac{\int_0^R \left(1 + \frac{r^2}{R^2}\gamma_R^2\right)^{1/2} 2\pi r dr}{\pi R^2}$$

$$B_{SR} = \left[\frac{2}{3}\gamma_R\left\{\left(1 + \gamma_R^{-2}\right)^{3/2} - \gamma_R^{-3}\right\}\right]^{1/2} \tag{5.51}$$

(b) Long rectangular channel

When the polymer melt emerges from a die with a rectangular section there will be swelling in both the width (T) and thickness (H) directions. By a similar analysis to that given above; expressions may be derived for the swelling in these two directions. The resulting equations are

$$B_{ST} = \left[\frac{1}{2}\left(1 + \gamma_R^2\right)^{1/2} + \frac{1}{2\gamma_R}\ln\left(\gamma_R + \left(1 + \gamma_R^2\right)^{1/2}\right)\right]^{1/3} \tag{5.52}$$

$$B_{SH} = B_{ST}^2 \tag{5.53}$$

Eqs. (5.51)–(5.53) can be cumbersome if they are to be used regularly so the relationships between swelling ratio and recoverable strain are often presented graphically as shown in Fig. 5.11.

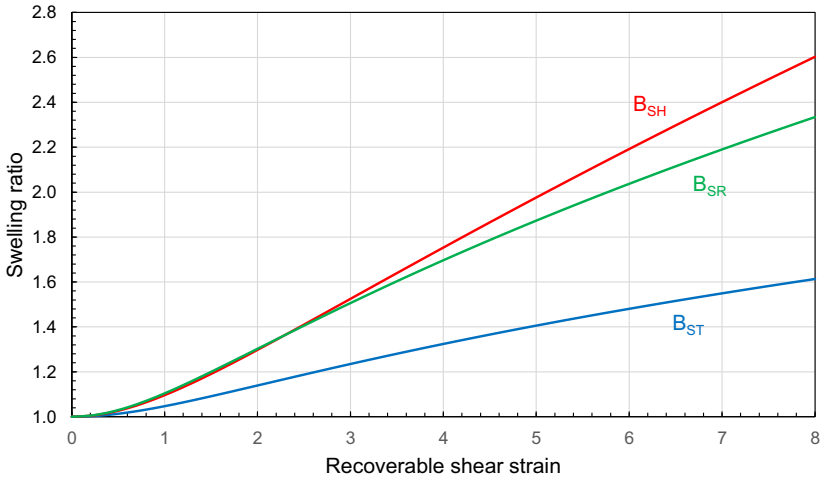


FIG. 5.11 Variation of swelling ratio for capillary and slit dies.

5.7.2 Swelling ratio due to tensile stresses

(a) short capillary (zero length)

Consider the annular element of fluid shown in Fig. 5.12. The true tensile strain ε_R in this element is given by

$$\varepsilon_R = \ln(1+\varepsilon)$$

where ε is the nominal strain (extension/original length)

$$\varepsilon_R = \ln\left(1+\left(\frac{dr^{'}-dr}{dr}\right)\right)$$

$$e^{\varepsilon_R} = 1+\left(\frac{dr^{'}-dr}{dr}\right)$$

$$(e^{\varepsilon_R}-1)dr+dr = dr^{'}$$

Now,

$$\frac{\text{area of swollen annulus}}{\text{original area of annulus}} = \frac{2\pi r dr^{'}}{2\pi r dr} = \frac{dr^{'}}{dr}$$

$$= \frac{(e^{\varepsilon_R}-1)dr+dr}{dr}$$

$$= e^{\varepsilon_R}$$

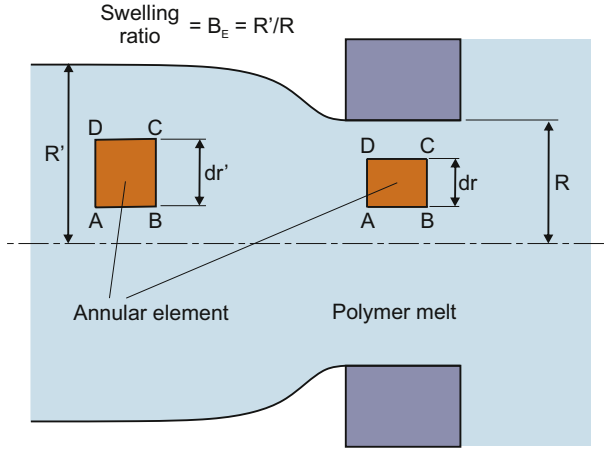


FIG. 5.12 Polymer melt emerging from a short die.

So from the definition of swelling ratio and using the subscript, *E,* to denote extensional stresses then

$$B_{ER}^2 = \frac{\text{area of swollen extrudate}}{\text{area of capillary}} = \frac{\int_0^R 2\pi r e^{\varepsilon_R} dr}{\int_0^R 2\pi r dr}$$

$$B_{ER} = (e^{\varepsilon_R})^{1/2} \tag{5.54}$$

(b) Short rectangular channel

By similar analysis it may be shown that for a short rectangular slit the swelling ratios in the width (T) and thickness (H) directions are given by

$$B_{ET} = (e^{\varepsilon_R})^{1/4} \tag{5.55}$$

$$B_{EH} = (e^{\varepsilon_R})^{1/2} \tag{5.56}$$

Although these expressions are less difficult to use than the expressions for shear, it is often convenient to have the relationships available in graphical form as shown in Fig. 5.13.

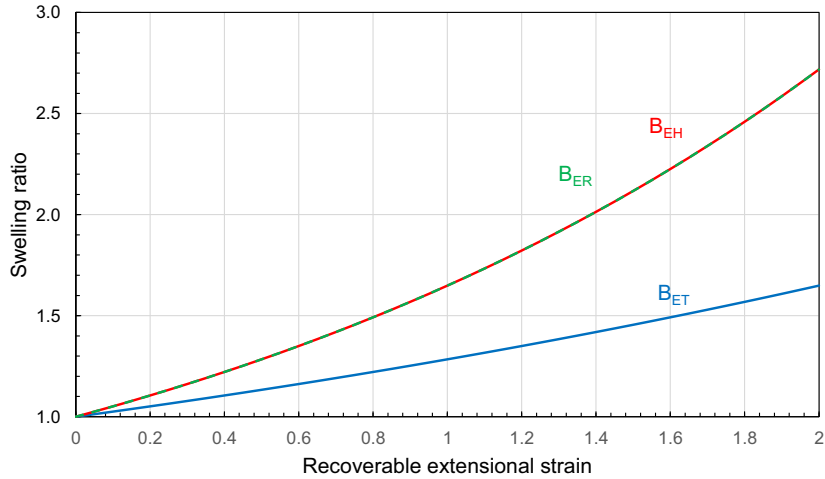


FIG. 5.13 Variation of swelling ratio for capillary and slit dies.

5.8 Residence and relaxation times

(a) Residence (or dwell) time

This refers to the time taken for the polymer melt to pass through the die or channel section. Mathematically it is given by the ratio

$$\text{Residence time}, t_R = \frac{\text{Volume of channel}}{\text{Volume flow rate}} \tag{5.57}$$

For the uniform channels analysed earlier, it is a simple matter to show that the residence times are:

Newtonian Flow

$$\text{Circular Cross Section} \quad t_R = \frac{8\eta L^2}{PR^2} \tag{5.58}$$

$$\text{Rectangular Cross Section} \quad t_R = \frac{12\eta L^2}{PH^2} \tag{5.59}$$

Power Law Fluid

$$\text{Circular Cross Section} \quad t_R = \left(\frac{3n+1}{n+1}\right)\frac{L}{V_0} \tag{5.60}$$

$$\text{Rectangular Cross Section} \quad t_R = \left(\frac{2n+1}{n+1}\right)\frac{L}{V_0} \tag{5.61}$$

(b) Relaxation (or natural) time

In Chapter 2 when the Maxwell and Kelvin models were analysed, it was found that the time constant for the deformations was given by the ratio of viscosity to modulus. This ratio is sometimes referred to as the Relaxation or Natural time and is used to give an indication of whether the elastic or the viscous response dominates the flow of the melt.

To do this, a *Deborah Number* $N_{\text{deb,}}$ has been defined as

$$N_{\text{deb}} = \frac{\text{Relaxation or Natural Time}}{\text{Timescale of the process}} \tag{5.62}$$

If $N_{\text{deb}} > 1$ then the process is predominantly elastic, whereas if $N_{\text{deb}} < 1$ then viscous effects dominate the flow.

5.9 Temperature rise in die

Power is the work done per unit time, where work in the simplest sense is defined as

$$\text{Work} = (\text{force}) \times (\text{distance})$$

Therefore

$$\text{Power} = (\text{force}) \times (\text{distance per unit time})$$

$$= (\text{Pressure drop} \times \text{area}) \times (\text{velocity})$$

but the volume flow rate, Q, is given by

$$\text{Q} = \text{area} \times \text{velocity}$$

$$\text{So Power} = P \cdot Q \tag{5.63}$$

where P is the pressure drop across the die.

Using this expression, it is possible to make an approximation for the temperature rise of the fluid during extrusion through a die. If it is assumed that all the work is changed into shear heating and that all the heat is taken up evenly by the polymer, then the work done may be equated to the temperature rise in the polymer.

$$\text{Power} = \text{Heat required to change temperature}$$

$$= \text{mass} \times \text{specific heat} \times \text{temperature rise}$$

So

$$PQ = \rho Q \times C_p \times \Delta T$$

$$\Delta T = \frac{P}{\rho C_p} \tag{5.64}$$

where ρ is the density of the fluid and C_p *is* its specific heat.

5.10 Experimental methods used to obtain flow data

In Section 5.11 design examples relating to polymer processing will be illustrated. In these examples the flow data supplied by material manufacturers is referred to, so this section shows how these data may be obtained.

The equipment used to obtain flow data on polymer melts may be divided into two main groups.

(a) Rotational Viscometers − these include the cone and plate and the concentric cylinder.
(b) Capillary Viscometer − the main example of this is the ram extruder.

5.10.1 Cone and plate viscometer

In this apparatus the plastic to be analysed is placed between a heated cone and a heated plate. The cone is truncated and is placed above the plate in such a way that the imaginary apex of the cone is in the plane of the plate. The angle between the side of the cone and the plate is small (typically $<5^\circ$).

The cone is rotated relative to the plate and the torque. *T,* necessary to do this is measured over a range of rotational rates, $\dot{\theta}$.

Referring to Fig. 5.14

$$\text{Area of annulus} = 2\pi r \cdot dr$$

$$\text{Force} = 2\pi r\tau \cdot dr$$

$$\text{Torque} = 2\pi r^2 \tau \cdot dr$$

$$\text{So Total Torque,} \quad T = \int_0^R 2\pi r^2 \tau \cdot dr$$

$$T = \left(\frac{2}{3}\right)\pi R^3 \tau \tag{5.65}$$

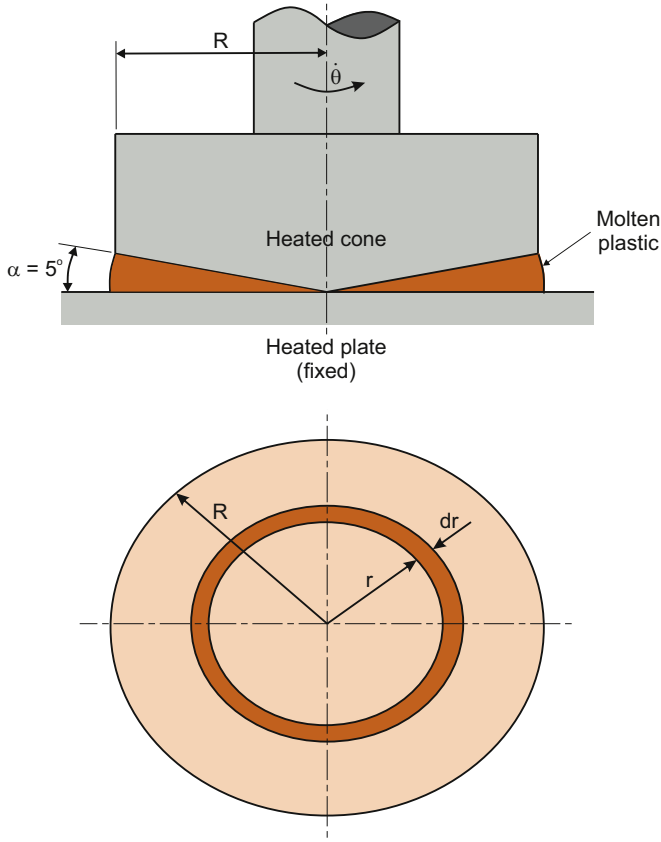


FIG. 5.14 Cone and plate viscometer.

$$\text{Also shear strain,} \quad \gamma = \frac{x}{h} = \frac{r\theta}{r\alpha} = \frac{\theta}{\alpha}$$

$$\text{Strain rate,} \quad \dot{\gamma} = \frac{\dot{\theta}}{\alpha} \tag{5.66}$$

$$\text{And since viscosity} \quad \eta = \frac{\tau}{\dot{\gamma}}$$

$$\eta = \frac{3T}{2\pi R^3} \cdot \frac{\alpha}{\dot{\theta}} \tag{5.67}$$

The disadvantage of this apparatus is that it is generally limited to strain rates in the region 10^{-2} to 10^{3} s^{-1} whereas in plastics processing equipment the strain rates are in the order of 10^{3} s^{-1} to 10^{5} s^{-1}.

5.10.2 Concentric cylinder viscometer

In this apparatus the polymer melt is sheared between concentric cylinders. The torque required to rotate the inner cylinder over a range of speeds is recorded so that viscosity and strain rates may be calculated.

Referring to Fig. 5.15

$$\text{Torque,} \quad T = 2\pi RL \cdot R \cdot \tau = 2\pi R^2 L\tau \tag{5.68}$$

$$\text{Strain rate,} \quad \dot{\gamma} = \frac{du}{dy} = \frac{2\pi RN}{H} \tag{5.69}$$

$$\text{Viscosity,} \quad \eta = \frac{\tau}{\dot{\gamma}} = \frac{TH}{4\pi^2 R^3 LN} \tag{5.70}$$

As in the previous case, this apparatus is usually restricted to relatively low strain rates.

5.10.3 Ram extruder

In this apparatus the plastic to be tested is heated in a barrel and then forced through a capillary die as shown in Fig. 5.16. Normally the ram moves at a

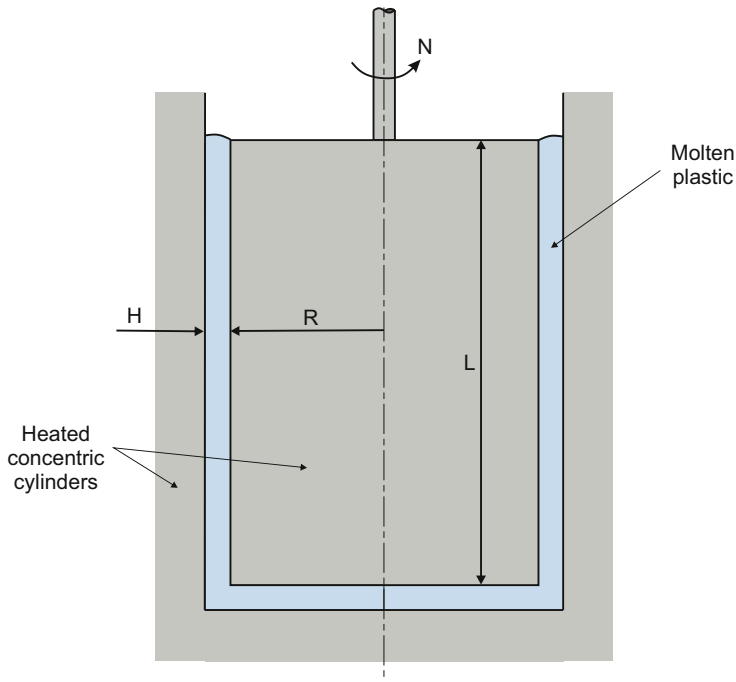


FIG. 5.15 Concentric cylinder viscometer.

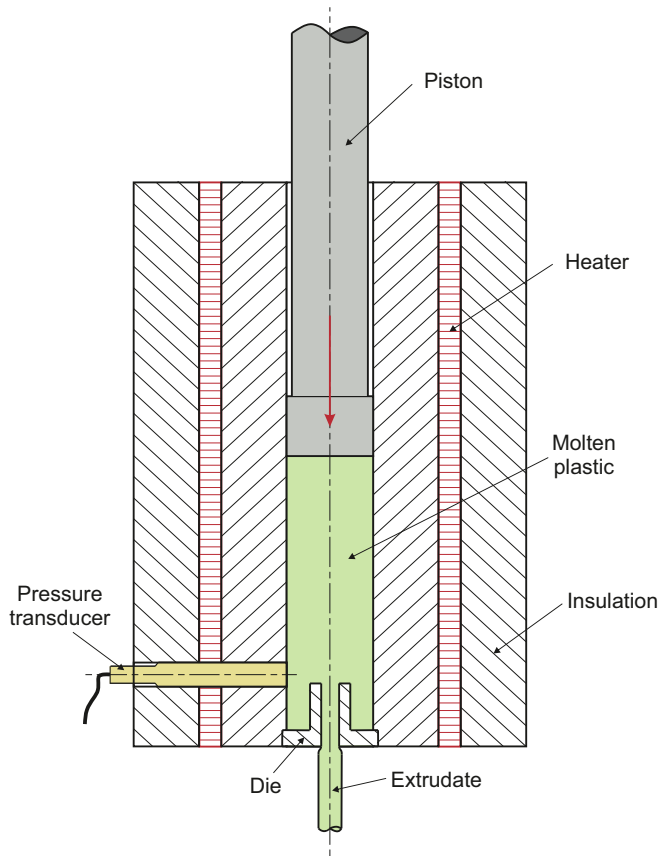


FIG. 5.16 Section through ram extruder.

constant velocity to give a constant volume flow rate, Q. From this it is conventional to calculate the shear rate from the Newtonian flow expression.

$$\dot{\gamma}_a = \frac{4Q}{\pi R^3}$$

Since it is recognised that the fluid is non-Newtonian, this is often referred to as the *apparent* shear rate to differentiate it from the *true* shear rate. If the pressure drop, P, across the die is also measured then the shear stress, τ, may be calculated from

$$\tau = \frac{PR}{2L}$$

This leads to a definition of apparent viscosity as the ratio of shear stress to apparent shear rate

$$\eta_a = \frac{\pi P R^4}{8LQ}$$

A plot of apparent viscosity against shear rate produces a unique flow curve for the melt as shown in Fig. 5.3. Occasionally this information may be based on the true shear rate. As shown in Section 5.4(a) this is given by

$$\dot{\gamma} = \left(\frac{3n+1}{4n}\right)\frac{4Q}{\pi R^3}$$

However, this then means that the true shear rate must always be used in the flow situation being analysed. Experience has shown that this additional complexity is unnecessary because if the Newtonian shear rate is correlated with flow data which has been calculated using a Newtonian shear rate, then no error is involved.

Note that rotational viscometers give true shear rates and if this is to be used with Newtonian based flow curves then, from above, a correction factor of $(4n/3n + 1)$ needs to be applied to the true shear rate.

The ratio $(3n + 1)/4n$ is called the Rabinowitsch Correction Factor and it is used to convert Newtonian shear rates to true shear rates.

There are two other points worth noting about this test. Firstly, the flow data is produced using a capillary die so that its use on channels of a different geometry would require a correction factor. However, in most cases of practical interest, the factor is not significantly different from 1 and so there is no justification for the additional complication caused by its inclusion.

Secondly, the pressure drop, P, in the above expression is the pressure drop due to shear flow along the die. If a pressure transducer is used to record the pressure drop as shown in Fig. 5.16, then it will also pick up the pressure losses at the die entry. This problem may be overcome by carrying out further tests using either a series of dies having different lengths or a die with a very short (theoretically zero) length. In the former case, the pressure drops for the various lengths of die may be extrapolated to give the pressure drop for entry into a die of zero length. In the second case this pressure is obtained directly by using the so-called zero length die. This is then subtracted from the measured pressure loss, P_L, on the long die being considered, so that

$$\tau = \frac{(P_L - P_0)R}{2L} \tag{5.71}$$

In addition, if the swelling of the extrudate is measured in each of these two tests then the swelling ratio using the long die will be B_{SR} and the swelling ratio using the short die will be B_{ER} (see Section 5.6). Using Eqs. (5.44) and

(5.47) this enables the shear and tensile components of the recoverable strains to be calculated and from them the shear and tensile moduli.

From this relatively simple test, therefore, it is possible to obtain complete flow data on the material as shown in Fig. 5.3. Note that shear rates similar to those experienced in processing equipment can be achieved. Variations in melt temperature and hydrostatic pressure also have an effect on the shear and tensile viscosities of the melt. An increase in temperature causes a decrease in viscosity and an increase in hydrostatic pressure causes an increase in viscosity. Typically, for low density polyethylene an increase in temperature of 40 °C causes a vertical shift of the viscosity curve by a factor of about 3. Since the plastic will be subjected to a temperature rise when it is forced through the die, it is usually worthwhile to check (by means of Eq. 5.64) whether or not this is significant. Fig. 5.2 shows the effect of temperature on the viscosity of polypropylene.

A change in pressure from atmospheric (= 0.1 MPa) to about 100 MPa (a pressure likely to be experienced during processing) causes a vertical shift of the viscosity curve by a factor of about 4 for LDPE. This effect may be important during processing because the material can be subjected to large changes in pressure in sections such as nozzles, gates, etc. However, it should be noted that in some cases the increase or decrease in pressure results in, or is associated with, an increase or decrease in temperatures so that the net effect on viscosity may be negligible.

Other factors such as the use of additives also have an effect on the shape of the flow curves. Flame retardants, if used, tend to decrease viscosity whereas pigments tend to increase viscosity. Fig. 5.17 shows flow curves for a range of plastics.

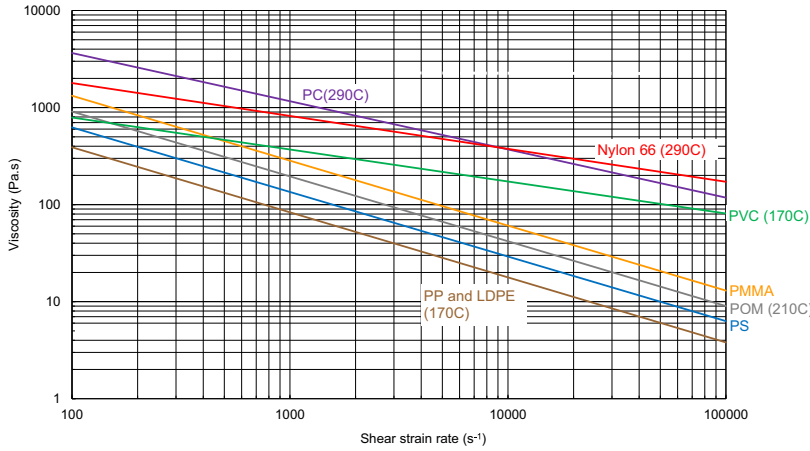


FIG. 5.17 Viscosity curves for a range of plastics (230 °C unless otherwise shown).

5.10.4 Melt Flow Rate (MFR) or Melt Flow Index (MFI)

The Melt Flow Rate Test (also called Melt Flow Index) is a common method used to characterise the processing behaviour of polymer melts. It is, in effect, a single point ram extruder test using standard testing conditions (e.g. BS 2782) as illustrated in Fig. 5.18. The polymer sample is heated in a barrel and then extruded through a standard die using pressure resulting from a standard

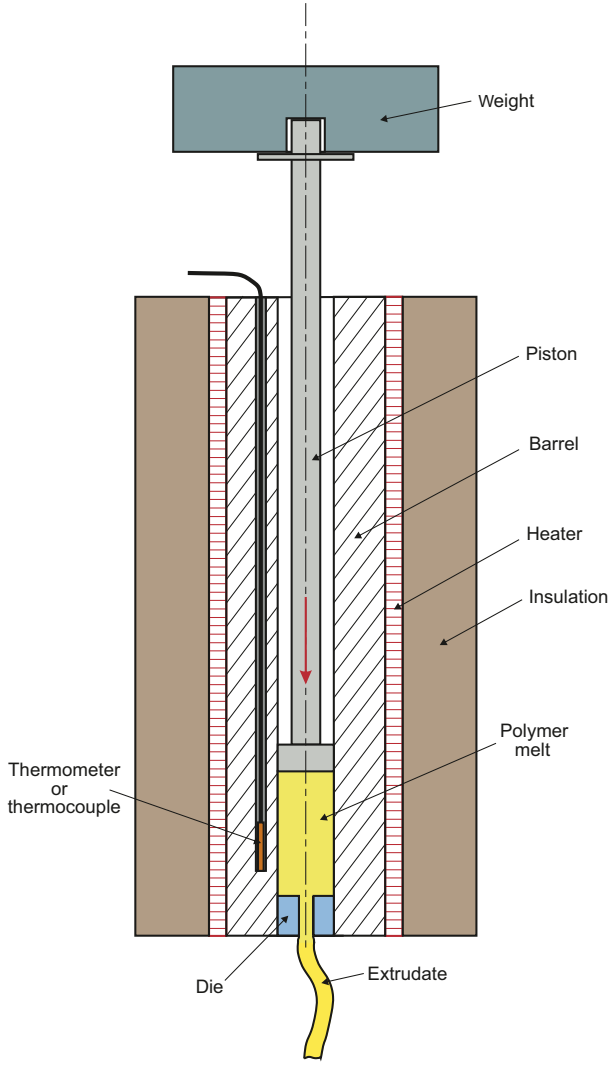


FIG. 5.18 Diagram of apparatus for measuring melt flow index.

weight on a piston. However, unlike the ram extruder test (Fig. 5.16), pressure is not measured and only the temperature of the melt is known. For this reason, the MFR or MFI test cannot be used to calculate melt viscosity, and instead it provides a means of comparing the flow properties of polymer melts under equivalent conditions. In a standard test the weight (in grams) of polymer extruded in 10 min is measured and this is quoted as the melt flow rate (MFR) of the polymer. This provides a very good indication of melt viscosity with high MFR meaning low viscosity, and low MFR meaning high viscosity. Originally the MFR test was developed as a rapid, low cost means of comparing the melt properties of thermoplastics, but today it is now accepted as a standard test for assessing the melt processability of thermoplastics and it is commonly quoted by polymer resin suppliers.

5.10.5 Flow defects

When a molten plastic is forced through a die it is found that under certain conditions there will be defects in the extrudate. In the worst case this will take the form of gross distortion of the extrudate, but it can be as slight as a dullness of the surface. In most cases flow defects are to be avoided since they affect the quality of the output and the efficiency of the processing operation. However, in some cases if the flow anomaly can be controlled and reproduced, it can be used to advantage – for example, in the production of sheets with matt surface finish. Flow defects result from a combination of melt flow properties, die design and processing conditions but some of the exact causes and mechanisms are not completely understood. The two most common defects are:

(a) Melt Fracture When a polymer melt is flowing through a die, there is a critical shear rate above which the extrudate is no longer smooth. The defect may take the form of a spiralling extrudate or a completely random configuration. With most plastics it is found that increasing the melt temperature or the L/D ratio of the die will increase the critical value of shear rate. It is generally believed that the distortion of the extrudate is caused by slip-stick mechanism between the melt and the die wall due to the high shear rates. If there is an abrupt entry to the die, then the tensile/shear stress history which the melt experiences is also considered to contribute to the problem.

(b) Sharkskin Although this defect is also a visual imperfection of the extrudate it is usually differentiated from melt fracture because the defects are perpendicular to the flow direction rather than helical or irregular. In addition, experience has shown that this defect is a function of the linear output rate rather than the shear rate or die dimensions. The most probable mechanism of sharkskin relates to the velocity of skin layers of the melt inside and outside the die. Inside the die the skin layers are almost stationary whereas when the extrudate emerges from the die there must be a

rapid acceleration of the skin layers to bring the skin velocity up to that of the rest of the extrudate. This sets up tensile stresses in the melt which can be sufficient to cause fracture.

5.11 Analysis of flow in some processing operations

Design methods involving polymer melts are difficult because the flow behaviour of these materials is complex. In addition, flow properties of the melt are usually measured under well-defined uniform conditions whereas unknown effects such as heating and cooling in processing equipment make service conditions less than ideal. However, sufficient experience has been gathered using the equations derived earlier that melt flow problems can be tackled quantitatively and with an accuracy which compares favourably with other engineering design situations. In this section a number of polymer processing methods will be analysed using the tools which have been assembled in this chapter. In some cases, the heating and cooling of the melt may have an important effect on the flow behaviour and methods of allowing for this are developed.

Example 5.2 In a plunger-type injection moulding machine the torpedo has a length of 40 mm, a diameter of 23 mm and is supported by three spiders. If, during moulding of polythene at 170 °C, the plunger moves forward at a speed of 15 mm/s, estimate the pressure drop along the torpedo and the shear force on the spiders. The barrel diameter is 25 mm.

Solution Assume that the flow is isothermal.

$$\text{Volume flow rate, } Q = area \times velocity$$

$$= \frac{\pi}{4}\left(25 \times 10^{-3}\right)^2 \times 15 \times 10^{-3}$$

$$= 7.36 \times 10^{-6} \text{ m}^3/\text{s}$$

The gap between the torpedo and the barrel may be considered as a rectangular slit with $T = (\pi \times 24 \times 10^{-3})$ m and $H = 1 \times 10^{-3}$ m

$$\text{So apparent strain rate, } \dot{\gamma} = \frac{6Q}{TH^2} = \frac{6 \times 7.36 \times 10^{-6}}{\pi \times 24 \times 10^{-3} \times \left(1 \times 10^{-3}\right)^2}$$

$$= 585 \text{ s}^{-1}$$

From Fig. 5.3, at this strain rate, $\eta = 400$ Pa s.

So $$\tau = \eta\dot{\gamma} = 400 \times 585 = 2.34 \times 10^5 \text{ Pa}$$

$$P = \frac{2L\tau}{H} = \frac{2 \times 40 \times 10^{-3} \times 2.34 \times 10^{5}}{1 \times 10^{-3}} = 18.7 \text{ MPa}$$

The force on the spider results from:

(a) the force on the torpedo due to the pressure difference across it and
(b) the force on the torpedo due to viscous drag.

Cross-sectional area of torpedo $= \pi r^2$

So force due to pressure $= \pi r^2 P$

$$= \pi\left(11.5 \times 10^{-3}\right)^2 \times 18.7 \times 10^{6}$$

$$= 7.8 \text{ kN}$$

Surface area of torpedo $= \pi DL$

Viscous drag force $= \pi DL\tau$

$$= \pi\left(23 \times 10^{-3}\right)\left(40 \times 10^{-3}\right)\left(2.34 \times 10^{5}\right)$$

$$= 0.68 \text{ kN}$$

So Total Force $= 8.48$ kN

Example 5.3 The output of polythene from an extruder is 30×10^{-6} m^3/s. If the breaker plate in this extruder has 80 holes, each being 4 mm diameter and 12 mm long, estimate the pressure drop across the plate assuming the material temperature is 170 °C at this point. The flow curves in Fig. 5.3 should be used.

Solution Assume the flow is isothermal.

$$\text{Flow rate through each hole} = \frac{30 \times 10^{-6}}{80} \text{m}^3/\text{s}$$

$$\text{So Apparent shear rate, } \dot{\gamma} = \frac{4Q}{\pi R^3}$$

$$= \frac{4 \times 30 \times 10^{-6}}{\pi \times 80 \times (2 \times 10^{-3})^3}$$

$$= 59.7 \text{ s}^{-1}$$

From Fig. 5.3 the shear stress, τ, is 1.2×10^5 Pa and since

$$\tau = \frac{PR}{2L}$$

$$P = \frac{2 \times 12 \times 10^{-3} \times 1.2 \times 10^{5}}{2 \times 10^{-3}}$$

$$= 1.44 \text{ MPa}$$

Example 5.4 Eight polypropylene mouldings, each weighing 10 g are to be moulded using the runner layout shown in Fig. 5.19. If the injection time is 2 s and the melt temperature is 210 °C, calculate the pressure at each cavity if the injection pressure at the sprue is 80 MPa. The density of the polypropylene is 909 kg/m^3 and the volume of the sprue is 5000 mm^3. Assume that the flow is isothermal and ignore the pressure losses at corners.

Solution Firstly it is necessary to determine the volume flow rate through the runners and gates. The total volume of the runners, gates and cavities may be calculated as follows:

$$\text{Volume of 8 cavities} = 8 \times 10 \times \frac{10^{-3}}{909} = 8.8 \times 10^{-5} \text{ m}^3$$

$$= 88 \times 10^{3} \text{ mm}^3$$

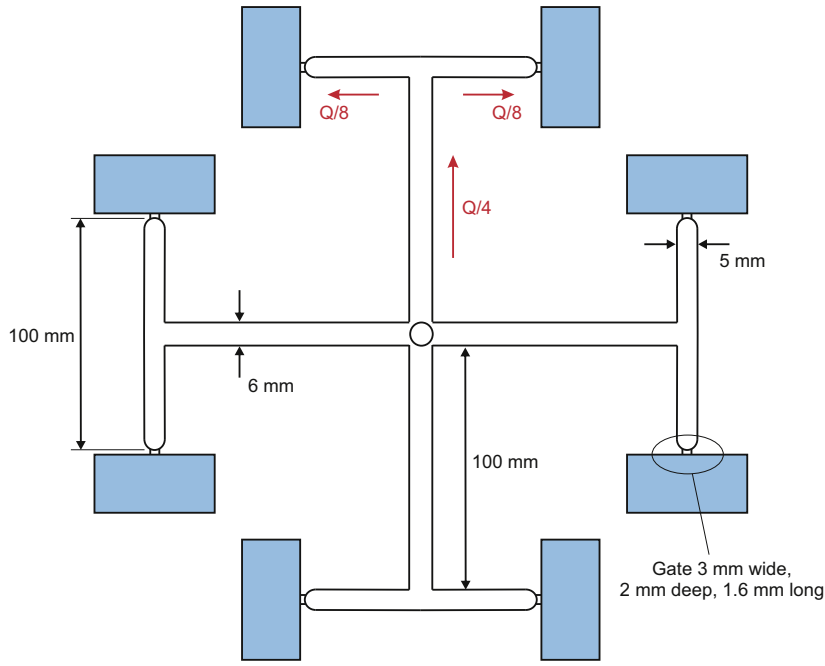


FIG. 5.19 Runner layout, Example 5.4.

$$\text{Volume of long runners} = 4 \times \pi R^2 \times L$$

$$= 4 \times \pi(3)^2 \times 100 = 11.3 \times 10^3 \ \text{mm}^3$$

$$\text{Volume of short runners} = 8 \times \pi(2.5)^2 \times 50 = 7.85 \times 10^3 \ \text{mm}^3$$

$$\text{Volume of sprue} = 5 \times 10^3 \ \text{mm}^3$$

$$\text{Total volume} = 112.2 \times 10^3 \ \text{mm}^3$$

The fill time is 2 s so the total volume flow rate, Q, is given by

$$Q = \frac{112.2 \times 10^3}{2} = 56.1 \times \frac{10^3 \ \text{mm}^3}{\text{s}} = 56.1 \times 10^{-6} \ \text{m}^3/\text{s}$$

To get the pressure loss in the runners and gates. The flow rate in the long runner is $Q/4$, hence:

(i) For long runners $\dot{\gamma} = \frac{4Q}{\pi R^3} = \frac{4 \times 56.1 \times 10^3}{4 \times \pi(3)^3} = 661 \ \text{s}^{-1}$

From the flow curves for polypropylene at 210 °C, at this shear rate, $\eta = 130$ Pa.s, so the shear stress, τ, is given by

$$\tau = 130 \times 661 = 85.9 \ \text{kPa} = \frac{PR}{2L}$$

Hence, Pressure loss, $P = \frac{2L\tau}{R} = \frac{2 \times 100 \times 85.9}{3} = 5.73 \ \text{MPa}$

(ii) For the short runners, the flow rate is Q/8, and so

$$\dot{\gamma} = 571 \ \text{s}^{-1}, \ \eta = 160 \ \text{Pa} \cdot \text{s}, \ \tau = 91.4 \ \text{kPa}$$

and these give the pressure loss = 3.66 MPa.

(iii) For the gates, the flow rate is Q/8 and so

$$\dot{\gamma} = \frac{6Q}{TH^2} = \frac{6 \times 56.1 \times 10^3}{8 \times 3 \times 2^2} = 3506 \ \text{s}^{-1}$$

$$\text{From the flow curves,} \quad \eta = 44 \ Pa.s, \tau = 154.3 \ \text{kPa}$$

So pressure loss, $P = \frac{2L\tau}{H} = \frac{2 \times 1.6 \times 154.3}{2} = 247$ kPa

Total pressure loss $= 5.73 + 3.66 + 0.247 = 5.73 + 3.66 + 0.247$

$= 9.64$ MPa

Thus, pressure available at cavity $= 80 - 9.64$

$= 70.4$ MPa

Example 5.5 In a polyethylene film blowing die the geometry of the die lips is as shown in Fig. 5.20. If the output is 300 kg/h and the density of the polythene is 760 kg/m^3, estimate the pressure drop across the die lips.

Solution

$$\text{Volume flow rate} = \frac{300}{60 \times 60 \times 760} = 109.6 \times 10^{-6} \text{ m}^3/\text{s}$$

The die lips may be considered in three Sections A, B and C and the total pressure drop is the sum of the losses in each.

Section A: Since this is of a uniform section there will only be a pressure drop due to shear.

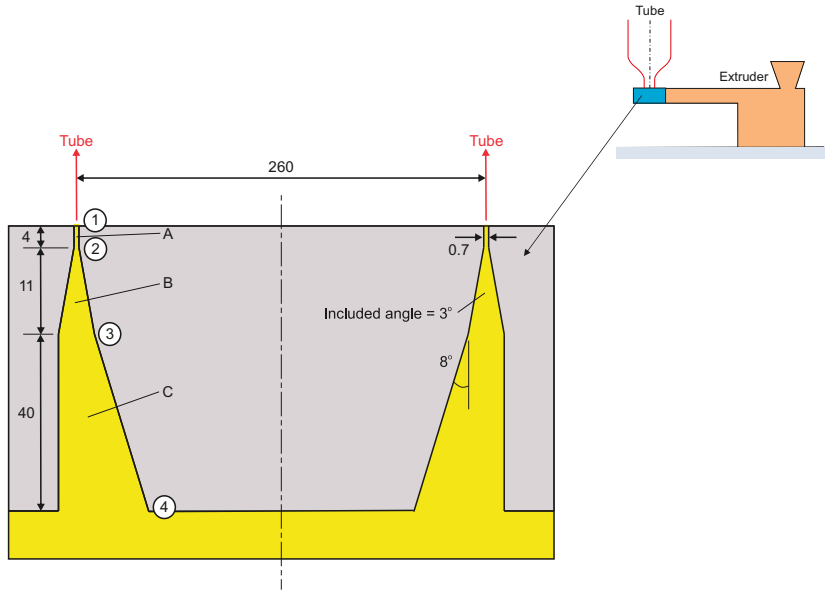


FIG. 5.20 Tube extrusion die.

For a rectangular slot, as shown earlier, the apparent shear rate, $\dot{\gamma}$ at A_1 is given by

$$\dot{\gamma} = \frac{6Q}{TH_1^2} = \frac{6 \times 109.6 \times 10^{-6}}{\pi(260 \times 10^{-3})(0.7 \times 10^{-3})^2} = 1.64 \times 10^3 \ \ \text{s}^{-1}$$

So from Fig. 5.3, $\tau = 3.3 \times 10^5$ Pa

$$P_{S_{12}} = \frac{2L\tau_1}{H_1}$$

$$= \frac{2 \times 4 \times 3.3 \times 10^5}{0.7}$$

$$= 3.77 \ \ \text{MPa}$$

Section B: This section is tapered so there will be pressure losses due to both shear and extensional flows.

From simple geometry $H_3 = H_2 + (2L \tan \alpha)$ where α is half the included angle and $L = 11$ mm.

$$H_2 = 0.7 \ \ \text{mm}, H_3 = 1.28 \ \ \text{mm}$$

$$\text{Now at B}_2, \quad \dot{\gamma} = 1.64 \times 10^3 \ \ \text{s}^{-1}$$

$$\dot{\varepsilon} = (\dot{\gamma} / 3)\tan \alpha = \frac{1}{3} \times 1.64 \times 10^3 \tan(1.5^\circ)$$

$$= 14 \ \ \text{s}^{-1}$$

At B_3,

$$\dot{\gamma} = \frac{6Q}{TH_3^2} = \frac{6 \times 109.6 \times 10^{-6}}{\pi \times 260 \times 10^{-3}(1.276 \times 10^{-3})^2}$$

$$= 494.5 \ \ \text{s}^{-1}$$

$$= \frac{1}{3}(494.5) \ \tan 1.5^\circ$$

$$= 4.3 \ \ \text{s}^{-1}$$

From Fig. 5.3 the flow curve can be taken as a straight line for the shear rate range 500 s^{-1} to 1600 s^{-1} and the power law index n may be taken as 0.33.

So from (5.45)

$$P_{S_{23}} = \frac{\tau_2}{2n\tan\alpha}\left[1-\left(\frac{H_2}{H_3}\right)^{2n}\right]$$

$$= \frac{3.3\times10^5}{2(0.3)\tan1.5}\left[1-\left(\frac{0.7}{1.28}\right)^{0.66}\right]$$

$$= 6.9 \text{ MPa}$$

Also from (5.46)

$$P_{E_{23}} = \frac{\sigma_2}{2}\cdot\left[1-\left(\frac{H_2}{H_3}\right)^2\right]$$

Now $\dot{\varepsilon} = 14s^{-1}$ so from Fig. 5.3 $\sigma_2 = 3.15\times10^6$ Pa (i.e. $2.25\times10^5\times14$)

$$P_{E_{23}} = \frac{3.15\times10^6}{2}\left[1-\left(\frac{0.7}{1.28}\right)^2\right]$$

$$= 1.1 \text{ MPa}$$

Section C: Although this section is tapered on one side only, since the angle is small the error in assuming it is tapered on both sides will be negligible. The included angle is taken as 8°.

$$H_4 = H_3 + L\tan 8^\circ$$

$$= 1.28 + 40\tan8^\circ = 6.9 \text{ mm}$$

At C_3

$$\dot{\gamma} = 494.5 \text{ s}^{-1}$$

$$\dot{\varepsilon} = \frac{1}{3}(494.5)\tan 4^\circ$$

$$= 11.52 \text{ s}^{-1}$$

At C_4

$$\dot{\gamma} = \frac{6Q}{TH_4^2} = \frac{6\times109.6\times10^{-6}}{\pi\times260\times10^{-3}\times(6.9\times10^{-3})^2} = 16.9 \text{ s}^{-1}$$

$$\dot{\varepsilon} = \frac{1}{3}(16.9)\tan 4^\circ$$

$$= 0.39 \text{ s}^{-1}$$

As before

$$P_{S_{34}} = \frac{\tau_3}{2n \tan \alpha} \cdot \left[1 - \left(\frac{H_3}{H_4}\right)^{2n}\right]$$

from Fig. 5.3, $\tau_3 = 2.1 \times 10^5$ Pa at $\dot{\gamma} = 494.5\ \text{s}^{-1}$

$$P_{S_{34}} = \frac{2.1 \times 10^5}{0.6 \tan 4^\circ}\left[1 - \left(\frac{1.28}{6.9}\right)^{0.66}\right]$$

$$= 3.36\ \text{MPa}$$

Also

$$P_{E_{34}} = \frac{\sigma_3}{2} \cdot \left[1 - \left(\frac{H_3}{H_4}\right)^2\right]$$

$\dot{\varepsilon} = 11.52\ \text{s}^{-1}$ so from Fig. 5.3 $\sigma_3 = 2.6 \times 10^6$ Pa (i.e. $2.25 \times 10^5 \times 11.52$)

$$P_{E_{34}} = \frac{2.6 \times 10^6}{2}\left[1 - \left(\frac{1.28}{6.9}\right)^2\right]$$

$$= 1.26\ \text{MPa}$$

In this case there will also be a pressure loss due to flow convergence at the die entry. This may be obtained from (5.47).

$$P_0 = \frac{4}{(3n+1)} \cdot \left(\frac{6Q}{TH_4^2}\right) \cdot (\eta\lambda)^{1/2}$$

At C_4, $\dot{\gamma} = \frac{6Q}{TH_4^2} = 16.9$, so $\eta = 4 \times 10^3$ Pa·s, $\lambda = 2.25 \times 10^5$ Pa·s

$$P_o = \frac{4}{1.9}(16.9)\left(4 \times 10^3 \times 2.25 \times 10^5\right)^{\frac{1}{2}}$$

$$= 1.07\ \text{MPa}$$

So the total pressure drop through the die is given by

$$P = 3.77 + 6.9 + 1.1 + 3.36 + 1.26 + 1.07$$

$$= 17.5\ \text{MPa}$$

Example 5.6 Estimate the dimensions of the tube which will be produced by the die in Example 5.5 assuming that there is no draw-down.

Solution Since the final section of the die lips is not tapered it may be assumed that the swelling at the die exit is due to shear effects only.

At exit,

$$\dot{\gamma} = \frac{6Q}{TH^2} = 1.64 \times 10^3 \ \text{s}^{-1}$$

From Fig. 5.3, $\tau = 3.3 \times 10^5$ Pa and $G = 5 \times 10^4$ Pa

So recoverable strain,

$$\gamma_R = \frac{\tau}{G} = \frac{3.3 \times 10^5}{5.0 \times 10^4} = 6.6$$

Then using Eqs. (5.52) and (5.53), or more conveniently Fig. 5.11, the swelling ratios may be obtained as

$$B_{SH} = 2.31 \ \text{ and } \ B_{ST} = 1.52$$

Therefore swollen thickness of film $= H_1 \times B_{SH}$

$$0.7 \times 2.31 = 1.62 \ \text{ mm}$$

and swollen diameter of bubble $= D \times B_{ST} = 260 \times 1.52 = 395$ mm.

Example 5.7 In many practical situations it is the dimensions of the output which are known or specified and it is necessary to work back (often using an iterative procedure) to design a suitable die.

Design a die which will produce plastic film 0.52 mm thick at a linear velocity of 20 mm/s. The lay-flat width of the film is to be 450 mm and it is known that a blow-up ratio of 1.91 will give the necessary orientation in the film. Assume that there is no draw-down.

Solution Using the terminology from the analysis of blow moulding in Section 4.2.5.

$$2 \times \text{Lay flat width} = \pi D_b$$

$$D_b = \frac{2 \times 450}{\pi} = 286.5 \ \text{ mm}$$

Now it makes the solution simpler to assume that the blow-up ratio is given by D_b/D_1 (i.e. rather than D_b/D_m). Also, this seems practical because the change from D_1 to D_b is caused solely by inflation whereas the change from D_m to D_b includes die swell effects.

$\therefore D_1 = 286.5/1.91 = 150$ mm.

Then, for constant volume

$$\pi D_1 h_1 = \pi D_b h_b$$

$$h_1 = \frac{286.5 \times 0.52}{150} = 1 \ \text{ mm}$$

So having obtained the dimensions of the tube to be produced, the procedure is to start by assuming that there is no die swell. This means that the die dimensions will be the same as those of the tube.

$$\text{Apparent shear rate, } \dot{\gamma} = \frac{6Q}{TH^2}$$

but volume flow rate, $Q = VTH$, where V is the velocity of the plastic melt.

$$\dot{\gamma} = \frac{6V}{H}$$

$$= \frac{6 \times 20}{1} = 120 \text{ s}^{-1}$$

from Fig. 5.3, $\tau = 1.3 \times 10^5$ Pa and $G = 3 \times 10^4$ Pa.
So recoverable shear strain, γ_R, is given by

$$\gamma_R = \frac{\tau}{G} = \frac{1.3 \times 10^5}{3 \times 10^4} = 4.33$$

Assuming that swelling results from shear effects only then from Fig. 5.13 at $\gamma_R = 4.33$, the swelling ratios are

$$B_{SH} = 1.81 \text{ and } B_{ST} = 1.35$$

The initial die dimension must now be adjusted to allow for this swelling.

$$\text{New die gap} = H' = \frac{1}{1.81} = 0.55 \text{ mm}$$

$$\text{New die circumference} = T' = \frac{\pi \times 150}{1.35} = 349 \text{ mm}$$

The volume flow rate, Q, will be constant so the velocity of the melt in the die will also be adjusted.

$$Q = VTH = V'T'H'$$

$$V' = \frac{VTH}{T'H'} = V \cdot B_{SH} \cdot B_{ST}$$

New shear rate,

$$\dot{\gamma} = \frac{6V'}{H'} = \frac{6 \times 20 \times 2 \times 1.35}{0.55} = 589 \text{ s}^{-1}$$

From Fig. 5.3, $\tau = 2.36 \times 10^5$ Pa and $G = 4 \times 10^4$ Pa

So $\gamma_R = 5.9$

and from Fig. 5.13

$$B_{SH} = 2.18 \text{ and } B_{ST} = 1.48$$

$$\text{So new die gap} = H'' = \frac{1}{2.18} = 0.459 \text{ mm}$$

$$\text{new die circumference} = T'' = \frac{\pi \times 150}{1.48} = 318 \text{ mm}$$

If this iterative procedure is repeated again the next values obtained are

$$\text{die gap, } H''' = 0.455 \text{ mm}$$

$$\text{die circumference, } T''' = \frac{\pi \times 150}{1.49} = 316 \text{ mm}$$

These values are sufficiently close to the previous values so the die exit dimensions are

$$\text{Gap} = 0.455 \text{ mm}$$

$$\text{Diameter} = \frac{\pi \times 150}{1.49 \times \pi} = 100.67 \text{ mm}$$

The shear rate, $\dot{\gamma}$, in the die land is

$$\dot{\gamma} = \frac{6 \times 20 \times 1.49 \times 2.2}{0.455}$$

$$= 864.5 \text{ s}^{-1}$$

From Fig. 5.3 it may be seen that this exceeds the shear rate for non-laminar flow (approximately 30 s^{-1}) so that the entry to this region would need to be streamlined. Fig. 5.3 also shows that the extensional strain rate, $\dot{\varepsilon}$ in the tapered entry region should not exceed about 15 s^{-1} if turbulence is to be avoided.

Therefore since

$$\dot{\varepsilon} = \frac{1}{3}\dot{\gamma}\tan\alpha$$

$$\alpha = \tan^{-1}\left(\frac{3\dot{\varepsilon}}{\dot{\gamma}}\right)$$

$$= \tan^{-1}\left(\frac{3 \times 15}{864.5}\right)$$

$$= 2.97^\circ$$

So the full angle of convergence to the die land must be less than $(2 \times 2.97^\circ) = 5.94^\circ$.

To complete the die design it is likely that a third tapered section will be necessary as shown in Fig. 5.20. This will be designed so that the entry to

the die is compatible with the outlet of the die body on the extruder. The maximum angle of convergence of this section can be estimated as shown earlier and the lengths of the two tapered sections selected to ensure the angle is not exceeded for the fixed die inlet dimension. If the length of the 5.94° tapered region is chosen as 10 mm it may be shown that the maximum angle of convergence for the entry to this taper is 58.5°. If the length of this section is fixed at 40 mm and the annular gap at the exit from the extruder is 16 mm, then a suitable angle of convergence would be about 40°.

Example 5.8 It is desired to blow mould a plastic bottle with a diameter of 60 mm and a wall thickness of 2 mm. If the extruder die has an annular slot of outside diameter = 32 mm and inside diameter = 28 mm, calculate the output rate needed from the extruder and recommend a suitable inflation pressure. Use the flow characteristics given in Fig. 5.3. Density of molten polythene = 760 kg/m^3.

Solution In the analysis of blow moulding in Section 4.2.7 (d), it was shown that the thickness, h, of the inflated bottle is given by

$$h = B_{ST}^3 h_d \left(\frac{D_d}{D_m}\right)$$

where h_d = die gap = 2 mm

D_m = mould diameter = 60 mm
D_d = die diameter = $^1/_2$ (28 + 32) = 30 mm

So

$$B_{ST}^3 = \frac{2 \times 60}{30 \times 2}$$

$$B_{ST} = 1.26$$

From Fig. 5.11 at $B_{ST} = 1.26$, $\gamma_R = 3.15$

So $3.15 = \tau/G$

From Fig. 5.3 it is now necessary to determine the combination of τ and G to satisfy this equation.

For example, at $\dot{\gamma} = 5\ \text{s}^{-1}$

$$G = 1.5 \times 10^4\ \text{Pa}, \quad \tau = 5 \times 8.8 \times 10^3 = 4.4 \times 10^4\ \text{Pa}$$

$$\text{So } \frac{\tau}{G} = 2.93$$

$$At\ \dot{\gamma} = 50\ \text{s}^{-1}$$

$$G = 2.5 \times 10^4 \text{ Pa}, \quad \tau = 5.9 \times 10^4 \text{ Pa}, \quad \frac{\tau}{G} = 4.2$$

$$At\ \dot{\gamma} = 10 \text{ s}^{-1}$$

$$G = 1.9 \times 10^4 \text{ Pa}, \quad \tau = 5.9 \times 10^4 \text{ Pa}, \quad \frac{\tau}{G} = 3.1$$

Therefore the latter combination is correct.

$$\dot{\gamma} = 10 = \frac{6Q}{TH^2}$$

and
$$Q = \frac{10 \times \pi \times 30 \times 2^2 \times 10^{-9}}{6} = 6.28 \times 10^{-7} \text{ m}^3/\text{s}$$

$$= 6.26 \times 10^{-7} \times 760 \times 3600 = 1.72 \text{ kg/h}$$

To calculate the inflation pressure, it is necessary to get the melt fracture stress. From Fig. 5.3 it may be seen that this is 4×10^6 Pa.

Therefore, since the maximum stress in the inflated bubble is the hoop stress, σ, the maximum inflation pressure, P, is given by

$$P = \frac{2h\sigma}{D_m} = \frac{2 \times 2 \times 4 \times 10^6}{60}$$

$$= 0.267 \text{ MPa}$$

Example 5.9 Calculate the time taken to inflate the bottle in the previous example if the inflation pressure is 50 kPa. The flow curves given in Fig. 5.3 may be used.

Solution It is necessary to derive an expression for the inflation time. Referring to Fig. 5.21 where R is the radius of the inflated tube at any time, t, and h_t is the wall thickness at this time, then a force balance on the shaded element gives (for unit length).

$$(Rd\theta)P_1 - (R + h_t)d\theta P_2 - 2\sigma h_t \sin\left(\frac{d\theta}{2}\right) = 0$$

Letting $\sin\left(\frac{d\theta}{2}\right) = \frac{d\theta}{2}$ and $P_2 = 0$, then

$$RP_1 = \sigma h_t \tag{5.72}$$

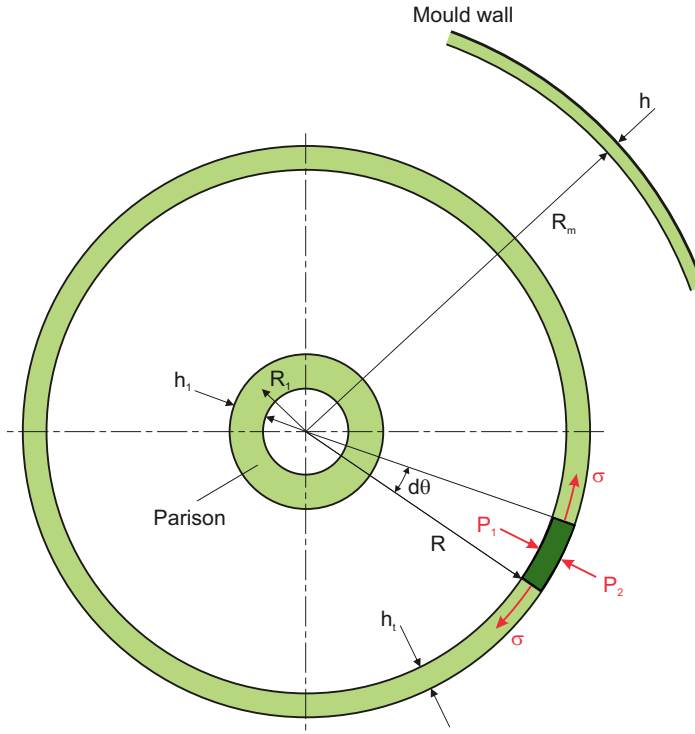


FIG. 5.21 Inflation of parison to mould wall.

Now $\sigma = \lambda\dot{\varepsilon}$

where λ is the tensile viscosity.

$\dot{\varepsilon}$ is the extensional strain rate and is given by

$$\dot{\varepsilon} = \frac{\text{change in length per unit time}}{\text{original length}} = \frac{(R + dR)d\theta - Rd\theta}{Rd\theta dt} = \frac{1}{R}\frac{dR}{dt}$$

Substituting into (5.72) we get

$$RP_1 = \frac{\lambda}{R}\frac{dR}{dt}h_t \tag{5.73}$$

Before this can be integrated, h_t needs to be expressed as a function of R or t. Assuming constant volume of the parison

$$Rh_t = R_1 h_1$$

Hence, we can write

$$\int_0^t dt = \int_{R_1}^{R_m} \frac{\lambda R_1 h_1}{P_1} \cdot \frac{dR}{R^3}$$

$$t = \frac{\lambda h_1}{2P_1 R_1} \left\{ 1 - \left(\frac{R_1}{R_m} \right)^2 \right\}$$

or expressing this in terms of the original die dimensions (see Blow Moulding, Section 4.2.7(d)),

$$\text{Inflation time,} \quad t = \frac{\lambda B_{ST} h_d}{P_1 D_d} \left\{ 1 - B_{ST}^2 \left(\frac{D_d}{D_m} \right) \right\} \tag{5.74}$$

Using the information given and with $\lambda = 2.2 \times 10^5$ Pa.s (from Fig. 5.3) then

$$t = \frac{2.2 \times 10^5 \times 1.26 \times 2}{50 \times 10^3 \times 30} \left\{ 1 - 1.26^2 \left(\frac{30}{60} \right) \right\}$$

$$t = 0.08\text{s}$$

Example 5.10 During the blow moulding of polythene bottles the parison is 0.3 m long and is left hanging for 5 s. Estimate the amount of sagging which occurs. The density of polythene is 760 kg/m^3

Solution Consider the small element of parison as shown as shown in Fig. 5.22.

(a) Elastic strain

From the relationship between stress, strain and modulus

$$\delta L = \frac{F dx}{AE}$$

$$= \frac{\rho \pi D_1 h_1 x dx}{\pi D_1 h_1 E}$$

$$\text{So total extension} \quad = \frac{\rho}{E} \int_0^L x dx = \frac{\rho L^2}{2E}$$

$$\text{So Elastic Strain} \quad = \varepsilon_R = \frac{\rho L}{2E}$$

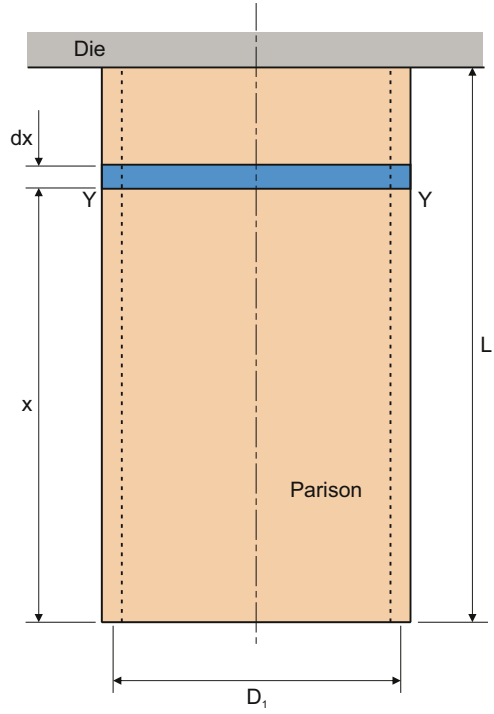


FIG. 5.22 Extruded parison for blow moulding.

(b) Viscous strain

$$\text{The stress on the element} = \frac{\text{force}}{\text{area}} = \frac{\text{weight below YY}}{\text{area}}$$

$$= \frac{\rho \pi D_1 h_1 dx}{\pi D_1 h_1} = \rho dx$$

$$\text{So total stress, } \sigma = \int_0^L \rho dx = \rho L$$

Now the viscous strain on the element is given by

$$\delta \varepsilon_v = \dot{\varepsilon} dt = \frac{\sigma}{\lambda} dt$$

$$\varepsilon_v = \int_0^t \frac{\sigma}{\lambda} dt = \int_0^t \frac{\rho L}{\lambda} dt = \frac{\rho L t}{\lambda}$$

Therefore the total strain, $\varepsilon = \varepsilon_R + \varepsilon_v$

$$= \frac{\rho l}{2E} + \frac{\rho L t}{\lambda}$$

$$\varepsilon = \rho L\left[\frac{1}{2E} + \frac{1}{\lambda}\right] \tag{5.75}$$

Note that this solution applies for values of t less than the relaxation time (λ/E) for the process. This is generally the case for blow moulding.

For the situation given,

$$\text{stress,} \qquad \sigma = \rho L = 760 \times 9.81 \times 0.3 = 2.24 \times 10^3 \text{ Pa}$$

From Fig. 5.3, $\lambda = 2.25 \times 10^5$ Pa.s.

$$\text{Also, since} \qquad \sigma = \lambda\dot{\varepsilon}, \dot{\varepsilon} = \frac{2.24 \times 10^3}{2.25 \times 10^5} = 0.01$$

Extrapolating to the left on Fig. 5.3, it may be found that at a strain rate of 0.01, $E = 1.9 \times 10^4$ Pa.

So characteristic time $= \lambda/E = 11.6 \text{ s}^{-1}$.

Therefore since the parison sag time is less than this, the above expression may be used to calculate the amount of stretching

$$\varepsilon = 760 \times 9.81 \times 0.3\left[\frac{1}{2 \times 1.9 \times 10^4} + \frac{5}{2.2 \times 10^5}\right] = 0.11$$

$$\text{So extension} = 0.11 \times 0.3 \text{ m}$$

$$= 33 \text{ mm}$$

5.12 Analysis of heat transfer during polymer processing

Most polymer processing methods involve heating and cooling of the polymer melt. So far the effect of the surroundings on the melt has been assumed to be small and experience in the situations analysed has proved this to be a reasonable assumption. However, in most polymer flow studies it is preferable to consider the effect of heat transfer between the melt and its surroundings. It is not proposed to undertake a detailed analysis of heat transfer techniques here, since these are dealt with in many standard texts on this subject. Instead some simple methods which may be used for heat flow calculations involving plastics are demonstrated.

Fourier's equation for non-steady heat flow in one dimension, *x,* is

$$\frac{\partial^2 T}{\partial x^2} = \frac{1}{\alpha}\frac{\partial T}{\partial t}$$

where T is temperature and α is the thermal diffusivity defined as the ratio of thermal conductivity, K, to the heat capacity per unit volume

$$\alpha = \frac{K}{\rho C_p}$$

where ρ is density and C_p is specific heat.

Most materials manufacturers supply data on the thermal diffusivity of their plastics but in the absence of any information a value of 1×10^{-7} m^2/s may be used for most thermoplastics (see Table 1.8 and Table 5.1).

Solutions to Fourier's equation are in the form of infinite series but are often more conveniently expressed in graphical form. In the solution the following dimensionless groups are used.

(1) Fourier Number,

$$F_o = \frac{\alpha t}{x^2} \tag{5.76}$$

where t is time and x is the radius of the sphere or cylinder (or half thickness of the/sheet) considered.

TABLE 5.1

Plastic	Moulding temperature (°C)	Mould temperature (°C)	Freeze-off temperature (°C)	Thermal diffusivity (m^2/s)
LDPE	230	30	90	1.1×10^{-7}
PLA Polypropylene	190 250	25 40	85 135	0.9×10^{-7} 1.1×10^{-7}
Polystyrene	230	50	130	0.8×10^{-7}
PVC	180	40	140	1.2×10^{-7}
POM	210	60	130	0.9×10^{-7}
Acrylic	250	50	160	0.9×10^{-7}
Polycarbonate	300	90	200	1.0×10^{-7}
Nylon 66	290	80	240	1.3×10^{-7}
ABS	230	60	140	0.9×10^{-7}

In the case of a flat sheet, if the heating/cooling is from one side only then the dimension, x, is taken as the full thickness.

(2) Temperature Gradient,

$$\Delta T = \frac{T_t - T_m}{T_i - T_m} \tag{5.77}$$

where T_i = Initial uniform temperature of the melt

T_m = Temperature of heating or cooling medium
T_t = Temperature at time t.

Fig. 5.23 show the solution to Fourier's equation in terms of the temperature gradient at the centre line of section considered and the Fourier Number for the cases of a flat sheet and a cylinder respectively. In each case it is assumed that there is no resistance to heat transfer at the boundary between the melt and the heating or cooling medium.

The way in which these data may be used is illustrated by the following example.

Example 5.11 A polyethylene injection moulding is in the form of a flat sheet 100 mm square and 3 mm thick. If the melt temperature is 230 °C, the mould temperature is 30 °C and the plastic may be ejected at a centre-line temperature of 90 °C, estimate:

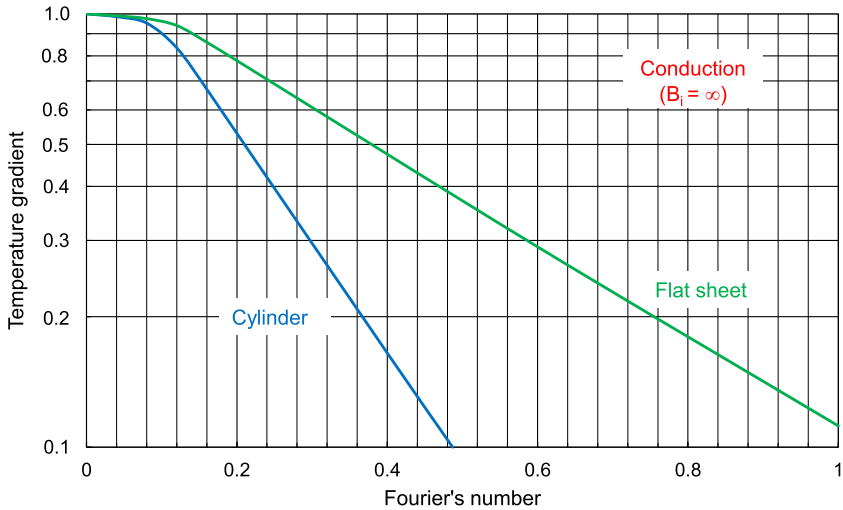


FIG. 5.23 Dimensionless temperature data for two geometries.

(a) the temperature of the material at the centre of the moulding after 7 s
(b) the time taken for the centre of the moulding to reach the ejection temperature of 90 °C
(c) the time taken for the centre of the moulding to cool to 60 °C in air at 20 °C after ejection from the mould. Comment on the meaning of the answer. The heat transfer coefficient for the air is 20 W/m^{2}K and the thermal conductivity of the polyethylene is 0.25 W/mK.

Solution (a) Fourier Number is

$$F_o = \frac{\alpha t}{x^2}$$

$$F_o = \frac{1 \times 10^{-7} \times 7}{(1.5 \times 10^{-3})^2}$$

$$= 0.31$$

From Fig. 5.23 the temperature gradient is 0.58

$$0.58 = \frac{T_t - 30}{230 - 30}$$

$$T_t = 146\ ^\circ\text{C}$$

(b) For freeze-off to occur the temperature gradient

$$\Delta T = \frac{T_t - T_m}{T_i - T_m}$$

$$\Delta T = \frac{90 - 30}{230 - 30} = 0.3$$

From Fig. 5.23, $F_o = 0.59$

$$0.59 = \frac{\alpha t}{x^2}$$

$$\text{or } t = \frac{0.59 \times (1.5 \times 10^{-3})^2}{1 \times 10^{-7}}$$

$$= 13.3\ \text{s}$$

(c) The above analysis relates to the situation where there is little resistance to heat transfer between the plastic and the heating/cooling medium, i.e. conduction. In situations where the plastic is in contact with a fluid such as

air, the main mode of heat transfer will be convection. The interrelationships between conduction and convection may be expressed by the Biot Number, B_i. This is given by

$$B_i = \frac{hx}{K}. \tag{5.78}$$

where h = heat transfer coefficient (typically 5−10 W/m^2 K for still air and 10−100 W/m^2 K for forced air)

K = thermal conductivity of the plastic
x = full or half thickness of the plastic as described above.

A large Biot Number means that conduction controls the energy transfer to/from the plastic and large temperature gradients will exist in the plastic. A small Biot Number means that convection is the dominant factor. The above analysis was for conduction heat transfer ($Bi \rightarrow \infty$). When the plastic moulding is taken out of the mould we need to check the value of B_i. In this case

$$B_i = \frac{20 \times 1.5 \times 10^{-3}}{0.25} = 0.12$$

The dimensionless temperature gradient is

$$\Delta T = \frac{60 - 20}{80 - 20} = 0.57$$

Fig. 5.24 shows the modified $\Delta T/F_o$ graph for a flat sheet for different values of B_i In this case $1/B_i = 8.33$. So from Fig. 5.24

$$F_o = 4 = \frac{\alpha t}{x^2}$$

$$t = \frac{4 \times (1.5 \times 10^{-3})^2}{1 \times 10^{-7}} = 90s$$

Hence the plastic cools by 140 °C (230 °C−90 °C) in 13.3 s when it is in contact with the mould but it takes 90 s to cool a further 30 °C when it emerges out into the air. This highlights the much faster cooling rate achieved in the mould.

Some typical moulding data for a range of plastics are given in Table 5.1. Note that the de-moulding temperature will be generally about 30 °C below the Freeze-off temperature in order to ensure that the moulding is sufficiently solid for handling.

The above analysis illustrates how to estimate the cooling time using the relationship between the temperature gradient ΔT and the Fourier Number F_o.

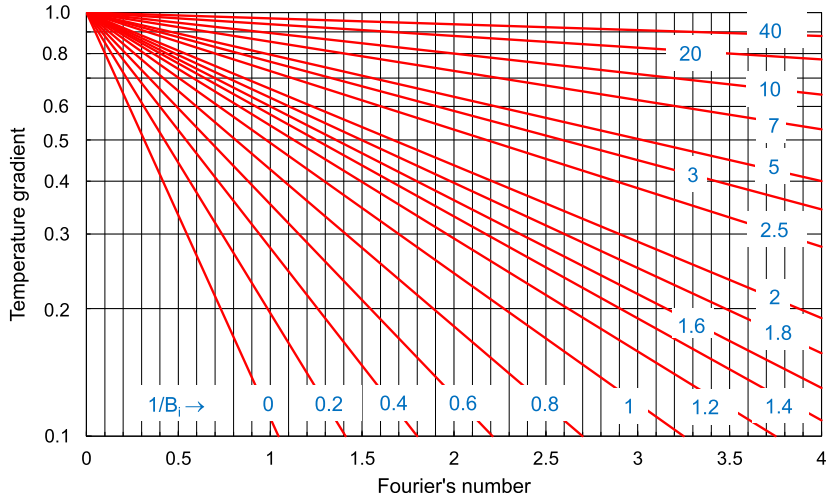


FIG. 5.24 Dimensionless temperature data for a flat sheet (conduction/convection).

A number of empirical relationships have also been proposed. Two of the more useful equations take the form

(a) for flat sheet

$$\text{time}, \quad t = \frac{4x^2}{\pi^2 \alpha} \ln\left(\frac{4}{\pi \cdot \Delta T}\right) \tag{5.79}$$

(b) for cylinder

$$\text{time}, \quad t = \frac{1.7r^2}{\pi^2 \alpha} \ln\left(\frac{1.7}{\Delta T}\right) \tag{5.80}$$

The reader may wish to check the predictions of freeze-off time for the data in the above example.

Example 5.12 Estimate the heat transfer from the die to the melt as it passes through the die land in Example 5.5.

Solution

$$\text{Volume of die land} = \pi DHL$$

$$= \left(\pi \times 260 \times 0.7 \times 4 \times 10^{-9}\right) \text{ m}^3$$

$$\text{Residence time} = \frac{\pi \times 260 \times 0.7 \times 4 \times 10^{-9}}{109.6 \times 10^{-6}}$$

$$= 2.08 \times 10^{-2} \text{ s}$$

$$\text{Fourier number} = \frac{\alpha t}{x^2}$$

$$F_o = \frac{1 \times 10^{-7} \times 2.08 \times 10^{-2}}{(0.35 \times 10^{-3})^2}$$

$$= 0.017$$

From Fig. 5.23 it may be seen that the centre line temperature gradient at this Fourier Number is almost 1.

$$\text{Since} \quad \Delta T = \frac{T_3 - T_2}{T_1 - T_2} \simeq 1$$

$$\text{then} \quad T_3 \simeq T_1$$

Thus the melt temperature after 2.08×10^{-2} s is the same as the initial melt temperature (T_1) so that as the melt passes through the die land it is relatively unaffected by the temperature of the die.

Any temperature rise which occurs in the melt as it passes through this section will be as a result of the work done on the melt and may be estimated using (5.64).

$$\text{Temperature rise} = \frac{P}{\rho C_p}$$

$$\text{So temperature rise} = \frac{3.66 \times 10^6}{760 \times 2.5 \times 10^3}$$

$$= 1.9 \ ^\circ\text{C}$$

Example 5.13 Derive an expression for the flow length of a power law fluid when it is injected at constant pressure into a rectangular section channel assuming

(a) the flow is isothermal
(b) there is freezing off as the melt flows (i.e. non-isothermal flow).

Solution (a) As shown earlier the flow rate of a power law fluid in a rectangular section is given by

$$Q = \left(\frac{n+1}{2n+1}\right) TH \left(\frac{n}{n+1}\right) \left(\frac{P}{\eta_0 \ell}\right)^{1/n} \left(\frac{H}{2}\right)^{(n+1)/n} \tag{5.81}$$

During any increment of time, *dt,* the volume of the fluid injected into the channel is *Qdt*. This will be equal to the increase in volume of the fluid in the channel

$$Qdt = THd\ell$$

So from above

$$TH\frac{d\ell}{dt} = \left(\frac{n}{2n+1}\right)TH\left(\frac{P}{\eta_0 \ell}\right)^{1/n}\left(\frac{H}{2}\right)^{(n+1)/n}$$

$$\therefore \int_0^L \ell^{1/n} d\ell = \left(\frac{n}{2n+1}\right)\left(\frac{P}{\eta_0}\right)^{1/n}\left(\frac{H}{2}\right)^{(n+1)/n}\int_0^t dt$$

$$\left(\frac{n}{n+1}\right)L^{(n+1)/n} = \left(\frac{n}{2n+1}\right)\left(\frac{P}{\eta_0}\right)^{1/n}\left(\frac{H}{2}\right)^{(n+1)/n}\cdot t$$

$$L = \left(\frac{n+1}{2n+1}\right)^{n(n+1)}\left(\frac{P}{\eta_0}\right)^{1/(n+1)}\left(\frac{H}{2}\right)\cdot t^{n(n+1)} \tag{5.82}$$

The volume flow rate at any instant in time may be determined by substituting for L in Eq. (5.81).

(b) If the melt is freezing off as it flows then the effective channel depth will be h instead of H as shown in Fig. 5.23. Therefore the above expression may be written as

$$\ell^{1/n} d\ell = \left(\frac{n}{2n+1}\right)\left(\frac{P}{\eta_0}\right)^{1/n}\left(\frac{h}{2}\right)^{(n+1)/n} dt \tag{5.83}$$

This equation cannot be integrated as simply as before because h is now a function of time. Fig. 5.26 shows how the depth of the cavity changes with time as the melt flows. Barrie has investigated this situation and concluded that the freezing-off could be described by a relation of the form

$$\Delta y = Ct^s \tag{5.84}$$

where C and s are constants and Δy is the thickness of the frozen layer as shown in Fig. 5.25. For most polymer melt flow situations, Barrie found that $s = 1/3$.

From (5.84) using the boundary condition that $t = t_f$ (freeze-off time) at

$$\Delta y = H/2$$

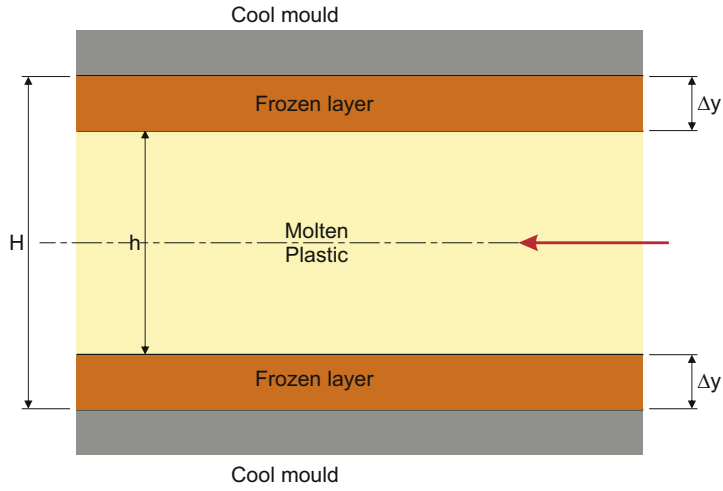


FIG. 5.25 Flow of molten polymer into a cold mould.

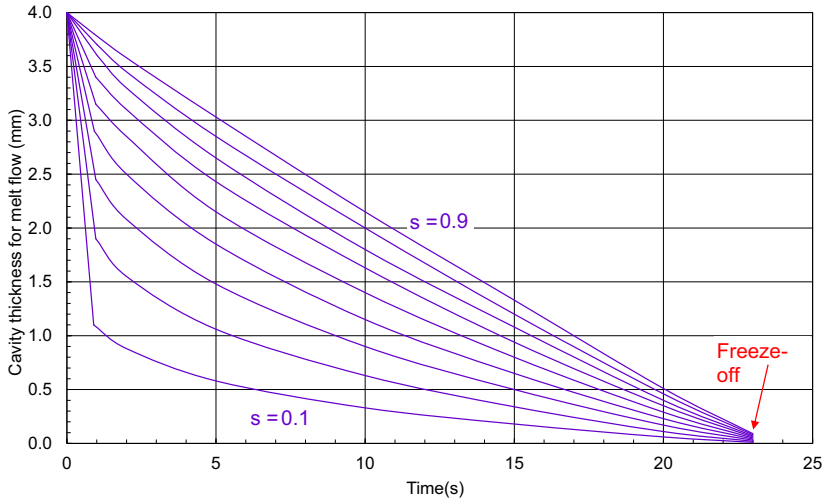


FIG. 5.26 Variation of cavity depth with time.

$$\text{Then } C = \left(\frac{H}{2t_f^{\frac{1}{3}}}\right)$$

also $2\Delta y = (H - h)$ so in (5.84)

$$\left(\frac{H-h}{2}\right)=\frac{H}{2}\left(\frac{t}{t_f}\right)^{\frac{1}{3}}$$

$$h=H\left(1-\left(\frac{t}{t_f}\right)^{\frac{1}{3}}\right) \tag{5.85}$$

So substituting this expression for h into (5.83), then

$$\ell^{1/n}d\ell=\left(\frac{n}{2n+1}\right)\left(\frac{P}{\eta_0}\right)^{1/n}\left(\frac{1}{2}\right)^{(n+1)/n}\left[H\left(1-\left(\frac{t}{t_f}\right)^{\frac{1}{3}}\right)\right]^{(n+1)/n}dt$$

This may then be integrated to give

$$\left(\frac{n}{n+1}\right)L^{(n+1)/n}=\left(\frac{n}{2n+1}\right)\left(\frac{P}{\eta_0}\right)^{1/n}\left(\frac{H}{2}\right)^{(n+1)/n}\times\left[6t_f\left(\frac{n}{4n+1}\right)\left(\frac{n}{3n+1}\right)\left(\frac{n}{2n+1}\right)\right]$$

$$\text{So}\quad L=\left(\frac{P}{\eta_0}\right)^{1/(n+1)}\frac{H}{2}\left[6t_f\left(\frac{n}{4n+1}\right)\left(\frac{n}{3n+1}\right)\left(\frac{n(n+1)}{(2n+1)^2}\right)\right]^{n/(n+1)} \tag{5.86}$$

Similar expressions may also be derived for a circular section channel and for the situation where the injection rate is held constant rather than the pressure (see questions at the end of the chapter). In practical injection moulding situations the injection rate would probably be held constant until a pre-selected value of pressure is reached. After this point, the pressure would be held constant and the injection rate would decrease.

Note that for a Newtonian fluid, $n=1$, so for the isothermal case, Eq. (5.82) becomes.

$$L=0.408\left(\frac{Pt}{\eta}\right)^{\frac{1}{2}}H$$

and for the non-isothermal case, Eq. (5.86) becomes

$$L=0.13\left(\frac{Pt_f}{\eta}\right)^{\frac{1}{2}}H$$

For the non-isothermal cases the freeze-off time, t_f, may be estimated by the method described in Example 5.11.

Example 5.14 A power law fluid with constants $\eta_0=1.2\times10^4$ Pa s and $n=0.35$ is injected through a centre gate into a disc cavity which has a depth of 2 mm and a diameter of 200 mm. If the injection rate is constant at

6×10^{-5} m^3/s, estimate the time taken to fill the cavity and the minimum injection pressure necessary at the gate for (a) Isothermal and (b) Non-isothermal conditions.

Solution (a) *Isothermal Situation.* If the volume flow rate is Q, then for any increment of time, dt, the volume of material injected into the cavity will be given by (Qdt). During this time period the melt front will have moved from a radius, r, to a radius ($r + dr$). Therefore a volume balance gives the relation

$$\mathrm{Qdt} = 2\pi \mathrm{rHdr}$$

where H is the depth of the cavity.

Since the volume flow rate, Q, is constant this expression may be integrated to give

$$\int_0^t dt = \frac{2\pi H}{Q}\int_0^R r dr$$

$$t = \frac{\pi R^2 H}{Q}$$

For the conditions given

$$t = \frac{\pi(100 \times 10^{-3})^2(2 \times 10^{-3})}{6 \times 10^{-5}}$$

$$= 1.05 \quad \mathrm{s}$$

It is now necessary to derive an expression for the pressure loss in the cavity. Since the mould fills very quickly it may be assumed that effects due to freezing-off of the melt may be ignored. In Section 5.5(b) it was shown that for the flow of a power law fluid between parallel plates

$$Q = \left(\frac{n+1}{2n+1}\right) T V_0 H$$

Now for the disc, $T = 2\pi r$ and substituting for V_0 from (5.34)

$$Q = \left(\frac{n+1}{2n+1}\right)\left(2\pi r H\left[-\left(\frac{n}{n+1}\right)\left(\frac{1}{\eta_0}\right)^{\frac{1}{n}}\left(\frac{dp}{dr}\right)^{\frac{1}{n}}\left(\frac{H}{2}\right)^{\frac{(n+1)}{n}}\right]\right)$$

$$dP = Q^n\left(\frac{2n+1}{2\pi n}\right)^n\left\{\frac{\eta_0(2)^{n+1}}{(H)^{2n+1}}\right\}\frac{dr}{r^n}$$

$$\int_{P_1}^{P_2} dP = \int_{R_1}^{R_2} -Q^n\left\{\frac{2n+1}{2\pi n}\right\}^n \frac{\eta_0(2)^{n+1}}{(H)^{2n+1}} \cdot \frac{dr}{r^n}$$

$$P_2 - P_1 = -Q^n \left\{ \frac{2n+1}{2\pi n} \right\}^n \frac{\eta_0(2)}{(H)^{2n+1}} \left[\frac{r^{1+n}}{1-n} \right]_{R_1}^{R_2}$$

$$= -Q^n \left\{ \frac{2n+1}{2\pi n} \right\} \frac{\eta_0(2)^{n+1}}{(1-n)H^{2n+1}} \left[R_2^{1-n} - R_1^{1-n} \right]$$

Now letting $P_1 = 0$ at $R_1 = R$ and $P_2 = P$ at $R_2 = r$

$$P = -Q^n \left\{ \frac{2n+1}{2\pi n} \right\} \frac{\eta_0(2)^{n+1}}{(1-n)H^{2n+1}} \left[R^{1-n} - r^{1-n} \right]$$

$$= Q^n \left\{ \frac{2n+1}{2\pi n} \right\} \frac{\eta_0(2)^{n+1}}{(1-n)H^{2n+1}} R^{1-n} \left(1 - \left(\frac{r}{R} \right)^{1-n} \right)$$

now $P = P_o$ at $r = 0$

$$P_0 = Q^n \left\{ \frac{2n+1}{2\pi n} \right\} \frac{\eta_0(2)^{n+1}}{(1-n)H^{2n+1}} R^{1-n}$$

So for the conditions given

$$P_0 = \left(6 \times 10^{-5}\right)^{0.35} \left(\frac{1.7}{0.7\pi} \right)^{0.35} \frac{(1.2 \times 10^4)(2)^{1.35}(100 \times 10^{-3})^{0.65}}{(2 \times 10^{-3})^{1.7}(0.65)}$$

$$= 12.42 \text{ MPa}$$

Note that if P_0 is substituted back into the expression for P then the expression used earlier (Chapter 4) to calculate the mould clamping force is obtained. That is

$$P = P_0 \left\{ 1 - \left(\frac{r}{R} \right)^{1-n} \right\}$$

(b) *Non-isothermal Situation.* In this case the injection pressure will need to be higher because as the melt flows the cavity effectively gets thinner due to the freezing-off of the melt as it makes contact with the relatively cold mould.

$$\Delta P = Q^n \left\{ \frac{2n+1}{2\pi n} \right\} \frac{\eta_0(2)^{n+1}}{(1-n)H^{2n+1}} R^{1-n}$$

but when non-isothermal conditions apply, $H = H(t)$, i.e. the cavity thickness varies with time due to the build up of a frozen layer at the mould.

As shown in the previous example, the variation of cavity thickness with time is given by

$$H(t) = H\left(1 - \left(\frac{t}{t_f}\right)^s\right)$$

where 's' is often taken as 1/3.

So
$$\Delta P = Q^n \left\{\frac{2n+1}{2\pi n}\right\} \frac{\eta_0 (2)^{n+1}}{(1-n)H^{2n+1}} \frac{R^{1-n}}{\left\{1 - \left(\frac{t}{t_f}\right)^{1/3}\right\}^{2n+1}}$$

For the conditions given, $T_i = 230\ ^\circ\text{C}$, $T_t = 90\ ^\circ\text{C}$, $T_m = 30\ ^\circ\text{C}$, the freeze-off time may be calculated as shown in Example 5.11. Thus $t_f = 5.8$ s.

Thus
$$\left\{1 - \left(\frac{t}{t_f}\right)^{1/3}\right\}^{2n+1} = \left\{1 - \left(\frac{1.05}{5.8}\right)^{1/3}\right\}^{1.7} = 0.24$$

So, for non-isothermal conditions

$$\Delta P = \frac{12.42}{0.24} = 51.3 \text{ MPa}$$

5.13 Calculation of clamping force

(a) Isothermal situation

It may be seen from the above analysis and that in Chapter 4 for the calculation of clamping force on an injection moulding machine the Mean Effective Pressure (MEP) across the cavity may be obtained from

$$(MEP)A = \pi R^2 P_0 \left\{\frac{1-n}{3-n}\right\} \tag{5.87}$$

where A = projected area (πR^2, for a disc mould).

Hence, for the isothermal situation

$$MEP = \left\{\frac{1-n}{3-n}\right\}\{Q^n\}\left\{\frac{2n+1}{2\pi n}\right\} \frac{\eta_0 (2)^{n+1}}{(1-n)H^{2n+1}} R^{1-n}$$

and for a constant injection rate, $Q = \pi R^2 H/t$

So,

$$MEP = \left(\frac{1-n}{3-n}\right)\left[\left(\frac{\pi}{t}\right)^n \left\{\frac{2n+1}{2\pi n}\right\} \frac{\eta_0\,(2)^{n+1}}{(1-n)}\left(\frac{R}{H}\right)^{n+1}\right]$$

$$= \frac{\pi^{n-1}}{t^n}\left\{\frac{(2n+1)(2)^{n+1}}{2n(3-n)}\right\}\eta_0\left(\frac{R}{H}\right)^{n+1}$$

$$MEP = \left\{\frac{(2n+1)\cdot 2^{n+1}\cdot \pi^{n-1}}{2n\cdot(3-n)}\right\} \frac{1}{t^n}\cdot\eta_0\cdot\left(\frac{R}{H}\right)^{n+1} \tag{5.88}$$

Thus for any plastic where the Power Law constants are known, the clamping force can be calculated for a given radius, R, cavity depth, H, and fill time, t.

Fig. 5.27 shows the variation of MEP with flow ratio (R/H) for spreading flow in discs of different depths. The material is polypropylene and the constant injection rate is 3.4×10^{-3} m^3/s. This is a high injection rate but has been chosen because the clamp forces predicted by this diagram are representative of those occurring in real moulding situations (even though it is based on isothermal conditions). Note that the clamp force is calculated simply by multiplying the mean effective pressure (MEP) by the projected area of the moulding, as illustrated in Chapter 4.

For plastics other than polypropylene it would be necessary to produce a similar set of curves using Eq. (5.88) and the Power Law data in Table 5.2.

(b) Non-isothermal situation

Once again

$$MEP = \left\{\frac{1-n}{3-n}\right\}Q^n\left\{\frac{2n+1}{2\pi n}\right\} \frac{\eta_0(2)^{n+1}}{(1-n)H^{2n+1}}R^{1-n}$$

but in this case, the thickness H is a function of time.

$$H(t) = H\left\{1-\left(\frac{t}{t_f}\right)^{\frac{1}{3}}\right\}$$

and the constant volume flow rate $Q = \pi R^2 H/t$ where t is the fill time for the cavity.

$$MEP = \left(\frac{1-n}{3-n}\right)\left(\frac{\pi}{t}\right)^n\left\{\frac{2n+1}{2\pi n}\right\} \frac{\eta_0(2)^{n+1}}{(1-n)}\left(\frac{R}{H}\right)^{n+1}\frac{1}{\left\{1-\left(\frac{t}{t_f}\right)^{1/3}\right\}^{2n+1}}$$

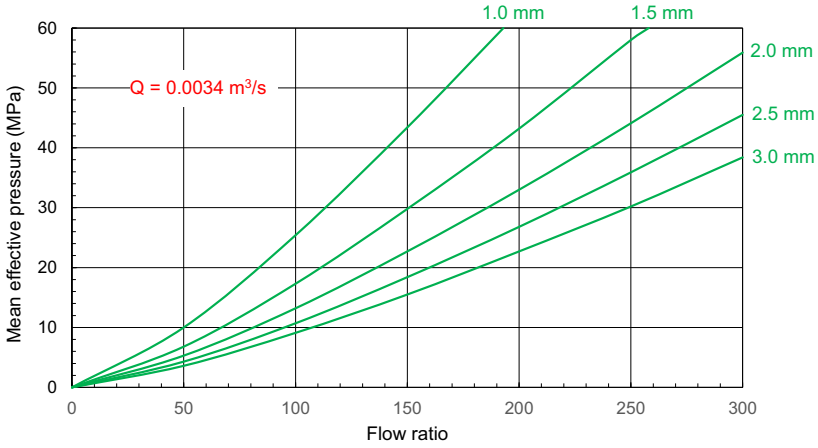


FIG. 5.27 Variation of cavity pressure with flow ratio.

TABLE 5.2 Typical power law parameters for plastics.

Material	Temperature (°C)	η_0 (Pa·s)	n
LDPE	170	0.85×10^4	0.33
PVC	170	0.36×10^4	0.67
Polypropylene	230	0.85×10^4	0.33
Acetal (POM)	210	2.0×10^4	0.33
Polystyrene	230	1.4×10^4	0.33
ABS	230	1.95×10^4	0.33
PMMA	230	3.0×10^4	0.33
Polycarbonate	290	3.6×10^4	0.5
Nylon 66	290	0.8×10^4	0.67

$$MEP = \left\{\frac{(2n+1)\cdot 2^{n+1}\pi^{n-1}}{2n(3-n)}\right\}\eta_0\left(\frac{R}{H}\right)^{n+1}\frac{1}{t^n\left\{1-\left(\frac{t}{t_f}\right)^{1/3}\right\}^{2n+1}} \tag{5.89}$$

Fig. 5.28 shows a comparison of the isothermal and non-isothermal situations for polypropylene. When pressure is plotted as a function of injection rate, it may be seen that for the isothermal situation the pressure increases as the injection rate increases. However, in the situation where the melt freezes

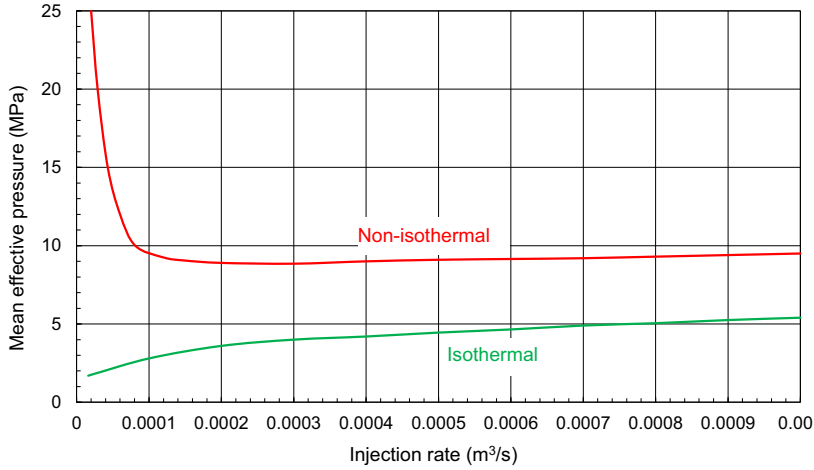


FIG. 5.28 Variation of cavity pressure loss with injection rate.

off as it enters the mould, the relationship is quite different. In this case the pressure is high at high injection rates, in a similar manner to the isothermal situation. In fact at extremely high injection rates the two curves would meet because the melt would enter the mould so fast it would not have time to be affected by the melt temperature.

However, in the non-isothermal case the pressure is also high at low injection rates. This is because slow injection gives time for significant solidification of the melt and this leads to high pressures. It is clear therefore that in the non-isothermal case there is an optimum injection rate to give minimum pressure. In Fig. 5.28 this is seen to be about 3.0×10^{-4} m^3/s for the situation considered here. This will of course change with melt temperature and mould temperature since these affect the freeze-off time, t_f, in the above equations.

Some typical values for η_0 and n are given in Table 5.2.

The viscosity flow curves for these materials are shown in Fig. 5.17. To obtain similar data at other temperatures then a shift factor of the type given in Eq. (5.27) would have to be used. The temperature effect for polypropylene is shown in Fig. 5.2.

Example 5.15 During injection moulding of low density polyethylene, 15 kg of material are plasticised per hour. The temperature of the melt entering the mould is 190 °C and the mould temperature is 40 °C. If the energy input from the screw is equivalent to 1 kW, calculate

(a) the energy required from the heater bands
(b) the flow rate of the circulating water in the mould necessary to keep its temperature at 40 ± 2 °C

Solution The steady flow energy equation may be written as

$$q - W = \Delta h \tag{5.90}$$

where q is the heat transfer per unit mass

W is the work transfer per unit mass
h is enthalpy

Enthalpy is defined as the amount of heat required to change the temperature of unit mass of material from one temperature to another. Thus the amount of heat required to change the temperature of a material between specified limits is the product of its mass and the enthalpy change.

The enthalpy of plastics is frequently given in graphical form. For a perfectly crystalline material there is a sharp change in enthalpy at the melting point due to the latent heat. However, for semi-crystalline plastics the rate of enthalpy change with temperature increases up to the melting point after which it varies linearly with temperature increases up to the melting point after which it varies linearly with temperature as shown in Fig. 5.29. For amorphous plastics there is only a change in slope of the enthalpy line at glass transition points. Fig. 5.29 shows that when LDPE is heated from 20 °C to 190 °C the change in enthalpy is 485 kJ/kg.

(a) In Eq. (5.90) the sign convention is important. Heat is usually taken as positive when it is applied to the system and work is positive when done by the system. Hence in this example where the work is done on the system by the screw it is regarded as negative work.

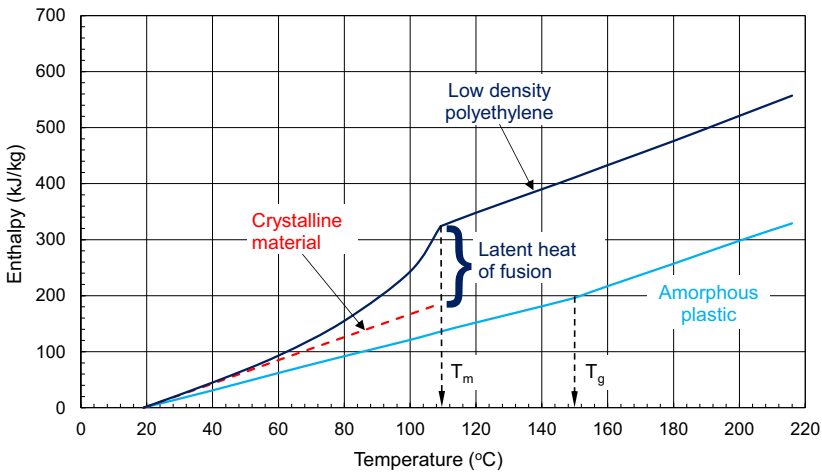


FIG. 5.29 Enthalpy variation with temperature.

So using (5.90) for a mass of 15 kg per hour

$$q-(-1)=15\left(485\times\frac{1}{60}\times\frac{1}{60}\right)$$

$$q=1.02\ \text{kW}$$

The heater bands are expected to supply this power.

(b) At the mould there is no work done so in terms of the total heat absorbed in cooling the melt from 190 °C to 40 °C.

$$q=m\Delta h$$

$$=15\left[(485-40)\frac{1}{60}\times\frac{1}{60}\right]$$

$$=1.85\ \text{kW}$$

This heat must be removed by the water circulating in the mould at a rate, Q

$$q=Q\Delta h$$

or by definition of enthalpy

$$q=QC_p\Delta T$$

where C_p is the specific heat (= 4.186 kJ/kg°C for water) and ΔT is the temperature change (= 4 °C i.e. ±2 °C)

$$1.85=Q\times 4.186\times 4$$

$$Q=0.11\ \text{kg/s}$$

$$=0.11\ \text{L/s}$$

It is also possible to estimate the number of cooling channels required. If the thermal conductivity of the mould material is K then the heat removed through the mould per unit time will be given by

$$q=\frac{K\cdot A(\Delta T)}{y}$$

where ΔT is the temperature between the melt and the circulating fluid, y is the distance of the cooling channels from the mould, and A is the area through which the heat is conducted to the coolant. This is usually taken as half the circumference of the cooling channel multiplied by its length.

$$q = \frac{K\pi DL(\Delta T)}{2y}$$

$$L = \frac{2yq}{K\pi D(\Delta T)}$$

The K value for steel is 48.3 J/m.s.°C, so assuming that the cooling channels have a diameter of 10 mm and they are placed 40 mm from the cavity, then

$$L = \frac{2 \times 40 \times 10^{-3} \times 1.85 \times 10^{3}}{11.5 \times 4.2 \times \pi \times 10 \times 10^{-3} \times (190 - 40)}$$

$$= 0.65 \text{ m}$$

If the length of the cavity is 130 mm then five cooling channels would be needed to provide the necessary heat removal.

Questions

5.1 In a particular type of cone and plate rheometer the torque is applied by means of a weight suspended on a piece of cord. The cord passes over a pulley and is wound around a drum which is on the same axis as the cone. There is a direct drive between the two. During a test on polythene at 190 °C the following results were obtained by applying a weight and, when the steady state has been achieved, noting the angle of rotation of the cone in 40 s. If the diameter of the cone is 50 mm and its included angle is 170°, estimate the viscosity of the melt at a shear stress of 10^4 Pa.

Weight (g)	**50**	**100**	**200**	**500**	**1000**	**2000**
Angle (θ°)	0.57	1.25	2.56	7.36	17.0	42.0

5.2 Derive expressions for the velocity profile, shear stress, shear rate and volume flow rate during the isothermal flow of a power law fluid in a rectangular section slit of width W, depth H and length L. During tests on such a section the following data was obtained.

Flow rate (kg/min)	**0.21**	**0.4**	**0.58**	**0.8**	**1.3**	**2.3**
Pressure drop (MPa)	1.8	3.0	4.0	5.2	7.6	12.0

If the channel has a length of 50 mm, a depth of 2 mm and a width of 6 mm, establish the applicability of the power law to this fluid and determine the relevant constants. The density of the fluid is 940 kg/m^3.

5.3 The viscosity characteristics of a polymer melt are measured using both a capillary rheometer and a cone and plate viscometer at the same temperature. The capillary is 2.0 mm diameter and 32.0 mm long. For volumetric flow rates of 70×10^{-9} m^3/s and 200×10^{-9} m^3/s, the pressures measured just before the entry to the capillary are 3.9 MPa and 5.7 MPa, respectively.

The angle between the cone and the plate in the viscometer is 3° and the diameter of the base of the cone is 75 mm. When a torque of 1.18 Nm is applied to the cone, the steady rate of rotation reached is observed to be 0.062 rad/s. Assuming that the melt viscosity is a power law function of the rate of shear, calculate the percentage difference in the shear stresses given by the two methods of measurement at the rate of shear obtained in the cone and plate experiment.

5.4 The correction factor for converting apparent shear rates at the wall of a circular cylindrical capillary to true shear rates is $(3n + 1)/4n$, where n is the power law index of the polymer melt being extruded.

Derive a similar expression for correcting apparent shear rates at the walls of a die whose cross-section is in the form of a very long narrow slit.

A slit die is designed on the assumption that the material is Newtonian, using apparent viscous properties derived from capillary rheometer measurements, at a particular wall shear stress, to calculate the volumetric flow rate through the slit for the same wall shear stress. Using the correction factors already derived, obtain an expression for the error involved in this procedure due to the melt being non-Newtonian. Also obtain an expression for the error in pressure drop calculated on the same basis. What is the magnitude of the error in each case for a typical power law index $n = 0.37$?

5.5 Polyethylene is extruded through a cylindrical die of radius 3 mm and length 37.5 mm at a rate of 2.12×10^{-6} m^3/s. Using the flow curves supplied, calculate the natural time of the process and comment on the meaning of the value obtained.

5.6 Polythene is passed through a rectangular slit die 5 mm wide, 1 mm deep at a rate of 0.7×10^{-9} m^3/s. If the time taken is 1 s, calculate the natural time and comment on its meaning.

5.7 In a plunger type injection moulding machine the torpedo has a length of 30 mm and a diameter of 23 mm. If, during the moulding of polythene at 170 °C (flow curves given), the plunger moves forward at a speed of 50 mm/s estimate the pressure drop along the torpedo. The barrel diameter is 25 mm.

5.8 The exit region of a die used to extrude a plastic section is 10 mm long and has the cross-sectional dimensions shown in Fig. 5.30. If the channel is being extruded at the rate of 3 m/min calculate the power absorbed in the die exit and the melt temperature rise in the die. Flow curves for the

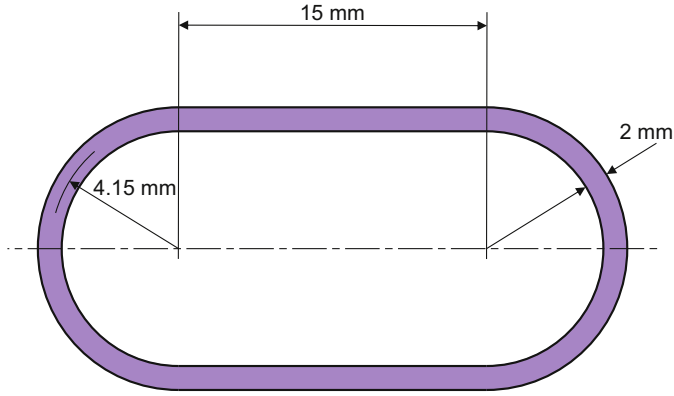


FIG. 5.30 Die exit for extruded section.

polymer melt are given in Fig. 5.3. The product ρC_p for the melt is 3.3×10^6.

5.9 The exit region of a die used to extrude a plastic channel section is 10 mm long and has the dimensions shown in Fig. 5.31. If the channel is being extruded at the rate of 3 m/min. Calculate the power absorbed in the die exit, and the dimensions of the extrudate as it emerges from the die. The flow curves in Fig. 5.3 may be used.

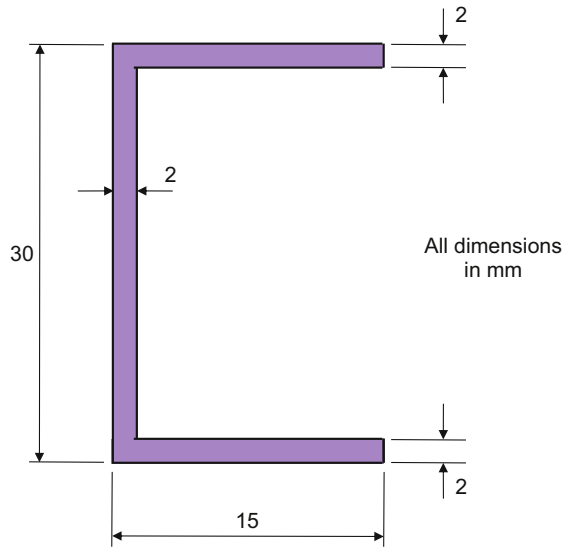


FIG. 5.31 Die exit for extruded channel.

5.10 During extrusion blow moulding of 60 mm diameter bottles the extruder output rate is 46×10^{-3} m^3/s. If the die diameter is 30 mm and the die gap is 1.5 mm calculate the wall thickness of the bottles which are produced. The flow curves in Fig. 5.3 should be used.

5.11 Polyethylene is injected into a mould at a temperature of 170 °C and a pressure of 100 MPa If the mould cavity has the form of a long channel with a rectangular cross-section 6 mm × 1 mm deep, estimate the length of the flow path after 1 s. The flow may be assumed to be isothermal and over the range of shear rates experienced (10^3–10^5 s^{-1}) the material may be considered to be a power law fluid.

5.12 Repeat the previous question for the situation in which the mould temperature is 60 °C and the freeze-off temperature is 128 °C. What difference would it make if it had been assumed that the material was Newtonian with a viscosity of 1.2×10^2 Pa·s.

5.13 During the blow moulding of polypropylene bottles, the parison is extruded at a temperature of 230 °C and the mould temperature is 50 °C. if the wall thickness of the bottle is 1 mm and the bottles can be ejected at a temperature of 120 °C estimate the cooling time in the mould.

5.14 An injection moulding is in the form of a flat sheet 100 mm square and 4 mm thick. The melt temperature is 230 °C, the mould temperature is 30 °C and the plastic may be ejected from the mould at a centre-line temperature of 90 °C. if the runner design criterion is that it should be ejectable at the same instant as the moulding, estimate the required runner diameter. The thermal diffusivity of the melt is 1×10^{-7} m^2/s.

5.15 For a particular polymer melt the power law constants are $= 40$ kN.s^n/m and $n = 0.35$. If the polymer flows through an injection nozzle of diameter 3 mm and length 25 mm at a rate of 5×10^{-5} m^3/s, estimate the pressure drop in the nozzle.

5.16 Polythene at 170 °C is used to injection mould a disc with a diameter of 120 mm and thickness 3 mm. A sprue gate is used to feed the material into the centre of the disc. If the injection rate is constant and the cavity is to be filled in 1 s estimate the minimum injection pressure needed at the nozzle. The flow curves for this grade of polythene are given in Fig. 5.3.

5.17 During the injection moulding of a polythene container having a volume of 4×10^{-6} m^3, the melt temperature is 170 °C, the mould temperature

is 50 °C and rectangular gates with a land length of 0.6 mm are to be used. If it is desired to have the melt enter the mould at a shear rate of 10^3 s^{-1} and freeze-off at the gate after 3 s, estimate the dimensions of the gate and the pressure drop across it. It may be assumed that freeze-off occurs at a temperature of 114 °C. The flow curves in Fig. 5.3 should be used.

5.18 Polyethylene at 170 °C passes through the annular die shown in Fig. 5.32, at a rate of 10×10^{-6} m^3/s. Using the flow curves provided and assuming the power law index $n = 0.33$ over the working section of the curves, calculate the total pressure drop through the die. Also estimate the dimensions of the extruded tube.

5.19 A polythene tube of outside diameter 40 mm and wall thickness 0.75 mm is to be extruded at a linear speed of 15 mm/s. Using the 170 °C polythene flow curves supplied, calculate suitable die exit dimensions.

5.20 The exit region of a die used to blow plastic film is shown in Fig. 5.33. If the extruder output is 100×10^{-6} m^3/s of polythene at 170 °C estimate the total pressure drop in the die between points A and C. Also calculate the dimensions of the plastic bubble produced. It may be assumed that there is no inflation or draw-down of the bubble. Flow data for polythene is given in Fig. 5.3.

5.21 A polyethylene moulding material at 170 °C passes along the channel shown in Fig. 5.34 at a rate of 4×10^{-6} m^3/s. Using the flow curves

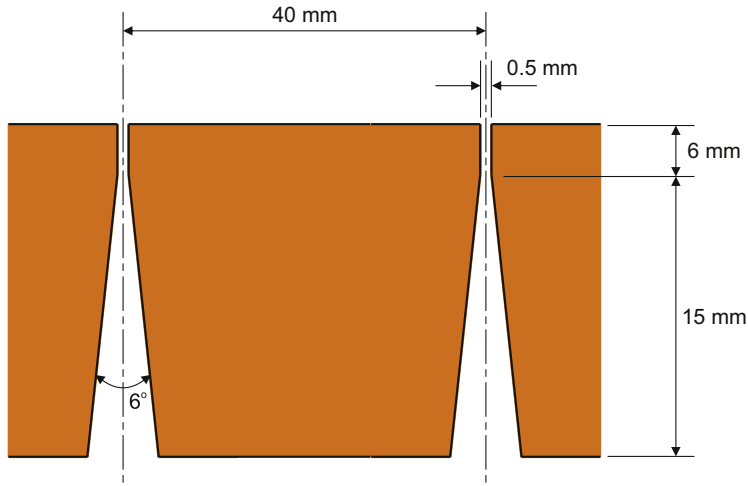


FIG. 5.32 Exit of annular die.

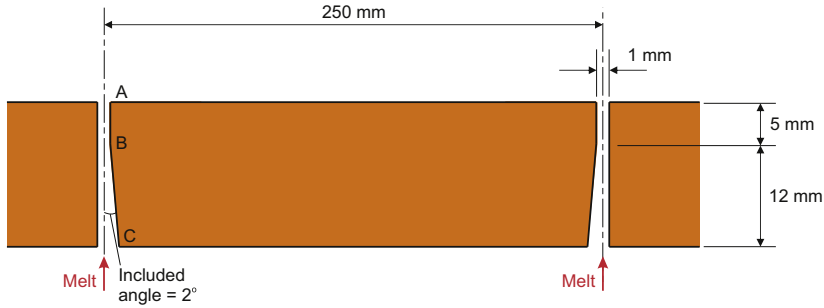


FIG. 5.33 Exit of blown film die.

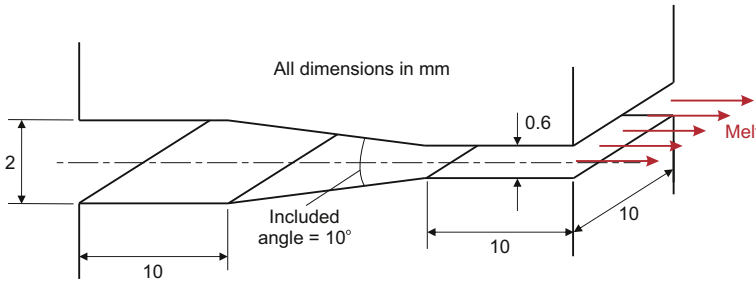


FIG. 5.34 Tapered channel.

given and assuming $n = 0.33$ calculate the pressure drop along the channel.

5.22 A power law plastic is injected into a circular section channel using a constant pressure, P. Derive an expression for the flow length assuming that
(a) the flow is isothermal
(b) the melt is freezing off as it flows along the channel.

5.23 A polymer melt is injected into a circular section channel under constant pressure. What is the ratio of the maximum non-isothermal flow length to the isothermal flow length in the same time for (a) a Newtonian melt and (b) a power law melt with index. $n = 0.3$.

5.24 A power law fluid with the constants $\eta_0 = 10^4$ Pa·s and $n = 0.3$ is injected into a circular section channel of diameter 10 mm. Show how the injection rate and injection pressure vary with time if:
(a) the injection pressure is held constant at 140 MPa
(b) the injection rate is held constant at 10^{-3} m^3/s.

The flow in each case may be considered to be isothermal.

5.25 Polyethylene at 170 °C is used to injection mould a flat plaque measuring 50 mm × 10 mm × 3 mm. A rectangular gate which is 4 mm × 2 mm with a land length of 0.6 mm is situated in the centre of the 50 mm side. The runners are 8 mm diameter and 20 mm long. The material passes from the barrel into the runners in 1 s and the pressure losses in the nozzle and sprue may be taken as the same as those in the runner. If the injection rate is fixed at 10^{-6} m^3/s, estimate (a) the pressure losses in the runner and gate and (b) the initial packing pressure on the moulded plaque. Flow curves are supplied.

5.26 A lace of polyethylene is extruded with a diameter of 3 mm and a temperature of 190 °C. If its centre-line must be cooled to 70 °C before it can be granulated effectively, calculate the required length of the water bath if the water temperature is 20 °C. The haul-off speed is 0.4 m/s and it may be assumed that the heat transfer from the plastic to the water is by conduction only.

5.27 Using the data in Tables 5.1 and 5.2, calculate the flow lengths which would be expected if the following materials were injected at 100 MPa into a wide rectangular cross-section channel, 1 mm deep. Materials – LDPE, polypropylene, polystyrene, PVC, POM, acrylic, polycarbonate, nylon 66 and ABS. Note that the answers will give an indication of the flow ratios for these materials. The flow should be assumed to be non-isothermal.

5.28 It is desired to blow mould a cylindrical plastic container of diameter 100 mm and wall thickness 2.5 mm. If the extruder die has an average diameter of 40 mm and a gap of 2 mm, calculate the output rate needed from the extruder. Comment on the suitability of an inflation pressure in the region of 0.4 MPa. The density of the molten plastic may be taken as 790 kg/m^3. Use the flow curves in Fig. 5.3.

5.29 During the blow moulding of polyethylene at 170 °C the parison is 0.4 m long and is left hanging for 1 s. Estimate the natural time for the process and the amount of sagging which occurs. The density of the melt may be taken at 730 kg/m^3.

5.30 The viscosity, η, of plastic melt is dependent on temperature, T, and pressure, P. The variations for some common plastics are given by equations of the form

$$\eta / \eta_R = 10^{B\Delta P} \text{ and } \eta/\eta_R = 10^{A\Delta T}$$

where $\Delta T = T - T_R$ (°C), $\Delta P = P - P_R$ (MPa), and the subscript R signifies a reference value. Typical values of the constants A and B are given below.

	Acrylic	Polypropylene	LDPE	Nylon	Acetal
A ($\times 10^{-3}$)	−28.32	−7.53	−11.29	−12.97	−7.53
B ($\times 10^{-3}$)	9.54	6.43	6.02	4.22	3.89

During flow along a particular channel the temperature drops by 40 °C and the pressure drops by 50 MPa. Estimate the overall change in viscosity of the melt in each case. Determine the ratio of the pressure change to the temperature change which would cause no change in viscosity for each of the above materials.

Bibliography

Pearson JRA: *Mechanics of polymer processing*, London, 1985, Elsevier Applied Science.

Progelhof RC, Throne JL: *Polymer engineering principles*, Munich, 1993, Hanser.

Osswald T, Hernandez-Ortiz JP: *Polymer processing: modeling and simulation*, Munich, 2006, Hanser.

Kumar A, Gupta RK: *Fundamentals of polymer engineering*, 2nd ed., New York, 2003, Marcel Dekker.

Tadmor Z, Gogos CG: *Principles of polymer processing*, 2nd ed., New York, 2006, Wiley.

Brydson JA: *Flow properties of polymer melts*, London, 1981, George Godwin.

Baird DG, Collias DI: *Polymer processing: principles and design*, 2nd ed., Wiley.

Grober H: *Fundamentals of heat transfer*, New York, 1961, McGraw-Hill.

Cogswell FN: *Polymer melt rheology*, London, 1981, George Godwin.

Carreau PJ, De Kee D, Chhabra RP, Munich, 1997, Hanser.

Rao NS, Schott NR: *Understanding plastics engineering calculations*, Munich, 2012, Hanser.

Muenstedt H, Schwarzl FR: *Deformation and flow of polymeric materials*, Heidelberg, 2014, Springer.

Solutions to questions

(2.1) Using the desirability factor D_f (Eq. 1.16)

$$D_f = \left(\frac{E^{1/3}}{\rho C}\right)$$

Material	E	ρ	C	D_f
Polypropylene	0.3	905	1	7.4×10^{-4}
uPVC (rigid)	2.1	1400	0.8	11.4×10^{-4}
ABS	1.2	1040	1.7	6×10^{-4}
Nylon 66	1.2	1140	2.5	3.7×10^{-4}
Polycarbonate	2.0	1150	2.2	5.5×10^{-4}
Acetal (copolymer)	1.0	1410	2.5	2.8×10^{-4}
Polysulphone	2.1	1240	10.0	1×10^{-4}

So uPVC would be the best choice on a cost basis.

(2.2) $L^3 = \dfrac{384EI\delta}{W}$

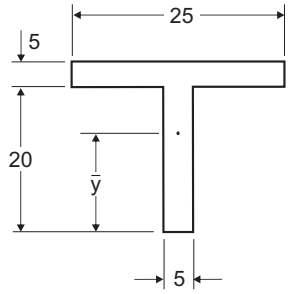
Weight, W = density × volume = $905 \times (2.25 \times 10^{-4}L) \times 9.81$ N = 2L N

From 1 week isochronous for polypropylene, $E = 427.5$ MPa

$$\text{So} \quad L^4 = \frac{384 \times 427.5 \times 10^6 \times 12.3 \times 10^{-9} \times 4 \times 10^{-3}}{2}$$

$$L = 1.417 \text{ m}$$

(2.3) $\bar{y} = 16.94$ mm



$$M = \frac{wL^2}{24} \text{where } w = \frac{W}{L}$$

$$\text{So, } \sigma = \frac{My}{I} = \frac{wL^2\bar{y}}{I} = \frac{2 \times 1.417^2 \times 16.94 \times 10^{-3}}{24 \times 12.3 \times 10^{-9}}$$
$$= 0.23 \text{ MPa}$$

At this stress, $E = 550$ MPa, so % error $= \dfrac{427.5 - 550}{427.5} = 28.7\%$

$$\text{So } \delta = \frac{WL^3}{384EI} = \frac{2 \times 1.417 \times 1.417^3}{384 \times 550 \times 10^6 \times 12.3 \times 10^{-9}} = 3.1 \text{ mm}$$

(2.4) From 3 year isochronous at 1.5%, $\sigma = 4.9$ MPa

$$\sigma_\theta = \frac{PR}{h} \text{ So } h = \frac{PR}{\sigma_\theta} = \frac{0.5 \times 40}{4.9} = 4.08 \text{ mm}$$

If the density = 905 kg/m^3 i.e. a reduction of 4 kg/m^3 then there would be a (4×4)% reduction in design stress. So new design stress = (0.84×4.9) MPa

$$\text{So} \qquad \text{New } h = \frac{0.5 \times 40}{4.9 \times 0.84} = 4.86 \text{ mm}$$

$$\text{Original weight} = 909 \times \pi \times 80 \times 4.08 \times 10^{-6}$$
$$\text{New weight} = 905 \times \pi \times 80 \times 4.86 \times 10^{-6}$$

$$\text{So } \% \text{ change} = \frac{(905 \times 4.86) - (909 \times 4.08)}{(909 \times 4.08)} \times 100 = +18.6\%$$

Note that this question involved a biaxial state of stress in the material and hence, strictly speaking, the creep curves used are not appropriate. However, creep curves for biaxial states of stress are rarely available, and one possible approach is to calculate an equivalent stress, σ_e, using a von Mises type criterion

$$\sigma_e = \frac{1}{\sqrt{2}} \sqrt{\left\{ (\sigma_1 - \sigma_2)^2 + (\sigma_2 - \sigma_3)^2 + (\sigma_3 - \sigma_1)^2 \right\}}$$

In the case of a cylinder under pressure, $\sigma_1 = PR/h$, $\sigma_2 = PR/2h$, $\sigma_3 = 0$, so

$$\sigma_e = \frac{\sqrt{3}}{2} \left(\frac{PR}{h} \right) = 0.866\sigma_\theta$$

In most cases it is probably sufficiently accurate to use σ_θ rather than σ_e and this approach will provide a built-in safety factor.

(2.5) Central Deflection,

$$\delta = \frac{WL^3}{48EI}$$

$$\text{Strain} = \frac{\sigma}{E} = \frac{My}{EI} = \left(\frac{W}{2}\right)\left(\frac{L}{2}\right)\left(\frac{d}{2}\right)\frac{1}{EI} = \frac{WLd}{8EI}$$

$$\text{So,} \quad \varepsilon = \frac{WL^3}{48EI} \quad \left(\frac{6d}{L^2}\right) = \frac{6\delta d}{L^2}$$

This strain will occur in the outer fibres at mid-span.

(2.6) For rotating pipe, $\sigma_\theta = \rho\omega^2 r^2$

$$\sigma_\theta = 909\left(\frac{2\pi \times 3000}{60}\right)^2 \left(150 \times 10^{-3}\right)^2 = 2 \text{ MPa}$$

It is necessary to know how long the material can withstand this stress before it reaches a strain of $\varepsilon_\theta = \Delta D/D = 1.2/300 = 0.4\%$
From the creep curves $t = 2.1 \times 10^6$ seconds = 24 days

(2.7) $\varepsilon_\theta = \dfrac{\Delta D}{D} = 2 \cdot \dfrac{\rho g H R}{2Eh}\left(= \dfrac{12.5}{1250} = 1\%\right)$

$$h = \frac{2\rho g H R^2}{E\Delta D}$$

From 1 year isochronous at 1% strain, $E = 360$ MPa. Making the 20% correction for change in density from 909 kg/m^3 to 904 kg/m^3, $E = 288$ MPa

$$\text{So} \quad h = \frac{2 \times 904 \times 9.81 \times 3 \times 0.625^2}{288 \times 10^6 \times 12.5 \times 10^{-3}} = 5.77 \text{ mm}$$

(2.8) From the 3 year isochronous curve for polypropylene, the initial modulus, $E = 466.7$ MPa. Making the $(5 \times 4)\%$ allowance for the different density, $E = 0.8 \times 466.7 = 373.3$ MPa.

$$h = \sqrt{\frac{P_c \times R^2}{0.365E}} = \sqrt{\frac{20 \times 10^3 \times 0.7^2}{0.365 \times 373.3 \times 10^6}} = 8.48 \text{ mm}$$

$$\text{Now} \quad \sigma = \frac{PR}{2h} = \frac{20 \times 10^3 \times 0.7}{2 \times 8.48 \times 10^{-3}} = 0.825 \text{ MPa}$$

At this stress the modulus has the same value as the initial modulus so no further iterations are necessary.

(2.9) The compressive stress in the bar is given by

$$\sigma = \frac{140}{(10 \times 10^{-3})^2} = 1.4 \text{ MPa}$$

$$\text{Now} \quad I = \frac{bd^3}{12} = \frac{10 \times 10^3}{12} = 833.3 \text{ mm}^4$$

$$\text{For buckling,} \quad E = \frac{P_c L^2}{\pi^2 I} = \frac{140 \times (225 \times 10^{-3})^2}{\pi^2 \times 833.3 \times 10^{-12}} = 861.7 \text{ MPa}$$

$$\therefore \ \varepsilon = \frac{\sigma}{E} = \frac{1.4 \times 10^6 \times 100}{861.7 \times 10^6} = 0.16\%$$

From the creep curves this strain is reached at 10^4 seconds

$$\text{So time} = \frac{10^4}{3600} = 2.78 \text{ hours}$$

(Note: $\varepsilon < 0.5\%$ so no correction to tensile creep data is needed).

(2.10) Critical Stress, $\sigma_c = \dfrac{P_c}{A} = \dfrac{4\pi^2 EI}{AL^2}$

and $I = \frac{wh^3}{12}$

So $$\sigma_c = \frac{4\pi^2 Ewh^3}{12whL^2} = \frac{\pi^2 E}{3}\left(\frac{h}{L}\right)^2$$

$$\frac{h}{L} = \sqrt{\frac{\pi^2}{3}\left(\frac{E}{\sigma_c}\right)}$$

For many plastics $\sigma_c/E = 30 \times 10^{-3}$ to 35×10^{-3} for short-term loading

So $$\frac{h}{L} = \sqrt{\frac{\pi^2}{3 \times 30 \times 10^{-3}}} = 10.5$$

For longer term loading, E will decrease more than σ_c so σ_c/E will get larger. This will cause the acceptable h/L to decrease.

(2.11) $P_c = \dfrac{\pi^2 EI}{L^2}$ So $\sigma_c = \dfrac{\pi^2 EI}{AL^2}$ and $\varepsilon_c = \dfrac{\pi^2 EI}{EAL^2} = \dfrac{\pi^2 I}{AL^2}$

Now for circular rod, $\varepsilon_c = \dfrac{\pi^2 d^2}{16L^2}$

So $$d = \sqrt{\frac{0.005 \times 16 \times 150^2}{\pi^2}} = 13.5 \text{ mm}$$

From 1 year isochronous at 0.5% strain, $E = 370$ MPa

So $$P_c = \frac{\pi^2 \times 370 \times \pi \times 13.5^4}{64 \times 150^2} = 227 \text{ N}$$

(2.12)

$h^2 = \dfrac{3(3+v)PR^2}{8\sigma} = \dfrac{3 \times 3.4 \times 40 \times 10^3 \times \left(75 \times 10^{-3}\right)^2}{8 \times 6 \times 10^6}$, $h = 6.91$ mm

From 1 year isochronous curve at a stress of 6 MPa, $E = 6/0.018 = 333.3$ MPa

So $$\delta = \frac{3 \times 0.6 \times 5.4 \times 40 \times 10^3 \times (75 \times 10^{-3})^2}{16 \times 333.3 \times 10^6 \times (6.91 \times 10^{-3})^3} = 7 \text{ mm}$$

(2.13) The maximum stress or strain is not specified so an iterative approach is needed.

From the 1 year isochronous for PP the initial modulus is 370 MPa

$$P = \frac{16Eh^3\delta}{3(1-v)(5+v)R^4} = \frac{16 \times 370 \times 10^6 \times (2.5 \times 10^{-3})^3 \times 4 \times 10^{-3}}{3 \times 0.6 \times 5.4 \times (32 \times 10^{-3})^4}$$
$$= 0.036 \text{ MPa}$$

So $$\sigma = \frac{3(3+v)PR^2}{8h^2} = \frac{3 \times 3.4 \times 0.0363 \times 32^2}{8 \times 2.5^2} = 7.58 \text{ MPa}$$

$$\text{but at} \quad \sigma = 7.58 \text{ MPa}, \quad E = \frac{7.58}{0.0248} = 305.6 \text{ MPa}$$

$$\text{So} \quad P = \frac{16 \times 2.5^3 \times 4}{3 \times 0.6 \times 5.4 \times 32^4}(305.6) = 3 \times 10^{-2} \text{ MPa}$$

$$\sigma = \frac{3 \times 3.4 \times 32^2}{8 \times 2.5^2}\left(3 \times 10^{-2}\right) = 6.27 \text{ MPa}$$

$$\text{but} \quad E = \frac{6.27}{0.0196} = 319.6 \text{ MPa} \rightarrow P = 3.14 \times 10^{-2} \rightarrow \sigma = 6.55 \text{ MPa}$$

$$E = 321.2 \text{ MPa} \rightarrow P = 3.15 \times 10^{-2} \text{MPa} \rightarrow \sigma = 6.58 \text{ MPa}$$

$$E = 321.2 \text{ MPa} \rightarrow P = 3.15 \times 10^{-2} \text{ MPa}$$

$$\varepsilon_\theta = \frac{\Delta D}{D} = \frac{PR}{2hE}(2 - v), \quad \text{So} \quad \Delta D = \frac{PR^2}{hE}(2 - v)$$

$$\text{So} \quad \Delta D = \frac{3.15 \times 10^{-2} \times 32^2}{2.5 \times 321.2}(1.6) = 6.43 \times 10^{-2} \text{ mm}$$

(2.14) $I = \dfrac{bd^3}{12} = \dfrac{12 \times d^3}{12} = d^3$

From the 1 year isochronous curve, the initial modulus = 370 MPa

$$\text{Now} \quad d^3 = \frac{5WL^3}{384E\delta} = \frac{5 \times 150 \times 200^3}{384 \times 370 \times 6} \quad \text{So} \quad d = 19.16 \text{ mm},$$

where $W = \omega L$

$$\sigma = \frac{My}{I} = \frac{WL}{16d^2} = \frac{150 \times 200}{16d^2} = 5.1 \text{ MPa}$$

$$\text{At} \quad \sigma = 5.1 \text{ MPa} \rightarrow E = 342.3 \text{ MPa} \rightarrow d = 19.67 \text{ mm}$$

$$\sigma = 4.85 \text{ MPa} \rightarrow E = 346.2 \text{ MPa} \rightarrow d = 19.6 \text{ mm}$$

$$\sigma = 4.88 \text{ MPa} \rightarrow E = 346.4 \text{ MPa} \rightarrow d = 19.6 \text{ mm}$$

(2.15) Once again an iterative type solution is required.

$$W = \frac{E(3)(1.5)}{\left\{0.48\left(\frac{1000}{40}\right)^{0.5}\left(\frac{40}{3}\right)^{1.22}\right\}} = 0.0795E$$

$$\sigma = \frac{2.4W}{3^2} = 0.267$$

From the 1 year isochronous curve, the initial modulus is 370 MPa

$$\text{So} \quad W = 29.43 \; N \rightarrow \sigma = 7.86 \text{ MPa} \rightarrow E = 302.3 \text{ MPa}$$

$$W = 24.03 \; N \rightarrow \sigma = 6.42 \text{ MPa} \rightarrow E = 324.1 \text{ MPa}$$

$$W = 25.76 \; N \rightarrow \sigma = 6.88 \text{ MPa} \rightarrow E = 317.0 \text{ MPa}$$

$$W = 25.2 \; N \rightarrow \sigma = 6.73 \text{ MPa} \rightarrow E = 317.4 \text{ MPa}$$

$$W = 25.2 \; N \rightarrow \sigma = 6.73 \text{ MPa}$$

So $W = 25.2$ N

(2.16) This is a stress relaxation problem but the isometric curves may be used.

From 2% isometric, after 10 seconds, $E = \dfrac{16.75}{0.02} = 837.5$ MPa

$$W = \frac{Ed^4\delta}{128(1+v)R^3N} = \frac{837.5 \times 3^4 \times 10}{128(1.4)5^3 \times 10} = 3 \; N$$

$$\text{After 1 week,} \quad E = \frac{8.55}{0.02} = 427.5 \text{ MPa}$$

$$\text{So} \quad W = \frac{427.5 \times 3^4 \times 10}{128(1.4)5^3 \times 10} = 1.55 \text{ N}$$

(2.17) From the 1 day isochronous curve, the maximum stress at which the material is linear is 4 MPa. This may be converted to an equivalent shear stress by the relation

$$\tau = \frac{\sigma}{2(1+v)} = \frac{4}{2(1.4)} = 1.43 \text{ MPa}$$

$$\text{Now} \quad \tau = \frac{16WR}{\pi d^3}, \text{ So} \quad d^3 = \frac{16 \times 3 \times 7.5}{\pi \times 1.43}$$

$$d = 4.31 \text{ mm}$$

$$\text{If} \quad \text{W} = 4.5 \text{ N}, \quad \tau = \frac{16 \times 4.5 \times 7.5}{\pi(4.31)^3} = 2.15 \text{ MPa}$$

Equivalent tensile stress $= \sigma = 2.15 \times 2 \times 1.4 = 6$ MPa.
From the 1 day isochronous at this stress,

$$E = \frac{6}{0.0094} = 638.3 \text{ MPa}$$

$$\delta = \frac{128(1+v)R^3N}{Ed^4} = \frac{K}{E}$$

$$\text{So} \quad \left(\frac{\delta_2 - \delta_1}{\delta_1}\right) = \left\{\frac{\frac{K}{E_2} - \frac{K}{E_1}}{\frac{K}{E_1}}\right\}$$

where $E_2 = 638.3$ MPa and

$$E_1 = \frac{1.4}{0.002} = 700 \text{ MPa}$$

So % change $= +9.67\%$

(2.18) At short times,

$$E = \frac{5.6}{0.004} = 1400 \text{ MPa}$$

Allowing for temperature, $E_{60} = 1400 \times 0.44 = 616$ MPa
Overall strain, $\varepsilon = \varepsilon_T - \varepsilon_\sigma = 0$

$$\varepsilon_T = \varepsilon_\sigma$$

$$\alpha \Delta T = \sigma / E = P/AE$$

$$\text{So} \quad P = AE\alpha\Delta T = \frac{\pi(10)^2}{4} \times 616 \times 1.35 \times 10^{-4} \times 40 = 261 \text{ N}$$

(Note: $\sigma = (261 \times 4)/\pi(10)^2 = 3.3$ MPa. Therefore since the strain is less than 0.5% no correction to the tensile data is needed for compressive loading).

After 1 year $E_{20} = 370$ MPa, $E_{60} = 222$ MPa

$$\text{So} \quad P = \frac{\pi(10)^2}{4} \times 222 \times 1.35 \times 10^{-4} \times 40 = 94 \text{ N}$$

(Note: Once again the strain is less than 0.5% so no correction is needed for compressive loading).

(2.19) $\varepsilon_\theta = \frac{\Delta D}{D} = \frac{0.05}{12} = 0.417\%$

From the 0.417% isometric curve, the stress after 1 year is 1.45 MPa
The pipe would leak if the hoop stress caused by atmospheric pressure (0.1 MPa) exceeded the stress in the pipe wall after 1 year.

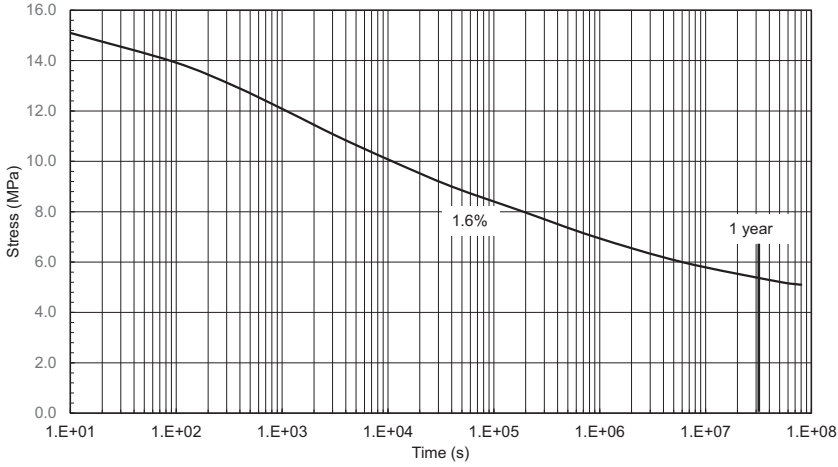
$$\text{For} \quad P = 0.1 \text{ MPa}, \quad \sigma_\theta = \frac{PR}{h} = \frac{0.1 \times 6}{1.5} = 0.4 \text{ MPa}$$

Hence, leakage would not occur.
When the pipe is cooled it will contract by an amount given by $\varepsilon_T = \alpha(\Delta T)$ and when this equals the fixed strain, ε_θ, the pipe would leak

$$\text{i.e.} \quad \Delta T = \frac{0.00417}{9 \times 10^{-5}} = 46.3^\circ\text{C}$$

So minimum temperature $= 20 - 46.3 = -26.3^\circ$C

(2.20) This is a stress relaxation problem, but the question states that creep data may be used



$$\text{Strain} = \frac{\Delta D}{D} = \frac{0.16}{10} = 1.6\%$$

Then from a 1.6% isometric taken from the creep curves it may be determined that the stress after 10 seconds is 15.1 MPa and after 1 year it is 5.4 MPa.

(a) Initial pressure at interface $= p = (h\sigma)/R = 1 \times 15.1/5 = 3.02$ MPa
Thus, normal force at interface, $F = p \times 2\pi RL = 3.02 \times 2\pi \times 5 \times 15 = 1.423$ kN
So axial force, $W = \mu F = 0.3 \times 1.423$ kN $= 0.427$ kN

(b) Similarly, after 1 year for $\sigma = 5.4$ MPa the axial force $W = 0.153$ kN.

(2.21) (a) As illustrated in Example 2.7, the extraction force, *F,* is given by

$$F = \pi\mu pDW$$

$$\text{So} \quad p = \frac{1.2 \times 10^3}{\pi(0.24)(40)(10)} = 4 \text{ MPa}$$

Treating the bush as a thick wall cylinder subjected to this value of external pressure, then Benham *et al.* show that at the outer surface of the bush, the stresses are:

$$\text{hoop stress, } \sigma_\theta = -p\left\{\frac{k^2+1}{k^2-1}\right\}$$

$$\text{radial stress, } \sigma_r = -p$$

Hence, the hoop strain, ε_θ, is given by

$$\varepsilon_\theta = \frac{\Delta R}{R} = \frac{\sigma_\theta}{E} - \frac{v\sigma_r}{E}$$

$$\Delta R = \frac{pR}{E}\left\{\left(\frac{k^2+1}{k^2-1}\right) - v\right\}$$

The negative sign simply means that this is a reduction.

$$\text{So} \quad \Delta R = \frac{4 \times 20}{2 \times 10^3}\left\{\left(\frac{1.14^2+1}{1.14^2-1}\right) - 0.4\right\}$$

$$\Delta R = 0.29 \text{ mm}$$

(b) $\Delta R = \alpha.R.\Delta T$

$$\Delta T = \frac{0.29}{100 \times 10^{-6} \times 20} = 143^\circ C$$

Hence the nylon bush would need to be cooled by 143°C to achieve the necessary contraction to have easy assembly. This suggests a cooled temperature of −123°C.

(c) At the bore of the bush, Benham *et al.* shows the stresses to be

$$\sigma_\theta = -\frac{2k^2p}{k^2-1}, \quad \sigma_r = 0$$

$$\text{hence} \quad \frac{\Delta r}{r} = \frac{\sigma_0}{E} - \frac{v\sigma_r}{E} = -\frac{2k^2p}{E(k^2-1)}$$

$$\Delta_r = \frac{-2(1.14)^2 17.5(4)}{2 \times 10^3(1.14^2-1)} = -0.3 \text{ mm}$$

Therefore, the internal diameter of the bush will be 35−2(0.3) = 34.4 mm.

(d) If the long-term modulus of the nylon is 1 GPa then for the same interference conditions, the interface pressure would be reduced to half its initial value ie 2 MPa. This means that the separation force would be half the design value i.e. 600 N.

(2.22) If the acetal ring is considered as a thick wall cylinder, then at the inner surface there will be hoop stresses and radial stresses if it is constrained in a uniform manner:

$$\text{hoop stress, } \sigma_\theta = p\left\{\frac{k^2+1}{k^2-1}\right\}$$

$$\text{radial stress, } \sigma_r = -p$$

where p is the effective internal pressure
k is the ratio of the outer to inner radii
Hence, the hoop strain, ε_θ, at the inner surface is given by

$$\varepsilon_\theta = \frac{\Delta r}{r} = \frac{\sigma_\theta}{E} - v\frac{\sigma_r}{E}$$

$$\text{So, } \quad \Delta r = \frac{pr}{E}\left\{\left(\frac{k^2+1}{k^2-1}\right)+v\right\}$$

When the bobbin is cooled by 60°C the effective constrained contraction of the inner surface of the acetal will be

$$\Delta r = (\alpha_a - \alpha_s) r \Delta T$$

$$\Delta r = (80-11)10^{-6}(10)(60) = 0.0414 \text{ mm}$$

So,

$$0.0414 = \frac{p(10)}{3\times 10^3}\left\{\left(\frac{1.5^2+1}{1.5^2-1}\right)+0.33\right\}$$

$$p = 4.24 \text{ MPa}$$

$$\text{hence,} \quad \sigma_\theta = p\left\{\frac{k^2+1}{k^2-1}\right\} = 4.24\left(\frac{3.25}{1.25}\right) = 11 \text{ MPa}$$

(2.23) Plot log $\dot{\varepsilon}$ vs. log σ and straight line confirms the Power Law with $A = 3 \times 10^{-11}$, $n = 0.774$

So $\varepsilon_t - \varepsilon_0 = \dot{\varepsilon}t = A\sigma^n t$

$$\varepsilon_t = 0.95 \times 10^{-2} + \left(3 \times 10^{-11}(5)^{0.774}\right)\left(9 \times 10^6 - 1 \times 10^6\right)$$
$$= 1.033\%$$

(2.24) A plot of log ε against log t is a straight line for $\sigma = 5.6$ MPa So $\varepsilon(t) = At^n$ where $A = 0.238$ and N $= 0.114$.
After 3 days ($= 2.59 \times 10^5$ seconds) strain $= 0.988\%$

$$F_r = \frac{\varepsilon(T) - \varepsilon_R(t)}{\varepsilon T} = \frac{0.988 - \varepsilon_R(t)}{0.988}$$

$$t_r = \frac{(2 \times 2.59 - 2.59) \times 10^5}{2.59 \times 10^5} = 1$$

So from (5) $F_r = 1 + t_R^n - (t_R + 1)^n$

$$1 - \frac{\varepsilon_R(t)}{0.988} = 1 + t_R^n - (t_R + 1)^n = 2 - (2)^{0.114}$$
$$0.988((2)^{0.114} - 1) = \varepsilon_r(t) = 0.0813\%$$

Alternatively: Strain after $2 \times 2.59 \times 10^5$ seconds $= 1.069\%$. Now recovery may be regarded as reversal of creep,
So residual strain $= 1.069 - 0.988 = 0.0812\%$

(2.25)

$$I = \frac{15 \times 15^3}{12} - \frac{10.5 \times 10.5^3}{12} + \frac{10.5}{12}\left(\frac{450}{909}\right)^2 (10.5)^3 = 3454.1 \text{ mm}^4$$

$$\text{For solid beam,} \quad I = \frac{D^4}{12} = 3454.1, \quad D = 14.27 \text{ mm}$$

Weight of solid beam $= 14.27^2 \times 10^{-6} \times 909 = 185.1$ g
Weight of foamed beam $= (4 \times 2.25 \times 12.75 \times 10^{-6} \times 909) + (450 \times 10.52 \times 10^{-6}) = 153.9$ g
% Saving $= 16.9\%$

(2.26)
$$\sigma = \frac{My}{I} = \frac{WL^2 \times 7.5}{24 \times 3126.3}$$

$$W = \frac{7 \times 3126.3 \times 24}{250^2 \times 7.5} = 1.12 \text{ kN/mm}$$

$$\text{From the 1 week isochronous,} \quad E = \frac{7}{0.015} = 466.7 \text{ MPa}$$

$$\delta = \frac{WL^4}{384EI} = \frac{1.12 \times 250^4}{384 \times 466.7 \times 3126.3} = 7.8 \text{ mm}$$

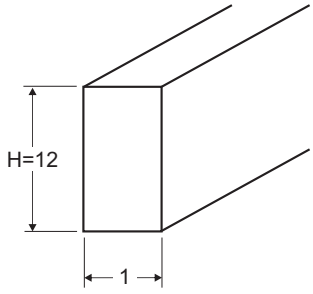
(2.27) Weight of solid beam $= 909 \times 12 \times 8 \times 300 \times 10^{-9} \times 10^3 = 26.18$ g Weight of composite $= (909 \times 2 \times 2 \times 12 \times 300 \times 10^{-6}) + (500 \times h12 \times 300 \times 10^{-6})$ $h = 7.27$ mm, so composite beam depth $= 11.27$ mm. The ratio of stiffnesses will *be* equal to the ratio of second moment of area

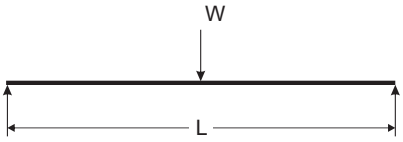
$$I_{solid} = \frac{bd^3}{12} = \frac{12 \times 8^3}{12} = 512 \text{ mm}^4$$

$$I_{composite} = \frac{12 \times 11.27^3}{12} - \frac{12 \times 7.27^3}{12} + \frac{\left(\frac{500}{900}\right)^2 12 \times 7.27^3}{12} = 1163.45 \text{ mm}^4$$

$$I_c/I_s = \frac{1163.45}{512} = 2.27$$

(2.28) (a) Solid





Consider a flexural loading situation as above,

$$\text{so} \quad \frac{W}{\delta} = \frac{48EI}{L^3} \propto EI$$

$$\text{So Solid} \quad EI = E_s\left(\frac{bd^3}{12}\right) = E_s\left(\frac{1 \times 12^3}{12}\right)$$

$$\text{Weight} = \rho_s \times H \times 1 \times 1 = \rho_s H = 12\rho_s$$

$$\text{Ratio} = \frac{E_s}{\rho_s}(12)$$

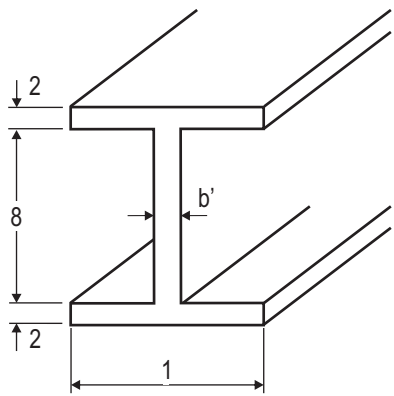
(b) Foamed

$$EI = E_f \left(\frac{bd^3}{12}\right) = \left(\frac{\rho_f}{\rho_s}\right) E_s \left(\frac{1 \times 12^3}{12}\right)$$

$$\text{Weight} = \rho_f \times H \times 1 \times 1 = 12\rho_f = \frac{12}{1.5}\rho_s$$

$$\text{Ratio} = \frac{E_s}{\rho_s}\left(\frac{12 \times 1.5}{1.5^2}\right) = \frac{E_s}{\rho_s}(8)$$

(c) Composite



$$b' = \left(\frac{E_f}{E_s}\right) \quad (I)$$

$$EI = E_s\left\{\frac{1 \times 2^3}{12} + (1 \times 2)(5)^2 + \frac{b'(8)^3}{12}\right\}$$

$$= E_s\left\{2(0.67 + 50) + \left(\frac{\rho_f}{\rho_s}\right)^2 \frac{(8)^3}{12}\right\} = 120.3E_s$$

$$\text{Weight} = \rho_s(4 + (8 \times 0.44)) \times 1 \times 1 = 7.56\ \rho_s$$

$$\text{Ratio} = \frac{120.3E_s}{7.56\rho_s} = (15.9)\frac{E_s}{\rho_s}$$

So ratio foam: solid: composite = 8:12:15.9

(2.29) (a) Sandwich Beam of Minimum Weight for a given stiffness (Fig. 2.19)

$$\text{deflection,}\quad \delta = \frac{KWL^3}{EI} \tag{1}$$

where K is a factor depending on loading and supports.

$$\text{For} \quad E_{skin} >> E_{core,} \quad EI \approx Ebdh^2/2$$

$$\delta = \frac{2KWL^3}{E_{skin}bdh^2}$$

$$\text{Total mass} \quad \text{m} = \rho_{\text{core}}bhL + 2\rho_{\text{skin}}bdL$$

From deflection Eq. (1)

$$d = \frac{2KWL^3}{E_{skin}bh^2\delta} \tag{2}$$

$$\text{So} \quad m = \rho_{core}bhL + \rho_{skin}\left(\frac{4KWL^4}{E_{skin}h^2\delta}\right)$$

To minimise the weight with respect to h, then $\partial m/\partial h = 0$

$$\frac{\partial m}{\partial h} = \rho_{core} bL - \frac{8\rho_{skin} KWL^4}{E_{skin}\delta h^3} = 0$$

Rearranging and substituting from (2) for KWL^3

$$\therefore \quad h^3 = \frac{4\rho_{skin} KWL^3}{E_{skin}\delta\rho_{core} b} = \frac{4\rho_{skin} dh^2}{\rho_{core}}$$

$$\therefore \quad \rho_{core} h = 4\rho_{skin} d$$

If weight of core $= \rho_{\text{core}} bhL$ and wight of skin $= 2\rho_{\text{skin}} bdL$,

then weight of core $= 2 \times$ weight of skin

(b) Sandwich Beam of Minimum Weight for a Given Strength

Assuming the core does not fail in shear, failure occurs in bending when the stress in the skin reaches its yield strength σ_y, i.e.

$$\sigma_y = \frac{M}{bdh}$$

where $M =$ bending moment.

Mass of beam

$$m = \rho_{\text{core}} bhL + 2\rho_{\text{skin}} bdL$$

Using

$$d = \frac{M}{bh\sigma_y}$$

$$m = \rho_{core} bhL + 2\rho_{skin}\left(\frac{LM}{h\sigma_y}\right)$$

To minimise the weight with respect to h, $\partial m/\partial h = 0$

$$\frac{\partial m}{\partial h} = \rho_{core} bL - 2\rho_{skin}\frac{LM}{h^2\sigma_y} = 0$$

$$\therefore \quad h^2 = \frac{2\rho_{skin}}{\rho_{core}}\frac{M}{b\sigma_y} = \frac{2\rho_{skin} d}{\rho_{core}}$$

$$\therefore \quad \rho_{\text{core}} \text{h} = 2\rho_{\text{skin}} d$$

or

$$\text{weight of core} = \text{weight of skin.}$$

(2.30)

(a) Maxwell

$$\varepsilon = \frac{\sigma_0}{\xi} + \dot{\varepsilon}t = \frac{\sigma_0}{\xi} + \frac{\sigma_0}{\eta}t$$

$$\varepsilon_{50} = \frac{12}{2000} + \frac{12 \times 10^6}{90 \times 10^9}(50) = 1.26\%$$

$$\varepsilon_{100} = \frac{12}{2000} + \frac{12 \times 10^6}{90 \times 10^9}(100) = 1.933\%$$

but $\dfrac{\sigma_0}{\xi} = 0.6\%$

$$\varepsilon_{150} = 1.933 - 0.6 = 1.333\%$$

(b) Voigt

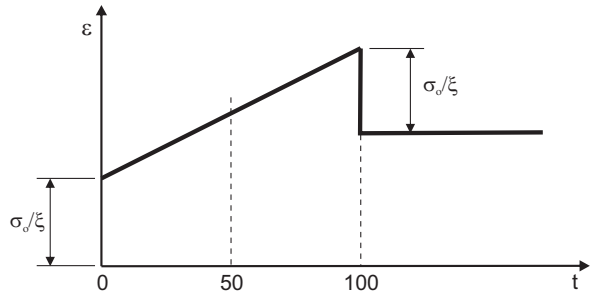
$$\varepsilon = \frac{\sigma_0}{\xi}\left(1 - e^{-(\xi t)/\eta}\right)$$

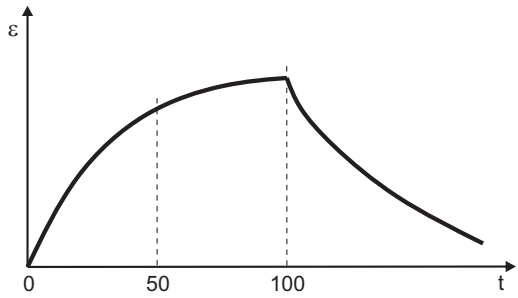
$$\varepsilon_{50} = \frac{12}{2000}\left(1 - e^{(-2\times 50)/90}\right) = 0.402\%$$

$$\varepsilon_{100} = \frac{12}{2000}\left(1 - e^{(-2\times 100)/90}\right) = 0.535\%$$

$$\varepsilon_{150} = \varepsilon_{100} e^{(\xi t)^{\eta}}$$

$$= 0.535 e^{(-2\times 50)/90} = 0.176\%$$





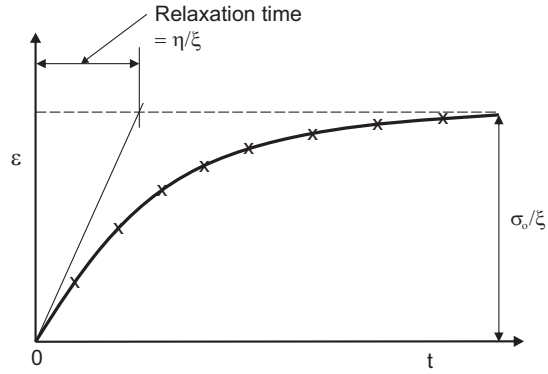
(2.31) Maxwell Strain (50 s) = Kelvin Strain (50 s)

$$\frac{\sigma_0}{\xi_1}+\frac{\sigma_0 t}{\eta_1} = \frac{\sigma_0}{\xi_2}\left(1-e^{(-\xi_2 t)/\eta_2}\right)$$

$$\text{So} \quad \xi_1 = \left[\frac{1}{\xi_2}\left(1-e^{(-\xi_2 t)/\eta_2}\right)-\frac{t}{\eta_1}\right]^{-1}$$

$$\xi_1 = \left[\frac{1}{2\times 10^9}\left(1-e^{(-2\times 50)/100}\right)-\frac{50}{200\times 10^9}\right]^{-1} = 15.1 \text{ GPa}$$

(2.32) From graph $\sigma_0/\xi = 0.01$



$$\text{So} \quad \xi = \frac{2}{0.01} = 200 \text{ MPa}$$

At $$\varepsilon = 0.0089, \text{t} = 3000 \text{ s}$$

$$0.0089 = 0.01\left\{1-e^{-3000(\xi/\eta)}\right\}$$

So

$$7.36\times 10^{-4} = \xi/\eta$$

$$\eta = 270 \text{ GPa.s}$$

Relaxation time $= \eta/\xi = 1350$ seconds

$$\text{for} \quad \sigma_0 = 4.5 \ \text{MPa}$$

$$\varepsilon = \frac{4.5}{200}\left\{1 - e^{(-1500)/1350}\right\} = 0.0151$$

(2.33) (a) Stress−Strain equations

$$\sigma_1 = \xi_1 \varepsilon_1$$

$$\sigma_2 = \xi_2 \varepsilon_2$$

$$\sigma_3 = \eta\, \dot{\varepsilon}_3$$

(b) Equilibrium equations

$$\sigma = \sigma_1 = \sigma_2 + \sigma_3$$

(c) Geometry of Deformation

$$\varepsilon = \varepsilon_1 + \varepsilon_2 \ \text{ and } \ \varepsilon_2 = \varepsilon_3$$

From above

$$\dot{\varepsilon} = \dot{\varepsilon}_1 + \dot{\varepsilon}_2$$

but

$$\dot{\varepsilon}_1 = \dot{\sigma}_1/\xi_1 \quad \text{and} \quad \dot{\varepsilon}_2 = (\sigma_1 / \eta) - (\xi_2 / \eta)\varepsilon_2 \ \text{ (from Kelvin model)}$$

$$\dot{\varepsilon} = \frac{\dot{\sigma}}{\xi_1} + \frac{\sigma}{\eta} + \frac{\xi_2}{\eta}(\varepsilon - \varepsilon_1)$$

$$\dot{\varepsilon} = \frac{\dot{\sigma}}{\xi_1} + \frac{\sigma}{\eta} - \frac{\xi_2}{\eta}\left(\varepsilon - \frac{\sigma}{\xi_1}\right)$$

$$\dot{\varepsilon} + \frac{\xi_2}{\eta}\varepsilon = \frac{\dot{\sigma}}{\xi_1} + \frac{\sigma}{\eta}\left(\frac{\xi_1 + \xi_2}{\xi_1}\right)$$

This is the governing equation for the Standard Model.
The solution to this differential equation will have the form

$$\varepsilon(t) = \frac{\sigma_0}{\xi_1} + \frac{\sigma_0}{\xi_2}\left(1 - e^{-t/T}\right)$$

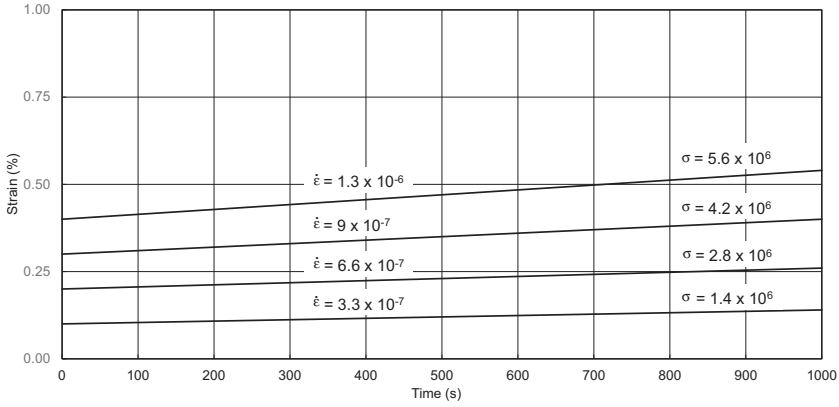
where $T = \eta/\xi_2$ and σ_0/ξ_1 is the initial strain when the stress is applied.
The unrelaxed creep modulus is obtained by putting $t = 0$.

Hence, unrelaxed modulus $E_U = \dfrac{\sigma_0}{\varepsilon(0)} = \xi_1$

The relaxed modulus is obtained by putting $t = \infty$.

Hence, relaxed modulus $E_R = \dfrac{\sigma_0}{\varepsilon(\infty)} = \dfrac{\xi_1\xi_2}{\xi_1 + \xi_2}$.

(2.34) From figure below redrawn from the creep curves



$$\eta = \frac{\sigma}{\dot{\varepsilon}} \simeq 4.3 \times 10^{12} \text{ Pa.s}$$

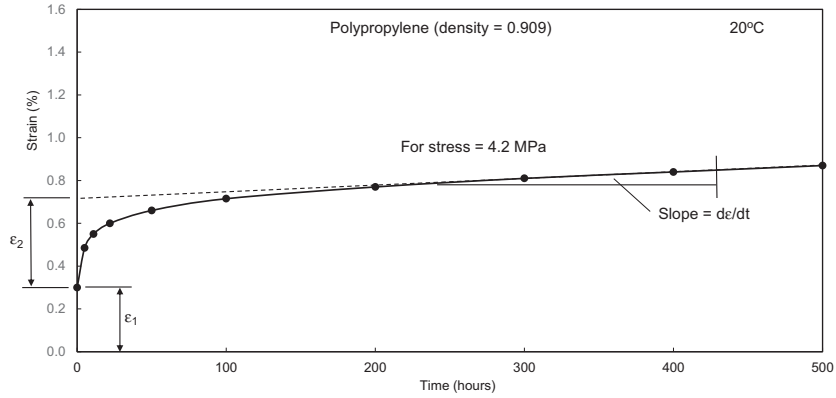
$$\xi = \frac{\sigma_0}{\varepsilon_0} = 1400 \times 10^6 \text{ Pa}$$

So from text using the fact that for a strain of 0.4%, $\sigma_0 \sim 5.5$ MPa (from creep data)

$$\sigma = \sigma_0 e^{(-\xi t)/\eta}$$

$$\sigma = 5.5e^{\left(-1400\times10^6\times900\right)/4.3\times10^{12}} = 4.1 \text{ MPa}$$

(2.35) From the graph below, and the theory of the 4-element model, $\xi_1 = \sigma_0/\varepsilon_1 = 4.2/0.003 = 1400$ MPa



$$\varepsilon_2 = \frac{\sigma_0}{\text{Retarded Creep}} = \frac{\sigma_0}{\varepsilon_2} = \frac{4.2}{(0.72-0.3)10^{-2}} = 1000 \text{ MPa}$$

$$\eta_1 = \frac{\sigma_0}{d\varepsilon/dt} = \frac{4.2}{3.167\times10^{-6}} = 1.326\times10^6 \text{(MPa).hr}$$

$$\eta_1 = 4.775\times10^9 \text{ MPa.s}$$

Finally from the expression for the 4-element model

$$\varepsilon = \frac{\sigma_0}{\xi_1} + \frac{\sigma_0 t}{\eta_1} + \frac{\sigma_0}{\xi_2}\left(1 - e^{-(\xi_2 t)/\eta_2}\right)$$

taking a value of strain from the *knee* of the curve

$$\varepsilon = 0.0055 \text{ at } t = 4\times10^4 \text{ seconds } (11.1 \text{ hrs})$$

$$\text{So } \quad \eta_2 = 4.525\times10^7 \text{ MPa.s}$$

$$\text{For } \quad \sigma = 5.6 \text{ MPa at } 3\times10^5 \text{ seconds}$$

$$\varepsilon = \frac{5.6}{1400} + \frac{5.6 \times 3 \times 10^5}{4.775 \times 10^9} + \frac{5.6}{1000}\left(1 - e^{-\left(1000 \times 3 \times 10^5\right)/4.525 \times 10^7}\right) = 0.99\%$$

(2.36)

$$E(t) = At^{-n}$$

$$\sigma(t) = Bt$$

$$\varepsilon(t) = \int_0^T \frac{1}{E(t)} \bullet \frac{d\sigma(t)}{dt} \bullet dt$$

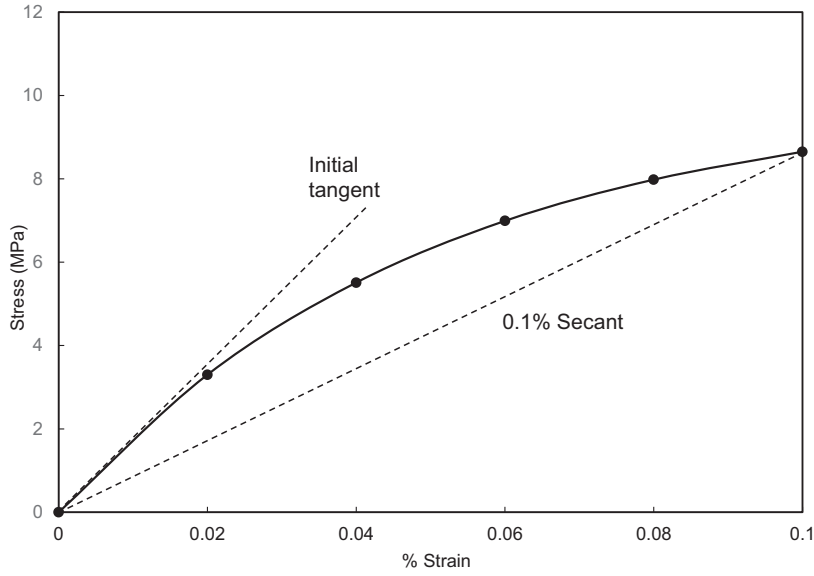
$$= \int_0^T \frac{t^n}{A} \bullet B dt$$

$$= \left[\frac{t^{n+1}}{A(n+1)} \bullet B\right]_0^T$$

$$\varepsilon(t) = \frac{BT^{n+1}}{A(n+1)}$$

This will be a non-linear response for all non-zero values of n.

(2.37) For the Maxwell Model



$$\dot{\varepsilon} = \frac{1}{\xi}\dot{\sigma} + \frac{1}{\eta}\sigma = K$$

$$\frac{d\sigma}{dt} + \frac{\xi\sigma}{\eta} = K\xi$$

$$\int_0^t \xi dt = \int_0^\sigma \left(\frac{1}{K - \dfrac{\sigma}{\eta}}\right) d\sigma$$

$$\xi t = -\eta \ln \left(K - \frac{\sigma}{\eta}\right) + \eta \ln K$$

$$\frac{\xi t}{\eta} = \ln \left(\frac{K}{K - \dfrac{\sigma}{\eta}}\right)$$

$$e^{(\xi t)/\eta} = \left(\frac{K}{K - \dfrac{\sigma}{\eta}}\right)$$

$$\sigma = K\eta\left(1 - e^{(-\xi t)/\eta}\right)$$

$$\text{Using} \quad \frac{\xi}{\eta} = \frac{20}{100} = 2 \times 10^{-2}$$

$$\text{and} \quad K\eta = 10^{-5} \times 1000 \times 10^3 = 10$$

Time (s)	Strain (%)	Stress (MPa)
20	0.02	3.3
40	0.04	5.51
60	0.06	6.99
80	0.08	7.98
100	0.1	8.65

initial tangent modulus = 7.00/0.0004 = 17.5 GPa
0.1% secant modulus = 8.65/0.001 = 8.65 GPa

Note that in this question an alternative solution may be carried out using the *creep modulus* but this causes slight inaccuracies.
Alternative Solution:

$$\sigma(t) = \int_0^t E(t-u)\frac{d\varepsilon(u)}{du}\bullet du$$

Now for Maxwell Model $E(t) = \dfrac{\xi\eta}{\eta + \xi t}$

So for case in question, the strain history is

$$0 < t < t_1 : \varepsilon(t) = Kt, \;\; d\varepsilon(u)/du = K$$

$$\text{So} \quad \sigma(t) = \int_0^{t_1} \frac{\xi\eta}{\eta + \xi(t_1 - u)}\bullet K \bullet du = \int_0^{t_1}\left(\frac{\xi\eta}{\eta + \xi t_1 - \xi u}\right)K du.$$

$$= K\xi\eta\left[\log_e(\eta + \xi t_1 - \xi u)\bullet\left(-\frac{1}{\xi}\right)\right]_0^{t_1}$$

$$\text{So} \quad \sigma(t) = K\eta\left[\log_e\left(\frac{\eta + \xi t_1}{\eta}\right)\right]$$

This equation predicts the following data

Time (s)	Strain (%)	Stress (MPa)
20	0.02	3.36
40	0.04	5.88
60	0.06	7.88
80	0.08	9.56
100	0.1	10.98

From a plot of this data

$$\text{Initial tangent modulus} = \frac{10}{0.00057} = 17.54 \text{ GPa}$$

$$0.1\% \text{ secant modulus} = \frac{10.98}{0.001} = 10.98 \text{ GPa}$$

(2.38) $\varepsilon(t_1) = K_1 t_1\left(\dfrac{1}{\xi} + \dfrac{t_1}{2\eta}\right)$

$$\varepsilon(40) = 0.5 \times 40\left(\frac{1}{3000} + \frac{40}{2 \times 45,000}\right) = 1.55\%$$

$$\varepsilon(t_2) = (K_1 T + K_2 T)\left(\frac{1}{\xi} + \frac{t_2}{\eta} - \frac{T}{2\eta}\right) - K_2 t_2\left(\frac{1}{\xi} + \frac{t_2}{2\eta}\right)$$

$$\varepsilon(70) = (0.5 \times 60 + 1 \times 60)\left(\frac{1}{3000} + \frac{70}{45,000} - \frac{60}{90,000}\right)$$

$$-70\left(\frac{1}{3000} + \frac{70}{90,000}\right)$$

$$= 3.22\%$$

$$\varepsilon(t_3) = \frac{K_1 T}{\xi\eta}\{\eta + \xi t_3 - 0.5\xi T\} - \frac{K_2(T' - T)}{\xi\eta}\{\eta + \xi t_3 - 0.5\xi(T' - T)\}$$

which, for $t_3 = 120$ s, $T = 60$ s and $T' = 90$ s, gives $\varepsilon(120) = 3\%$

(2.39)

$$\varepsilon(t_1) = K_1 t_1\left(\frac{1}{\xi} + \frac{t_1}{2\eta}\right)$$

$$\varepsilon(60) = 0.4 \times 60\left(\frac{1}{3500} + \frac{60}{2 \times 50,000}\right) = 2.12\%$$

$$\varepsilon(t_2) = K_1 t'\left(\frac{1}{\xi} + \frac{t_2}{\eta} - \frac{t'}{2\eta}\right) - \frac{\Delta\sigma}{E(t_2 - t')}$$

$$= K_1 t'\left(\frac{1}{\xi} + \frac{t_2}{\eta} - \frac{t'}{2\eta}\right) - \frac{\Delta\sigma(\eta + (t_2 - t'))}{\xi\eta}$$

$$\varepsilon(130) = 0.4(100)\left(\frac{1}{3500} + \frac{130}{50,000} - \frac{100}{100,000}\right)$$

$$- \frac{10(50,000 + 350(30))}{3500 \times 50,000}$$

$$= 6.61$$

(2.40) (a)

$$\varepsilon(u_1) = \int_0^{u_1} \frac{1}{E(t-t_1)} \cdot \frac{d\sigma(t)}{dt} \cdot dt$$

$$\sigma(t) = \frac{20}{800} \cdot t, \quad \frac{d\sigma(t)}{dt} = \frac{20}{800}$$

$$\varepsilon(u_1) = \int_0^{u_1} \frac{1}{E(t-0)} \cdot \frac{20}{800} dt$$

$$= \int_0^{u_1} \frac{t^{0.05}}{10^3} \frac{20}{800} dt$$

$$\varepsilon(500) = \left[\frac{t^{1.05}}{1.05 \times 1000} \cdot \frac{20}{800} \right]_0^{500}$$

$$= 0.0162 = 1.62\%$$

(b) After 800 s, the change in stress is (−Kt) where $K = \frac{20}{800}$. So

$$\varepsilon(u_2) = \int_0^{u_2} \frac{1}{E(t-t_1)} \cdot \frac{d\sigma(t)}{dt} \cdot dt + \int_{t_2}^{u_2} \frac{1}{E(t-t_2)} \cdot \frac{d\sigma(t)}{dt} \cdot dt$$

$$= \int_0^{u_2} \frac{t^{0.05}}{10^3} \cdot K \cdot dt + \int^{u_2} t_2 \frac{(t-t_2)^{0.05}}{10^3} \cdot (-K) dt$$

$$= \left[\frac{t^{1.05}}{1.05 \times 10^3} \cdot K \right]_0^{u_2} - \left[\frac{(t-t_2)^{1.05}}{1.05 \times 10^3} \cdot K \right]_{t_2}^{u_2}$$

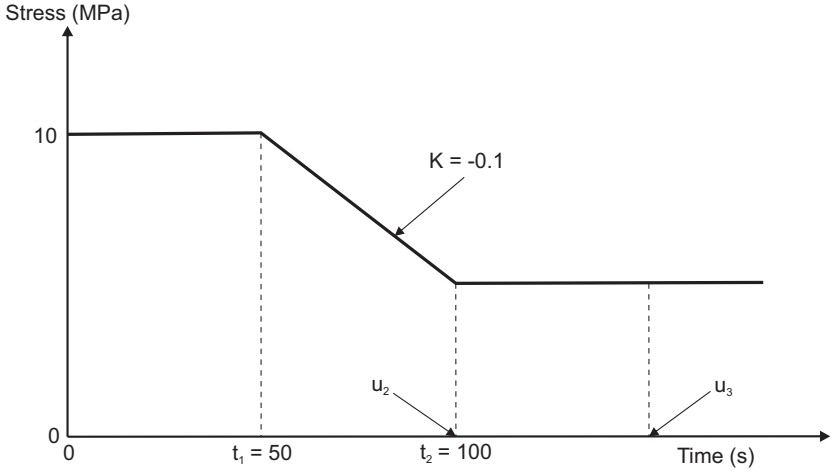
then for $u_2 = 1000$ s, $t_2 = 800$ s

$$\varepsilon(1000) = 0.0336 - 6.21 \times 10^{-3} = 0.0274 = 2.74\%$$

(2.41) For a Kelvin – Voigt model

$$E(t) = \xi \left[1 - e^{-t/T} \right]^{-1}$$

where $T = \eta/\xi = 30$



(a) Using Boltzmanns Superposition Principle

$$\varepsilon(u_2) = \frac{\sigma_0}{\xi}\left(1 - e^{-u_2/T}\right) + \int_{t_1}^{u_2} \frac{1}{E(t-t_1)} \cdot \frac{d\sigma(t)}{dt} \cdot dt$$

where

$$\sigma(t) = -Kt \quad \text{so} \quad \frac{d\sigma(t)}{dt} = -K$$

$$\varepsilon(u_2) = \frac{\sigma_0}{\xi}\left(1 - e^{-u_2/T}\right) - K\int_{t_1}^{u_2} \frac{\left[1 - e^{-t/T} \cdot e^{-t_1/T}\right]}{\xi} dt$$

$$= \frac{\sigma_0}{\xi}\left(1 - e^{-u_2/T}\right) - K\left[\frac{t + T \cdot e^{t_1/T} \cdot e^{-t/T}}{\xi}\right]_{t_1}^{u_2}$$

$$\varepsilon(90) = \frac{10}{12 \times 10^3}\left(1 - e^{-90/30}\right) - 0.1\left[\left(\frac{90 + 30e^{-40/30}}{12 \times 10^3}\right) - \left(\frac{50 + 30}{12 \times 10^3}\right)\right]$$

$$\varepsilon(90) = 6.43 \times 10^4 = 0.064\%$$

$$\text{(b) } \varepsilon(u_3) = \frac{\sigma_0}{\xi}\left(1 - e^{-u_3/T}\right) + \int_{t_1}^{u_3} \frac{1}{E(t-t_1)} \frac{d\sigma(t)}{dt} dt + \int_{t_2}^{u_3} \frac{1}{E(t-t_2)} \frac{d\sigma(t)}{dt} dt$$

For the period after t_2 (= 100 s) the change in stress is Kt.

So $\dfrac{d\sigma(t)}{dt} = K$ for this third period

$$\varepsilon(u_3) = \frac{\sigma}{\xi}\left(1 - e^{-u_3/T}\right) + \int_{t_1}^{u_3} \frac{\left(1 - e^{-t/T} \cdot e^{-t_1/T}\right)}{\xi} \times (-K) dt \int_{t_2}^{u_3} \frac{\left(1 - e^{-t_2/T}\right)}{\xi} K\, dt$$

$$\varepsilon(u_3) = \frac{\sigma_0}{\xi}\left(1 - e^{-u_3/T}\right) - K\left[\frac{\left(t + T \cdot e^{-\frac{t_1}{T}} \cdot e^{-\frac{t}{T}}\right)}{\xi}\right]_{t_1}^{u_3} + K\left[\frac{\left(t + T \cdot e^{-\frac{t_2}{T}} \cdot e^{-\frac{t}{T}}\right)}{\xi}\right]_{t_2}^{u_3}$$

Substituting $u_3 = 150\,\text{s}, K = 0.1, t_1 = 50\,\text{s}, t_2 = 100\,\text{s}$

$\varepsilon(150) = 4.49 \times 10^{-4} = 0.045\%$

(2.42) $\varepsilon(t) = \sum_{i=0}^{i=N} \sigma_i \left\{\dfrac{1}{E(t-u_i)}\right\}$ where $E(t-u_i) = \dfrac{\xi\eta}{\eta + \xi(t-u_i)}$

So,

$$\varepsilon(4500) = 10\left\{\frac{\eta + \xi(4500-0)}{\xi\eta}\right\} + 10\left\{\frac{\eta + \xi(4500-1000)}{\xi\eta}\right\}$$

$$-15\left\{\frac{\eta + \xi(4500-2000)}{\xi\eta}\right\} + 20\left\{\frac{\eta + \xi(4500-3000)}{\xi\eta}\right\}$$

$$-25\left\{\frac{\eta + \xi(4500-4000)}{\xi\eta}\right\}$$

$$= \frac{10}{\xi\eta}\{\eta + 4500\xi + \eta + 3500\xi - 1.5\eta - 3750\xi + 2\eta + 3000\xi - 2.5\eta - 1250\xi\}$$

$$= \frac{10}{\xi\eta}\{6000\xi\} = \frac{60,000}{4 \times 10^6} = 1.5\%$$

(2.43) From the information provided

$$F_r = \frac{\varepsilon_c(T) - \varepsilon_r(t)}{\varepsilon_c(T)} = \frac{0.8 - 0.058}{0.8} = 0.9275$$

also

$$t_R = \frac{t - T}{T} = \frac{200 - 100}{100} = 1$$

but,

$$F_r = 1 + t_R^n - (t_R + 1)^n$$

$$0.9275 = 1 + 1 - (2)^n \rightarrow n = 0.1$$

Also, since $\varepsilon_c(100) = 0.8\%$ and $\varepsilon_c(100) = A(100)^{0.1}$

then $A = 0.504766$ (for $\sigma = 10$ MPa)

Therefore after 2400 seconds at 10 MPa

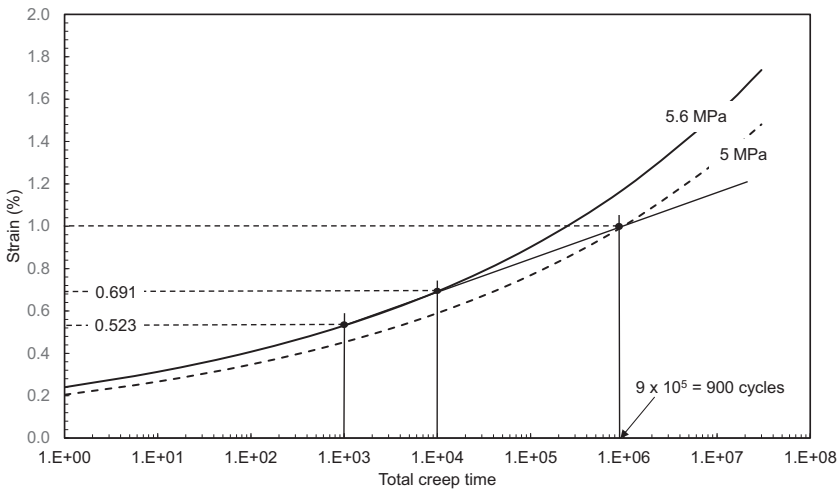
$$\varepsilon(2400) = 0.504766\ (2400)^{0.1} = 1.1\%$$

For 2400 seconds on and 7200 seconds off, $t' = 9600$ seconds.

$$\text{So} \quad \varepsilon_r\left(9.6 \times 10^4\right) = \varepsilon_c(2400) \sum_{x=1}^{x=10} \left[\left(\frac{t'x}{T}\right)^n - \left(\frac{t'x}{T} - 1\right)^n \right]$$

$$\varepsilon_r\left(9.6 \times 10^4\right) = 1.1 \sum_{x=1}^{x=10} \left[(4x)^n - (4x - 1)^n\right] = 0.108\%$$

(2.44) From question (2.20) at 5.6 MPa the grade of PP may be represented by $\varepsilon\ (t) = 0.238(t)^{0.114}$



So, after 1000 seconds, $\varepsilon(t) = 0.523\%$
After 10 cycles in the given sequence ($t' = 1500$ seconds)

$$\varepsilon\left(1.5 \times 10^4\right) = (0.523) + 0.523 \sum_{x=1}^{x=10} \left[(1.5x)^{0.114} - (1.5x - 1)^{0.114}\right] = 0.691\%$$

Then if a straight line is drawn from the point 0.523, 1000 to 0.691, 10,000 on Fig. 2.5 then this may be extrapolated to 1% strain which occurs at approximately $t = 9 \times 10^5$ seconds. This is the total creep time (ignoring recovery) and so the number of cycles for this time is

$$(9 = 10^5)/1000 = 900 \text{ cycles}$$

Notes

$$\text{1000 cycles} \quad \begin{cases} \varepsilon_c\left(1.5 \times 10^6\right) = 0.495\% \\ \varepsilon_r\left(1.5 \times 10^6\right) = 1.018\% \end{cases}$$

$$\text{1500 cycles} \quad \begin{cases} \varepsilon_c\left(2.25 \times 10^6\right) = 0.5329\% \\ \varepsilon_r\left(2.25 \times 10^6\right) = 1.056\% \end{cases}$$

Equivalent modulus after 900 cycles = 5/0.01 = 500 MPa.

(2.45) For the PP creep curves in Fig. 2.5, $n = 0.114$ at $\sigma = 7$ MPa, $\varepsilon_c\ (2.16 \times 10^4) = 0.99\%$ after 11 cycles of creep (10 cycles of load removal), $t = 66$ hrs $= 2.37 \times 10^5$ s (using equation in spreadsheet program) $\varepsilon_c\ (2.37 \times 10^5) = 1.105\%$

A line joining 0.99, 2.16×10^4 to 1.105, 2.375×10^6 on Fig. 2.5 allows strain at 365 days (i.e. 365 days @ 6 hrs per day $= 7.88 \times 10^6$ seconds) to be extrapolated to 1.29%. The spreadsheet predicts

$$\varepsilon_c\ (7.88 \times 10^6) = 1.294\%$$

at $\sigma = 8.4$ MPa, $\varepsilon_c\ (2.37 \times 10^5) = 1.406\%$ and $\varepsilon_c\ (2.16 \times 10^4) = 1.26\%$

Extrapolation on Fig. 2.5 to 7.88×10^6 seconds gives $\varepsilon_c\ (7.88 \times 10^6) = 1.62\%$. Spreadsheet gives $\varepsilon_c\ (7.88) \times 1(0^6) = 1.64\%$
Extrapolation between these two values to get $\varepsilon_c\ (7.88 \times 10^6) = 1.5\%$ gives $\sigma = 7.8$ MPa.
So since

$$\sigma = \frac{pD}{2h},\ h = \frac{0.5 \times 150}{2 \times 7.8} = 4.8 \text{ mm}$$

For continuous loading for 1 year ($= 3.15 \times 10^7$ s) the design stress would be 5.08 MPa which gives $h = 7.38$ mm

$$\text{So material saving} = \frac{7.38 - 4.8}{7.38} = 35\%$$

(2.46)

$$\sigma = \sigma_0 e^{i(\omega t+\delta)}$$

$$\varepsilon = \varepsilon_0 e^{i\omega t}$$

As shown in the previous question, the governing equation for this type of Standard Linear Solid is given by:

$$\dot{\varepsilon} + \frac{\xi_2}{\eta}\varepsilon = \frac{\dot{\sigma}}{\xi_1} + \frac{\sigma}{\eta}\left(\frac{\xi_1 + \xi_2}{\xi_1}\right)$$

$$\varepsilon_0 i\omega e^{i\omega t} + \frac{\xi_2}{\eta}\varepsilon_0 e^{i\omega t} = \frac{1}{\xi_1}\sigma_0 i\omega e^{i(\omega t+\delta)} + \left(\frac{\xi_1 + \xi_2}{\xi_1 \eta}\right)\sigma_0 e^{i(\omega t+\delta)}$$

Dividing across by $\varepsilon_0 e^{i\omega t}$ and letting $E^* = \dfrac{\sigma_0 e^{i(\omega t+\delta)}}{\varepsilon_0 e^{i\omega t}}$
Then E^* is given by

$$E^* = \frac{\xi_1\eta\omega i + \xi_1\xi_2}{(\xi_1 + \xi_2) + \eta\omega i}$$

Multiplying top and bottom by the conjugate of the denominator,

$$E^* = \frac{\xi_1\xi_2(\xi_1 + \xi_2) + \eta^2\omega^2\xi_1 + [(\xi_1 + \xi_2)\omega\xi_1\eta - \xi_1\xi_2\eta\omega]i}{(\xi_1 + \xi_2)^2 + \eta^2\omega^2}$$

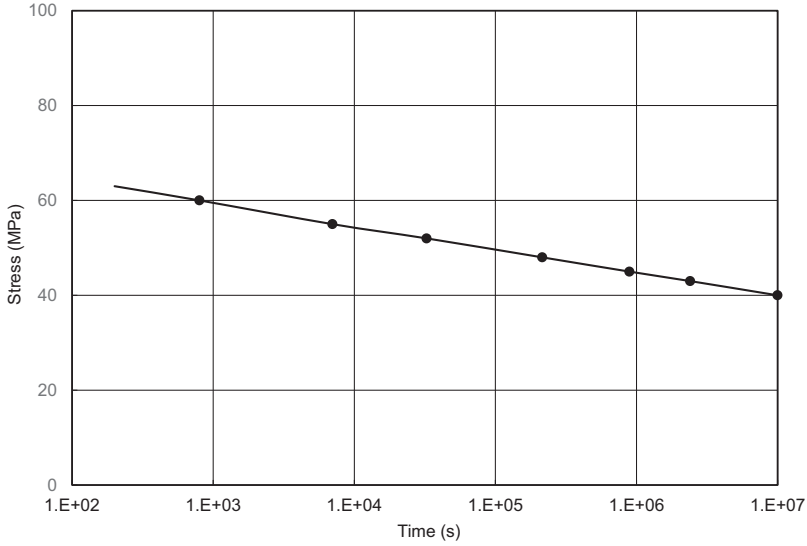
Hence

$$E_1 = \frac{\xi_1\xi_2(\xi_1 + \xi_2) + \eta^2\omega^2\xi_1}{(\xi_1 + \xi_2)^2 + \eta^2\omega^2}$$

$$E_2 = \frac{(\xi_1 + \xi_2)\omega\xi_1\eta - \xi_1\xi_2\eta\omega}{(\xi_1 + \xi_2)^2 + \eta^2\omega^2}$$

$$\tan\delta = \frac{E_2}{E_1} = \frac{(\xi_1 + \xi_2)\omega\xi_1\eta - \xi_1\xi_2\eta\omega}{\xi_1\xi_2(\xi_1 + \xi_2) + \eta^2\omega^2\xi_1}$$

(2.47) The straight line graph of stress against log (time) confirms the relationship



$$\left.\begin{array}{c}\text{At } t = 800, \sigma = 60 \\ \text{At } t = 8.9 \times 10^5, \sigma = 45\end{array}\right\} \quad \begin{array}{c}\text{So, } B = 0.467(\text{MPa})^{-1} \\ A = 1.225 \times 10^5 s\end{array}$$

(2.48) Zhurkov-Bueche equation gives

$$t = t_0 e^{(U_0 - \gamma\sigma)/RT}$$

comparing this with $t = A^{-B\sigma}$

$$t = t_0 e^{U_0/RT} \text{ and } B = \gamma/RT$$

$$\text{So} \quad t_0 = \frac{A}{exp\left(\frac{U_0}{RT}\right)} = \frac{1.225 \times 10^{15}}{exp\left(\frac{150 \times 10^3}{8.314 \times 293}\right)} = 2.22 \times 10^{-12}\text{m}^3\text{s}$$

Also $\gamma = BRT = 0.467 \times 8.314 \times 293 \times 10^{-6} = 1137.6 \times 10^{-6}$ m^3/mol

So at $\sigma = 44$ MPa, $T = 40°$C

$$t = 2.22 \times 10^{-12}\, exp\left(\frac{150 \times 10^3 - 1137.6 \times 10^{-6} \times 44 \times 10^6}{8.314 \times 313}\right) = 1.06 \times 10^5\text{s}$$

(2.49) 3 years $= 0.95 \times 10^8$ seconds

From Fig. 2.73 creep rupture strength = 8 MPa
Using a safety factor of 1.5 the design stress = 8/1.5 = 5.33 MPa for the pipe, hoop stress = *PR/h*

$$5.33 = \frac{0.5(100)}{h}$$

$$h = 9.4 \text{ mm}$$

(2.50) The critical defect size in the material may be calculated from

$$K_{Ic} = \sigma(\pi a_c)^{\frac{1}{2}}$$

$$a_c = \left(\frac{2}{20}\right)^2 \frac{1}{\pi} = 3.18 \text{ mm}$$

$$t_f = \frac{2}{C(\sigma)^m \pi^{(1/2)m}(m-2)} \left\{ a_i^{1-(1/2)m} - a_c^{1-(1/2)m} \right\}$$

$$3.15 \times 10^7 = \frac{2}{3 \times 10^{-11}(20)^{3.2}(1.2)\pi^{1.6}} \left\{ a_i^{-0.6} - \left(3.18 \times 10^{-3}\right)^{-0.6} \right\}$$

$$a_i = 0.631 \text{ mm}$$

(2.51) acrylic,

$$r_p = \frac{1}{2\pi}\left(\frac{K_{Ic}}{\sigma_y}\right)^2 = \frac{(0.023)^2}{2\pi} = 0.084 \text{ mm}$$

ABS,

$$r_p = \frac{(0.13)^2}{2\pi} = 2.69 \text{ mm}$$

polypropylene,

$$r_p = \frac{(0.2)^2}{2\pi} = 6.37 \text{ mm}$$

(2.52) Using fracture mechanics

$$K_{1c} = \sigma(\pi a_c)^{1/2}$$

$$a_c = \left(\frac{K_{1c}}{\sigma}\right)^2 \frac{1}{\pi}$$

Table 3.1 gives K_{1c} for acrylic as 0.9−1.6 $MN/m^{-(3/2)}$

$$a_c = \left(\frac{0.9}{57}\right)^2 \frac{1}{\pi} = 0.08 \text{ mm(up to 0.25 mm)}$$

So inherent flaw sizes are probably in the range 0.16−0.5 mm.

(2.53) Stress range $= \dfrac{FL}{60}$

$$\text{Stress amplitude} = \text{mean stress} = \frac{FL}{120}$$

To allow for mean stress use

$$\sigma_a = \sigma_f \left\{1 - \frac{\sigma_m}{\sigma_c}\right\} \tag{1}$$

Now at 1×10^7 cycles $\sigma_f = 16$ MPa

also 1×10^7 cycles at $5H_f$ represents 2×10^6 seconds

So

$$\sigma_c = 42 \text{ MPa}$$

In (1)

$$\frac{FL}{120} = \frac{16}{2}\left\{1 - \frac{FL}{120 \times 42}\right\}$$

So

$$F = 16.13 \text{ N}$$

(2.54) Bending stress $= \dfrac{My}{I}$

$$\text{So} \quad \sigma_m = \frac{1 \times d/2}{\pi d^4/64} = \frac{32}{\pi d^3} \text{ Pa}$$

$$\sigma_a = \frac{32 \times 0.75}{\pi d^3} \text{ Pa}$$

but

$$\sigma_a = \sigma_f \left(1 - \frac{\sigma_m}{\sigma_c}\right)$$

$$2.5\left(\frac{32 \times 0.75}{\pi d^3}\right) = 25 \times 10^6 \left(1 - \frac{32 \times 2.5}{\pi d^3 \times 35 \times 10^6}\right)$$

So

$$d = 11.43 \text{ mm}$$

if $K_f = 2$

$$2.5 \times \left(\frac{32. \times 0.75}{\pi d^3}\right) = \frac{25 \times 10^6}{2} \left(1 - \frac{32 \times 2.5}{\pi d^3 \times 35 \times 10^6}\right)$$

$$d = 13.1 \text{ mm}$$

(2.55) $\sigma_f = 43.4 - 3.8 \log 10^7 = 16.8$ MPa
At 5 Hz, 10^7 cycles would take 2×10^6 seconds
from (2.47) $t = 1.225 \times 10^{15} e^{-0.467\sigma} c$ So $\sigma_c = 43.3$ MPa

Now

$$\sigma_m = \frac{500 \times 4}{\pi (10)^2} = 6.37 \text{ MPa}$$

$$\sigma_a = \frac{M_y}{I} = \frac{64M(5 \times 10^{-3})}{\pi (10 \times 10^{-3})^4} = 10.2 \times 10^6 M(\text{Pa})$$

$$\text{So} \quad \sigma_a = \sigma_f \left(1 - \frac{\sigma_m}{\sigma_c}\right)$$

$$2 \times 10.2 \times 10^6 M = \frac{16.8 \times 10^6}{1.8}\left(1 - \frac{6.37. \times 2}{43.3}\right)$$

$$M = 0.32 \quad \text{Nm}$$

(2.56) Maximum stress $= \dfrac{P}{\pi r^2} + \dfrac{4(Pe)r}{\pi T^4}$

$$\text{Minimum stress} = -\frac{P}{2\pi r^2} - \frac{4(Pe)r}{\pi T^4}$$

$$\sigma_m = \frac{\sigma_{max+}\sigma_{min}}{2} = \frac{P}{2\pi r^2} - \frac{4(Pe)r}{\pi r^4}$$

$$\sigma_a = \frac{\sigma_{max-}\sigma_{min}}{2} = \frac{1}{2}\left(\frac{3P}{2\pi r^2} - \frac{12Per}{2\pi r^4}\right)$$

$$\sigma_a = \sigma_f\left(1 - \frac{\sigma_m}{\sigma_c}\right)$$

$$\sigma_f = 43.4 - 3.8\,log\left(1 \times 10^8\right) = 13 \quad \text{MPa}$$

At 10 Hz, 10^8 cycles would take 10^7 seconds so from $t = 1.225 \times 10^{15}$ exp $(-0.467\sigma_c)$, $\sigma_c = 39.9$ MPa

So $$2.5 \times \frac{1}{2}\left(\frac{3P}{2\pi r^2} + \frac{12Per}{2\pi r^4}\right) = 13 \times 10^6\left(1 - \frac{2.5 \times 10^6}{39.9}\left(\frac{P}{4\pi r^2} + \frac{Per}{4\pi r^2}\right)\right)$$

from which $P = 235.7$ N

(2.57) $$K_t = 1 + 2(c/r)^{1/2}$$

$$3.5 = 1 + 2(c/0.25)^{1/2} \rightarrow c = 0.39 \text{ mm}$$

(2.58) 4.5 kg = 44.145 N

(i) loss of energy due to friction, etc = (44.145) (0.3−0.29) = 0.44 J

(ii) energy absorbed due to specimen fracture = (44.145) (0.29−0.2) = 3.973 J

$$\text{impact strength} = \frac{3.973}{(12 \times 2)10^{-6}} = 165.5 \ \text{kJ/m}^2$$

(iii) Initial pendulum energy $= 0.25 \times 44.145 = 11.036$ J

Loss of energy due to friction + specimen fracture $= 0.44 + 3.947 = 4.414$ J

Remaining energy $= 11.036 - 4.414 = 6.6218$

$$\text{So height of swing} = \frac{6.6218}{44.145} = 0.15 \ \text{m}$$

(2.59) $$K = \frac{P}{Wh}(\pi a)^{1/2}\left[1.12 - 0.23\left(\frac{a}{w}\right) + 10.6\left(\frac{a}{w}\right)^2 - 21.7\left(\frac{a}{w}\right)^3 + 30.4\left(\frac{a}{w}\right)^4\right]$$

So

$$1.75 \times 10^6 = \frac{P}{100 \times 5 \times 10^{-6}}\left(\pi \times 10 \times 10^{-3}\right)^{1/2}\left[f\left(\frac{a}{w}\right)\right]$$

where

$$\left[f\left(\frac{a}{w}\right)\right] \simeq 1$$

$$\text{So} \quad P = 4.89 \ \text{kN}$$

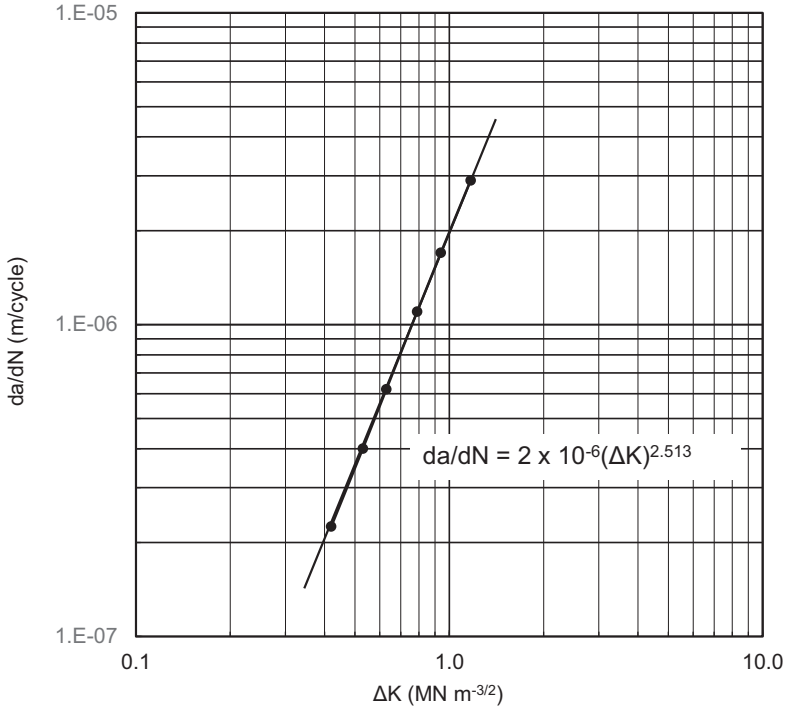
(2.60) $K_c = \sigma\sqrt{\pi a_c} \rightarrow a_c = \left(\frac{1.6}{10}\right)^2 \frac{1}{\pi} = 8.15\text{mm}$

from Eq. (2.119)

$$N = \frac{2\left(\left(8.15 \times 10^{-3}\right)^{-0.66} - \left(25 \times 10^{-6}\right)^{-0.66}\right)}{2 \times 10^{-6}(10)^{3.22}\pi^{1.66}(-1.32)}$$

$$= 57,794 \ \text{cycles} = 16.05 \ \text{hours}$$

(2.61) $$N = \frac{2\left[\left(\left(\frac{K_c}{\sigma}\right)^2 \frac{1}{\pi}\right)^{1-(1/2)n} - a_i^{1-(1/2)n}\right]}{c\sigma^n \pi^{n/2}(2-n)}$$



from the graph $\frac{da}{dN} = 2 \times 10^{-6}(\Delta K)^{2.513}$

$$\sigma^{2.513} = \frac{\left(\left(\frac{1.8^2}{\pi\sigma^2}\right)^{-0.256} - \left(20 \times 10^{-6}\right)^{-0.256}\right)}{2 \times 10^{-6} \times 10^{6} \times \pi^{1.256}(-0.513)}$$

$$\sigma = 2.13 \quad \text{MPa}$$

(2.62) For a sheet, $K = \sigma_f (\pi a)^{1/2}$
where $\sigma_f =$ fatigue limit. Knowing K this would give the critical defect size, $a_{c,}$ in the material. Equating this to the critical version of the expression for the pressure vessel

$$\sigma_f(\pi a_c)^{\frac{1}{2}} = 2\sigma_\theta(2a_c)^{\frac{1}{2}}$$

$$\sigma_\theta = \sigma_f\left(\frac{\pi^{\frac{1}{2}}}{2\sqrt{2}}\right) = 10\left(\frac{\pi^{\frac{1}{2}}}{2\sqrt{2}}\right) = 0.627 \quad \text{MPa}$$

Now,

$$\sigma_\theta = \frac{PD}{2h} \rightarrow P = \frac{2h\sigma_\theta}{D}$$

$$P = \frac{2 \times 4 \times 0.627}{120} = 41.8 \text{ kPa}$$

(3.1) The energy absorbing ability of a material is given by

$$U = \frac{1}{2}\sigma\varepsilon = \frac{1}{2}\frac{\sigma^2}{E}$$

Hence the following table may be drawn up

	σ	*E*	$\sigma^2/2E$
Carbon (HS)	2.89	229	1.82×10^{-2}
Carbon (HM)	2.16	392	0.595×10^{-2}
Kevlar	3.0	129	3.49×10^{-2}
E-Glass	2.03	80	2.58×10^{-2}
S-Glass	3.32	93	5.9×10^{-2}
UHMWPE	4.2	120	7.4×10^{-2}

From this table it may be seen that carbon fibre has low energy absorbing capability compared with the other fibres. However, the other fibres including the thermoplastic (UHMWPE) are not as stiff. Hence it is quite common to use hybrid fibre composites, e.g. glass and carbon fibres together or thermoplastics with glass or carbon in order to get a better combination of properties.

(3.2) It is necessary to calculate the volume fraction for each of the fibres. Firstly for the carbon

$$V_{fc} = \frac{\dfrac{20}{1800}}{\dfrac{20}{1800} + \dfrac{30}{2540} + \dfrac{50}{1300}} = 0.181$$

Similarly for the glass fibres

$$V_{fg} = \frac{\dfrac{30}{2540}}{\dfrac{20}{1800} + \dfrac{30}{2540} + \dfrac{50}{1300}} = 0.192$$

Hence, using the rule of mixtures

$$\begin{aligned}\rho_c &= 0.181(1800) + 0.192(2540) + 0.627(1300)\\ &= 1629 kg/m^3\end{aligned}$$

(3.3) $\rho_f = 1800$ kg/m^3, $\rho_m = 1250$ kg/m^3, $\rho_c = 1600$ kg/m^3
Using rule of mixtures

$$\rho_c = \rho_f V_f + \rho_m(1 - V_f)$$

$$1600 = 1800V_f + 1250(1 - V_f)$$

$$V_f = 0.636$$

to get weight fraction

$$W_f = \frac{\rho_f}{\rho_c} V_f = \frac{1800}{1600}(0.636) = 0.716$$

hence

$$W_m = 0.284$$

Weight ratio W_m: $W_f = 0.284$: 0.716
Hence for 1 kg epoxy, the weight of carbon = 2.52 kg

(3.4) Using rule of mixtures

$$\rho_c = \rho_f V_f + \rho_m V_m = 2540(0.5) + 1250(0.4) = 2024 \text{ kg/m}^3$$

$$E_c = E_f V_f + E_m V_m = 80(0.6) + 6.1(0.4) = 50.44 \text{ GPa}$$

$$K_c = K_f V_f = 1.05(0.6) + 0.25(0.4) = 0.73 \text{W/m}^\circ K$$

(3.5) Using the rule of mixtures

$$E_c = E_f V_f + E_m(1 - V_f) = 120(0.4) + 6(0.6) = 51.6 \text{GPa}$$

Also,

$$\sigma_c = \sigma_f V_f + \sigma_m(1 - V_f)$$

but

$$\varepsilon_c = \varepsilon_m = \varepsilon_f$$

$$\frac{\sigma_c}{E_c} = \frac{\sigma_m}{E_m} = \frac{\sigma_f}{E_f} \rightarrow \left(\frac{E_f}{E_m}\right)\sigma_m = \sigma_f$$

So

$$\sigma_c = \frac{E_f}{E_m}(\sigma_m)V_f + \sigma_m(1 - V_f)$$

$$50 = 20(\sigma_m)0.4 + \sigma_m(0.6)$$

$$\sigma_m = 5.8 \text{ MPa}, \ \sigma_f = 20(5.8) = 116.3 \text{ MPa}$$

(3.6) In the composite

$$\varepsilon_f = \varepsilon_c$$

$$\frac{\sigma_f}{E_f} = \frac{\sigma_c}{E_c}$$

$$\frac{\sigma_f}{\sigma_c} = \frac{E_f}{E_c}$$

$$\frac{F_f A_c}{F_c A_f} = \frac{E_f}{E_f V_f + E_m V_m}$$

$$\frac{F_f}{F_c} = \frac{E_f/E_m}{E_f/E_m + V_m/V_f} = \frac{40}{40 + 1}$$

$$F_f = 97.6\% F_c$$

(3.7) $\sigma_c = \sigma_f V_f + \sigma_m(1 - V_f)$

Since $$\varepsilon_c = \varepsilon_m = \varepsilon_f \quad \text{then} \quad \frac{\sigma_c}{E_c} = \frac{\sigma_m}{E_m} = \frac{\sigma_f}{E_f}$$

i.e. $$\sigma_f = \sigma_m\left(\frac{E_f}{E_m}\right)$$

So $$\sigma_c = \sigma_m\left(\frac{E_f}{E_m}\right)V_f + \sigma_m(1 - V_f)$$

$$= 60(25)0.3 + 60(0.7) = 492 \quad \text{MPa}$$

Also $$E_c = E_f V_f + E_m(1 - V_f)$$

$$= (76 \times 0.3) + \frac{76}{25}(0.7) = 24.93 \quad \text{GPa}$$

(3.8)

(i) $v_{12} = v_f V_f + v_m(1 - V_f)$

$$= (0.23)(0.58) + 0.35(0.42)$$
$$= 0.28$$

(ii) $E_1 = E_f V_f + E_m V_m = 230(0.58) + 3.8(0.42) = 135 \quad \text{GPa}$

$$E_2 = \frac{E_f E_m}{V_f E_m + V_m E_f} = \frac{(230)(3.8)}{(0.58)(3.8) + (0.42)(230)} = 8.8 \quad \text{GPa}$$

$$v_{21} = v_{12} = 0.28\left(\frac{8.8}{135}\right) = 0.02$$

(3.9) The local compliance matrix is

$$S = \begin{bmatrix} \frac{1}{E_1} & \frac{v_{12}}{E_1} & 0 \\ \frac{v_{12}}{E_1} & \frac{1}{E_2} & 0 \\ 0 & 0 & \frac{1}{G_{12}} \end{bmatrix} \quad \text{and} \quad Q = S^{-1}$$

$$\overline{Q} = T_\sigma^{-1} \cdot Q \cdot T_\varepsilon \quad \text{and} \quad \overline{S} = \overline{Q}^{-1}$$

Then

$$\begin{bmatrix} \varepsilon_x \\ \varepsilon_y \\ \gamma_{xy} \end{bmatrix} = \overline{S} \begin{bmatrix} \sigma_x \\ \sigma_y \\ \tau_{xy} \end{bmatrix}$$

$$\overline{S} = \begin{bmatrix} 8.81 \times 10^{-5} & -2.72 \times 10^{-5} & -5.44 \times 10^{-5} \\ -2.72 \times 10^{-5} & 1.04 \times 10^{-4} & -4.05 \times 10^{-5} \\ -5.44 \times 10^{-5} & -4.05 \times 10^{-5} & 1.70 \times 10^{-4} \end{bmatrix} m^2/\text{MN}$$

Directly by matrix manipulation

$$\varepsilon_x = 2.238 \times 10^{-3} \quad \varepsilon_y = 7.578 \times 10^{-4} \quad \gamma_{xy} = -2.241 \times 10^{-3}$$

and

$$E_x = \frac{1}{\overline{S}_{11}}, \quad E_y = \frac{1}{\overline{S}_{22}}, \quad G_{xy} = \frac{1}{\overline{S}_{66}}, \quad v_{xy} = -E_x \cdot \overline{S}_{21}, \quad v_{yx} = -E_y \cdot \overline{S}_{12}$$

Alternatively using the Constitutive Equation Approach

$$A = \overline{Q} \cdot h$$

$$A = \begin{bmatrix} 2.78 \times 10^4 & 1.17 \times 10^4 & 1.16 \times 10^4 \\ 1.17 \times 10^4 & 2.06 \times 10^4 & 8.624 \times 10^3 \\ 1.16 \times 10^4 & 8.62 \times 10^3 & 1.45 \times 10^4 \end{bmatrix}$$

Also,

$$a = A^{-1} \text{ (since } [B] = 0)$$

$$a = \begin{bmatrix} 5.87 \times 10^{-5} & -1.81 \times 10^{-5} & -3.63 \times 10^{-5} \\ -1.81 \times 10^{-5} & 6.99 \times 10^{-5} & -2.7 \times 10^{-5} \\ -3.63 \times 10^{-5} & -2.7 \times 10^{-5} & 1.13 \times 10^{-4} \end{bmatrix} \text{ mm/N}$$

$$E_x = \frac{1}{a_{11} \cdot h}, \quad E_y = \frac{1}{a_{22} \cdot h}, \quad G_{xy} = \frac{1}{a_{66} \cdot h}, \quad v_{xy} = \frac{-a_{12}}{a_{11}}, \quad v_{yx} = \frac{-a_{12}}{a_{22}}$$

$$E_x = 11.3 \text{ GPa}, \quad E_y = 9.53 \text{ GPa}, \quad G_{xy} = 5.8 \text{ GPa}$$

$$v_{xy} = 0.308 \quad v_{yx} = 0.259$$

For the applied Forces N_x and N_y

$$\begin{bmatrix} \varepsilon_x \\ \varepsilon_y \\ \gamma_{xy} \end{bmatrix} = a \cdot \begin{bmatrix} N_x \\ N_y \\ N_{xy} \end{bmatrix} \left(= a \cdot \begin{bmatrix} \sigma_x \\ \sigma_y \\ \tau_{xy} \end{bmatrix} \cdot h \right)$$

$$\varepsilon_x = 2.238 \times 10^{-3} \quad \varepsilon_y = 7.578 \times 10^{-4} \quad \gamma_{xy} = -2.241 \times 10^{-3}$$

(3.10) (i) The properties of the ply in the fibre and transverse directions are

$$E_1 = 200 \text{ GPa}$$
$$E_2 = 11 \text{ GPa}$$
$$G_{12} = 8 \text{ GPa}$$
$$v_{12} = 0.32$$

The local compliance matrix is

$$S = \begin{bmatrix} \frac{1}{E_1} & -\frac{v_{12}}{E_1} & 0 \\ -\frac{v_{12}}{E_1} & \frac{1}{E_2} & 0 \\ 0 & 0 & \frac{1}{G_{12}} \end{bmatrix} \text{ and } Q = S^{-1}$$

So, $$\overline{Q} = T_\sigma^{-1} \cdot Q \cdot T_\varepsilon \text{ and } \overline{S} = Q^{-1}$$

Then

$$\begin{bmatrix} \varepsilon_x \\ \varepsilon_y \\ \gamma_{xy} \end{bmatrix} = \overline{S} \cdot \begin{bmatrix} \sigma_x \\ \sigma_y \\ \tau_{xy} \end{bmatrix}$$

$$\overline{S} = \begin{bmatrix} 3.13 \times 10^{-5} & -6.45 \times 10^{-6} & -4.28 \times 10^{-5} \\ -6.45 \times 10^{-6} & 7.42 \times 10^{-5} & -3.15 \times 10^{-5} \\ -4.28 \times 10^{-5} & -3.15 \times 10^{-5} & 1.05 \times 10^{-4} \end{bmatrix} m^2/\text{MN}$$

Directly by matrix manipulation

$$\varepsilon_x = 2.507 \times 10^{-3}, \quad \varepsilon_y = 5.164 \times 10^{-4}, \quad \gamma_{xy} = -3.424 \times 10^{-3}$$

and

$$E_x = \frac{1}{\overline{S}_{11}}, \quad E_y = \frac{1}{\overline{S}_{22}}, \quad G_{xy} = \frac{1}{\overline{S}_{66}}, \quad v_{xy} = -E_x \cdot \overline{S}_{21}, \quad v_{yx} = -E_y \cdot \overline{S}_{12}$$

$$E_x = 3.19 \text{ GPa}, \quad E_y = 13.5 \text{ GPa}, \quad G_{xy} = 9.5 \text{ GPa},$$

$$v_{xy} = 0.206, \quad v_{yx} = 0.087$$

Alternatively using the Constitutive Equation Approach

$$A = \overline{Q} \cdot h$$

$$A = \begin{bmatrix} 2.42 \times 10^5 & 7.2 \times 10^4 & 1.19 \times 10^5 \\ 7.2 \times 10^4 & 5.22 \times 10^4 & 4.48 \times 10^4 \\ 1.19 \times 10^5 & 4.48 \times 10^4 & 8.09 \times 10^4 \end{bmatrix} \text{N/mm}$$

$$D = \overline{Q} \cdot \frac{h^3}{12}$$

$$D = \begin{bmatrix} 8.07 \times 10^4 & 2.4 \times 10^4 & 3.99 \times 10^4 \\ 2.4 \times 10^4 & 1.74 \times 10^4 & 1.49 \times 10^4 \\ 3.99 \times 10^4 & 1.49 \times 10^4 & 2.69 \times 10^4 \end{bmatrix} \text{ Nmm}$$

$$a = A^{-1}$$

$$a = \begin{bmatrix} 1.56 \times 10^{-5} & -3.22 \times 10^{-6} & -2.14 \times 10^{-5} \\ -3.22 \times 10^{-6} & 3.71 \times 10^{-5} & -1.58 \times 10^{-5} \\ -2.14 \times 10^{-5} & 1.58 \times 10^{-5} & 5.27 \times 10^{-5} \end{bmatrix} \text{ mm/N}$$

$$d := D^{-1}$$

$$d = \begin{bmatrix} 4.7 \times 10^{-5} & -9.68 \times 10^{-6} & -6.42 \times 10^{-5} \\ -9.68 \times 10^{-6} & 1.11 \times 10^{-4} & -4.73 \times 10^{-5} \\ -6.42 \times 10^{-5} & -4.73 \times 10^{-5} & 1.58 \times 10^{-4} \end{bmatrix} (\text{Nmm})^{-1}$$

$$E_x = \frac{1}{a_{11} \cdot h}, \quad E_y = \frac{1}{a_{22} \cdot h}, \quad G_{xy} = \frac{1}{a_{66} \cdot h} \nu_{xy} = \frac{-a_{12}}{a_{11}} \nu_{yx} = \frac{-a_{12}}{a_{22}}$$

$$E_x = 31.9 \text{ GPa}, \quad E_y = 13.5 \text{ GPa}, \quad G_{xy} = 9.5 \text{ GPa}$$

$$\nu_{xy} = 0.206, \quad \nu_{yx} = 0.087$$

It may be seen that these agree with the previous values.
For the applied Force N_x

$$\begin{bmatrix} \varepsilon_x \\ \varepsilon_y \\ \gamma_{xy} \end{bmatrix} = a \cdot \begin{bmatrix} N_x \\ N_y \\ N_{xy} \end{bmatrix} \left(= a \cdot \begin{bmatrix} \sigma_x \\ \sigma_y \\ \tau_{xy} \end{bmatrix} \cdot h \right)$$

$$\varepsilon_x = 2.507 \times 10^{-3} \quad \varepsilon_y = -5.164 \times 10^{-4} \quad \gamma_{xy} = -3.424 \times 10^{-3}$$

For the applied Moment $M_x = 180$ Nm/m

$$\begin{bmatrix} \kappa_x \\ \kappa_y \\ \kappa_{xy} \end{bmatrix} = d \cdot \begin{bmatrix} M_x \\ M_y \\ M_{xy} \end{bmatrix} \quad \text{and} \quad \nu_{yx} = \frac{-\kappa_x}{\kappa_y}, \quad \nu_{xy} = \frac{-\kappa_y}{\kappa_x}$$

$$\kappa_x = 8.46m^{-1}, \quad \kappa_y = -1.743m^{-1}, \quad \kappa_{xy} = -12m^{-1},$$

$$v_{yx} = 4.854, \quad v_{xy} = 0.206$$

It may be seen that when the moment is applied, the major Poisson's ratio v_{xy} corresponds as it should to the value when the in-plane stress, σ_x, is applied.

(ii) If an additional moment M_y is applied, then the D and d matrices do not change and so once again

$$\begin{bmatrix} \kappa_x \\ \kappa_y \\ \kappa_{xy} \end{bmatrix} = d \bullet \begin{bmatrix} M_x \\ M_y \\ M_{xy} \end{bmatrix} \quad \text{and} \quad v_{xy} = \frac{-\kappa_y}{\kappa_x}, \quad v_{yx} = \frac{-\kappa_x}{\kappa_y}$$

$$\kappa_x = 6.04 \text{ m}^{-1}, \quad \kappa_y = -26 \text{ m}^{-1}, \quad \kappa_{xy} = -23 \text{ m}^{-1}$$

$$v_{yx} = 0.23, \quad v_{xy} = 4.32$$

(3.11)

(i) Symmetric
(ii) Non-symmetric (there is an uneven number of plies)
(iii) Symmetric (could also be written as $[0/90/45/-45_3/-45_3/45/90/0]_T$

(3.12) This is treated as a 4 layer situation with

$$h_0 = -0.7, \quad h_1 = -0.2, \quad h_2 = 0, \quad h_3 = 0.2, \quad h_4 = 0.7 \text{ mm}$$

For

$$\overline{Q}_1 = \begin{bmatrix} 4.16 \times 10^3 & 1.66 \times 10^3 & 0 \\ 1.66 \times 10^3 & 4.16 \times 10^3 & 0 \\ 0 & 0 & 1.25 \times 10^3 \end{bmatrix}, \quad \overline{Q}_2 = \begin{bmatrix} 683.5 & 239.5 & 0 \\ 239.5 & 683.5 & 0 \\ 0 & 0 & 222.2 \end{bmatrix}$$

Material A *Material B*

$$\overline{Q}_4 = \overline{Q}_1 \quad \text{and} \quad \overline{Q}_3 = \overline{Q}_2$$

As the laminate is symmetrical, $B = 0$ and

$$A = \sum_{f=1}^{4} \overline{Q_f} \cdot (h_f - h_{f-1}) \quad \text{and} \quad a = A^{-1}$$

$$A = \begin{bmatrix} 4.44 \times 10^3 & 1.76 \times 10^3 & 0 \\ 1.76 \times 10^3 & 4.44 \times 10^3 & 0 \\ 0 & 0 & 1.33 \times 10^3 \end{bmatrix} \text{N/mm}$$

$$a = \begin{bmatrix} 2.67 \times 10^{-4} & -1.06 \times 10^{-4} & 0 \\ -1.06 \times 10^{-4} & 2.67 \times 10^{-4} & 0 \\ 0 & 0 & 7.46 \times 10^{-4} \end{bmatrix} \text{mm/N}$$

The strains are then obtained from

$$\begin{bmatrix} \varepsilon_x \\ \varepsilon_y \\ \gamma_{xy} \end{bmatrix} = a \bullet \begin{bmatrix} N_x \\ N_y \\ N_{xy} \end{bmatrix}$$

$$\varepsilon_x = 3.028 \times 10^{-3}, \varepsilon_y = 8.257 \times 10^{-3}, \gamma_{xy} = 0.016$$

and the stresses are given by

Stresses in Material A

$$\begin{bmatrix} \sigma_{ax} \\ \sigma_{ay} \\ \tau_{axy} \end{bmatrix} = \overline{Q}_1 \cdot \begin{bmatrix} \varepsilon_x \\ \varepsilon_y \\ \gamma_{xy} \end{bmatrix} \quad \sigma_{ax} = 26.38 \text{ MPa} \quad \sigma_{ay} = 39.45 \text{ MPa}$$

$$\tau_{axy} = 19.6 \text{ MPa}$$

Stresses in Material B

$$\begin{bmatrix} \sigma_{bx} \\ \sigma_{by} \\ \tau_{bxy} \end{bmatrix} = \overline{Q}_2 \bullet \begin{bmatrix} \varepsilon_x \\ \varepsilon_y \\ \gamma_{xy} \end{bmatrix} \quad \sigma_{bx} = 4.04 \text{ MPa} \quad \sigma_{by} = 6.36 \text{ MPa}$$

$$\tau_{bxy} = 3.48 \text{ MPa}$$

(3.13) *Compliance Matrix* *Stiffness Matrix*

$$S = \begin{bmatrix} \frac{1}{E_1} & -\frac{\nu_{12}}{E_1} & 0 \\ -\frac{\nu_{12}}{E_1} & \frac{1}{E_2} & 0 \\ 0 & 0 & \frac{1}{G_{12}} \end{bmatrix} \qquad Q = S^{-1}$$

Overall Stiffness Matrix *Overall Compliance Matrix*

$$Q = T_\sigma^{-1} \cdot Q \cdot T_\varepsilon \qquad \overline{S} = \overline{Q}^{-1}$$

The Extension Stiffness Matrix is then obtained from

$$[A] = 0.4\overline{Q}(-60) + 0.4\overline{Q}(-30) + 0.4\overline{Q}(0) + 0.4\overline{Q}(30) + 0.4\overline{Q}(60) + 0.4\overline{Q}(90)$$

which gives

$$A = \begin{bmatrix} 1.36 \times 10^5 & 4.19 \times 10^4 & 0 \\ 4.19 \times 10^4 & 1.36 \times 10^5 & 0 \\ 0 & 0 & 4.71 \times 10^4 \end{bmatrix} \text{N/mm}$$

As $[B] = 0$ in this symmetric laminate, the compliance matrix is obtained by inverting $[A]$

$$a = \begin{bmatrix} 8.10 \times 10^{-6} & -2.49 \times 10^{-6} & 0 \\ -2.49 \times 10^{-6} & 8.10 \times 10^{-6} & 0 \\ 0 & 0 & 2.11 \times 10^{-5} \end{bmatrix} \text{N/mm}$$

The stiffness terms in the global directions are (for $h = 2.4$ mm)

$$E_x = \frac{1}{a_{11} \cdot h}, \quad E_x = 5.14 \times 10^4 \text{ MPa}$$

$$E_y = \frac{1}{a_{22} \cdot h}, \quad E_y = 5.14.10^4 \text{ MPa}$$

$$G_{xy} = \frac{1}{a_{66} \cdot h}, \quad G_{xy} = 1.96.10^4 \text{ MPa}$$

$$\nu_x = \frac{a_{12}}{a_{22}}, \qquad \nu_x = 0.308$$

$$\nu_y = \frac{a_{12}}{a_{22}}, \qquad \nu_y = 0.308$$

and the strains may be obtained as

$$\begin{bmatrix} \varepsilon_x \\ \varepsilon_y \\ \gamma_{xy} \end{bmatrix} = a \bullet \begin{bmatrix} \sigma_x \\ \sigma_y \\ \tau_{xy} \end{bmatrix} \bullet h$$

$$\varepsilon_x = 1.94 \times 10^{-3}, \varepsilon_y = -5.98 \times 10^{-4}, \gamma_{xy} = -1.12 \times 10^{-7}$$

(3.14) Using the *S* and *Q matrices* to calculate $\overline{S}$ and $\overline{Q}$ for each layer, then

$$A = \sum_{f=1}^{8} \overline{Q}_f \bullet (h_f - h_{f-1}), a = A^{-1}$$

$$B = \frac{1}{2} \bullet \sum_{f=1}^{8} \overline{Q}_f \bullet \left[(h_f)^2 - (h_{f-1})^2 \right], \; D = \frac{1}{3} \bullet \sum_{f=1}^{8} \overline{Q}_f \bullet \left[(h_f)^3 - (h_{f-1})^3 \right], d = D^{-1}$$

$$\begin{bmatrix} \varepsilon_x \\ \varepsilon_y \\ \varepsilon_{xy} \end{bmatrix} = a \bullet \begin{bmatrix} N_x \\ N_y \\ N_{xy} \end{bmatrix} = a \bullet \begin{bmatrix} \sigma_x \\ \sigma_y \\ N_{xy} \end{bmatrix} \bullet H \; \textit{where } H \; = \textit{full thickness of laminate}$$

$$\varepsilon_x = 8.989 \times 10^{-4}, \varepsilon_y = -1.286 \times 10^{-3}, \gamma_{xy} = 1.774 \times 10^{-4}$$

Note, to assist the reader, the values of the terms in the matrices are

$$A = \begin{bmatrix} 4.65 \times 10^5 & 2.47 \times 10^5 & 0 \\ 2.47 \times 10^5 & 2.82 \times 10^5 & 0 \\ 0 & 0 & 2.81 \times 10^5 \end{bmatrix} \text{N/mm} \qquad \text{B} = \begin{bmatrix} 0 & 0 & 0 \\ 0 & 0 & 0 \\ 0 & 0 & 0 \end{bmatrix}$$

$$a = \begin{bmatrix} 4.03 \times 10^{-6} & -3.54 \times 10^{-6} & 0 \\ -3.54 \times 10^{-6} & 6.65 \times 10^{-6} & 0 \\ 0 & 0 & 3.54 \times 10^{-6} \end{bmatrix} \text{mm/N}$$

(3.15) Taking the x-direction as the hoop direction

$$\sigma_x = \frac{Pr}{t} = \frac{3 \times 600}{3} = 600 \quad \text{MPa}$$

$$\sigma_y = \frac{Pr}{2t} = \frac{3 \times 600}{6} = 300 \quad \text{MPa}$$

From the data given

Compliance Matrix *Stiffness Matrix*

$$S = \begin{bmatrix} \frac{1}{E_1} & -\frac{v_{12}}{E_1} & 0 \\ -\frac{v_{12}}{E_1} & \frac{1}{E_2} & 0 \\ 0 & 0 & \frac{1}{G_{12}} \end{bmatrix} \qquad Q = S^{-1}$$

Overall Stiffness Matrix *Overall Compliance Matrix*

$$\overline{Q}(\theta) = T_\sigma^{-1} \cdot Q \cdot T_\varepsilon \qquad \overline{S}(\theta) = \overline{Q}(\theta)^{-1}$$

$$\overline{Q}(60) = \begin{bmatrix} 9.82 \times 10^3 & 6.95 \times 10^3 & 2.71 \times 10^3 \\ 6.95 \times 10^3 & 2.21 \times 10^4 & 7.91 \times 10^3 \\ 2.71 \times 10^3 & 7.91 \times 10^3 & 7.50 \times 10^3 \end{bmatrix}$$

The Extension Stiffness matrix is then given by

$$A = 2 \cdot \overline{Q}(60) + 2 \cdot \overline{Q}(-60) + 6 \cdot \overline{Q}(0)$$

$$A = \begin{bmatrix} 2.35 \times 10^5 & 4.25 \times 10^4 & 0 \\ 4.25 \times 10^4 & 1.37 \times 10^5 & 0 \\ 0 & 0 & 4.80 \times 10^4 \end{bmatrix}$$

The compliance matrix is obtained by inverting [A]

$$a = A^{-1}$$

$$a = \begin{bmatrix} 4.49 \times 10^{-6} & -1.39 \times 10^{-6} & 0 \\ -1.39 \times 10^{-6} & 7.70 \times 10^{-6} & 0 \\ 0 & 0 & 2.08 \times 10^{5} \end{bmatrix}$$

and the strains may be obtained as

$$\begin{bmatrix} \varepsilon_x \\ \varepsilon_y \\ \gamma_{xy} \end{bmatrix} = a \bullet \begin{bmatrix} \sigma_x \\ \sigma_y \\ \tau_{xy} \end{bmatrix} \bullet 10$$

$$\varepsilon_x = 0.023 \quad \text{or} \quad 2.3\%$$

$$\varepsilon_y = 0.015 \ \text{ or } \ 1.5\%$$

$$\gamma_{xy} = 0$$

(3.16) (a) This is a symmetric laminate and the $\overline{Q}$ terms are as follows:

$$\overline{Q}_1 = \begin{bmatrix} 8.77 \times 10^4 & 2.98 \times 10^4 & 4.31 \times 10^4 \\ 2.98 \times 10^4 & 2.22 \times 10^4 & 1.35 \times 10^4 \\ 4.31 \times 10^4 & 1.35 \times 10^4 & 2.96 \times 10^4 \end{bmatrix}$$

$$\overline{Q}_2 = \begin{bmatrix} 8.77 \times 10^4 & 2.98 \times 10^4 & -4.31 \times 10^4 \\ 2.98 \times 10^4 & 2.22 \times 10^4 & -1.35 \times 10^4 \\ -4.31 \times 10^4 & -1.35 \times 10^4 & 2.96 \times 10^4 \end{bmatrix}$$

$$\overline{Q}_3 = \begin{bmatrix} 8.77 \times 10^4 & 2.98 \times 10^4 & -4.31 \times 10^4 \\ 2.98 \times 10^4 & 2.22 \times 10^4 & -1.35 \times 10^4 \\ -4.31 \times 10^4 & -1.35 \times 10^4 & 2.96 \times 10^4 \end{bmatrix}$$

$$\overline{Q}_4 = \begin{bmatrix} 8.77 \times 10^4 & 2.98 \times 10^4 & 4.31 \times 10^4 \\ 2.98 \times 10^4 & 2.22 \times 10^4 & 1.35 \times 10^4 \\ 4.31 \times 10^4 & 1.35 \times 10^4 & 2.96 \times 10^4 \end{bmatrix}$$

The *A, B, D* matrices are

$$A = \sum_{f=1}^{4} \overline{Q}_f \bullet (h_f - h_{f-1})$$

$$B = \frac{1}{2} \cdot \sum_{f=1}^{4} \overline{Q}_f \cdot \left[(h_f)^2 - (h_{f-1})^2 \right] \quad D = \frac{1}{3} \cdot \sum_{f=1}^{4} \overline{Q}_f \left[(h_f)^3 - (h_{f-1})^3 \right]$$

So that with

$$h_0 = -0.2, \quad h_1 = -0.1, \quad h_2 = 0, \quad h_3 = 0.1, \quad h_4 = 0.2$$

The *A, B, D* matrices and hence the a^{-1}, d^{-1}, matrices may be determined as:

$$A = \begin{bmatrix} 3.51 \times 10^4 & 1.19 \times 10^4 & 0 \\ 1.19 \times 10^4 & 8.88 \times 10^3 & 0 \\ 0 & 0 & 1.18 \times 10^4 \end{bmatrix}$$

$$a = \begin{bmatrix} 5.25 \times 10^{-5} & -7.06 \times 10^{-5} & 0 \\ -7.06 \times 10^{-5} & 2.07 \times 10^{-4} & \ddot{u} \\ 0 & 0 & 8.42 \times 10^{-5} \end{bmatrix}$$

$$B = \begin{bmatrix} 0 & 0 & 0 \\ 0 & 0 & 0 \\ 0 & 0 & 0 \end{bmatrix} \quad b = \begin{pmatrix} 0 & 0 & 0 \\ 0 & 0 & 0 \\ 0 & 0 & 0 \end{pmatrix} \quad \beta = \begin{pmatrix} 0 & 0 & 0 \\ 0 & 0 & 0 \\ 0 & 0 & 0 \end{pmatrix}$$

$$D = \begin{pmatrix} 467.9 & 159.3 & 172.7 \\ 159.3 & 118.5 & 54.2 \\ 172.7 & 54.2 & 158.2 \end{pmatrix}$$

$$d = \begin{bmatrix} 5.58 \times 10^{-3} & -5.59 \times 10^{-3} & -4.18 \times 10^{-3} \\ -5.59 \times 10^{-3} & 0.016 & 7.62 \times 10^{-4} \\ -4.18 \times 10^{-3} & 7.62 \times 10^{-4} & 0.011 \end{bmatrix}$$

Then using

$$\begin{bmatrix} \varepsilon_x \\ \varepsilon_y \\ \gamma_{xy} \\ \kappa_x \\ \kappa_y \\ \kappa_{xy} \end{bmatrix} = \begin{bmatrix} a_{11} & a_{12} & a_{16} & b_{11} & b_{12} & b_{16} \\ a_{21} & a_{22} & a_{26} & b_{21} & b_{22} & b_{26} \\ a_{61} & a_{62} & a_{66} & b_{61} & b_{62} & b_{66} \\ \beta_{11} & \beta_{12} & \beta_{16} & d_{11} & d_{12} & d_{16} \\ \beta_{21} & \beta_{22} & \beta_{26} & d_{21} & d_{22} & d_{26} \\ \beta_{61} & \beta_{62} & \beta_{66} & d_{61} & d_{62} & d_{66} \end{bmatrix} \begin{bmatrix} N_x \\ N_y \\ N_{xy} \\ M_x \\ M_y \\ M_{xy} \end{bmatrix}$$

The strains and curvatures are thus

$$\varepsilon_x = 2.101 \times 10^{-3}, \quad \varepsilon_y = -2.825 \times 10^{-3}, \quad \gamma_{xy} = 0,$$

$$\kappa_x = 0, \quad \kappa_y = 0, \quad \kappa_{xy} = 0$$

(b) This laminate is unsymmetrical. In the above analysis, $\overline{Q}_2$ and $\overline{Q}_3$ are reversed and this has the effect of making $[B] \neq 0$. The matrix values are.

$$A = \begin{bmatrix} 3.51 \times 10^4 & 1.19 \times 10^4 & 0 \\ 1.19 \times 10^4 & 8.88 \times 10^3 & 0 \\ 0 & 0 & 1.18 \times 10^4 \end{bmatrix}$$

$$a = \begin{bmatrix} 5.75 \times 10^{-5} & -7.15 \times 10^{-5} & 0 \\ -7.15 \times 10^{-5} & 2.07 \times 10^{-4} & 0 \\ 0 & 0 & 9.74 \times 10^{-5} \end{bmatrix}$$

$$B = \begin{pmatrix} 0 & 0 & -863.8 \\ 0 & 0 & -271 \\ -863.8 & -271 & 0 \end{pmatrix}$$

$$b = \begin{bmatrix} 0 & 0 & 1.91 \times 10^{-4} \\ 0 & 0 & -3.49 \times 10^{-5} \\ 1.91 \times 10^{-4} & -3.49 \times 10^{-5} & 0 \end{bmatrix}$$

$$\beta = \begin{bmatrix} 0 & 0 & 1.91 \times 10^{-4} \\ 0 & 0 & -3.49 \times 10^{-5} \\ 1.91 \times 10^{-4} & -3.49 \times 10^{-5} & 0 \end{bmatrix}$$

$$D = \begin{pmatrix} 467.9 & 159.3 & 0 \\ 159.3 & 118.5 & 0 \\ 0 & 0 & 158.2 \end{pmatrix}$$

$$d = \begin{bmatrix} 4.31 \times 10^{-3} & -5.36 \times 10^{-3} & 0 \\ -5.36 \times 10^{-3} & 0.016 & 0 \\ 0 & 0 & 7.30 \times 10^{-3} \end{bmatrix}$$

Using the above equation relating strains and curvatures to N and M we get

$$\varepsilon_x = 2.3 \times 10^{-3}, \quad \varepsilon_y = -2.86 \times 10^{-3}, \quad \gamma_{xy} = 0$$

$$\kappa_x = 0, \ \kappa_y = 0 \quad \text{and} \quad \kappa_{xy} = 7.67 \times 10^{-3}\text{mm}^{-1}$$

The difference in this case therefore is that we start to see some twisting of the laminate due to the non-symmetric nature of the lay-up.

(3.17) This is a non-symmetric laminate. The $\overline{Q}$ matrices are given in the text and the A, B and D matrices are determined from

$$A = \sum_{f=1}^{3} \overline{Q}_f \cdot (h_f - h_{f-1})$$

$$B = \frac{1}{2} \cdot \sum_{f=1}^{3} \overline{Q}_f \cdot \left[(h_f)^2 - (h_{f-1})^2 \right] \quad D = \frac{1}{3} \cdot \sum_{f=1}^{3} \overline{Q}_f \cdot \left[(h_f)^3 - (h_{f-1})^3 \right]$$

$$h_0 = -0.15, \ h_1 = -0.075, \ h_2 = 0.075, \ h_3 = 0.15$$

and a, b, β, d are determined from

$$\begin{bmatrix} a & b \\ \beta & d \end{bmatrix} = \begin{bmatrix} A & B \\ B & D \end{bmatrix}^{-1}$$

The strains and curvatures are then obtained from

$$\begin{bmatrix} \varepsilon_x \\ \varepsilon_y \\ \gamma_{xy} \\ \kappa_x \\ \kappa_y \\ \kappa_{xy} \end{bmatrix} = \begin{bmatrix} a_{11} & a_{12} & a_{16} & b_{11} & b_{12} & b_{16} \\ a_{21} & a_{22} & a_{26} & b_{21} & b_{22} & b_{26} \\ a_{61} & a_{62} & a_{66} & b_{61} & b_{62} & b_{66} \\ \beta_{11} & \beta_{12} & \beta_{16} & d_{11} & d_{12} & d_{16} \\ \beta_{21} & \beta_{22} & \beta_{26} & d_{21} & d_{22} & d_{26} \\ \beta_{61} & \beta_{62} & \beta_{66} & d_{61} & d_{62} & d_{66} \end{bmatrix} \begin{bmatrix} N_x \\ N_y \\ N_{xy} \\ M_x \\ M_y \\ M_{xy} \end{bmatrix} \quad \text{where } N_x = 30\,\text{N/mm}$$

from which

$$\varepsilon_x = 2.77 \times 10^{-3}, \quad \varepsilon_y = 2.55 \times 10^{-3}, \quad \gamma_{xy} = -1.026 \times 10^{-3}$$

$$\kappa_x = 0.015\ \text{mm}^{-1}, \quad \kappa_y = -0.021\ \text{mm}^{-1}, \quad \kappa_{xy} = 0.021\ \text{mm}^{-1}$$

The values in the relevant matrices are

$$A = \begin{bmatrix} 2.73 \times 10^4 & 8.06 \times 10^3 & 3.13 \times 10^3 \\ 8.06 \times 10^3 & 7.44 \times 10^3 & 1.48 \times 10^3 \\ 3.13 \times 10^3 & 1.48 \times 10^3 & 8 \times 10^3 \end{bmatrix}$$

$$a = \begin{bmatrix} 9.23 \times 10^{-5} & -8.51 \times 10^{-5} & -3.42 \times 10^{-5} \\ -8.51 \times 10^{-5} & 2.54 \times 10^{-4} & -3.94 \times 10^{-5} \\ -3.42 \times 10^{-5} & -3.94 \times 10^{-5} & 1.98 \times 10^{-4} \end{bmatrix}$$

$$B = \begin{pmatrix} -619.1 & 255.0 & -352.5 \\ 255.0 & 108.9 & -167.0 \\ -352.5 & -167.0 & 254.9 \end{pmatrix}$$

$$b = \begin{bmatrix} 5.07 \times 10^{-4} & -6.88 \times 10^4 & 6.84 \times 10^{-4} \\ -6.08 \times 10^{-4} & 3.85 \times 10^{-4} & 2.12 \times 10^{-4} \\ -3.23 \times 10^{-5} & 5.84 \times 10^{-4} & -1.31 \times 10^{-3} \end{bmatrix}$$

$$B = \begin{bmatrix} 5.07 \times 10^{-4} & -6.08 \times 10^{-4} & -3.23 \times 10^{-4} \\ -6.88 \times 10^{-4} & 3.85 \times 10^{-4} & 5.84 \times 10^{-4} \\ 6.84 \times 10^{-4} & 2.12 \times 10^{-4} & -1.31 \times 10^{-3} \end{bmatrix}$$

$$D = \begin{pmatrix} 236.0 & 47.7 & -29.3 \\ 47.7 & 50.3 & -13.9 \\ -29.3 & -13.9 & 47.2 \end{pmatrix}$$

$$d = \begin{bmatrix} 8.37 \times 10^{-3} & -8.00 \times 10^{-3} & 4.65 \times 10^{-3} \\ -8.00 \times 10^{-3} & 0.031 & -2.68 \times 10^{-3} \\ 4.65 \times 10^{-3} & -2.68 \times 10^{-3} & 0.036 \end{bmatrix}$$

(3.18) (a) **Maximum Stress Criterion**
The local stresses are given by

$$\begin{bmatrix} \sigma_1 \\ \sigma_2 \\ \tau_{12} \end{bmatrix} = T_\sigma \begin{bmatrix} \sigma_x \\ \sigma_y \\ \tau_{xy} \end{bmatrix}, \quad \begin{bmatrix} \sigma_1 \\ \sigma_2 \\ \tau_{12} \end{bmatrix} = \begin{bmatrix} 61.6 \\ 38.4 \\ -29.4 \end{bmatrix} \text{MPa}$$

$$\frac{\widehat{\sigma}_{IT}}{\sigma_1} = 20.1, \quad \frac{\widehat{\sigma}_{2T}}{\sigma_2} = 0.52, \quad \frac{\widehat{\widehat{\tau}}_{12}}{\tau_{12}} = 1.36$$

As the second term is less than 1, a tensile failure in the 2-direction would be expected.

(b) **Maximum Strain Criterion**
From the data given

$$\widehat{\varepsilon}_{IT} = 2.49 \times 10^{-3}, \quad \widehat{\varepsilon}_{2T} = 3.777 \times 10^{3}, \quad \widehat{\varepsilon}_{IC} = 5.84 \times 10^{-5}$$
$$\widehat{\varepsilon}_{2C} = 5.66 \times 10^{-3}, \quad \widehat{\gamma}_{12} = 7.14 \times 10^{-3}$$

The 1−2 strains are given by

$$\begin{bmatrix} \varepsilon_1 \\ \varepsilon_2 \\ \gamma_{12} \end{bmatrix} = S \bullet \begin{bmatrix} \sigma_1 \\ \sigma_2 \\ \tau_{12} \end{bmatrix} \quad \text{So,} \quad \begin{bmatrix} \varepsilon_1 \\ \varepsilon_2 \\ \gamma_{12} \end{bmatrix} = \begin{bmatrix} 0.1 \\ 7.2 \\ -5.25 \end{bmatrix} 10^{-3}$$

$$\frac{\widehat{\varepsilon}_{IT}}{\varepsilon_1} = 24.9, \quad \frac{\widehat{\varepsilon}_{2T}}{\varepsilon_2} = 0.5, \quad \frac{\widehat{\gamma}_{12}}{\gamma_{12}} = 1.36$$

Hence once again a failure is predicted in the 2-direction.

(c) **Tsai−Hill Criterion**

The Tsai − Hill equation gives

$$\dot{\gamma} \propto Q \quad \text{and} \quad \tau \propto \dot{\gamma}^n \propto Q^n$$

Therefore failure is predicted.

(3.19) (i) For an applied stress of $\sigma_x = 1$ MPa, the stresses in the 1−2 direction are given by

$$\begin{bmatrix} \sigma_1 \\ \sigma_2 \\ \tau_{12} \end{bmatrix} = T_\sigma \begin{bmatrix} \sigma_x \\ \sigma_y \\ \tau_{xy} \end{bmatrix} \quad \text{So} \quad \begin{bmatrix} \sigma_1 \\ \sigma_2 \\ \tau_{12} \end{bmatrix} = \begin{bmatrix} 0.75 \\ 0.25 \\ -0.433 \end{bmatrix} \text{MPa}$$

$$\frac{\widehat{\sigma}_{IT}}{\sigma_1} = 1867, \quad \frac{\widehat{\sigma}_{2T}}{\sigma_2} = 200, \quad \frac{\widehat{\tau}_{12}}{\tau_{12}} = 92.4$$

Hence an applied stress of $\sigma_x = 92$ MPa would initiate a shear failure before tensile or compressive failures occurred.

(ii) Maximum Strain Criterion

From the data given

$$\widehat{\varepsilon}_{IT} = \frac{\widehat{\sigma}_{IT}}{E_1} = 0.035, \widehat{\varepsilon}_{2T} = \frac{\widehat{\sigma}_{2T}}{E_2} = 5.56 \times 10^{-3}$$

$$\widehat{\varepsilon}_{IC} = \frac{\widehat{\sigma}_{IC}}{E_1} = 5.5 \times 10^{-3}, \quad \widehat{\varepsilon}_{2C} = \frac{\widehat{\sigma}_{2C}}{E_2} = 0.011$$

$$\widehat{\gamma}_{12} = \frac{\widehat{\gamma}_{12}}{G_{12}} = 0.01$$

Also,

$$\begin{bmatrix} \varepsilon_1 \\ \varepsilon_2 \\ \gamma_{12} \end{bmatrix} = S \begin{bmatrix} \sigma_1 \\ \sigma_2 \\ \tau_{12} \end{bmatrix} \quad \text{So} \quad \begin{bmatrix} \varepsilon_1 \\ \varepsilon_2 \\ \gamma_{12} \end{bmatrix} = \begin{bmatrix} 1.68 \\ 2.19 \\ -10.8 \end{bmatrix} 10^{-5}$$

$$\frac{\widehat{\varepsilon}_{IT}}{\varepsilon_1} = 2082, \quad \frac{\widehat{\varepsilon}_{2T}}{\varepsilon_2} = 253, \quad \frac{\widehat{\gamma}_{12}}{\gamma_{12}} = 92.4$$

Hence once again a stress of $\sigma_x = 92$ MPa is the limiting condition.

(iii) Tsai − Hill Criterion

Letting X be the multiplier for σ_x

$$\left(\frac{X \bullet \sigma_1}{\widehat{\sigma}_{IT}}\right)^2 - \left(\frac{X^2 \bullet \sigma_1 \sigma_2}{\widehat{\sigma}_{IT}}\right)^2 + \left(\frac{X\sigma_2}{\sigma_{2T}}\right)^2 + \left(\frac{X\tau_{12}}{\widehat{\tau}_{12}}\right)^2 = 1$$

Solving for X gives $X = 83.8$.
Hence the limiting condition is $\sigma_x = 83$ MPa.

(3.20) Let $N_x = 1.2$ N/mm (i.e. $\sigma_x = 1$ N/mm^2).
By calculating the matrix $[a]$ we get (for 30°ply).

$$\begin{bmatrix} \varepsilon_x \\ \varepsilon_y \\ \gamma_{xy} \end{bmatrix} = a \begin{bmatrix} N_x \\ N_y \\ N_{xy} \end{bmatrix} = \begin{bmatrix} 1.235 \\ -1.248 \\ 0 \end{bmatrix} \times 10^{-5}$$

Then

$$\begin{bmatrix} \varepsilon_1 \\ \varepsilon_2 \\ \gamma_{12} \end{bmatrix} = T_\varepsilon \begin{bmatrix} \varepsilon_x \\ \varepsilon_y \\ \gamma_{xy} \end{bmatrix} = \begin{bmatrix} 6.14 \\ -6.27 \\ -21.5 \end{bmatrix} \times 10^{-6}$$

$$\frac{\widehat{\varepsilon}_{IT}}{\varepsilon_1} = 2379, \quad \frac{\varepsilon_{2c}}{\varepsilon_2} = 3624, \quad \frac{\widehat{\gamma}_{12}}{\gamma_{12}} = 606$$

Hence the limiting condition is $\sigma_x = 606$ MPa.
Also,

$$\begin{bmatrix} \sigma_x \\ \sigma_y \\ \tau_{xy} \end{bmatrix} = \overline{Q}_f \begin{bmatrix} \varepsilon_x \\ \varepsilon_y \\ \gamma_{xy} \end{bmatrix} \quad \text{and} \quad \begin{bmatrix} \sigma_1 \\ \sigma_2 \\ \tau_{12} \end{bmatrix} = T_\sigma \begin{bmatrix} \sigma_x \\ \sigma_y \\ \tau_{xy} \end{bmatrix}$$

which gives

$$\begin{bmatrix} \sigma_1 \\ \sigma_2 \\ \tau_{12} \end{bmatrix} = \begin{bmatrix} 0.787 \\ -0.039 \\ -0.148 \end{bmatrix} \text{ MPa}$$

$$\frac{\widehat{\sigma}_{IT}}{\sigma_1} = 2415, \quad \frac{\widehat{\sigma}_{2C}}{\sigma_2} = 5102, \quad \frac{\widehat{\tau}_{12}}{\tau_{12}} = 606$$

Hence the Maximum Stress Criterion also predicts $\sigma_x = 606$ MPa as the limiting condition.
For the Tsai−Hill Criterion, letting $X =$ multiplier on stress σ_x, then solving

$$\left(\frac{X \bullet \sigma_1}{\widehat{\sigma}_{IT}}\right)^2 - \left(\frac{X^2 \bullet \sigma_1 \sigma_2}{\widehat{\sigma}_{IT}}\right)^2 + \left(\frac{X\sigma_2}{\sigma_{2T}}\right)^2 + \left(\frac{X\tau_{12}}{\widehat{\tau}_{12}}\right)^2 = 1$$

gives $X = 583$.
This predicts a stress of $\sigma_x = 583$ MPa.
If this is repeated for all the plies then we get

TABLE Q3.20 Maximum permissible values of σ_x, to cause failure in each ply.

Ply	Max. stress or Max. strain	Tsai−Hill
$\theta = 0°$	$\sigma_x = 1201$ MPa	$\sigma_x = 1067$
$\theta = -30°$	$\sigma_x = 606$ MPa	$\sigma_x = 583$
$\theta = 30°$	$\sigma_x = 606$ MPa	$\sigma_x = 583$

The limiting condition is thus $\sigma_x = 583$ MPa as predicted by Tsai−Hill.

(3.21)
$$K_c = \sigma(\pi a_c)^{1/2}\left(\frac{W}{\pi a}\tan\left(\frac{\pi a}{W}\right)\right)^{1/2}$$

$$= \frac{P}{Wb}(\pi a_c)^{1/2}\left(\frac{W}{\pi a}\tan\left(\frac{\pi a}{W}\right)\right)^{1/2}$$

$$43 = \frac{P}{30 \times 5}\left(\pi \times 5 \times 10^{-3}\right)^{1/2}(1.05)$$

$$P = 49 \text{ kN}$$

(3.22) $CSM: \; K_c = \sigma(\pi a_c)^{1/2} \rightarrow a_c = \left(\frac{13.5}{80}\right)^2 \frac{1}{\pi} = 9.06 \times 10^{-3}$ m

$$N = \frac{2\left((9.06 \times 10^{-3})^{-5.35} - (1000 \times 10^{-6})^{-5.35}\right)}{3.3 \times 10^{-18}(80)^{12.7}\pi^{6.35}(-10.7)}$$

$$= 3 \times 10^5 \text{ cycles}$$

Woven Roving:

$$a_c = 34.9 \times 10^{-3}, \text{ so in a similar way}$$

$$N = 1.14 \times 10^6 \text{ cycles}$$

(4.1) $Q_D = \frac{1}{2}\pi^2 D^2 NH \sin\phi \cos\phi$

$$= \frac{1}{2}\pi^2(50 \times 10^{-3})^2(100/60)(2.4 \times 10^{-3})\sin 17.7 \cos 17.7$$

$$= 1.43 \times 10^{-5} \text{ m}^3/\text{s}$$

$$Q_P = \frac{\pi D H^3 \sin^2\phi}{12\eta}\left(\frac{P}{L}\right)$$

$$= \frac{\pi(50 \times 10^{-3})(2.4 \times 10^{-3})^3 \sin^3 17.7}{12(200)}\left(\frac{20 \times 10^6}{1}\right)$$

$$= 1.67 \times 10^{-6} \text{ m}^3/\text{s}$$

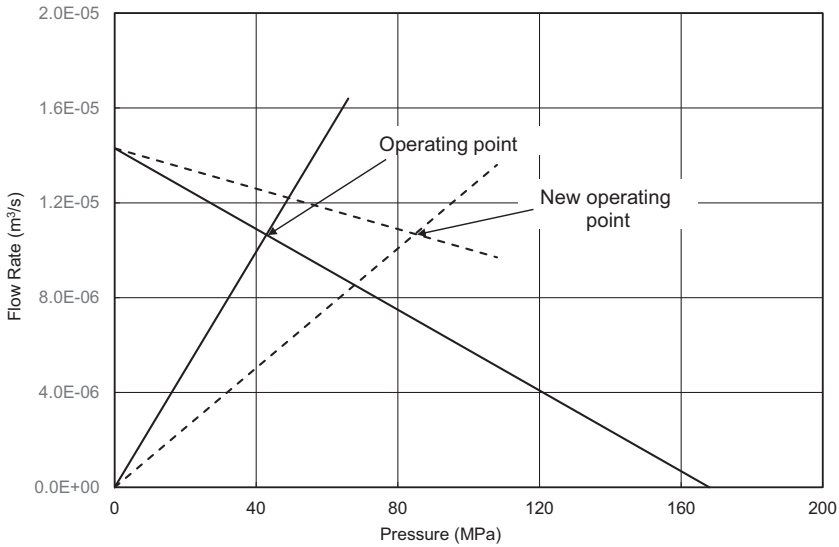
$$\text{Total flow } Q_D - Q_P = 1.26 \times 10^{-5} \text{ m}^3/\text{s}$$

The shear rate in the metering zone will be given by

$$\dot{\gamma} = \frac{V_d}{H} = \frac{\pi DN \cos\varphi}{H} = \frac{\pi(50 \times 10^{-3})(100/60)\cos 17.7}{2.4 \times 10^{-3}}$$

$$\dot{\gamma} = 104\ s^{-1}$$

(4.2) For the die,



$$Q = \frac{\pi P R^4}{8L\eta} = KP$$

where

$$K = \frac{\pi R^4}{8L\eta} = \frac{\pi(1.5)^4 10^{-9}}{8 \times 40 \times 200 \times 10^{-6}} = 2.485 \times 10^{-7}\ \left(\frac{m^s/s}{MPa}\right)$$

for the extruder,

$$P_{max} = \frac{6\pi\eta LDN}{H^2 \tan\phi}$$

$$P_{max} = \frac{6\pi \times 200 \times 10^{-6} \times 1000 \times 50 \times 100}{60 \times (2.4)^2 \times 0.3191} = 171\ \ \text{MPa}$$

$$Q_{max} = \frac{1}{2}\pi^2 D^2 NH \sin\phi \cos\phi = 1.436 \times 10^{-5}\text{m}^3\text{s}$$

From graph, operating point is

$$P = 43\ \text{MPa},\ Q = 1.075\ \text{m}^3/\text{s}$$

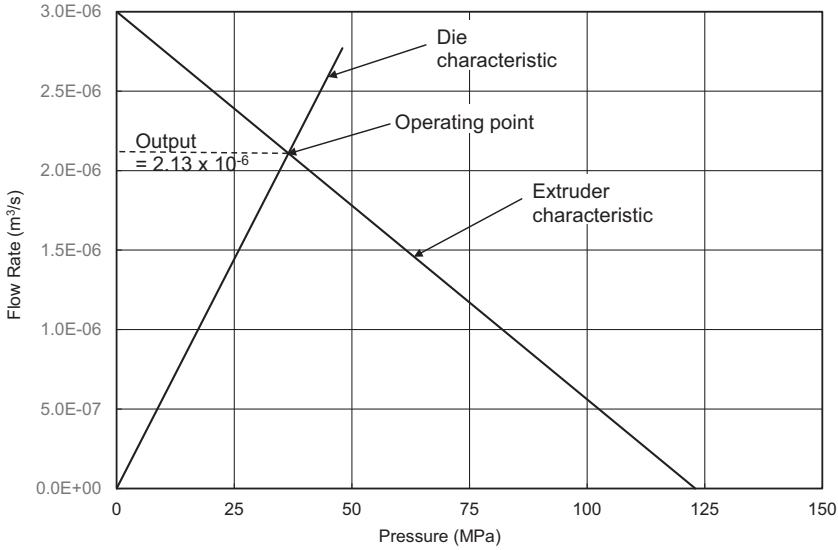
New operating point is

$$P = 85 \text{ MPa}, \; Q = 1.075 \text{ m}^3/\text{s}$$

(4.3) Extruder : $Q_{max} = \frac{1}{2}\pi^2 D^2 NH \sin\phi \cos\phi$

$$= \frac{1}{2}\pi^2 (25)^2 \left(\frac{100}{60}\right)(2)\sin 17°42' \cos 17°42'$$

$$= 2.98 \times 10^{-6} \text{ m}^3/\text{s}$$



$$P_{max} = \frac{6\pi\eta LDN}{H^2 \tan\phi}$$

$$= \frac{6\pi(25)(500)\left(\frac{100}{60}\right)\left(400 \times 10^{-6}\right)}{2^2 \times \tan 17°42'}$$

$$= 123 \quad \text{MPa}$$

Die:

$$Q = 2\left\{\frac{\pi R^4}{8\eta L_d}\right\}P$$
$$= 2\left\{\frac{\pi(0.75)^4}{8 \times 400 \times 10^{-6} \times 10}\right\}P$$

Hence the characteristics shown may be drawn.
The operating point is at the intersection of the two characteristics.

$$\text{Output, } \; Q = 2.13 \times 10^{-6}\text{m}^3/\text{s}$$

(4.4) $Q = \frac{1}{2}\pi D^2 NH \sin\phi \cos\phi - \pi DH^3 \sin^2\phi\left(\frac{P}{12\eta L}\right)$

But

$$Q = \frac{K_1 P}{\eta}$$

So

$$Q = \frac{1}{2}\pi D^2 NH \sin\phi \cos\phi - \frac{\pi DH^3 \sin^2\phi}{12\eta} \bullet \frac{Q\eta}{K_1 L}$$

$$Q = \frac{AH \sin\phi \cos\phi}{1 + BH^3 \sin^2\phi}$$

where

$$A = \frac{1}{2}\pi^2 D^2 N \text{and } B = \frac{\pi D}{12LK_1}$$

So

$$\frac{dQ}{d\phi} = \frac{(1 + BH^3 \sin^2\phi)AH(2\cos^2\phi - 1) - AH \sin\phi \cos\phi(2H^3 B \sin\phi \cos\phi)}{(1 + BH^3 \sin^2\phi)} = 0$$

$$\left(1 + BH^3 \sin^2\phi\right)\left(2\cos^2\phi - 1\right) = 2H^3 B \sin^2\phi \cos^2\phi \qquad (1)$$

Also

$$\frac{dQ}{dH} = \frac{(1 + BH^3 \sin^2 \phi)A \sin \phi \cos \phi - AH \sin \phi \cos \phi (3BH \sin^2 \phi)}{(1 + BH^3 \sin^2 \phi)} = 0$$

So

$$\left(1 + BH^3 \sin^2 \phi\right) = 3BH^3 \sin^2 \phi \qquad (2)$$

Using (2) in (1)
Thus

$$\left(3BH^3 \sin^2 \phi\right)\left(2 \cos^2 \phi - 1\right) = 2H^3 B \sin^2 \phi \cos^2 \phi$$

$$\left(3BH^3 \sin^2 \phi\right)(\cos 2\,\phi) = 2H^3 B \sin^2 \phi \cos^2 \phi$$

$$2 \cos 2\,\phi = 2 \cos^2 \phi \rightarrow 3\left(1 - 2 \sin^2 \phi\right) = 2\left(1 - \sin^2 \phi\right)$$

which can be solved to give $\phi = 30^\circ$

Also

$$\left[1 + BH^3 \sin^2 \phi\right] = 3BH^3 \sin^2 \phi$$

$$H^3 = \frac{1}{2B \sin^2 \phi} = \frac{2}{B}$$

$$H = \left[\frac{24K_1 L}{\pi D}\right]^{\frac{1}{3}}$$

(4.5) $F = \pi R^2 P_0 \left(\frac{m}{m+1}\right) = \pi(0.25)^2 \left(50 \times 10^6\right)\left(\frac{0.6}{2.6}\right)$

$= 2.26\ MN$

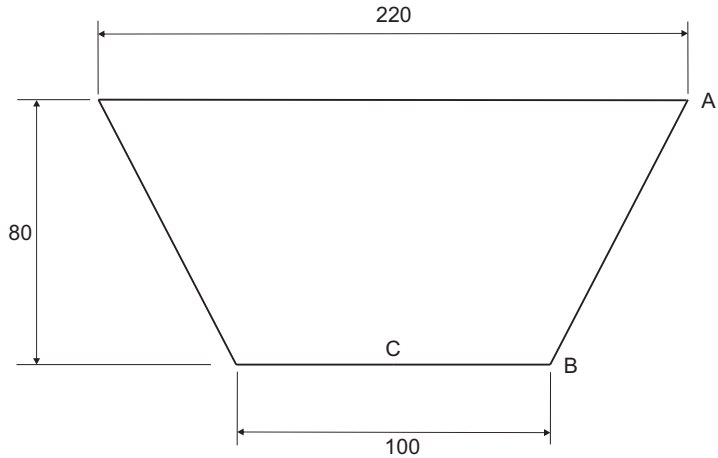
(4.6) $AB = 100$ mm

Flow ratio $= \frac{CBA}{3} = \frac{150}{3} = 50$

Clamp force $= \pi R^2 P_0 \left(\frac{m}{m+2}\right)$

$= \pi(110)^2 140\left(\frac{0.5}{2.5}\right)$

$= 1.06$ MN



(4.7)

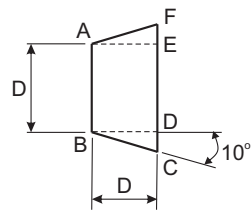
(i) $$\frac{c.s.a.}{s.a.} = \frac{1/4\pi D^2}{\pi D} = 0.25D$$

(ii) $DC = D\tan 10^\circ$, $BC = D/\cos 10^\circ$

$c.s.a. = D^2 + D^2 \tan 10^\circ = D^2(1 + \tan 10^\circ)$

$s.a. = 2D + 2D/\cos 10^\circ + 2D \tan 10^\circ$

$$\frac{c.s.a}{s.a.} = \frac{D^2(1 + \tan 10^\circ)}{2D\,(1 + (\cos 10^\circ)^{-1} + \tan 10^\circ)} = 0.268\text{D}$$



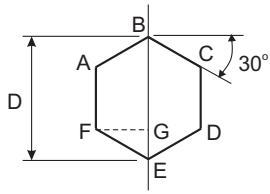
(iii)

$$FG = (D/4)\tan 30^\circ$$

$$c.s.a. = D^2(1.5)/4 \tan 30^\circ$$

$$s.a. = 6(D/2) = 3D$$

$$\frac{c.s.a.}{s.a.} = \frac{D}{8 \tan 30^\circ} = 0.216D$$

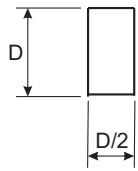


(iv)

$$c.s.a. = D^2/2$$

$$s.a. = 2D + D = 3D$$

$$\frac{c.s.a.}{s.a.} = \frac{D^2}{6D} = 0.167D$$



(4.8) $V_d = 2\pi RN = \frac{2\pi \times 0.15 \times 5}{60} = 0.078 \text{ m/s}$

$$Q = \frac{2000kg}{hour} = 0.396 \times 10^{-3} \text{ m}^3/\text{s}$$

but

$$Q = HWV_d \quad So \ H = \frac{0.396 \times 10^{-3}}{1 \times 0.078} = 5.04 \text{ mm}$$

$$x = \sqrt{(5.04 - 4.5)150} = 9 \text{ mm}$$

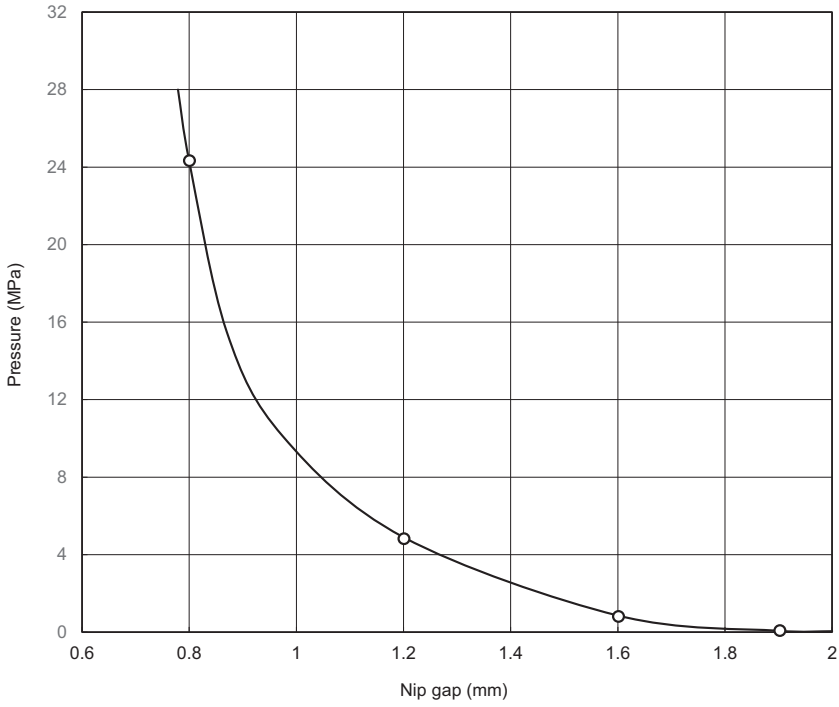
Now

$$w = 1.786(i.e.\ x/H)$$

So

$$P_{max} = \frac{3 \times 1.5 \times 10^4 \times 0.078}{4.5 \times 10^{-3}}(3.57 - 0.64(1.786 + 5.77(0.33)))$$
$$= 0.93 \quad \text{MPa}$$

(4.9) For $H_0 = 0.8, x = \sqrt{(H - H_0)^R} = 10.9$ mm, $w = 5.45$



$P_{max} = 24.3$ MPa (same equation as above)

For $H_0 = 1.2 \ \text{mm}, P_{max} = 4.9 \ \text{MPa}$

For $H_0 = 1.6 \ \text{mm}, P_{max} = 0.86 \ \text{MPa}$

For $H_0 = 1.9 \ \text{mm}, P_{max} = 0.073 \ \text{MPa}$

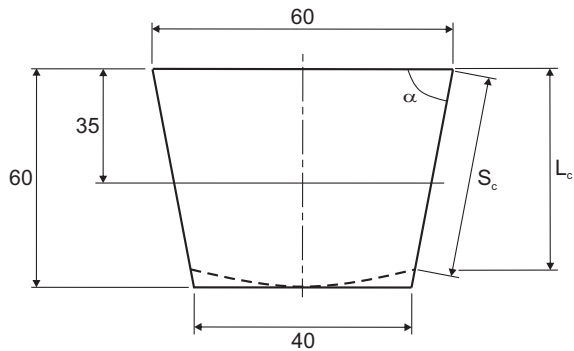
(4.10) Initial volume of sheet $= \left(\frac{\pi D^2}{4}\right)4 = \pi D^2$

Since the dome formed is a free surface it may be assumed to have a constant thickness, t

$$\text{Final volume} = \left(\frac{\pi D^2}{2}\right)t$$

$$\frac{\pi D^2}{2}t = \pi D^2 \rightarrow t = 2 \ \text{mm}$$

(4.11) $$\alpha = \tan^{-1}\left(\frac{60}{10}\right) = 80.54^\circ$$



$$L = 35 \ \text{um}, t_0 = 3 \ \text{mm}$$

$$H = 30 \tan \beta = 180$$

$$t_{AA} = t_0\left(\frac{1+\cos\alpha}{2}\right)\left(\frac{H-L}{H}\right)^{\sec\alpha-1}$$
$$= 0.58 \quad \text{mm}$$

When sheet just touches the base.

$$S_c = (D(1+\cos\alpha)/\sin\alpha) - R = 40.82$$

So

$$L_c = 40.27 \quad \text{mm and thus} \quad t_B = 0.48 \quad \text{mm}$$

(4.12) (a) $B_{SH} = 1.8$ So Parison thickness $= 1.8 \times 2 = 3.6$ mm

$B_{ST} = \sqrt{1.8} = 1.34$, Parison diameter $= 38 \times 1.34 = 50.98$ mm

(b) $h = B_{ST}^3\, h_d\left(\frac{D_d}{D_m}\right) = (1.34)^3 \times 2 \times \left(\frac{38}{70}\right) = 2.62$

(c) $P = \frac{2\sigma h}{D_m} = \frac{2\times10\times2.62}{70} = 0.75$ MPa

(4.13) $$\frac{O_{MD}}{O_{TD}} = \frac{\text{die gap}}{\text{film thickness} \times (\text{blow} - \text{up})^2} = 2$$

So

$$\text{blow} - \text{up} = \sqrt{\frac{1}{0.1 \times 2}} = 2.24$$

$$D_{\text{bubble}} = 2.24 \times 99 = 221.76 \text{ mm}$$

$$\text{Lay flat width} = \frac{\pi D_b}{2} = 348.3 \text{ mm}$$

(4.14)

$$\Delta P = \frac{6\eta VL(2h-H)}{H^3}$$
$$= \frac{6 \times 100 \times 0.5 \times 6 \times 10^{-2}(0.6-0.5)10^{-3}}{(0.5)^3 \times 10^{-9}}$$
$$= 14.4 \quad \text{MPa}$$

(4.15) $\left(\frac{T_0-T}{T_0-T_i}\right) = \exp\left(\frac{-h\beta t}{\rho C_p}\right) = \exp\left(\frac{-h\alpha t}{Hk}\right)$

where $\alpha = k/\rho C_p$ = thermal diffusivity and H = wall thickness = $1/\beta$

$$\frac{300-250}{300-23} = \exp\left(\frac{-28.4 \times 8.6 \times 10^{-5}\, t}{3 \times 10^{-3} \times 230}\right)$$

$$t = 484.4 \text{ s} = 8.07 \text{ minutes}$$

$$\frac{300-250}{300-23} = \exp\left(\frac{-28.4 \times 8.6 \times 10^{-5} t}{3 \times 10^{-3} \times 230}\right)$$

$$t = 484.4 \text{ s} = 8.07 \text{ minutes}$$

(4.16) volume $= \frac{\text{mass}}{\rho} = \frac{150 \times 10^{-3}}{1200}\text{m}^3$

So,
$$\pi R^3 H = \frac{150 \times 10^{-3} \times 10^9}{1200}$$

$$H = \frac{150 \times 10^6}{\pi \times 1200 \times (150)^2} = 1.77 \quad \text{mm}$$

Also

$$t = \frac{3\eta V^2}{8\pi F H^4} = \frac{3 \times 10^4 \times \left(150 \times 10^6\right)^2}{8\pi \times 10^6 \times 100 \times 10^3 \times 1.77^4 \times (1200)^2} = 19 \quad \text{s}$$

(5.1) $\tau = \frac{3T}{2\pi R^3} = \frac{3}{2}\frac{WR}{\pi R^3} = \frac{3W}{2\pi R^2} = 7.49 \quad \text{W}$

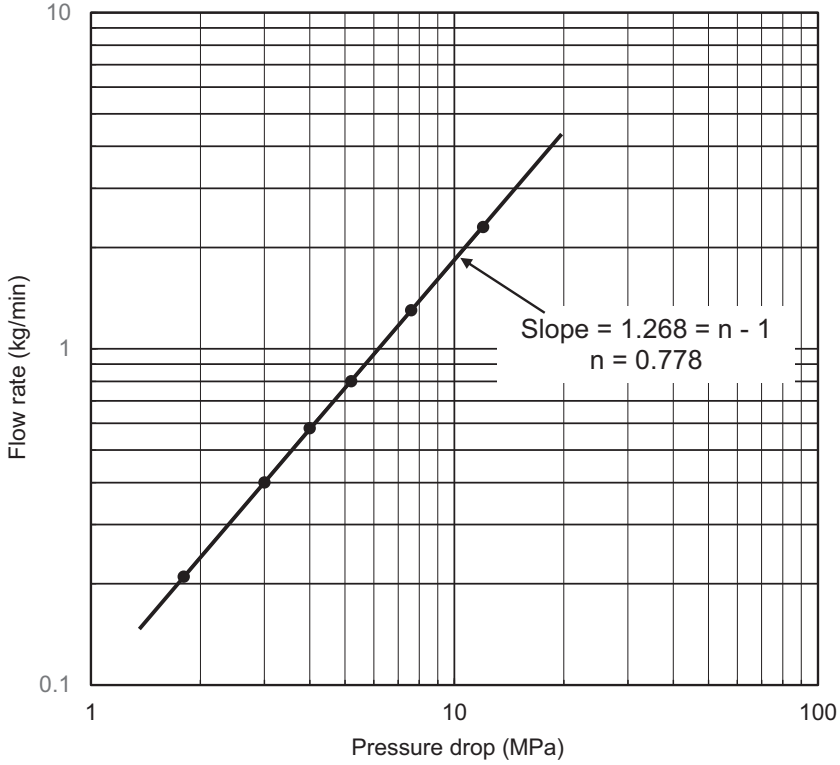
Also

$$\dot{\gamma} = \frac{\dot{\theta}}{\alpha} = \frac{\theta}{40 \times 5} = \frac{\theta}{200}$$

W(g)	τ(Pa)	θ	$\dot{\gamma}$ (s^{-1})	$\eta = \tau/\dot{\gamma}$
50	374.5	0.57	2.85×10^{-3}	1.31×10^5
100	749	1.25	6.25×10^{-3}	1.2×10^5
200	1498	2.56	1.28×10^{-2}	1.17×10^5
500	3745	7.36	3.68×10^{-2}	1.02×10^5
1000	7490	17.0	8.5×10^{-2}	8.8×10^4
2000	14980	42.0	0.21	7.13×10^4

A graph of η vs. τ gives $\tau = 1 \times 10^4$ *Pa and* $\eta = 8 \times 10^4$ *Pa.s*

(5.2) For a Power Law fluid $\dot{\gamma} \propto (\tau)^{1/n}$



So,

$$Q \propto (\Delta P)^{1/n}$$

or

$$\log Q \propto 1/n \log \Delta P$$

So the slope of a graph of (log Q) against (log ΔP) will be a straight line of slope $1/n$ if the Power Law is obeyed. From the attached graph $1/n = 1.268$ so $n = 0.7886$

Consider the point, $Q = 0.8$ kg/min and $\Delta P = 5.2$ MPa.

$$\tau = \frac{H(\Delta P)}{2L} = \frac{2 \times 10^{-3} \times 5.2 \times 10^{6}}{2 \times 50 \times 10^{-3}} = 1.04 \times 10^{5} \text{ Pa}$$

Now

$$\dot{\gamma} = \left(\frac{2n+1}{3n}\right) \frac{6Q}{TH^2} = \left(\frac{2(0.7886)+1}{3(0.7886)}\right) \left(\frac{6 \times 0.8 \times 10^{6}}{60 \times 0.94 \times 6 \times 2^2}\right) = 3863 \text{ s}^{-1}$$

but

$$\tau = \tau_0 \dot{\gamma}^n$$

So

$$\tau_0 = \frac{1.04 \times 10^{5}}{(3863)^{0.7886}} = 154.3$$

(5.3) *Cone and Plate*

$$\text{True shear rate, } \dot{\gamma} = \frac{\dot{\theta}}{\alpha} = \frac{0.062 \times 180}{3\pi} = 1.18 \text{ s}^{-1}$$

$$\text{Shear Stress, } \tau = \frac{3T}{2\pi R^3} = \frac{3 \times 1.18}{2\pi \times (37.5 \times 10^{-3})^3} = 10.7 \text{ kPa}$$

Ram Extruder

$$Q = 70 \times 10^{9} \left\{ \begin{array}{l} \dot{\gamma} = \dfrac{4Q}{\pi R^3} = \dfrac{4 \times 70 \times 10^{-9}}{\pi \times 10^{-9}} = 89.1 \text{ s}^{-1} \\ \tau = \dfrac{PR}{2L} = \dfrac{3.9 \times 10^{6} \times 1}{2 \times 32} = 60.9 \text{ kPa} \end{array} \right\}$$

$$Q = 200 \times 10^9 \left\{ \begin{array}{l} \dot{\gamma} = \dfrac{4 \times 200 \times 10^{-9}}{\pi \times 10^{-9}} = 254.6 \ \ \mathrm{s}^{-1} \\ \tau = \dfrac{5.7 \times 10^6 \times 1}{2 \times 32} = 89.1 \ \ \mathrm{kPa} \end{array} \right\}$$

but

$$\tau = \tau_0 \dot{\gamma}^n$$

$$\left(\frac{60.9}{89.1}\right) = \left(\frac{89.1}{254.6}\right)^n$$

So $n = 0.362$ and $\tau_0 = 11.98$
Now the cone and plate gives true shear rate whereas the ram extruder uses apparent shear rate. The Non-Newtonian correction factor is

$$\left(\frac{4n}{3n+1}\right) = \left(\frac{4 \times 0.362}{3(0.362)+1}\right) = 0.69$$

Therefore the true shear rate on the cone and plate is equivalent to a shear rate of 0.69 (1.18) = 0.817 on the ram extruder
At

$$\dot{\gamma} = 0.817 \quad \tau = 11.98(0.817)^{0.362} = 11.13 \ \ \mathrm{kPa}$$

$$\%\ \text{difference} = \frac{11.13 - 10.7}{10.7} = 4.06\%$$

(5.4) If the material is assumed Newtonian and the shear rates are equated then

$$\frac{6Q_2}{TH^2} = \frac{4Q_1}{\pi R^3}$$

$$Q_2 = \frac{4TH^2Q_1}{6\pi R^3} \tag{1}$$

If the material is non-Newtonian then the true shear rates should be equated

$$\left(\frac{2n+1}{3n}\right)\frac{6Q_2}{TH^2} = \left(\frac{3n+1}{4n}\right)\frac{4Q_1}{\pi R^3}$$

$$Q_2 = \left(\frac{3n+1}{4n}\right)\left(\frac{3}{2n+1}\right)\frac{4TH^2Q_1}{6\pi R^3} \tag{2}$$

So for $n = 0.37$ correction factor $= 0.9094$
Error $= 1-0.9094 = 0.0906 \rightarrow 9.06\%$

Now $\dot{\gamma} \propto Q$ and $\tau \propto \dot{\gamma}^n \propto Q^n$

and $P \propto \tau$ then $P \propto Q^n$

So $\text{Correction Factor} = \left(\left(\frac{3n+1}{4n}\right)\left(\frac{3n}{2n+1}\right)\right)^n$

for

$$n = 0.37 \text{ Factor} = 0.9655$$
$$\text{Error} = 1 - 0.9655 = 0.0345 \rightarrow 3.45\%$$

(5.5) $\dot{\gamma} = \frac{4Q}{\pi R^3} = \frac{4 \times 2.12 \times 10^{-6}}{\pi(3 \times 10^{-3})^3} = 100\ \text{s}^{-1}$

From flow curves

$$\eta = 1.3 \times 10^3 \text{ Pa.s}, \; G = 3 \times 10^4 \text{ Pa}$$

So

$$\text{Natural time} = \frac{\eta}{G} = \frac{1.3 \times 10^3}{3 \times 10^4} = 4.3 \times 10^{-2}\text{s}$$

$$\text{Dwell time} = \frac{V}{Q} = \frac{\pi(3 \times 10^{-3}) \times 37 \times 10^{-3}}{2.12 \times 10^{-6}} = 0.5 \text{ s}$$

So flow is mostly plastic.

(5.6) $\dot{\gamma} = \dfrac{6Q}{TH^2} = \dfrac{6 \times 0.75 \times 10^{-9}}{(5 \times 10^{-3})(1 \times 10^{-3})^2} = 0.9 \text{ s}$

From flow curves $\eta = 2 \times 10^4$ Pa.s, $G = 1 \times 10^4$ Pa
So

$$\text{Natural time} = \frac{\eta}{G} = 2 \text{ seconds}$$

Dwell time = 1 second so flow is predominantly elastic.

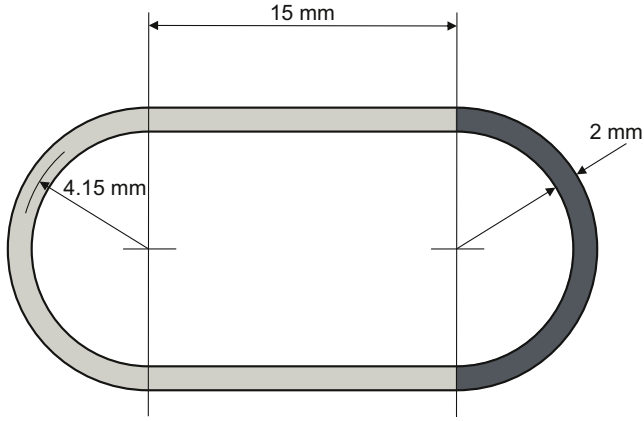
(5.7) $Q = AV = \frac{\pi}{4} \times 25^2 \times 10^{-6} \times 50 \times 10^{-3} = 24.54 \times 10^{-6}\text{m}^3/\text{s}$

$$\dot{\gamma} = \frac{6Q}{TH^2} = \frac{6 \times 24.54 \times 10^{-6}}{\pi \times 25 \times 10^{-3} \times 1 \times 10^{-6}} = 1953 \text{ s}^{-1}$$

From flow curves at $\dot{\gamma} = 1953 \text{ s}^{-1}$, $\tau = 3.2 \times 10^5$ Pa.

$$\tau = \frac{PH}{2L} \rightarrow P = \frac{3.2 \times 10^5 \times 2 \times 30}{1} = 19.2 \text{ MPa}$$

(5.8) Flow rate = 3 m/min



$$\text{Area} = 2\{(15+15)+\pi(8.3)\} = 112\times10^{-6}\text{m}^2$$

$$Q = \frac{3\times112\times10^{-6}}{60} = 5.6\times10^{-6}\text{m}^3/\text{s}$$

$$\dot{\gamma} = \frac{6Q}{TH^2} = \frac{6\times5.6\times10^{-6}}{(30+26)\times2^2\times10^{-9}}$$
$$= 150 \ \ \text{s}^{-1}$$

from flow curves, at $\dot{\gamma} = 150\ \text{s}^{-1}$, $\tau = 1.5\times10^5$ Pa

$$\Delta P = \frac{2L\tau}{H} = \frac{2\times10\times1.5\times10^5}{2} = 1.5 \ \ \text{MPa}$$

$$\text{Power} = PQ$$

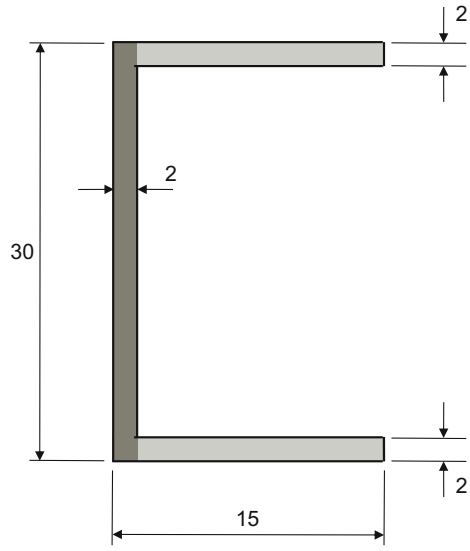
$$\text{Power} = 1.5\times10^6\times5.6\times10^{-6}$$

$$= 8.4\ \text{NM/s} \ \ (= 8.4\ \text{W})$$

The temperature rise ΔT is then given by

$$\Delta T = \frac{\Delta P}{\rho C_p} = \frac{1.5 \times 10^6}{3.3 \times 10^6} = 0.45^\circ\text{C}$$

(5.9) Flow rate = 3 m/min



$$\text{Area} = (30 \times 2) + 2(13 \times 2) = 112 \times 10^{-6}\text{m}^2$$

$$Q = \frac{3 \times 112 \times 10^{-6}}{60} = 5.6 = 10^{-6}\text{m}^3/\text{s}$$

$$\dot{\gamma} = \frac{6Q}{TH^2} = \frac{6 \times 5.6 \times 10^{-6}}{(30 + 26) \times 2^2 \times 10^{-9}} = 150 \text{ s}^{-1}$$

from flow curves, at $\dot{\gamma} = 150$ s^{-1}, $\tau = 1.5 \times 10^5$ Pa

$$\Delta P = \frac{2L\tau}{H} = \frac{2 \times 10 \times 1.5 \times 10^5}{2} = 1.5 \text{ MPa}$$

$$\text{Power} = PQ$$

$$= 1.5 \times 10^6 \times 5.6 \times 10^{-6}$$

$$= 8.4 \frac{\text{Nm}}{\text{s}} = 8.4 \text{ W}$$

From flow curves, at $\dot{\gamma} = 150$

$$G = 3.05 \times 10^4 \text{ Pa}$$

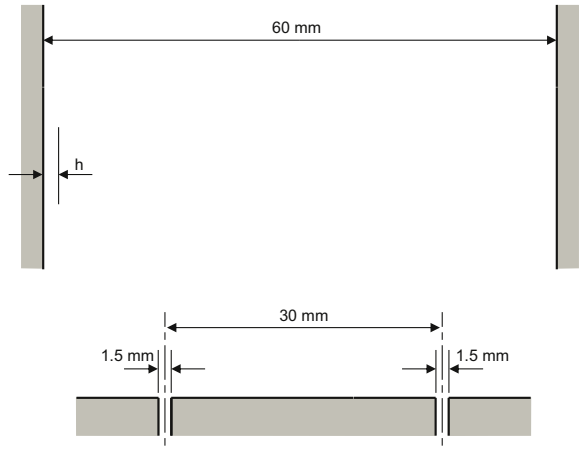
So,

$$\gamma_R = \tau / G = 4.92$$

From graphs for swell ratio $B_{ST} = 1.41$, $B_{SH} = 1.99$

Thus approximate dimensions of extrudate would be 42.3 mm deep × 21.2 mm wide × 3.98 mm thick.

(5.10) $\dot{\gamma} = \dfrac{6Q}{TH^2}$



$$= \frac{6 \times 46 \times 10^{-3}}{(\pi \times 30)(1.5 \times 10^{-3})^2}$$

$$= 1.3 \times 10^3 \text{ s}^{-1}$$

So from the flow curves, at $\dot{\gamma} = 1300 \ \ s^{-1}$

$$\tau = 2.6 \times 10^5 \text{ Pa}$$

$$G = 5 \times 10^4 \text{ Pa}$$

$$\gamma_R = \frac{\tau}{G} = 5.2$$

From swell ratio curves

at $\gamma_R = 5.2$, $B_{ST} = 1.41$, $B_{SH} = 2$

$$h = B_{ST}^2 hd \left(\frac{D_d}{D_m}\right)$$

$$h = (1.41)^2(1.5)\left(\frac{30}{60}\right) = 1.5 \text{ mm}$$

(5.11) From the flow curves, $\eta_0 = 3 \times 10^4$ and $n = 0.33$

$$L = \left(\frac{n+1}{2n+1}\right)^{n/(n+1)} \left(\frac{P}{\eta_0}\right)^{1/(n+1)} \left(\frac{H}{2}\right)^{n/(n+1)}$$

$$L = \left(\frac{1.33}{1.66}\right)^{0.33/1.33} \left(\frac{100 \times 10^6}{3 \times 10^4}\right)^{1/1.33} \left(\frac{1}{2}\right)^{0.33/1.33} = 355 \ \ \text{mm}$$

(5.12) $L = \left(\frac{P}{\eta_0}\right)^{1/(n+1)} \left(\frac{H}{2}\right) 6t_f \left(\frac{n}{4n+1}\right) \ \left(\frac{n}{3n+1}\right) \ \left(\frac{n(n+1)}{(2n+1)^2}\right)^{n/(n+1)}$

$$\Delta T = \frac{T_3 - T_2}{T_1 - T_2} = \frac{128 - 60}{170 - 60} = 0.62 \rightarrow F_0 = 0.295 = \frac{\alpha t_f}{x^2}$$

So

$$t_f = \frac{0.295 \times 0.5^2 \times 10^{-6}}{10^{-7}} = 0.74 \quad \text{seconds}$$

$$L = \left(\frac{100 \times 10^6}{3 \times 10^4}\right)^{\frac{1}{1.33}} \left(\frac{1}{2}\right) \left(\frac{6 \times 0.74 \times 0.33^3 \times 1.33}{1.32 \times 1.99 \times 1.66^2}\right)^{\frac{0.33}{1.33}} = 80.6 \quad \text{mm}$$

For a Newtonian fluid, $n = 1$

$$L = 0.13\left(\frac{Pt_f}{\eta}\right)^{1/2} H = 0.13\left(\frac{100 \times 10^6 \times 0.74}{1.2 \times 10^2}\right)^{1/2} = 101.9 \quad \text{mm}$$

(5.13) $$\Delta T = \frac{120 - 5}{230 - 50} = 0.39$$

So,

$$F_0 = 0.48 = \frac{\alpha t}{x^2} \quad \text{where} \quad x = 1 \text{ mm}$$

$$t = \frac{0.48 \times 1 \times 10^{-6}}{1 \times 10^{-7}} = 4.8 \quad \text{seconds}$$

(5.14) $$\Delta T = \frac{T_3 - T_2}{T_1 - T_2} = \frac{90 - 30}{230 - 30} = 0.3$$

$$F_0 = 0.58 = \frac{\alpha t}{x^2}$$

$$t = \frac{0.58 \times (2 \times 10^{-3})^2}{1 \times 10^{-7}} = 23.2 \quad \text{s}$$

for the runner, ΔT also equals 0.3 so $F_0 = 0.29$. To cause freeze-off in 23.2 seconds then

$$0.29 = \frac{1 \times 10^{-7} \times 23.2}{R^2}$$

$$= 2.83 \quad \text{mm}, \quad \text{runner diameter} = 5.66 \ \text{mm}$$

(5.15) Since the power law equations are going to be used rather than the flow curves, it is necessary to use the true shear rates.
i.e.

$$\dot{\gamma} = \left(\frac{3n+1}{4n}\right) \frac{4Q}{\pi R^3} = \left(\frac{3(0.35)+1}{4(0.35)}\right)\left(\frac{4 \times 5 \times 10^{-5}}{\pi \times 1.5^3 \times 10^{-9}}\right)$$

$$= 2.76 \times 10^4 \text{s}^{-1}$$

Now

$$\tau = \tau_0 \dot{\gamma}^n = 40 \times 10^3 \left(2.76 \times 10^4\right)^{0.35} = 1.43 \ \text{MPa}$$

Now

$$\tau = \frac{PR}{2L} \ \ So \ \ P = \frac{2L\tau}{R} = \frac{2 \times 25 \times 1.43}{1.5} = 47.8 \ \text{MPa}$$

(5.16) Volume flow rate,

$$Q = \frac{\pi R^2 H}{t} = \frac{\pi(60 \times 10^{-3})^2 (3 \times 10^{-3})}{1} = 3.39 \times 10^{-5} \ \text{m}^3/\text{s}$$

From Fig. 5.3, $\eta_0 = 3 \times 10^4$ Pa.s (i.e. η at $\dot{\gamma} = 1 \ \text{s}^{-1}$) and $n = 0.33$.
So from illustrative example (5.14)

$$P = Q^n \left(\frac{2n+1}{2n\pi}\right)^n \frac{\eta_0 (2)^{n+1} R^{1-n}}{(H)^{2n+1}(1-n)}$$

$$= 1.05 \quad \text{MPa}$$

(5.17) $\Delta T = \dfrac{114-50}{170-50} = 0.531 \rightarrow F_0 = 0.35 = \dfrac{\alpha t}{x}$

$$x = \sqrt{\frac{1 \times 10^{-7} \times 3}{0.35}} = 0.926 \quad \text{mm}$$

$$\text{gate depth} = 2x = 1.85 \quad \text{mm}$$

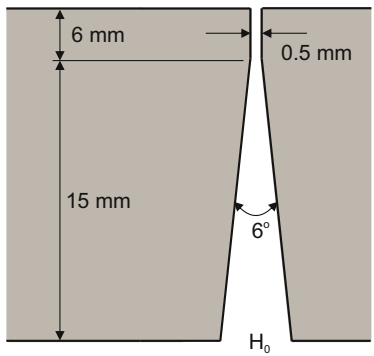
Now

$$\dot{\gamma} = \frac{6Q}{TH^2} \rightarrow T = \frac{6Q}{\dot{\gamma}H^2} = \frac{6 \times 4 \times 10^{-6} \times 10^9}{1000 \times 3 \times 1(1.85)^3} = 1.26 \quad \text{mm}$$

From Fig. 5.3 at $\dot{\gamma} = 1000\ \text{s}^{-1}$, $\tau = 2.9 \times 10^5$ Pa

$$\tau = \frac{PH}{2L} \quad \text{so} \quad P = \frac{2L\tau}{H} = \frac{2 \times 0.6 \times 2.9 \times 10^5}{1.85} = 0.19 \quad \text{MPa}$$

(5.18) $H_0 = H_1 + 2L \tan \alpha$



$$H_0 = 0.5 + 30 \tan 3^\circ = 2.07 \quad \text{mm}$$

$$T = \pi D = 40\pi = 126 \quad \text{mm}$$

$$\dot{\gamma}_1 = \frac{6Q}{TH^2} = \frac{6 \times 10 \times 10^{-6}}{126 \times 10^{-3}(0.5 \times 10^{-3})^2} = 1910 \text{ s}^{-1}$$

$$\dot{\gamma}_3 = 1910\left(\frac{0.5}{2.07}\right)^2 = 111 \text{ s}^{-1}, \quad \dot{\varepsilon}_3 = \frac{1}{3}(111)\tan 3^\circ = 2 \text{ s}^{-1} \rightarrow \sigma_3$$

$$= 0.45 \text{ MPa}$$

$$\dot{\varepsilon}_2 = \frac{1}{3}\dot{\gamma}_2 \tan\alpha = \frac{1}{3(1910)\tan 3^\circ} = 33 \text{ s}^{-1} \rightarrow \sigma_2 = 7.5 \text{ MPa}$$

For the tapered section,

$$P_0 = \frac{4\dot{\gamma}(n\lambda)^{1/2}}{(3n+1)} = \frac{4 \times 111\left(1150 \times 2.25 \times 10^5\right)^{1/2}}{1.99}$$

$$= 3.6 \text{ MPa}$$

$$P_s = \frac{\tau_1}{2_n \tan\alpha}\left(1 - \left(\frac{H_1}{H_0}\right)^{2n}\right) = \frac{3.6 \times 10^5}{0.66 \tan 3^\circ}\left(1 - \left(\frac{0.5}{2.07}\right)^{0.66}\right)$$

$$= 6.3 \text{ MPa}$$

$$P_E = \frac{1}{2}\sigma_1\left(1 - \left(\frac{H_1}{H_0}\right)^2\right) = \frac{1}{2} \times 7.5\left(1 - \left(\frac{0.5}{2.07}\right)^2\right)$$

$$= 3.53 \text{ MPa}$$

Parallel Section,

$$P_s = \frac{2L\tau}{H} = \frac{2 \times 6 \times 10^{-3} \times 3.6 \times 10^5}{0.5 \times 10^{-3}} = 8.6 \text{ MPa}$$

$$\text{Total Pressure loss} = 22.1 \text{ MPa}$$

At exit,

$$\dot{\gamma} = 1910 \quad \text{So} \quad \tau = 3.6 \times 10^5 \text{ Pa}, G = 5 \times 10^4 \text{ Pa}$$

So

$$\gamma_R = \frac{36}{.5} = 7.2 \rightarrow B_H = 2.43, B_T = 1.56$$

So wall thickness = 1.21 mm, diameter = 62.4 mm

(5.19) Assuming no swelling at the die exit

$$\dot{\gamma} = \frac{6V}{H} = \frac{6 \times 15 \times 10^{-3}}{0.75 \times 10^{-3}} = 120\ \text{s}^{-1}$$

From the flow curves, $\tau = 1.3 \times 10^5$ Pa, $G = 3 \times 10^4$ Pa

So $\gamma_R = \tau/G = 4.4$ and so $B_H = 1.85$, $B_T = 1.36$

$$\therefore \quad \text{New } H = \frac{0.75 \times 10^{-3}}{1.85} = 0.41 \times 10^{-3}\ \text{m}$$

$$\text{New} \quad V = 15 \times 10^{-3} \times 1.85 \times 1.36 = 37.7 \times 10^{-3}\ \text{m/s}$$

So,

$$\dot{\gamma} = \frac{6. \times 37.7 \times 10^{-3}}{0.41 \times 10^{-3}} = 552\ \text{s}^{-1}$$

This gives

$$\tau = 2.2 \times 10^5\ \text{Pa},\ G = 4 \times 10^4\ \text{Pa}$$

So,

$$\gamma_R = 5.5 \quad \text{and} \quad B_H = 2.08,\ B_T = 1.455$$

$$\text{New} \quad H = \frac{0.75 \times 10^{-3}}{2.08} = 0.36 \times 10^{-3}\ \text{m}$$

$$\text{New} \quad V = 15 \times 2.08 \times 1.455 \times 10^{-3} = 45.39 \times 10^{-3}\ \text{m/s}$$

So,

$$\dot{\gamma} = \frac{6 \times 45.39}{0.36} = 756.6\ \text{s}^{-1}$$

And so on until the iteration converges, at which point

$$H = 0.405 \times 10^{-3}\ \text{m},\ D = 29.2\ \text{mm}$$

(5.20) $\dot{\gamma} = \dfrac{6Q}{TH_1} = \dfrac{6 \times 100 \times 10^{-6}}{\pi(250 \times 10^{-3})(1 \times 10^{-3})^2} = 764 \ \ \mathrm{s}^{-1}$

so from flow curves $\tau = 2.4 \times 10^5$ Pa

$$P_{s1} = \frac{2L\tau}{H} = \frac{2 \times 5 \times 2.4 \times 10^5}{1} = 2.4 \ \ \mathrm{MPa}$$

$$H_3 = H_2 + 2L \tan \alpha \ \left(\text{where} \ \ \alpha = \frac{1}{2}\text{angle} \right)$$

$$H_3 = 1 + 2(12)\tan(1)^\circ = 1.42 \ \ \mathrm{mm}$$

At

$$B_2, \dot{\bar{\gamma}} = 764 s^{-1}, \dot{\varepsilon} = \frac{1}{3}\dot{\gamma} \tan \alpha$$

$$= \frac{1}{3}(764)\tan(1) = 4.45 \ \ \mathrm{s}^{-1}$$

So

$$P_{s_2} = \frac{\tau_2}{2n \tan \alpha}\left[1 - \left(\frac{H_2}{H_3}\right)^{2n}\right]$$

$$= \frac{2.4 \times 10^5}{2(0.33)\tan(1)}\left[1 - \left(\frac{1}{1.42}\right)^{0.66}\right]$$

$$= 4.3 \ \ \mathrm{MPa}$$

$$P_{E_2} = \frac{\sigma_2}{2}\left[1 - \left(\frac{H_2}{H_3}\right)^2\right]$$

$$= \frac{1 \times 10^6}{2}\left[1 - \left(\frac{1}{1.42}\right)^2\right]$$

$$= 0.25 \ \ \mathrm{MPa}$$

$$\text{Total Pressure loss} = 6.95 \quad \text{MPa}$$

At die exit,

$$\dot{\dot{\gamma}} = \frac{6Q}{TH^2} = \frac{6 \times 100 \times 10^{-6}}{\pi(250 \times 10^{-3}) \times (1 \times 10^{-3})^2}$$

$$= 764 \quad \text{s}^{-1}$$

From flow curves,

$$\tau = 2.4 \times 10^5 \ \text{Pa}$$

$$G = 4.1 \times 10^4 \ \text{Pa}$$

$$\gamma_R = \frac{\tau}{G} = \frac{2.4 \times 10^5}{4.1 \times 10^4} = 5.85$$

From swelling ratio curves

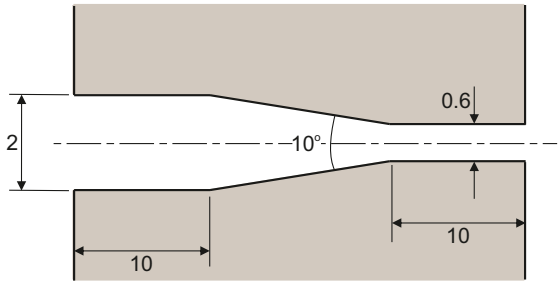
$$B_{SH} = 2.19 \quad \text{and} \quad B_{ST} = 1.48$$

So

$$\text{Bubble thickness} = 1 \times 2.19 = 2.19 \text{ mm}$$

$$\text{Bubble diameter} = 250 \times 1.48 = 370 \text{ mm}$$

(5.21) $\dot{\gamma}_1 = \dfrac{6Q}{TH^2} = \dfrac{6 \times 4 \times 10^{-6}}{10^{-2}(2 \times 10^{-3})^2}$



$$= 600 \ \ \text{s}^{-1}$$

$$\dot{\gamma}_4 = 6667 \ \ \text{s}^{-1}$$

$$\dot{\varepsilon}_2 = \frac{1}{3}\dot{\gamma}_2 \tan \alpha$$

$$= \frac{1}{3}(600)\tan 5^\circ$$

$$= 17.5 \ \ \text{s}^{-1}$$

$$\dot{\varepsilon}_3 = 194 \ \ \text{s}^{-1}$$

$$P_0 = \frac{4\dot{\gamma}(\eta\lambda)^{1/2}}{3n+1} = \frac{4 \times 600\left(4 \times 10^2 \times 2.25 \times 10^5\right)^{1/2}}{1.99} = 11.4 \ \ \text{MPa}$$

$$P_{s1} = \frac{2L\tau}{H} = \frac{2 \times 10^{-2} \times 2.4 \times 10^5}{2 \times 10^{-3}} = 2.4 \ \ \text{MPa}$$

$$P_{s2} = \frac{\tau_3}{2n \tan \alpha}\left(1 - \left(\frac{H_3}{H_2}\right)^{2n}\right) = \frac{5.7 \times 10^5}{0.66 \tan 5}\left(1 - \left(\frac{0.6}{2}\right)^{0.66}\right) = 5.4 \ \ \text{MPa}$$

$$P_E = \frac{1}{2}\sigma_3\left(1 - \left(\frac{H_3}{H_2}\right)^2\right) = \frac{1}{2}\left(43.6 \times 10^6\right)\left(1 - \left(\frac{0.6}{2}\right)^2\right) = 19.8 \ \ \text{MPa}$$

$$P_{s3} = \frac{2L\tau}{H} = \frac{2 \times 10 \times 10^{-3} \times 5.7 \times 10^5}{0.6 \times 10^{-3}} = 19 \ \ \text{MPa}$$

Total pressure loss = 58 MPa

(5.22) (a) As shown in the text, the flow rate of a power law fluid in a circular section is given by

$$Q = \left(\frac{n+1}{3n+1}\right)\ \pi R^2\left(\frac{n}{n+1}\right)\ \left(\frac{P}{2\ell\eta_0}\right)^{1/n} R^{(n+1)/n} \tag{1}$$

Now for a volume flow rate, Q, the volume in any increment of time, *dt, is* Qdt and this is equal to $\pi R^2 d\ell$

$$Qdt = \pi R^2 d\ell$$

So from Eq. (1)

$$\pi R^2 d\ell = \left(\frac{n}{3n+1}\right)\ \pi R^2\left(\frac{P}{2\ell\eta_0}\right)^{1/n} R^{(n+1)/n} dt$$

$$\ell^{1/n} d\ell = \left(\frac{n}{3n+1}\right)\ \left(\frac{P}{2\eta_0}\right)^{1/n} R^{(n+1)/n} dt$$

$$\frac{n\ell}{(n+1)} = \left(\frac{n}{3n+1}\right)\ \left(\frac{P}{2\eta_0}\right)^{1/n} R^{(n+1)/n} t$$

So

$$\ell = \left(\frac{n+1}{3n+1}\right)^{n/n+1}\left(\frac{P}{2\eta_0}\right)^{1/(n+1)} R t^{n/(n+1)}$$

(b) If the cross-section is freezing-off then the radius of the channel will be changing with time and is given by

$$r = R\ \left(1 - \left(\frac{t}{t_f}\right)^{1/3}\right)$$

So since

$$\frac{d\ell}{dt} = \left(\frac{n}{3n+1}\right)\ \left(\frac{P}{2\ell\eta_0}\right)^{1/n} r^{(n+1)/n}$$

i.e.

$$\frac{d\ell}{dt} = \left(\frac{n}{3n+1}\right)\ \left(\frac{P}{2\ell\eta_0}\right)^{1/n}\left(R\ \left(1 - \left(\frac{t}{t_f}\right)^{1/3}\right)\right)^{(n+1)/n}$$

So

$$\ell^{1/n} d\ell = \left(\frac{n}{3n+1}\right)\ \left(\frac{P}{2\ell n_o}\right)^{1/n} R^{(n+1)/n}\left(\left(1 - \left(\frac{t}{t_f}\right)^{1/3}\right)\right)^{(n+1)/n} dt$$

$$\frac{n\ell^{(n+1)/n}}{(n+1)} = \left(\frac{n}{3n+1}\right)\left(\frac{P}{2\eta_0}\right)^{1/n} R^{(n+1)/n}\left(6t_f\left(\frac{n}{4n+1}\right)\left(\frac{n}{3n+1}\right)\left(\frac{n}{2n+1}\right)\right)$$

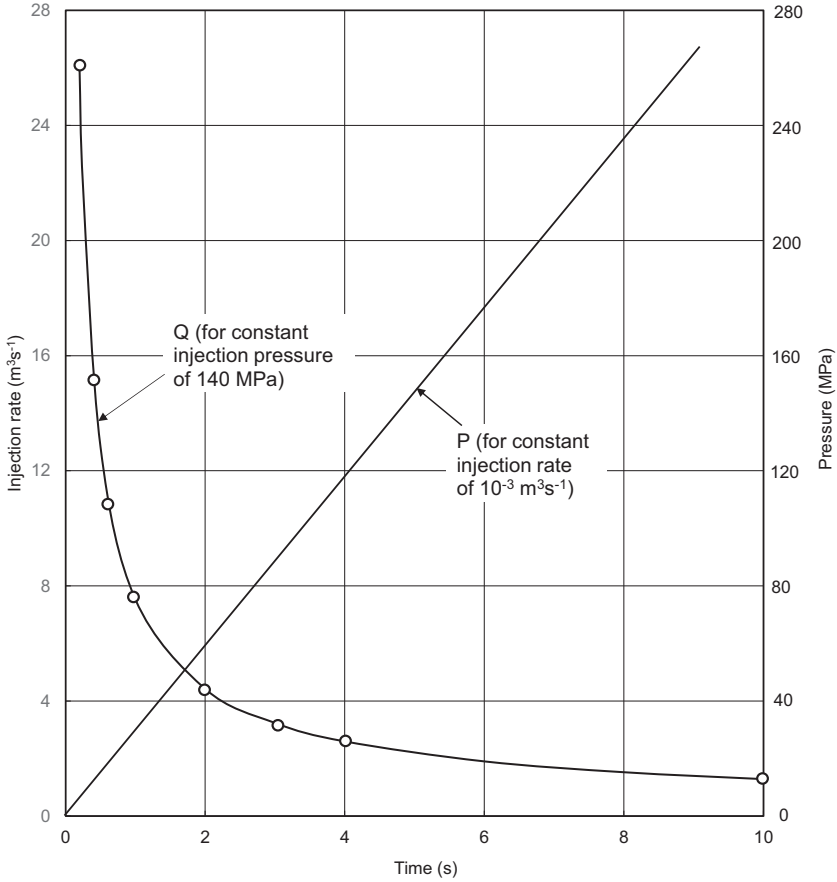
$$\ell = \left(\frac{P}{2\eta_0}\right)^{1/(n+1)} R\left(6t_f\left(\frac{n}{4n+1}\right)\left(\frac{n(n+1)}{(3n+1)^2}\right)\left(\frac{n}{2n+1}\right)\right)^{n/(n+1)}$$

(5.23) From the equations in the previous example

$$\frac{\ell f}{\ell} = \left(6\left(\frac{n}{4n+1}\right)\left(\frac{n}{3n+1}\right)\left(\frac{n}{2n+1}\right)\right)^{n/(n+1)}$$

For a Newtonian fluid $n = 1$ so $\ell_f/\ell = 0.316$
For a Non-Newtonian fluid, $n = 0.3\ell_f/\ell = 0.424$

(5.24) (a) As shown in the previous examples, if the pressure is held constant



$$\ell = \left(\frac{n+1}{3n+1}\right)^{n/(n+1)} \left(\frac{P}{2\eta_0}\right)^{1/(n+1)} Rt^{n/(n+1)}$$

but

$$Q = \left(\frac{n+1}{3n+1}\right)\ \pi R^2 \left(\frac{n}{n+1}\right)\ \left(\frac{P}{2\ell\eta_0}\right)^{1/n} R^{(n+1)/n}$$

So substituting for ℓ gives

$$Q = \left(\frac{n+1}{3n+1}\right)^{n/(n+1)} \pi R^3 \left(\frac{n}{n+1}\right)\ \left(\frac{P}{2\eta_0 t}\right)^{1/(n+1)}$$

$$= \left(\frac{1.3}{1.9}\right)^{0.3/1.3} \pi\left(5\times10^{-3}\right)^3 \left(\frac{0.3}{1.3}\right)\ \left(\frac{140\times10^6}{2\times10^4 t}\right)^{1/1.3} = \frac{7.53\times10^{-5}}{t^{0.769}}$$

(b) As shown in the text for the flow of a power law fluid in a capillary

$$Q = \left(\frac{n+1}{3n+1}\right)\ \left(\frac{\dfrac{dR}{d\ell}}{2\eta_0}\right)^{1/n} R^{(n+1)/n}\pi R^2\left(\frac{n}{n+1}\right)$$

$$2\eta_0 Q^n = \left(\frac{n}{3n+1}\right)^n \left(\frac{dP}{d\ell}\right)\pi^n R^{3n+1}$$

but

$$Qdt = \pi R^2 d\ell \quad So \quad d\ell = (Qdt)/\pi R^2$$

$$\therefore \quad 2\eta_0 Q^n = \left(\frac{\pi n}{3n+1}\right)^n \frac{dP}{Qdt}\bullet\pi R^2 \bullet R^{3n+1}$$

$$2\eta_0 Q^n dt = \left(\frac{\pi n}{3n+1}\right)^n \pi R^{3n+3} \cdot dP$$

which may be integrated to give

$$P = \frac{2\eta_0 Q^{n+1}}{\pi R^{3n+3}} \left(\frac{3n+1}{\pi n}\right)^n t = \frac{2 \times 10^4 \left(7 \times 10^{-5}\right)^{1.3}}{\pi (5 \times 10^{-3})^{3.9}} \left(\frac{1.9}{0.3\pi}\right)^{0.3} t$$

$$= (29.36t) \text{ MPa}$$

The variations of Q and P in each case are shown in the attached graph.

(5.25) Volume of cavity $= 50 \times 10 \times 3 \times 10^{-9}$ m^3

So time to fill this $= 1.5$ seconds

Gate: volume $= 2 \times 4 \times 0.6 \times 10^{-9}$ m^3

So time to pass through $= 4.8 \times 10^{-3}$ seconds

$$\dot{\gamma} = \frac{6Q}{TH^2} = \frac{6 \times 10^{-6} \times 10^9}{4 \times 2^2} = 375 \text{ s}^{-1}$$

From flow curves, $\tau = 2.1 \times 10^5$ Pa

$$\therefore \quad P = \frac{2L\tau}{H} = \frac{2 \times 0.6 \times 2.1 \times 10^5}{2} = 0.13 \text{ MPa}$$

Runner: volume $= \pi(4)^2 \times 20 \times 10^{-9}$ m^3

time to fill this $= 1$ second

$$\dot{\gamma} = \frac{4Q}{\pi R^3} = \frac{4 \times 1 \times 10^{-6} \times 10^9}{\pi (4)^3} = 20 \text{ s}^{-1}$$

So

$$\tau = 7.6 \times 10^4 \text{ Pa} \rightarrow P = \frac{2 \times 20 \times 7.6 \times 10^4}{5} = 0.6 \text{ Pa}$$

Sprue, etc: time to pass through $= 1$ second

pressure loss $= 0.6$ MPa

Total time to fill $= 1 + 1 + 1.5 = 3.5$ seconds

Now, as shown in previous example, for a constant flow rate situation the pressure build-up in the machine is given by

$$P = \frac{2\eta_0 Q^{n+1}}{\pi R^{3n+3}} \left[\frac{3n+1}{\pi n}\right]^n t$$

For P_E, $n = 0.33$ and $\eta_0 = 3 \times 10^4$ (from flow curves)

$$P = \frac{2 \times 3 \times 10^4 \left(1 \times 10^{-6}\right) 1.33}{\pi (4 \times 10^{-3})^{3.99}} \left[\frac{1.99}{0.33\pi}\right]^{0.33} \quad t \; = \; 1.34 \times 10^6 \; \; t$$

Therefore after 3.5 seconds $P = 4.7$ MPa.

But Pressures losses $= (0.6 + 0.6 + 0.13) = 1.33$ MPa

So packing pressure $= 3.37$ MPa

(5.26) The temperature gradient,

$$\Delta T = \frac{T_t - T_m}{T_i - T_m}$$

$$\Delta T = \frac{70 - 20}{190 - 20} \; = \; 0.29$$

From Fig. 5.23,

$$F_0 \; = 0.29 \; = \frac{\alpha t}{x^2}$$

$$t = \frac{0.29 \times (1.5 \times 10^{-3})^2}{1 \times 10^{-7}} \; = \; 6 \text{ s}$$

Since the haul-off speed is 0.4 m/s, the water bath would need to be at least (0.4×6) m long i.e. 2.4 m.

(5.27) Using the equation derived in the text:

$$\frac{L}{H} = \frac{1}{2}\left(\frac{P}{\eta_0}\right)^{\frac{1}{n+1}} \left[6t_f \left(\frac{n}{4n+1}\right)\left(\frac{n}{3n+1}\right)\left(\frac{n(n+1)^2}{(2n+1)}\right)\right]^{\frac{n}{n+1}}$$

where the freeze-off time may be calculated from

$$t_f \; = \frac{4x^2}{\pi^2 \alpha} \ln\left[\frac{4}{\pi}\left(\frac{T_m - T_M}{T_f - T_M}\right)\right]$$

Using the data given, the flow ratios will be

Material	*Flow Ratio (L/H)*
LDPE	240
polypropylene	220
polystyrene	165
PVC	60
POM	121
acrylic	86
polycarbonate	32
Nylon 66	30
ABS	123

Note the η_0 and n data from Table 5.2 has been used even though the temperatures quoted are not always the same as the moulding temperature.

(5.28)
$$h = B_{ST}^3 h_d \left(\frac{D_d}{D_m}\right)$$

So
$$B_{ST} = \sqrt[3]{\frac{2.5 \times 100}{2 \times 40}} = 1.46$$

From Fig. 5.11 at $B_{ST} = 1.46$, $\gamma_R = 5.5 = \tau/G$
From the flow curves the value of shear stress to give $\tau/G = 5.5$ is $\tau = 2.25 \times 10^5$ Pa (also $G = 4.1 \times 10^4$ Pa). From the flow curves at $\tau = 2.25 \times 10^5$ Pa,

$$\dot{\gamma} = 620 = \frac{6Q}{TH^2} \rightarrow Q = 52 \times 10^{-6} \text{m}^3/\text{s} = 147 \text{ kg/hour}$$

$$P = \frac{2\sigma h}{D_m} = \frac{2 \times 2.5 \times 4 \times 10^6}{100} = 0.2 \times 10^6 \text{ Pa}$$

So the suggested pressure would cause melt fracture.

(5.29) Stress $= \rho L = 730 \times 9.81 \times 0.4 = 2.86 \times 10^4$ Pa
From flow curves $\lambda = 2.25 \times 10^5$ and $E = 4.6 \times 10^4$
So characteristic time $= \lambda/E = 4.95$
Also

$$\varepsilon = \rho L\left(\frac{1}{2E}+\frac{t}{\lambda}\right) = 730 \times 9.81 \times 0.4\left[\frac{1}{2 \times 4.6 \times 10^4}+\frac{1}{2.25 \times 10^5}\right] = 0.044$$

So

$$\delta L = 0.044 \times 0.4 = 0.017 \text{ m} = 17 \text{ mm}$$

(5.30) For the overall change of temperature and pressure

$$\eta / \eta_R = 10^{A\Delta T+B\Delta P}$$

For acrylic,

$$\eta / \eta_R = 10^{[(28.32\times-40)+(9.54\times-50)]10^{-3}} = 4.53$$

Similarly for the others $\eta/\eta_R = 0.95$, 1.415, 2.03 and 1.28.
Also for

$$\eta / \eta_R = 1, A\Delta T = -B\Delta P$$

For acrylic

$$\frac{\Delta P}{\Delta T} = \frac{28.32}{9.54} = 2.97 \text{ MPa}/^oC$$

Similarly for the others $(\Delta P)/(\Delta T) = 1.17$, 1.87, 3.07 and 1.93.

Appendix A

Structure of plastics

A.1 Structure of long molecules

Polymeric materials consist of long chain-like molecules. Their unique structural configuration affects many of their properties and it is useful to consider in more detail the nature of the chains and how they are built up. The simplest polymer to consider for this purpose is polyethylene. During the polymerisation of the monomer ethylene, the double bond (see Fig. A.1) is opened out enabling the carbon single bonds to link up with neighbouring units to form a long chain of CH_2 groups as shown in Fig. A.2. This is a schematic representation and conceals the fact that the atoms are joined to each other at an angle as shown in Fig. A.3.

In all the groups along the chain, the bond angle is fixed. It is determined by considering a carbon atom at the centre of a regular tetrahedron and the four covalent bonds are in the directions of the four corners of the tetrahedron. This sets the bond angle at 109° 28′ as shown in Fig. A.4 and this is called the tetrahedral angle.

For a typical molecular weight of 300,000 there are about 21,000 carbon atoms along the backbone of the chain. Since the length of the C-C bond is 0.154×10^{-9} m the dimensions of an extended zig-zag chain would be about 2700 mm long and 0.3 mm diameter. This gives an idea of the long thread-like nature of the molecules. It must be remembered, however, that in any

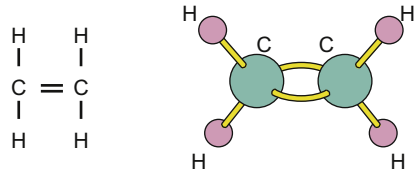


FIG. A.1 Ethylene monomer.

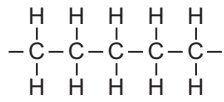


FIG. A.2 Polyethylene molecule.

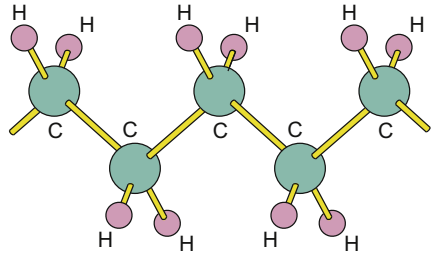


FIG. A.3 Polyethylene molecule.

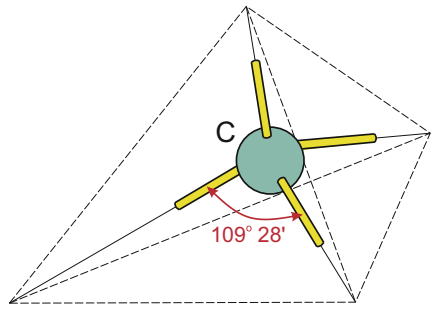


FIG. A.4 Tetrahedral angle.

particular polymer, not all molecular chains have the same length. The length of each chain depends on a series of random events during the polymerisation process. One chain may grow rapidly in a region with an abundant supply of monomer whereas other chains stop growing prematurely as the supply of monomer dries up. This means that a particular sample of synthetic polymer will not have a unique value for its molecular weight. Instead statistical methods are used to determine an average molecular weight and the molecular weight distribution.

A.2 Conformation of the molecular chain

The picture presented so far of the polyethylene chain being of a linear zig-zag geometry is an idealised one. The conformation of a molecular chain is in fact random provided that the bond tetrahedral angle remains fixed. This is best illustrated by considering a piece of wire with one bend at an angle of 109° 28′ as shown in Fig. A.5.

If the horizontal arm is rotated about its axis, the other arm will form a cone of revolution. On the polyethylene molecule, the bent wire is similar to the carbon backbone of the chain with carbon atoms at positions 1, 2 and 3. Due to the rotation of the bond 2−3, atom 3 may be anywhere around the base of the cone of revolution. Similarly, the next bond will form a cone of revolution with atom 3 as the apex and atom 4 anywhere around the base of this

cone. Fig. A.6 illustrates how the random shape of the chain is built up. The hydrogen atoms have been omitted for clarity.

In practice the picture can take on a further degree of complexity if there is chain branching. This is where a secondary chain initiates from some point along the main chain as shown in Fig. A.7. In rubbers and thermosetting materials these branches link up to other chains to form a three-dimensional network.

So far, the structure of polymers has been described with reference to the material with the simplest molecular structure, i.e. polyethylene. The general principles described also apply to other polymers and the structures of several of the more common polymers are shown in Fig. A.8.

It will be seen from this that a variety of atoms can be present along the carbon backbone and indeed carbon atoms may also be replaced, as in the cases of nylon, acetal and PLA. During polymerisation it is possible to direct the way in which monomers join on to a growing chain. This means that side groups (X) may be placed randomly (**atactic**) or symmetrically along one side

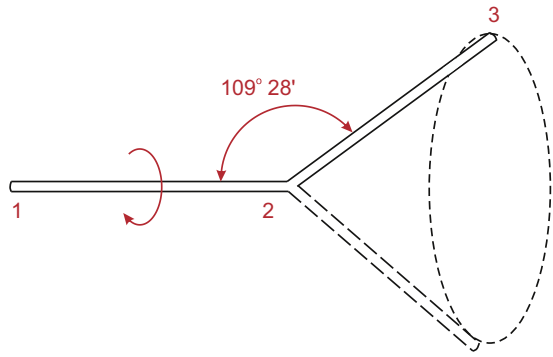


FIG. A.5 Rigid joint at fixed angle.

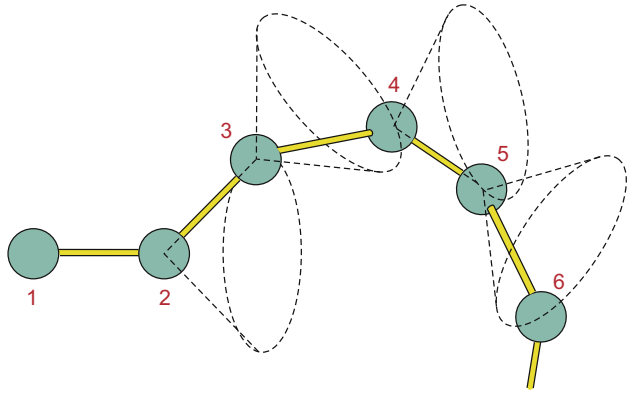


FIG. A.6 Random conformation of carbon backbone on molecular chain.

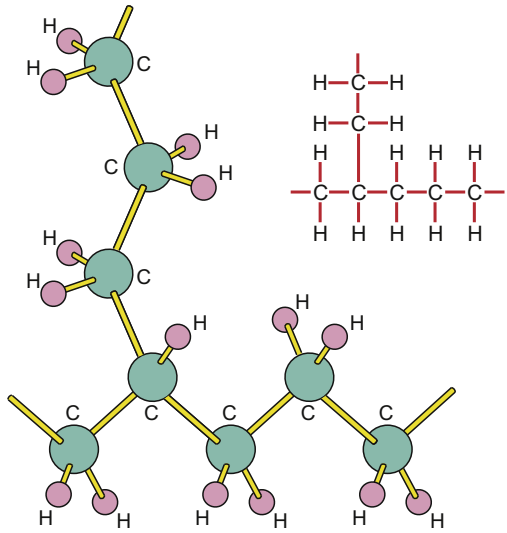


FIG. A.7 Chain branch in polyethylene.

of the chain (**isotactic**) or in regular alternating pattern along the chain **(syndiotactic)** as shown in Fig. A.9. A good example of this is polypropylene (see Fig. A.10) which in the atactic form is an amorphous material of little commercial value but in the isotactic form is an extremely versatile large tonnage plastic material.

Polymers can also be produced by combining two or more different monomers in the polymerisation process. If two monomers are used the product is called a **copolymer** and the second monomer is usually included in the reaction to enhance the properties of the polymer produced by the first monomer alone. It is possible to control the way in which the monomers (A and B) link up and there are four main configurations which are considered useful. These are:

(1) Alternating — A — B — A — B — A — B —

(2) Random — A — A — B — A — A — A — B — B — A —

(3) Block — A — A — A — B — B — B — B — B — B — A — A —

(4) Graft

```
        B
        |
— A — A — A — A — A — A — A —
          |       |
          B       B
          |       |
                  B
                  |
                  B
```

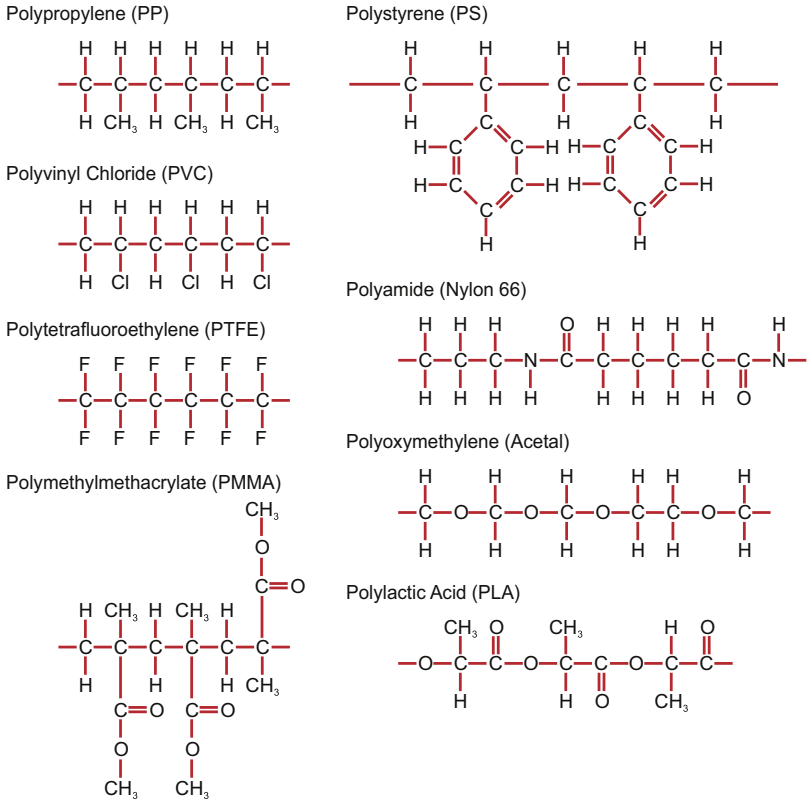


FIG. A.8 Chain structures of common polymers.

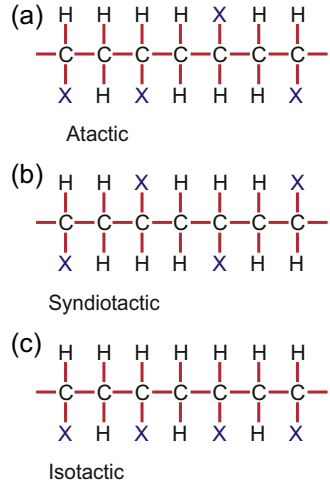


FIG. A.9 Possible molecular structures.

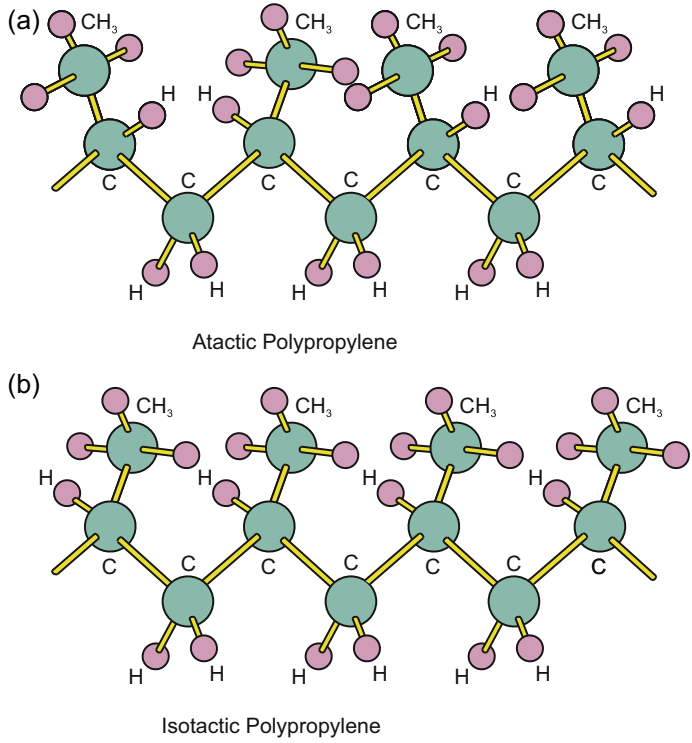


FIG. A.10 Polypropylene structures.

A.3 Arrangement of molecular chains

A picture of an individual molecular chain has been built up as a long randomly twisted thread-like molecule with a carbon backbone. It must be realised, however, that each chain must co-exist with other chains in the bulk material and the arrangement and interaction of the chains has a considerable effect on the properties of the material. Probably the most significant factor is whether the material is *crystalline* or *amorphous.* At first glance it may seem difficult to imagine how the long randomly twisted chains could exist in any uniform pattern. In fact, X-ray diffraction studies of many polymers show sharp features associated with regions of three-dimensional order (crystallinity) and diffuse features characteristic of disordered (amorphous) regions. By considering the polyethylene molecule again it is possible to see how the long chains can physically co-exist in an ordered crystalline fashion. This is illustrated in Fig. A.11.

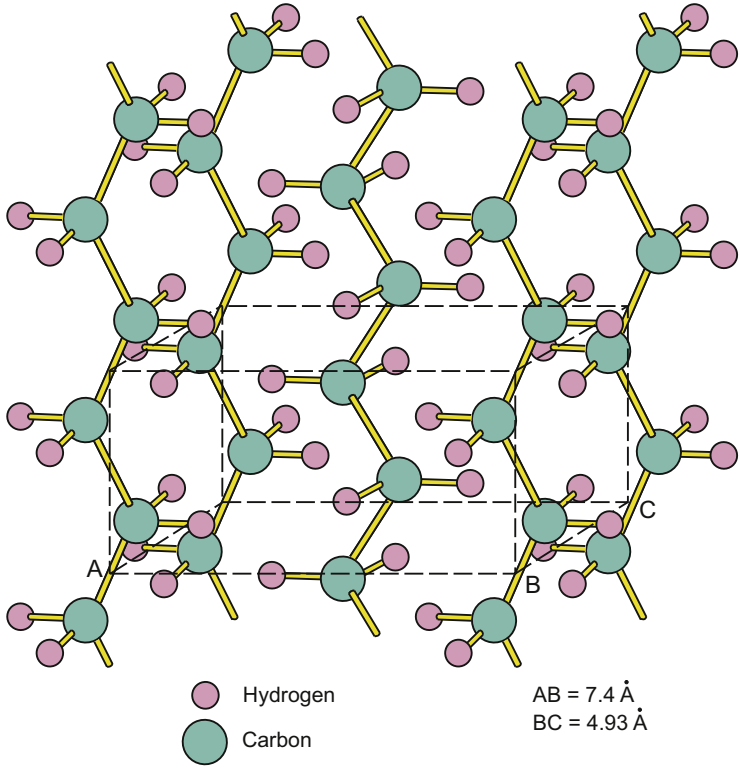


FIG. A.11 Crystalline structure of polyethylene.

During the 1940s it was proposed that partially crystalline polymers consisted of regions where the molecular chains were gathered in an ordered fashion whereas adjacent regions had a random distribution of chains. The crystalline regions were considered to be so small that an individual chain could contribute to both crystalline and amorphous areas as shown in Fig. A.12. This was known as the **Fringed Micelle Model** and was generally accepted until the late 1950s when for the first time single polymer crystals were prepared from solution. These crystals took the form of thin platelets, their thickness being about 10 mm and their lateral dimensions as large as 0.01 mm. The most important discovery from the growth of these single crystals was that the chains were aligned perpendicular to the flat faces of the platelet. Since the length of an individual chain could be 1000 times greater than the thickness of the platelet the only conclusion was that the chains were folded.

Appropriately, this was called the **Folded Chain Theory** and is illustrated in Fig. A.13. There are several proposals to account for the co-existence of crystalline and amorphous regions in the latter theory. In one case, the

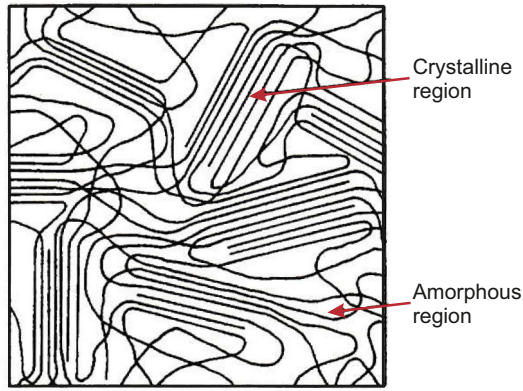


FIG. A.12 Fringed micelle model.

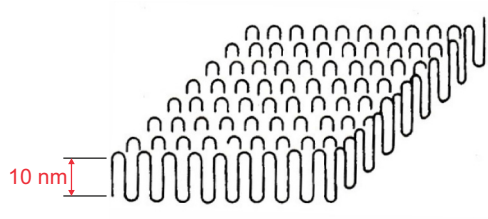


FIG. A.13 Folded chain model.

structure is considered to be a totally crystalline phase with defects. These defects which include such features as dislocations, loose chain ends, imperfect folds, chain entanglements etc., are regarded as the diffuse (amorphous) regions viewed in X-ray diffraction studies. As an alternative it has been suggested that crystalline (folded chains) and amorphous (random chains) regions can exist in a similar manner to that proposed in the fringed micelle theory. Therefore, in the complex structure of partially crystalline polymers, the crystalline regions consist of aligned and folded chains and the amorphous regions consist of crystal defects and randomly entangled chains.

Many crystalline polymers when viewed in cross polarised light, display characteristic Maltese crosses due to the presence of spherulites. These spherulites, shown in Fig. A.14, may vary in size from fractions of a micron to several millimetres in diameter, depending on the cooling rate from the melt. Slow cooling tends to produce larger spherulites than fast cooling. It is believed that the spherulites grow in all directions from a central nucleus, by the twisting of the folded chain platelets as shown in Fig. A.15. The size of a spherulite will be limited by the growth of adjacent spherulites. If the polymer melt is cooled very quickly it may undercool, i.e. remain molten at a

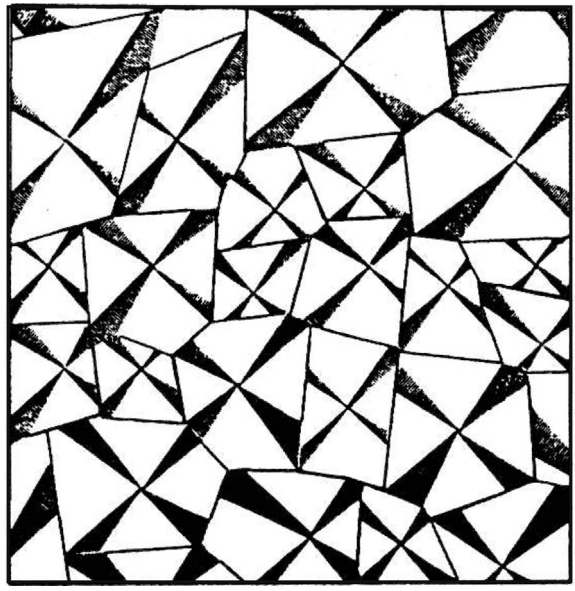


FIG. A.14 Typical illustration of spherulites.

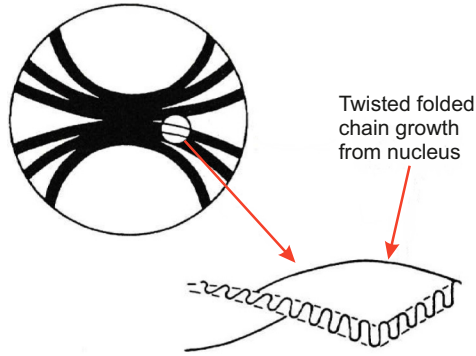


FIG. A.15 Structure of spherulite.

temperature below its melting point. This results in a shower of nucleation sites becoming available and a mass of spherulites will start to grow. The solid polymer will then consist of a large number of small spherulites.

The ease with which a polymer will form into crystalline regions depends on the structure of the molecular chain. It can be seen, for example, that if the polyethylene molecule has a high degree of branching then it makes it difficult to form into the ordered fashion shown in Fig. A.11. Also, if the side groups are large, it is not easy for a polymer with an atactic structure to form ordered

regions. On the other hand, isotactic and syndiotactic structures do have sufficient symmetry to be capable of crystallisation.

Another important feature of long chain molecules is the ease with which they can be rearranged by the application of stress. If a plastic is stretched the molecules will tend to align themselves in the direction of the stress and this is referred to as **orientation.** Molecular orientation leads to anisotropy of mechanical properties. This can be used to advantage in the production of fibres and film or may be the undesirable result of a moulding process. However, it is important that orientation should not be confused with crystallinity. It is possible to have an orientated polymer which shows no evidence of crystalline regions when X-ray diffraction studies are carried out. Equally, a polymer may be crystalline but optical measurements will show no signs of orientation. Orientation can be introduced into plastics such as polyethylene and polypropylene (both semi-crystalline) by cold drawing at room temperature. Other brittle plastics such as polymethyl methacrylate and polystyrene (both amorphous) cannot be cold drawn but can be drawn at elevated temperatures.

Appendix B

Solution of differential equations

The following type of differential equation is encountered in the text, for example, in the analysis of the models for viscoelastic behaviour:

$$A\frac{dy}{dx} + By - C = 0$$

where A, B and C are constants.

This has the solution

$$y = \frac{C}{B} - \frac{K}{B}e^{-Bx/A}$$

where the constant 'K' can be determined from the known boundary conditions in the specific case.

Appendix C

Stress/strain relationships

(i) Uniaxial stresses

When a material is subjected to a uniaxial stress (Fig. C.1), there will be a strain in the direction of the stress and a strain of the opposite sense in the perpendicular directions. The latter is referred to as the Poisson's Ratio effect.

$$\varepsilon_x = \frac{1}{E}\sigma_x$$

where E = modulus of material.

$$\varepsilon_y = -\nu\left(\frac{1}{E}\cdot\sigma_x\right)$$

where ν = Poisson's ratio (typical values are given in , Chapter 2).

$$\varepsilon_z = -\nu\left(\frac{1}{E}\cdot\sigma_x\right)$$

The z-direction is perpendicular to the page. For simplicity the material is assumed to be isotropic, i.e. same properties in all directions. However, in some cases for plastics and almost always for fibre composites, the properties

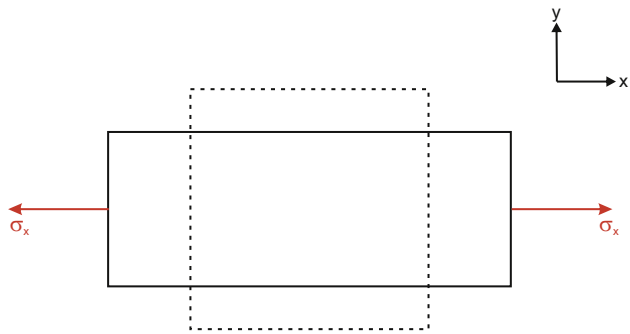


FIG. C.1 Uniaxial stress.

will be anisotropic. Thus, E and v will have different values in the x, y and z directions. Also, it should be remembered that only at short times can E and v be assumed to be constants. They will both change with time and so for long-term loading, appropriate values should be used.

(ii) Biaxial stresses

If the material is subjected to biaxial stresses in both the x and y directions (Fig. C.2) then the strains will be

$$\varepsilon_x = \frac{1}{E}\sigma_x - v\frac{1}{E}\sigma_y$$

That is, the total strain will be the sum of the tensile strain due to σ_x and the negative strain due to the Poisson's ratio effect caused by σ_y.

Similarly

$$\varepsilon_y = \frac{1}{E}\sigma_y - v\frac{1}{E}\sigma_x$$

$$\varepsilon_z = -\frac{v}{E}(\sigma_x + \sigma_y)$$

This situation is sometimes referred to as *plane stress* because there are only stresses in one plane. It is important to note, however, that there are strains in all three co-ordinate directions.

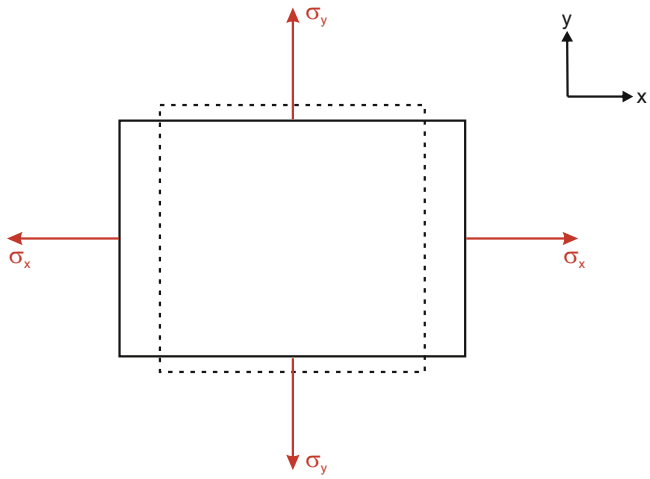


FIG. C.2 Biaxial stresses.

(iii) Triaxial stresses

If there are stresses in the *x, y* and *z* directions then the above approach is continued so that

$$\varepsilon_x = \frac{1}{E}\sigma_x - \nu\frac{1}{E}\sigma_y - \nu\frac{1}{E}\sigma_z = \frac{1}{E}\sigma_x - \frac{\nu}{E}(\sigma_y + \sigma_z)$$

$$\varepsilon_y = \frac{1}{E}\sigma_y - \frac{\nu}{E}(\sigma_x + \sigma_z)$$

$$\varepsilon_z = \frac{1}{E}\sigma_z - \frac{\nu}{E}(\sigma_y + \sigma_x)$$

In the above situation, if the stresses are such that $\varepsilon_z = 0$ then this condition is referred to as *plane strain.* This is because strains are experienced in only one plane even though there are stresses in all three co-ordinate directions.

Appendix D

Stresses in cylindrical shapes

(i) In a thin wall cylinder ($r > 10\ h$, shown in Fig. D.1) subjected to internal pressure, p, the stresses are given by

$$\sigma_\theta = \frac{pr}{h}$$

$$\sigma_a = \frac{pr}{2h}$$

$$\sigma_r = -p\ (at\ \ bore)$$

$$\sigma_r = 0\ (at\ \ outside)$$

Note that σ_r is small compared to σ_θ or σ_a and so it is often ignored.

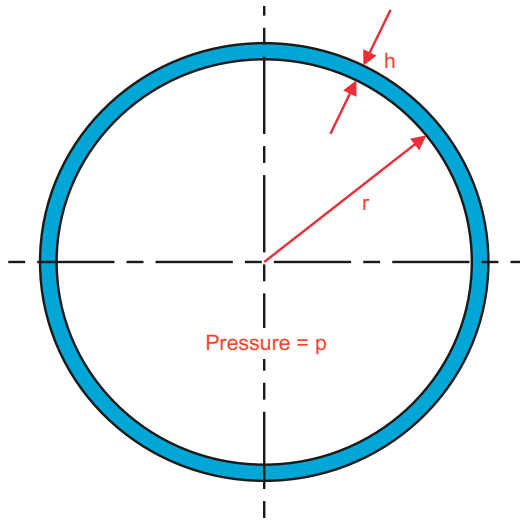


FIG. D.1 Thin-walled cylinder subjected to internal pressure.

Hoop strain,

$$\varepsilon_\theta = \frac{\Delta r}{r} = \frac{1}{E}\sigma_\theta - \frac{v}{E}\sigma_a$$

$$\varepsilon_\theta = \frac{pr}{Eh}\left\{1 - \frac{v}{2}\right\} = \frac{pr}{2Eh}\{2 - v\}$$

Axial strain,

$$\varepsilon_a = \frac{1}{E}\sigma_a - \frac{v}{E}\sigma_\theta$$

$$\varepsilon_a = \frac{pr}{2Eh}\{1 - 2v\}$$

(ii) In a thick wall cylinder subjected to both internal and external pressures the stresses are given by

$$\sigma_\theta = \frac{1}{k^2 - 1}\left\{p_i\left(1 + \frac{r_0^2}{r^2}\right) - p_0 k \left(1 + \frac{r_i^2}{r^2}\right)\right\}$$

$$\sigma_r = \frac{1}{k^2 - 1}\left\{p_i\left(1 - \frac{r_0^2}{r^2}\right) - p_0 k \left(1 - \frac{r_i^2}{r^2}\right)\right\}$$

where $k = r_0/r_i$.

The axial stress will depend on the end constraints, but if we consider the most common situation where there are end caps and the cylinder is free to change in length then for internal pressure only (i.e. $p_0 = 0$):

$$\sigma_a = \frac{p_i}{k^2 - 1}$$

For the zero external pressure situation, the axial strain will be given by

$$\varepsilon_a = \frac{1}{E}\sigma_a - \frac{v}{E}\sigma_r - \frac{v}{E}\sigma_\theta$$

$$\varepsilon_a = \frac{(1 - 2v)}{(E(k^2 - 1))}(p_i)$$

Appendix E

Introduction to matrix algebra

E.1 Matrix definitions

A matrix is an array of terms as shown below:

$$[A] = \begin{bmatrix} a_{11} & a_{12} & a_{13} & \dots & a_{1n} \\ a_{21} & a_{22} & a_{23} & \dots & a_{2n} \\ a_{31} & a_{32} & a_{33} & \dots & a_{3n} \\ \vdots & \vdots & \vdots & \vdots & \vdots \\ a_{m1} & a_{m2} & a_{m3} & \dots & a_{mn} \end{bmatrix}$$

If $n = 1$ then we have a matrix consisting of a single column of terms and this referred to as a *column matrix*. If $m = 1$ then the matrix is called a *row matrix*.

If in the analysis of a problem there is a set of simultaneous equations then the use of matrices can be a very convenient shorthand way of expressing and solving the equations. For example, consider the following set of equations:

$$\begin{aligned} y_1 &= a_{11}x_1 + a_{12}x_2 + a_{13}x_3 + \cdots + a_{1n}x_n \\ y_2 &= a_{21}x_1 + a_{22}x_2 + a_{23}x_3 + \cdots + a_{2n}x_n \\ y_3 &= a_{31}x_1 + a_{32}x_2 + a_{33}x_3 + \cdots + a_{3n}x_n \\ &\vdots \\ y_m &= a_{m1}x_1 + a_{m2}x_2 + a_{m3}x_3 + \cdots + a_{mn}x_n \end{aligned}$$

These may be written in matrix form as follows:

$$\{y\} = [A]\{x\} \tag{E.1}$$

where $\{y\}$ and $\{x\}$ are column matrices.

E.2 Matrix multiplication

The matrix Eq. (E.1) involves the multiplication of the matrices $[A]$ and $\{x\}$. To do this one must apply the simple rules of *matrix multiplication*. These are:

(*a*) two matrices may only be multiplied if the number of columns in the first is equal to the number of rows in the second;
(*b*) the terms in the product matrix resulting from the multiplication of matrix $[A]$ with a matrix $[B]$ are given by

$$c_{ij} = \sum_{k=1}^{n} a_{ik} b_{kj} \tag{E.2}$$

The use of these rules is illustrated in the following example:

$$\begin{bmatrix} a_{11} & a_{12} \\ a_{21} & a_{22} \end{bmatrix} \begin{bmatrix} b_{11} & b_{12} & b_{13} \\ b_{21} & b_{22} & b_{23} \end{bmatrix} = \begin{bmatrix} (a_{11}b_{11} + a_{12}b_{21}) & (a_{11}b_{12} + a_{12}b_{22}) & (a_{11}b_{13} + a_{12}b_{23}) \\ (a_{21}b_{11} + a_{22}b_{21}) & (a_{21}b_{12} + a_{22}b_{22}) & (a_{21}b_{13} + a_{22}b_{23}) \end{bmatrix}$$

Suppose

$$[A] = \begin{bmatrix} 2 & 4 \\ 6 & 8 \end{bmatrix}, \quad [B] = \begin{bmatrix} 1 & 2 & 3 \\ 3 & 2 & -1 \end{bmatrix}$$

Then

$$[C] = [A][B] = \begin{bmatrix} 14 & 12 & 2 \\ 30 & 28 & 10 \end{bmatrix}$$

E.3 Matrix addition and subtraction

Matrix algebra also involves the *addition and subtraction* of matrices. The rules for this are as follows:

(*a*) matrices may only be added or subtracted if they are of the same order, i.e. they each contain the same number of rows and columns;
(*b*) the terms in the resulting matrix are given by

$$c_{ij} = a_{ij} \pm b_{ij} \tag{E.3}$$

The following example illustrates the use of these rules:

$$\begin{bmatrix} d_{11} & d_{12} & d_{13} \\ d_{21} & d_{22} & d_{23} \end{bmatrix} \begin{bmatrix} b_{11} & b_{12} & b_{13} \\ b_{21} & b_{22} & b_{23} \end{bmatrix} = \begin{bmatrix} (d_{11} \pm b_{11}) & (d_{12} \pm b_{12}) & (d_{13} \pm b_{13}) \\ (d_{21} \pm b_{21}) & (d_{22} \pm b_{22}) & (d_{23} \pm b_{23}) \end{bmatrix}$$

Suppose

$$[D] = \begin{bmatrix} -2 & 4 & 5 \\ 6 & 8 & -3 \end{bmatrix} \quad [B] = \begin{bmatrix} 1 & 2 & 3 \\ 3 & 2 & -1 \end{bmatrix}$$

Then

$$[E] = [D] + [B] = \begin{bmatrix} -1 & 6 & 8 \\ 9 & 10 & -4 \end{bmatrix}$$

$$[F] = [D] - [B] = \begin{bmatrix} -3 & 2 & 2 \\ 3 & 6 & -2 \end{bmatrix}$$

E.4 Inversion of a matrix

Referring back to the set of simultaneous equations at the beginning of this appendix, the objective is usually to solve these for the unknown x terms. This is where the use of matrices has a major advantage because referring to Eq. (E.1) we may rewrite this as

$$\{x\} = [A]^{-1}\{y\} \tag{E.4}$$

This equation expresses the solution to the set of simultaneous equations in that each of the unknown x terms is now given by a new matrix $[A]^{-1}$ multiplied by the known y terms. The new matrix is called the *inverse* of matrix $[A]$. The determination of the terms in the inverse matrix is beyond the scope of this brief introduction. Suffice to say that it may be obtained very quickly on a computer and hence the solution to a set of simultaneous equations is determined quickly using Eq. (E.4).

E.5 Symmetric matrix

A square matrix is one in which the number of columns is equal to the number of rows. An important type of square matrix which arises quite often in the

finite element method is a *symmetric matrix*. Such matrices possess the property that $a_{ij} = a_{ji}$. An example of such a matrix is given below:

$$\begin{bmatrix} 2 & 4 & 7 & -3 \\ 4 & 5 & 1 & 9 \\ 7 & 1 & 6 & -5 \\ -3 & 9 & -5 & 4 \end{bmatrix}$$

which is often written as

$$\begin{bmatrix} 2 & 4 & 7 & -3 \\ & 5 & 1 & 9 \\ \text{sym.} & & 6 & -5 \\ & & & 4 \end{bmatrix}$$

Appendix F

Abbreviations for some common polymers

ABS	Acrylonitrile butadiene styrene
ASA	Acrylonitrile styrene acrylade
CA	Cellulose acetate
CAB	Cellulose acetate butyrate
CAP	Cellulose acetate propionate
CN	Cellulose nitrate
CP	Cellulose propionate
EC	Ethyl cellulose
EP	Epoxide, epoxy
EVA	Ethylene vinyl acetate
FEP	Fluorinated ethylene propylene
HDPE	High density PE
HIPS	High impact PS
LDPE	Low density PE
LLDPE	Linear low density PE
MDPE	Medium density PE
MF	Melamine-formaldehyde
PA	Polyamide
PAEK	Polyaryletherketone
PAI	Polyamide-imide
PAN	Polyacrylonitrile
PB	Polybutene-l
PBA	Poly(butylene acrylate)
PBS	Polybutylene succinate
PBT	Poly(butylene terephthalate)
PC	Polycarbonate
PCL	Polycaprolactone
PCTEE	Polychlorotrifluoroethylene
PE	Polyethylene
PEEK	Polyetheretherketone
PEI	Polyether-imide
PEK	Polyetherketone
PES	Polyethersulfone
PET	Poly(ethylene terephthalate)
PF	Phenol-formaldehyde
PHA	Polyhydroxyalkanoate

PI	Polyimide
PIB	Polyisobutylene
PLA	Polylactic acid
PMMA	Poly(methyl methacrylate), acrylic
PMP	Poly-4-methylpentene-1
POM	Polyoxymethylene: polyformaldehyde, acetal
PP	Polypropylene
PPE	Polyphenylene ether
PPO	Polyphenylene oxide
PPS	Poly(phenylene sulphide)
PPSU	Poly(phenylene sulphone)
PS	Polystyrene
PSU	Polysulfone
PTFE	Polytetrafluoroethylene
PUR	Polyurethane
PVAC	Poly(vinyl acetate)
PVAL	Poly(vinyl alcohol)
PVB	Poly(vinyl butyral)
PVC	Poly(vinyl chloride)
PVDC	Poly(vinylidene chloride)
PVDF	Poly(vinylidene fluoride)
PVFM	Poly(vinyl formal)
PVK	Polyvinylcarbazole
SAN	Styrene Acrylonitrile
SBR	Styrene butadiene rubber
SBS	Styrene-butadiene-styrene
UF	Urea-formaldehyde
UHMWPE	Ultra-high molecular weight polyethylene
UP	Unsaturated polyester

Index

'*Note*: Page numbers followed by "f" indicate figures and "t" indicate tables.'

A

ABS. *See* Acrylonitrile butadiene styrene (ABS)
Acetals. *See* Polyoxymethylene (POM)
Acrylonitrile butadiene styrene (ABS), 9–10, 17, 53, 153, 389–390
Additive manufacturing techniques, 387–392
  FFF, 389–390, 390f
  SLA, 388–389
  SLS, 390–392, 391f
  3D printing techniques, 392
Adiabatic process, 287
Alcryn, 54
Aliphatic polyesters, 19
Amino plastics, 11, 54
Amorphous plastics, 5–6, 52–54, 590–591
Amorphous polyethylene terephthalate (aPET), 50–52, 357–358
Amorphous polymers, 357–358
Antioxidants, 3
Antistatic agents, 3
aPET. *See* Amorphous polyethylene terephthalate (aPET)
Apparent shear rate, 442
Apparent viscosity, 420–421
Arnitel, 54
Aspect ratio, 199
Assisted injection moulding, 344–348
Atactic groups, 587–588
Autoclave moulding, 398
Automatic processes
  centrifugal casting, 404
  filament winding, 403
  injection moulding, 405
  pultrusion, 404
Automotive industry, 12

B

Bakelite, 2, 54
Bending stiffness matrix, 226
Bending stress, 523–524
Bi-directional fibre composites, 198, 198t
Biaxial stresses, 598–599, 598f
Biaxially orientated forms of polyamide (BOPA), 318–319
Biaxially orientated forms of polyethylene (BOPE), 318–319
Biaxially orientated forms of polyethylene terephthalate (BOPET), 318–319
Biaxially orientated forms of polylactic acid (BOPLA), 318–319
Biaxially orientated forms of polypropylene (BOPP), 9–10, 318–319
Biaxially orientated plastics, 318–321
  reactive extrusion, 321
Binder jetting 3D printing, 392
Bio-degradable plastics, 19. *See also* Reinforced plastics
  amorphous plastics, 52–54
  characteristics, 47–56
  semi-crystalline plastics, 47–52
  thermosetting plastics, 54–56
  TPRs, 54
Biodegradation, 31
Blow moulding, 101, 306–312, 376
  analysis, 309–311, 310f
  extrusion, 306–309
    stretch, 311–312
  injection, 349–351
    stretch blow moulding, 312
Blowing agents, 3, 13
Blown Film Extrusion process, 304
BMC. *See* Bulk moulding compound (BMC)
Bolster, 331
Boltzmann superposition principle, 116–117, 516
BOPA. *See* Biaxially orientated forms of polyamide (BOPA)
BOPE. *See* Biaxially orientated forms of polyethylene (BOPE)
BOPET. *See* Biaxially orientated forms of polyethylene terephthalate (BOPET)

BOPP. *See* Biaxially orientated forms of polypropylene (BOPP)
Brintrup equation, 208
Brittle failures, 153
Brittleness temperature, 174
Bulk modulus, 76
Bulk moulding compound (BMC), 13
Butyl rubber, 14

C

Calcium stearate, 4
Calendering, 372–376
  analysis, 373–376
Capillary viscometer, 439
Carbon fibre-reinforced plastics (CFRP), 13
Carbon fibres, 195–197
Cariflex, 54
Carreau model, 422
Cast Film Extrusion, 304
Celluloid, 2
Cellulose, 19
Central crack of length in sheet of finite width, 150
Central deflection, 491
Centrifugal casting, 404
CFD. *See* Computational fluid dynamics (CFD)
CFRP. *See* Carbon fibre-reinforced plastics (CFRP)
Chain lengths, 5
Chemical attack, 29–31
Chemical blowing agents, 3, 13
Chopped strand mat (CSM), 262–263, 395
Clamping force calculation
  isothermal situation, 475–476
  non-isothermal situation, 476–481
Clamping systems, 328
Co-extrusion, 315–318, 316f
  co-extruded barrier sheet structure, 319f
  transmission rates
    of plastic packaging films, 319t
    for range of plastics, 318t
Coefficient of thermal expansion, 81
COI. *See* Critical oxygen index (COI)
Cold crystallisation, 357–358
Cold drawing, 61–62
Cold press moulding, 398–399
Column matrix, 603
Commodity thermoplastics, 8–9
Compatible polymer blends, 17
Complex modulus, 133, 133f
Compliance, 145
  matrix, 211
Composites, 11–13
  analysis
    of continuous fibre, 200–209
    of multi-layer isotropic materials, 248–253
    of non-symmetric laminates, 253–256
    of short fibre, 256–263
  approach to analysis of unidirectional, 217–224
  beam, 503–504
  creep behaviour of fibre reinforced plastics, 263
  deformation behaviour
    of laminates, 232–235, 237–248
    of reinforced plastics, 195
    of single ply or lamina, 209–216, 224–232
  fatigue behaviour of reinforced plastics, 269–271
  fibre reinforcement forms, 199–200
  impact behaviour of reinforced plastics, 271
  matrix, 198–199
  reinforcement, 195–198
  steps to predicting stiffness of symmetric laminates, 235–237
  strength of fibre composites, 263–269
  tensile behaviour of fibres, 197f
Compression moulding, 383–386, 400
Compression zone, 281–282
Compressive stress, 492
Computational fluid dynamics (CFD), 422
Computer-aided simulation, 411
Concentric cylinder viscometer, 441, 441f
Cone and plate viscometer, 439–440, 440f
Coni-cylindrical dies, isothermal flow in, 426–431
  drop due to extensional flow, 428–429
  pressure drop
    at die entry, 429–431
    due to shear, 426–428
Constitutive equation approach, 531–536
Continuous changes of stress, 119–125
Continuous fibre composite analysis, 200–209
  longitudinal properties, 200
    equilibrium equation, 200
    geometry of deformation equation, 201
    stress–strain relationships, 201–205

properties perpendicular to longitudinal axis, 206
equilibrium equation, 206
geometry of deformation equation, 206–207
stress–strain relationships, 207–209
Continuous fibres, 195
Copolymer, 588–590
Corrugation dimensions, 101
Costs, 45–56
selection for stiffness at minimum cost, 47
selection for strength at minimum cost, 45–47
Counter-rotating twin screw extruder, 298, 299t
Coupling agents, 3
Coupling matrix, 239
cPET. *See* Crystalline polyethylene terephthalate (cPET)
Crack extension force, 144
Crack-like defect, 143
Crazing, 157
in plastics, 159–160
Creep, 28, 59–60, 105–106, 108–109, 114
behaviour of fibre reinforced plastics, 263
compliance, 70
contraction ratio, 77
creep-strain equations, 65–66
curves, 64–65, 64f–65f, 67–69, 490, 509
for acetal, 128f
data, 497–498
failure of plastics, 156–160
crazing in plastics, 159–160
fracture mechanics approach to creep fracture, 159
modulus, 67–69, 68f, 106, 108–109, 128–129, 511–513
rupture, 29, 156
data, 157
strain, 126–127
Critical defect size in material, 522
Critical fibre length, 258–259
Critical oxygen index (COI), 41–42
Critical strain energy release rate, 144
Critical stress, 492–493
intensity factor, 152
Critical value (V_{crit}), 203
Cross-linked polyethylene (XLPE), 49–50
Cross-linking of chains, 7–8
Crystalline, 590–591
plastics, 5–6, 34
polymers, 357–358
structure of polyethylene, 591f
Crystalline polyethylene terephthalate (cPET), 50–52, 357–358
CSM. *See* Chopped strand mat (CSM)
Cyclic frequency effect, 162–164

D

Dashpot, 104
Deborah Number (N_{deb}), 438
Deformation behaviour
of laminates, 232–235
of reinforced plastics, 195
of single ply or lamina, 209–216
Deformation equation, geometry of, 201, 206–207, 508
Kelvin or Voigt Model, 107–110
Maxwell model, 105–107
standard linear solid, 114–116
Degradation, 29–31
physical or chemical attack, 29–31
Degree of polymerisation, 2
Design methods for plastics using deformation data, 66–80
isochronous and isometric graphs, 66–70
pseudo-elastic design method for plastics, 71–80
Desirability factor, 27, 47, 51t, 55t, 489
Die characteristics, 293–294, 294f
Die geometries, 294–297
Differential equations, solution of, 106–107, 110, 595
Digital light processing (DLP), 392
Dimensionless temperature gradient, 467, 468f
Discontinuous fibres, 195
Distribution tube runner system, 338
DLP. *See* Digital light processing (DLP)
DMC. *See* Dough Moulding Compounds (DMC)
'Double-bubble' orientation process, 320–321
Dough Moulding Compounds (DMC), 383, 395, 400–401
Drag flow, 287–289
Drape vacuum forming, 360–362, 362f
Draw-down process, 305
Dual-sheet thermoforming. *See* Twin-sheet thermoforming
Ductility, 27
factor, 155
Dwell time. *See* Residence time
Dyes, 4

Dynamic loading of plastics, 131–137. *See also* Intermittent loading
Dynamic moduli, 133
Dyneema® fibres, 195–197

E

EBM. *See* Extrusion blow moulding (EBM)
Edge cracks in plate of finite width, 150
Effective creep modulus, 128–129
Elastic
  behaviour of polymer melts, 432–436
  stored energy, 145
  strain, 461
Elastollan, 54
Elastomeric alloys, 16–17
Elastomers, 3, 14–17
Electro-magnetic interference (EMI), 40, 344
4-Element model theory, 510
Empirical approach, 125–131
Endurance limit, 162–164
Energy absorbing ability of material, 528
Energy approach to fracture, 143–148
Engineering strain, 60
Engineering stress, 60
Engineering thermoplastics, 9–10
Enthalpy, 479
Environmental stress cracking (ESC), 31
Epoxides, 56
Epoxies (EP), 11
  resins, 56
Equilibrium equation, 200, 206, 508
  Kelvin or Voigt model, 107
  Maxwell model, 104
  standard linear solid, 113
Equivalent stress, 490
Equivalent tensile stress, 496
ESC. *See* Environmental stress cracking (ESC)
Ethylene monomer, 585f
Ethylene vinyl alcohol (EVA), 17, 317–318
Ethylene-propylene rubber, 14
EVA. *See* Ethylene vinyl alcohol (EVA)
EVOH. *See* Ethylene vinyl alcohol (EVA)
Extenders, 4
Extension stiffness matrix, 538–541
Extensional stiffness matrix, 225, 234, 239, 249
External gas
  external gas-assisted injection moulding, 346
  injection, 346
Extraction force, 498–500
Extruder
  characteristics, 293–294, 294f
  flow analysis in, 287–292
  processing methods based on, 300–321
Extrusion, 280–321
  die geometries, 294–297
  extruder/die characteristics, 293–294
  flow analysis in extruder, 287–292
  flow mechanism, 286–287
  processing methods based on extruder, 300–321
    biaxially orientated plastics, 318–321
    blow moulding, 306–312
    co-extrusion, 315–318, 316f
    extrusion coating processes, 312–314
    fibre spinning, 314–315
    film extrusion, 303–306
    granule production/compounding, 300–301
    profile production, 302–303
    reactive extrusion, 321
  single screw extrusion features, 280–286, 281f
  stretch blow moulding, 311–312
  twin screw extruder features, 297–299
Extrusion blow moulding (EBM), 349–351

F

Fabrication costs, 45
Failure stress, 153
Fatigue, 29
  behaviour of reinforced plastics, 269–271
  limit, 162–164
  of plastics, 160–170
    cyclic frequency effect, 162–164
    fracture mechanics approach, 168–170
    fracture surface, 161f
    mean stress effect, 165–167
    stress system effect, 167–168
    testing control mode effect, 165
    waveform effect, 164–165
Feed zone, 281
FEP. *See* Fluorinated ethylene propylene (FEP)
FFF. *See* Fused filament fabrication (FFF)
Flow
  curves, 565, 569
  rate, 566–567
  ratios, 583

Fibre
composite strength, 263–269
reinforcement forms in composites, 199–200
spinning, 314–315
Fibre reinforced plastics, creep behaviour of, 263
Filament winding, 403
Fillers, 4
Film extrusion, 303–306
Fire retardant, 41
Flame retardants, 4
Flammability, 41
Flexural stiffness, 95
Flow analysis
in extruder, 287–292
in processing operations, 447–463
elastic strain, 461
viscous strain, 462–463
Flow defects, 446–447
Flow mechanism, 286–287
Fluorinated ethylene propylene (FEP), 10
Fluoropolymers, 10
Foamed beam, 503
Folded Chain Theory, 592, 592f
Food packaging, 317–318
products, 366
Force equilibrium, 238
Fourier Number, 464
Fourier's equation for non-steady heat flow, 463–464
Fractional recovery, 126–127
Fracture behaviour
of plastics, 153–155
of unreinforced plastics, 141–142
Fracture mechanics approach, 523
to creep fracture, 159
to fatigue, 168–170
to impact, 176–180
Fracture toughness. See Critical stress intensity factor
Freeze-off time, 582
Frictional properties, 31–33
Fringed micelle model, 591, 592f
Fused Deposition Modelling® (FDM). *See* Fused filament fabrication (FFF)
Fused filament fabrication (FFF), 389–390, 390f

G

Gas, 13
gas-assisted injection moulding, 346
Gate, 329–332
GFRP. *See* Glass fibre-reinforced plastics (GFRP)
Glass, 197
fibres, 13
glass-filled nylon, 173
glass–rubber transition, 34
Glass fibre-reinforced plastics (GFRP), 13
Glass reinforced plastics (GRP), 269–270
Glass transition temperature (T_g), 34, 357–358
Glass-mat thermoplastics (GMT), 12
Granule production/compounding, 300–301
GRP. *See* Glass reinforced plastics (GRP)

H

Halpin–Tsai equation, 207–209
Hand lay-up method, 396
HD-PE. *See* High density polyethylene (HD-PE)
Heat stabilisers, 4
Heat transfer analysis during polymer processing, 463–475, 464t
High density polyethylene (HD-PE), 5, 49
High impact polystyrene (HIPS), 53–54
High modulus (HM), 195–197
High performance plastics, 10
HIPS. *See* High impact polystyrene (HIPS)
HM. *See* High modulus (HM)
Hoop strain, 498–500
Hoop stress, 500
Hot press mouldings, 399–401
Hot runner moulds, 336–337
Hydrolysis, 30, 326
Hytrel, 54

I

IBM. *See* Injection blow moulding (IBM)
IMD. *See* In-Mould Decoration (IMD)
IML. *See* In-Mould Labelling (IML)
Impact behaviour of plastics, 170–180
fracture mechanics approach to impact, 176–180
impact test methods, 174–176
miscellaneous factors, 174
of reinforced plastics, 271
stress concentration effect, 170–173
temperature effect, 173–174
Impact strength, 172, 176
In-Mould Decoration (IMD), 356–357
In-Mould Labelling (IML), 308–309, 355–357

In-plane behaviour of symmetric laminate, 232–235
Incompatible blends, 17
Infrared lamps (IR lamps), 351
Injection blow moulding (IBM), 349–351
  moulded PET, 9–10
Injection moulding, 321–322, 405
  advanced injection moulding technologies, 353–357
    IML, 355–357
    microcellular injection moulding, 357
    micromoulding, 353–354
    overmoulding, 354–355
    SCORIM, 357
  assisted, 344–348
  details of process, 322–329
  IBM, 349–351
  moulds, 329–342
  reaction, 348–349, 349f
  sandwich moulding, 344
  structural foam, 342–344
  of thermosetting materials, 351–353
Injection stretch blow moulding (ISBM), 312, 349–351
Insert moulding, 354–355
Insulated runner moulds, 338
Intermittent loading, 116–131
  empirical approach, 125–131
  superposition principle, 116–125
Internal gas
  injection, 346
  internal gas-assisted injection moulding, 346
Inversion of matrix, 605
IR lamps. *See* Infrared lamps (IR lamps)
ISBM. *See* Injection stretch blow moulding (ISBM)
Isochronous curve, 66–67
Isochronous graphs, 66–70, 69f
Isomerism, 5
Isometric curve, 66–67, 495–496
Isometric graphs, 66–70, 69f
Isotactic groups, 587–588
Isothermal flow
  in channels
    Newtonian fluid, 414–419
    non-Newtonian fluids, 423–426
  in non-uniform channels, 426–432
Isothermal process, 287
Isothermal situation, 475–476
Izod and Charpy tests, 176

K

Kelvin or Voigt Model, 107–110, 515–517
  equilibrium equation, 107
  geometry of deformation equation, 107–110
  response of, 109f
  stress–strain relations, 107
Kevlar, 13, 17–18, 195–197

L

Labels, 308–309
Laminated object manufacturing (LOM), 392
Laminates
  deformation behaviour of, 232–235, 237–248
    analysis of laminates, 238–248
    convention for defining thicknesses and positions of plies, 237–238
    in-plane behaviour of symmetric laminate, 232–235
    from unidirectional plies, 232
  strength of, 267–269
Lateral strain ratio, 77
LCP. *See* Liquid crystal polymers (LCP)
LD-PE. *See* Low density polyethylene (LD-PE)
Leakage flow, 291–292
LEFM. *See* Linear elastic fracture mechanics (LEFM)
LFRT. *See* Long fibre reinforced thermoplastics (LFRT)
Limiting oxygen index (LOI). *See* Critical oxygen index (COI)
Linear elastic fracture mechanics (LEFM), 148–149, 152
Linear low density polyethylene (LLD-PE), 5, 49
Liquid crystal polymers (LCP), 17–18
LLD-PE. *See* Linear low density polyethylene (LLD-PE)
Load transfer length, 258
Load/no-load cycle, 125
Local compliance matrix, 531–536
Local stresses, 546
Logarithmic scales, 412
LOM. *See* Laminated object manufacturing (LOM)
Long fibre reinforced thermoplastics (LFRT), 12, 394

Long molecule structure, 585–586
Long-term testing of plastics, 64–66
Low density polyethylene (LD-PE), 5, 47–49
Lubricants, 4

M

Machined surfaces, 174
Manual processing methods
  autoclave moulding, 398
  hand lay-up method, 396
  spray-up method, 396–398
Matched die forming, 366
Material width, 177–178
Material's resistance to crack growth, 155
Mathematical models of viscoelastic behaviour, 103–116
  complex models, 110–112
  Kelvin or Voigt Model, 107–110
  Maxwell model, 104–107
  standard linear solid, 113–116
Matrix, 198–199, 603
  addition and subtraction, 604–605
  inversion, 605
  multiplication, 604
  symmetric matrix, 605–606
  thermoplastics, 198–199
  thermosets, 198
Maximum strain criterion, 264–267, 546–548
Maximum stress criterion, 263, 265–267, 525, 546
Maximum volume fraction (V_{max}), 204
Maxwell and Kelvin models, 438
Maxwell model, 104–107, 511–513
  equilibrium equation, 104
  geometry of deformation equation, 105–107
  response of, 106f
  stress–strain relations, 104
Maxwell strain, 507
MDF. *See* Medium density fibreboard (MDF)
MDPE. *See* Medium density PE (MDPE)
Mean effective pressure (MEP), 475
  power law parameters for plastics, 477t
Mean stress, 523
  effect, 165–167
Mechanical behaviour of plastics, 59
  creep failure of plastics, 156–160
  design methods for plastics using deformation data, 66–80
  dynamic loading of plastics, 131–137
  energy approach to fracture, 143–148
  fatigue of plastics, 160–170
  fracture behaviour
    of plastics, 153–155
    of unreinforced plastics, 141–142
  impact behaviour of plastics, 170–180
  intermittent loading, 116–131
  long-term testing of plastics, 64–66
  mathematical models of viscoelastic behaviour, 103–116
  multi-layer mouldings, 85–89
  ribbed section design, 94–100
  short-term testing of plastics, 61–64
  snap fits design, 90–94
  stiffening mechanisms in other moulding situations, 101–103
  stress concentration, 142–143
  stress intensity factor approach to fracture, 148–152
  thermal stresses and strains, 81–85
  time–temperature superposition, 138–141
  viscoelastic behaviour of plastics, 60
Medium density fibreboard (MDF), 54
Medium density PE (MDPE), 153
Melamine formaldehyde (MF), 11
Melamine formaldehyde, 54
Melt flow index (MFI). *See* Melt flow rate test (MFR test)
Melt flow rate test (MFR test), 31, 445–446
Melt flow theory, 411
Melt fracture, 446
Melt processing methods, 411–412
Melting temperature (T_m), 357–358
MEP. *See* Mean effective pressure (MEP)
Metering zone, 282–286
MF. *See* Melamine formaldehyde (MF)
MFR test. *See* Melt flow rate test (MFR test)
Microcellular injection moulding, 357
Microcellular plastics, 343
Micromoulding, 353–354
Minimum stress, 525
Modified polyphenylene oxide, 54
Modulus
  of material, 60
  modulus–time curves for range of temperatures, 138
Molecular chain
  arrangement of, 590–594
  conformation of, 586–590, 587f
Molecular orientation, 594
Molten plastic, 446–447

Moment equilibrium, 239
Monomers, 2
Moulded plastics, 161
Moulding methods, 101
Moulds, 329–342
  clamping force, 338–342
  gates, 331–332
  runners, 332–333
  sprue, 333
  temperature control, 333–342
    hot runner moulds, 336–337
    insulated runner moulds, 338
    multi-daylight moulds, 335–336
  venting, 333
Multi-daylight moulds, 335–336
Multi-layer isotropic material analysis, 248–253
Multi-layer mouldings, 85–89

N

Nanocellular foams, 343
Natural fibres, 314–315
Natural materials, 2
Natural rubbers, 14
Natural time. *See* Relaxation time
Neck Ring process, 311–312
Necking, 157
Negative forming, 360
Neoprene, 14
Newtonian analysis, 280
Newtonian flow, 437
Newtonian fluid, 412, 414–419. *See also* Non-Newtonian fluids
  flow along channel of uniform circular cross-section, 414–417
    fluid element in capillary, 415f
  flow between parallel plates, 417–419, 419f
Non-isothermal situation, 476–481
Non-linear viscoelastics, 60
Non-Newtonian fluids. *See also* Newtonian fluid
  power law fluid flow
    along uniform circular cross-section channel, 423–424
    between parallel plates, 424–426
Non-Newtonian model, 411
Non-symmetric laminates analysis, 253–256, 544–546
Non-uniform channels, isothermal flow in, 426–432
  flow in coni-cylindrical dies, 426–431
  flow in wedge shaped die, 431–432
Nozzle, 326–327
Nucleating agents, 4
Nylon 66, properties of fibre reinforced, 198–199, 199t
Nylons, 50, 153

O

Olefinic TPR, 16–17
Olefinics, 54
Operating point, 551–553
Overmoulding, 354–355
Oxidation, 30

P

PAEK. *See* Polyaryletherketones (PAEK)
PAES. *See* Polyarylethersulfones (PAES)
Parison moulding, 306–307, 349–351
Parkesine, 2
Partially crystalline plastics, 5–6
Partially incompatible blends, 17
PBI. *See* Polybenzimidazole (PBI)
PBS. *See* Polybutylene succinate (PBS)
PBT. *See* Polybutylene terephthalate (PBT)
PC. *See* Polycarbonate (PC)
PCL. *See* Polycaprolactone (PCL)
PEBA. *See* Polyester block amide (PEBA)
Pebax, 54
PEEK. *See* Polyetheretherketone (PEEK)
PEK. *See* Polyetherketones (PEK)
Pellethane, 54
Pendulum impact tests, 175, 175f
Penny shaped internal crack, 150
Percolation network, 40
Perfluoroalkoxy fluoropolymer (PFA fluoropolymer), 10
Permeability, 42
Permeation constant, 42
PES. *See* Polyethersulphone (PES)
PET. *See* Polyethylene terephthalate (PET)
PFA fluoropolymer. *See* Perfluoroalkoxy fluoropolymer (PFA fluoropolymer)
PHAs. *See* Polyhydroxyalkanoates (PHAs)
PHB. *See* Poly-3-hydroxybutyrate (PHB)
Phenol-formaldehyde, 2, 54
Phenolics, 11, 54
Physical attack, 29–31
Physical blowing agents, 3, 13
PI. *See* Polyimides (PI)
Pigments, 4

Pin gates, 332
PLA. *See* Polylactic acid (PLA)
Plane
  strain, 599
  stress, 599
Plasticisers, 4
Plastics, 1–3, 279, 317–318
  alloys, 18t
  to designer, 8–19
  moulding methods, 411
  polymeric materials, 2–8
  selection, 19–56
    costs, 45–56
    degradation, 29–31
    electrical properties, 39
    mechanical properties, 20–29
    optical properties, 41
    processing, 43–44
    recyclability, 44–45
    special properties, 39–43
    thermal properties, 34–39
    wear resistance and frictional properties, 31–33
Plate constitutive equations, 226–232, 240, 248–253
Plug assisted forming, 364
Plug-assisted thermoforming, 364–366
Ply properties in fibre and transverse directions, 533–536
PMMA. *See* Polymethyl methacrylate (PMMA)
Poisson's ratio, 77, 208, 246–247
  effect, 597
Poly-3-hydroxybutyrate (PHB), 19
Polyamides, 50, 54, 389–390
Polyaryletherketones (PAEK), 10
Polyarylethersulfones (PAES), 10
Polybenzimidazole (PBI), 10
Polybutylene succinate (PBS), 19
Polybutylene terephthalate (PBT), 52
Polycaprolactone (PCL), 19
Polycarbonate (PC), 9–10, 53, 153, 164, 389–390
Polyester block amide (PEBA), 391–392
Polyesters, 54, 56
Polyetheretherketone (PEEK), 31–32, 52, 198–199, 391–392
Polyetherketones (PEK), 10
Polyethersulphone (PES), 31–32, 53–54
Polyethylene, 5, 594
  chain branch in, 588f
  chain structures, 6f
  molecule, 585f–586f
Polyethylene terephthalate (PET), 5, 8–9, 50–52
Polyhydroxyalkanoates (PHAs), 19
Polyimides (PI), 10
Polylactic acid (PLA), 5, 19, 52, 389–390
Polymer melt flow analysis
  behaviour, 412–414
    flow curves for polyethylene, 414f
    relations between shear stress and shear rate, 412f
    viscosity curves for polypropylene, 413f
  clamping force calculation, 475–481
  elastic behaviour of polymer melts, 432–436
  experimental methods for obtaining flow data, 439–447
    concentric cylinder viscometer, 441, 441f
    cone and plate viscometer, 439–440, 440f
    flow defects, 446–447
    MFR and MFI, 445–446
    ram extruder, 441–444, 442f
  flow analysis in processing operations, 447–463
  heat transfer analysis during polymer processing, 463–475
  isothermal flow in channels
    Newtonian fluid, 414–419
    non-Newtonian fluids, 423–426
  isothermal flow in non-uniform channels, 426–432
  relaxation time, 438
  residence time, 437–438
  rheological models for, 419–423
  swelling ratio
    due to shear stresses, 433–434
    due to tensile stresses, 435–436
  temperature rise in die, 438–439
Polymeric materials, 2–8, 585
  thermoplastic materials, 5–6
  thermosetting plastics, 7–8
Polymerisation, 2
Polymers, 2–3, 364–366, 391–392, 588–590
  alloys, 17
  blends, 17
  chain structures, 589f
  processing, 411, 463–475

Polymethyl methacrylate (PMMA), 53
Polymethylpentene, 173
Polynomial of Muenstedt, 422
Polyoxymethylene (POM), 9–10, 50
Polyphenylene oxide (PPO), 9–10, 54
Polyphenylene sulphide (PPS), 10, 30–32, 198–199
Polyphthalamides (PPA), 10
Polypropylene (PP), 50, 594
  crystalline structure of, 591f
  structures, 590f
Polystyrene (PS), 53, 154–155, 389–392
Polysulphone (PSU), 9–10
Polytetrafluoroethylene (PTFE), 10, 50
Polyurethanes (PU), 11, 54, 56
Polyvinyl chloride (PVC), 4–5, 8–9, 52–53
Polyvinylidene fluoride (PVDF), 31–32
POM. *See* Polyoxymethylene (POM)
Power, 438
Power law, 419–420
  equations, 571
  fluid, 438, 561
  fluid flow
    between parallel plates, 424–426
    along uniform circular cross-section channel, 423–424
PP. *See* Polypropylene (PP)
PPA. *See* Polyphthalamides (PPA)
PPO. *See* Polyphenylene oxide (PPO)
PPS. *See* Polyphenylene sulphide (PPS)
Pre-form moulding, 349–351, 399–400
Pressure bag moulding, 396
Pressure drop
  at die entry, 429–431
  due to extensional flow, 428–429
  due to shear, 426–428
Pressure flow, 289–291
Pressure forming, 363
Processing of plastics, 279–280
  additive manufacturing techniques, 387–392
  calendering, 372–376
  compression moulding, 383–386
  extrusion, 280–321
  injection moulding, 321–357
  processing reinforced thermoplastics, 392–394
  processing reinforced thermosets, 394–405
  rotational moulding, 376–383
  thermoforming, 357–371
  transfer moulding, 386–387
Production injection mould, 331
Profile production, 302–303
Proteins, 19
PS. *See* Polystyrene (PS)
Pseudo-elastic design method for plastics, 71–80
PSU. *See* Polysulphone (PSU)
PTFE. *See* Polytetrafluoroethylene (PTFE)
PU. *See* Polyurethanes (PU)
Pultrusion, 404
PV ratings, 33
PVC. *See* Polyvinyl chloride (PVC)
PVDF. *See* Polyvinylidene fluoride (PVDF)

R

Rabinowitsch Correction Factor, 443
Radial stress, 500
Ram extruder, 441–444, 442f
Rapid prototyping techniques, 387–388
Reaction injection moulding (RIM), 348–349, 349f
Reactive extrusion, 321
Recovery, 107, 109–110, 115–116
  behaviour, 28
Recyclability, 44–45
Reduced time, 126
Reinforced plastics. *See also* Bio-degradable plastics
  deformation behaviour of, 195
  fatigue behaviour of, 269–271
  impact behaviour of, 271
Reinforced reaction injection moulding (RRIM), 348
Reinforced thermoplastics processing, 392–394
Reinforced thermosets, 12
  processing, 394–405
    automatic processes, 403–405
    manual processing methods, 396–398
    semi-automatic processing methods, 398–403
Reinforcement, 4, 195–198
Relaxation, 60, 106–107, 109, 114
Relaxation modulus, 67–69, 68f
Relaxation time, 106–107, 438, 507–508
Relaxed modulus, 69
Release agents, 4
Residence time, 437–438
Residual strain, 127
Resin injection, 401–402

Retardation time, 108
Rheological models for polymer melt flow, 419–423
  applying Carreau model to polypropylene, 422
  comparison of models for flow behaviour, 421f
Ribbed section design, 94–100
RIM. *See* Reaction injection moulding (RIM)
Roll-stack, 302
Rotational moulding, 101, 376–383
  slush moulding, 382–383
Rotational viscometers, 439
Rotosim®, 382
Row matrix, 603
RRIM. *See* Reinforced reaction injection moulding (RRIM)
Rule of mixtures, 529
Runners, 329–333

S

Sandwich beam of minimum weight, 504–505
Sandwich moulding, 344
Santoprene, 54
SBR. *See* Styrene-butadiene rubber (SBR)
SCF. *See* Supercritical fluid (SCF)
SCORIM. *See* Shear controlled orientation in injection moulding (SCORIM)
Screws, 325–326
Secant modulus, 21–22
Selective laser sintering (SLS), 390–392, 391f
Self-extinguishing, 41
Semi-automatic processing methods
  cold press moulding, 398–399
  hot press mouldings, 399–401
  resin injection, 401–402
  vacuum injection, 402–403
Semi-crystalline plastics, 5–6, 47–52
Semi-elliptical surface flaw, 150
Shape memory polymers (SMP), 18
Sharkskin, 446–447
Shear controlled orientation in injection moulding (SCORIM), 357
Shear modulus, 76
  of fibres, 208
Shear stresses, swelling ratios due to, 433–434
Sheet moulding compound (SMC), 13, 395, 400
Shift factor, 138–141
Short fibre composites
  analysis of, 256–263
  fibre lengths, 260–263
Short-term testing of plastics, 61–64
Side gate, 332
Silicone rubber, 14
Simple Newtonian model, 373, 411
Single edge cracks in plate of finite width, 150
Single plies
  deformation behaviour of, 209–216, 224–232
  loading off fibre axis, 212–216, 227–232
    using matrix notation, 212
  loading on fibre axis, 209–212, 224–226
  strength of, 265–267
    maximum strain criterion, 265–266
    maximum stress criterion, 265
    Tsai–Hill criterion, 266–267
Single screw extrusion, 280–286, 281f
  compression zone, 281–282
  feed zone, 281
  metering zone, 282–286
Sinusoidal variation of stress and strain, 132, 132f
Sizing, 198
SLA. *See* Stereolithography (SLA)
Slow burning, 41
SLS. *See* Selective laser sintering (SLS)
Slush moulding, 382–383
SMC. *See* Sheet moulding compound (SMC)
SMP. *See* Shape memory polymers (SMP)
Snap fits design, 90–94
Solid beam, 502–504
Solprene, 54
Spherulites, 593f
Spinneret, 314–315
Spray-up method, 396–398
Spring, 104
Sprue, 329–331, 333
  gates, 332
Standard linear solid, 113–116, 520
  equilibrium equation, 113
  geometry of deformation equation, 114–116
  stress–strain relations, 113
Starches, 19
Static fatigue, 156
Stereolithography (SLA), 388–389
Stiffening mechanisms in other moulding situations, 101–103
Stiffness
  enhancement factor, 101
  matrix, 212

Stiffness (*Continued*)
of plastics, 20–22
material selection for, 27–29
Strain
creep, 126–127
elastic, 461
engineering, 60
plane, 599
recovery, 125–126
residual, 127
thermal, 81–85
time-dependent residual, 125–126
transformation matrix, 214
viscous, 462–463
Strength
desirability factor, 22
of fibre composites, 263–269
of laminates, 267–269
of plastics, 20
material selection, 22–26
of single plies, 265–267
Stress
concentration, 142–143, 143f
effect, 170–173
factor, 143
continuous changes of, 119–125
in cylindrical shapes, 601–602
history, 119–120
intensification effect, 153
intensity factor approach to fracture, 148–152
plane, 599
range, 523
relaxation, 29
step changes of, 116–119
system effect, 167–168
thermal, 81–85
transformation matrix, 213
Stress–strain curves for polypropylene, 67f
Stress–strain equations, 508–509
Stress–strain graph for plastics, 20–21
Stress–strain relationships, 201–205, 207–209
biaxial stresses, 598–599, 598f
Kelvin or Voigt model, 107
Maxwell model, 104
standard linear solid, 113
triaxial stresses, 599
uniaxial stresses, 597–598, 597f
Stress–strain–time curves for polypropylene, 67f
Stress–time curves for polypropylene, 68f
Structural foams, 13–14, 15t
injection moulding, 342–344
Structure of plastics
molecular chain
arrangement of, 590–594
conformation of, 586–590, 587f
possible molecular structures, 589f
structure of long molecules, 585–586
Styrene-butadiene rubber (SBR), 14
Styrenics, 54
block copolymer, 14–16, 16f
Supercritical fluid (SCF), 357
Superposition principle, 116–125
continuous changes of stress, 119–125
step changes of stress, 116–119
Swelling ratio, 432–433
due to shear stresses
long capillary, 433–434
long rectangular channel, 434
due to tensile stresses
short capillary, 435–436
short rectangular channel, 436
Symmetric laminate, 541–544
stiffness, 235–237
Symmetric matrix, 605–606
Syndiotactic groups, 587–588

T

Tangent modulus, 21–22
Tape laying process, 393–394
Temperature
effect, 173–174
gradient, 465, 582
rise in die, 438–439
'Tensar geogrid' system, 318–319
Tensile modulus, 76
Tensile stresses, swelling ratio due to, 435–436
Tensile test, 61, 64–65
Tenter frame, 319–320
Testing control mode effect, 165
Tetrahedral angle, 585, 586f
Thermal stresses and strains, 81–85
Thermoforming, 101, 357–371
analysis, 368–371
matched die forming, 366
plug-assisted thermoforming, 364–366
pressure forming, 363
temperatures for common polymers, 359t
twin-sheet thermoforming, 366–368
vacuum forming, 360–363

Thermoplastic elastomers (TPEs), 14–16, 54
Thermoplastic polyurethanes (TPUs), 321, 389–392
Thermoplastic rubbers (TPRs), 14–16, 54
  physical characteristics, 28t
Thermoplastics, 198–199
  materials, 5–6, 20
Thermosets, 10–11, 164, 198
Thermosetting
  injection moulding of thermosetting materials, 351–353
  plastics, 7–8, 11, 54–56
  polyesters, 11
  polyimides, 11
Thick-gauge thermoforming, 359–360
Thin-gauge thermoforming, 359–360
Three plate mould. *See* Multi-daylight moulds
Three point bending, 152
Three-point loading, 63, 63f
3D printing, 388, 392
Time dependence of strength of plastics, 158
Time-dependent residual strain, 125–126
Time-temperature superposition, 138–141
Toggle, 328–329
Toughness, 29, 144
TPEs. *See* Thermoplastic elastomers (TPEs)
TPRs. *See* Thermoplastic rubbers (TPRs)
TPUs. *See* Thermoplastic polyurethanes (TPUs)
Transfer moulding, 386–387
Trial and error methods, 411
Triaxial stresses, 170–171, 171f, 599
Tsai–Hill criterion, 264, 266–267, 547–548
Twin screw extruders, 297–299
Twin-sheet thermoforming, 366–368

U

UF. *See* Urea formaldehyde (UF)
Ultra-high molecular weight polyethylene (UHMW-PE), 5, 9–10, 33
Ultraviolet (UV)
  radiation, 30
  stabilisers, 4
Uniaxial stresses, 597–598, 597f
Unidirectional composites, 217–224
Unidirectional fibre composites, elastic properties for, 209, 210t
Unidirectional plies, laminates from, 232
  in-plane behaviour of symmetric laminate, 232–235
Unplasticised polyvinyl chloride (uPVC), 9–10, 52–53
Unreinforced plastics, fracture behaviour of, 141–142
Unrelaxed modulus, 69
Unsymmetrical laminate, 543–544
uPVC. *See* Unplasticised polyvinyl chloride (uPVC)
Urea formaldehyde (UF), 11, 54

V

Vacuum bag moulding, 396
Vacuum forming, 360–363
Vacuum injection, 402–403
Venting, 333
Vestamid, 54
Viscoelastic behaviour of plastics, 60, 71
Viscosity of fluid, 60
Viscous strain, 462–463
Volume flow rate, 417, 571
Volume fraction, 199–200, 203, 528–529
Volume of cavity, 581
von Mises criterion, 296, 490
Vulcanisation, 14
Vulcanised rubbers, 14

W

Water-assisted injection moulding, 347–348
Waveform effect, 164–165
Wear resistance, 31–33
Weathering, 30
Wedge shaped die, isothermal flow in, 431–432
Weight fraction, 529
Whitening, 157
WLF equation, 139

X

XLPE. *See* Cross-linked polyethylene (XLPE)

Y

Young's modulus, 21–22

Z

Zero length die, 443
Zhurkov-Bueche equation, 521

FOURTH EDITION

PLASTICS ENGINEERING

ROY J. CRAWFORD AND PETER J. MARTIN

Plastics Engineering, Fourth Edition presents the essentials on the properties and processing behaviour of plastics and composites. The book gives engineers and technologists a sound understanding of fundamental principles without the introduction of unduly complex levels of mathematics or chemistry and thereby set plastics in their proper context as engineering materials. Over 200 analytical examples are included to demonstrate how basic engineering principles in design, mechanics of materials, fluid mechanics and thermodynamics may be applied to modern plastic materials. Early chapters discuss the types of plastics and composites currently available and describe how designers select a material for a particular application. Later chapters guide the reader through the mechanical behaviour of the materials to the detailed analysis of their major processing techniques and the underlying principles of polymer melt flow. All techniques are illustrated with numerous worked examples within each chapter.

This updated edition has been thoroughly revised to reflect major changes and developments in plastic and composite materials that have occurred since the previous edition, with new illustrations throughout and updated sections on new technologies. Plastics Engineering, Fourth Edition is an ideal resource for plastics and composites engineers, manufacturing engineers, plastics technologists, processing engineers, design engineers and product engineers involved with plastic or composite material development or modification. It also serves as a key text for undergraduate and postgraduate engineers in mechanical and aerospace manufacturing, and related disciplines where the study of plastics and composites is part of the degree programme.

KEY FEATURES

- Gives new engineers and technologists a thorough understanding of the essential properties and processing behaviour of plastics and composites
- Presents an outstanding source of foundational information for students, early-career engineers and researchers
- Demonstrates how basic engineering principles in design, mechanics of materials, fluid mechanics and thermodynamics may be applied to the properties, processing and performance of modern plastic materials

ABOUT THE AUTHORS

Roy J. Crawford was Vice Chancellor of the University of Waikato, New Zealand. Prior to this he was Pro-Vice-Chancellor for Research at Queen's University Belfast in Northern Ireland, United Kingdom. At Queen's University, Dr. Crawford was responsible for establishing the Polymer Processing Research Centre which included the Research Group on rotational moulding of plastics, which he also founded. In 1998, he was elected as a Fellow of the Royal Academy of Engineering, and in 2005, he was elected as a Fellow of the Society of Plastics Engineers. In the 2015 Queen's Birthday Honours, Dr. Crawford was appointed a Companion of the New Zealand Order of Merit, for services to tertiary education. Dr. Crawford sadly passed away in 2016.

Peter J. Martin is a Reader in Mechanical Engineering and Director of the Polymer Processing Research Centre at Queen's University Belfast. After joining Queen's University in 1991, his early research work focussed on extrusion and thermoforming, but his interests have since grown to encompass most forms of manufacturing with plastics and composites materials. Dr. Martin has lectured on plastics for more than 25 years and he has published numerous papers and articles in the area of plastics engineering. Dr. Martin is a Fellow of the Institution of Mechanical Engineers.

ELSEVIER

B H

Butterworth-Heinemann
An imprint of Elsevier
elsevier.com/books-and-journals

ISBN 978-0-08-100709-9

9 780081 007099